Torsion of a Circular Shaft With Diametrically Opposite Flat Sides

By W. J. CARTER[1] and J. B. OLIPHINT,[2] AUSTIN, TEXAS

The solutions for torsional stress and torsional stiffness of circular shafts with flat sides which are presented in this paper have been obtained by means of the relaxation technique. The solutions for both shear stress and torsional stiffness are given for four ratios of flat side dimension to diameter of the shaft. The stress for a very small flat has been obtained by use of a hydrodynamic analogy to the torsion problem. A comparison of the results obtained is made with those given by Ōkubo.

Introduction

THE problem of the elastic torsional behavior of prismatical bars has been studied extensively by many investigators. Saint Venant showed that all such problems may be reduced to a solution of Poisson's equation over the cross section

$$\nabla^2\psi = \frac{\partial^2\psi}{\partial x^2} + \frac{\partial^2\psi}{\partial y^2} = -2G\theta \quad \ldots\ldots\ldots\ldots [1]$$

where θ is the unit angular twist of the bar in radians, G is the shear modulus of the material, psi, and ψ is the stress function for the cross section. The shear stress is the gradient of the "ψ-surface," that is, the shear stress is $\partial\psi/\partial n$, where n is the direction normal to the boundary. The contour lines of the ψ-surface are lines of shear stress direction. The torsional stiffness of the cross section M_t is given by the expression

$$M_t = 2\int\int \psi\, dx\, dy \quad \ldots\ldots\ldots\ldots [2]$$

The exact solution of Equation [1] has been obtained for only a comparatively small number of cross sections, circles, ellipses, equilateral triangles, and so forth. The shear stress and torsional stiffness of most sections must be obtained either by some sort of approximate solution or by a numerical solution of Equation [1].

The relaxation technique has been employed by the authors in obtaining the solution for cross sections of the type shown in Fig. 1. The relaxation technique has been discussed in great detail elsewhere (1, 2)[3] and consequently will not be described here.

Maximum Shear Stress and Torsional Stiffness of Flattened Shafts

The cross sections for which solutions were obtained are like that of Fig. 1. A net spacing of $^1/_{16}r$ was used. The results are given in Table 1.[4]

TABLE 1 VALUES OF MAXIMUM SHEAR STRESS AND TORSIONAL STIFFNESS

$\frac{w}{r}$	α	τ_{max}	M_t
$\frac{7}{8}$	28.95°	1.34 $G\theta w$	1.357 $G\theta r^4$
$\frac{3}{4}$	41.40°	1.57 $G\theta w$	1.076 $G\theta r^4$
$\frac{5}{8}$	51.30°	1.71 $G\theta w$	0.733 $G\theta r^4$
$\frac{1}{2}$	60.00°	1.86 $G\theta w$	0.438 $G\theta r^4$

It is believed that the values for the maximum shear stress τ_{max}, and the values of the torsional stiffness given in Table 1 are accurate to within 2 or 3 per cent. The maximum stress in all cases is found at the center of the flat side.

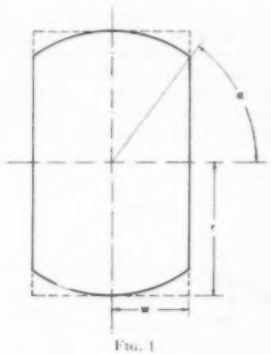

Fig. 1

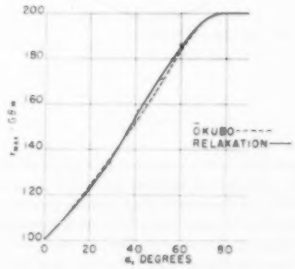

Fig. 2

Fig. 2 shows the values of τ_{max} plotted versus α. For comparison, the results obtained by Okubo (3) are also shown.

[4] τ_{max} = maximum shear stress.

---

[1] Associate Professor of Mechanical Engineering, University of Texas. Mem. ASME.

[2] Research Engineer, Military Physics Research Laboratory, University of Texas.

[3] Numbers in parentheses refer to the Bibliography at the end of the paper.

Contributed by the Applied Mechanics Division and presented at the Spring Meeting, Seattle, Wash., March 24–26, 1952, of The American Society of Mechanical Engineers.

Discussion of this paper should be addressed to the Secretary, ASME, 29 West 39th Street, New York, N. Y., and will be accepted until October 10, 1952, for publication at a later date. Discussion received after the closing date will be returned.

Note: Statements and opinions advanced in papers are to be understood as individual expressions of their authors and not those of the Society. Manuscript received by ASME Applied Mechanics Division, June 25, 1951. Paper No. 52—8-2.

Okubo's results were obtained by the use of an approximate solution employing a variation of the technique given by Shepherd (4). It is seen that the agreement is very good. For values of α greater than 60 deg, τ_{max} for the flattened shaft is essentially the same as for a rectangle which would enclose the flattened shaft (the rectangle is shown by dotted lines in Fig. 1).

The determination of τ_{max} for small values of α by the relaxation method would be much more laborious than for the cases listed. Such solutions would require the use of a much finer net spacing, thus multiplying the number of operations to be performed. This difficulty is always met when the behavior near a small irregularity such as a small flat or a small keyway radius is to be investigated by the relaxation method.

Calculation of Torsional Stress for Small Flats by Hydrodynamic Analogy

Greenhill (5) has shown that the stress function ψ is mathematically identical with the stream function of the motion of an ideal fluid circulating with uniform vorticity in a tube of the same cross section as the twisted bar. The velocity distribution in the hydrodynamical model is mathematically identical with the shear distribution in the twisted bar. For the case of a circular shaft with a small semicircular groove parallel to the axis of the shaft, the maximum flow velocity around the groove in the tube would be approximately twice the flow velocity on the tube wall far removed from the groove. It then may be concluded that a small semicircular groove very nearly doubles the maximum shearing stress in a shaft.

The fluid velocity increase across a small flat on the tube wall can be determined as follows: (*a*) The ideal fluid flow around a nonrotating circular cylinder can be transformed by the Kármán-Trefftz transformation (6) into the flow around a biconvex airfoil at zero angle of attack; (*b*) the flow around the biconvex airfoil can be transformed by the bilinear transformation into a flow pattern corresponding to the flow over the tube wall and flat. It should be noted that such a scheme would be valid only for small flats, since the airfoil flow satisfies Laplace's equation and will have a singularity at the center when transformed to the circle.

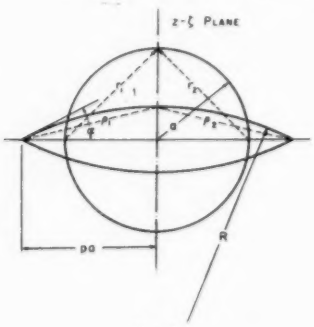

Fig. 3

The Kármán-Trefftz transformation which transforms the flow around a nonrotating circular cylinder into the flow around a biconvex airfoil at zero degrees angle of attack is of the form

$$Z = pa\,\frac{(\zeta + a)^p + (\zeta - a)^p}{(\zeta + a)^p - (\zeta - a)^p} \qquad [3]$$

The Z-plane is the plane of the flow around the biconvex airfoil and the ζ-plane is the plane of the flow around the circular cylinder, Fig. 3. The exponent p has the value $p = 2(1 - \alpha/\pi)$. If V is the free-stream velocity far removed from the airfoil, it may be shown that the maximum flow velocity on the biconvex airfoil is

$$V_p = 2V\,\frac{\rho_1\rho_2}{r_1 r_2} \qquad [4]$$

where V_p is the velocity at the center of the biconvex airfoil. For this special case

$$\rho_1\rho_2 = 2a^2$$

$$r_1 = r_2 = \frac{pa}{\cos\alpha} \cong \frac{pa}{1 - \dfrac{\alpha^2}{2!}}, \quad \text{for small } \alpha \qquad [5]$$

$$r_1 r_2 = \frac{\left[2a\left(1 - \dfrac{\alpha}{\pi}\right)\right]^2}{\left(1 - \dfrac{\alpha^2}{2!}\right)^2} \cong \frac{4a^2\left(1 - \dfrac{2\alpha}{\pi} + \dfrac{\alpha^2}{\pi^2}\right)}{(1 - \alpha^2)}, \quad \text{for small } \alpha \qquad [6]$$

$$\frac{\rho_1\rho_2}{r_1 r_2} = \frac{2a^2(1 - \alpha^2)}{4a^2\left(1 - \dfrac{2\alpha}{\pi} + \dfrac{\alpha^2}{\pi^2}\right)} = \frac{1 - \alpha^2}{2\left(1 - \dfrac{2\alpha}{\pi} + \dfrac{\alpha^2}{\pi^2}\right)} \qquad [7]$$

$$V_p = \frac{V(1 - \alpha^2)}{\left(1 - \dfrac{2\alpha}{\pi} + \dfrac{\alpha^2}{\pi^2}\right)} \qquad [8]$$

The complex transformation which maps three distinct points Z_1, Z_2, and Z_3 into any three desired points w_1, w_2, and w_3 that are distinct is known as the bilinear or Mobius transformation. This transformation is

$$\frac{(w - w_1)(w_2 - w_3)}{(w - w_3)(w_2 - w_1)} = \frac{(Z - Z_1)(Z_2 - Z_3)}{(Z - Z_3)(Z_2 - Z_1)} \qquad [9]$$

In this instance it is desired to transform $Z_1 = 1$ into $w_1 = 1$, $Z_2 = ih$ into $w_2 = 0$, and $Z_3 = -1$ into $w_3 = -1$. Such a transformation will map the upper portion of the biconvex airfoil into a straight line corresponding to the flat and the center streamline approaching the biconvex airfoil into a circle corresponding to the tube wall, Fig. 4.

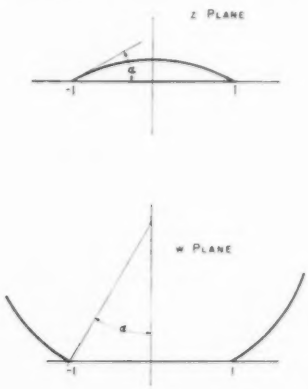

Fig. 4

The maximum flow velocity across the flat is found by multiplying Equation [7] by $(dZ)/(dw)$. A differentiation of Equation [5] yields

$$\frac{dZ}{dw} = \frac{(Z_2 - Z_3)(Z_3 - Z_1)(w_1 - w_3)}{(w_2 - w_3)(w_3 - w_1)(Z_1 - Z_3)} \quad [10]$$

and upon substitution there results

$$\frac{dZ}{dw} = h^2 + 1 \quad [11]$$

For small α

$$h = R(1 - \cos\alpha) \cong R\left[1 - \left(1 - \frac{\alpha^2}{2!}\right)\right] = \frac{R\alpha^2}{2}. \quad [12]$$

Also

$$R = \frac{1}{\sin\alpha} \cong \frac{1}{\alpha}, \text{ for small } \alpha \quad [13]$$

Thus $h = \alpha/2$, from which

$$\frac{dZ}{dw} = \frac{\alpha^2}{4} + 1 \quad [14]$$

It may be now stated that the stress at a small flat is

$$\tau_{max} = \frac{G\theta r(1 - \alpha^2)\left(\frac{\alpha^2}{4} + 1\right)}{\left(1 - \frac{2\alpha}{\pi} + \frac{\alpha^2}{\pi^2}\right)} \cong \frac{G\theta r\left(1 - \frac{3}{4}\alpha^2\right)}{\left(1 - \frac{2\alpha}{\pi} + \frac{\alpha^2}{\pi^2}\right)} \quad [15]$$

Equation [15] has been used in drawing the curve for τ_{max} for the portion of the curve in Fig. 2 from $\alpha = 0$ deg to $\alpha = 7.5$ deg. It should be noted that α must be expressed in radians for substitution in Equation [15].

BIBLIOGRAPHY

1 "Relaxation Methods," by Sir R. V. Southwell, Oxford University Press, Oxford, England, 1946.

2 "The Torsion of Solid and Hollow Prisms in the Elastic and Plastic Range by Relaxation Methods," by F. S. Shaw, Report ACA-11, Australian Council for Aeronautics, Melbourne, Australia, 1944.

3 "Torsion ' a Circular Shaft With a Number of Longitudinal Notches," by H. Okubo, JOURNAL OF APPLIED MECHANICS, Trans. ASME, vol. 72, 1950, pp. 359–362.

4 "The Torsion and Flexure of Shafting With Keyways of Cracks," by W. M. Shepherd, Proceedings of the Royal Society of London, series A, vol. 138, 1932, pp. 607–634.

5 "Hydromechanics," by Sir A. G. Greenhill, Encyclopaedia Britannica, Cambridge University Press, New York, N. Y., eleventh edition, vol. 14, 1910, pp. 115–135.

6 "Théorie et Traces des Profils d'ailes sustentatrices," by A. Toussaint and E. Carafoli, Extrait du Bulletin de la Chambre Syndicale des Industries Aéronautiques, Librairie Aéronautique, Paris, France, 1928, pp. 50–53 and 60–65.

Optimum Single Propellers in Radially Varying, Incompressible Inflow[1]

By FRANK LANE,[2] STATE COLLEGE, PA.

The Betz process for minimizing the energy loss of single propellers is extended to the propeller operating in radially varying inflow, with a view toward the development of optimum stern propulsion for bodies of revolution. Assuming the usual lifting-line treatment of the propeller blades, an application of the isoperimetric problem in the calculus of variations is directed toward minimizing the energy loss while maintaining constant total thrust. Resulting expressions describe the optimum radial distribution of induced velocity in terms of an undetermined multiplier. The magnitude of the required total thrust, in turn, fixes the value of this multiplier, making the solution determinate. Inclusion of blade-profile drag at a later point in the development serves to determine an optimum propeller diameter for minimum over-all energy loss. The method gains in accuracy as the ratio of blade number to advance ratio increases, due to an approximation in the relation between the circulation and induced velocity.

The following nomenclature is used in the paper:

- B = number of blades
- C_d = section drag coefficient
- C_l = section lift coefficient
- F = correction factor for finite blade number
- J_l = advance ratio based on reference length l; $V_0/nl = J_l$
- l = reference length; some characteristic length of the inflow velocity function
- n = propeller rotational speed; revolutions per second (rps)
- P_{use} = useful power, neglecting blade-profile drag
- P_{in} = input power, neglecting blade-profile drag
- $P_{use(d)}$ = useful power including profile-drag effect
- $P_{in(d)}$ = input power including profile-drag effect
- Q = torque
- r = local radius
- R = tip radius of propeller or of trailing vortex sheets
- T = thrust
- V_0 = velocity of advance of propeller relative to undisturbed fluid
- V = variable axial inflow velocity, a function of relative radius, r/l
- V_e = resultant of relative incident and induced velocities
- w = induced velocity
- w_a = axial component of w
- w_t = tangential component of w
- Γ = circulation or bound vorticity per blade
- Γ^∞ = circulation per blade as $B \to \infty$
- ϕ = angle between resultant velocity V_e and plane of propeller
- Φ = value of ϕ at outside radius of propeller or vortex sheets
- ρ = fluid density
- ω = propeller angular velocity; radians per second
- λ = Lagrange undetermined multiplier
- ϵ = arctan (C_d/C_l)
- η = efficiency, P_{use}/P_{in}, neglecting profile drag
- η_d = efficiency, $P_{use(d)}/P_{in(d)}$, including profile drag

Subscripts:

- a = axial component
- h = hub
- d = including drag
- l = tangential component
- u = ultimate wake

Introduction

The conditions on induced-velocity distribution and bound vorticity for the optimum propeller acting in an undisturbed fluid have been developed to a high degree by Betz, Prandtl, Goldstein, and Theodorsen.[3, 4, 5] The well-known requirement that for maximum efficiency the trailing vortex sheets move as solid helicoids under the influence of their own induced velocities was derived first by Betz under the restriction of light loading and extended later by Theodorsen to include the case of moderate loading. Circulation functions corresponding to this optimum distribution of induced velocity were developed by Prandtl and Goldstein. This paper describes an extension of the optimizing process to propellers operating in axially symmetric, nonuniform inflow, such as might be encountered in the wake of a body of revolution. Given a prescribed inflow and required values of thrust and operating advance ratio (based on some characteristic dimension of the inflow rather than on the usual propeller diameter), a method is presented whereby the optimum induced-velocity distribution and the corresponding bound vorticity function may be derived. Moreover, consideration of blade-profile drag fixes an optimum propeller diameter for minimum total energy loss. Certain assumptions are introduced during the optimizing process in order to simplify the development, but a final re-evaluation of the resulting formulas justifies these earlier assumptions.

Outline of Problem and General Method of Solution

Fig. 1(*a*) illustrates the axial component of a radially varying

[1] This work was sponsored by the U. S. Navy Department under Contract NOrd 7958.

[2] Associate Professor, Engineering Research, Ordnance Research Laboratory, The Pennsylvania State College.

Presented at the National Conference of the Applied Mechanics Division, State College, Pa., June 19–21, 1952, of The American Society of Mechanical Engineers.

Discussion of this paper should be addressed to the Secretary, ASME, 29 West 39th Street, New York, N. Y., and will be accepted until October 10, 1952, for publication at a later date. Discussion received after the closing date will be returned.

Note: Statements and opinions advanced in papers are to be understood as individual expressions of their authors and not those of the Society. Manuscript received by ASME Applied Mechanics Division, November 7, 1951. Paper No. 52—APM-23.

[3] "Schraubenpropeller mit geringstem Energieverlust; mit einem Zusatz von L. Prandtl," by A. Betz, Goettinger Nachrichten, 1919. Reprinted in Prandtl and Betz, "Vier Abhandlungen zur Hydrodynamik und Aerodynamik," Göttingen, Germany, 1927.

[4] "On the Vortex Theory of Screw Propellers," by S. Goldstein, Proceedings of the Royal Society of London, England, series A, vol. 123, 1929, pp. 440–465.

[5] "Theory of Propellers," by T. Theodorsen, McGraw-Hill Book Company, Inc., New York, N. Y., 1948.

inflow relative to the plane in which a propeller is to operate. The reference velocity V_0, with respect to which all velocities will be made dimensionless, represents the velocity of advance of the propeller relative to the undisturbed fluid. The reference length l may be taken as any characteristic length of the velocity distribution or of the body causing the disturbance. Only the axial component V of the symmetric inflow is considered in the present development, since the radial inflow component is effective

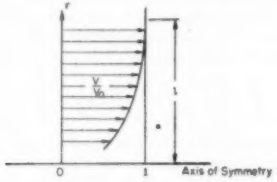

FIG. 1(*a*) AXIAL COMPONENT OF INFLOW VELOCITY RELATIVE TO PROPELLER PLANE

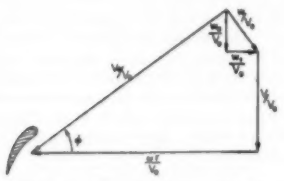

FIG. 1(*b*) BLADE-ELEMENT VELOCITY DIAGRAM

chiefly in increasing the wake contraction. The wake-contraction effect, in turn, is minimized by expressing the circulation function in terms of the ratio of local radius to the radius of the outer edge of the trailing vorticity. It must be assumed, however, that the radial inflow component is small relative to the axial inflow. It is assumed further that the major portion of the velocity defect $(V_0 - V)$ in the inflow is frictional in origin and that the departure of static pressure from its free-stream value is relatively small. This implies that the increase in axial velocity downstream is brought about almost entirely by propeller action rather than by any potential velocity regain which would occur even in the absence of the propeller.

Shown in Fig. 1(*b*) is a typical dimensionless blade-element velocity diagram at some relative radius r/l. The induced velocities, shown as dimensionless quantities, are dependent upon the degree and type of loading to which the propeller is subjected. Optimizing propeller efficiency resolves itself into the determination of the most favorable radial distribution of these induced velocities and of the corresponding circulation function.

Proceeding from the incident flow conditions just described, the method of optimizing is as follows: Expressions for thrust, torque, power input, and useful power are developed in terms of general distributions of induced velocity and bound vorticity after replacing each blade by a lifting line of bound vorticity. With the aid of Prandtl's relation between induced velocity and bound vorticity and with the usual geometrical restrictions on induced velocities, the integral expressions for useful power and input power are rewritten in terms of induced-velocity components. An application of the calculus of variations is then directed toward minimizing input power while holding constant the thrust or useful power. The resulting expression prescribes a radial distribution of induced velocity for optimum efficiency. The introduction of blade-profile drag is postponed until a later stage where it is useful in determining the most favorable propeller diameter for minimum total energy loss.

EXPRESSIONS FOR THRUST, TORQUE, AND POWER

Keeping the induced-velocity and bound-vorticity functions perfectly general for the moment, we can express the total thrust and torque of a B-bladed propeller, neglecting friction, as follows

$$\text{Thrust} = T = V_0^2 l^2 \rho B \int_{r_h/l}^{R/l} \frac{\Gamma}{V_0 l} \left(\frac{\omega r - w_i}{V_0} \right) d\left(\frac{r}{l}\right) \quad [1]$$

$$\text{Torque} = Q = V_0^2 l^3 \rho B \int_{r_h/l}^{R/l} \frac{r}{l} \frac{\Gamma}{V_0 l} \left(\frac{V + w_a}{V_0} \right) d\left(\frac{r}{l}\right) \quad [2]$$

These integrations are carried out over the extent of the blade radius from hub to tip.

Useful power is given by the product of thrust T and advance velocity V_0, while input power equals the torque Q multiplied by angular velocity ω.

The optimizing problem consists in minimizing the input power while maintaining constant useful power or thrust. In order to perform this operation, it is necessary to determine functional relations between circulation and induced velocity as well as the relation between the induced-velocity components themselves.

RELATION BETWEEN CIRCULATION FUNCTION AND INDUCED VELOCITY

For a fictitious infinite-bladed propeller, the relation between circulation or bound vorticity Γ, and induced velocity is given directly by elementary considerations of vortex continuity and Stokes' theorem. The expression for circulation per blade as B approaches infinity is

$$\frac{\Gamma^\infty}{lV_0} = \frac{4\pi}{B} \left(\frac{r}{l}\right) \frac{w_i}{V_0} \quad [3]$$

where w_i is the tangential component of induced velocity at the propeller plane. This component builds up to its ultimate value of $2w_i$ immediately downstream from the propeller plane.

For single propellers operating in undisturbed fluid two methods are available for extending the infinite-blade circulation function to the case of a finite blade number. Goldstein[4] solved the exact potential problem for a system of rigid helicoidal laminae in a uniform axial flow. This corresponds physically to the solution for a finite-bladed propeller with the Betz-type optimum induced-velocity distribution. Goldstein's solution, while rigorous for propellers operating in undisturbed fluid, proves to be too cumbersome to handle in the optimizing process, and is no longer exact for the condition of nonuniform inflow with its rotational character. Prandtl[3] in an earlier treatment, derived an approximate relation between circulation and induced velocity, the approximation becoming more exact as the ratio of blade number to advance ratio increases. This relation also applies only to the Betz-type induced-velocity distribution and was, of course, derived for the case of the propeller in an undisturbed fluid. In view of its susceptibility to an application of the variational calculus, Prandtl's approximation is chosen for the present optimizing treatment. The use of this relation in radially varying inflow will be justified later. The results of Prandtl's work may be expressed in terms of a single factor F, by which the infinite-bladed circulation function is multiplied to allow for the effect of finite blade number. Thus

$$\left.\begin{aligned} \Gamma &= F\Gamma^\infty \\ &= F \frac{4\pi}{B} r w_i \end{aligned}\right\} \quad [4]$$

where

$$F = \frac{2}{\pi} \arccos \left[\exp \left\{ \frac{-B\left[1 - \left(\frac{r}{R}\right)_u\right]}{2 \sin \Phi_u} \right\} \right] \quad \ldots\ldots [5]$$

Here r/R denotes local radius divided by tip radius, and Φ is the angle ϕ evaluated at the tip radius. The subscript u is employed in Equation [5] to indicate that the quantities $(r/R)_u$ and Φ_u must be evaluated in the ultimate wake, or sufficiently far downstream for the induced velocities to have attained their ultimate values. Assuming, however, that any wake contraction will be nearly uniform, r/R at the propeller plane will be closely equal to $(r/R)_u$ at the corresponding point in the ultimate wake, i.e., on the same trailing vortex element. Thus

$$\left(\frac{r}{R}\right)_u \cong \left(\frac{r}{R}\right) \quad \ldots\ldots [6]$$

for the same trailing vortex element. The ultimate wake value ϕ_u of the angle ϕ at any radius may be evaluated closely by making the usual assumption that both w_a and w_t, the axial and tangential induced-velocity components, respectively, increase by a factor of 2 from the propeller plane to the ultimate wake.

The application of Prandtl's finite-blade correction factor to a propeller operating in a nonuniform inflow requires some justification. A close scrutiny of Prandtl's development indicates that three conditions are necessary in order to apply the results with any degree of confidence: (1) The vortex sheets downstream from the propeller must move as rigid helicoids under the influence of their own induced velocities. (2) The quotient B/J_t must be large in order that Prandtl's approximation to the flow about the vortex-sheet edges approach the true solution. (3) The form of the inflow-velocity function should be fairly flat toward the propeller-blade tips in order to approximate effectively the conditions of Prandtl's two-dimensional flow model. The requirement of high B/J_t values is entirely compatible with high efficiency, since induced tip losses decrease as B/J_t increases. Restriction to low velocity-gradient magnitudes in the propeller-tip region is consistent with normal wake forms for bodies of revolution and with the relative propeller diameters R/l which result from the present development. The requirement that the vortex sheets move as rigid helicoids in the ultimate wake can only be assumed to hold for the present. Fortunately, it will appear later from the results of the optimizing treatment that this condition is met fairly closely when the propeller operates with its optimum distribution of induced velocities. Hence we proceed in the development with Equations [4] and [5] providing the necessary relation between circulation and induced velocity. Under the assumption that w_a and w_t increase by a factor of 2 from the propeller plane to the ultimate wake, we may write

$$\tan \Phi_u = \tan \phi_u \Big]_{r/R=1} = \frac{V + 2w_a}{\omega r - 2w_t}\Big]_{r/R=1} \quad \ldots\ldots [7]$$

Equation [7] must be regarded as arising from a hypothetical extension of conditions at the propeller into an idealized ultimate wake for the sole purpose of applying the Prandtl correction factor. Discrepancies in the angle Φ_u due to the assumptions involved in Equation [7] are minimized in the determination of F by the form in which this angle appears in Equation [5].

Solution of the Isoperimetric Problem

Using the relation between circulation and induced velocity, the expressions for useful power and input power may be written

$$P_{use} = V_0^3 l^2 \rho \int_{r_h/l}^{R/l} 4\pi \frac{r}{l} \frac{w_t}{V_0} F \left(\frac{\omega r - w_t}{V_0}\right) d\left(\frac{r}{l}\right) \quad \ldots [8]$$

$$P_{in} = V_0^3 l^2 \rho \int_{r_h/l}^{R/l} 4\pi \frac{r}{l} \frac{w_t}{V_0} F \frac{\omega r}{V_0} \left(\frac{V + w_a}{V_0}\right) d\left(\frac{r}{l}\right) \quad \ldots [9]$$

It is important to note here that the finite blade factor F is independent of local induced velocities at radius r, but depends only upon tip values of induced velocity in so far as these affect the angle Φ_u.

The immediate aim of the optimizing process is the development of some relation between the induced-velocity components whereby the input power may be minimized while useful power is held constant. This may be expressed formally in the notation of the calculus of variations as

$$\int \delta \left[\frac{dP_{in}}{d(r/l)} - \lambda \frac{dP_{use}}{d(r/l)} \right] d\left(\frac{r}{l}\right) = 0 \quad \ldots\ldots [10]$$

Here δ denotes variation and λ is the Lagrange undetermined multiplier. If we express the bracketed portion of Equation [10] entirely in terms of relative radius r/l and one quantity which is a function of r/l, the formal solution of Equation [10] will provide the conditions on this function necessary to satisfy our optimizing relation. We choose the tangential induced-velocity component w_t as the function of r/l most easily handled, and express the input and useful power integrands entirely in terms of r/l and $w_t(r/l)$. The circulation function Γ is already in the required form. It remains to express the axial induced-velocity component w_a in terms of the tangential component w_t. This is accomplished by following the usual assumption that the total induced velocity w_u is closely normal to the resultant velocity V_{eu} in the ultimate wake. The requirement that w_u be normal to V_{eu} is expressed as

$$\tan \phi_u \Big]_{r/l} = \frac{V + 2w_a}{\omega r - 2w_t}\Big]_{r/l} = \frac{2w_t}{2w_a}\Big]_{r/l} \quad \ldots\ldots [11]$$

From Equations [11] the following relations may be written

$$\left.\begin{aligned} \frac{w_a}{V_0}\left(\frac{V + 2w_a}{V_0}\right) &= \frac{w_t}{V_0}\left(\frac{\omega r - 2w_t}{V_0}\right) \\ \frac{\partial w_a}{\partial w_t} &= \left(\frac{\omega r - 4w_t}{V + 4w_a}\right) \end{aligned}\right\} \quad \ldots\ldots [12]$$

Now the operation indicated by Equation [10] may be performed in the following manner

$$\frac{\partial}{\partial w_t}\left[\frac{dP_{in}\left(\frac{r}{l}, w_t\right)}{d(r/l)} - \lambda \frac{dP_{use}\left(\frac{r}{l}, w_t\right)}{d(r/l)}\right] = 0 \quad \ldots [13]$$

$$\frac{\partial}{\partial w_t}\left[\frac{r}{l}\frac{w_t}{V_0} F \frac{\omega r}{V_0}\left(\frac{V + w_a}{V_0}\right) - \lambda \frac{r}{l}\frac{w_t}{V_0} F\left(\frac{\omega r - w_t}{V_0}\right)\right] = 0 \quad \ldots [14]$$

$$\frac{\omega r}{V_0}\left[\frac{V + w_a}{\omega r - 2w_t} + \left(\frac{w_t}{\omega r - 2w_t}\right)\left(\frac{\omega r - 4w_t}{V + 4w_a}\right)\right] = \lambda \quad \ldots [15]$$

Equation [15] is the desired relation, indicating that the quantity on the left must remain constant over the radius of the propeller blade for optimum efficiency. It can be shown, further, from this relation that the assumption of rigid helicoidal motion of the vortex sheets in the ultimate wake, under the influence of induced velocities, is quite closely approximated for values of w_a and w_t which are reasonably small relative to the reference velocity V_0. This serves as justification for the use of Prandtl's F-factor for nonuniform inflow in the present case.

Application of Optimizing Equation to Propeller Design

Equation [15] merely places a condition of constancy on the left-hand expression, the magnitude of this constant depending on the value of the undetermined multiplier λ. The problem

becomes determinate, however, upon the specification of a required value of total thrust. For any fixed value of λ, Equations [12] and [15] may be solved simultaneously for w_a and w_t at any relative radius in terms of the radius itself and V_0 which is a known function of relative radius. Choice of a propeller (relative) tip radius R/l will then allow the computation of the blade factor F, and ultimately the value of the thrust integral. It is thus found that for each of a range of possible values of λ, a corresponding relative tip radius will provide the required thrust. This suggests immediately the possibility of carrying the optimizing process one step further and determining an optimum relative tip radius. The logical approach is to find several combinations of λ and R/l each of which provides the required thrust, plot efficiency as a function of R/l or λ, and choose the peak of the efficiency curve. Actually, however, unless profile drag is incorporated into the expressions for thrust and power, only a lower limit on R/l will arise from this procedure when applied to inflow velocities normally encountered with slender bodies of revolution. The inclusion of profile drag, on the other hand, results in a curve of efficiency with a well-defined maximum and a corresponding optimum tip radius.

At this point, therefore, it becomes expedient to introduce profile drag into the expressions for useful and input power. Letting $\tan \epsilon$ denote the ratio C_d/C_l at any radius, the expressions for thrust and power are modified as follows

$$P_{use(d)} = V_0 \Omega^2 \rho \int_{r_h/l}^{R/l} \frac{4\pi r}{l} \frac{w_t}{V_0} F \frac{(\omega r - w_t)}{V_0} (1 - \tan \epsilon \tan \phi)\, d\left(\frac{r}{l}\right) \quad [8a]$$

$$P_{in(d)} = V_0 l^2 \rho \int_{r_h/l}^{R/l} \frac{4\pi r}{l} \frac{\omega r}{V_0} \frac{w_t}{V_0} F \left(\frac{V + w_a}{V_0}\right) \left(1 + \frac{\tan \epsilon}{\tan \phi}\right) d\left(\frac{r}{l}\right) \quad [9a]$$

The determination of an optimum tip radius is then performed in the following manner: Several values of λ are chosen, and the corresponding distributions of induced velocity are determined from Equations [12] and [15]. For each value of λ several trial values of tip radius R/l are chosen and the corresponding F-factors are determined. The values of $\tan \epsilon$ can be estimated closely from a knowledge of the desired lift-coefficient magnitudes and typical drag-coefficient information. Then the thrust can be determined from Equation [8a] and plotted for each value of tip radius at a fixed value of λ. The intersection of this plot with the value of required thrust gives the desired tip radius. For this radius, input power is found from Equation [9a], and the quotient $P_{use(d)}/P_{in(d)}$ gives the value of efficiency η_d. This process is repeated for each of several values of λ. Finally, a plot is made of efficiency versus either λ or the corresponding value of R/l, and the peak efficiency determines the optimum tip radius.

It can be shown, for practical values of $\tan \epsilon$ and for usual wake forms $V(r/l)$, that the introduction of profile drag into the development at an earlier stage alters the optimum induced-velocity distribution to a negligible extent, while complicating the entire procedure considerably.[5] Furthermore, the approximate methods necessary for estimating $\tan \epsilon$, while not sufficiently accurate for final performance calculations, are adequate for the optimum tip-radius determination.

Typical Results and Interpretation

Shown in Fig. 2 is an inflow-velocity function as measured close to the tail of a body of revolution with 7:1 fineness ratio. Also illustrated is the corrected velocity function, which will be explained later. In this particular instance the reference length l is taken as the maximum radius of the body causing the disturbance. The propeller-optimizing calculations described herein were carried out in detail for this velocity function at an advance ratio of $J_l = 1.675$, with a thrust requirement equal to the body drag plus an interference correction. Some of the results of these calculations are of sufficient interest to merit inclusion in the present discussion.

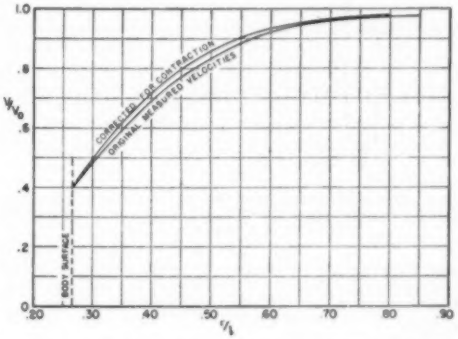

Fig. 2 Axial Inflow-Velocity Functions V/V_0 Versus r/l

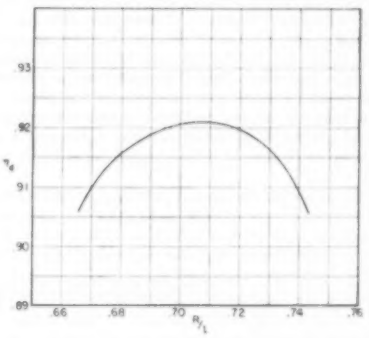

Fig. 3 Curve of Efficiency Versus Tip Radius for Constant Thrust and Optimum Induced-Velocity Distribution

It should be noted first that the velocity function in Fig. 2 satisfies the requirement of a small gradient outboard in the neighborhood of the propeller-blade tips. Application of the optimizing procedure led to a set of pairs, λ and R/l, for each of which the prescribed value of total thrust was attained, using Equation [8a] with an estimated distribution of $\tan \epsilon$. The resulting curve, Fig. 3, of efficiency η_d as a function of tip radius shows a well-defined maximum. A relative tip radius of $R/l = 0.708$ with its corresponding value of λ will then give the minimum total energy loss for a propeller operating at the specified thrust in the inflow-velocity function of Fig. 2 at $J_l = 1.675$.

Finally, Fig. 4 shows the radial distribution of axial and tangential induced-velocity components for the peak efficiency conditions found from Fig. 3, while Fig. 5 indicates the degree of departure of the vortex sheets in the ultimate wake from true heli-

[5] The author is indebted to D. J. Gildea, formerly of the Pennsylvania State College, for this portion of the investigation.

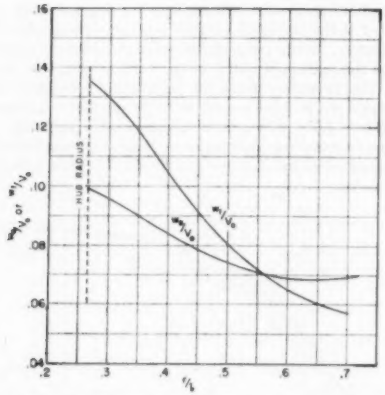

FIG. 4 RADIAL DISTRIBUTION OF RELATIVE AXIAL AND TANGENTIAL INDUCED-VELOCITY COMPONENTS CALCULATED FOR λ CORRESPONDING TO PEAK EFFICIENCY OF FIG. 3

coidal form ($r_i \tan \phi_i$ = const). The relatively large values of w_t/V_0 in the inboard region, Fig. 4, explain the minor departure of the trailing vorticity from true helicoidal form in this region, Fig. 5.

REFINEMENTS AND CORRECTIONS

In performing an actual propeller-design calculation based on the theory presented here, several refinements are necessary:

(1) If the propeller is located close to the tail of the propelled body, the thrust required for self-propulsion must be somewhat larger than the bare-body drag, due to interference effects. The propeller, in effect, induces a negative pressure field over the afterportion of the body, thereby causing an effective increase in drag. This correction can be estimated in terms of the drag and need not be incorporated into the optimizing scheme as a local function of w_t/V_0.

(2) The inflow-velocity function measured or calculated at the plane of the propeller must be altered to allow for upstream contraction due to axial induced velocities. Fig. 2 shows, in addition to the original measured inflow-velocity function, the final contracted distribution corresponding to the loading of Fig. 4. The upstream contraction effect could be considered an integral

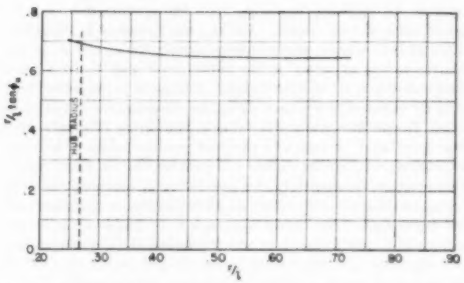

FIG. 5 PLOT OF (r/l) TAN ϕ_w TO DETERMINE DEPARTURE OF ULTIMATE VORTICITY FROM TRUE HELICOIDAL FORM

part of the optimizing operation, and an attempt made to include it in the form $\partial V/\partial w_t$ in the isoperimetric problem; however, while the actual *existence* of the contraction correction has a marked effect on the induced velocities for specified thrust, the *change* in the correction for slightly varying distribution of induced velocities at constant total thrust should introduce only a higher-order effect on the optimum induced-velocity function.

Repeated trials may be used to refine the estimate of tan ϵ if greater accuracy is desired. Based on a first estimate of tan ϵ the optimizing process may be carried through to the point of a tentative choice of airfoil sections. This allows a better estimate of the radial distribution of tan ϵ, and a recalculation based on the new values will be sufficiently accurate for design purposes. It should be noted that the profile-drag estimate affects only the latter stages of the optimizing process, i.e., the optimum diameter calculation, and has no influence upon the induced-velocity calculations for various λ-values.

One final problem arises whenever the ratio of propeller hub diameter to tip diameter becomes large. This difficulty is not confined to the treatment of propellers in nonuniform inflow, but exists for propellers with large hub-to-tip diameter ratios operating in undisturbed fluid as well. The fault lies in the failure of either the Prandtl or the Goldstein circulation functions to satisfy hub boundary conditions, since both of these theories are based on an effectively zero hub-to-tip diameter ratio. Further investigation of this effect is necessary to provide design information for propellers with relatively large hubs operating either in nonuniform inflow or in undisturbed fluid.

A Progressing-Wave Approach to the Theory of Blast Shock[1]

By R. G. NEWTON,[2] CAMBRIDGE, MASS.

This paper deals with a theoretical description of the motion of a spherical shock wave in a homogeneous medium, such as a blast shock in free air. In order to facilitate such a treatment, a simple assumption concerning the flow is made. The concept of a "progressing wave" as used in this paper is explained and compared with that used by other authors. A simple assumption is made about the motion of the progressing wave, and on its basis an ordinary second-order differential equation for the shock front is derived. Conservation of energy in the shock sphere reduces this to an ordinary first-order differential equation. Examination of the asymptotic behavior of the wave reveals that the original assumption in its simplest form contradicts conservation of energy. The original assumption is then suitably modified and the resulting new equations derived, including asymptotic values. Values for the high-pressure approximation, i.e., near the center of the explosion, are derived, and finally asymptotic as well as high-pressure values are derived for the pressure decay behind the shock front.

Nomenclature

The following nomenclature is used in the paper:

- u = particle velocity
- ρ = density
- p = pressure
- c = velocity of sound
- T = temperature
- R = radius of shock sphere, i.e., distance of shock front from center
- U = velocity of shock front divided by sound velocity in gas at rest in front of shock, i.e., Mach number of shock velocity
- $V = R/c_0 t$ = ratio of distance shock front has traveled to distance a sound wave would have traveled in same time interval

Subscripts t and r denote partial differentiation with respect to time or radial distance, respectively. A subscript 0 denotes a value in the still gas in front of the shock; a subscript 1 denotes a value directly behind the shock, i.e., a limit as one approaches the shock discontinuity from behind; λ is the ratio of the specific heats of the gas in question, with the value 1.4 for air at atmospheric pressure.

Introduction

In attempting to find the distance-time curve of a spherical shock front resulting from an explosion in a free gas at rest, one is confronted with the usual problem in the theory of shock waves, namely, that of several simultaneous, nonlinear partial differential equations with boundary conditions which partly lie on an unknown boundary (the shock curve) determined by these conditions (the Rankine-Hugoniot relations). It is essential that the differential equations themselves do not imply at all the position of the shock discontinuity but that, in case there is to be a shock, all they imply is that a discontinuity must occur somewhere within certain limits (between the two branches of the limiting line, the envelope of the characteristics). The exact position of the discontinuity is determined only by the additional Rankine-Hugoniot relations. For this reason it is not advisable to make any kind of assumption as to the flow behind the shock front in which the shock itself, a breakdown of the flow equations after all, plays any particularly distinguished role.

Since it is impossible to obtain an ordinary differential equation for the shock front from the flow equations and the Rankine-Hugoniot relations alone, it is imperative, in order to obtain such an ordinary differential equation, to make some arbitrary but reasonable assumptions about the "wave form" of the flow, or some other kind of auxiliary assumption in its place. A progressing-wave assumption of a simple type has been made by G. I. Taylor.[3] His approach, however, gives the shock front a distinguished position in the wave form, as, for example, the peak pressure is assumed to follow an equation of the form

$$p/p_0 = R^{-\alpha} f(x)$$

with $x = r/R$; similarly for the density and particle velocity. Such assumptions can be written in the following form

$$u = f_1 W(\eta),\ \rho = f_2 \Omega(\eta),\ p = f \Pi(\eta),\ \eta = r^{-k} t$$

as is done in Courant and Friedrichs.[4] Here the f are suitable, simple functions for the purpose of distorting the wave. (These are necessary, since a constant-wave amplitude is inconsistent with the Rankine-Hugoniot relations in the spherical case.) The original idea, of course, is to attempt the satisfaction of the flow equations with such assumptions in which η_1 is constant, i.e., the shock front moves in such a way that $R = \text{const}\ (t^{1/k})$. That is what Taylor does and which is possible, as he recognizes, only in the high-pressure approximation, i.e., near the center of the explosion.

In keeping with the idea not to assign to the shock breakdown of the equations of flow any distinguished role, we shall adopt Courant-Friedrichs' way of writing the wave assumption, but we shall no longer assume that η_1 is constant. In other words, the point $\eta = 1$ will now travel with a trajectory different from that of the shock front; the wave will still stay "similar," but it is now broken off, independently of the similarity assumption of the flow, by the shock discontinuity.

[1] This work was done at the Ballistic Research Laboratory, Aberdeen Proving Ground, during the summer of 1950.

[2] Department of Physics, Harvard University.

Presented at the National Conference of the Applied Mechanics Division, State College, Pa., June 19-21, 1952, of The American Society of Mechanical Engineers.

Discussion of this paper should be addressed to the Secretary, ASME, 29 West 39th Street, New York, N. Y., and will be accepted until October 10, 1952, for publication at a later date. Discussion received after the closing date will be returned.

Note: Statements and opinions advanced in papers are to be understood as individual expressions of their authors and not those of the Society. Manuscript received by ASME Applied Mechanics Division, July 27, 1951. Paper No. 52—APM-18.

[3] "The Formation of a Blast Wave by a Very Intense Explosion," by G. I. Taylor, British Ministry of Home Security, RC 210.

[4] "Supersonic Flow and Shock Waves," by R. Courant and K. O. Friedrichs, Interscience Publications, New York, N. Y., 1948, p. 419.

The distorting factors in the flow have to be chosen judiciously in order for the conservation of excess energy enclosed in the shock sphere (which we must assume in the case of an instantaneous explosion) to lead to a useful mathematical relation. The energy in excess over the heat energy originally contained in the shock sphere is given by

$$E = 4\pi \int_0^R \left(\frac{1}{2} u^2 \rho + \frac{p - p_0}{\gamma - 1} \right) r^2 \, dr$$

As it stands, the fact that $dE/dt = 0$ does not lead to any useful mathematical relation, as it is impossible to eliminate the integral involved. It naturally suggests itself to adopt such assumptions for the form of the flow that, after introduction of a suitable variable of integration, one can eliminate the integral between the expression for the energy and the differential equation of its constancy. Such are the distorting factors used by Courant and Friedrichs,[4] and we shall follow them.

Flow Assumption and Differential Equation

The differential equations for spherical flow are [5]

$$u_t + uu_r + p_r/\rho = 0 \quad [1]$$

$$\rho_t + u\rho_r + \rho(u_r + 2u/r) = 0 \quad [2]$$

$$(p\rho^{-\gamma})_t + u(p\rho^{-\gamma})_r = 0 \quad [3]$$

where we assume that we are dealing with a perfect gas and therefore set

$$c^2 = \gamma \, p/\rho \quad [4]$$

The Rankine-Hugoniot relations are as follows [6]

$$u_1 = \frac{2c_0}{\gamma + 1} \frac{U^2 - 1}{U} \quad [5]$$

$$p_1/p_0 = [2\gamma U^2 + (1 - \gamma)]/(\gamma + 1)$$

or

$$(p_1 - p_0)/p_0 = \frac{2\gamma}{\gamma + 1} (U^2 - 1) \quad [6]$$

$$\rho_1/\rho_0 = [U^2(\gamma + 1)]/[U^2(\gamma - 1) + 2] \quad [7]$$

$$(c_1/c_0)^2 = [2\gamma U^2 - (\gamma - 1)][U^2(\gamma - 1) + 2]/U^2(\gamma + 1)^2 \quad [8]$$

The flow will be assumed to be of the following form

$$u = \frac{r}{t} W(\eta) \quad [9]$$

$$p = \frac{r^{k+2}}{t^2} \Pi(\eta) \quad [10]$$

$$\rho = r^k \Omega(\eta) \quad [11]$$

and, in accordance with Equation [4]

$$c = \frac{r}{t} C(\eta) \quad [12]$$

with

$$\eta = r^{-\lambda} t \quad [13]$$

After straightforward calculation one obtains the equation [7]

$$D\eta W_\eta = A(W, C) \quad [14]$$

with

$$D = (1 - \lambda W)^2 - \lambda^2 C^2 \quad [15]$$

$$A = (1 - W)(1 - \lambda W)W - \lambda \left(3\lambda W - \frac{\mu}{\gamma} \right) C^2 \quad [16]$$

$$\mu = 2\lambda - 2 - k \quad [17]$$

We now combine the shock relations, Equations [5] to [8] with [9] to [12], equating the values of the total time derivatives of our variables directly behind the shock front as obtained from Equations [5] to [8] with the respective ones obtained from Equations [9] to [12]. Thus we eliminate $W\eta$ between these results and Equation [14] and express P_1, C_1, W_1, and η_1 in terms of R, t, U, and $\dot{U}$. The result, after some cumbersome computations, is an ordinary second-order differential equation for the shock front

$$\dot{U}tP(U, V) = Q(U, V) \quad [18]$$

where P and Q are the following polynomials

$$\left.\begin{aligned} P(U, V) &= a_{10}V + a_{21}V^2U + a_{12}VU^2 + a_{20}V^3U^2 + a_{14}VU^4 \\ &\quad + a_{34}V^3U^4 + a_{25}V^2U^5 + a_{16}V^1U^6 \\ Q(U, V) &= b_{11}VU + b_{03}U^3 + b_{22}V^2U^2 + b_{13}V^1U^3 + b_{04}U^4 \\ &\quad + b_{24}V^2U^4 + b_{15}VU^5 + b_{06}U^6 + b_{26}V^2U^6 \\ &\quad + b_{17}VU^7 + b_{08}U^8 \end{aligned}\right\} \quad [19]$$

with the coefficients

$$\left.\begin{aligned} a_{10} &= 4\lambda^2\gamma(\gamma + 1) \\ a_{21} &= 8\lambda\gamma(\gamma + 1) \\ a_{12} &= 2\lambda^2\gamma(\gamma + 1)(\gamma - 5) \\ a_{20} &= 2\gamma(\gamma + 1)^2 \\ a_{14} &= -2\lambda^2\gamma(\gamma + 1)(\gamma + 3) \\ a_{34} &= 2\gamma(\gamma + 1)^2 \\ a_{25} &= -8\lambda\gamma(\gamma + 1) \\ a_{16} &= 4\lambda^2\gamma(\gamma + 1)(2 - \gamma) \end{aligned}\right\} \quad [20]$$

and

$$\left.\begin{aligned} b_{11} &= 4\lambda\gamma(1 - 3\gamma + \lambda\gamma + \lambda) \\ b_{02} &= 8\lambda^2\gamma(\gamma - 1) \\ b_{22} &= 2(\gamma + 1)[2\lambda\gamma - 2\gamma - \mu(\gamma - 1)] \\ b_{13} &= 2\lambda[-7\lambda\gamma - 6\lambda\gamma^2 + \lambda\gamma^3 + 22\gamma^2 + \gamma - 3\gamma^3 \\ &\quad + \mu(\gamma^2 - 1)] \\ b_{04} &= 4\lambda^2\gamma(3 - 8\gamma + \gamma^2) \\ b_{24} &= (\gamma + 1)[6\gamma - 2\gamma^2 + 2\lambda\gamma^2 - 6\lambda\gamma \\ &\quad + \mu(6\gamma - 1 - \gamma^2)] \\ b_{15} &= \lambda[-10\gamma - 40\gamma^2 + 8\lambda\gamma^2 + 14\lambda\gamma + 18\gamma^3 \\ &\quad - 6\lambda\gamma^3 + \mu(\gamma^3 - 5\gamma^2 - 5\gamma + 1)] \\ b_{06} &= 4\lambda^2\gamma(8\gamma - 3\gamma^2 - 1) \\ b_{26} &= 2\gamma(\gamma^2 - 1)(1 - \lambda + \mu) \\ b_{17} &= 2\lambda\gamma(\gamma - 1)[22\gamma + 2\lambda - 6\gamma - 2 - \mu(\gamma + 1)] \\ b_{08} &= 8\lambda^2\gamma^2(\gamma - 1) \end{aligned}\right\} \quad [21]$$

We now have to adjust the constants λ and k so that the shock velocity approaches the sound velocity in the free gas at large distances; i.e., we demand that

$$\lim U = \lim V = 1 \quad \text{as} \quad t \to \infty$$

Therefore, since we must have $\dot{U}t \to 0$ as $t \to \infty$ we must demand that $Q(1, 1) = 0$. But from Equation [21]

$$Q(1, 1) = (2\lambda - 2 - k)(1 - \lambda)(\gamma + 1)^2 \quad [22]$$

using Equation [17]. Since this must vanish, it follows that unless $\lambda = 1$

$$k = 2(\lambda - 1) \quad [23]$$

On the other hand, for very large values of U compared to 1,

[5] V., e.g., ibid., p. 418; or "Progress Report on Theory of Shock Waves," by v. Neuman, OSRD 1140.
[6] Reference (2), p. 123f.
[7] Reference (2), p. 419.

Equations [19] reduce to the high-pressure approximation

$$\dot{U}tV(a_{14}V^2 + a_{25}UV + a_{16}U^2) = U^2(b_{25}V^2 + b_{17}UV + b_{08}U^2) \quad [24]$$

This equation has a solution of the form $R = c_0At^\beta$, where β must satisfy the equation

$$\beta^2(a_{14} - b_{08}) + \beta^2(a_{25} - a_{16} - b_{17}) + \beta(a_{34} - a_{25} - b_{26}) - a_{34} = 0 \quad [25]$$

Conservation of Energy

We shall now consider the energy integral of Equations [19] in accordance with the assumption that the excess energy in the shock sphere over the enclosed heat energy of the still gas is constant and equal to the energy released by the blast. This energy is

$$E = 4\pi \int_0^R \left(\frac{1}{2}u^2\rho + \frac{p - p_0}{\gamma - 1}\right) r^2\, dr \quad [26]$$

Substituting Equations [9] to [11] in this and then using η as the variable of integration, we obtain

$$E = \frac{-4\pi t^{\frac{k+5}{\lambda}-2}}{\lambda} \int^{tR^{-\lambda}} \left(\frac{1}{2}W^2\Omega + \frac{\Pi - \Pi_0}{\gamma - 1}\right) d\eta\eta^{-\frac{k+5}{\lambda}-1} \quad [26a]$$

We differentiate this with respect to the time, substitute the boundary values from Equations [5] to [11], set $dE/dt = 0$, and eliminate the integral between the result and Equation [26a]. The result can be written in the following manner

$$4\gamma E_0 t^{-3} = \frac{V^2(V - \lambda U)}{k + 5 - 2\lambda} f(U) + V^2\left(\frac{3\lambda}{k + 5 - 2\lambda}U - V\right)(\gamma + 1)$$

with

$$f(U) = [4\gamma(\gamma - 1)U^4 - (1 - 10\gamma + 5\gamma^2)U^2 + 2(\gamma - 1)^2]/[U^2(\gamma - 1) + 2]$$

Now, as $t \to \infty$, the left-hand side tends to zero, while U and V tend to 1. Hence we must have

$$\frac{k + 2 - 2\lambda}{k + 5 - 2\lambda} = 0$$

and thus again the condition, Equation [23].

There is, however, one exceptional case: If $k + 5 - 2\lambda = 0$ then the integral in the foregoing equation can be eliminated only together with E. But again obtaining dE/dt, equating it to zero, then in the resulting equation (which does not contain the integral any longer) setting $t = \infty$, $U = V = 1$, we get the contradictory equation

$$(\gamma + 1)^2(1 - \lambda) + \lambda(\gamma + 1)^2 = 0$$

Therefore the case $k + 5 - 2\lambda = 0$ must be excluded and Equation [23] must hold, as we now see, unconditionally. Notice from Equation [26a] that if $k + 5 - 2\lambda = 0$, then $\eta_1 = \text{const}$. That is Taylor's case and cannot be satisfied for the entire shock curve but, as we see, leads to a contradiction at $t \to \infty$.

By the use of Equation [23] the first-order differential equation of the conservation of energy becomes, after some simplification

$$\left(U^2 + \frac{2}{\gamma - 1}\right)E_0 = V^2t^3(V - \lambda U)(U^2 - 1)\left(U^2 + \frac{3 - \gamma}{2(\gamma - 1)}\right) \quad [27]$$

with

$$E_0 = \frac{3(\gamma^2 - 1)}{16\pi} E/c_0^5\rho_0 \quad [28]$$

We notice from this that as $R \to 0$, U must tend to infinity, since otherwise the right-hand side would tend to zero, while the left-hand side remains greater than some positive constant. Hence, near the origin, the high-pressure approximation always holds, provided that we allow R to tend to zero, i.e., in case we consider a point explosion.

Asymptotic Behavior

We shall now consider the asymptotic behavior of the shock front. Since $U \to 1$ as $t \to \infty$, we set $U = 1 + \epsilon'$, and $R = c_0(t + \nu + \epsilon)$, and $V = 1 + \nu t^{-1} + \epsilon t^{-1}$, where ν is a constant, and $\epsilon' \to 0$ as $t \to \infty$. Then Equation [27] becomes

$$\left(\frac{\gamma + 1}{\gamma - 1} + 2\epsilon' + \epsilon'^2\right)E_0 = (t^3 + 2\nu t^2 + 2\epsilon t^2 + \nu^2 t + 2\nu\epsilon t + \epsilon^2)[(1 - \lambda)t + \nu + \epsilon - \lambda t\epsilon'](2\epsilon' + \epsilon'^2)\left(\frac{\gamma + 1}{\gamma - 1}\frac{1}{2} + 2\epsilon' + \epsilon'^2\right) \quad [29]$$

Now we let $t \to \infty$ and neglect terms of higher order than the first one occurring. We then have to distinguish between two possible cases as follows:

Case A, $\lambda \neq 1$. Then Equation [29] yields $\epsilon \sim Bt^{1-\lambda}$. We have to substitute this in Equations [19]. The left-hand side of Equations [19] behaves asymptotically as

$$-6Bt^{-\lambda}P(1, 1) = -24\gamma(\gamma + 1)^2(1 - \lambda^2)Bt^{-\lambda}$$

The constant term, $Q(1, 1)$, on the right-hand side of Equations [19] vanishes because of Equation [23]. The coefficients of t^{-1} and t^{-2} on the right also are seen to vanish by substitution of Equations [21] and [23]. Now the coefficient of $t^{-\lambda}$ is, after some computation, seen to be

$$8\gamma(\gamma + 1)^2(\lambda - 1)(3\lambda - 1)B$$

Since we see that the coefficients of $t^{-\lambda}$ are not equal on both sides, this case must be excluded.

Case B, $\lambda = 1$. Then Equation [29] yields asymptotically $\epsilon = -Bt^{-1}$, $\epsilon' = Bt^{-2}$, $\epsilon'' = -2Bt^{-3}$. Again we substitute in Equations [19]. Since for $P(1, 1) = 0$, the asymptotic behavior of the left-hand side is as $-16\gamma(\gamma + 1)^2Bvt^{-3}$, as is found by the use of Equations [20]. On the right, the coefficients of t^3, t^{-1}, and t^{-2} vanish, while that of t^{-3} is $-8\gamma(\gamma + 1)^2\nu B$, which again is not equal to that on the left unless $\nu = 0$. But $\nu = 0$, together with the fact that the shock front never advances with a velocity less than c, implies that $U \times \text{const} = c_0$, which is impossible. Thus we have to conclude that the assumptions, Equations [9] to [11] are not compatible with the conservation of energy. That is to say, we cannot assume that the central point of the similarity, so to speak, namely, the point defined by $\eta = 1$, moves with such a simple equation of motion as $r - \lambda t = \text{const}$.

More General Flow Assumption

We shall now attempt to satisfy the equations of flow, shock, and conservation of energy by letting the parameters λ and k in Equations [9] to [11] be functions of the time

$$\lambda = \lambda(t),\ k = k(t)$$

It then develops that we have to modify Equation [10] slightly in order to have the pressure tend to a constant value throughout space as the time tends to infinity. Our present assumptions will then be the following

$$u = \frac{r}{t} W(\eta) \quad [30]$$

$$p = p_0 + \frac{r^{k+2}}{t^2} \Pi(\eta) \quad [31]$$

$$\rho = r^k \Omega(\eta) \quad [32]$$

$$\eta = r^{-\lambda(k)} t \quad [33]$$

It is apparent from Equation [26a] that it is impossible to eliminate the integral between [26a] and the equation $dE/dt = 0$, unless $(k + 5)/\lambda = \text{const}$. Therefore we shall assume this. For later convenience we define a constant α so that

$$(k + 5)/\lambda = 2 - 3\alpha \quad [34]$$

We also introduce a function of the time by the definition

$$\delta = (1 - \lambda - \lambda' t \log R)/\lambda \quad [35]$$

i.e., so that

$$\lambda' t \log R = 1 - \lambda(1 + \delta)$$

where the prime indicates differentiation with respect to the time.

Just as in the section, Conservation of Energy, we have to consider separately the special case $\alpha = 0$. It then follows from Equation [26a] that $\eta_1 = \text{const}$. We then see from Equation [9] that $u_1 = \text{const} \times R/t$, and as $t \to \infty$, $R/t \to c_0$ and thus $u_1 \to \text{const} \neq 0$, which contradicts Equation [5]. The case $\alpha = 0$ therefore must be excluded.

Now for $\alpha \neq 0$ Equation [27] will be modified in the following way

$$\left(U^2 + \frac{2}{\gamma - 1}\right) \alpha E_0 = \lambda V^2 t^2 [U - V(1 + \delta)]$$
$$(U^2 - 1)\left(U^2 + \frac{3 - \gamma}{2(\gamma - 1)}\right) \quad [36]$$

With E_0 as defined by Equation [28].

Assumptions, Equations [30] to [33], of course, also modify the original second-order Equation [18], and Equations [14] to [16]. Straightforward computation shows that the form of Equations [18] and [19] is retained, but that the coefficients (which, through λ, become time dependent) now are the following

$$\left.\begin{aligned}
a_{10} &= 2(\gamma + 1) \\
a_{21} &= 4(\gamma + 1)(1 + \delta) \\
a_{12} &= (\gamma + 1)(\gamma - 5) \\
a_{32} &= (\gamma + 1)^2 (1 + \delta)^2 \\
a_{14} &= -(\gamma + 1)(\gamma + 3) \\
a_{34} &= (\gamma + 1)^2 (1 + \delta)^2 \\
a_{25} &= -4(\gamma + 1)(1 + \delta) \\
a_{16} &= 2(\gamma + 1)(2 - \gamma)
\end{aligned}\right\} \quad [37]$$

$$\left.\begin{aligned}
b_{11} &= 2[2(1 - \gamma) + \delta(1 - 3\gamma)] \\
b_{05} &= 4(\gamma - 1) \\
b_{22} &= -2(\gamma + 1)(1 + \delta)[3(\alpha + 1) + 4\delta] \\
b_{13} &= 2\gamma(11 - \gamma) + 6\alpha(\gamma + 1) + \delta(-3\gamma^2 + 28\gamma + 7) \\
b_{01} &= 2(\gamma^2 - 8\gamma + 3) \\
b_{24} &= (\gamma + 1)(3 - \gamma)[3(\alpha + 1) + 4\delta](1 + \delta) \\
b_{15} &= 9\gamma^2 - 22\gamma - 7 - 3\alpha(3 - \gamma)(\gamma + 1) \\
&\quad + 2\delta(6\gamma^2 - 13\gamma - 7) \\
b_{08} &= 2(-3\gamma^2 + 8\gamma - 1) \\
b_{28} &= (\gamma^2 - 1)[3(\alpha + 1) + 4\delta](1 + \delta) \\
b_{17} &= -(\gamma - 1)[(7\gamma + 3) + 3\alpha(\gamma + 1) + \delta(9\gamma + 5)] \\
b_{38} &= 4\gamma(\gamma - 1)
\end{aligned}\right\} \quad [38]$$

From Equations [37] and [38] it follows that

$$P(1, 1) = 2(\gamma + 1)^2(2 + \delta)\delta \text{ and } Q(1, 1) = 0$$

Hence the necessary condition for U to tend to 1 as t tends to infinity is fulfilled.

Asymptotic Values

We shall again consider the asymptotic behavior of the shock front. For that purpose we again set $U = 1 + \epsilon'$, $V = 1 + \nu t^{-1} + \epsilon t^{-1}$, $R = c_0(t + \nu + \epsilon)$, with $\epsilon' \to 0$ as $t \to \infty$. We express δ in terms of U, R, and t from Equation [36]

$$\delta = (U/V - 1) - 2E_0\alpha[(\gamma - 1)U^2 + 2)]$$
$$[2(\gamma - 1)U^2 + 3 - \gamma]\lambda V^2 t^2 (U^2 - 1)$$

Then we let t tend to infinity, i.e., $U \to 1$, $V \to 1$, and, keeping only the highest order terms, obtain

$$\delta \sim \epsilon' - \frac{\nu}{t} - \frac{\epsilon}{t} + \ldots - \frac{\alpha E_0}{\epsilon' t^2} + \ldots \quad [39]$$

On the other hand, if we substitute Equations [37] and [38] in [18] and [19], reorder and keep the highest terms only, we obtain

$$\left.\begin{aligned}
&\delta^2[\epsilon'' t - 4\epsilon' + \ldots] + \delta[2\epsilon'' t - (1 + 3\alpha)\epsilon' + \ldots] \\
&-4\epsilon'\epsilon'' t + 2\nu\epsilon'' + 2\epsilon\epsilon'' + 3\epsilon'' \frac{\nu^2}{t} + 3\epsilon'' \frac{\epsilon^2}{t} + 6\frac{\nu\epsilon}{t}\epsilon'' \\
&-(1 + 3\alpha)\left(\frac{\nu\epsilon'}{t} + \frac{\epsilon\epsilon'}{t} - \epsilon'^2\right) + \ldots = 0
\end{aligned}\right\} \quad [40]$$

Substituting Equation [39] in this, multiplying out, canceling terms, and keeping the highest terms only, we get the following

$$2\nu^2(\epsilon'' t - \epsilon') + \frac{E_0^2\alpha^2}{2\epsilon' t^4}\left(\frac{\epsilon'' t}{\epsilon'} - 4\right) - \epsilon'\epsilon'' t^2$$
$$-\alpha E_0 t^{-1}\left(\frac{\epsilon'' t}{\epsilon'} - \frac{1 + 3\alpha}{2}\right) + \ldots = 0 \quad [41]$$

Which of these terms predominates for large t is a priori not determined.

Now let us set $\epsilon' = Bt^{-s} + \ldots$ and try to satisfy Equation [41]. Then we notice that the first term is of the order t^{-s}, the second of the order t^{s-3}, the third of the order $t^{2(1-s)}$, and the fourth of the order t^{-3}. Therefore we distinguish between the following possibilities:

(*a*) If $s \leq 2$, then the third term predominates over the first and second, and therefore it must be canceled by the fourth. Hence it follows that

$$s = 3/2 \text{ and } B^2 = -\alpha(4 + 3\alpha)E_0/3$$

Since $E_0 > 0$ and $B > 0$ we must have $-\alpha(4 + 3\alpha) > 0$, and thus $-4/3 < \alpha < 0$.

(*b*) If $2 \leq s < 3$, then the last term in Equation [41] predomi-

nates over all the others and therefore we must have $\epsilon''t/\epsilon' - (1 + 3\alpha)/2 = 0$ and hence $s = -(1 + 3\alpha)/2$, $\alpha = -(2s + 1)/3$. This means, by hypothesis, that $-7/3 < \alpha \leq -5/3$.

(*c*) If $s = 3$, then the last and the second term are of the same order and hence we must have $7\alpha E_0 = (7 + 3\alpha)B$. It follows that in this case either $\alpha > 0$ or $\alpha < -7/3$.

(*d*) If $s > 3$, then the second term predominates over all the others; but since then $\epsilon''t/\epsilon' = 4$, this case is impossible.

As the values of α involved in all these cases are distinct from one another, we can state the result in the following manner:

If $\alpha > 0$, then $s = 3$
If $0 > \alpha > -4/3$, then $s = 2/3$
If $-4/3 \geq \alpha > -5/3$, then there is no solution
If $-5/3 \geq \alpha > -7/3$, then $s = -(1 + 3\alpha)/2$
If $-7/3 > \alpha$, then $s = 3$.

We see from this and Equation [39] that $\delta \to 0$, and, therefore, by Equation [35], $\lambda \to 1$ as $t \to \infty$, except when $\alpha > 0$, or when $\alpha < -7/3$. The problem now is to decide on a suitable value for α.

At the end of the flow, i.e., in the limit as $t \to \infty$, there cannot be a pressure gradient left over anywhere in space. But the flow Equations [1] to [3] leave the question a priori open whether there will be a density and temperature gradient (via the velocity of sound) left. Since such a permanent gradient is thermodynamically impossible, we shall assume that the flow equations do not imply it either, in spite of the fact that the Rankine-Hugoniot relations (in addition to Equations [5] to [8]) contain the statement of a permanent entropy increase across the shock front. Equation [32] then shows that α must be equal to -1, provided one assumes that it is between zero and $-7/3$. (From the point of view of our similarity assumption it is most reasonable to assume that $\lambda \to 1$ as $t \to \infty$, and then, as seen from Equation [35], $\delta \to 0$.) From Equation [34] we see that, if we hold r fixed and let t tend to infinity, ρ tends, by Equation [32], to $r^{-2(1+\alpha)/\alpha}\Omega(\infty)$, which is independent of r if and only if $\alpha = -1$. Therefore we shall adopt this value for α.

Applying Case (*a*), substituting $\alpha = -1$, and using the value of E_0 given by Equation [28], we find

$$B^2 = (\gamma^2 - 1)E/16\pi c_0^5\rho_0 = (\gamma^2 - 1)E/16\pi\gamma c_0^5 p_0$$

and hence

$$U \sim 1 + \frac{1}{4}\left(\frac{\gamma^2 - 1}{\pi\gamma}\right)^{1/5}(c_0 t)^{-2/5}(E/p_0)^{1/5}$$

Since $R \to c_0 t$ as $t \to \infty$, we can write this as

$$U \sim 1 + \frac{1}{4}\left(\frac{\gamma^2 - 1}{\pi\gamma}\right)^{1/5} R^{-2/5}(E/p_0)^{1/5} \quad \ldots\ldots [42]$$

and from Equations [5] to [8] we get the asymptotic values of pressure, density, sound velocity, and particle velocity. Writing Δ to denote the difference in the values in front and directly behind the shock, we obtain[8]

$$\Delta p \sim \sqrt{\frac{\gamma}{\pi}\frac{\gamma - 1}{\gamma + 1}}\, R^{-3/5}(Ep_0)^{1/5} \quad \ldots\ldots [43]$$

which for air yields (with $\gamma = 7/5$)

$$\Delta p \sim 0.272\, R^{-3/5}(Ep_0)^{1/5} \quad \ldots\ldots [43a]$$

[8] This result may be compared to Kirkwood's, which is $\Delta p \sim P_1 R^{-1}(\log R/R_1)^{-1/5}$; v. John G. Kirkwood and Stuart Brinkley, Jr., "Theory of the Propagation of Shock Waves From Explosive Sources in Air and Water." OSRD No. 4918, NDRC No. A-318.

$$\Delta\rho \sim \rho_0 \sqrt{\frac{1}{\pi\gamma}\frac{\gamma - 1}{\gamma + 1}}\, R^{-3/5}(E/p_0)^{1/5} \quad \ldots\ldots [44]$$

and for air

$$\frac{\Delta\rho}{\rho_0} \sim 0.195\, R^{-3/5}(E/p_0)^{1/5} \quad \ldots\ldots [44a]$$

$$u_1 \sim \sqrt{\frac{1}{\pi}\frac{\gamma - 1}{\gamma + 1}}\, R^{-3/5}(E/\rho_0)^{1/5} \quad \ldots\ldots [45]$$

and for air

$$u_1 \sim 0.224\, R^{-3/5}(E/\rho_0)^{1/5} \quad \ldots\ldots [45a]$$

$$\Delta c \sim \frac{3\gamma - 2}{4}\sqrt{\frac{1}{\pi}\frac{\gamma - 1}{\gamma + 1}}\, R^{-3/5}(E/\rho_0)^{1/5} \quad \ldots\ldots [46]$$

and for air

$$\Delta c \sim 0.127\, R^{-3/5}(E/\rho_0)^{1/5} \quad \ldots\ldots [46a]$$

Since for an ideal gas $c^2 = \gamma kT$, where k is the universal gas constant divided by the effective molecular weight of the gas,[9] we can, by means of Equation [46], express the asymptotic value of the rise in temperature across the shock front. For small Δc we see from the above relation that $\Delta T \sim 2c_0\Delta c/k\gamma$ and therefore

$$\Delta T \sim \frac{3\gamma - 2}{2k}\sqrt{\frac{1}{\gamma\pi}\frac{\gamma - 1}{\gamma + 1}}\, R^{-3/5}\frac{(Ep_0)^{1/5}}{\rho_0} \quad \ldots\ldots [47]$$

High-Pressure Approximation

We shall now consider the shock values near the center of the explosion, regarding the blast as a point explosion. For values of $U >> 1$, Equation [36] simplifies to

$$\alpha E_0 = \lambda V^2 t^3[U - V(1 + \delta)] \quad \ldots\ldots [48]$$

which has a solution of the form $R = c_0 A t^\beta$. Then

$$\alpha E_0 = \lambda(\beta - 1 - \delta)\beta^2 A^5 t^{\beta s - 2} \quad \ldots\ldots [48a]$$

where we simply write δ for $\delta(0)$. This shows that unless $\beta = 1 + \delta$, we must have $\beta = 2/5$. Now from Equation [35] we notice that unless $\lambda \to 0$ or $\lambda \to \infty$ as $t \to 0$, both of which cases it is reasonable to reject, we must have in the limit as $t \to 0$, $\lambda(1 + \delta) = 1$. Taylor's simple similarity assumption is therefore again the one in which in the limit as $t \to 0$, $\beta\lambda = 1$. In that case we get immediately from Equation [26*a*] $\alpha = 0$, and also $\beta = 2/5$. We thus get a result similar to Taylor's for the high-pressure approximation, although we use a quite different similarity assumption.

We have seen before that near the center of the blast Equation [18] reduces to Equation [24], which also has a solution of the form $R = c_0 A t^\beta$. β must then satisfy Equation [25], which, after substitution of Equations [37] and [38] and reordering, becomes

$$(\beta - 1 - \delta)\{(1 + \delta)(1 + \gamma)[(5 - 3\gamma)\beta - (\lambda + 1)] - \beta[2(-3\gamma^2 + 3\gamma + 2)\beta - 2(\gamma + 1) + 3\alpha(\gamma^2 - 1)]\} = 0 \quad \ldots\ldots [49]$$

Hence here again $\beta = 1 + \delta$, i.e., $\beta\lambda = 1$, the Taylor case, is a solution. On the other hand, if $\beta\lambda \neq 1$, then Equation [48] yields, with $\beta = 2/5$

$$1 + \delta = \frac{2/5[2(-6\gamma^2 + \gamma - 1) + 15\alpha(\gamma^2 - 1)]}{(5 - 11\gamma)(\gamma + 1)}$$

[9] Reference (2), p. 9.

and from this λ, as $\lambda = 1/(1 + \delta)$. From Equations [48a] and [28] we then obtain the following value for A (using $\alpha = -1$)

$$A^5 = C^5 E/c_0^5 \rho_0 \quad [50]$$

with

$$C^5 = \frac{75}{512\pi} \frac{\gamma + 1}{2\gamma + 1} (27\gamma^2 - 2\gamma - 13) \quad [50a]$$

Then, by Equation [5] and straightforward calculation

$$p_1 = \frac{8}{25} \frac{C^5}{\gamma + 1} ER^{-3}$$

and thus near the center of the blast

$$p_1 = \frac{3}{64\pi} \frac{27\gamma^2 - 2\gamma - 13}{2\gamma + 1} ER^{-3} \quad [51]$$

In air, if we neglect the change in γ for high pressures

$$p_1 = 0.146\ ER^{-3}$$

On the other hand, in the limit as $\gamma \to 1$, toward which γ tends as the pressure increases to infinity (for air γ is actually rather close to 1 for pressures of, say, 1000 psi) this becomes

$$p_1 = 0.0596\ ER^{-3}$$

The Pressure Decay

Now we shall consider briefly the pressure decay behind the shock front. From the flow equations and the Rankine-Hugoniot relations one can, by straightforward computation, derive the following equation for the slope of the pressure curve behind the shock front

$$p_{1t}(U^2 - 1)[U^2(\gamma - 1) + 2] = \frac{2\gamma p_0}{\gamma + 1} U \left\{ U[2(3\gamma - 2)U^4 + (11 - \gamma)U^2 - (\gamma + 3)] + \frac{2c_0}{\gamma + 1} \frac{U^2 - 1}{R} [2\gamma U^2 - (\gamma - 1)][U^2(\gamma - 1) + 2] \right\} \quad [52]$$

By setting $U = 1 + \epsilon'$ and neglecting terms in powers of ϵ' higher than 1, we get the asymptotic expression for p_{1t}

$$p_{1t} \sim \frac{4\gamma}{\gamma + 1} p_0 \left(\frac{\epsilon'' t}{\epsilon'} + 1 \right) t^{-1} \quad [53]$$

unless $\epsilon'' t/\epsilon' + 1 = 0$. Therefore, by our value of ϵ' derived in the foregoing ($\epsilon' = Bt^{-3/5}$)

$$p_{1t} \sim -\frac{2\gamma}{\gamma + 1} p_0 t^{-1}$$

or

$$p_{1t} \sim -\frac{2\gamma}{\gamma + 1} p_0 c_0 R^{-1} \quad [54]$$

Near the center, on the other hand, Equation [52] yields

$$p_{1t} = \frac{2\gamma p_0}{\gamma^2 - 1} U \left[U\, 2(3\gamma - 2) + \frac{4\gamma(\gamma - 1)}{\gamma + 1} c_0 U^3/R \right]$$

Now setting $R = c_0 A t^{2/5}$, with A given by Equation [50], we obtain the following

$$p_{1t} = -C_1 \frac{E^{2/5}}{\rho_0^{1/5}} R^{-11/5} \quad [55]$$

with

$$C_1 = \frac{5\gamma^2 + 7\gamma - 6}{256} \frac{\gamma + 1}{\gamma - 1} \left[\frac{3}{2\pi} \frac{27\gamma^2 - 2\gamma - 13}{(2\gamma + 1)(\gamma + 1)} \right]^{2/5}$$

Conclusions

The progressing-wave approach used here seems to be compatible with the flow equations and conservation of energy inside the shock sphere. Since, however, the exact motion of the wave, i.e., say, the motion of the point $\eta = 1$, which is determined by the equation $r - \lambda(t)t = 1$, is not known independently of the differential equations of the shock front, the latter contain a still unknown function. One may then regard the two Equations [18] and [36], originally one an integral of the other, as two ordinary differential equations for the two unknown functions of t, R, and λ. The blast-shock problem would be solved completely if these two equations were solved for R and λ.

On the Stresses in a Rotating Disk of Variable Thickness

By TI-CHIANG LEE,[1] TAIWAN, CHINA

This paper presents an analytic solution of the stresses in a rotating disk of variable thickness. By introducing two parameters, the profile of the disk is assumed to vary exponentially with any power of the radial distance from the center of the disk. In some respects this solution may be considered as a generalization of Malkin's solution, but it differs essentially from the latter in the method of solution. Here, the stresses are solved through a stress function instead of being solved directly. The required stress function is expressed in terms of confluent hypergeometric functions. Numerical examples are also shown for illustration.

Introduction

THE problem of analyzing the stresses in a rotating disk of variable thickness occurs frequently in machine design, especially in the design of turbines. As early as 1895 an analytic solution was obtained by Chree (1)[2] for a rotating disk in the shape of a flat ellipsoid of revolution. In 1912 an approximate solution was developed by Donath (2) in which the disk is assumed to be divisible into parts, and each part is considered as a flat disk of constant thickness. Further development of this approximate solution was made by Grammel (3) in 1923. A different approximate solution was given by Stodola (4) in 1924, in which the profile of the disk is assumed to be a hyperbolic curve. For an actual disk, the approximation is obtained by dividing the disk concentrically into parts and fitting each part to the hyperbolic curve. In 1934 Malkin (5) developed an analytic solution expressed in infinite series for disks of two particular exponential profiles. Another approximate solution was suggested by Bisshopp (6) in 1944, in which the actual disk is replaced by portions of circular cones.

It may be mentioned that each of the approximate solutions mentioned is, in fact, a lengthy process, and indeed a considerable amount of labor is required in obtaining the required numerical solution. Naturally, Chree's solution no longer will be applicable if the profile of the disk is substantially different from a flat ellipsoid of revolution. Malkin's solution is restricted to two particular exponential profiles only, which lie between the conical and hyperbolic profiles. In the present solution the profile of the disk is assumed to vary exponentially with *any* power of the radial distance from the center of the disk. It is in this sense that it may be considered as a generalization of Malkin's solution. However, it is not a mere generalization since it differs essentially from Malkin's solution in that the stresses in the disk are solved through a stress function instead of being solved directly. As will be described later, the differential equation for the stress function is first transformed to an equation of confluent hypergeometric type so that it can be solved in terms of the confluent hypergeometric functions. The constants of integration involved in the solution are adjusted to satisfy the given boundary conditions. The stresses are then derived readily from the stress function. Finally, the solution is discussed and illustrated by some numerical examples.

Differential Equation

Consider a circular rotating disk of radius a with a central hole of radius b. Let (r, θ) be the polar co-ordinates referred to the center of the disk as the origin—r being a dimensionless variable measured by the unit a. Let the thickness of the disk be denoted by h, also a dimensionless variable measured by the unit a. For the present radially symmetrical disk, h is a function of r only.

In the subsequent analysis it is assumed that the stresses in the disk do not vary across the thickness of the disk, and also that the weight of the disk is negligible in comparison with the centrifugal force produced by rotation. Under these assumptions, the state of stress in the disk may be specified by a stress function ϕ, a function of r only, which satisfies the following differential equation (7)

$$r^3\frac{d^3\phi}{dr^3} + r\frac{d\phi}{dr} - \phi - \frac{r^3}{h}\frac{dh}{dr}\frac{d\phi}{dr} + \nu\frac{r}{h}\frac{dh}{dr}\phi = -(3+\nu)ph r^3 \quad [1]$$

where ν is the Poisson's ratio of the material of the disk, and $p = \rho\omega^2 a^2$, ω being the angular velocity and ρ the density of the disk.

The radial and tangential stresses in the disk are then given by

$$\sigma_r = \frac{\phi}{hr}, \qquad \sigma_\theta = \frac{1}{h}\frac{d\phi}{dr} + pr^2 \quad [2]$$

Method of Solution

Suppose that the thickness of the disk is given as a function of r as follows

$$h = c\exp(kr^s) \quad [3]$$

where c is the "hypothetic" thickness at the center of the disk, k and s being the parametric constants. A doubly infinite family of curves can be obtained by varying these two constants. When k and s are both positive or both negative, h increases with increase of r; but when k and s have different signs, it decreases with increase of r. The latter case only is of practical significance. In particular, when k vanishes, it is a flat disk of uniform thickness.

Substitute this value of h into the preceding equation and further write

$$\phi = pcrW(t) \quad [4]$$

where

$$t = kr^s \quad [5]$$

It then appears that the function W satisfies the following differential equation of confluent hypergeometric type (8)

[1] Research Engineer, Aeronautical Research Laboratory.

[2] Numbers in parentheses refer to the Bibliography at the end of the paper.

Presented at the National Conference of the Applied Mechanics Division, State College, Pa., June 19–21, 1952, of The American Society of Mechanical Engineers.

Discussion of this paper should be addressed to the Secretary, ASME, 29 West 39th Street, New York, N. Y., and will be accepted until October 10, 1952, for publication at a later date. Discussion received after the closing date will be returned.

Note: Statements and opinions advanced in papers are to be understood as individual expressions of their authors and not those of the Society. Manuscript received by ASME Applied Mechanics Division, July 12, 1950. Paper No. 52—APM-6.

$$t\frac{d^2W}{dt^2} + (\gamma - t)\frac{dW}{dt} - \alpha W = \frac{(\gamma-1)(2-2\gamma+\alpha)}{2k^{\gamma-1}} t^{\gamma-2}e^t \quad [6]$$

where

$$\gamma = 1 + \frac{2}{s}, \qquad \alpha = \frac{1-\nu}{s} \quad [7]$$

The general solution of this equation may be written as follows

$$W(t) = AP(t) + BQ(t) + R(t) \quad [8]$$

where R is a particular integral of the solution and P and Q are the complementary functions; A and B being the constants of integration. It can be shown readily that the particular integral R may be given by

$$R(t) = -\frac{(\gamma-1)t^{\gamma-2}}{2k^{\gamma-1}} e^t\left[1 + \frac{(2-\gamma)(3-2\gamma)}{(3-2\gamma+\alpha)t} + \frac{(2-\gamma)(3-\gamma)(3-2\gamma)(4-2\gamma)}{(3-2\gamma+\alpha)(4-2\gamma+\alpha)t^2} + \cdots\right] \quad [9]$$

The series in the brackets terminates whenever γ is an integer or half an odd integer. For instance: When $\gamma = 2$ or $3/2$, all the terms vanish except the first term; when $\gamma = 3$, all vanish except the first two terms; and when $\gamma = 4$ or $5/2$, all vanish except the first three terms. It may be mentioned that the cases $\gamma = 5/2$ and 4 are, in fact, identical to the Malkin's first and second exponential profiles, respectively, provided that k is negative and ν is equal to $1/3$. It also may be mentioned that when γ is neither an integer nor half an odd integer, the function R may be expressed in an alternative form as follows

$$R(t) = \frac{2-2\gamma+\alpha}{4(\gamma-1)k^{\gamma-1}} e^t t^{\gamma-1}\left[1 - \frac{2\gamma-1-\alpha}{\gamma(2\gamma-1)}t + \frac{(2\gamma-1-\alpha)(2\gamma-\alpha)}{\gamma(\gamma+1)(2\gamma-1)2\gamma}t^2 - \cdots\right] \quad [10]$$

It is readily seen that the function P may be given by the following confluent hypergeometric function

$$P(t) = {}_1F_1(\alpha, \gamma, t) = 1 + \frac{\alpha}{1!\gamma}t + \frac{\alpha(\alpha+1)}{2!\gamma(\gamma+1)}t^2 + \cdots \quad [11]$$

Furthermore, the function Q may be given by

$$Q(t) = t^{1-\gamma}{}_1F_1(\alpha-\gamma+1, 2-\gamma, t) \quad [12]$$

These two solutions are independent of each other as long as γ is not an integer. However, when γ is an integer, they become dependent. An independent solution may then be obtained by Frobenius' method (9) as follows: For $\gamma \geq 2$

$$Q(t) = \frac{\Gamma(\gamma-\alpha)}{\Gamma(1-\alpha)}\left[{}_1F_1(\alpha, \gamma, t)\log|t| + (-1)^\gamma G(\alpha, \gamma, t) - (-1)^\gamma H(\alpha, \gamma, t)\right] \quad [13]$$

where

$$G(\alpha, \gamma, t) = 1 + \frac{\alpha t}{1!\gamma}[\psi_1(\alpha) - \psi_1(1) - \psi_\gamma(1)] + \frac{\alpha(\alpha+1)t^2}{2!\gamma(\gamma+1)}[\psi_2(\alpha) - \psi_2(1) - \psi_{\gamma+1}(1)] + \cdots \quad [14]$$

$$H(\alpha, \gamma, t) = 1 + \psi_{\gamma-1}(1) + (\gamma-1)!(\gamma-2)! \times\left[\frac{1}{(1-\alpha)t} + \frac{1}{(1-\alpha)(2-\alpha)t^2} + \cdots + \frac{1}{(1-\alpha)(2-\alpha)\cdots(\gamma-1-\alpha)t^{\gamma-1}}\right] \quad [15]$$

in which, for $n \geq 1$

$$\psi_n(\alpha) = \sum_{m=1}^{n}\frac{1}{\alpha+m-1} \quad [16]$$

The Stresses

Let the radius of the central hole be denoted by $r = \lambda$. Suppose that the external periphery of the disk is under the action of a constant pull q, while the internal periphery is free from any traction. The boundary conditions are thus

$$(\sigma_r)_{r=\lambda} = 0, \qquad (\sigma_r)_{r=1} = q \quad [17]$$

The two constants of integration are readily found as follows

$$A = \frac{Q(k)R(u) - Q(u)R(k) + vQ(u)}{P(k)Q(u) - P(u)Q(k)} \quad [18]$$

$$B = -\frac{P(k)R(u) - P(u)R(k) + vP(u)}{P(k)Q(u) - P(u)Q(k)} \quad [19]$$

where

$$u = k\lambda^s, \qquad v = qe^k/p$$

Consequently, the radial and tangential stresses are given by

$$\left.\begin{aligned}\sigma_r &= p[AP(t) + BQ(t) + R(t)]e^{-t}\\ \sigma_\theta &= \sigma_r + pr^2 + \frac{2pt}{\gamma-1}[AP'(t) + BQ'(t) + R'(t)]e^{-t}\end{aligned}\right\} \quad [20]$$

where the prime sign denotes, as usual, the derivative of the function with respect to the variable t.

For a solid disk without a central hole, the function Q may be omitted from the general solution, that is

$$W(t) = AP(t) + R(t) \quad [21]$$

The second boundary condition of Equation [17] then gives

$$A = \frac{v - R(k)}{P(k)} \quad [22]$$

Consequently

$$\left.\begin{aligned}\sigma_r &= \frac{p}{P(k)}[P(k)R(t) - R(k)P(t) + vP(t)]e^{-t}\\ \sigma_\theta &= \sigma_r + pr^2 + \frac{2pt}{(\gamma-1)P(k)}[P(k)R'(t) - R(k)P'(t) + vP'(t)]e^{-t}\end{aligned}\right\} \quad [23]$$

It appears that both the radial and tangential stresses in a rotating disk are always tensile in nature. In a solid disk the maximum radial and tangential stresses occur at the center of the disk and are equal in magnitude. While at any other point the tangential stress is always greater than the radial stress. In a disk with a central hole, the tangential stress decreases from a maximum at the periphery of the hole to a minimum at the outer periphery, while the radial stress increases from zero at the periphery of the hole to a maximum and then decreases to the given boundary value at the outer periphery. The tangential stress

TABLE 1 $P(t) = {}_1F_1(\alpha, \gamma, t)$; $t = kr^s$, FOR $\gamma = 2$, $\alpha = 0.35$

r	$k = -1$	$k = -0.8$	$k = -0.6$	$k = -0.4$	$k = -0.2$
0.1	0.99825	0.99860	0.99895	0.99930	0.99965
0.2	0.99306	0.99444	0.99582	0.99721	0.99860
0.3	0.98456	0.98760	0.99066	0.99375	0.99686
0.4	0.97298	0.97823	0.98356	0.98896	0.99444
0.5	0.95860	0.96652	0.97461	0.98289	0.99135
0.6	0.94176	0.95269	0.96396	0.97559	0.98760
0.7	0.92287	0.93701	0.95177	0.96176	0.98322
0.8	0.90230	0.91977	0.93820	0.95766	0.97823
0.9	0.88048	0.90124	0.92343	0.94718	0.97265
1	0.85779	0.88713	0.90766	0.93584	0.96652

TABLE 2 $Q(t)$; $t = kr^s$, FOR $\gamma = 2$, $\alpha = 0.35$

r	$k = -1$	$k = -0.8$	$k = -0.6$	$k = -0.4$	$k = -0.2$
0.1	9.6361×10	1.2136×10^2	1.6303×10^2	2.4636×10^2	4.9636×10^2
0.2	2.2271×10	2.8518×10	3.8932×10	5.9754×10	1.2226×10^2
0.3	8.9165	1.1690×10	1.6316×10	2.5571×10	5.3345×10
0.4	4.4347	5.9922	8.5912	1.3794×10	2.9414×10
0.5	2.4765	3.4712	5.1325	8.4603	1.8455×10
0.6	1.4886	2.1784	3.3310	5.6409	1.2580×10
0.7	9.4456×10^{-1}	1.4516	2.2987	3.9984	9.0943
0.8	6.2738×10^{-1}	1.0172	1.6674	2.9685	6.8736
0.9	4.3521×10^{-1}	7.4614×10^{-1}	1.2629	2.2942	5.3832
1	3.1559×10^{-1}	5.7155×10^{-1}	9.9461×10^{-1}	1.8348	4.3421

TABLE 3 $P'(t) = {}_1F_1'(\alpha, \gamma, t) = \frac{\alpha}{2}\,{}_1F_1(1+\alpha, 1+\gamma, t)$; $t = kr^s$, FOR $\gamma = 2$, $\alpha = 0.35$

r	$k = -1$	$k = -0.8$	$k = -0.6$	$k = -0.4$	$k = -0.2$
0.1	0.17421	0.17437	0.17452	0.17469	0.17485
0.2	0.17189	0.17219	0.17312	0.17373	0.17437
0.3	0.16810	0.16945	0.17082	0.17220	0.17359
0.4	0.16297	0.16528	0.16765	0.17005	0.17251
0.5	0.15668	0.16014	0.16369	0.16735	0.17112
0.6	0.14942	0.15412	0.15902	0.16412	0.16945
0.7	0.14141	0.14740	0.15372	0.16093	0.16750
0.8	0.13286	0.14011	0.14790	0.15627	0.16529
0.9	0.12400	0.13243	0.14165	0.15175	0.16283
1	0.11503	0.12788	0.13507	0.14689	0.16013

TABLE 4 $Q'(t)$; $t = kr^s$; FOR $\gamma = 2$, $\alpha = 0.35$

r	$k = -1$	$k = -0.8$	$k = -0.6$	$k = -0.4$	$k = -0.2$
0.1	9.9346×10^2	1.5543×10^3	2.7669×10^3	6.2337×10^3	2.4967×10^4
0.2	6.0854×10^2	9.5604×10^2	1.7088×10^3	3.8651×10^3	1.5544×10^4
0.3	1.1612×10^2	1.8376×10^2	3.3078×10^2	7.5343×10^2	3.0502×10^3
0.4	3.4954×10	5.5910×10	1.0169×10^2	2.3901×10^2	9.5620×10^2
0.5	1.3404×10	2.1752×10	4.0112×10	9.3662×10	3.8700×10^2
0.6	5.9524	9.8467	1.8450×10	4.3731×10	1.8391×10^2
0.7	2.9095	4.9212	9.4306	2.2811×10	9.7564×10
0.8	1.5191	2.6405	5.1864	1.2819×10	5.6059×10
0.9	7.4001×10^{-1}	1.4919	3.0138	7.6414	3.4218×10
1	4.7119×10^{-1}	8.7257×10^{-1}	1.8276	4.7647	2.1897×10

TABLE 5 THE MAXIMUM TANGENTIAL STRESS $(\sigma_\theta)_{max}/p$ FOR $\gamma = 2$, $\alpha = 0.35$

k	q/p	$\lambda = 0$ (solid disk)	$\lambda \to 0$	$\lambda = 0.1$	$\lambda = 0.3$	$\lambda = 0.5$
-1	0	0.286	0.571	0.588	0.664	0.763
	1/8	0.339	0.678	0.700	0.803	0.965
	1/4	0.393	0.786	0.812	0.943	1.167
-0.8	0	0.308	0.617	0.632	0.700	0.789
	1/8	0.372	0.744	0.763	0.859	1.011
	1/4	0.435	0.870	0.894	1.018	1.233
-0.6	0	0.329	0.659	0.672	0.728	0.803
	1/8	0.405	0.810	0.827	0.912	1.051
	1/4	0.481	0.961	0.983	1.096	1.299
-0.4	0	0.355	0.709	0.716	0.764	0.826
	1/8	0.444	0.888	0.902	0.974	1.100
	1/4	0.534	1.067	1.085	1.185	1.375
-0.2	0	0.382	0.765	0.771	0.801	0.846
	1/8	0.488	0.976	0.986	1.042	1.149
	1/4	0.594	1.188	1.201	1.283	1.451
0	0	0.413	0.825	0.827	0.841	0.869
	1/8	0.538	1.075	1.079	1.116	1.202
	1/4	0.663	1.325	1.332	1.390	1.535

is always greater than the radial stress at the same point, the larger the hole the smaller the radial stress. In the limiting case of a thin ring the radial stress becomes negligible in comparison with the tangential stress. In the other limiting case when the hole is very small, the maximum tangential stress reaches a value twice as large as that in a corresponding solid disk. In all cases it appears that the tangential stress at the periphery of the hole or at the center of a solid disk is greatest in magnitude. This stress is thus of great importance in practical design.

Numerical Examples

As an illustration, the case $\gamma = 2$ (i.e. $s = 2$) will be worked out in detail. For convenience, ν is taken as 0.3. The values of the confluent hypergeometric functions $P(t)$ and $Q(t)$ and also their derivatives are shown in Tables 1 to 4. A and B are then readily calculated for any given value of q/p, and also are the radial and tangential stresses. A typical example of the stress distribution in a free rotating disk of $\lambda = 0.3$ is shown in Fig. 1. The maximum stress or the tangential stress at the periphery of the hole for different λ and q/p are given in Table 5 and also shown graphically in Fig. 2.

In applying the results to practical design, the Malkin's example will be taken for further illustration: A disk is to be calculated for $b = 6.75$ in., and $a = 18.75$ in. The thickness at

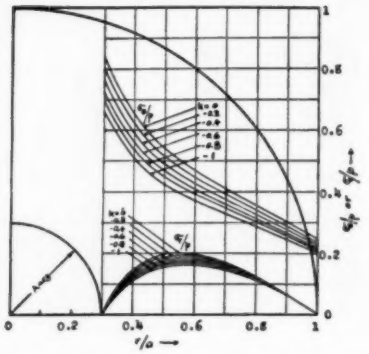

FIG. 1 RADIAL AND TANGENTIAL STRESSES IN A FREE ROTATING DISK; $\lambda = 0.3$ ($s = 2$)

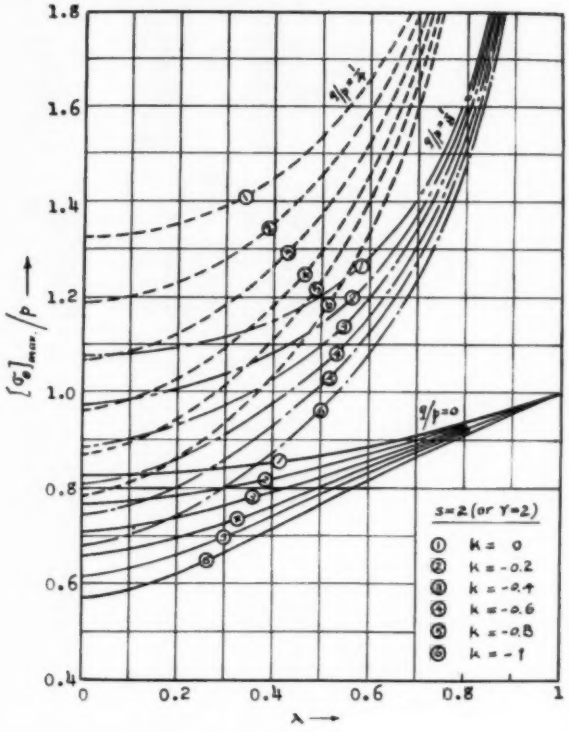

FIG. 2 (*right*) MAXIMUM TANGENTIAL STRESS IN A DISK WITH A CENTRAL HOLE

the external periphery is 4 in. The working speed is 3600 rpm, and the pull exerted on the external periphery at 20 per cent overspeed is 13,000 psi. Thus we have

$$\lambda = 0.36$$
$$p = 52{,}740 \text{ psi}$$
$$q = 13{,}000 \text{ psi}$$
$$q/p = 1/4 \text{ very nearly}$$

In Malkin's calculation, the allowable stress is taken to be 52,500 psi. The thickness at the periphery of the hole is found to be 10 in., both for his first and second exponential profiles. From this value the profile for $s = 2$ (i.e., $\gamma = 2$) gives $k = -1.025$. For simplicity, a round value $k = -1$ will be taken, which gives a thickness of 9.55 in. at the periphery of the hole. For this value of k and $\lambda = 0.36$, $q/p = 1/4$, it can be read directly from Fig. 2 that

$$[\sigma_\theta]_{max} = 0.994\ p = 52{,}400 \text{ psi}$$

which is slightly lower than the allowable stress.

The foregoing example is, nevertheless, a fortunate one since the result can be read directly from the graph. In general, the procedure may be as follows: (*a*) Read $(\sigma_\theta)_{max}/p$ from Fig. 2 for the given values of k and λ, by interpolation if necessary, corresponding to $q/p = 0$, 1/8, 1/4, or any two of them, respectively. (*b*) Plot them against q/p. They should lie in a straight line. (*c*) Read $(\sigma_\theta)_{max}/p$ for the given value of q/p.

ACKNOWLEDGMENT

The author wishes to express his sincere gratitude to Dr. C. B. Ling for his valuable suggestions and frequent help during the course of the work.

BIBLIOGRAPHY

1 "Stress in a Rotating Ellipsoid," by C. Chree, Proceedings of the Royal Society of London, England, vol. 58, 1895, p. 39.

2 "Die Berechnung Rotierender Scheiben und Ringe," by M. Donath, Berlin, Germany, 1912.

3 "Einneues Verfahren zur Berechnung Rotierender Scheiben," by R. Grammel, *Dinglers Polytechnical Journal*, vol. 338, 1923, pp. 217–219.

4 "Steam and Gas Turbine," by A. Stodola, Peter Smith, New York, N. Y., vol. 2, 1945, pp. 386 and 397–398.

5 "Design and Calculation of Steam-Turbine Disk Wheels," by I. Malkin, Trans. ASME, vol. 56, paper APM—56-8, 1934, pp. 585–600.

6 "Stress Coefficients for Rotating Disks of Conical Profile," by K. E. Bisshopp, JOURNAL OF APPLIED MECHANICS, Trans. ASME, vol. 66, 1944, pp. A-1-9.

7 "Theory of Elasticity," by S. Timoshenko, McGraw-Hill Book Company, Inc., New York, N. Y., 1934, pp. 66–70.

8 "Functions of a Complex Variable," by E. T. Copson, Oxford University Press, London, England, 1935, pp. 260–261.

9 "A Treatise on Differential Equations," by A. R. Forsyth, Cambridge University Press, London, England, sixth edition, 1928, pp. 250–251.

Investigation of Annular Liquid Flow With Cocurrent Air Flow in Horizontal Tubes

By A. E. ABRAMSON,[1] CLEVELAND, OHIO

Visual observations and flow analysis were made of annular liquid flow with cocurrent air flow in horizontal tubes. The effect of liquid properties and air-stream conditions on the characteristics of the liquid flow were observed. The results are presented in form of shadowgraph pictures of the liquid flow. Analysis of the flow system related the characteristics of the liquid flow to the flow conditions.

Nomenclature

The following nomenclature is used in the paper:

D = inside diameter of tube, ft
g = acceleration due to gravity, 32.2 fps per sec
u = velocity parallel to axis of tube, fps
u_b = bulk or average velocity at cross section of tube, fps
W = flow rate, lb per sec
w = flow rate per unit length, lb/sec/ft
y = distance from tube wall, ft
μ_0 = absolute viscosity of fluid at wall, lb-sec per sq ft
ρ = mass density, lb-sec^2/ft^4
ρ_b = bulk or average density at cross section of tube, lb-sec^2/ft^4
ρ_0 = mass density of fluid at wall, lb-sec^2/ft^4
τ_0 = shear stress in fluid at wall, psf

Subscripts:

fr = on friction pressure gradient
g = gas flow
l = liquid flow

Dimensionless parameters:

f = friction factor, $\dfrac{D\left(\dfrac{dp}{dx}\right)_{fr}}{2\rho_b u_b^2}$

u^+ = velocity parameter, $\dfrac{u}{\sqrt{\tau_0/\rho_0}}$

y^+ = wall-distance parameter, $\dfrac{\sqrt{\tau_0/\rho_0}}{\mu_0/\rho_0}\,y$

w^+ = flow-rate parameter, $\dfrac{W}{\pi D g \mu_0}$

Introduction

During the past decade considerable interest has been shown in film cooling, particularly in the rocket-engine application. Film cooling is accomplished by establishing a film or layer of liquid between the hot gases and the confining wall, the film of liquid thus shielding the wall from the hot-gas stream. The over-all flow system therefore consists of the simultaneous flow of a gas and a liquid with the liquid flowing as an annulus or film along the duct wall, and the gas flows at high velocities through the central core. This flow system is termed annular liquid flow with cocurrent gas flow and is one of several types of two-phase, two-component flow systems. An understanding of the annular liquid-flow system is therefore desirable for its application to film cooling.

Considerable research has been conducted on the simultaneous flow of a gas and a liquid. Martinelli and co-workers have indicated several types of flow encountered in two-phase, two-component flow and have proposed a general correlation for determining pressure drop during cocurrent two-phase flow.[2,3] Bergelin also has indicated flow characteristics of gas-liquid mixtures, made pressure-drop determinations, and has given a summary of progress in the field of gas-liquid flow.[4] Whereas these investigations cover several types of cocurrent two-phase flow over a considerable range of flow conditions, very little information is available on annular liquid flow in the flow range encountered in the film cooling of rocket engines. As an aid to a more complete understanding of annular liquid flow and its relation to film cooling in this flow range, visual studies were conducted recently at the NACA Lewis laboratory. The object of this investigation was to determine by visual observation the effect of liquid properties, liquid-flow rate, and air-flow conditions on the characteristics of the annular liquid flow.

Apparatus

The apparatus and flow system used for the investigation are shown schematically in Fig. 1. The flow system consists of a combustion-air supply, jet-engine combustor, mixing section, test section, and exhaust system. Gasoline was burned with the air in the combustor to furnish a hot-gas source for tests at elevated gas-stream temperatures. However, the majority of the tests were conducted at ambient-air temperatures. The test section consists of an approach section, a liquid injector, and a transparent duct. The approach section is 40 in. long and of the same diameter as the transparent duct. The liquid injector was designed to give a uniform circumferential distribution of the liquid. Three different transparent ducts were used for the investigation: a 4-in. and a 2-in-diam lucite duct and a 4-in-diam pyrex duct for tests at elevated gas temperatures. The ducts were 48 in. long.

The visual studies were accomplished by shadowgraph photo-

[1] Aeronautical Research Scientist, Lewis Flight Propulsion Laboratory, National Advisory Committee for Aeronautics, Cleveland Airport.

Presented at the National Conference of the Applied Mechanics Division, State College, Pa., June 19–21, 1952, of The American Society of Mechanical Engineers.

Discussion of this paper should be addressed to the Secretary, ASME, 29 West 39th Street, New York, N. Y., and will be accepted until October 10, 1952, for publication at a later date. Discussion received after the closing date will be returned.

Note: Statements and opinions advanced in papers are to be understood as individual expressions of their authors and not those of the Society. Manuscript received by ASME Applied Mechanics Division, July 2, 1951. Paper No. 52—APM-11.

[2] "Proposed Correlation of Data for Isothermal Two-Phase, Two-Component Flow in Pipes," by R. W. Lockhardt and R. C. Martinelli, *Chemical Engineering Progress*, vol. 45, 1949, pp. 39–45; discussion, pp. 45–48.

[3] "Isothermal Pressure Drop for Two-Phase Two-Component Flow in a Horisontal Pipe," by R. C. Martinelli, L. M. K. Boelter, T. H. M. Taylor, E. G. Thomsen, and E. H. Marrin, Trans. ASME, vol. 66, 1944, pp. 139–151.

[4] "Flow of Gas-Liquid Mixtures," by O. P. Bergelin, *Chemical Engineering*, vol. 56, May, 1949, pp. 104–106.

graphs, high-speed motion pictures, and visual observations with the aid of a stroboscopic light.

An optical device was developed to determine the thickness of the liquid film. Calibrations using thin glass plates indicated that the device was capable of measurements to 0.005 in.

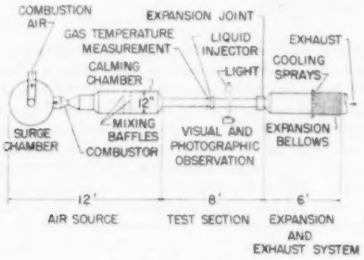

FIG. 1 FLOW SYSTEM

PROCEDURE

The experimental procedure was as follows: The desired gas-stream condition was established in the test section. Liquid was then introduced through the injector and the liquid flow increased until the inner surface of the duct was covered with a liquid film. The liquid-film surface was observed with the aid of a stroboscopic light and as the liquid flow was increased in small increments, a description of the liquid surface was recorded. The liquid-film surface gradually became disturbed as the liquid flow was increased. A transition region of liquid flow from a relatively smooth to a definitely disturbed condition was determined for most of the liquids. To obtain a photographic record of the flow disturbances, shadowgraph and high-speed motion pictures were taken of the liquid flow for various test conditions.

The flow conditions covered the following ranges:

Air mass velocity, lb/(sec) (sq ft)	30.6–108
Air temperature, deg F	80, 800
Liquid flow, lb/(sec) (ft)	0.027–0.270

Water containing various quantities of detergent (aerosol) and water-ethylene-glycol solutions were used in the experiments. The liquids used and their properties at the temperatures during the experiments are listed in Table 1.

TABLE 1 PROPERTIES OF LIQUIDS USED FOR INVESTIGATION

Liquid	Temperature, deg F	Absolute viscosity, (lb-sec)/(sq ft)	Surface tension, (dynes/cm)
Water	80	1.84×10^{-5}	72
Water	210	0.606	57
Water and 0.004 per cent detergent	80	1.84	55
Water and 0.025 per cent detergent	80	1.84	45
Water and 0.050 per cent detergent	80	1.84	41
Water and 0.085 per cent detergent	80	2.05	36
Water and 0.150 per cent detergent	80	2.07	33
Water and 12 per cent ethylene glycol	80	2.72	70
Water and 53 per cent ethylene glycol	80	7.74	62
Water and 98 per cent ethylene glycol	80	31.4	54

RESULTS

Velocity and Thickness of the Liquid Films. The liquid film established on the inside surface of the duct was very thin for the range of test conditions. Computed values of the thickness were from 0.005 to 0.0005 in. with corresponding surface velocities of the liquid of 10 to 35 fps. The method used in calculating the surface velocity or thickness of the liquid film is given in the Appendix. The velocity of the liquid-surface disturbances was measured from the high-speed motion pictures and agreed favorably with the calculated values.

Attempts at direct measurement of the liquid-film thickness using the optical device described in the apparatus showed the thickness to be less than the sensitivity of the instrument (0.005 in.) which substantiates the order of magnitude of the computed values.

Description of Water-Film Disturbances. Observations, using a stroboscopic light, of water films on the inside surface of transparent tubes revealed changes in appearance of the water flow for different water-flow rates. With constant air-stream conditions, the water flow appeared essentially smooth at the low water-flow rates; whereas there were disturbances having the appearance of waves on the surface at the higher flow rates. The change in appearance of the water flow occurs gradually as the water-flow rate increases. Figs. 2 and 3 show shadowgraph pictures of the water flow for increasing flow rates at two air flows. The photographs are arranged to show three regions involved in the changing appearance of the water flow as the flow increases; (*a*) smooth flow (no appreciable disturbance); (*b*) transition from small traces of disturbance to appreciable and consistent clearly visible disturbances; and (*c*) increasing number and magnitude of the disturbances. Although the change from smooth to a disturbed condition of the water film was gradual, water flows defining this transition region could be determined readily.

Effect of Flow Variables on Liquid-Film Characteristics. Experiments were conducted to determine the effect of several variables on the values of liquid-flow rate over which the liquid-flow transition occurred and on the appearance of the liquid flow. The variables investigated were air-mass velocity, air temperature, tube diameter, liquid surface tension, and liquid viscosity. The values of the liquid flow per circumferential length defining the transition region for the different flow conditions are listed in Tables 2 and 3.

Variations in air-mass velocity at ambient temperature resulted in no appreciable change in the water flow per circumferential length defining the transition region for the three different transparent tubes, Table 2. There was, however, as shown in Figs. 2 and 3, a change in the appearance of the water-flow disturbances with air-mass velocity. The disturbances appear smaller and more numerous at the higher air-mass velocity.

A comparison of the transition region for the lucite and pyrex tubes, Table 2 indicates the transition region starts at a slightly lower water flow for the lucite tube.

The transition region for various air-mass velocities using the 4-in. and 2-in-diam lucite tubes is given in Table 2. The results show no appreciable difference in liquid flow per circumferential length defining the transition region for the two tube diameters. The disturbances had the same appearance for corresponding air-mass velocities.

Significant information on the effect of air temperature on the transition region could not be determined because water flows in

TABLE 2 EFFECT OF AIR-MASS VELOCITY, TUBE SURFACE, AND TUBE DIAMETER ON LIQUID-FLOW TRANSITION REGION

(Conditions: liquid, water; air temperature, 80 F)

Air-mass velocity lb/(sec) (sq ft)	Liquid-flow transition region[a] lb/(sec) (ft)		
	Pyrex tube	Lucite tube	
	4 in.	4 in.	2 in.
30.6	0.052–0.063	0.035–0.065	0.037–0.060
44.5	0.052–0.068	0.040–0.068	0.038–0.063
70.0	0.050–0.068	0.037–0.073	0.038–0.062
108	0.048–0.068	0.035–0.070	0.038–0.062

[a] From visual observations.

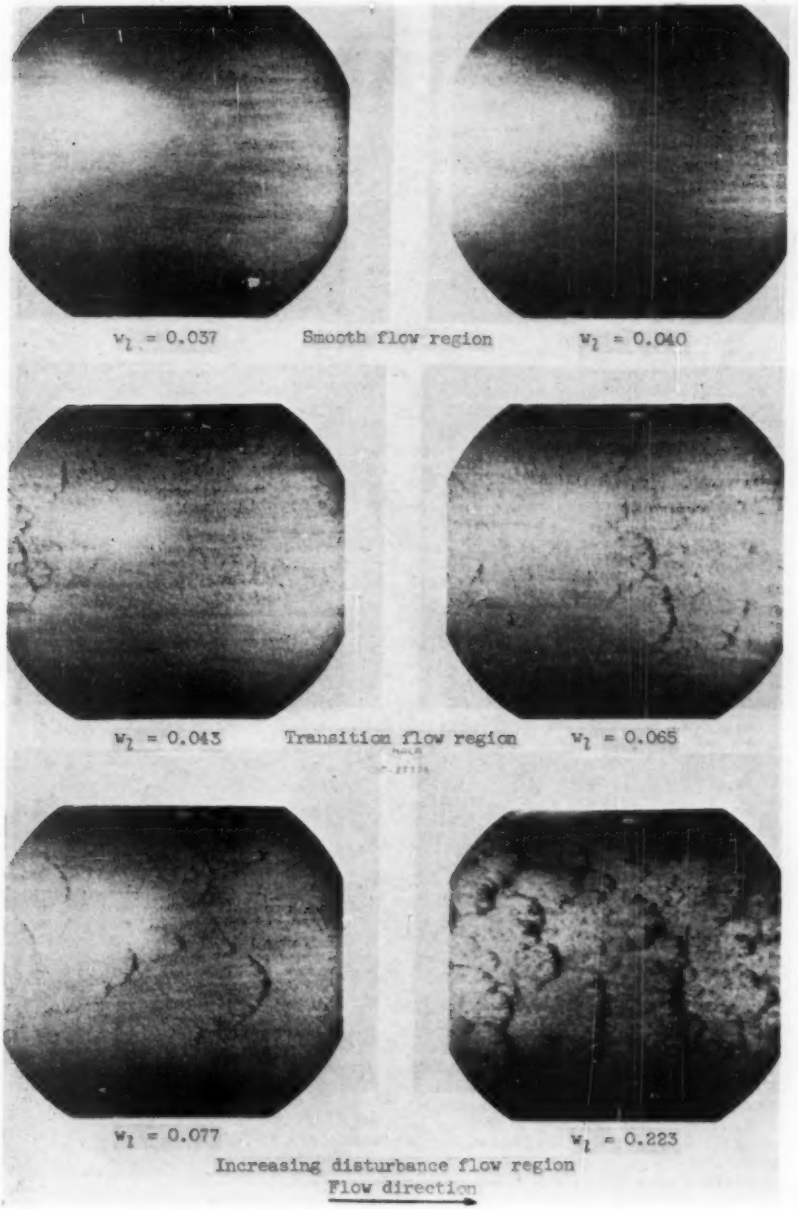

FIG. 2 SHADOWGRAPH PICTURES OF ANNULAR WATER FLOW WITH COCURRENT AIR FLOW IN HORIZONTAL TUBE
(Air-mass velocity, 44.5 lb/sec-ft²; air temperature, 80 F; lucite tube diameter, 4 in.)

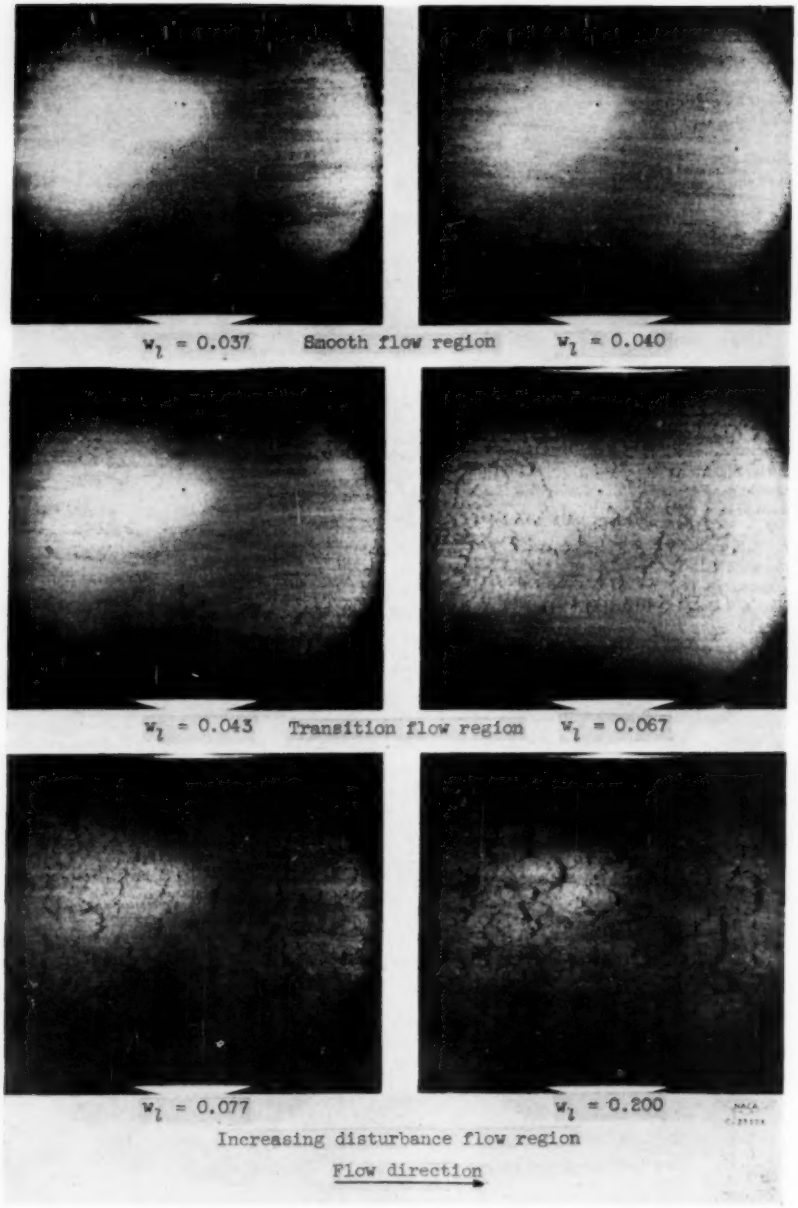

FIG. 3 SHADOWGRAPH PICTURES OF ANNULAR WATER FLOW WITH COCURRENT AIR FLOW IN HORIZONTAL TUBE
(Air-mass velocity, 70.0 lb/sec-ft²; air temperature, 80 F; lucite tube diameter, 4 in.)

this region were too low to form a liquid film along the entire length of the tube at high air temperatures and thus prevent the tube from overheating. However, flow disturbances accompanying the higher water flows were observed at elevated air temperatures. Fig. 4 shows shadowgraph pictures of the water flow at air temperatures of 80 and 800 F for the same air flow. The pictures indicate that the disturbances had the same appearance at the different air-stream temperatures; apparently there is no boiling or appreciable effect on the liquid-film surface due to vaporization.

The liquid-flow disturbances using aqueous glycol solutions to vary viscosity were observed to differ from those using water. The disturbances became less wavelike in appearance, smaller in size, and less distinct with increased viscosity. Fig. 5 shows shadowgraph pictures of the flow of a 53 per cent glycol-water solution at various liquid flows and indicates that the development of the surface disturbances is very gradual with increased liquid flow. Because of this gradual increase in liquid-surface disturbances with the more viscous solutions, it was difficult to define a transition region as observed with water. However, as the viscosity was increased, higher liquid flows were required before appreciable disturbances were observed.

Variation in liquid-surface tension was obtained using water-detergent solutions. A slight increase in the liquid flow for the start of the transition region and an increase in the magnitude of the transition region were observed with decreasing liquid-surface tension as indicated in Table 3. The liquid-surface disturbances had essentially the same appearance as those observed using water. This was indicative only of water-detergent solutions for which the surface tension was larger than one half that of water. The flow of liquids having a higher concentration of detergent which resulted in a liquid-surface tension less than one half that of water had the following characteristics: At low liquid flows small areas of roughened surface appeared and as the liquid flow was increased the size and intensity of the disturbances increased with the entire surface becoming disturbed. No disturbances appearing as waves were detected over the flow range investigated.

TABLE 3 EFFECT OF LIQUID SURFACE TENSION ON LIQUID-FLOW TRANSITION REGION

(Conditions: tube, pyrex; air-mass velocity, 44.5 lb/sec/sq ft; air temperature, 80 F)

Liquid (per cent by weight detergent in water)	Absolute viscosity at 80 F, (lb-sec)/(sq ft)	Surface tension at 80 F, (dynes/cm)	Liquid-flow transition region,[a] lb/(sec) (ft)
0.000	1.84×10^{-5}	72	0.052–0.068
0.004	1.84	55	0.057–0.082
0.025	1.84	45	0.063–0.090
0.050	1.84	41	0.067–0.090
0.095	2.05	36	0.063–0.097
0.150	2.07	33	Not determined

[a] From visual observations.

(*a*) Air temperature, 80 F; water flow, 0.093 lb per sec per ft; lucite tube diameter, 4 in.

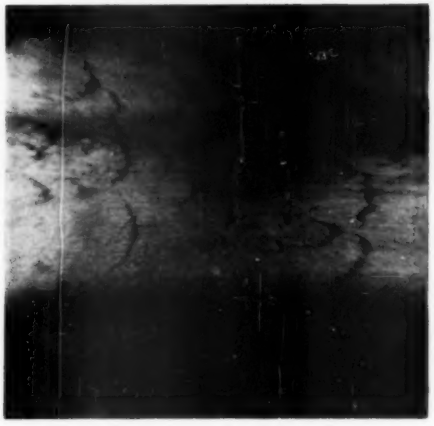

(*b*) Air temperature, 800 F; water flow, 0.130 lb per sec per ft; pyrex tube diameter, 4 in.

FIG. 4 SHADOWGRAPH PICTURES OF ANNULAR WATER FLOW WITH COCURRENT AIR FLOW IN HORIZONTAL TUBE AT DIFFERENT AIR TEMPERATURES

(Air-mass velocity, 44.5 lb/sec-ft².)

RELATION BETWEEN DISTURBANCES AND FLOW CONDITIONS

By analysis, the surface disturbances of the liquid film were found to originate when the thickness of the liquid film enters a flow region where turbulent forces predominate over the viscous forces. Plots of the generalized velocity distribution for fully developed flow in smooth tubes, as given elsewhere,[5,6] are shown in Fig. 6 and this distribution is assumed applicable to the liquid film. The flow regions where the viscous or turbulent forces predominate are defined by the value of the wall-distance parameter y^+. Viscous forces predominate in the laminar layer ($y^+ < 3$); turbulent forces in the turbulent core ($y^+ > 30$); and both laminar and turbulent forces are present in the intermediate region ($3 < y^+ < 30$).[5,6]

For the purposes of this investigation, it is convenient to place the results in terms of a flow rate parameter w^+, as the liquid flow was measured for each test condition. This parameter is obtained as follows: Consider the continuity equation in the region near the wall where a velocity gradient is present, Fig. 7. The

[5] "Analytical and Experimental Investigation of Adiabatic Turbulent Flow in Smooth Tubes," by R. G. Deissler, NACA TN 2138, 1950.

[6] "The Analogy Between Fluid Friction and Heat Transfer," by Th. von Kármán, Trans. ASME, vol. 61, 1939, pp. 705–710.

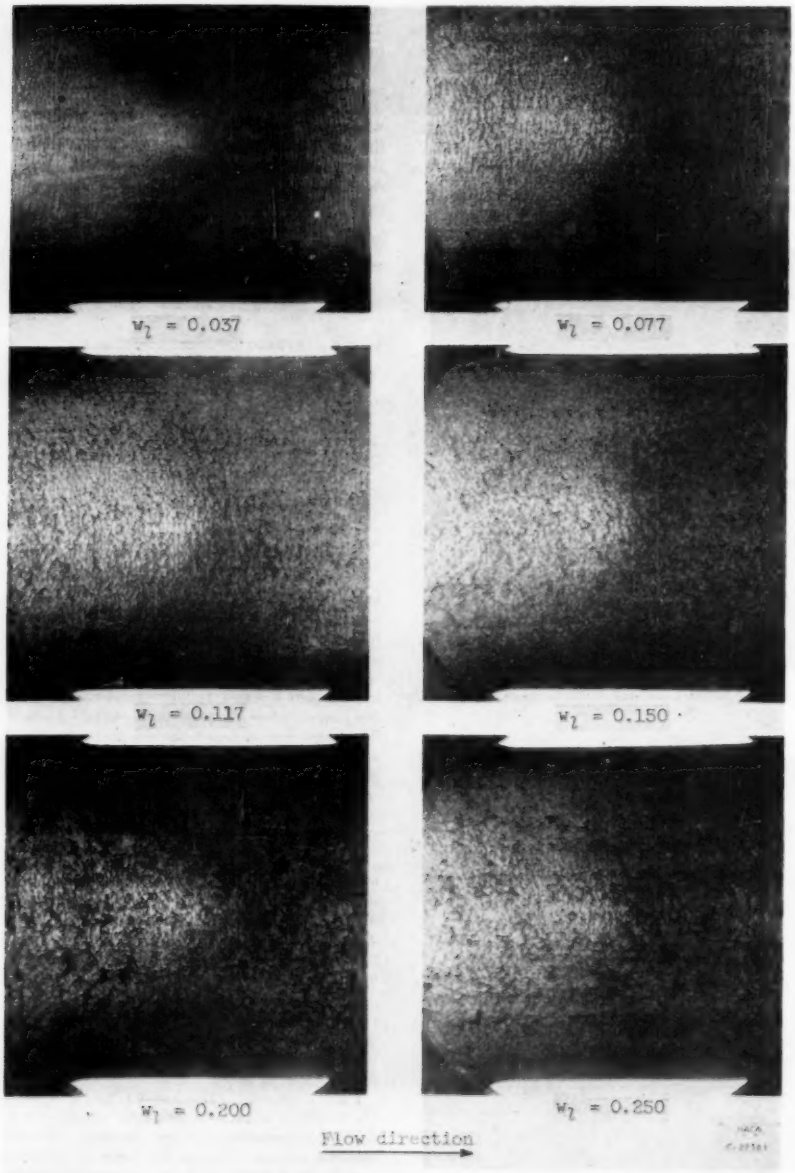

FIG. 5 SHADOWGRAPH PICTURES OF ANNULAR LIQUID FLOW OF 53 PER CENT GLYCOL-WATER SOLUTION WITH COCURRENT AIR FLOW IN HORIZONTAL TUBE
(Air-mass velocity, 44.5 lb/sec-ft^2; air temperature, 80 F; lucite tube diameter, 4 in.)

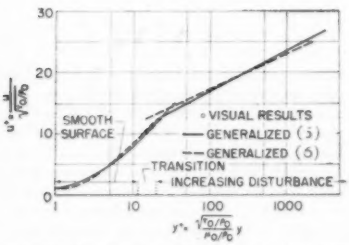

FIG. 6 ASSOCIATION OF VISUAL FLOW REGIONS WITH GENERALIZED VELOCITY DISTRIBUTION

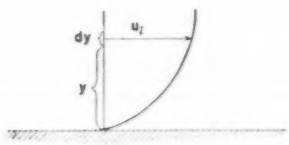

FIG. 7

flow per unit width w_l, though the element dy is given by the relation

$$dw_l = g\rho u_l \, dy \quad \ldots\ldots [1]$$

Substituting the dimensionless parameters u^+ and y^+, which are defined as

$$u^+ = \frac{u}{\sqrt{\tau_0/\rho_0}}$$

$$y^+ = \frac{\sqrt{\tau_0/\rho_0}}{\mu_0/\rho_0} y$$

in Equation [1] and assuming a constant density across the liquid film gives the relation

$$\int^{w_l} dw_l = g\,\mu_0 \int_0^{y^+} u^+ dy^+$$

Thus

$$\frac{w_l}{g\,\mu_0} = \int_0^{y^+} u^+ dy^+ \quad \ldots\ldots [2]$$

The flow per unit width w_l can be approximated for a circular duct by dividing the total liquid flow W_l by the circumference of the duct. The flow rate parameter w^+ is thus obtained from Equation [2] as

$$w^+ = \frac{W_l}{\pi D g\,\mu_0} = \int_0^{y^+} u^+ dy^+$$

The value of

$$\int_0^{y^+} u^+ dy^+$$

can be evaluated for any desired value of y^+ by graphical integration of the curve in Fig. 6. The result of this graphical integration for various values of y^+ is shown in Fig. 8.

Values of the flow-rate parameter w^+ were calculated for the median liquid flows defining the transition region as listed in Tables 2 and 3. The corresponding values of y^+ were obtained from Fig. 8 and plotted on the generalized velocity distribution in Fig. 6. The highest and lowest values of y^+ defining the transition region are also shown in Fig. 6 by the dotted lines and indicate that for the various test conditions the observed transition region occurred between $y^+ = 12$ and $y^+ = 21$. The previously defined flow regions, as shown in Fig. 2, may be associated with Fig. 6 as follows: At values of $y^+ < 12$, the liquid film appears relatively smooth. In the region $12 < y^+ < 21$, a surface disturbance develops on the liquid film. For values of $y^+ > 21$, the disturbance increases with y^+ to the limit of the test conditions at $y^+ = 80$. The approximate liquid flow at which the surface disturbances initially occur can be obtained using a flow-rate parameter w^+ of 90, which corresponds to $y^+ = 15$.

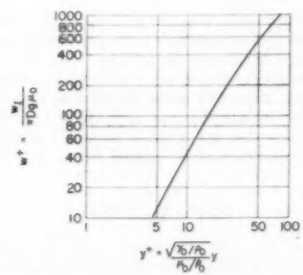

FIG. 8 VARIATION OF DIMENSIONLESS FLOW-RATE PARAMETER WITH WALL-DISTANCE PARAMETER

For a film-cooling application of annular liquid flow with cocurrent gas flow the presence of the liquid-film disturbances could affect the heat transfer to the liquid film. The disturbance on the liquid film (at the gas-liquid interface) would tend to eliminate the laminar sublayer of the gas stream that exists in smooth pipe flow and thus lower the thermal resistance of the gas-stream boundary layer. Also, the presence of the liquid disturbances increases the area of the liquid exposed to the gas stream. Both of these effects would increase the heat transfer to the liquid.

Conclusion

For annular liquid flow with cocurrent gas flow, the liquid flow is relatively smooth until the liquid-flow rate is sufficient for the thickness of the liquid annulus to enter the flow region where the turbulent forces predominate over the viscous forces; disturbances then develop on the liquid film. The approximate liquid-flow rate for this transition can be predicted.

Appendix

Calculation of Velocity and Thickness of Liquid Film

For annular liquid flow with cocurrent gas flow in a horizontal duct, the velocity or the thickness of the annular liquid film can be calculated using the dimensionless parameters u^+ and y^+ from Fig. 6, which were obtained from von Kármán.[6]

Velocity Calculation. The parameter u^+ is defined as

$$u^+ = \frac{u}{\sqrt{\frac{\tau_0}{\rho_0}}} \quad \ldots\ldots [3]$$

The friction velocity $\sqrt{\tau_0/\rho_0}$ for a homogeneous fluid flowing in a duct is given by the equation

$$\sqrt{\tau_0/\rho_0} = u_b\sqrt{f/2} \quad \ldots\ldots [4]$$

For annular liquid flow with cocurrent gas flow, however, Equation [4] must be modified. This modification is accomplished

by referring the friction velocity $\sqrt{\tau_0/\rho_0}$ to the liquid annulus and by considering the gas flow to be replaced by a fictitious flow of the same liquid as in the annulus. Then the restriction is imposed that the pressure drop per unit length must be the same for the fictitious liquid flow as for the gas flow with the friction factor f for the actual conditions applying to each case. This restriction means that the dynamic pressures of the fictitious liquid flow and gas flow must be equal or

$$u_{b,l} = \sqrt{\frac{\rho_{b,g}}{\rho_{b,l}}}\, u_{b,g}$$

Substituting for the velocity in Equation [4] and combining the result with Equation [3] give the following relation for the liquid surface velocity

$$u_l = u^+_l \sqrt{\frac{f}{2}} \sqrt{\frac{\rho_{b,g}}{\rho_{b,l}}}\, u_{b,g} \quad \ldots\ldots\ldots\ldots\ldots\ldots [5]$$

Thickness Calculation. The parameter y^+ is defined as

$$y^+ = \frac{\sqrt{\tau_0/\rho_0}}{\mu_0/\rho_0}\, y$$

Again, referring the expression for y^+ to the liquid annulus and expressing the friction velocity τ_0/ρ_0 in terms of the gas-stream velocity give the following relation for the liquid-film thickness

$$y_l = y^+_l \frac{\mu_{0,l}}{\rho_{0,l}} \sqrt{\frac{2}{f}} \sqrt{\frac{\rho_{b,l}}{\rho_{b,g}}} \frac{1}{u_{b,g}} \quad \ldots\ldots\ldots\ldots\ldots\ldots [6]$$

All of the variables appearing in Equations [5] and [6], except the friction factor, are known for any given conditions. The friction factor for annular liquid flow with cocurrent gas flow is unavailable from experimental data for the range of conditions investigated in this paper. Extrapolation of the data by Lockhardt[2] and Bergelin[4] indicates that the friction factor for the conditions reported herein is in the order of 2 to 4 times that of single-phase flow in a smooth duct for the same gas-stream Reynolds number.

For convenience, a flow-rate parameter defined as $w^+ = W/\pi D g \mu_0$ is used for the calculations. It is the integral of the curve in Fig. 6 and is plotted as a function of y^+ in Fig. 8.

Calculation Procedure. The following procedure is used to determine the velocity and the thickness of the annular liquid film:

1 Determine the value of the flow-rate parameter $\dfrac{W}{\pi D g \mu_0}$.

2 Using this value, employ Fig. 8 to obtain the corresponding value of y^+_l.

3 The corresponding value of u^+_l is then obtained from Fig. 6.

4 The velocity or the thickness of the liquid film can then be determined from Equation [5] or [6], respectively.

An Airy Integral Analysis of Beam Columns With Distributed Axial Loading Having a Fixed Line of Action

By C. M. TYLER, JR.,[1] AND J. G. CHRISTIANO,[2] PITTSBURGH, PA.

An analytic method of solution of beam columns with partial uniformly distributed axial loading whose line of action does not change as the column deflects is developed in terms of Airy integral functions. This method is valid when the beam bending moment can be expressed or approximated piecewise as a polynomial. A numerical example is included and also tables of the necessary Airy integral functions and their first derivatives.

Nomenclature

The following nomenclature is used in the paper:

x = axial co-ordinate
x_1 = dimensionless transformed axial co-ordinate
l = length of member
$M(x)$ = actual bending moment at x
$W(x)$ = bending moment at x due to transverse loads treating member as a rigid body
$y(x)$ = deflection at x
$P(x)$ = axial load at x
P_1 = smaller end load, applied at $x = 0$; positive if compressive
P_2 = larger end load, applied at $x = l$; positive if compressive
EI = stiffness of member
$C_1 = P_1 l^2/EI$
$C_2 = (P_2 - P_1) l^2/EI$
$\lambda = C_2^{2/3}/l^2$, a parameter of a linear transformation

$$Ai(x_1) = \frac{1}{\pi}\int_0^\infty \cos\left(\frac{1}{3}t^3 + x_1 t\right) dt, \text{ Airy integral function}$$

$$Bi(x_1) = \frac{1}{\pi}\int_0^\infty \left[e^{\left(-\frac{1}{3}t^3 + x_1 t\right)} + \sin\left(\frac{1}{3}t^3 + x_1 t\right)\right] dt, \text{ Airy integral function}$$

$$Gi(x_1) = \frac{1}{\pi}\int_0^\infty \sin\left(\frac{1}{3}t^3 + x_1 t\right) dt, \text{ Airy integral function}$$

$x_0 = -C_2^{1/3} P_1/(P_2 - P_1)$, value of x_1 when $x = 0$
$x_l = -C_2^{1/3} P_2/(P_2 - P_1)$, value of x_1 when $x = l$
$\alpha, \beta, \gamma, \delta$ = arbitrary constants
b_0, b_1, b_2, b_3 = coefficients of beam-loading polynomial
b_0', b_1', b_2', b_3' = values of b_0, b_1, b_2, b_3 valid for only a portion of beam length

$$Ai'(x_1) = \frac{d}{dx_1}[Ai(x_1)]$$

$$Bi'(x_1) = \frac{d}{dx_1}[Bi(x_1)]$$

$$Gi'(x_1) = \frac{d}{dx_1}[Gi(x_1)]$$

N = beam loading

Introduction

Beam columns may have distributed axial loadings that act in three distinct ways as follows:

(*a*) The line of action of the axial loading may remain fixed as the column deflects.

(*b*) The axial loading may deflect with the column and have its line of action parallel to its undeflected position.

(*c*) The axial loading may deflect with the column and act along the tangent of the column deflection curve.

Each of these possibilities leads to separate problems inasmuch as the resulting differential equations are different. In the case of fixed line of action the reactions do not change as the column deflects, thus leading to the simplest differential equation. This type of loading is obtained when the surrounding structure induces a moment to offset that produced by the deflection of the column. A simple example would be when the distributed axial loading is provided by a web which in turn is loaded through a slip joint. This case (*a*) will be the subject matter of the present paper.

The differential equations for the beam columns of case (*a*) can be solved either in terms of Bessel functions or Airy integral functions. Airy integral functions yield a more concise solution inasmuch as the particular solution does not have to be constructed but can be written down as readily as the complementary solution. The case of the axial load deflecting with the column also can be solved using Airy integral functions; practical numerical solutions, however, must await the tabulation of integrals of the Airy integral functions. Incidentally, if the curvature of the beam column is of one sign, solutions obtained herein for case (*a*) can be considered as conservative approximations to cases (*b*) and (*c*).

The following analysis applies to straight structural members of uniform stiffness having axial end loads whose difference is balanced by a uniformly distributed loading along the axis of the member. The member may or may not have a transverse loading. The assumptions are made that the curvature may be considered as equal to the second derivative of the deflection with respect to the axial co-ordinate, and that the lines of action of the loads do not change as the member deflects.

At any point x on the axis of a beam column the actual bending moment may be taken as the bending moment due to trans-

[1] Assistant Professor of Mechanical Engineering, Carnegie Institute of Technology. Jun. ASME.

[2] Assistant Professor of Mathematics, University of Pittsburgh.

Presented at the National Conference of the Applied Mechanics Division, State College, Pa., June 19–21, 1952, of THE AMERICAN SOCIETY OF MECHANICAL ENGINEERS.

Discussion of this paper should be addressed to the Secretary, ASME, 29 West 39th Street, New York, N. Y., and will be accepted until October 10, 1952, for publication at a later date. Discussion received after the closing date will be returned.

NOTE: Statements and opinions advanced in papers are to be understood as individual expressions of their authors, and not those of the Society. Manuscript received by ASME Applied Mechanics Division, May 2, 1951. Paper No. 52—APM-8.

verse loads plus the product of the axial load and the deflection; Thus

$$M(x) = W(x) + P(x)\,y(x)$$

For straight beam columns with partially distributed column loading, Fig. 1, this becomes

$$M(x) = W(x) + [P_1 + (P_2 - P_1)\,x/l]\,y(x) \quad [1]$$

FIG. 1 FORM OF COLUMN LOADING FOR BEAM COLUMNS UNDER CONSIDERATION

All terms on the right of this equation are calculable by statics except the deflection $y(x)$. The basic differential equation for the deflection is

$$\frac{d^2y}{dx^2} = -\frac{M(x)}{EI}$$

Substituting the expression for $M(x)$ from Equation [1], this becomes

$$\frac{d^2y}{dx^2} = -\frac{W(x)}{EI} - \left(\frac{P_1}{EI} + \frac{P_2 - P_1}{EI}\,\frac{x}{l}\right) y(x) \quad [2]$$

Too often in the theory of beam columns the differential equation

$$\frac{d^2y}{dx^2} = f(x, y)$$

is of such nature that its solution is difficult, if not impossible. In these cases numerical methods can be used (1).[2]

For the case at hand an analytic solution will be effected by reducing the differential equation to the form

$$\frac{d^2y}{dx_1^2} = x_1 y + f(x_1)$$

whose solution is known in terms of recently tabulated Airy integral functions (2, 3).

METHOD OF ANALYSIS

Equation [2] can be rewritten as

$$\frac{d^2y}{dx^2} + \left(\frac{C_1}{l^2} + \frac{C_2}{l^3}\,x\right) y = -\frac{W(x)}{EI}$$

This may be changed to the desired form by a linear transformation involving a parameter λ

$$x_1 = -\frac{1}{\lambda}\left(\frac{C_1}{l^2} + \frac{C_2}{l^3}\,x\right)$$

then

$$\frac{d^2y}{dx^2} = \frac{d}{dx_1}\left(\frac{dy}{dx_1}\,\frac{dx_1}{dx}\right)\frac{dx_1}{dx} = \frac{C_2^2}{\lambda^3 l^6}\,\frac{d^2y}{dx_1^2}$$

and Equation [2] becomes

$$\frac{C_2^2}{\lambda^3 l^6}\,\frac{d^2y}{dx_1^2} - \lambda x_1 y = -\frac{W(x)}{EI}$$

[2] Numbers in parentheses refer to the Bibliography at the end of the paper.

The left side will have the desired form if

$$\lambda^3 l^6/C_2^2 = 1 \text{ or } \lambda = C_2^{2/3}/l^2$$

The transformation is now

$$x_1 = -C_1 C_2^{-4/3} - C_2^{1/3}\,x/l = -C_2^{1/3}\left(\frac{P_1}{P_2 - P_1}\right) - C_2^{1/3}\,\frac{x}{l}$$

and inversely

$$x = -C_2^{1/3} l x_1 - l C_1 C_2^{-1} = -C_2^{-1/3} l x_1 - l\left(\frac{P_1}{P_2 - P_1}\right)$$

Applying this transformation Equation [2] becomes

$$\frac{d^2y}{dx_1^2} - x_1 y = -\frac{W(x) l^2}{C_2^{2/3} EI} = F(x_1) \quad [3]$$

If the transverse loading is such that the right side of Equation [3] can be written or approximated by a third-degree polynomial, which is the case here, Equation [3] takes the form

$$\frac{d^2y}{dx_1^2} - x_1 y = F(x_1) = b_0 + b_1 x_1 + b_2 x_1^2 + b_3 x_1^3$$

the solution of which is known to be (4)

$$y(x_1) = \alpha Ai(x_1) + \beta Bi(x_1) - (b_0 + 2b_2)\pi Gi(x_1) - b_1 - b_2 x_1 - b_3 x_1^2 \quad [4]$$

In this expression $Ai(x_1)$, $Bi(x_1)$, and $Gi(x_1)$ are Airy integral functions, and α and β are arbitrary constants. The constants are evaluated using the following boundary conditions:
When

$$x = 0,\ x_1 = -C_2^{1/3}\,\frac{P_1}{P_2 - P_1} = x_0, \text{ and } y = 0$$

When

$$x = l,\ x_1 = -C_2^{1/3}\,\frac{P_1}{P_2 - P_1} = x_l, \text{ and } y = 0$$

For these boundary conditions the constants are

$$\alpha = \frac{\begin{vmatrix} (b_0 + 2b_2)\pi Gi(x_0) + b_1 + b_2 x_0 + b_3 x_0^2 & Bi(x_0) \\ (b_0 + 2b_2)\pi Gi(x_l) + b_1 + b_2 x_l + b_3 x_l^2 & Bi(x_l) \end{vmatrix}}{\begin{vmatrix} Ai(x_0) & Bi(x_0) \\ Ai(x_l) & Bi(x_l) \end{vmatrix}}$$

$$\beta = \frac{\begin{vmatrix} Ai(x_0) & (b_0 + 2b_2)\pi Gi(x_0) + b_1 + b_2 x_0 + b_3 x_0^2 \\ Ai(x_l) & (b_0 + 2b_2)\pi Gi(x_l) + b_1 + b_2 x_l + b_3 x_l^2 \end{vmatrix}}{\begin{vmatrix} Ai(x_0) & Bi(x_0) \\ Ai(x_l) & Bi(x_l) \end{vmatrix}}$$

If the transverse loading is discontinuous, the right side of Equation [3] can be treated piecewise as polynomials. The pieces of the deflection curve can be fitted together by determining the arbitrary constants such that the slope and deflection at the left of a loading discontinuity are equal to those at the right of the discontinuity. This technique is illustrated in the numerical example. In the event that there are numerous discontinuities or, if a third-degree polynomial is not a good approximation, the analysis is perhaps better made by a numerical method (1).

With the deflection $y(x)$ known, the bending moment $M(x)$ can be found by Equation [1].

Elastic Stability of Members

A beam column of the type considered will become unstable when the determinant

$$\begin{vmatrix} Ai(x_0) & Bi(x_0) \\ Ai(x_l) & Bi(x_l) \end{vmatrix} = 0$$

The lowest numerical values of $C_2^{1/3}$ at which this occurs have been calculated and are plotted against the ratio of P_1 to P_2 as Fig. 2. These values agree with those calculated by Timoshenko using Bessel functions within the accuracy of his calculations (3). When P_1 is negative (tension) and numerically greater than P_2, the critical value of $C_2^{1/3}$ may be taken as equal to $2.34(1 - P_1/P_2)$.

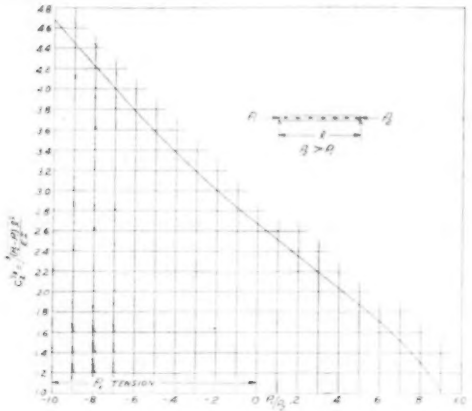

Fig. 2 Lowest Critical Values of $C_2^{1/3}$ Representing Simplest Mode of Buckling

Numerical Applications

As an aid in making numerical calculations, exact expressions for the coefficients b_0, b_1, b_2, and b_3 are given in Table 1 for several simple beam loadings. More complicated beam loadings can be constructed by adding the coefficients for the simple cases.

In Table 2 numerical values of $Ai(x_1)$, $Bi(x_1)$, $\pi Gi(x_1)$ and their first derivatives are presented for the interval $-10 \leq x_1 \leq +5$. This will cover all stable cases of compression members when $P_1/P_2 \leq 0.90$ and also a range of tension and part tension members.

The values of $Ai(x_1)$, $Bi(x_1)$, $Ai'(x_1)$, and $Bi'(x_1)$ have been taken from or calculated from related functions tabulated in the 8-place table by J. C. P. Miller (2). Values of $\pi Gi(x_1)$ have been calculated from values of $Gi(x_1)$ or a related function tabulated by R. S. Scorer (3). The derivatives of this function have been obtained numerically by using Bickley's tables for numerical differentiation (6).

Example

The following was chosen as an example because it involves a part tension axial loading and a discontinuous transverse loading, illustrating the technique of matching pieces of the deflection curve.

Fig. 3 represents a beam column with a 5000-lb tension load at one end, a 15,000-lb compression load at the other end, and a 2000-lb beam load 14 in. from the right support.

Fig. 3 Loading of Example Beam Column

For this example

$$C_2 = \frac{(P_2 - P_1)l^2}{EI} = \frac{(15{,}000 + 5000) \times 40^2}{4 \times 10^6} = 8$$

The value of x_1 for the left end is

$$-C_2^{1/3}\frac{P_1}{P_2 - P_1} = -8^{1/3}\frac{-5000}{15{,}000 + 5000} = +0.50$$

The value of x_1 for the right end is

$$-C_2^{1/3}\frac{P_2}{P_2 - P_1} = -8^{1/3}\frac{15{,}000}{15{,}000 + 5000} = -1.50$$

From Table 1 the constants on the right-hand side of Equation [3] are

$$b_0 = \frac{Nbl^2}{C_2^{2/3}EI}\frac{P_1}{P_2 - P_1} = \frac{2000 \times 14 \times 40^2}{4 \times 4 \times 10^6} \times \frac{-5000}{15{,}000 + 5000} = -0.700$$

$$b_1 = \frac{Nbl^2}{C_2EI} = \frac{2000 \times 14 \times 40^2}{8 \times 4 \times 10^6} = +1.400$$

$$b_0' = -\frac{Nal^2}{C_2^{2/3}EI}\frac{P_2}{P_2 - P_1} = -\frac{2000 \times 26 \times 40^2}{4 \times 4 \times 10^6} \times \frac{15{,}000}{15{,}000 + 5000} = -3.900$$

$$b_1' = -\frac{Nal^2}{C_2EI} = -\frac{2000 \times 26 \times 40^2}{8 \times 4 \times 10^6} = -2.600$$

From Equation [4] the expressions for the two pieces of the deflection curve to the left and to the right of the beam load are, respectively

$$y = \alpha Ai(x_1) + \beta Bi(x_1) - b_0\pi Gi(x_1) - b_1$$
$$y = \gamma Ai(x_1) + \delta Bi(x_1) - b_0'\pi Gi(x_1) - b_1'$$

The four constants α, β, γ, and δ can be evaluated using the boundary conditions

$x = 0$, $x_1 = 0.50$; $y = 0$

$$0 = \alpha Ai(0.50) + \beta Bi(0.50) + 0.700\pi Gi(0.50) - 1.400$$

$x = 40$ in., $x_1 = -1.50$; $y = 0$

$$0 = \gamma Ai(-1.50) + \delta Bi(-1.50) + 3.900\pi Gi(-1.50) + 2.600$$

$x = 26$ in., $x_1 = -0.80$; $y^- = y^+$

$$\alpha Ai(-0.80) + \beta Bi(-0.80) + 0.700\pi Gi(-0.80) - 1.400 = \gamma Ai(-0.80) + \delta Bi(-0.80) + 3.900\pi Gi(-0.80) + 2.600$$

$x = 26$ in., $x_1 = -0.80$; $\left(\frac{dy}{dx}\right)^- = \left(\frac{dy}{dx}\right)^+$

and $\left(\frac{dy}{dx_1}\right)^- = \left(\frac{dy}{dx_1}\right)^+$

TABLE 1 EXPRESSIONS FOR COEFFICIENTS

(a) Beam Loading	b Coefficients	
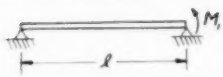	$b_0 = \frac{M_1 l^2}{C_2^{2/3} EI} \frac{P_1}{P_2 - P_1}$	$b_1 = \frac{M_1 l^2}{C_2 EI}$
	$b_0 = -\frac{M_1 l^2}{C_2^{2/3} EI} + \frac{(M_2 - M_1) l^2}{C_2^{2/3} EI} \frac{P_1}{P_2 - P_1}$	$b_1 = \frac{(M_2 - M_1) l^2}{C_2 EI}$
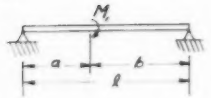	$b_0 = -\frac{M_1 l^2}{C_2^{2/3} EI} \frac{P_1}{P_2 - P_1}$	$0 \le x \le a$
	$b_1 = -\frac{M_1 l^2}{C_2 EI}$	$0 \le x \le a$
	$b_0' = -\frac{M_1 l^2}{C_2^{2/3} EI} \frac{P_2}{P_2 - P_1}$	$a \le x \le l$
	$b_1' = -\frac{M_1 l^2}{C_2 EI} = b_1$	$a \le x \le l$
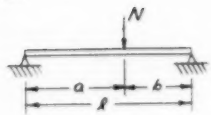	$b_0 = \frac{Nbl^2}{C_2^{2/3} EI} \frac{P_1}{P_2 - P_1}$	$0 \le x \le a$
	$b_1 = \frac{Nbl^2}{C_2 EI}$	$0 \le x \le a$
	$b_0' = \frac{-Nal^2}{C_2^{2/3} EI} \frac{P_2}{P_2 - P_1}$	$a \le x \le l$
	$b_1' = -\frac{Nal^2}{C_2 EI}$	$a \le x \le l$
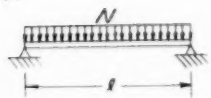	$b_0 = \frac{Nl^2}{2C_2^{2/3} EI} \frac{P_1}{P_2 - P_1} \frac{P_2}{P_2 - P_1}$	
	$b_1 = \frac{Nl^3}{C_2 EI} \left(\frac{1}{2} + \frac{P_1}{P_2 - P_1} \right)$	
	$b_2 = \frac{Nl^3}{2C_2^{4/3} EI}$	
	$b_0 = \frac{Nl^2}{2C_2^{2/3} EI} \frac{P_1}{P_2 - P_1} \left[(2b + a) + \frac{l^2}{a} \frac{P_1}{P_2 - P_1} \right]$	$0 \le x \le a$
	$b_1 = \frac{Nl^2}{C_2 EI} \left[\frac{2b + a}{2} + \frac{l^2}{a} \frac{P_1}{P_2 - P_1} \right]$	$0 \le x \le a$
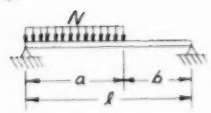	$b_7 = \frac{Nl^4}{2aC_2^{4/3} EI}$	$0 \le x \le a$
	$b_0' = -\frac{Nal^2}{2C_2^{2/3} EI} \frac{P_2}{P_2 - P_1}$	$a \le x \le l$
	$b_1' = -\frac{Nal^2}{2C_2 EI}$	$a \le x \le l$

$$\alpha Ai'(-0.80) + \beta Bi'(-0.80) + 0.700\pi Gi'(-0.80) = \gamma Ai'(-0.80) + \delta Bi'(-0.80) + 3.900\pi Gi'(-0.80)$$

Substituting the numerical values of the Airy integral functions, four equations in the four constants are obtained

$$0.23169\alpha + 0.85428\beta = -0.700 \times 0.76881 + 1.400 = +0.86183$$

$$0.46426\gamma - 0.19178\delta = -3.900(-1.14709) - 2.600 = +1.87365$$

$$0.52357(\alpha - \gamma) + 0.21983(\beta - \delta) = (-0.700 + 3.900)(-0.08168) + 1.400 + 2.600 = 3.73862$$

$$-0.10581(\alpha - \gamma) + 0.56353(\beta - \delta) = (-0.700 + 3.900)\,1.33968 = 4.28698$$

TABLE 2 NUMERICAL VALUES OF AIRY INTEGRAL FUNCTIONS

x_1	$Ai(x_1)$	$Ai'(x_1)$	$Bi(x_1)$	$Bi'(x_1)$	$\pi Gi(x_1)$	$\pi Gi'(x_1)$
0.0	+0.35503	-0.25882	+0.61493	+0.44829	+0.64395	+0.46945
- 0.1	.38085	.25696	.57000	.45121	.59190	.57250
- 0.2	.40628	.25103	.52451	.45939	.52927	.68087
- 0.3	.43090	.24055	.47798	.47188	.45560	.79315
- 0.4	.45423	.22503	.43002	.48773	.37057	.90757
- 0.5	+0.47573	-0.20408	+0.38035	+0.50593	+0.27408	+1.02203
- 0.6	.49485	.17736	.32879	.52540	.16625	1.13410
- 0.7	.51100	.14464	.27527	.54500	+ .04744	1.12791
- 0.8	.52357	.10581	.21983	.56353	- .08168	1.33968
- 0.9	.53196	.06091	.16264	.57975	.22011	1.42679
- 1.0	+0.53556	-0.01016	+0.10400	+0.59238	-0.36654	+1.49886
- 1.1	.53381	+ .04603	+ .04433	.60012	.51926	1.55228
- 1.2	.52619	.10703	- .01582	.60171	.67625	1.58343
- 1.3	.51227	.17199	.07577	.59593	.83509	1.58885
- 1.4	.49170	.23982	.13472	.58166	.99305	1.56529
- 1.5	+0.46426	+0.30919	-0.19178	+0.55791	-1.14709	+1.50993
- 1.6	.42986	.37854	.24596	.52389	1.29390	1.42052
- 1.7	.38861	.44612	.29620	.47906	1.43001	1.29551
- 1.8	.34076	.51000	.34141	.42315	1.55180	1.13427
- 1.9	.28680	.56809	.38047	.35624	1.65566	0.93719
- 2.0	+0.22741	+0.61826	-0.41230	+0.27880	-1.73809	+0.70585
- 2.1	.16348	.65834	.43590	.19169	1.79579	.44313
- 2.2	.09615	.68624	.45036	+ .09623	1.82581	+ .15327
- 2.3	.02671	.70003	.45493	- .00581	1.82572	- .15812
- 2.4	- .04333	.69802	.44905	.11223	1.79370	.48401
- 2.5	-0.11233	+0.67885	-0.43242	-0.22042	-1.72871	-0.81613
- 2.6	.17850	.64134	.40501	.32740	1.63058	1.14506
- 2.7	.24004	.58601	.36709	.42990	1.50015	1.46047
- 2.8	.29510	.51221	.31929	.52445	1.33930	1.75142
- 2.9	.34191	.42118	.26259	.60752	1.15105	2.00675
- 3.0	-0.37881	+0.31458	-0.19829	-0.67561	-0.93951	-2.21544
- 3.1	.40438	.19482	.12807	.72545	.70986	2.36717
- 3.2	.41744	.06503	- .05391	.75412	.46828	2.45275
- 3.3	.41718	- .07096	+ .02199	.75927	- .22177	2.46471
- 3.4	.40319	.20875	.09711	.73920	+ .02203	2.39778
- 3.5	-0.37553	-0.34344	+0.16894	-0.69312	+0.25507	-2.24936
- 3.6	.33478	.46986	.23487	.62117	.46920	2.01994
- 3.7	.28201	.58273	.29235	.52461	.65648	1.71342
- 3.8	.21886	.67688	.33905	.40582	.80955	1.33723
- 3.9	.14742	.74756	.37289	.26830	.92197	0.90242

(Continued on page 280)

TABLE 2 (*Continued*)

x_1	$Ai(x_1)$	$Ai'(x_1)$	$Bi(x_1)$	$Bi'(x_1)$	$\pi Gi(x_1)$	$\pi Gi'(x_1)$
- 4.0	-0.07027	-0.79063	+0.39223	-0.11667	+0.98856	-0.42346
- 4.1	+0.00968	.80287	.39594	+ .04348	1.00577	+ .08211
- 4.2	.08921	.78222	.38347	.20576	0.97192	.59423
- 4.3	.16500	.72749	.35495	.36320	.88744	1.09103
- 4.4	.23370	.64085	.31123	.50859	.75498	1.54981
- 4.5	+0.29215	-0.52336	+0.25387	+0.63474	+0.57949	+1.94806
- 4.6	.33750	.37953	.18585	.73494	.36809	2.26466
- 4.7	.36737	.21499	.10795	.80329	+ .12990	2.48109
- 4.8	.38004	- .03677	+ .02571	.83509	- .12429	2.58262
- 4.9	.37454	+ .14696	- .05775	.82722	.38246	2.55942
- 5.0	+0.35076	+0.32719	-0.13837	+0.77841	-0.63188	+2.40754
- 5.1	.30953	.49459	.21209	.68949	.85975	2.12891
- 5.2	.25258	.63990	.27503	.56346	1.05389	1.73492
- 5.3	.18257	.75458	.32372	.40556	1.20339	1.24009
- 5.4	.10293	.83122	.35532	.22307	1.29933	0.66799
- 5.5	+0.01778	+0.86420	-0.36781	+0.02511	-1.33536	+0.04718
- 5.6	- .06833	.85003	.36017	- .17784	1.30823	- .58934
- 5.7	.15062	.78782	.33246	.37441	1.21816	1.20588
- 5.8	.22435	.69743	.28589	.55300	1.06894	1.76598
- 5.9	.28512	.52963	.22283	.70248	0.86801	2.23403
- 6.0	-0.32915	+0.34594	-0.14670	-0.81290	-0.62611	-2.58067
- 6.1	.35351	+ .13836	- .06182	.87623	.35682	2.77878
- 6.2	.35642	- .08107	+ .02679	.88698	- .07587	2.81177
- 6.3	.33735	.29899	.11374	.84276	+ .19977	2.67209
- 6.4	.29714	.50148	.19354	.74461	.45289	2.36303
- 6.5	-0.23802	-0.67495	+0.26101	-0.59717	+0.66720	-1.89912
- 6.6	.16353	.80712	.31160	.40857	.82840	1.30593
- 6.7	- .07831	.88791	.34173	- .19010	.92525	-0.61896
- 6.8	+ .01210	.91030	.34908	+ .04438	.95051	+ .11829
- 6.9	.10169	.87103	.33284	.27926	.90155	.85679
- 7.0	+0.18428	-0.77101	+0.29376	+0.49824	+0.78081	+1.54531
- 7.1	.25404	.61553	.23425	.68542	.59582	2.13388
- 7.2	.30585	.41412	.15822	.82651	.35887	2.57763
- 7.3	.33577	- .18010	+ .07087	.90998	+ .08634	2.84039
- 7.4	.34132	+ .07028	- .02160	.92813	- .20234	2.89787
- 7.5	+0.32178	+0.31881	-0.11246	+0.87780	-0.48604	+2.74023
- 7.6	.27825	.54672	.19493	.76096	.74341	2.37359
- 7.7	.21372	.73605	.26267	.58474	.95453	1.82042
- 7.8	.13285	.87116	.31030	.36123	1.10252	1.11865
- 7.9	+ .04170	.94004	.33388	+ .10670	1.17500	+0.31943

(*Continued on page 281*)

TABLE 2 (*Continued*)

x_1	$Ai(x_1)$	$Ai'(x_1)$	$Bi(x_1)$	$Bi'(x_1)$	$\pi Gi(x_1)$	$\pi Gi'(x_1)$
- 8.0	-0.05271	+0.93556	-0.33125	-0.15945	-1.16519	-0.51633
- 8.1	.14291	.85622	.30230	.41616	1.07272	1.32243
- 8.2	.22160	.70660	.24904	.64232	0.90391	2.03259
- 8.3	.28223	.49728	.17551	.81860	.67144	2.58603
- 8.4	.31959	.24422	- .08752	.92911	.39360	2.93288
- 8.5	-0.33029	-0.03231	+0.00775	-0.96297	-0.09291	-3.03893
- 8.6	.31311	.30933	.10236	.91548	+ .20564	2.88942
- 8.7	.26920	.56290	.18820	.78883	.47666	2.49123
- 8.8	.20205	.77061	.25778	.59221	.69654	1.87326
- 8.9	.11727	.91289	.30483	.34136	.84561	1.08492
- 9.0	-0.02213	-0.97566	+0.32495	-0.05740	+0.91004	-0.19255
- 9.1	+ .07496	.95150	.31603	+ .23484	.88325	+ .72583
- 9.2	.16527	.84067	.27858	.50894	.76678	1.58720
- 9.3	.24047	.65149	.21571	.73928	.57040	2.31107
- 9.4	.29348	.39986	.13294	.90349	.31151	2.82717
- 9.5	+0.31910	-0.10810	+0.03779	+0.98471	+0.01368	+3.08259
- 9.6	.31465	+ .19695	- .06091	.97350	- .29530	3.04758
- 9.7	.28024	.48629	.15379	.86898	.58603	2.71946
- 9.8	.21887	.73154	.23186	.67937	.83025	2.12397
- 9.9	.13624	.90781	.28738	.42147	1.00365	1.31397
-10.0	+0.04024	+0.99627	-0.31468	+0.11941	-1.08840	+0.36523
0.0	+0.35503	-0.25882	+0.61493	+0.44829	+0.64395	+0.46945
0.1	.32920	.25713	.65986	.45151	.68601	.37282
0.2	.30370	.25241	.70546	.46179	.71875	.28339
0.3	.27881	.24515	.75249	.48005	.74294	.20170
0.4	.25474	.23583	.80177	.50728	.75936	.12802
0.5	+0.23169	-0.22491	+0.85428	+0.54457	+0.76881	+0.06244
0.6	.20980	.21279	.91106	.59314	.77211	+ .00484
0.7	.18916	.19985	.97333	.65441	.77004	- .04501
0.8	.16985	.18641	1.04242	.73001	.76335	.08749
0.9	.15189	.17276	1.11987	.82190	.75277	.12304
1.0	+0.13529	-0.15915	+1.20742	+0.93244	+0.73896	-0.15217
1.1	.12005	.14577	1.30707	1.06441	.72253	.17544
1.2	.10613	.13279	1.42113	1.22123	.70405	.19341
1.3	.093475	.12033	1.55228	1.40699	.68401	.20666
1.4	.082038	.10851	1.70366	1.62664	.66286	.21575
1.5	+0.071750	-0.097382	+1.87894	+1.88621	+0.64098	-0.22123
1.6	.062537	.086996	2.08247	2.19300	.61871	.22362
1.7	.054325	.077375	2.31941	2.55585	.59634	.22340
1.8	.047036	.068525	2.59587	2.98554	.57411	.22101
1.9	.040594	.060437	2.91918	3.49517	.55220	.21685

(*Continued on page 282*)

TABLE 2 (*Continued*)

x_1	$Ai(x_1)$	$Ai'(x_1)$	$Bi(x_1)$	$Bi'(x_1)$	$\pi Gi(x_1)$	$\pi Gi'(x_1)$
2.0	+0.034924	-0.053030	+3.29810	+4.10068	+0.53078	-0.21128
2.1	.029953	.046457	3.74315	4.82155	.50998	.20464
2.2	.025610	.040497	4.26704	5.68154	.48988	.19718
2.3	.021832	.035173	4.88506	6.70974	.47056	.18916
2.4	.018556	.030439	5.61577	7.94179	.45206	.18078
2.5	+0.015726	-0.026251	+6.48166	+9.42142	+0.43441	-0.17222
2.6	.013289	.022561	7.5191	11.202	.41762	.16362
2.7	.011199	.019326	8.7344	13.351	.40168	.15510
2.8	.0094105	.016500	10.1953	15.949	.38659	.14674
2.9	.0078863	.014042	11.943	19.099	.37233	.13862
3.0	+.0065911	-.011913	+14.037	+22.922	+0.35886	-0.13081
3.1	.0054940	.010076	16.555	27.578	.34616	.12332
3.2	.0045674	.0084957	19.587	33.258	.33419	.11619
3.3	.0037873	.0071425	23.248	40.202	.32291	.10944
3.4	.0031323	.0059871	27.680	48.714	.31228	.10307
3.5	+.0025841	-.0050044	+33.056	+59.165	+0.30228	-0.09709
3.6	.0021265	.0041712	39.593	72.072	.29285	.09148
3.7	.0017456	.0034670	47.561	87.891	.28397	.08623
3.8	.0014294	.0028738	57.295	107.45	.27560	.08133
3.9	.0011677	.0023757	69.216	131.78	.26769	.07677
4.0	+.00095156	-.0019586	+83.847	+161.93	+0.26023	-0.07253
4.1	.00077363	.0016106	101.846	199.42	.25318	.06858
4.2	.00062750	.0013210	124.04	246.15	.24651	.06491
4.3	.00050779	.0010807	151.46	304.50	.24019	.06151
4.4	.00040997	.00088188	185.43	377.55	.23420	.05834
4.5	+.00033025	-.00071786	+227.59	+469.14	+0.22851	-0.05541
4.6	.00026543	.00058291	280.04	584.23	.22311	.05268
4.7	.00021286	.00047218	345.43	729.15	.21797	.05014
4.8	.00017033	.00038158	427.13	911.97	.21307	.04778
4.9	.00013599	.00030761	529.43	1143.1	.20841	.04559
5.0	+.00010834	-.00024740	+657.79	+1435.8	+0.20395	-0.04354

The last pair of equations can be solved simultaneously for $(\alpha - \gamma)$ and $(\beta - \delta)$. With these values known the first two equations can be solved simultaneously for α and β or γ and δ. These values are

$$\alpha = 4.2124, \quad \beta = -0.1336, \quad \gamma = 0.5543, \quad \delta = -8.4279$$

With these constants evaluated the deflection curve is

$$y = 4.2124Ai(x_1) - 0.1336Bi(x_1) + 0.700\pi Gi(x_1) - 1.400; \qquad 0 \leq x \leq 26 \text{ in.}, \quad +0.50 \geq x_1 \geq -0.80$$

$$y = 0.5543Ai(x_1) - 8.4279Bi(x_1) + 3.900\pi Gi(x_1) + 2.600; \qquad 0.26 \text{ in.} \leq x \leq 40 \text{ in.}, \quad -0.80 \geq x_1 \geq -1.50$$

Numerical values of the deflection and the actual bending moments are given in Table 3 for 20 points along the axis of the beam column.

Nonuniformly Distributed Axial Load

The technique of matching deflection curves, as illustrated in the previous example, also can be used for more complicated axial loadings. When the running axial load is distributed uniformly over a portion of the length or has several varying magnitudes, the deflection curves can be matched at the points where the magnitude changes.

As an example consider the beam column in Fig. 4(*a*). The general form of the deflection curve from $0 \leq x \leq a$ will be given by simple loading in Fig. 4(*b*). This is known to be (7)

$$y = \alpha \sin \sqrt{\frac{P}{EI}}\, x + \beta \cos \sqrt{\frac{P}{EI}}\, x - \frac{Nx}{2P} + \frac{Nx^2}{2Pl} - \frac{NEI}{P^2l}$$

TABLE 3 NUMERICAL VALUES OF DEFLECTION AND ACTUAL BENDING MOMENT FOR EXAMPLE BEAM COLUMN

1 Axial co-ordinate, x, in.	2 x_1	3 Deflection, $y(x)$, in.	4 $P(x)$, lb	5 $P(x)\ y(x)$	6 $W(x)$, in-lb	7 Actual bending moment, $M(x)$, in-lb
0	+0.50	0	—5000	0	0	0
2	+0.40	0.059	—4000	—240	1400	1160
4	+0.30	0.194	—3000	—580	2800	2220
6	+0.20	0.289	—2000	—580	4200	3620
8	+0.10	0.379	—1000	—380	5600	5220
10	0	0.464	0	0	7000	7000
12	—0.10	0.543	+1000	540	8400	8940
14	—0.20	0.612	+2000	1220	9800	11020
16	—0.30	0.669	+3000	2010	11200	13210
18	—0.40	0.714	+4000	2860	12600	15460
20	—0.50	0.745	+5000	3730	14000	17730
22	—0.60	0.757	+6000	4540	15400	19940
24	—0.70	0.749	+7000	5240	16800	22040
26	—0.80	0.719	+8000	5750	18200	23950
28	—0.90	0.666	+9000	5990	15600	21590
30	—1.00	0.631	+10000	6310	13000	19310
32	—1.10	0.497	+11000	5470	10400	15870
34	—1.20	0.398	+12000	4780	7800	12580
36	—1.30	0.266	+13000	3460	5200	8660
38	—1.40	0.135	+14000	1890	2600	4490
40	—1.50	0	+15000	0	0	0

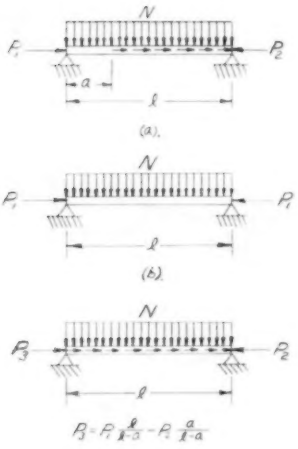

FIG. 4 EQUIVALENT LOADINGS FOR EXAMPLE NONUNIFORMLY DISTRIBUTED AXIAL-LOAD BEAM COLUMN

The form of the deflection curve from $a \leq x \leq l$ will be given by the loading in Fig. 4(*c*). From Table 1 and Equation [4] this is

$$y(x_1) = \gamma Ai(x_1) + \delta Bi(x_1) - \frac{Nl^2}{2(C_2{}^3/_2)EI}\left(\frac{P_3}{P_1 - P_3}\frac{P_2}{P_1 - P_3}\right)\pi Gi(x_1) - \frac{Nl^2}{C_2EI}\left(\frac{1}{2} + \frac{P_3}{P_1 - P_3}\right) - \frac{Nl^2}{2C_2{}^1/_2EI}\,x_1$$

The constants α, β, γ, and δ now can be evaluated by the conditions that the deflection is zero at the ends and the slope and deflection of the two curves must be the same when $x = a$.

BIBLIOGRAPHY

1 "Analysis of Straight and Curved Beam Columns," by C. M. Tyler, Jr., and J. G. Christiano, JOURNAL OF APPLIED MECHANICS, Trans. ASME, vol. 73, 1951, pp. 283–284.

2 "The Airy Integral," by J. C. P. Miller, British Association for the Advancement of Science, Mathematical Tables Part-Volume B Cambridge University Press, London, England, 1946.

3 "Numerical Evaluation of Integrals of the Form $I = \int_{x_1}^{x_2} f(x)e^{i\phi(x)}\,dx$ and the Tabulation of the Function $Gi(x) = 1/\pi \int_0^\infty \sin(uz + \overline{1/3}u^3)du$," by R. S. Scorer, *The Quarterly Journal of Mechanics and Applied Mathematics*, vol. 3, March, 1950, pp. 107–112.

4 "Notes on the Solution of the Equation $y'' - xy = f(x)$," by J. C. P. Miller and Z. Mursi, *The Quarterly Journal of Mechanics and Applied Mathematics*, vol. 3, March, 1950, pp. 113–118.

5 "Theory of Elastic Stability," by S. Timoshenko, McGraw-Hill Book Company, Inc., New York, N. Y., 1936, p. 122.

6 "Formulae for Numerical Differentiation," by W. G. Bickley, *The Mathematical Gazette*, vol. 25, 1941, pp. 19–27.

7 "Strength of Materials," by S. Timoshenko, D. Van Nostrand Company, Inc., New York, N. Y., second edition, 1941, p. 30.

The Concept of Complex Damping

By N. O. MYKLESTAD,[1] URBANA, ILL.

In this paper it is shown that if the hysteresis loop for a material has a particular shape the damping can be considered adequately by multiplying the modulus of elasticity of the material by the complex number e^{2bi} where $2b$ is called the complex damping factor. For small values of b it is shown that both for free and forced vibrations of a simple spring-mass system the motion in the case of complex damping is the same as in the case of viscous damping, with $b = c/c_{cr}$, except that in the steady-state case the phase angles are slightly different. Also, it is shown how complex damping may be applied to cases of forced vibrations of uniform rods and beams. The greatest advantage of using complex damping, however, is in numerical calculations of forced vibrations of engine crankshafts, airplane wings, and other types of structures; and for such calculations it already has been extensively used.

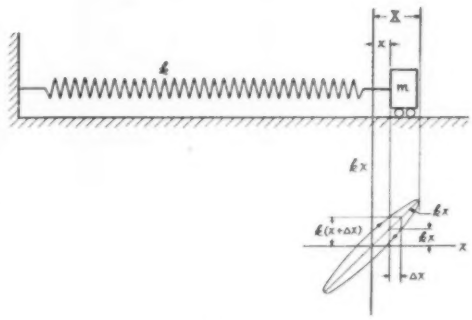

Fig. 1

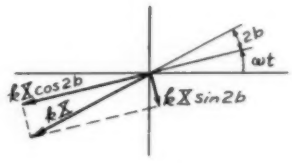

Fig. 2

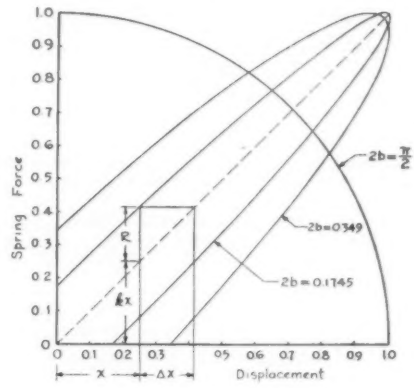

Fig. 3

Complex Damping

CONSIDER the simple spring-mass system in Fig. 1 in which the spring has a hysteresis loop as shown in the bottom part of the figure for steady-state harmonic motion of the mass given by

$$x = Xe^{i\omega t} \quad [1]$$

If there is no damping the spring force is kx, but with damping the spring force may be written as $k(x + \Delta x)$, as shown in Fig. 1. By means of Equation [1] the spring force may be written as

$$k(x + \Delta x) = kXe^{i\omega(t + \Delta t)} \quad [2]$$

If the quantity $\omega\Delta t$ is constant for a particular hysteresis loop, the damping is called complex with a complex damping factor

$$2b = \omega\Delta t \quad [3]$$

and Equation [2] may be written

$$k(x + \Delta x) = ke^{2bi}Xe^{i\omega t} = ke^{2bi}x \quad [4]$$

It is seen that in this case the damping is taken care of adequately by replacing k by a complex spring constant

$$\bar{k} = ke^{2bi} \quad [5]$$

and using kx for the spring force.

This is illustrated in Fig. 2 where it is seen that the rotating vector representing the complex spring force is an angle $2b$ ahead of the one representing the real spring force. This means that the effective spring force has been reduced from kx to $kx \cos 2b$, and at the same time a damping force $kx \sin 2b$ has been introduced in phase with the velocity. In Fig. 3 are shown several hysteresis loops for complex damping. The loops are elliptical in shape and the limiting case is a circle, for which $2b = \pi/2$.

Free Vibration of a Simple Spring-Mass System

If the damping is so small that the motion of the mass is essentially harmonic during one period, the differential equation of the motion may be written as

---

[1] Professor of Theoretical and Applied Mechanics, University of Illinois. Mem. ASME.

Presented at the National Conference of the Applied Mechanics Division, State College, Pa., June 19–21, 1952, of The American Society of Mechanical Engineers.

Discussion of this paper should be addressed to the Secretary, ASME, 29 West 39th Street, New York, N. Y., and will be accepted until October 10, 1952, for publication at a later date. Discussion received after the closing date will be returned.

Note: Statements and opinions advanced in papers are to be understood as individual expressions of their authors and not those of the Society. Manuscript received by ASME Applied Mechanics Division, September 24, 1951. Paper No. 52—APM-15.

$$m\ddot{x} + ke^{2bi}x = 0 \quad [6]$$

The complete solution to this differential equation is

$$x = A_0 e^{-\omega_n \beta t} e^{i\omega_n \alpha t} + B_0 e^{\omega_n \beta t} e^{-i\omega_n \alpha t} \quad [7]$$

where

$$\omega_n = \sqrt{k/m} \quad [8]$$

$$\alpha = \cos b \quad [9]$$

$$\beta = \sin b \quad [10]$$

From Equation [7] it looks as if the motion is unstable owing to the term $e^{\omega_n \beta t}$, which increases indefinitely as t increases. However, the term $e^{-i\omega_n \alpha t}$ indicates that in this case the cycle is in the negative direction from that given by Equation [1], making the damping force in Fig. 2 negative. The second term on the right-hand side of Equation [7] therefore does not represent complex damping and hence has no physical connection with reality.

Considering only the real part, and putting $A_0 = A_0 e^{-i\gamma_0}$, Equation [7] may now be written

$$x = A_0 [e^{-\omega_n \beta t} e^{i(\omega_n \alpha t - \gamma_0)}]_R = A_0 e^{-\omega_n \beta t} \cos(\omega_n \alpha t - \gamma_0) \quad [11]$$

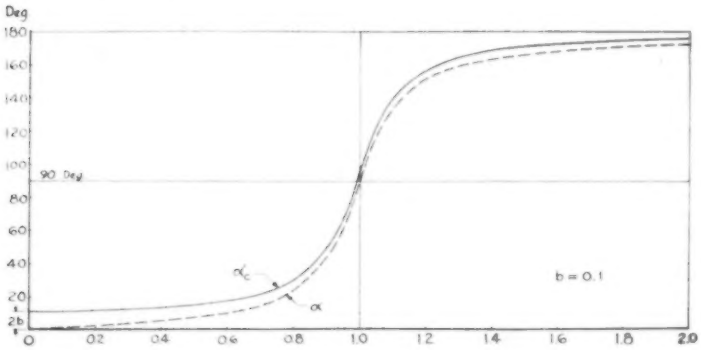

FIG. 4

Since the only practically significant cases are those where b is a small quantity one may put

$$\alpha \approx 1 - \frac{1}{2}b^2 \approx \sqrt{1 - b^2} \quad [12]$$

$$\beta \approx b \quad [13]$$

Equation [11] then becomes

$$x = A_0 e^{-b\omega_n t} \cos\left(\sqrt{1 - b^2}\,\omega_n t - \gamma_0\right) \quad [14]$$

which is identical with the case of viscous damping, for which the coefficient of viscous damping is

$$c = 2b\sqrt{km} \quad [15]$$

and the viscous damping factor b is the ratio of c to the critical damping coefficient $c_{cr} = 2\sqrt{km}$.

FORCED VIBRATION OF A SIMPLE SPRING-MASS SYSTEM

Assume now that the mass in Fig. 1 is acted on by a driving force $Fe^{i\omega t}$ and that a steady state has been reached. The differential equation then becomes

$$m\ddot{x} + ke^{2bi}x = Fe^{i\omega t} \quad [16]$$

which has the particular solution

$$x = \bar{X}e^{i\omega t} \quad [17]$$

$$\bar{X} = \frac{x_{st}e^{-ia_c}}{\sqrt{1 - 2r^2\cos 2b + r^4}} \quad [18]$$

$$x_{st} = F/k \quad [19]$$

$$r = \omega/\omega_n = \omega\sqrt{m/k} \quad [20]$$

$$\alpha_c = \tan^{-1}\frac{\sin 2b}{\cos 2b - r^2} \quad [21]$$

For small values of b Equations [18] and [21] may be written

$$\bar{X} = \frac{x_{st}e^{-ia_c}}{\sqrt{(1 - r^2)^2 + 4b^2r^2}} \quad [22]$$

$$\alpha_c = \tan^{-1}\frac{2b}{1 - r^2 - 2b^2} \quad [23]$$

and it is interesting to note that the amplitude of forced vibration is identical with that for viscous damping with a viscous-damping factor $b = c/c_{cr}$, but that the phase angle α_c is different from the phase angle $\alpha = \tan^{-1}(2br/1 - r^2)$ obtained for viscous damping. The phase angles α and α_c are plotted in Fig. 4 and it is seen that α_c never becomes zero, nor is it 90 deg at resonance. It does approach 180 deg for large values of r, however, just as does the phase angle α in the case of viscous damping.

A common way of writing so-called structural damping is by multiplying the spring constant k by the complex number $1 + 2bi$, or more commonly $1 + gi$, which is approximately the same as complex damping when b is small. This form of damping, however, has no real physical explanation based upon a known observation such as the hysteresis loop. If it is applied to a free-vibration problem it gives a frequency of damped free vibration which is higher than the natural frequency, and if applied to a forced-vibration problem it gives a peak amplitude at the natural frequency itself, neither of which conforms to observation.

FORCED VIBRATION OF SLENDER ROD

The displacement $u(x,t)$ for the case shown in Fig. 5 with no damping considered is given as

$$u = \frac{LF\sin\dfrac{\beta x}{L}}{AE\beta\cos\beta}e^{i\omega t} \quad [24]$$

where L is the length of the rod, F the amplitude of the harmonic driving force, A the cross-sectional area, E the modulus of elasticity, and

$$\beta = \omega L\sqrt{\rho/E} \quad [25]$$

ρ being the mass density. In the case of complex damping it is merely necessary to replace E by the complex quantity Ee^{2bi} in

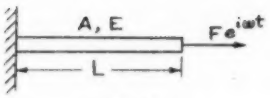

FIG. 5

Equation [24]. The important term in Equation [24] is the cos β-term since this becomes zero when

$$\beta = \frac{2r - 1}{2}\pi$$

for any integer value of r, making $u = \infty$ for the case of no damping. Since damping is only of importance in the vicinity of resonance assume $r = 1$ and

$$\beta = \beta_n^{(1)} = \omega L\sqrt{\rho/E} = \frac{\pi}{2} \quad \ldots\ldots [26]$$

Replacing E by Ee^{2bi} gives

$$\beta' = \omega L\sqrt{\rho/E}\, e^{-bi} = \frac{\pi}{2}e^{-bi} \quad \ldots\ldots [27]$$

The value of $\cos \beta'$ may then be written

$$\cos\beta' = \cos\left(\frac{\pi}{2}\cos b\right)\cosh\left(\frac{\pi}{2}\sin b\right) + i\sin\left(\frac{\pi}{2}\cos b\right)\sinh\left(\frac{\pi}{2}\sin b\right) \quad \ldots\ldots [28]$$

For small values of b this may be approximated by

$$\cos\beta' \approx i\sinh\frac{\pi b}{2} \approx \frac{\pi b i}{2} \quad \ldots\ldots [29]$$

Since replacing β by β' and E by Ee^{2bi} in the other terms of Equation [24] does not appreciably affect the amplitude, this latter may be written approximately as

$$|u| = \frac{4LF\sin\dfrac{\pi x}{2L}}{AE\pi^2 b} \quad \ldots\ldots [30]$$

and at the end of the rod the amplitude becomes

$$|u|_{x=L} = \frac{4LF}{\pi^2 AEb} \quad \ldots\ldots [31]$$

Forced Vibration of Uniform Cantilever Beam

Consider the uniform cantilever beam shown in Fig. 6 acted on by the driving force $Fe^{i\omega t}$ at its free end. If there is no damping the deflection $y(x,t)$ is

$$y = \frac{L^3F}{2EI\beta^3(1 + \cosh\beta\cos\beta)}\left[(\sinh\beta + \sin\beta)\left(\cosh\frac{\beta x}{L} - \cos\frac{\beta x}{L}\right) - (\cosh\beta + \cos\beta)\left(\sinh\frac{\beta x}{L} - \sin\frac{\beta x}{L}\right)\right]e^{i\omega t} \quad \ldots [32]$$

where

$$\beta = \sqrt[4]{\frac{\rho A\omega^2 L^4}{EI}} \quad \ldots\ldots [33]$$

ρ the mass density, A the cross-sectional area, I the moment of inertia of the cross-sectional area, and L the length of the beam. The effect of a small amount of damping on the amplitude of y

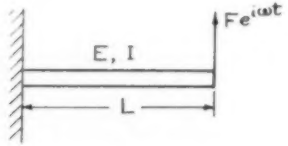

FIG. 6

will be appreciable only in the neighborhood of resonance, or when $1 + \cosh\beta\cos\beta = 0$, and, therefore, only this last term need be modified by the damping. Replacing E by Ee^{2bi} gives

$$\beta' = \sqrt[4]{\frac{\rho A\omega^2 L^4}{EI}}\, e^{-1/2bi} = \beta e^{-1/2bi} \quad \ldots\ldots [34]$$

and

$$\cosh\beta' = \cosh\left(\beta\cos\frac{b}{2}\right)\cos\left(\beta\sin\frac{b}{2}\right) - i\sinh\left(\beta\cos\frac{b}{2}\right)\sin\left(\beta\sin\frac{b}{2}\right) \approx \cosh\beta\cos\frac{b\beta}{2} - i\sinh\beta\sin\frac{b\beta}{2} \quad \ldots\ldots [35]$$

$$\cos\beta' = \cos\left(\beta\cos\frac{b}{2}\right)\cosh\left(\beta\sin\frac{b}{2}\right) + i\sin\left(\beta\cos\frac{b}{2}\right)\sinh\left(\beta\sin\frac{b}{2}\right) \approx \cos\beta\cosh\frac{b\beta}{2} + i\sin\beta\sinh\frac{b\beta}{2} \quad \ldots\ldots [36]$$

The only modified term in Equation [33] then becomes

$$1 + \cosh\beta'\cos\beta' \approx 1 + \left(\cosh\beta\cos\frac{b\beta}{2} - i\sinh\beta\sin\frac{b\beta}{2}\right)\left(\cos\beta\cosh\frac{b\beta}{2} + i\sin\beta\sinh\frac{b\beta}{2}\right) \quad \ldots\ldots [37]$$

Considering only the case of resonance with the first natural mode, for which $\beta = \beta_n^{(1)} = 1.875$, the value of $b\beta/2$ is small for small values of b, and as an approximation, then, Equation [37] may be written

$$1 + \cosh\beta'\cos\beta' \approx 1 + \cosh\beta\cos\beta + \left(\frac{b\beta}{2}\right)^2\sinh\beta\sin\beta + i\frac{b\beta}{2}(\cosh\beta\sin\beta - \sinh\beta\cos\beta) \approx 0.938\, ib$$

$$(\cosh 1.875\sin 1.875 - \sinh 1.875\cos 1.875) = 3.88ib \quad \ldots [38]$$

The absolute value of the displacement at the end of the beam then becomes

$$|y|_{x=L} = \frac{0.161L^3F}{EI\,b} \quad \ldots\ldots [39]$$

Large Deflections of Circular Plates

By M. STIPPES[1] and A. H. HAUSRATH[2]

This paper contains a solution of von Kármán's equations for a uniformly loaded, simply supported circular plate. The method used to obtain the solution is the perturbation procedure. Series expansions for the deflection and stresses in the plate are obtained. The legitimacy of these expansions is demonstrated in the Appendix. Critical values of stress and deflection are presented in graphical form. Furthermore, tables of coefficients for the afore-mentioned series are presented if anyone desires to extend the results which are presented here.

Nomenclature

The following nomenclature is used in the paper:

w = deflection normal to plane of plate
F = Airy's stress function for middle surface of plate
E = Young's modulus
h = thickness of plate
ν = Poisson's ratio
$D = Eh^3/12\,(1-\nu^2)$
q = normal load per unit of area
$\lambda = qa^4/Dh$

$$\nabla^2 = \frac{\partial^2}{\partial \xi^2} + \frac{\partial^2}{\partial \eta^2} \qquad \nabla^4 = \nabla^2\nabla^2$$

$$\tau(u, v) = \frac{\partial^2 u}{\partial \xi^2}\frac{\partial^2 v}{\partial \eta^2} + \frac{\partial^2 u}{\partial \eta^2}\frac{\partial^2 v}{\partial \xi^2} - 2\frac{\partial^2 u}{\partial \xi \partial \eta}\frac{\partial^2 v}{\partial \xi \partial \eta}$$

Introduction

Consider a flat plate occupying a region R and bounded by a curve Γ. The equations for large deflections as given by von Kármán can be written as

$$\left.\begin{aligned} \nabla^4\phi &= -\frac{1}{2}\tau(\psi, \psi) \\ \nabla^4\psi &= \lambda f(\xi, \eta) + 12(1-\nu^2)\tau(\psi, \phi) \end{aligned}\right\} \text{ in } R \ldots . \quad [1]$$

where

$$\xi = \frac{x}{a}, \quad \eta = \frac{y}{a}, \quad F = Eh^3\phi, \quad w = h\psi, \quad \lambda = \frac{qa^4}{Dh} \ldots . \quad [2]$$

If the plate is simply supported, then the appropriate boundary conditions are given by

$$\phi = 0, \quad \frac{\partial\phi}{\partial n} = 0, \quad \psi = 0, \quad M_n(\psi) \equiv \nu\nabla^2\psi + (1-\nu)\left[\frac{\partial^2\psi}{\partial\xi^2}\cos^2\alpha + \frac{\partial^2\psi}{\partial\xi\partial\eta}\sin 2\alpha + \frac{\partial^2\psi}{\partial\eta^2}\sin^2\alpha\right] = 0$$

on Γ . . . [3]

We shall presume, for the moment, that ϕ, ψ depend analytically on λ. (The demonstration of this assumption will be relegated to the Appendix.) With this assumption, we have

$$\phi = \sum_{p=0}^{\infty} \lambda^p \phi_p(\xi, \eta) \qquad \psi = \sum_{q=0}^{\infty} \lambda^q \psi_q(\xi, \eta) \ldots . \quad [4]$$

and Conditions [3] become

$$\left.\begin{aligned} \phi_p = 0, \quad \frac{\partial\phi_p}{\partial n} = 0, \quad \psi_q = 0, \quad M_n(\psi_q) = 0 \end{aligned}\right\} \text{ for all } p,q \text{ on } \Gamma. \quad [5]$$

Substituting [4] in [1] and utilizing the identity theorem for power series, we find that ϕ_0, ψ_0 must satisfy

$$\nabla^4\phi_0 = -\tfrac{1}{2}\tau(\psi_0, \psi_0)$$
$$\nabla^4\psi_0 = 12(1-\nu^2)\tau(\psi_0, \phi_0)$$

From these, we readily obtain

$$\int\int_R \left\{2(\nabla^2\phi_0)^2 + \frac{1}{12(1-\nu^2)}\left[(\nabla^2\psi_0)^2 + (1-\nu)\tau(\psi_0, \psi_0)\right]\right\} d\xi d\eta = 0$$

from which it follows that

$$\phi_0 \equiv 0 \qquad \psi_0 \equiv 0 \text{ in } R$$

This implies that the expansion for ϕ contains only even powers of λ and that of ψ contains only odd powers of λ. Interpreted physically, no load produces no deflection, and a reversal of the load changes the sign of the deflection but leaves the membrane stresses unaltered.

We have then to solve the system of equations

$$\left.\begin{aligned} \nabla^4\psi_1 &= f(\xi, \eta) \\ \nabla^4\phi_{2p} &= -\tfrac{1}{2}\sum_{k=1}^{p}\tau(\psi_{2k-1}, \psi_{2(p-k)+1}) \\ \nabla^4\psi_{2p+1} &= 12(1-\nu^2)\sum_{k=1}^{p}\tau(\phi_{2p}, \psi_{2(p-k)+1}) \end{aligned}\right\} \quad p = 1, 2, \ldots, \infty.$$

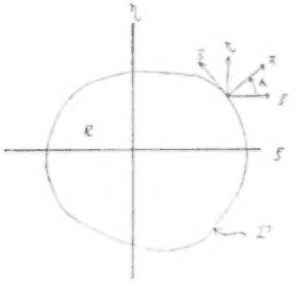

Fig. 1

[1] Associate Professor of Applied Mechanics, Washington University, St. Louis, Mo.

[2] Research Associate, Theoretical and Applied Mechanics, University of Illinois, Urbana, Ill. Jun. ASME.

Presented at the National Conference of the Applied Mechanics Division, State College, Pa., June 19–21, 1952, of The American Society of Mechanical Engineers.

Discussion of this paper should be addressed to the Secretary, ASME, 29 West 39th Street, New York, N. Y., and will be accepted until October 10, 1952, for publication at a later date. Discussion received after the closing date will be returned.

Note. Statements and opinions advanced in papers are to be understood as individual expressions of their authors and not those of the Society. Manuscript received by ASME Applied Mechanics Division, August 13, 1951. Paper No. 52—APM-12.

Circular Plate

We shall consider here only the uniformly loaded circular plate in detail. To this end, we have for a circular plate of radius a

$$\nabla^4 f \equiv L(f) \equiv \frac{1}{\rho}\frac{d}{d\rho}\left\{\rho\frac{d}{d\rho}\left[\frac{1}{\rho}\frac{d}{d\rho}\left(\rho\frac{df}{d\rho}\right)\right]\right\}$$

$$\tau(f, g) \equiv \frac{1}{\rho}\frac{d}{d\rho}\left(\frac{df}{d\rho}\frac{dg}{d\rho}\right)$$

where ρ is the dimensionless radius. The boundary conditions become

$$\phi_p = 0,\ \frac{d\phi_p}{d\rho} = 0,\ \psi_q = 0,\ \frac{d^2\psi_q}{d\rho^2} + \frac{\nu}{\rho}\frac{d\psi_q}{d\rho} = 0 \text{ for } \rho = 1 \quad [6]$$

and ϕ_p, ψ_q are regular for $\rho = 0$.

With these boundary conditions, we find that if [a]

$$\left.\begin{aligned}
L(\phi_{2p}) &= -\frac{1}{2}\sum_{k=1}^{p}\tau(\psi_{2k-1},\ \psi_{2(p-k)+1}) \\
&= \sum_{m=0}^{2(2p-1)} P_{2m}{}^{2p}\rho^{2m} \\
L(\psi_1) &= 1 \\
L(\psi_{2p+1}) &= 12(1-\nu^2)\sum_{k=1}^{p}\tau(\phi_{2k},\ \psi_{2(p-k)+1}) \\
&= \sum_{m=0}^{4p} Q_{2m}{}^{2p+1}\rho^{2m} \\
\phi &= \sum_{p=1}^{\infty}\lambda^{2p}\phi_{2p}(\rho),\quad \phi_{2p}(\rho) = \sum_{m=0}^{8p} C_{2m}{}^{2p}\rho^{2m} \\
\psi &= \sum_{q=0}^{\infty}\lambda^{2q+1}\psi_{2q+1}(\rho) \\
\psi_{2q+1}(\rho) &= \sum_{m=0}^{4(2q+1)} C_{2m}{}^{2q+1}\rho^{2m} \\
& p,q = 1,2,\ldots
\end{aligned}\right\} \quad [7]$$

then

$$\left.\begin{aligned}
\psi_1 &= \frac{1}{64}\left[\frac{5+\nu}{1+\nu} - \frac{2(3+\nu)}{1+\nu}\rho^2 + \rho^4\right] \\
\phi_{2p} &= \sum_{m=0}^{2(2p-1)}\left\{\frac{(m+1) - (m+2)\rho^2 + \rho^{2m+4}}{16\,(m+1)^2(m+2)^2}\right\} P_{2m}{}^{2p} \\
\psi_{2q+1} &= \sum_{m=0}^{4p}\left\{\frac{(m+1)\,(2m+5+\nu)}{16(1+\nu)\,(m+1)^2(m+2)^2}\right. \\
&+ \left.\frac{-(m+2)\,(2m+3+\nu)\,\rho^2 + (1+\nu)\rho^{2m+4}}{16(1+\nu)\,(m+1)^2(m+2)^2}\right\} Q_{2m}{}^{2p+1}
\end{aligned}\right\} \quad [8]$$

The dimensionless maximum deflection is given by

$$\psi_{\max} = \frac{1}{64}\frac{5+\nu}{1+\nu}\lambda + \sum_{p=1}^{\infty}\lambda^{2p+1}\sum_{m=0}^{4p}\frac{(m+2)\,(2m+3+\nu) - (1+\nu)}{16(1+\nu)\,(m+1)^2(m+2)^2} Q_{2m}{}^{2p+1} \quad [9]$$

The radial bending stress at the center is

$$\frac{\sigma_r{}^b a^2}{Eh^2} = \frac{1}{2(1-\nu^2)}\left\{\frac{3+\nu}{16}\lambda + \sum_{p=1}^{\infty}\lambda^{2p+1}\sum_{m=0}^{4p}\frac{(2m+3+\nu)}{8(m+1)^2(m+2)} Q_{2m}{}^{2p+1}\right\} \quad [10]$$

and the radial membrane stress at the center is

$$\frac{\sigma_r{}^m a^2}{Eh^2} = -\sum_{p=1}^{\infty}\lambda^{2p}\sum_{m=0}^{2(2p-1)}\frac{P_{2m}{}^{2p}}{8(m+1)^2(m+2)} \quad [11]$$

The computations for the deflection were carried out to the seventh power of λ and those for the stress function to the sixth power of λ.

The series, Equation [9], as far as the calculations have been carried, is an alternating series. Furthermore, at

$$\lambda = \frac{32(1+\nu)}{5+\nu}$$

the terms of this series, to the point of truncation, are strictly monotonic decreasing. Since we were not able to demonstrate the validity of either of these statements for the entire series, we offer the following bounds on the absolute error involved in truncating the series after the linear term with reservations

$$\left|\lambda^3\sum_{m=0}^{4}\frac{(m+2)\,(2m+3+\nu) - (1+\nu)}{16\,(1+\nu)\,(m+1)^2\,(m+2)^2} Q_{2m}{}^3 - \lambda^5\sum_{m=0}^{8}\frac{(m+2)\,(2m+3+\nu) - (1+\nu)}{16(1+\nu)\,(m+1)^2\,(m+2)^2} Q_{2m}{}^5\right| <$$

$$|\text{Absolute error}| < \left|\lambda^3\sum_{m=0}^{4}\frac{(m+2)\,(2m+3+\nu) - (1+\nu)}{16(1+\nu)\,(m+1)^2(m+2)^2} Q_{2m}{}^3\right|$$

(We emphasize that this result is subject to the assumption

[a] Where $P_{2m}{}^{2p}$, $Q_{2m}{}^{2p+1}$ are coefficients of the powers of ρ and not Legendre polynomials.

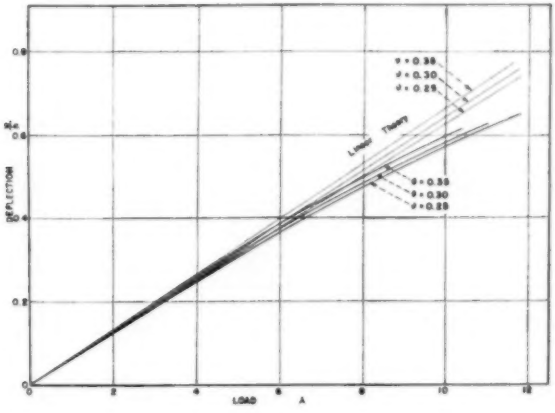

FIG. 2

stated previously.) If these results are valid, they give an indication of the range of utilizability of the linear theory which is usually quoted in references as deflections less than one half the thickness of the plate.

Figs. 2 and 3 indicate the Relations [9], [10], and [11]. Tables 1 and 2 give the appropriate values of the various constants used in the computations if anyone desires to carry the calculations beyond the point presented here.

Appendix

To show that the Expansions [4] are legitimate, at least for small values of λ, it is convenient to convert the system [1], [3] into a nonlinear integral equation for the derivative of ψ. Consider then, the Green's functions for the following systems

$$L(\phi) = 0;\ \phi = 0,\ \frac{d\phi}{d\rho} = 0\ \ \rho = 1$$

$$L(\psi) = 0;\ \psi = 0,\ \frac{d^2\psi}{d\rho^2} + \frac{\nu}{\rho}\frac{d\psi}{d\rho} = 0\ \ \rho = 1$$

and ϕ, ψ are regular at $\rho = 0$. These Green's functions will be denoted by $K_1^*(\rho, \xi)$, $K_2^*(\rho, \xi)$, respectively. They have the following forms

$$K_1^*(\rho, \xi) = \frac{\xi(1 - \xi^2)(1 + \rho^2)}{8} + \frac{\xi(\rho^2 + \xi^2)\log \xi}{4} \qquad \rho < \xi$$

$$K_1^*(\rho, \xi) = \frac{\xi(1 - \rho^2)(1 + \xi^2)}{8} + \frac{\xi(\xi^2 + \rho^2)\log \rho}{4} \qquad \rho > \xi$$

$$K_2^*(\rho, \xi) = \frac{\xi(1 - \xi^2)[(3 + \nu) - (1 - \nu)\rho^2]}{8(1 + \nu)} + \frac{\xi(\rho^2 + \xi^2)\log \xi}{4} \qquad \rho < \xi$$

$$K_2^*(\rho, \xi) = \frac{\xi(1 - \rho^2)[(3 + \nu) - (1 - \nu)\xi^2]}{8(1 + \nu)} + \frac{\xi(\xi^2 + \rho^2)\log \rho}{4} \qquad \rho > \xi$$

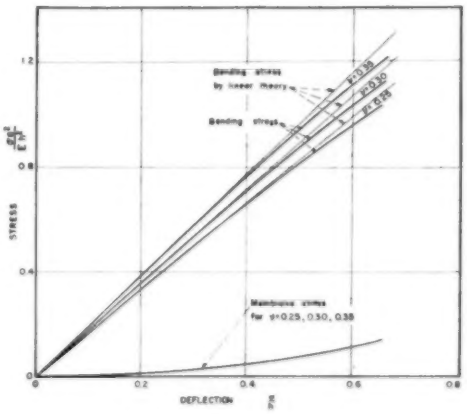

FIG. 3

It is convenient to introduce the quantities $K_1(\rho, \xi)$; $K_2(\rho, \xi)$ defined by

$$K_1(\rho, \xi) = \frac{2K_1^*(\rho, \xi)}{\xi} \qquad K_2(\rho, \xi) = \frac{2K_2^*(\rho, \xi)}{\xi}$$

Utilizing these quantities, we obtain the following equation for

$$\Gamma(\rho) = \frac{d\psi}{d\rho}$$

$$\Gamma(\rho) = \lambda \int_0^1 \frac{\partial K_2^*(\rho, \xi)}{\partial \rho} f(\xi)\, d\xi$$

$$- \frac{3(1 - \nu^2)}{2} \int_0^1 \int_0^1 \frac{\partial^2 K_2(\rho, \xi)}{\partial \rho \partial \xi} \frac{\partial^2 K_1(\xi, \eta)}{\partial \xi \partial \eta} \Gamma^2(\eta)\Gamma(\xi)\, d\eta\, d\xi$$

TABLE 1 CONSTANTS USED IN COMPUTATIONS

	ν	p^2_{2n}	p^4_{2n}	p^6_{2n}	q^3_{2n}	q^5_{2n}	q^7_{2n}
		$\times 10^{-2}$	$\times 10^{-5}$	$\times 10^{-7}$	$\times 10^{-5}$	$\times 10^{-5}$	$\times 10^{-8}$
	0.25	-2.64062	8.79922	-4.15079	-4.63577	2.08044	-11.03887
$n = 0$	0.30	-2.51710	7.84294	-3.18192	-4.16050	1.67578	-7.94581
	0.35	-2.40857	6.48469	-2.43252	-3.72403	1.34273	-5.67448
		$\times 10^{-2}$	$\times 10^{-4}$	$\times 10^{-6}$	$\times 10^{-2}$	$\times 10^{-5}$	$\times 10^{-7}$
	0.25	4.06250	-2.56015	1.42186	1.56348	-8.69189	5.00715
$n = 1$	0.30	3.96635	-2.24449	1.11810	1.41802	-7.09351	3.66008
	0.35	3.87732	-1.96496	0.875680	1.28221	-5.78568	2.65290
		$\times 10^{-2}$	$\times 10^{-4}$	$\times 10^{-6}$	$\times 10^{-2}$	$\times 10^{-5}$	$\times 10^{-7}$
	0.25	-1.17188	2.67456	-1.88674	-1.16043	10.64014	-7.19901
$n = 2$	0.30	-1.17188	2.39120	-1.50967	-1.07570	8.84673	-5.37048
	0.35	-1.17188	2.11570	-1.20218	-0.989396	7.30574	-3.98872
			$\times 10^{-4}$	$\times 10^{-6}$	$\times 10^{-3}$	$\times 10^{-5}$	$\times 10^{-7}$
	0.25		-1.55810	1.59773	2.97547	-6.93962	5.94885
$n = 3$	0.30		-1.21174	1.13751	2.81983	-5.86666	4.61789
	0.35		-1.09406	0.920490	2.65808	-4.92222	3.39566
			$\times 10^{-5}$	$\times 10^{-7}$	$\times 10^{-4}$	$\times 10^{-5}$	$\times 10^{-7}$
	0.25		3.27378	-7.67462	-2.86102	2.76783	-3.51402
$n = 4$	0.30		3.02911	-6.26685	-2.77710	2.37252	-2.55285
	0.35		2.79126	-5.15101	-2.67791	2.02411	-1.95732
			$\times 10^{-6}$	$\times 10^{-7}$		$\times 10^{-5}$	$\times 10^{-7}$
	0.25		-3.95179	2.37012		-1.46872	1.34111
$n = 5$	0.30		-3.74508	1.99648		-1.29145	1.05469
	0.35		-3.53026	1.66944		-1.12476	0.819567
			$\times 10^{-7}$	$\times 10^{-8}$		$\times 10^{-7}$	$\times 10^{-8}$
	0.25		2.08616	-5.00728		9.48788	-4.09890
$n = 6$	0.30		2.02497	-4.30113		8.52127	-3.28243
	0.35		1.96264	-3.66385		7.57173	-2.59498
				$\times 10^{-8}$		$\times 10^{-8}$	$\times 10^{-9}$
	0.25			1.16904		-7.62105	7.43502
$n = 7$	0.30			1.02709		-7.01055	6.06172
	0.35			0.893809		-6.37240	4.87568
				$\times 10^{-10}$		$\times 10^{-9}$	$\times 10^{-9}$
	0.25			-7.56192		2.80644	-1.73739
$n = 8$	0.30			-6.79152		2.54421	-1.44778
	0.35			-6.03472		2.45870	-1.18858
				$\times 10^{-11}$			$\times 10^{-10}$
	0.25			4.42499			1.83540
$n = 9$	0.30			4.07082			1.56419
	0.35			3.69999			1.31211
				$\times 10^{-12}$			$\times 10^{-11}$
	0.25			-1.22078			-1.14922
$n = 10$	0.30			-1.15021			-1.00186
	0.35			-1.06982			-0.858428
							$\times 10^{-13}$
	0.25						4.90414
$n = 11$	0.30						4.37896
	0.35						3.83819
							$\times 10^{-14}$
	0.25						-1.26162
$n = 12$	0.30						-1.15382
	0.35						-1.03455

TABLE 2 CONSTANTS USED IN COMPUTATIONS

	ν	c^1_{2n}	c^2_{2n}	c^3_{2n}	c^4_{2n}	c^5_{2n}	c^6_{2n}	c^7_{2n}
		$\times 10^{-2}$	$\times 10^{-4}$	$\times 10^{-5}$	$\times 10^{-7}$	$\times 10^{-7}$	$\times 10^{-9}$	$\times 10^{-9}$
	0.25	6.56250	-2.86797	-6.84903	7.61090	3.14916	-3.38023	-1.69241
n = 0	0.30	6.37020	-2.70836	-7.42301	6.43316	2.45248	-2.52442	-1.17029
	0.35	6.19210	-2.56469	-6.43651	5.43891	1.87170	-1.89759	-0.80828
		$\times 10^{-2}$	$\times 10^{-4}$	$\times 10^{-4}$	$\times 10^{-6}$	$\times 10^{-7}$	$\times 10^{-9}$	
	0.25	-8.12500	6.33952	1.36373	-1.78880	-5.25810	8.01290	
n = 1	0.30	-7.93270	6.00360	1.18858	-1.61861	-4.12348	6.06971	
	0.35	-7.75460	5.70080	1.04206	-1.28940	-3.22062	4.58624	
		$\times 10^{-2}$	$\times 10^{-4}$	$\times 10^{-5}$	$\times 10^{-6}$	$\times 10^{-7}$	$\times 10^{-9}$	
	0.25	1.56250	-4.12598	-7.24340	1.37488	3.25069	-6.48561	
n = 2	0.30	1.56250	-3.93298	-6.50078	1.17868	2.61841	-4.97174	
	0.35	1.56250	-3.75839	-5.81880	1.01009	2.09801	-3.80060	
			$\times 10^{-5}$	$\times 10^{-6}$	$\times 10^{-7}$	$\times 10^{-7}$	$\times 10^{-9}$	
	0.25		7.05295	2.714316	-4.44470	-1.50898	2.46851	
n = 3	0.30		6.88502	2.461836	-3.89669	-1.23151	1.94115	
	0.35		6.73145	2.226062	-3.41137	-0.999250	1.52028	
			$\times 10^{-6}$	$\times 10^{-6}$	$\times 10^{-7}$	$\times 10^{-8}$	$\times 10^{-10}$	
	0.25		-5.08626	-5.03659	1.16076	4.61812	-8.18899	
n = 4	0.30		-5.08626	-4.66017	1.03351	3.83975	-6.55240	
	0.35		-5.08626	-4.29426	0.918273	3.17089	-5.21768	
				$\times 10^{-7}$	$\times 10^{-8}$	$\times 10^{-9}$	$\times 10^{-10}$	
	0.25			4.64917	-2.09078	-10.84316	2.18396	
n = 5	0.30			4.40598	-1.89334	-9.16666	1.77736	
	0.35			4.15324	-1.70947	-7.69096	1.45827	
				$\times 10^{-8}$	$\times 10^{-9}$	$\times 10^{-9}$	$\times 10^{-11}$	
	0.25			-1.98682	2.27546	1.91495	-5.26016	
n = 6	0.30			-1.92854	2.10356	1.64758	-4.55177	
	0.35			-1.85966	1.93838	1.40563	-3.57709	
					$\times 10^{-10}$	$\times 10^{-10}$	$\times 10^{-12}$	
	0.25				-1.40015	-5.20381	8.39753	
n = 7	0.30				-1.32691	-4.57573	7.07371	
	0.35				-1.25080	-3.98512	5.91498	
					$\times 10^{-12}$	$\times 10^{-11}$	$\times 10^{-13}$	
	0.25				4.15769	1.89092	-9.97943	
n = 8	0.30				4.03573	1.69828	-8.57209	
	0.35				3.89159	1.50904	-7.30196	
						$\times 10^{-13}$	$\times 10^{-13}$	
	0.25					-9.18819	1.40944	
n = 9	0.30					-8.45215	1.23829	
	0.35					-7.68278	1.07760	
						$\times 10^{-14}$	$\times 10^{-15}$	
	0.25					2.16546	-5.83481	
n = 10	0.30					2.04022	-5.24037	
	0.35					1.89715	-4.65642	
							$\times 10^{-16}$	
	0.25						2.28564	
n = 11	0.30						2.10254	
	0.35						1.91116	
							$\times 10^{-18}$	
	0.25						-4.37894	
n = 12	0.30						-4.12581	
	0.35						-3.83636	

If

$$\int_0^1 \frac{\partial K_2^*(\rho, \xi)}{\partial \rho} f(\xi) d\xi = F(\rho);$$

$$-\frac{3(1-\nu^2)}{2} \frac{\partial^2 K_2(\rho, \xi)}{\partial \rho \partial \xi} \frac{\partial^2 K_1(\xi, \eta)}{\partial \xi \partial \eta} = M(\rho, \xi, \eta)$$

it is easy to obtain the following

$$\text{Max} \mid F(\rho) \mid < \frac{P}{9} \qquad \text{Max} \mid M(\rho, \xi, \eta) \mid < 3$$

where $P = \text{Max} \mid f(\xi) \mid$ for $0 \leqslant \rho \leqslant 1, 0 \leqslant \xi \leqslant 1, 0 \leqslant \eta \leqslant 1$. (These are not the best possible upper bounds but have been chosen for convenience.) The method of successive approximation gives us

$$\Gamma_1(\rho) = \lambda F(\rho)$$

$$\Gamma_{2k+1}(\rho) = \lambda F(\rho) + \int_0^1 \int_0^1 M(\rho, \xi, \eta) \Gamma_{2k-1}^2(\eta) \Gamma_{2k-1}(\xi) d\eta d\xi$$

If we let ϵ be the smallest positive root of

$$\epsilon = Q + 3\epsilon^3$$

where $Q = \lambda P/9$ (and the existence of a positive root is guaranteed if $0 \leqslant Q \leqslant \frac{2}{9}$), then

$$\Gamma_1(\rho) = \lambda F(\rho) < \epsilon$$
$$\Gamma_3(\rho) < Q + 3\epsilon^3 = \epsilon$$
$$\Gamma_{2k+1}(\rho) < Q + 3\epsilon^3 = \epsilon$$

so that each $\Gamma_{2k+1}(\rho)$ is analytic. Now let

$$\Gamma(\rho) = \Gamma_1(\rho) + [\Gamma_3(\rho) - \Gamma_1(\rho)] + \ldots + [\Gamma_{2k+1}(\rho) - \Gamma_{2k-1}(\rho)] + \ldots\ldots [12]$$

From the previous assumptions it follows that

$$\mid \Gamma_{2k+1}(\rho) - \Gamma_{2k-1}(\rho) \mid \leqslant 9\epsilon^2 \text{ Max} \mid \Gamma_{2k-1} - \Gamma_{2k-3} \mid$$

Hence the Series [12] is absolutely and uniformly convergent, provided $\epsilon \leqslant \epsilon_0 < 1/2$. Since, now, each of the successive approximations is an analytic function of λ, it follows that the limit function $\Gamma(\rho)$ is expandable in a power series in λ, so that a representation of the form

$$\Gamma(\rho) = \sum_{q=0}^{\infty} \lambda^{2q+1} \Psi_{2q+1}(\rho)$$

is legitimate.

Moreover

$$\psi(\rho) = \lambda \int_0^1 K_2^*(\rho, \xi) f(\xi) d\xi + \lim_{k \to \infty} \int_0^1 \int_0^1 M(\rho, \xi, \eta) \Gamma_{2k+1}^2(\rho) \Gamma_{2k+1}(\xi) d\eta d\xi$$

so that

$$\psi(\rho) = \sum_{q=0}^{\infty} \lambda^{2q+1} \psi_{2q+1}(\rho)$$

is permissible along with the representation for the second derivatives of ψ, ϕ.

Conclusions

The method of perturbations is a valid procedure for the solution of the problem considered here provided that the load parameter is sufficiently small. In view of the fact that the bound obtained for λ is not the best possible one, we have proceeded in the engineering spirit and used the series to predict results beyond the values of λ as given in the Appendix. As compared to the method for solving a similar problem presented by Stewart Way, the method has the disadvantage of a solution appearing as a fairly slowly convergent series at the points of interest in the plate. On the other hand, it does show the direct dependence of significant quantities on the load parameter. The method also has the advantage that it can be used directly to compute deflections in the sense of von Kármán for concentrated loads which, to the authors' knowledge, have not been treated theoretically in the literature.

References

1 "Ordinary Differential Equations," by E. L. Ince, Dover Publications, New York, N. Y., 1944.

2 "Vorlesungen uber einige Klassen Nichtlinearer Integralgleichungen und Integro-Differentialgleichungen," by L. Lichtenstein, Julius Springer, Berlin, Germany, 1931.

3 "Theory of Plates and Shells," by S. Timoshenko, McGraw-Hill Book Company, Inc., New York, N. Y., 1940.

Bending of Elastoplastic Circular Plates With Large Deflection

By P. M. NAGHDI,[1] ANN ARBOR, MICH.

A general theory for the elastoplastic bending of thin circular plates with polar symmetrical loading is developed, and a numerical integration method is given for the complete solution of problems within the scope of the general theory. In the development of the theory, stress-strain relations of the deformation type (theory of plastic deformation) are employed. As special examples, simply supported circular plates with a central concentrated loading are considered. Using a stress-strain curve for 24S-T aluminum which is determined experimentally, numerical solutions for bending moments, membrane forces, and deflections are obtained for two cases. In one case, the plate experiences large elastic deformation and in the second case, the plate undergoes large elastoplastic deformation. Several plate specimens, made of the same sheet of 24S-T aluminum for which the foregoing stress-strain curve was determined, are tested and a comparison is made between the theoretically determined and the experimentally obtained values of deflection.

Introduction

THE behavior of large deformation of thin plates in the elastic range has been considered by Way (1),[2] Levy (2), Jen (3), Perry (4), Chien (5, 6), and others.

The problem of plastic bending of thin plates, until recently, has received very little attention. However, several contributions have been made by Russian investigators, in particular Ilyushin (7) and Sokolovsky (8, 9), who considered the small deformation of plastic plates. In addition, Trifan (10) who considered the small plastic deformation of circular plates based on two different theories of plasticity, namely, the theory of plastic flow and the theory of plastic deformation, should also be mentioned.

It is the purpose of this paper to investigate the problem of large deformation of thin elastoplastic circular plates due to polar symmetrical transverse loading. In the development of the theory, the following assumptions are made:

1 The material is homogeneous.

2 The material is isotropic.

3 Both the bending strains and the membrane strains are small in comparison with unity.

In this work, Latin indexes will have the range 1, 2, 3, and we shall use Greek indexes for the range 1, 2; also, the summation convention will be employed whenever needed, so that a repeated index implies summation over all the values the index may take.

General Theory of Elastoplastic Bending of Thin Circular Plates With Polar Symmetrical Loading

Let us consider a thin circular plate in the strained state as shown in Fig. 1, and let us choose co-ordinate axes $x_i (i = 1, 2, 3)$

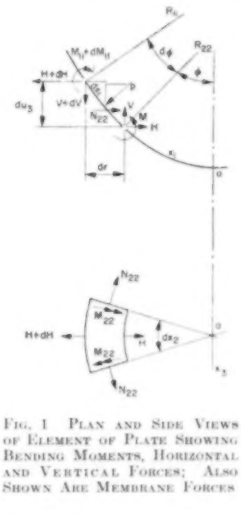

FIG. 1 PLAN AND SIDE VIEWS OF ELEMENT OF PLATE SHOWING BENDING MOMENTS, HORIZONTAL AND VERTICAL FORCES; ALSO SHOWN ARE MEMBRANE FORCES

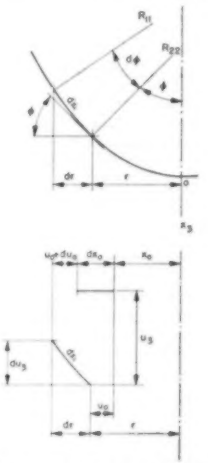

FIG. 2 SIDE VIEW OF ELEMENT OF PLATE IN UNDEFORMED AND IN DEFORMED STATE

with the origin in the middle plane of the plate such that x_1 is along the deflected surface, x_2 is the polar angle, and x_3 is along the axis of symmetry of the strained plate measured downward. It should be noted that this co-ordinate system is nonorthogonal and may be regarded as a set of imbedded co-ordinates in the deformed plate. Since for a thin plate the normal component of the stress tensor along the x_3 axis is either negligible or vanishes, it follows that $\sigma_{33} = 0$ everywhere.

(*a*) *Kinematics of Middle Surface.* It is well known that when the deflection u_3 is large in comparison with the thickness of the plate, its middle surface is stretched under the action of membrane forces and the radial distance x_0 of the plate in the unstrained state will suffer a displacement u_0, as indicated in Fig. 2, so that the radial distance r in the strained state is given by

$$r = x_0 + u_0 \qquad [a]$$

Further, in view of polar symmetry, u_2 vanishes everywhere in the plate.

It should be recalled that u_1 is the displacement along the principal direction x_1 and that, in general, $u_1 \neq u_3$. In fact, it is

---

[1] Assistant Professor of Engineering Mechanics, University of Michigan. Jun. ASME.

[2] Numbers in parentheses refer to the Bibliography at the end of the paper.

Presented at the National Conference of the Applied Mechanics Division, State College, Pa., June 19–21, 1952, of THE AMERICAN SOCIETY OF MECHANICAL ENGINEERS.

Discussion of this paper should be addressed to the Secretary, ASME, 29 West 39th Street, New York, N. Y., and will be accepted until October 10, 1952, for publication at a later date. Discussion received after the closing date will be returned.

NOTE: Statements and opinions advanced in papers are to be understood as individual expressions of their authors and not those of the Society. Manuscript received by ASME Applied Mechanics Division, August 20, 1951. Paper No. 52—APM-16.

only for small deformation (linear) theory that one may assume $u_1 = u_0$.

The following relations are self-evident from a geometrical consideration of the middle surface

$$\cos \phi = dr/dx_1 \quad [b]$$

$$\sin \phi = du_3/dx_1 \quad [c]$$

$$\tan \phi = -du_3/dr \quad [1]^3$$

$$\frac{1}{R_{11}} = d\phi/dx_1 \quad [d]$$

$$\frac{1}{R_{22}} = \frac{\sin \phi}{r} \quad [e]$$

where $1/R_{11}$ and $1/R_{22}$ are the curvatures.

Equations [d] and [e] are exact and may be obtained from the well-known expressions for the curvatures, namely

$$\frac{1}{R_{11}} = \frac{\partial^2 u_3}{\partial r^2} \Big/ \left[1 + \left(\frac{\partial u_3}{\partial r}\right)^2\right]^{3/2}; \quad \frac{1}{R_{22}} = \frac{1}{r}\frac{du_3}{dx_1}$$

With the aid of Equation [d] the differential arc length dx_1 may be written as

$$dx_1 = [(dr)^2 + (du_3)^2]^{1/2} = \sec \phi \, dr \quad [f]$$

Since both membrane and bending-strain tensors are infinitesimal, the total strain tensor η_{ij} is given by

$$\eta_{ij} = e_{ij} + \epsilon_{ij} \quad [g]$$

The membrane strains e_{11} and e_{22} along the principal directions x_1 and x_2 in the conventional manner, Fig. 2, are given by

$$e_{11} = \frac{dx_1 - dx_0}{dx_0} \quad [h]$$

$$e_{22} = \frac{u_0}{x_0} \quad [2]$$

Denoting by e_{00} the membrane strain along the radius x_0, we have

$$e_{00} = \frac{dr - dx_0}{dx_0} = \frac{dr}{dx_0} - 1 \quad [k]$$

Now with Equations [b] and [h] du_0 may be written as

$$du_0 = \frac{[(1 + e_{11}) \cos \phi - 1]}{(1 + e_{11}) \cos \phi} dr \quad [3]$$

In the theory of elastic plates and elastoplastic beams, it is a fundamental hypothesis that plane cross sections normal to the middle plane remain plane and normal to the middle surface during bending. Assuming that this hypothesis also remains valid for elastoplastic plates, we have for the bending-strain tensor

$$\epsilon_{\alpha\beta} = x_3 \frac{1}{R_{\alpha\beta}} \quad [l]$$

$1/R_{\alpha\beta}$ being the curvature tensor.

It is clear that since $\epsilon_{\alpha\beta}$ are principal strains, $\epsilon_{12} = 0$. Moreover, since $\sigma_{33} = 0$, both ϵ_{33} and e_{33} are determined directly from the stress-strain relations.

[3] Only the equations which are directly used in the solution of a specific problem are numbered. All other equations are lettered.

(*b*) *Equations of Equilibrium.* The equations of equilibrium for the element shown in Fig. 1 in terms of bending moments and forces normal and perpendicular to the radial sections of the deflected surface of the plate are

$$\left.\begin{aligned} &d(rV) + (rp) \cos \phi \, dx_1 = 0 \\ &d(rH) - N_{22} dx_1 + (rp) \sin \phi \, dx_1 = 0 \\ &d(rM_{11}) - M_{22} dr - (rV) dr - (rH) \sin \phi \, dx_1 = 0 \end{aligned}\right\} \quad [m]$$

Or, by Equations [b] and [c], they become

$$d(rV) + pr \, dr = 0 \quad [4]$$

$$d(rH) - N_{22} \sec \phi \, dr + p \tan \phi \, r dr = 0 \quad [5]$$

$$d(rM_{11}) - M_{22} dr + rH \tan \phi \, dr = 0 \quad [6]$$

where

$$V = Q_1 \cos \phi - N_{11} \sin \phi$$
$$H = Q_1 \sin \phi + N_{11} \cos \phi$$

from which

$$N_{11} = H \cos \phi - V \sin \phi \quad [7]$$

It should be noted that incorporation of Equation [7] into Equations [m], with an adjustment of notation, yields those given by Timoshenko (11) for a shell having the form of a surface of revolution.

(*c*) *Stress-Strain Relations.* Two alternative theories of plasticity, namely, a theory of plastic flow and a theory of plastic deformation, are in current use for elastoplastic materials. As applied to strain-hardening materials, the theory of plastic flow, advanced by Prager (12, 13, 14) and others, is based upon the assumption that the rate of change of strain is uniquely determined by the existing stress and its time rate of change. The theory of plastic deformation, on the other hand, developed by Hencky (15) for perfectly plastic materials, modified by Nadai (16) and von Mises (17), and recently in a more general form, suggested and used by Gleyzal (18, 19), is based upon the assumption that the rate of change of strain in the plastic state, as in the elastic state, is uniquely determined by the state of stress.

Neither of the theories is exact, but both predict the same results when the stress history does not involve rotation of the principal directions of stress and strain. This may be evidenced from the work of Trifan (10, 20) who, using both theories, obtained identical results for the small deformation theory of thin circular plates.

Assuming that the material is isotropic so that the principal directions of stress and strain coincide, the total strain tensor η_{ij} is given by

$$\eta_{ij} = -\left(\frac{\nu}{E} + \frac{1/2}{\psi}\right)\sigma_{KK}\delta_{ij} + \left(\frac{1+\nu}{E} + \frac{3/2}{\psi}\right)\sigma_{ij} \quad [n]$$

where δ_{ij} is the Kronecker delta defined by

$$\delta_{ij} = \begin{cases} 1 \text{ if } i = j \\ 0 \text{ if } i \neq j \end{cases}$$

and

$$\psi = \frac{3\tau(\gamma)}{\gamma^p}$$

γ^p being the plastic octahedral shear strain.

It is not difficult to show from Relation [n] that the plastic volume change vanishes, i.e., $\eta^p{}_{ii} = 0$, and that further

$$\frac{\eta_{11} - \eta_{22}}{\sigma_{11} - \sigma_{22}} = \frac{\eta_{22} - \eta_{33}}{\sigma_{22} - \sigma_{33}} = \frac{\eta_{33} - \eta_{11}}{\sigma_{33} - \sigma_{11}}$$

which is usually associated with the assumption that at any one point the principal axes of stress and strain coincide. If we let

$$\frac{E}{\psi} = \lambda(\gamma) \quad \ldots\ldots [p]$$

the three principal stress-strain relations of Equation [n] become

$$\eta_{ij} = -\frac{(\nu + \lambda/2)}{E}\sigma_{kk}\delta_{ij} + \frac{\left(1 + \nu + \frac{3\lambda}{2}\right)}{E}\sigma_{ij} \quad \ldots [q]$$

Now solving for the principal stresses and recalling that $\sigma_{33} = 0$, we obtain

$$\left.\begin{aligned}\sigma_{11} &= \frac{E(1+\lambda)}{[(1+\lambda)^2 - (\nu + \lambda/2)^2]}\left(\eta_{11} + \frac{\nu + \lambda/2}{1+\lambda}\eta_{22}\right)\\ \sigma_{22} &= \frac{E(1+\lambda)}{[(1+\lambda)^2 - (\nu + \lambda/2)^2]}\left(\eta_{22} + \frac{\nu + \lambda/2}{1+\lambda}\eta_{11}\right)\end{aligned}\right\} \quad \ldots [r]$$

where $\eta_{\alpha\beta} = \epsilon_{\alpha\beta} + \epsilon_{\alpha\beta}$ and the third Equation [n] yields

$$\eta_{33} = -\mu(\eta_{11} + \eta_{22}) \quad \ldots\ldots [s]$$

where

$$\mu = \frac{(\nu + \lambda/2)(1 + \nu + 3\lambda/2)}{[(1+\lambda)^2 - (\nu + \lambda/2)^2]} \quad \ldots\ldots [t]$$

By substitution of Equations [r] into the usual relation of bending moments in terms of the stress tensor, namely

$$M_{\alpha\beta} = \int_{-h/2}^{+h/2} \sigma_{\alpha\beta}\, x_3\, dx_3$$

we obtain the following moment-curvature relations

$$\left.\begin{aligned}M_{11} &= D_1\frac{1}{R_{11}} + D_2\frac{1}{R_{22}}\\ M_{22} &= D_1\frac{1}{R_{22}} + D_2\frac{1}{R_{11}}\end{aligned}\right\} \quad \ldots\ldots [u]$$

Or, with the aid of Equations [d] and [e], they may be written as

$$d(\sin\phi) = \frac{D_1 M_{11} - D_2 M_{22}}{D_1^2 - D_2^2}\,dr \quad \ldots\ldots [8]$$

$$M_{22} = \frac{D_2}{D_1}M_{11} + \left(D_1 - D_2\frac{D_2}{D_1}\right)\left(\frac{\sin\phi}{r}\right) \quad \ldots\ldots [9]$$

where

$$\left.\begin{aligned}D_1 &= \int_{-h/2}^{+h/2} \frac{E(1+\lambda)}{[(1+\lambda)^2 - (\nu+\lambda/2)^2]}\, x_3^2\, dx_3\\ D_2 &= \int_{-h/2}^{+h/2} \frac{E(\nu+\lambda/2)}{[(1+\lambda)^2 - (\nu+\lambda/2)^2]}\, x_3^2\, dx_3\end{aligned}\right\} \quad \ldots [10]$$

D_1 and D_2 may be termed the "equivalent rigidities" of the plate. Since $\lambda = \lambda(\gamma)$, it then follows that D_1 and D_2 are functions of the octahedral shear strain γ as well as the thickness of the plate.

Similarly, substitution of Equations [r] into the usual relation of membrane forces in terms of the stress tensor, namely

$$N_{\alpha\beta} = \int_{-h/2}^{+h/2} \sigma_{\alpha\beta}\, dx_3$$

yields the following membrane force-membrane strain relations

$$\left.\begin{aligned}N_{11} &= E_1\epsilon_{11} + E_2\epsilon_{22}\\ N_{22} &= E_1\epsilon_{22} + E_2\epsilon_{11}\end{aligned}\right\} \quad \ldots\ldots [11]$$

or

$$\left.\begin{aligned}\epsilon_{11} &= \frac{E_1 N_{11} - E_2 N_{22}}{E_1^2 - E_2^2}\\ \epsilon_{22} &= \frac{E_1 N_{22} - E_2 N_{11}}{E_1^2 - E_2^2}\end{aligned}\right\} \quad \ldots\ldots [12]$$

where

$$\left.\begin{aligned}E_1 &= \int_{-h/2}^{+h/2} \frac{E(1+\lambda)}{[(1-\lambda)^2 - (\nu+\lambda/2)^2]}\, dx_3\\ E_2 &= \int_{-h/2}^{+h/2} \frac{E(\nu+\lambda/2)}{[(1+\lambda)^2 - (\nu+\lambda/2)^2]}\, dx_3\end{aligned}\right\} \quad \ldots [13]$$

E_1 and E_2, similar to D_1 and D_2, are also functions of the octahedral shear strain and the thickness of the plate. We may refer to them as the "equivalent moduli."

The total octahedral shear strain γ may be expressed as a function of η_{11} and η_{22} as follows

$$\gamma = \frac{\sqrt{2}}{3}[(1 + \mu + \mu^2)(\eta_{11} + \eta_{22})^2 - 3\eta_{11}\eta_{22}]^{1/2} \quad \ldots [14]$$

where μ is defined by Equation [t].

Since, within the elastic range the plastic octahedral shear strain γ^p must vanish, then $\psi = \frac{3\tau}{\gamma^p} \to \infty$ and by Equation [p], λ vanishes. Thus we note that in the limit Equations [8], [9], [10], [11], [12], and [13] reduce to the corresponding known relations for elastic materials.

To assist the reader in retaining the basic equations in mind, Table 1 provides a comparison between the equivalent rigidities and the equivalent moduli for elastoplastic materials and the corresponding rigidities and moduli for perfectly elastic materials.

TABLE 1 COMPARISON OF FACTORS IN ELASTOPLASTIC AND ELASTIC MATERIALS

Rigidities and moduli for elastoplastic materials	Rigidities and moduli for elastic materials
$D_1 = \int_{-h/2}^{+h/2} \frac{E(1+\lambda)}{[(1+\lambda)^2 - (\nu+\lambda/2)^2]}\, x_3^2 dx_3$	$\frac{Eh^3}{12(1-\nu^2)}$
$\frac{D_2}{D_1} = \frac{\int_{-h/2}^{+h/2} \frac{(1+\lambda)}{[(1+\lambda)^2 - (\nu+\lambda/2)^2]}\, x_3^2\, dx_3}{\int_{-h/2}^{+h/2} \frac{(\nu+\lambda/2)}{[(1+\lambda)^2 - (\nu+\lambda/2)^2]}\, x_3^2\, dx_3}$	ν
$E_1 = \int_{-h/2}^{+h/2} \frac{E(1+\lambda)}{[(1+\lambda)^2 - (\nu+\lambda/2)^2]}\, dx_3$	$\frac{Eh}{1-\nu^2}$
$\frac{E_2}{E_1} = \frac{\int_{-h/2}^{+h/2} \frac{(1+\lambda)}{[(1+\lambda)^2 - (\nu+\lambda/2)^2]}\, dx_3}{\int_{-h/2}^{+h/2} \frac{(\nu+\lambda/2)}{[(1+\lambda)^2 - (\nu+\lambda/2)^2]}\, dx_3}$	ν

(d) Numerical Solution. It is clear that Equations [1 to 14] inclusive, if solved together for a given load and for given boundary conditions, would constitute the solution of the problem in question. The equations of compatibility will be satisfied identically if one formulates a numerical procedure in terms of displacements. To obtain successive approximation by numerical integration for any given problem, it is necessary to rewrite Equations [1 to 14] in summation form with the aid of the boundary conditions, and further, to replace the differential radial element dr by a corresponding finite length Δr. It is assumed in the

following numerical integration procedure that this has been done:

Steps in Numerical Procedure:

1 Divide the radius of the plate from center line to the boundary into a number of finite elements Δr, not necessarily all equal.

2 Assume a set of values for $\sin \phi$, M_{22}, N_{22}, E_1, E_2, D_1, and D_2.

3 Calculate V from Equation [4].

4 Calculate H from Equation [5].

5 Calculate N_{11} from Equation [7].

6 Calculate ϵ_{11} from the first of Equations [12] and steps 5 and 2.

7 Calculate u_0 from Equation [3].

8 Calculate ϵ_{22} from Equation [2].

9 Calculate M_{11} from Equation [6] and steps 2 and 4.

10 Calculate $\sin \phi$ from Equation [8] and steps 9 and 2.

11 Calculate E_1, E_2, D_1, and D_2 from Table 1 or from Equations [10] and [13].

12 Calculate M_{22} from Equation [9] and steps 9, 10, and 11.

13 Calculate N_{22} from the second of Equations [11] and steps 6, 8, and 11.

14 Calculate u_3 from Equation [1] and step 10.

15 Repeat steps 3 through 14, using values obtained in steps 10, 11, 12, and 13, to replace the values assumed in step 2 for the first cycle of computation until the values of $\sin \phi$ do not change by more than the desired accuracy of solution.

We shall now elaborate on some of the individual steps which require further clarification. In step 2, reasonable values of ϕ, M_{22}, and N_{22} should be assumed from existing elastic solutions, or they may be obtained by energy methods, and so forth. Caution must be exercised not to assume zero values for N_{22} (or for any other estimated quantity) in the first cycle of computation, if rapid convergence is to be expected. The values of E_1, E_2, D_1, and D_2 for the elastoplastic plate in the first cycle of computation may be assumed to be the same as those for the corresponding elastic plate. These functions are constant for elastic plates and thus it is clear that step 11 should be omitted throughout the computation if the plate is to remain elastic.

In steps 12 and 13, M_{22} and N_{22} are calculated after new values for $\sin \phi$, E_1, E_2, D_1, and D_2, defined in Table 1, along the radius of the plate, it is necessary to know the variation of $\lambda(\gamma)$ along the x_3-axis, i.e., across the thickness of the plate. For a given stress-strain relation in tension, an octahedral shear stress-shear strain curve can be constructed according to the procedure developed by Shepherd (21), whose results have been verified experimentally.

With the octahedral shear stress-shear strain curve (for the purpose of discussion, a typical diagram is shown in Fig. 3) constructed, we are able to plot μ

$$\frac{(1 + \lambda)}{[(1 + \lambda)^2 - (\nu + \lambda/2)^2]}$$

and

$$\frac{(\nu + \lambda/2)}{[(1 + \lambda)^2 - (\nu + \lambda/2)^2]}$$

versus octahedral shear strain γ. Again, for the purpose of discussion, sketches of these curves appear in Figs. 4, 5, and 6, respectively.

We shall now determine the variation of the octahedral shear strain along the thickness of the plate. We recall that the middle surface of the plate is stretched, thus causing the neutral axis of the plate to shift from the origin of the stress-strain curve. If the values of the octahedral shear strain at the top, middle, and bottom of the surface of the plate are denoted by $\bar{\gamma}$, γ_0, and $\underline{\gamma}$, respectively, and if we assume that the stress-strain curve is the same in tension as in compression, we have

$$\bar{\gamma} = \Gamma_{\max} - \gamma_0 \quad [15]$$

$$\underline{\gamma} = \Gamma_{\max} + \gamma_0 \quad [16]$$

where, by Equations [14], (g), and (l)

$$\Gamma = \frac{\sqrt{2}}{3}\left[(1 + \mu + \mu^2)\left(\frac{1}{R_{11}} + \frac{1}{R_{22}}\right)^2 - \frac{3}{R_{11}R_{22}}\right]^{1/2} x_3 \quad [17]$$

and

$$\gamma_0 = \frac{\sqrt{2}}{3}\left[(1 + \mu + \mu^2)(\epsilon_{11} + \epsilon_{22})^2 - 3\epsilon_{11}\epsilon_{22}\right]^{1/2} \quad [18]$$

If each of the equations for $\Gamma_{\max}$ and γ_0 are solved simultaneously with

$$\mu = \frac{(\nu + \lambda/2)(1 + \lambda + 3\lambda/2)}{(1 + \lambda)^2 - (\nu + \lambda/2)^2}$$

the solution may be plotted as indicated by the broken-line curves in Fig. 4. The points of intersection of these dashed-line curves and the solid-line curve (μ versus γ) determine the values of $\Gamma_{\max}$ and γ_0 and hence by Equations [15] and [16], $\bar{\gamma}$ and $\underline{\gamma}$ are determined.

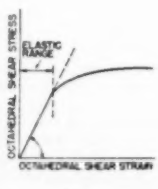

FIG. 3

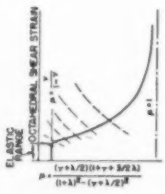

FIG. 4

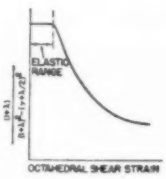

FIG. 5

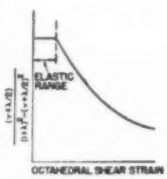

FIG. 6

SCHEMATIC DIAGRAMS SHOWING VARIATIONS OF OCTAHEDRAL SHEAR STRESS, VERSUS OCTAHEDRAL SHEAR STRAIN

$$\mu = \frac{(\nu + \lambda/2)(1 + \nu + 3\lambda/2)}{(1 + \lambda)^2 - (\nu + \lambda/2)^2}, \quad \frac{(1 + \lambda)}{(1 + \lambda)^2 - (\nu + \lambda/2)^2}, \text{ and } \frac{(\nu + \lambda/2)}{(1 + \lambda)^2 - (\nu + \lambda/2)^2}$$

(Also shown in Fig. 4 is a sketch of plot of $\Gamma_{\max}$ and γ_0 for various values of μ.)

It is of interest to note that values of μ have the range $\nu/(1-\nu) \leqq \mu < 1$, where the lower limit corresponds to perfectly plastic material for which Poisson's ratio has the value of $^1/_2$.

Thus, with known values of $\bar{\gamma}$, γ_0, and $\underline{\gamma}$ as functions of x_3, and since the shear stress-shear strain relation is one to one, the variation of γ across the thickness of the plate is determined uniquely.

It is now clear that the values of

$$\frac{(1+\lambda)}{(1+\lambda)^2-(\nu+\lambda/2)^2}$$

and

$$\frac{(\nu+\lambda/2)}{(1+\lambda)^2-(\nu+\lambda/2)^2}$$

at every point along the thickness of the plate can be determined from curves in Figs. 5 and 6; and therefore, the evaluation of the equivalent rigidities and of the equivalent moduli, given in Table 1, readily follows.

Simply Supported Circular Plates With a Central Concentrated Load

As an application of the theory developed, we shall now obtain solutions to simply supported circular plates of uniform thickness, Fig. 7, for two different loads—one which would result in

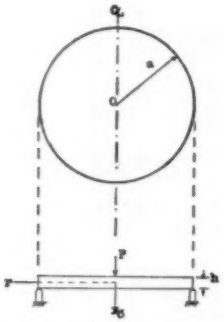

Fig. 7 Circular Plate With Central Concentrated Load

large elastoplastic deformation. These simple examples were chosen in the light of their simplicity for experimental verification of results.

The boundary conditions of this particular example are as follows

At $r = a$

$$V = P/2\pi a$$
$$M_{11} = N_{11} = 0$$
$$u_3 = 0$$

At $r = 0$

$$\phi = 0$$
$$u_0 = 0$$

Using the foregoing boundary conditions and remembering that there is a concentrated load rather than distributed pressure, the basic equations, written in summation form, are as follows

$$u_3 = \sum_0^a \tan\phi\,\Delta r - \sum_0^r \tan\phi\,\Delta r \qquad [1a]$$

$$e_{22} = u_3/x_0 \qquad [2a]$$

$$u_0 = \sum_0^r \frac{[(1+e_{11})\cos\phi - 1]}{(1+e_{11})\cos\phi}\,\Delta r \qquad [3a]$$

$$rV = P/2\pi \qquad [4a]$$

$$rH = \sum_0^r N_{22}\sec\phi\,\Delta r - \sum_0^a N_{22}\sec\phi\,\Delta r \qquad [5a]$$

$$rM_{11} = \left[\sum_0^r M_{22}\Delta r - \sum_0^a M_{22}\Delta r\right] - \frac{P}{2\pi}(a-r) + \left[\sum_0^a rH\tan\phi\,\Delta r - \sum_0^r rH\tan\phi\,\Delta r\right] \qquad [6a]$$

$$N_{11} = H\cos\phi - V\sin\phi \qquad [7a]$$

$$\sin\phi = \sum_0^r \frac{M_{11} - \frac{D_2}{D_1}M_{22}}{D_1 - \frac{D_2}{D_1}D_2} \qquad [8a]$$

$$M_{22} = \frac{D_2}{D_1}M_{11} + \left(D_1 - \frac{D_2}{D_1}D_2\right)\left(\frac{\sin\phi}{r}\right) \qquad [9a]$$

$$N_{11} = E_1 e_{11} + E_2 e_{22} \qquad [11a]$$

$$e_{22} = \frac{E_1 N_{22} - E_2 N_{11}}{E^2_1 - E^2_2} \qquad [12a]$$

The general numerical procedure, outlined in the foregoing, will be employed to obtain numerical solutions for the following two cases:

1 Load $P = 20$ lb for the plate to undergo large elastic deformation only.

2 Load $P = 500$ lb for the plate to suffer large elastoplastic deformation.

The plate material was assumed to be of 24S-T aluminum (Young's modulus $E = 10.0 \times 10^6$ psi and Poisson's ratio $\nu = 0.3$), and its dimensions were chosen to be 10 in. diam with thickness of 0.065 in.

It was desired to use an actual stress-strain curve in the solution rather than a hypothetical one. For this purpose, two sets of specimens were made of rolled thin sheet of 24S-T aluminum which appeared to be orthotropic. The specimens, $8.5 \times 8.5 \times 0.65$ in. in size with 2-in. gage length were tested for both sets in tension. The stress-strain curves obtained from the two sets of specimens were found to be identical except for a very small deviation around the knee. On the basis of this, as well as comparison of the reduced moduli of the material in bending, as discussed by Timoshenko (22), it appeared reasonable to assume that the material is isotropic. The stress-strain curve was, therefore, taken as the average of the curves of the two specimens determined experimentally, as shown in Fig. 8.

From the tensile stress-strain curve and the procedure of Shepherd, the octahedral shear stress-shear strain curve, Fig. 8, was constructed. Using this last curve, the graph of μ

$$\frac{(1+\lambda)}{(1+\lambda)^2-(\nu+\lambda/2)^2}$$

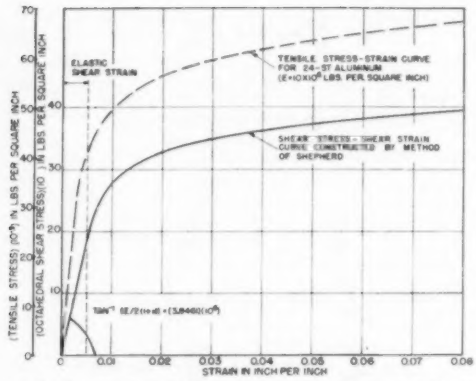
ELASTIC SHEAR STRAIN
TENSILE STRESS-STRAIN CURVE FOR 24-ST ALUMINUM (E=10X10⁶ LBS. PER SQUARE INCH)
SHEAR STRESS-SHEAR STRAIN CURVE CONSTRUCTED BY METHOD OF SHEPHERD
(TENSILE STRESS) (10³) IN LBS PER SQUARE INCH
(OCTAHEDRAL SHEAR STRESS)(10) IN LBS PER SQUARE INCH
STRAIN IN INCH PER INCH

FIG. 8 TENSILE STRESS-TENSILE STRAIN AND OCTAHEDRAL SHEAR STRESS-SHEAR STRAIN CURVES FOR 24S-T ALUMINUM

and

$$\frac{(\nu + \lambda/2)}{(1 + \lambda)^2 - (\nu + \lambda/2)^2}$$

respectively, versus γ, the octahedral shear strain. Fig. 9, was obtained.

In computing the two cases mentioned for the first few cycles of computation it was assumed that a small rigid plug was inserted at the center of the plate. Once fair results were obtained, the plug was removed and the computation for the simply supported plate with a concentrated loading was carried out for at least two more cycles. The results of the solutions for the bending moments and the membrane forces, and the deflections for each of the two cases are presented in Figs. 10 and 11. In addition, the results of the final cycle of computation for the elastoplastic case (load = 500 lb) are given in Table 2.

COMPARISON OF ANALYTICAL WITH EXPERIMENTAL RESULTS

In order to demonstrate the validity of the theory developed, circular plate specimens were made of the same sheet of 24S-T

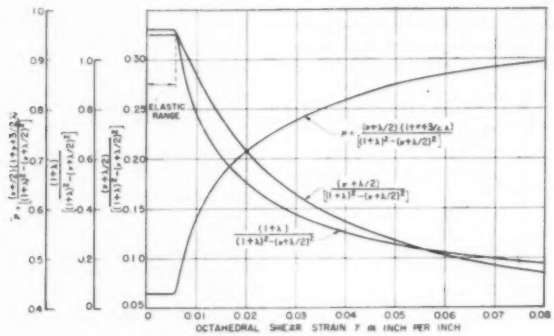

FIG. 9 VARIATION OF PARAMETER μ,

$$\frac{(1 + \lambda)}{(1 + \lambda)^2 - (\nu + \lambda/2)^2} \quad \text{and} \quad \frac{(\nu + \lambda/2)}{(1 + \lambda/2)^2 - (\nu + \lambda/2)^2}$$

VERSUS OCTAHEDRAL SHEAR STRAIN γ FOR 24S-T ALUMINUM
($E = 10 \times 10^6$ psi, $\nu = 0.3$.)

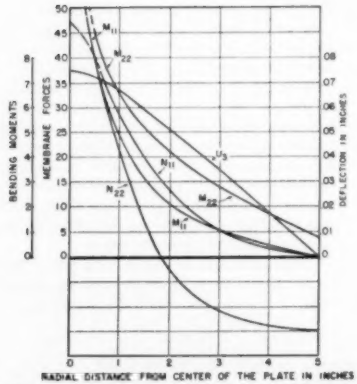

FIG. 10 SOLUTION FOR SIMPLY SUPPORTED CIRCULAR PLATE WITH CONCENTRATED LOADING OF 20 LB

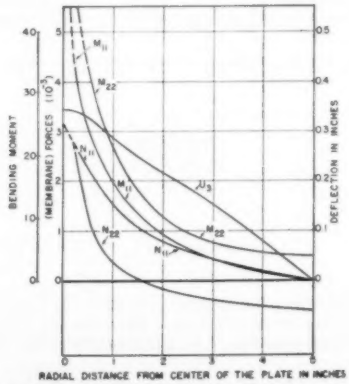

FIG. 11 SOLUTION FOR SIMPLY SUPPORTED CIRCULAR PLATE WITH CONCENTRATED LOADING OF 500 LB

TABLE 2 RESULTS OF FINAL COMPUTATION FOR ELASTOPLASTIC CASE

r	Δr	Sin φ	Cos φ	tan φ	M_{11}	N_{11}	$E_1 \times 10^{-4}$	$E_2 \times 10^{-4}$	D_1	D_2
0		0	1	0	(42)	(2800)	571.5830	189.8810	158.2587	60.1168
	1/8									
1/8		0.02200	0.99975	0.02200	40.33	2764	602.7500	199.3220	171.7036	63.1693
	1/8									
1/4		0.04051	0.99917	0.04053	38.32	2599	632.2600	203.1240	185.2253	65.7069
	1/4									
1/2		0.07335	0.99730	0.07356	34.15	1300	695.4540	204.1650	199.8320	68.4700
	1/2									
1		0.08531	0.99635	0.08554	21.34	375	695.8900	212.0430	236.4190	73.6420
	1/2									
1 1/2		0.07407	0.99727	0.07417	14.62	20	714.2857	214.2857	251.4880	75.4464
	1/2									
2		0.05367	0.99856	0.05374	8.41	—150				
	1/2									
2 1/2		0.06276	0.99802	0.06288	7.26	—310				
	1/2									
3		0.06949	0.99757	0.06965	6.37	—400				
	1/2									
3 1/2		0.07138	0.99745	0.07156	5.27	—460				
	1/2									
4		0.07858	0.99690	0.07882	4.81	—525				
	1/2									
4 1/2		0.08011	0.99678	0.08036	4.22	—575				
	1/2									
5		0.08034	0.99676	0.08060	3.71	—600				

Constant ←for elastic portion→ of plate

Constant ←for elastic portion→ of plate

Constant ←for elastic portion→ of plate

Constant ←for elastic portion→ of plate

r	Δr	V	N_{11}	$\sum_0^r M_{11}\Delta r$	$\sum_0^a M_{11}\Delta r$	$\sum_0^r r H \tan\varphi \Delta r$	$\sum_0^a r H \tan\varphi \Delta r$	M_{11}	$e_{11} \times 10^3$	$[(1+e_{11})\cos\varphi - 1] \times 10^3$
0		—	(2800)	—65.7547		455		(42)	3.6967	3.6967
	1/8	636.6384	2775.2965	—60.5922		453.3562		38.6412	3.4882	3.2372
1/8										
	1/8	318.3192	2634.9086	—55.7472		442.2516		34.0016	3.2870	2.0376
1/4										
	1/4	159.1596	2232.2571	—46.6296		416.7207		24.0002	3.1793	+0.4704
1/2										
	1/2	79.5798	1515.1351	—32.2597		366.5789		15.9855	2.2504	—1.4080
1										
	1/2	53.0532	1063.1530	—22.7665		317.7953		10.8813	1.6355	—1.0989
1 1/2										
	1/2	39.7899	782.4330	—17.0090		270.7484		7.5617	1.2729	—0.1689
2										
	1/2	31.8319	577.6523	—13.0900		224.5395		5.0249	1.0317	—0.9504
2 1/2										
	1/2	26.5266	418.8020	— 9.6794		179.3372		3.4772	0.8473	—1.5847
3										
	1/2	22.7370	294.7593	— 6.7673		133.1169		2.0168	0.6842	—1.8676
3 1/2										
	1/2	19.8949	194.0783	— 4.2452		87.8250		1.0309	0.5385	—2.5632
4										
	1/2	17.6844	118.8947	— 1.9844		44.0238		0.5006	0.4361	—2.7853
4 1/2										
	1/2	15.9459	0	0		0		0	0.7490	—2.4934
5										

r	Δr	$w_0 \times 10^3$	$e_{22} \times 10^3$	$\bar{\gamma}$	γ_2	$\bar{\gamma}$	$\sum_0^r \tan\varphi \Delta r$	w
0		0	—	0.01001	0.00476	0.01952	0	0.3464
	1/8	0.4333	3.4664	0.00950	0.00325	0.01600	0.00137	0.3450
1/8								
	1/4	0.7629	3.0516	0.00840	0.00275	0.01390	0.00528	0.3411
1/4								
	1/2	1.0764	2.1528	0.00700	0.00241	0.01182	0.01954	0.3269
1/2								
	1/2	0.8420	0.8420	0.00510	0.00193	0.00896	0.05931	0.2871
1								
	1/2	0.1903	0.1268	0.00410	0.00075	0.00560	0.09923	0.2472
1 1/2								
	1/2	—0.1266	—0.0633				0.13121	0.2152
2								
	1/2	—0.4064	—0.1625				0.16036	0.1861
2 1/2								
	1/2	—1.0402	—0.3467				0.19349	0.1530
3								
	1/2	—1.9032	—0.5437				0.22879	0.1177
3 1/2								
	1/2	—3.0109	—0.7527				0.26628	0.0801
4								
	1/2	—4.3480	—0.9662				0.30617	0.0403
4 1/2								
	1/2	—5.0677	—1.1335				0.34640	0
5								

←Elastic range→

←Elastic range→

←Elastic range→

aluminum from which the tensile specimens mentioned in the foregoing were cut. The plate specimens were $10^1/_8$ in. diam with an average thickness of 0.65 in. These plates were cut so that their diameters were $^1/_8$ in. larger than those considered in the analytical solution so that they could be supported adequately.

The apparatus used to test the plate specimens consisted of a 6-in. length of 9-in-ID steel pipe to afford a simple support for the circular plates. One edge of the supporting cylinder was tapered to a 60-deg slope on a lathe and then was very slightly rounded with a file. The concentrated load was applied to the center of the plates by means of a 1-in-diam steel rod. This load rod had one end turned to a point in the lathe and the other end fashioned to fit into the head of the testing machine. The deflections of the test plates were measured at four points along the radii of the plates by means of dial indicators which were affixed to the plates and the load rod.

For comparison of the analytical with the experimental deflections, the theoretical curves for loads of 20 lb and 500 lb are plotted, and the experimental points corresponding to each curve are marked as shown in Fig. 12. It is apparent from Fig. 12

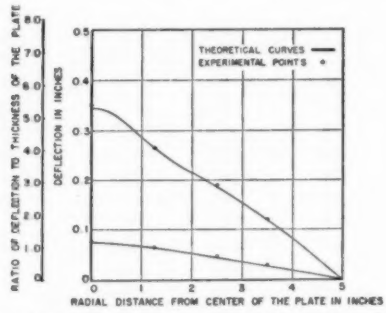
RATIO OF DEFLETION TO THICKNESS OF THE PLATE
DEFLECTION IN INCHES
THEORETICAL CURVES
EXPERIMENTAL POINTS
RADIAL DISTANCE FROM CENTER OF THE PLATE IN INCHES

FIG. 12 COMPARISON OF ANALYTICAL WITH EXPERIMENTAL RESULTS

that the agreement between the theoretical and experimental results is very good, since the maximum deviation is less than 5 per cent near the concentrated load.

CONCLUSION

A general theory for the bending with large deflection of elastoplastic thin circular plates with polar symmetrical loading is developed, two special examples using this theory are solved, and the validity of the theory is verified by experiment.

BIBLIOGRAPHY

1 "The Bending of Circular Plates With Large Deflections," by S. Way, Trans. ASME, vol. 56, 1934, pp. 627–636.

2 "Bending of Rectangular Plates With Large Deflections," by S. Levy, NACA Technical Notes 846, 847, 1942.

3 "Bending of Circular Plates," by S. Jen, PhD Thesis, University of Michigan, Ann Arbor, Mich., 1948.

4 "The Bending of Thin Elliptic Plates," by C. L. Perry, Proceedings of Third Symposia in Applied Mathematics, *Elasticity*, McGraw-Hill Book Company, Inc., New York, N. Y., 1950.

5 "Large Deflection of a Circular Clamped Plate Under Uniform Pressure," by W. Chien, *Chinese Journal of Physics*, December, 1947.

6 "Asymptotic Behavior of a Thin Clamped Circular Plate Under Uniform Normal Pressure at Very Large Deflection," by W. Chien, The Science Reports of National Tsing Hua University, Peiping, China, April, 1948.

7 "Some Problems in the Theory of Plastic Deformations," by A. S. Ilyushin, *Prikl. Mat. Mekh.*, vol. 7, 1943, pp. 245–272.

8 "Elastic-Plastic Bending of Circular and Annular Plates," by W. W. Sokolovsky, *Prikl. Mat. Mekh.*, vol. 8, 1944, pp. 141–166.

9 "The Theory of Plasticity—An Outline of Work Done in Russia," by W. W. Sokolovsky, JOURNAL OF APPLIED MECHANICS, Trans. ASME, vol. 68, 1946, pp. A-1–10.

10 "On the Plastic Bending of Circular Plates Under Uniform Transverse Loads," by D. Trifan, Technical Report No. 8, Contract NTONR-358 T.O.I., Brown University, Providence, R. I., 1948.

11 "Theory of Plates and Shells," by S. Timoshenko, McGraw-Hill Book Company, Inc., New York, N. Y., 1940.

12 "On Isotropic Materials With Continuous Transition From Elastic to Plastic State," by W. Prager, Proceedings of the Fifth International Congress of Applied Mechanics, Cambridge, Mass., 1948, pp. 234–237.

13 "A New Mathematical Theory of Plasticity," by W. Prager, *Prikl. Mat. Mekh.*, vol. 2, 1947, pp. 419, 428.

14 "On Mechanical Behavior of Metals in Strain Hardening Range," G. H. Handelman, C. C. Lin, and W. Prager, *Quarterly of Applied Mathematics*, vol. 4, 1947, pp. 397–407.

15 "Zur Theorie Plastischer Deformationen und der Rierdurch in Material Hervorguerufenen Nachspanungen," by H. Hencky, *Zeitschrift für angewandte Mathematik und Mechanik*, vol. 4, 1924, pp. 323–334.

16 "Plasticity, a Mechanics of the Plastic State of Matter," by A. Nadai, McGraw-Hill Book Company, Inc., New York, N. Y., 1950.

17 "Mechanik der festen Korper in plastisch deformablen Zustand," by R. von Mises, Gottlinger Nachrichten, 1913.

18 "General Stress-Strain Laws of Elasticity and Plasticity," by A. Gleyzal, JOURNAL OF APPLIED MECHANICS, Trans. ASME, vol. 68, 1946, pp. A-261–264.

19 "Plastic Deformation of Circular Diaphragm Under Pressure," by A. Gleyzal, JOURNAL OF APPLIED MECHANICS, Trans. ASME, vol. 70, 1948, pp. 288–296.

20 "A New Theory of Plastic Flow," by D. Trifan, *Quarterly of Applied Mathematics*, vol. 7, 1949, pp. 201–211.

21 "Plastic Stress-Strain Relations," by W. M. Shepherd, Proceedings of The Institution of Mechanical Engineers, War Emergency Issue No. 39, vol. 159, 1948, pp. 95–99.

22 "Strength of Materials," Part 2, by S. Timoshenko, D. Van Nostrand Company, Inc., New York, N. Y., 1947.

Forced Lateral Vibration of Beam Carrying a Concentrated Mass

By W. H. HOPPMANN, 2ND,[1] BALTIMORE, MD

In this paper a study is made of the problem of the lateral vibration of a simply supported beam with a concentrated mass attached at its mid-point. A force assumed to act at the mass in a direction normal to the length of the beam is represented by a sinusoidally time-varying function. The homogeneous form of the Bernoulli-Euler beam equation is solved considering the problem as one with time-dependent boundary conditions. To represent an important case of forced vibrations the solution is transformed to give the deflection and bending strain caused by a pulse type of load. Curves are plotted whereby the contributions to deflection and strain from the higher modes of vibration may be examined as functions of the ratio of attached mass to mass of beam. Results of computations for a specific beam and set of masses are presented, as well as experimental results for the same beam with similar pulse-type loads applied. Oscillograms show rather trenchantly the slow transition of the mass-beam system toward a one-degree-of-freedom system as the concentrated mass is increased.

Nomenclature

The following nomenclature is used in the paper:

E = Young's modulus of elasticity
I = moment of inertia of cross section of beam about neutral axis
A = area of cross section of beam
ρ = mass per unit volume
l = length of beam
m = reduced mass of beam (one-half total mass)
M = concentrated mass fixed to beam
n = number of nth mode of vibration of beam
p_n = circular frequency of nth mode of vibration of beam with mass M attached
t = time
P_0 = amplitude of sinusoidal driving force (also amplitude of sinusoidal pulse)
T = length of time sinusoidal pulse is assumed to act on beam
$w(x, t)$ = deflection of beam
$\epsilon(x, t)$ = strain at outer fiber of beam

$$Q_n = \frac{p_n T}{2\pi}$$

$\Phi(Q_n)$ = dimensionless function of Q_n

$\Psi\left(\frac{k_n l}{2}\right)$ = dimensionless function of $\frac{k_n l}{2}$

$\Omega\left(\frac{k_n l}{2}\right)$ = dimensionless function of $\frac{k_n l}{2}$

$$a = \sqrt{\frac{EI}{\rho A}}$$

$$\omega = \frac{\pi}{T}$$

$$k_n = \sqrt{\frac{p_n}{a}}$$

$$\lambda = \sqrt{\frac{\omega}{a}}$$

$$R = \frac{M}{2m} = \text{mass ratio}$$

Introduction

It has been the practice in engineering for many years to consider vibrating shafts and beams carrying concentrated masses as elastic systems of finite number of degrees of freedom depending upon the number of masses (1).[2] This assumption is usually made necessary by the complexity of calculations required for a practical case. In some instances this assumption may be quite satisfactory but there is no a priori justification for it and indeed in the important cases of sharp transient loading it is highly misleading.

It seems then instructive to examine a technically important and representative case with the view of evaluating the assumption. For this purpose a study is made of a simply supported beam with a concentrated mass attached at its mid-point. A sinusoidally time-varying force is assumed to act on the mass in a direction normal to the length of the beam. From the solution of this problem the solution for a sinusoidal pulse is derived easily.

In a paper by E. H. Lee a single energy criterion was developed for the purpose of evaluating the assumption that a beam may be considered as a single-degree-of-freedom system (2). While this criterion was reasonably easy to develop for a uniform simply supported beam, it is not so for cases in which the shape functions are not orthogonal; and the frequency roots must be obtained from a complicated transcendental equation as in the present case. Therefore it is proposed to examine deflection ratios and strain ratios directly as indications of how far the vibrating system diverges from a single-degree-of-freedom system. This procedure may be preferred because interest normally centers in the deflection and the strain caused by forced vibrations.

Analytical Formulation of Problem

The beam carrying a concentrated mass is shown in Fig. 1. The ends of the beam are hinged. The constant cross-sectional area of the beam is A. The moment of inertia I is also constant. The density is designated by ρ. The driving force is $P_0 \sin \omega t$.

Symmetrical vibrations only are excited in this case so it is sufficient to determine the deflection w only for one half of the beam as shown in Fig. 2. This arrangement is also suitable for

[1] Associate Professor, The Johns Hopkins University. Mem. ASME.

Presented at the National Conference of the Applied Mechanics Division, State College, Pa., June 19–21, 1952, of The American Society of Mechanical Engineers.

Discussion of this paper should be addressed to the Secretary, ASME, 29 West 39th Street, New York, N. Y., and will be accepted until October 10, 1952, for publication at a later date. Discussion received after the closing date will be returned.

Note: Statements and opinions advanced in papers are to be understood as individual expressions of their authors and not those of the Society. Manuscript received by ASME Applied Mechanics Division, August 13, 1951. Paper No. 52—APM-20.

[2] Numbers in parentheses refer to the Bibliography at the end of the paper.

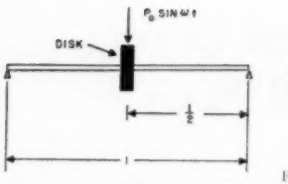

FIG. 1 GENERAL ARRANGEMENT OF BEAM

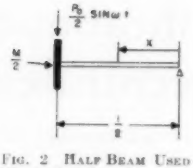

FIG. 2 HALF BEAM USED WITH BOUNDARY CONDITIONS OF PROBLEM

treating the vibration problem as one with time-dependent boundary conditions.

Neglecting the effects of shearing forces and rotatory inertia on the deflection, the differential equation used to describe the motion is as follows

$$EI \frac{\partial^4 w}{\partial x^4} + \rho A \frac{\partial^2 w}{\partial t^2} = 0 \quad \ldots\ldots\ldots\ldots\ldots\ldots [1]$$

Inasmuch as the beam is assumed to be initially at rest and the vibrations are symmetrical, the boundary conditions, in accord with Fig. 2, and the initial conditions are

$$\left.\begin{aligned} &w(0, t) = 0 \qquad \left.\frac{\partial^2 w}{\partial^2 x^2}\right|_{x=0} = 0 \\ &\left.\frac{\partial w}{\partial x}\right|_{x=l/2} = 0 \qquad EI \left.\frac{\partial^3 w}{\partial x^3}\right|_{x=l/2} = \frac{M}{2}\frac{\partial^2 w}{\partial t^2} - \frac{P_0}{2}\sin \omega t \\ &w(x, 0) = 0 \qquad \left.\frac{\partial w}{\partial t}\right|_{t=0} = 0 \end{aligned}\right\} \quad \ldots [2]$$

If the amplitude P_0 of the driving force is assumed to be zero the solution of Equation [1] may be obtained by separation of variables so that

$$w = \sum (A_n \sin k_n x + B_n \cos k_n x + C_n \sinh k_n x + D_n \cosh k_n x) \sin p_n t \ldots [3]$$

and satisfying the boundary conditions so that all constants A_n, B_n, C_n, and D_n are not zero, the frequency equation is

$$\frac{M}{2m}\frac{k_n l}{2}\left(\tan \frac{k_n l}{2} - \tanh \frac{k_n l}{2}\right) - 2 = 0 \quad \ldots\ldots\ldots [4]$$

This equation is the same as that given by von Kármán and Biot (3). In order to be consistent with usage for zero mass ratio and symmetrical vibration, the consecutive roots of this equation will be labeled 1, 3, 5 . .

The deflection at any point along the beam can be written

$$w = \sum_1^\infty C_n(\sinh k_n x - \alpha_n \sin k_n x) \sin p_n t \ldots\ldots [5]$$

where

$$\alpha_n = \frac{\cosh \frac{k_n l}{2}}{\cos \frac{k_n l}{2}}$$

Now to obtain a solution for the case in which a driving force acts at $x = \frac{l}{2}$; write as a solution

$$w = w_0 + \sum_1^\infty C_n(\sinh k_n x - \alpha_n \sin k_n x) \sin p_n t \ldots [6]$$

The portion given by the infinite series satisfies the differential equation and the boundary conditions when the driving force is absent.

Let $w_0 = g(x) \sin \omega t$ so that w_0 satisfies the differential equation and all boundary conditions (4). This method which is quite useful was first presented by Duhamel in 1834 (5) and applied in the case of the transverse vibrations of a simply supported beam without concentrated mass by Phillips in 1864 (6). The conditions on w_0 determine the form of $g(x)$ and the required solution then becomes

$$w = \frac{P_0\left(\frac{\sin \lambda x}{\cos \frac{\lambda l}{2}} - \frac{\sinh \lambda x}{\cosh \frac{\lambda l}{2}}\right)\sin \omega t}{\left[4EI\lambda^3 - M\omega^2\left(\tan \frac{\lambda l}{2} - \tanh \frac{\lambda l}{2}\right)\right]} - \frac{2P_0\omega}{a^2}\sum_1^\infty \frac{\left(\sinh k_n x - \frac{\cosh \frac{k_n l}{2}}{\cos \frac{k_n l}{2}} \sin k_n x\right)\sin p_n t}{p_n \cosh \frac{k_n l}{2}(\lambda^4 - k_n^4)\left[\frac{4m}{k_n l} - \frac{k_n l}{4} M\left(\frac{1}{\cosh^2 \frac{k_n l}{2}} - \frac{1}{\cos^2 \frac{k_n l}{2}}\right)\right]} \quad \ldots [7]$$

The forced-vibration portion is in closed form. If we expand it in a sine series the solution may be written

$$w = \frac{1}{\left[4EI\lambda^3 - M\omega^2\left(\tan \frac{\lambda l}{2} - \tanh \frac{\lambda l}{2}\right)\right]}\sum_1^\infty \frac{-8P_0\lambda^2 \sin \frac{n\pi}{2} \sin \frac{n\pi x}{l} \sin \omega t}{l\left(\lambda^4 - \frac{n^4\pi^4}{l^4}\right)} - \frac{2P_0\omega}{a^2}\sum_1^\infty \frac{\left(\sinh k_n x - \frac{\cosh \frac{k_n l}{2}}{\cos \frac{k_n l}{2}} \sin k_n x\right)\sin p_n t}{p_n \cosh \frac{k_n l}{2}(\lambda^4 - k_n^4)\left[\frac{4m}{k_n l} - \frac{k_n l}{4} M\left(\frac{1}{\cosh^2 \frac{k_n l}{2}} - \frac{1}{\cos^2 \frac{k_n l}{2}}\right)\right]} \quad \ldots\ldots [8]$$

If $M = 0$, Equation [8] agrees with that given by Timoshenko (7) for the case of the uniform simply supported beam.

To obtain the solution for a sinusoidal pulse given by

$$\left.\begin{aligned} F &= P_0 \sin \omega t \qquad 0 < t \leq T \\ &= 0 \qquad\qquad t > T \end{aligned}\right\} \quad \ldots\ldots\ldots\ldots [9]$$

simply write

$$w = w(t) + w(t - T) \qquad \text{for } t > T \quad \ldots\ldots\ldots [10]$$

The Mass-Beam as a One-Degree-of-Freedom System

The deflection of the mass-beam system is given by Equation [7] or by Equation [10]. The bending strains may be obtained from these by differentiating twice with respect to the space variable x. To determine a convenient form for investigating how close a given mass-beam system approaches to one which might be called a single-degree-of-freedom system, equations for the maxima of strain and deflection in each mode will be given in terms of specific functions which are then plotted for ready reference. The deflections and strains are given for those cases in which the driving force is assumed to have finally become zero after a time T. Such an assumption applies especially to the case of a pulse duration short compared with period of the fundamental.

Now for the position $x = \frac{l}{2}$ we may write the amplitude of deflection contribution from each mode

$$w_{n\max} = \frac{2P_0 l^2}{Ma\omega} \Phi(Q_n)\ \Psi\left(\frac{k_n l}{2}\right)$$

where

$$Q_n = \frac{p_n T}{2\pi}$$

$$\Phi(Q_n) = \frac{\cos \pi Q_n}{1 - 4Q_n^2}$$

$$\Psi\left(\frac{k_n l}{2}\right) = \frac{\left(\tanh \frac{k_n l}{2} - \tan \frac{k_n l}{2}\right)}{\left(\frac{k_n l}{2}\right)^3 \left[\left(\tanh \frac{k_n l}{2} - \tan \frac{k_n l}{2}\right) + \frac{k_n l}{2}\left(\frac{1}{\cosh^2 \frac{k_n l}{2}} - \frac{1}{\cos^2 \frac{k_n l}{2}}\right)\right]} \quad [11]$$

The function Φ is plotted in Fig. 3 and the function Ψ in Fig. 4.

In a similar manner the amplitude of bending strain from each mode may be written

$$\epsilon_{n\max} = \frac{8i^2 c}{Ma\omega} \Phi(Q_n)\ \Omega\left(\frac{k_n l}{2}\right)$$

where

$$\Omega\left(\frac{k_n l}{2}\right) = \frac{\left(\tanh \frac{k_n l}{2} + \tan \frac{k_n l}{2}\right)}{\left[\left(\tanh \frac{k_n l}{2} - \tan \frac{k_n l}{2}\right) + \frac{k_n l}{2}\left(\frac{1}{\cosh^2 \frac{k_n l}{2}} - \frac{1}{\cos^2 \frac{k_n l}{2}}\right)\right]} \quad [12]$$

The function Ω is plotted in Fig. 5.

To facilitate the use of the functions Φ, Ψ, and Ω in determining the contributions to deflection and to strain from each mode, the frequency roots $k_n l$ are plotted as continuous functions of the mass ratio $R = M/2m$. In order to compact the curves giving the frequency numbers into a reasonable space an auxiliary func-

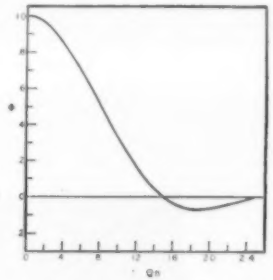

Fig. 3 Displacement Function and Strain Function Φ

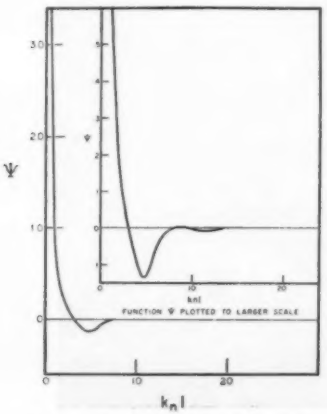

Fig. 4 Displacement Function Ψ

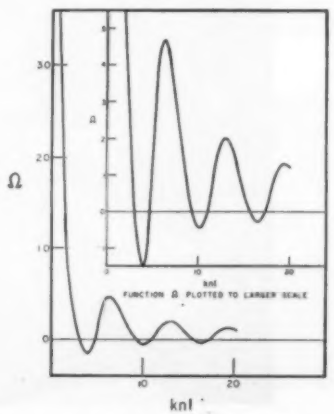

Fig. 5 Strain Function Ω

tion N of R is plotted in Fig. 6. The frequency numbers $k_n l$ are then given as follows

$$k_n l = N + (n - 1)\pi, \quad n = 1, 3, 5, \ldots\ldots\ldots [13]$$

It may be observed that the curve for $n = 1$ (fundamental) runs asymptotic to the R-axis. All of the other curves run asymptotic to the line $N = \pi/2$.

A remark may be made concerning the zeros of the functions Ψ and Ω. For the function Ψ the 1st, 3rd, etc., zeros correspond to a mass ratio of zero while the remaining zeros correspond to mass ratio of infinity. For the function Ω the 1st, 3rd, etc., zeros correspond to a mass ratio of zero, while the remaining zeros are only incidental zeros of the plotted continuous function. The latter zeros correspond to no admissible values of $k_n l$.

Experiments

Strains and deflections were measured on an experimental beam. For the purpose a 1-in. × 1-in. bar of cold-rolled steel 57 in. long with a solid steel disk affixed at its mid-length was mounted on ball-bearing supports. In the tests five sizes of steel disks were used. The maximum thickness was about $1^1/_2$ in. and the maximum diameter was 10 in. A rectangular hole was machined near the center of each disk so that it could be wedged tightly onto the bar with a suitable pair of wedges. Mass ratios investigated were approximately 0, $^1/_4$, $^1/_2$, 1, 2, and 3.

The load was applied by dropping a 1-lb steel ball onto the uppermost point of the disk. The ball was made to strike the disk with a predetermined speed. The test speeds were about 4 fps, 5.6 fps, and 7.2 fps. Theoretical discussion of force of impact is given in the literature (8).

The assumption of simple support was investigated by driving the beam with an electromagnet supplied from an oscillator and checking the calculated resonant frequencies. The experimental and theoretical frequencies checked within a few per cent.

The maximum deflections were measured at the middle of the beam with a special micrometer and indicator-light arrangement.

The calibrated bending strains obtained with standard resistance-wire strain-gage equipment were photographed with an F 1.5 Leica camera from the face of a single-sweep oscilloscope. The triggering was accomplished by interrupting a light beam with the falling steel ball. Strains were measured near the middle of the beam about 1 in. from the face of the attached disk on the lower beam surface. A few checks were made by strain gages on the upper beam surface. Test setup and apparatus are shown in Fig. 7.

The contact times of ball and disk during impact were measured with a chronometer and while they vary with the given mass of disk as well as for any one disk a good indicated average is about 0.16 millisec. The total range of variation was from 0.13 millisec to 0.20 millisec.

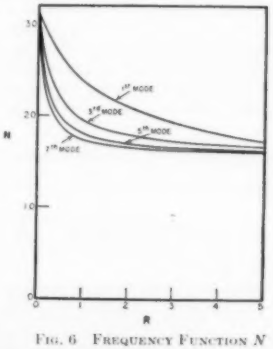

Fig. 6 Frequency Function N

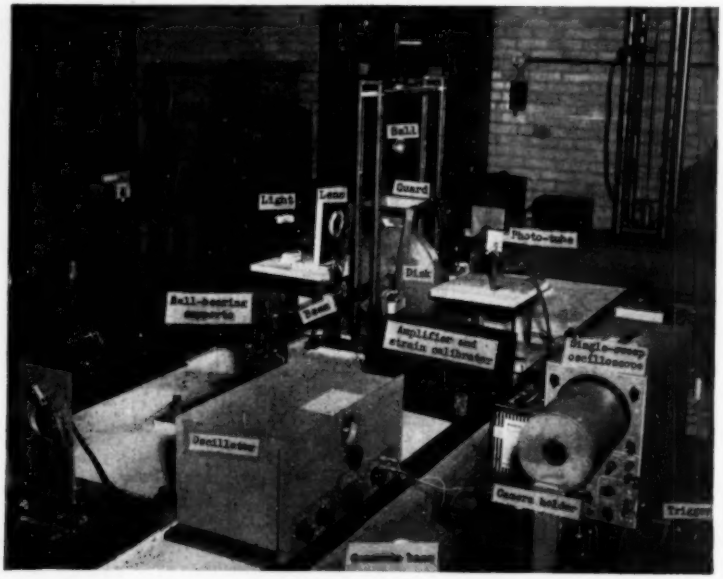

Fig. 7 Test Setup and Apparatus

A summary of experimental results is given in Table 1 and typical oscillograms in Fig. 8. These will be discussed later.

Numerical Examples

For the purpose of comparison with the experimental results the strains for the same beam and mass ratios were computed using the theoretical equations derived in this paper. A constant time of contact of 0.13 millisec was assumed for all of the six mass-beam systems investigated. The strains were computed over a time interval approximately equal to one quarter of the fundamental period of each system, assuming a pulse-type loading. The results are shown in Fig. 8. The number of modes taken shows on each chart.

TABLE 1 MAXIMA OF MEASURED DISPLACEMENTS AND STRAINS

Mass ratio $R = \frac{M}{2m}$	Velocity of impact, fps: 4.0 Deflection, in.	4.0 Strain $\times 10^4$	5.6 Deflection, in.	5.6 Strain $\times 10^4$	7.2 Deflection, in.	7.2 Strain $\times 10^4$
0	0.028	1.85	0.040	2.20	0.050	—
.24	—	0.97	—	1.46	—	1.77
.48	0.039	0.80	0.051	1.16	0.068	1.45
.97	0.037	0.61	0.045	0.87	0.058	1.05
2.03	0.027	0.59	0.039	0.71	0.048	0.84
2.95	0.023	0.40	0.032	0.55	0.045	.64

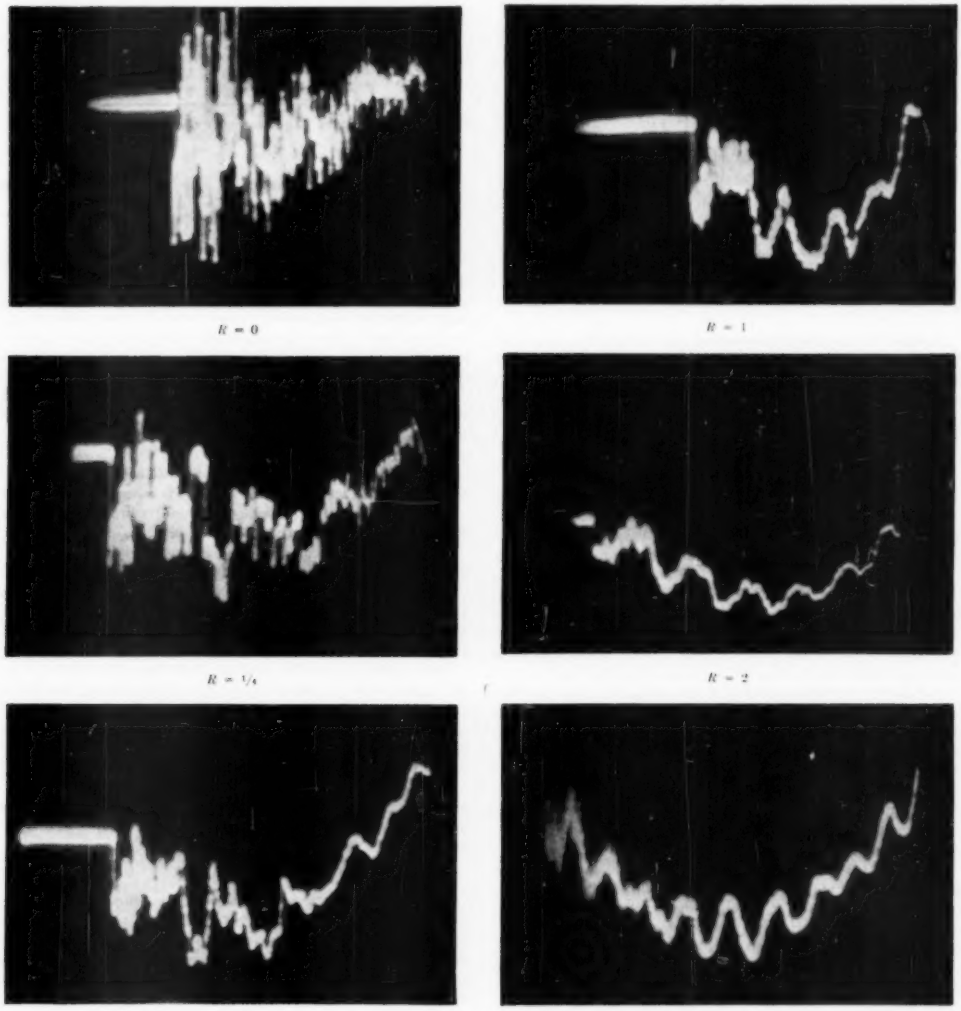

$R = 0$ $R = 1$ $R = 1/4$ $R = 2$ $R = 1/2$ $R = 3$

Fig. 8 Oscillograms of Strain Variation With Time for Various Mass Ratios R
(Each oscillogram represents strain for period of time corresponding to about half period of fundamental.)

TABLE 2 ESTIMATED DISPLACEMENT RATIOS AND STRAIN RATIOS FOR TEST BEAM

Mass ratio $R = \frac{M}{2m}$	Ratio of third —mode to fundamental— Displacement	Strain	Ratio of fifth —mode to fundamental— Displacement	Strain
0.5	0.03	0.63	0.00	0.45
1.0	0.02	0.60	0.00	0.40
2.0	0.01	0.37	0.00	0.24
5.0	0.00	0.27	0.00	0.16

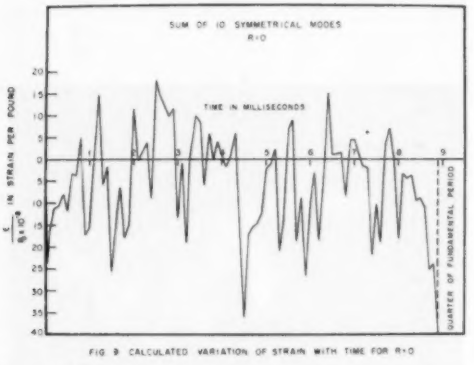

FIG. 9 CALCULATED VARIATION OF STRAIN WITH TIME FOR R=0

FIG. 9 CALCULATED VARIATION OF STRAIN WITH TIME FOR $R = 0$

In order to illustrate the results obtained with the curves for Φ, Ψ, Ω, and N, given in Figs. 3 to 6, inclusive, the W_{max} and ϵ_{max} for the first, third, and fifth modes of the experimental beam were estimated and the ratios are given in Table 2. The calculations were for mass ratios $^1/_2$, 1, 2, and 5. These results are discussed in the next section.

Discussion of Results

In Table 1 it can be seen that the maximum strain near the mid-length of the beam decreases sharply with increasing mass ratio and that it increases with increasing velocity of impact as might be expected. The deflections have the same general characteristics except that there is a small and unexpected decrease in deflection in going from $R = 0.24$ to $R = 0$. It was surmised that this effect might be caused by the nature of the surface of contact but attaching some very small blocks of steel to the beam with small C-clamps and then dropping the ball onto these blocks gave approximately the same deflections as for zero mass.

The oscillograms shown in Fig. 8 correspond to a time interval equal to approximately the half-period of the fundamental in each case. The strain calibrations vary somewhat from case to case so no attempt should be made to compare absolute values. The oscillograms are presented mainly for the purpose of demonstrating how the strain detail varies with increasing mass ratio R. It is quite clear that the oscillogram showing the largest mass ratio would still not be classed as one belonging to a single-degree-of-freedom system.

Several examples of the calculated strains are shown as Figs. 9 and 10. They are for about one half of the time interval given in the oscillograms. For general detail, they show rather remarkable agreement with the oscillograms. For zero mass ratio a relative maximum of strain occurs near the end of time of impact but this diminishes markedly as the mass ratio is increased.

Deflection and strain ratios obtained for the beam under discussion with the aid of the auxiliary functions Φ, Ψ, Ω, and N show that for deflections the beam might be considered as one of single degree of freedom but certainly not for the strains. These results given in Table 2 required only a few minutes for calculation by aid of the plotted functions.

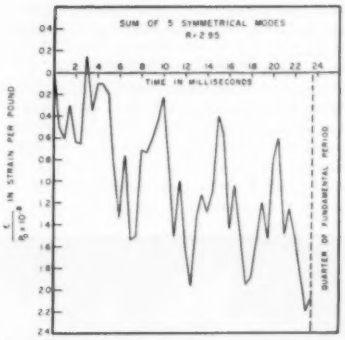

FIG. 10 CALCULATED VARIATION OF STRAIN WITH TIME FOR $R = 2.95$

Conclusions

Equations have been derived for bending deflection and strain in a simply supported beam carrying a concentrated mass at its mid-length caused by a harmonic force applied to the concentrated mass. Strains computed by means of this theory have been compared with those experimentally determined for a specific beam and set of concentrated masses, and very good general agreement has been found.

Auxiliary functions have been plotted so that in a short length of time one might investigate a beam-mass system of the type studied and determine how closely it conformed to a single-degree-of-freedom system.

Application of these functions in the case of the experimental beam tested predicts that as far as strain is concerned it certainly cannot be construed as a single-degree-of-freedom system. This clearly agrees with the experimental results.

The method of auxiliary functions developed in the paper obviously could be applied to many classes of vibration problems. Criteria based upon strain would then be available to check the assumption that a system is one of a single degree of freedom. Such a program would consist mainly of systematic computations of sets of functions.

The experimental results indicate that damping does not erase the higher modes in the period of time corresponding to the first quarter-cycle of the fundamental. This fact is considered to be of utmost importance in any mechanical shock problems. It indicates that protection by damping in very short intervals of time after a transient force is applied is far from being complete.

By theory it has been found that for a constant sinusoidal pulse the maximum strain decreases very sharply for increasing mass ratio. This conclusion is also in agreement with the experimental results.

Acknowledgments

The author wishes to acknowledge the sponsorship of the Office of Naval Research, Navy Department, Washington, D. C. He also wishes to express appreciation to Mr. Tse-Sun Chow for aid in computing the strain-time curves and especially to Mr. Joshua Greenspon, a graduate student, for considerable assistance with computations and with the experiments.

BIBLIOGRAPHY

1 "Mechanical Vibrations," by J. P. Den Hartog, McGraw-Hill Book Company, Inc., New York, N. Y., 1934, p. 137.

2 "The Impact of a Mass Striking a Beam," by E. H. Lee, JOURNAL OF APPLIED MECHANICS, Trans. ASME, vol. 62, 1940, p. A-129.

3 "Mathematical Methods in Engineering," by Th. von Kármán and M. A. Biot, McGraw-Hill Book Company, Inc., New York, N. Y., 1940, p. 290.

4 "Beam Vibrations With Time-Dependent Boundary Conditions," by R. D. Mindlin and L. E. Goodman, JOURNAL OF APPLIED MECHANICS, Trans. ASME, vol. 72, 1950, pp. 377–380.

5 "Sur les Vibrations d'un systeme quelconque de points materiels," by J. M. C. Duhamel, *Journal de l'École Polytechnique*, Cahiers 23, Paris, France, vol. 14, 1834, pp. 1–36.

6 "Solution de divers problemes de Mécanique . . . . ," by M. Phillips, *Journal de Mathematiques*, Paris, France, 2 sèrie, vol. 9, 1864, pp. 25–83.

7 "Vibration Problems in Engineering," by S. Timoshenko, second edition, D. Van Nostrand Company, Inc., New York, N. Y., 1937, p. 350.

8 "Impact of a Mass on a Damped Elastically Supported Beam," by W. H. Hoppmann, 2nd, JOURNAL OF APPLIED MECHANICS, Trans. ASME, vol. 70, 1948, pp. 125 and 128.

Large Plastic Deformations of Beams Under Transverse Impact[1]

By E. H. LEE[2] and P. S. SYMONDS,[3] PROVIDENCE, R. I.

A comparatively simple method of analysis is developed to determine the deformations in a beam subjected to lateral impact of such a magnitude that plastic strains large compared with elastic strains occur. A useful approximation to the motion then can be obtained by neglecting elastic strains and considering rigid-body motion of segments of the beam joined at plastic hinges where the entire deformation takes place. A method of analyzing such a situation is described and applied to a beam subjected to central impact. The approximate final permanent deformation is obtained; this includes deformation during application of the load, and plastic flow which continues afterward when the kinetic energy of the motion generated by the impact is transformed into additional plastic deformation. A criterion is given for conditions when this type of theory can be expected to provide a satisfactory analysis. The method of solution provides an interesting analogy to the concept of static determinacy which has been used in the analysis of quasi-static plastic-flow problems.

Introduction and Basic Assumptions

THE analysis given here represents an attempt to calculate the permanent deformation of a bar of ductile material subjected to a transverse impact force. It is shown that idealizations can be introduced which can be expected to yield a satisfactory approximation, with a comparatively simple method of analysis, for the case when the plastic strains produced are large compared with elastic strains.

The analysis is based on the assumption of a moment-curvature relation of the type shown in Fig. 1(*a*). This considers the beam to be rigid until the limit bending moment M_0 is reached, under which moment unrestricted bending can occur. Thus elastic strains are ignored, and we have what is usually termed a "plastic-rigid" theory in contrast to the corresponding elastic-plastic theory illustrated by *B* in Fig. 1(*b*). In general, it can be expected that the plastic-rigid assumption is a reasonable approximation to the behavior of an elastic-plastic material if large plastic strains occur, so that the initial elastic curvature is negligible in comparison with the total curvature. No general statement can be made concerning the comparison of solutions based on the two types of hypothesis, but in the few particular cases for which the elastic-plastic problem has been solved[4] the solution has been found to approach that based on the plastic-rigid theory as the maximum strain becomes appreciably larger than the elastic strains. According to this consideration, a criterion is detailed in the section Preliminary Results and Discussion, indicating in what circumstances the present analysis is likely to provide a satisfactory approximation. However, the assessment of the reliability of such an analysis must rest ultimately upon comparison either with tests, or with predictions of more complete elastic-plastic solutions when these can be developed.

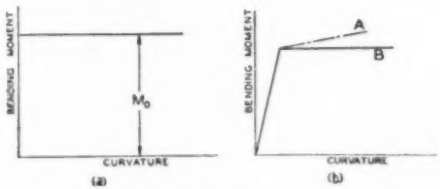

FIG. 1

The physical significance of the limit moment M_0 is that of the "fully plastic moment" of the plastic theory of quasi-static bending of beams. The moment M_0 corresponds to the spread of plastic regions over the whole cross section of the beam, with the fibers on one side of the neutral axis at the yield stress in tension and those on the other side at the yield stress in compression. M_0 usually can be taken equal to $\sigma_y Z_p$, where σ_y is the yield stress and Z_p the sum of the first moments of the upper and lower halves of the section area about the neutral axis. If strain hardening is neglected the quantity M_0 represents an upper limit which the bending moment approaches as the curvature increases indefinitely.[6] Thus finite changes of slope can occur in a very short segment of the beam so that the beam can take on a sharp kink at a section where the fully plastic moment is approached closely. A "plastic hinge" is said to occur at such a section and free rotations are allowed at the constant moment M_0. The present assumption, that the bar has an infinite rigidity at any section until the limit moment M_0 is reached there, after which arbitrarily large curvatures can occur, may appear unrealistic because the theoretical fully plastic moment is, in fact, only approached asymptotically. Thus sharp kinks and plastic hinges are only

[1] The suggestion of applying the approach adopted in this paper was made by W. Prager and some of the preliminary analytical work was carried out by W. W. Murray, both of Brown University. The results presented were obtained in the course of research conducted under Contract N7onr-35810 sponsored by the Office of Naval Research.

[2] Professor of Applied Mathematics, Brown University. Mem. ASME.

[3] Associate Professor of Engineering, Brown University. Mem. ASME.

Presented at the National Conference of the Applied Mechanics Division, State College, Pa., June 19–21, 1952, of THE AMERICAN SOCIETY OF MECHANICAL ENGINEERS.

Discussion of this paper should be addressed to the Secretary, ASME, 29 West 39th Street, New York, N. Y., and will be accepted until October 10, 1952, for publication at a later date. Discussion received after the closing date will be returned.

NOTE: Statements and opinions advanced in papers are to be understood as individual expressions of their authors and not those of the Society. Manuscript received by ASME Applied Mechanics Division, November 7, 1951. Paper No. 52—APM-21.

[4] References (1)[5] and (2) give examples of static stress and strain distribution problems, and similar consideration for a dynamic problem has recently been carried out by M. Conroy (3) at Brown University on the basis of the elastic-plastic solution for constant velocity impact on an infinite beam due to Duwez, Clark, and Bohnenblust (5).

[5] Numbers in parentheses refer to the Bibliography at the end of the paper.

[6] The relation shown in Fig. 1(*a*) can be considered as an approximation for a strain-hardening material, in which case M_0 is a suitable average moment based on the amount of plastic flow occurring. Such an approximation is satisfactory if the rate of strain hardening of the material is small.

approached, not strictly realized. However, despite their somewhat idealized nature, these concepts have been shown to provide powerful analytical methods which can be used to good advantage in predicting the statical loads on redundant beams and frames at which the deflection starts to increase at a much more rapid rate per unit load increment than at lower loads (4). A similar analysis can be applied to dynamic problems. The neglecting of elastic deformation eliminates the influence of elastic vibrations on the bending moment distribution. The present approximation is based on the assumption that if much larger curvatures occur than are possible in elastic vibrations, the error in replacing the elastic motion of each segment between yield hinges by rigid body motion will not be appreciable.

A method of analysis for constant velocity impact on an infinite beam of arbitrary bending moment-curvature relation has been given by Duwez, Clark, and Bohnenblust (5), and numerical examples evaluated for linear elastic and plastic relations as illustrated by A and B in Fig. 1(b). Attempts to extend this type of analysis to satisfy end conditions for beams of finite length have not as yet been successful, nor can the analysis deal with any type of impact other than that in which a constant velocity is imposed at one cross section. Moreover, the method only determines the behavior while the impact force is applied, and does not permit analysis of the motion after the impact load has been removed. The present analysis based on the more idealized plastic-rigid moment-curvature relation of Fig. 1(a), permits general impact on finite beams to be considered in a comparatively simple manner, including the motion after the impact force has ceased to act. To illustrate the theory the problem of a pulse of force applied at the mid-point of a uniform beam with free ends (Fig. 2) will be treated. The force pulse is assumed to have a triangular shape, as shown in Fig. 3. It is found that, owing to the kinetic energy of deformation generated during the impact, plastic flow continues, in general, after the magnitude of the applied force has returned to zero.

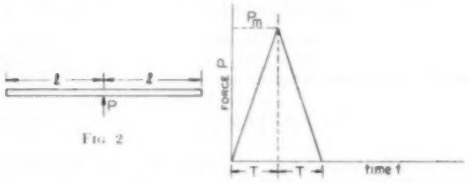

FIG. 2

FIG. 3

In the present problem of the bending of a plastic-rigid beam, if the positions and senses of relative rotation of plastic hinges are assumed, bending moments of magnitude M_0 and corresponding signs must occur at these points. Moreover, since M_0 is the largest magnitude of the moment which the beam can carry, the magnitude of the moment must have a (stationary) maximum value at a plastic hinge and so the shearing force must be zero if no external force acts there. Hence both the bending moment and shearing force are known at all plastic hinges. This enables the equations of motion for the rigid segments of the beam between the hinges to be written down. Thus the force interactions between rigid segments depend in a very simple way on the kinematics of the beam, and we obtain a force determinate situation. However, it is necessary to check that the velocities deduced from the equations of motion do maintain the existence of the assumed plastic hinges. If, for example, the relative angular velocity at a particular hinge falls to zero, and thus the hinge disappears, this hinge must be removed in the force analysis and a different force determinate set of equations obtained. Unfortunately, as is shown in the next section, this simple force determinacy permits direct calculation of the accelerations only if the plastic hinges are at rest, for otherwise the equations of motion contain a term involving the velocity of the hinge along the beam.

To illustrate the foregoing discussion in the case of the problem treated here, Fig. 2, the beam is assumed to move as a rigid body when the force is first applied, Fig. 4. The bending moments

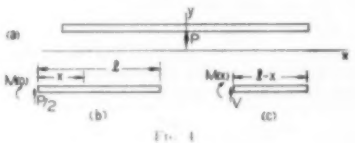

FIG. 4

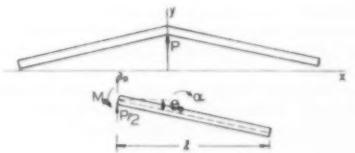

FIG. 5

METHOD OF ANALYSIS

The analysis of stress distributions in the theory of plasticity has been influenced largely by the concept of static determinacy, and while this concept has enabled the solution of many problems to be obtained, it also has led, when used incorrectly, to many erroneous solutions which have appeared in the literature (see reference 6 for a discussion of this question in the case of plane strain). Static determinacy is based on the combination of the yield condition for plastic flow with the equilibrium equations to determine the stress distribution without the consideration of displacements. However, since the yield condition does depend on the plastic flow taking place, in general it is necessary to consider the kinematics of the problem to insure that the statically determinate solution is compatible with plastic flow actually occurring, and it is the failure to make this check that has led to errors in the literature. A similar situation arises in the present analysis, but since we are concerned with the equations of motion rather than of equilibrium, we will term the concept "force determinacy."

corresponding to this rigid-body motion can be determined easily, and, if the bending moment is everywhere less in magnitude than M_0, the assumed kinematics is compatible with the bending moment-curvature relation, and the correct motion is obtained. With increasing force P, a value may be reached for which the analysis as given determines the limit moment magnitude M_0 at the center. Thereafter a plastic hinge must be assumed at the center, Fig. 5, the moment of magnitude M_0 is prescribed there, and the translational and angular accelerations of the two halves of the beam are determined directly from the equations of motion. The angular accelerations determine the relative angular velocity at the hinge and provide a check on its continued existence. Then the single hinge at the center will give the correct solution as long as the bending moment in the assumed rigid region does not exceed M_0.

If the force begins to decrease while only the central hinge exists, the relative angular velocity generated during the impact will maintain the existence of the hinge at force magnitudes less than that required to generate it. In fact, the hinge may persist even

after the force has dropped to zero. The corresponding equations of motion thus continue to apply even though the force magnitudes are those which initially determined rigid-body translation of the whole beam. Thus, although the system is force determinate at each stage, the particular equations to be used depend on the kinematics as well as the forces, so that both aspects must be taken into account. The continued rotation at plastic hinges after the impact force has decreased to zero represents absorption in plastic flow of the kinetic energy generated during the impact and causes increased deformation after the impact.

Dynamical Equations

Under the assumptions just discussed, as the force increases from zero its first effect is to cause a translation of the bar parallel to itself, Fig. 4. This initial translational motion is termed the "first phase" of the motion. The accelerations of all points of the bar are given by

$$a = \frac{P}{2ml} \quad [1]$$

The inertial forces in the bar produce shear forces and bending moments. Positive bending moments are defined as indicated in Fig. 4(*b*) and (*c*). In the first phase the constant acceleration has the effect of a uniformly distributed loading, and the bending moment is given by

$$M(x) = -\frac{m(l-x)^2}{2}\,a$$

where x is measured from the middle of the beam. The magnitude of the bending moment has a maximum at the middle of the beam, where the bending moment is

$$M(0) = -\frac{ml^2}{2}\,a = -\frac{Pl}{4} \quad [2]$$

This first phase of the motion ends when the central moment reaches the value $-M_0$. Thus when the load P reaches the value $4M_0/l$ the bar ceases to translate parallel to itself as the load is further increased.

It is convenient to introduce the symbol μ for the dimensionless combination Pl/M_0 which represents a loading parameter. Thus the first phase ends when μ attains the value

$$\mu \equiv \frac{Pl}{M_0} = 4 \quad [3]$$

The "second phase" of the motion commences when the central moment reaches the limit moment M_0. In this phase the two halves of the bar remain rigid but rotate with respect to each other, making the angle θ_0 with the horizontal, Fig. 5. Let a_0 denote the linear acceleration of the center of the bar, and $\alpha_0 = d^2\theta_0/dt^2$ denote the angular acceleration of the right-hand half, θ_0 being positive when the bar rotates clockwise. Assuming θ_0 to remain small, the equations of motion are

$$\frac{P}{2} = ml\left(a_0 - \frac{1}{2}\,l\alpha_0\right); \quad \frac{Pl}{4} - M_0 = \frac{ml^2}{12}\,\alpha_0 \quad [4]$$

Solving these for a_0 and α_0 we obtain

$$a_0 = \frac{M_0}{ml^2}\left(\frac{2Pl}{M_0} - 6\right) = \frac{M_0}{ml^2}\,(2\mu - 6) \quad [5]$$

$$l\alpha_0 = \frac{M_0}{ml^2}\left(\frac{3Pl}{M_0} - 12\right) = \frac{M_0}{ml^2}\,(3\mu - 12) \quad [6]$$

This second phase continues only so long as each half of the bar moves as a rigid body, which means under the present assumptions only so long as the bending moment at no further cross section reaches the magnitude M_0. In the second phase the bending moment at a section at a distance x from the middle of the beam is given by

$$M(x) = \frac{Px}{2} - M_0 - \frac{mx^2a_0}{2} + \frac{mx^2\alpha_0}{6} \quad [7]$$

It is a straightforward matter to find where the maximum value of $M(x)$ occurs. The maximum bending moment occurs at the point where $V = dM/dx = 0$, and is found by solving the quadratic equation

$$V = \frac{dM}{dx} = \frac{P}{2} - mxa_0 + \frac{mx^2\alpha_0}{2} = 0 \quad [8]$$

Inserting expressions for a_0 and α_0, the appropriate solution of Equation [8] is found to be

$$\frac{x}{l} = \frac{\mu}{3(\mu - 4)} \quad [9]$$

where μ is the loading parameter Pl/M_0. This value of x is substituted into Equation [7] to give the expressions for the maximum moment. Then the value of P at which the second phase terminates can be found by setting the expression for the maximum bending moment equal to M_0. This yields a cubic equation which is written most simply in terms of $\mu \equiv Pl/M_0$ as follows

$$2\mu^3 - 63\mu^2 + 432\mu - 864 = 0 \quad [10]$$

The only real root of Equation [10] is found to be

$$\mu = 22.9 \quad [11]$$

and from Equation [9] the cross section where the limit moment M_0 first occurs is found to be at a distance

$$x = 0.404l \quad [12]$$

Thus the second phase of the motion occurs while $\mu = Pl/M_0$ lies in the range

$$4 \leq \mu \leq 22.9 \quad [13]$$

During this phase each half of the bar acquires a certain angular velocity $\dot{\theta}_0$ and angular displacement θ_0. These quantities as well as the linear velocities and displacements are readily obtained by integration. The velocities and displacement magnitudes depend on the rate at which P increases with time, as will be discussed later; the accelerations, however, depend only on the instantaneous value of the force.

The "third phase" of the motion starts when the loading parameter μ reaches the value 22.9, corresponding to the limit moment M_0 being reached at a section $0.404l$ from the mid-point on either side of the mid-point. As the load is increased further, the limit moment M_0 occurs at sections slightly closer to the mid-point. In other words, the hinge point on either side moves toward the center as the load increases. This may not be evident immediately but is a consequence of the dynamical equations applying to the segments to right and left of the hinge, Fig. 6, together with the equation expressing kinematic conditions across the hinge point.

Consider an instant when the hinge is at a typical distance x_h, Fig. 6(*a*), from the center. An infinitesimal rotation occurs of the segment on one side of x_h with respect to that on the other as the hinge moves a distance dx_h. As soon as the hinge has moved to its new position, the moment at the original section at

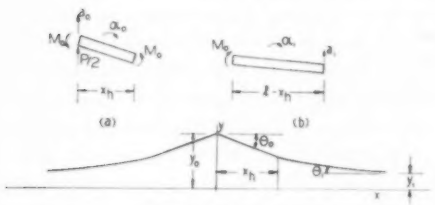

FIG. 6

x_h drops to a value below M_0 and no further rotation occurs there. To see this, consider the other alternative, namely, that in the region through which the hinge has moved the moment remains at the value M_0. This cannot occur since a region of constant moment must have zero shear, and this would be possible only with zero accelerations at all points in the region. Thus the segments to right and left of the hinge point move as rigid bodies. Although hinge action occurs as the moment reaches the value M_0 at successive sections, the relative rotations at each section are infinitesimal, and the slope angle changes continuously through the segment through which the hinge has passed. In fact, the curvature generated is equal to the relative angular velocity divided by the velocity of motion of the hinge along the beam.

We first write the kinematic equations at the hinge point. On physical grounds the transverse displacements must be continuous across this section, but it is not evident a priori that either velocities or accelerations are continuous. It is shewn in the Appendix that the velocities are continuous, but that the accelerations are discontinuous because the hinge point moves.

It is convenient to introduce notation appropriate to the actual type of motion, which for each half of the original bar is that of two rigid bars of length x_h, $l - x_h$, hinged (momentarily) at x_h. For the right-hand half of the bar we write[7]

$\omega_0 = \dot{\theta}(x < x_h)$ = angular velocity of segment to left of hinge
$\omega_1 = \dot{\theta}(x > x_h)$ = angular velocity of segment to right of hinge
$\alpha_0 = \ddot{\theta}(x < x_h)$ = angular acceleration of segment to left of hinge
$\alpha_1 = \ddot{\theta}(x > x_h)$ = angular acceleration of segment to right of hinge

Then the velocity and acceleration formulas, as derived in the Appendix, are as follows

$$x < x_h: \quad \dot{y} = \dot{y}_0 - \omega_0 x \qquad [14]$$

$$\ddot{y} = \ddot{y}_0 - \alpha_0 x \qquad [15]$$

$$x > x_h: \quad \dot{y} = \dot{y}_0 - \omega_0 x_h - \omega_1(x - x_h) \qquad [16]$$

$$\ddot{y} = \ddot{y}_0 - \alpha_0 x_h - \alpha_1(x - x_h) - \dot{x}_h(\omega_0 - \omega_1). \qquad [17]$$

It will be noted that the velocity is continuous across the hinge but that, in general, the acceleration is not.

We next write the equations of motion of the two segments to right and left of the hinge, free-body diagrams of which are shown in Fig. 6 (*a*) and (*b*). The force equations, for example, are derived by equating total force on each segment to the mass of the segment multiplied by its average acceleration; although the mass of the segment is changing, the transverse velocities are continuous at the hinge section so that increments of mass appear with the appropriate momentum. Denoting the accelerations at $x = 0$ and at $x = l$ by a_0 and a_1, respectively, the equations are

$$\frac{1}{2}P = mx_h\left(a_0 - \frac{1}{2}\alpha_0 x_h\right) \qquad [18]$$

$$\frac{1}{4}Px_h - 2M_0 = \frac{mx_h^2}{12}\alpha_0 \qquad [19]$$

$$0 = m(l - x_h)\left[a_1 + \frac{1}{2}\alpha_1(l - x_h)\right] \qquad [20]$$

$$M_0 = \frac{m(l - x_h)^2}{12}\alpha_1 \qquad [21]$$

The following additional relation between the quantities a_0, α_0, a_1, α_1, x_h is obtained from the kinematic conditions Equations [15] and [17]

$$(a_0 - \alpha_0 x_h) - [a_1 + \alpha_1(l - x_h)] = \dot{x}_h(\omega_0 - \omega_1) \qquad [22]$$

This expresses the fact that the acceleration just to the left of the hinge section exceeds that just to the right by the amount $\dot{x}_h(\omega_0 - \omega_1)$.

These equations can be simplified somewhat by introducing the dimensionless variables

$$\mu = \frac{Pl}{M_0}$$

$$\xi = \frac{x_h}{l}$$

Then Equations [18] to [21] can be rewritten as follows, expressing the accelerations as functions of μ and ξ

$$\frac{a_0}{l} = \frac{M_0}{ml^2}\left(\frac{2\mu}{\xi} - \frac{12}{\xi^2}\right) \qquad [23]$$

$$\alpha_0 = \frac{M_0}{ml^2}\left(\frac{3\mu}{\xi^2} - \frac{24}{\xi}\right) \qquad [24]$$

$$\frac{a_1}{l} = \frac{-M_0}{ml^2}\,\frac{6}{(1-\xi)^2} \qquad [25]$$

$$\alpha_1 = \frac{M_0}{ml^2}\,\frac{12}{(1-\xi)^3} \qquad [26]$$

$$\frac{M_0}{ml^2}\left[\frac{\mu}{\xi} - \frac{12}{\xi^2} + \frac{6}{(1-\xi)^2}\right] = -\dot{\xi}(\omega_0 - \omega_1) \qquad [27]$$

The solution of these equations is complicated by the presence of the term $-\dot{\xi}(\omega_0 - \omega_1)$ in Equation [27]. If this term were missing then we would have five simultaneous algebraic equations for the five unknowns a_0, α_0, a_1, α_1, and ξ. Thus μ and ξ would be related in a simple manner, and all the accelerations could be expressed easily in terms of ξ and thus implicitly in terms of μ. Then it would require only straightforward numerical quadratures to obtain the velocity and displacement values at any instant. The fact that the relation between μ and ξ actually involves unknown quantities $\dot{\xi}$, ω_0, and ω_1 means that the velocities and displacements are not obtainable by direct integration.

One method of successive approximations would start by setting the term $\dot{\xi}(\omega_0 - \omega_1)$ zero in Equation [27]. A first approximate solution would be obtained by solving Equations [23] to [27] with this condition. The resulting accelerations would be integrated numerically to yield $(\omega_0 - \omega_1)$ and $\dot{\xi}$, and this function $\dot{\xi}(\omega_0 - \omega_1)$ then would be inserted in Equation [27]. Again, the equations would be solved, yielding a new function $\dot{\xi}(\omega_0 - \omega_1)$. The process would be repeated until no appreciable change in $\dot{\xi}(\omega_0 - \omega_1)$ is produced by a further iteration.

Another method would be to use step-by-step integration of Equations [23] to [27]. Values μ_1 and ξ_1 at some time t_1 would be used to compute accelerations at this instant, from Equations [23] to [26]. The angular velocities then would be computed for

[7] Dots indicate differentiation with respect to time.

a time $t_2 = t_1 + \Delta t$, by writing, for example, $(\omega_b)_2 = (\omega_b)_1 + (\alpha_b)_1 \Delta t$. This would enable $(\omega_b - \omega_1)$ to be computed at t_2. Then Equation [27] would be solved by repeated trials to obtain values μ_2 and ξ_2 corresponding to time t_2. Having these, the accelerations at t_2 would be evaluated, and new computations of ω_b and ω_1 at time t_2 would be made, using for example, $(\omega_b)_2 = (\omega_b)_1 + \frac{1}{2}[(\alpha_b)_1 + (\alpha_b)_2]\Delta t$. After recomputation of ξ_2 and μ_2 the process would be repeated to obtain values at a new time $t_3 = t_2 + \Delta t$, and so forth.

Conditions When Load Is Decreasing

In the foregoing it was assumed that the force is increasing continuously. We now consider what happens after the force has reached the maximum value P_m, corresponding to $\mu_m = P_m l/M_0$. It is evident that the Equations [23] to [27] apply so long as the moment at an interior section retains the value M_0, i.e., so long as the free-body diagrams in Fig. 6 (a) and (b), are correct. In other words, they apply until the plastic hinge at $x = x_h$ disappears. It will be noted that as the force decreases the relative angular accelerations of a segment near the center with respect to a segment near the tip decreases and becomes negative, but there still will be, for a certain time after P starts to decrease, a positive angular velocity of one segment with respect to the other. The free-body diagrams in Fig. 6 must hold until this relative angular velocity is reduced to zero. This concludes the third phase of the motion. The time when this occurs will depend upon the maximum value of the load and the pulse duration time $2T$.

If the peak force is large enough, there still will be a relative angular velocity $\omega_b - \omega_1$ when the force has decreased from its peak value to zero. In this case the hinge point continues to move while the force is zero until the angular velocities are equalized. Then the outer hinges disappear, although further bending at the middle hinge point continues. The final position of the outer hinge in this case is obtained by solving Equation [27] with $\mu = 0$ and $\dot{\xi}(\omega_b - \omega_1) = 0$. The result is

$$\xi_{max} = 2 - \sqrt{2} = 0.586 \quad [28]$$

This gives the maximum distance from the center which the hinge attains, but it goes this far out only if the force decreases to zero before the angular velocity difference $\omega_b - \omega_1$ is absorbed. Fig. 7 shows the range of variation of the hinge position.

In the "fourth phase" there is no hinge action except at the mid-point. The free-body diagrams in Fig. 5 again are appropriate (it is assumed that deflections are sufficiently small so that the permanent distortions in the two halves of the bar do not affect this formulation). Eventually the angular velocity ω_b decreases to zero. Then the hinge action at the mid-point also ceases, and the bar thereafter translates as a rigid body, with no further deformation. The final plastic strain is then the permanent deformation caused by the impact.

Preliminary Results and Discussion

The exact determination of the accelerations and their integration to obtain velocities and displacements requires either a process of successive approximation or step-by-step numerical integration as discussed in the previous section. To indicate the general form of results, quantities specifying the final permanent deformation are shown in Figs. 8 and 9, computed according to Equations [25] to [27] with the term $\dot{\xi}(\omega_b - \omega_1)$ rejected in Equation [27]. Thus the results presented are correct prior to the formation of the second hinge and form a first approximation to the correct solution thereafter. In the region in which they represent a first approximation only, when the maximum force

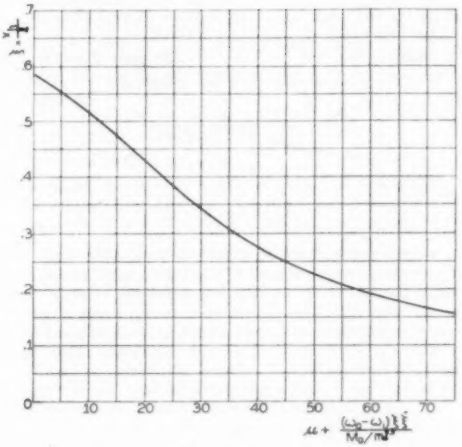

Fig. 7

P_m has a value such that $\mu_m = P_m l/M_0$ exceeds 22.9, the curves are shown dashed.

Fig. 8 shows the variation of the final deformation parameters, the central angle θ_0, and the relative displacement $y_0 - y_1$ between the mid-point of the beam and the tip, as functions of the maximum load parameter $P_m l/M_0$. These quantities are plotted nondimensionally, so that these results apply for arbitrary values of the length, mass, limit moment, and duration of impact. Thus for the same P_m, increase of the duration of impact $2T$ gives the same nondimensional parameters plotted but increased values for the actual quantities θ_0 and $(y_0 - y_1)$ in direct proportion to T^2.

Fig. 8 indicates that for forces less than that required to generate a second hinge, these two deformation parameters have the same value. With the appearance of the second hinge, curvature due to the second hinge in the opposite direction to that at the central hinge causes a reduction of the $(y_0 - y_1)$ parameter below the θ_0 parameter. The curves indicate only a small effect due to the second hinge until the maximum force P_m has increased considerably, and though in this region these curves are only a first approximation to the correct solution, this small difference indicates that the term omitted will be small, and the approximation thus can be expected to be a good one. Where the curves separate, the influence of the second hinge, and thus the term omitted from the analysis, can be expected to be appreciable.

Fig. 9 shows how one of the damage parameters, corresponding to θ_0, increases with time during and after the impact. The curves for $\mu_m = 12$, 20 are correct since only a central hinge is formed, but for $\mu_m = 24$, 30, and 38, they form an approximation once μ has exceeded 22.9 in the earlier part of the impact. It is seen that in all cases the angle of bend continues to increase after the end of impact, when the kinetic energy of distortion is absorbed in plastic flow. This enhanced plastic flow during unloading is seen to be more marked for higher values of μ, although these figures need to be confirmed when the exact solution is obtained.

It was stated in the first section that the type of analysis by which these results are obtained can be expected to supply a satisfactory approximation for the actual elastic-plastic problem if the final strains are large compared with elastic strains. A criterion based on this concept can be written down readily by

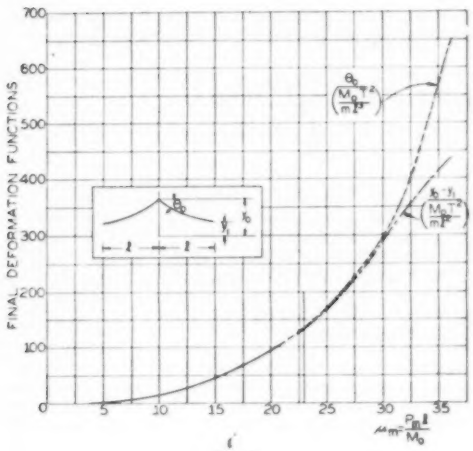

FIG. 8

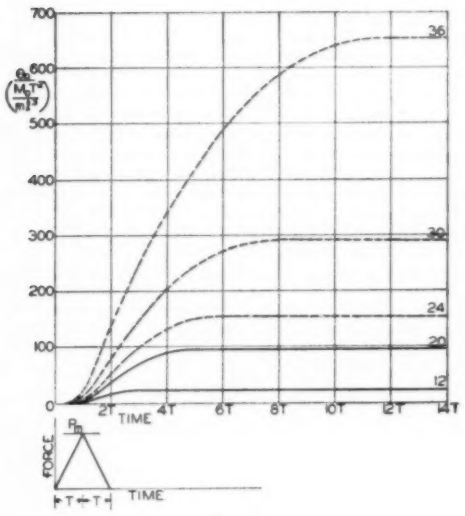

FIG. 9

requiring the plastic work done at the central hinge to be large compared with the maximum elastic energy which could be stored in the beam in bending when the whole beam is subject to the limit moment M_0. If this is so, then on the average over the whole length, plastic deformation will be large compared with any possible elastic deformations, and correspondingly larger than actual distributions of elastic bending strain during the motion of the elastic-plastic beam. This criterion is

$$M_0\theta_0 >> \frac{M_0 l}{2EI} \quad \ldots\ldots [29]$$

and this reduces to

$$\frac{\theta_0}{M_0T^2/ml^2} >> \frac{1}{2.5}\frac{\tau^2}{T^2} \quad \ldots\ldots [30]$$

where τ is the fundamental period of elastic vibration of the free-free beam. For a given beam and a given value of maximum force P_m, this sets a lower limit on the duration impact time T, above which the present analysis can be expected to give satisfactory results.

An additional obvious limitation is that the deformation must be sufficiently small for the usual small deflection beam theory to be applicable. Values of θ_0 up to, say, 10 deg presumably would involve reasonable approximations in this respect.

BIBLIOGRAPHY

1 "The Theory of Combined Plastic and Elastic Deformation With Particular Reference to a Thick Tube Under Internal Pressure," by R. Hill, E. H. Lee, and S. J. Tupper, Proceedings of the Royal Society, series A, vol. 191, 1947, pp. 278–303.

2 "General Features of Plastic-Elastic Problems as Exemplified by Some Particular Solutions," by R. Hill, JOURNAL OF APPLIED MECHANICS, Trans. ASME, vol. 71, 1949, pp. 295–300.

3 "Plastic-Rigid Analysis of Long Beams Under Transverse Impact Loading," by M. Conroy, Brown University Technical Report, A11-63, September, 1951.

4 "Recent Progress in the Plastic Methods of Structural Analysis," by P. S. Symonds and B. G. Neal, *Journal of The Franklin Institute*, vol. 252, 1951, pp. 383–407, 469–492.

5 "The Behavior of Long Beams Under Impact Loading," by P. E. Duwez, D. S. Clark, and H. F. Bohnenblust, JOURNAL OF APPLIED MECHANICS, Trans. ASME, vol. 72, 1950, pp. 27–34.

6 "The Theoretical Analysis of Metal-Forming Problems in Plane Strain," by E. H. Lee, JOURNAL OF APPLIED MECHANICS, Trans. ASME, vol. 74, 1952, pp. 97–103.

Appendix

CONTINUITY CONDITIONS AT TRAVELING HINGE

The analysis is based on the usual theory of small displacements. If y is the transverse displacement at a given (fixed) point x, then for small displacements y can be written as

$$y = y_0 - \int_0^x \theta(x')dx' \quad \ldots\ldots [31]$$

where y_0 is the displacement at the mid-point of the beam and $\theta(x)$ is the slope angle (positive if corresponding to clockwise rotation). Let $x_h(t)$ denote the distance of the hinge point from the beam center. Then for $x \leq x_h$ we obtain the transverse velocities by differentiation, thus

$$x \leq x_h: \quad \dot{y} = \dot{y}_0 - \int_0^x \dot{\theta}(x')dx' \quad \ldots\ldots [32]$$

where a dot indicates differentiation with respect to time. However, to find velocities for $x \geq x_h$ we must take account of the fact that the angular velocity $\dot{\theta}$ is discontinuous at the hinge point, so we must write

$$x \geq x_h: \quad y = y_0 - \int_0^{x_h} \theta\, dx' - \int_{x_h}^x \theta\, dx'$$

$$\dot{y} = \dot{y}_0 - \int_0^{x_h} \dot{\theta}\, dx' - \dot{x}_h\theta(x_h^-) - \int_{x_h}^x \dot{\theta}\, dx' + \dot{x}_h\theta(x_h^+). \quad [33]$$

Here x_h^- and x_h^+ designate sections just to the left and just to the right, respectively, of the hinge section. But the slope angle θ is continuous at the hinge, as was deduced in the section Dynamical Equations, hence the foregoing result reduces to

$$x \geq x_h: \quad \dot{y} = \dot{y}_0 - \int_0^{x_h} \dot{\theta}\, dx' - \int_{x_h}^x \dot{\theta}\, dx' \quad \ldots\ldots [34]$$

If we set $x = x_h$ in Equations [32] and [34], in both cases we have

$$x = x_h: \quad \dot{y} = \dot{y}_0 - \int_0^{x_h} \dot{\theta}(x')dx' \quad \ldots\ldots\ldots [35]$$

Thus the transverse velocity is continuous across the hinge section.

Differentiating Equations [32] and [34] again to obtain transverse accelerations, we obtain

$$x \leq x_h: \quad \ddot{y} = \ddot{y}_0 - \int_0^{x} \ddot{\theta}(x')dx' \quad \ldots\ldots\ldots [36]$$

$$x \geq x_h: \quad \ddot{y} = \ddot{y}_0 - \int_0^{x_h} \ddot{\theta}(x')dx' - \dot{x}_h\dot{\theta}(x_h^-) - \int_{x_h}^{x} \ddot{\theta}(x')dx' + \dot{x}_h\dot{\theta}(x_h^+) \ldots [37]$$

If x is put equal to x_h it is seen that the two formulas give different values for the acceleration at the hinge section; we have

$$\ddot{y}(x_h^-) = \ddot{y}_0 - \int_0^{x_h} \ddot{\theta}(x')dx' \quad \ldots\ldots\ldots [38]$$

$$\ddot{y}(x_h^+) = \ddot{y}_0 - \int_0^{x_h} \ddot{\theta}(x')dx' - \dot{x}_h[\dot{\theta}(x_h^-) - \theta(x_h^+)] \ldots [39]$$

Thus there is a discontinuity in the acceleration across the hinge. Equation [39] is equivalent to Equation [17] in the text.

The need for such a discontinuity can be seen alternatively by considering the relative displacement at x_h^- and x_h^+. The relative displacement must be zero for all time, so that all time derivatives must be zero. Expressing this in terms of partial derivatives with respect to x and t, shows that the discontinuity in angular velocity across the hinge implies a discontinuity in acceleration and curvature.

The Free Oscillation of the Centrifugal Pendulum With Wide Angles[1]

By F. R. E. CROSSLEY,[2] NEW HAVEN, CONN.

The pendulum torsional vibration absorber, designed usually in the bifilar form, has proved very effective in its purpose, especially in radial aircraft engines. The ordinary theory is based on an assumption of small angles of swing of the pendulum, and this assumption simplifies the equations of motion to linear form. However, wide angles of swing have actually been observed in most installations. Two previous analyses have been made of the wide angle swing, but have shown only the usual lengthening of the period due to wide swing of a gravity-controlled pendulum. Here it is demonstrated that the longer period due to wide angles will be offset by taking a heavier pendulum on a given carrier, for this shortens the period tremendously, as shown in Fig. 2.

THE motion of any type of centrifugal pendulum, be it swinging as in the bifilar types of Sarazin and Chilton, or rolling in an eccentric circular track, as in the puck type of Salomon, may be analyzed through the motion of its equivalent simple pendulum. To obtain the equivalence, certain relations between moments of inertia and mass, between relative velocities of rolling on a track and rotating around the carrier center have to be considered, but such is in theory a fairly elementary matter. These may be found in references (1, 7, 10).[3] Consequently in this paper only the simple pendulum is considered.

The pendulum is to be considered as a mass m, concentrated at the end of a simple pendulum of length L. This pendulum is mounted freely at a point on the carrier disk, at radius R from the center of rotation of the disk. Thus, when the carrier, which has moment of inertia I_c, rotates at a steady speed Ω, the moment of inertia of the system will be $I_c + m(R + L)^2$, for the pendulum will fly around radially outward.

We consider a varying torque applied to the carrier shaft, so that the position of the carrier is given by

$$\theta = \Omega t + \alpha \ldots\ldots [1]$$

where α is an angle of vibration, probably small. This will cause a change in the radially outward position of the pendulum, so that it makes an angle φ relative to the carrier. These dimensions are shown in Fig. 1.

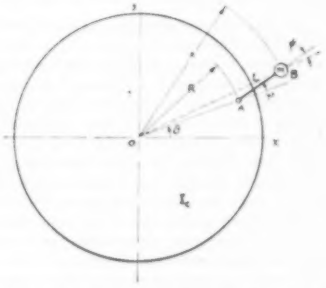

FIG. 1 SCHEMATIC DIAGRAM OF SIMPLE CENTRIFUGAL PENDULUM SYSTEM

MOTION WITH SMALL ANGLE SWING

When the angle φ is presumed small, the analysis of the motion is simple. A very full treatment of the design problems is given by Ker Wilson (1) both for "resonance" and "inertia" tuning, and a theoretical analysis is given by Den Hartog (2) and others (3, 4). Suffice it to say that for small angle φ, the circular frequency of motion of the pendulum is given by

$$\omega = \Omega \sqrt{R/L} \ldots\ldots [2]$$

so that if the exciting torque is of harmonic order n, that is, of frequency $\omega = n\Omega$, resonance will occur throughout the speed range provided

$$n = \sqrt{R/L} \ldots\ldots [3]$$

For this important ratio we use the symbol $a = \sqrt{R/L}$. The small angle φ is defined by Ker Wilson as preferably limited to ± 10 deg, but in no case allowed to exceed ± 20 deg. Steiglitz (5), however, allows ± 22 deg. The arguments are based upon the change in period of a pendulum in a gravity field, as it swings at wide angles.

DIFFERENTIAL EQUATIONS OF WIDE-ANGLE MOTION

These equations will be derived by the Lagrangian method, The square of the velocity of the particle m is

$$v^2 = (R\dot{\theta})^2 + L^2(\dot{\theta} + \dot{\varphi})^2 + 2RL\dot{\theta}(\dot{\theta} + \dot{\varphi})\cos\varphi \ldots [4]$$

Hence the kinetic energy of the system is

$$T = \frac{1}{2} I_c \dot{\theta}^2 + \frac{1}{2} m v^2 \ldots\ldots [5]$$

Now if we consider either that the force of gravity is small in comparison with the large centrifugal-force field, or that the carrier is rotating about a vertical axis, the potential energy of the system is at all times zero. There must be some external excitation in the form of a torque on the carrier to start an oscillation, but this will not continue in the case of a free vibration.

We apply the Lagrangian equation

---

[1] Most of this analysis was written in partial fulfillment of the requirements of the Yale School of Engineering for the degree of doctor of engineering.

[2] Assistant Professor of Mechanical Engineering, Yale School of Engineering, Yale University. Mem. ASME.

[3] Numbers in parentheses refer to the Bibliography at the end of the paper.

Presented at the National Conference of the Applied Mechanics Division, State College, Pa., June 19–21, 1952, of THE AMERICAN SOCIETY OF MECHANICAL ENGINEERS.

Discussion of this paper should be addressed to the Secretary, ASME, 29 West 39th Street, New York, N. Y., and will be accepted until October 10, 1952, for publication at a later date. Discussion received after the closing date will be returned.

NOTE: Statements and opinions advanced in papers are to be understood as individual expressions of their authors and not those of the Society. Manuscript received by ASME Applied Mechanics Division, December 14, 1951. Paper No. 52—APM-17.

$$\frac{d}{dt}\left(\frac{\partial T}{\partial \dot{q}}\right) - \frac{\partial T}{\partial q} = 0$$

where the obvious variables for the generalized co-ordinate q are θ and φ, and so obtain the two equations of motion

$$[I_e + m(R^2 + L^2 + 2RL\cos\varphi)]\ddot{\theta} + m(L^2 + RL\cos\varphi)\ddot{\varphi} - mRL\sin\varphi\,(2\dot{\varphi}\dot{\theta} + \dot{\varphi}^2) = 0 \quad [6]$$

$$mL^2\ddot{\varphi} + mL(L + R\cos\varphi)\ddot{\theta} + mRL\dot{\theta}^2\sin\varphi = 0 \quad [7]$$

Now two previous analyses of this have been published. Den Hartog (6) uses the d'Alembertian approach, so that his equations appear different.[4] Porter[5] has the same equations.

However, in both these papers it is assumed that it is possible to reduce the carrier motion to steady rotation, as appeared in the small angle approximation. As a result, in Equation [7] the middle term drops out and there remains the ordinary equation of a pendulum with solution in elliptic functions. Both then substitute this answer in Equation [6], to find an externally applied torque which will be necessary to justify their assumption of steady rotation. Of course this involves an exact ratio of amplitudes of a series of torque harmonics, and it is unlikely that any engine will understand and comply!

Porter also makes the analysis allowing the carrier to have a simple harmonic oscillation superimposed on steady rotation.[6]

We proceed here without any assumption of θ, to find the natural period of the free oscillation, and hope later in a sequel paper to describe the forced steady-state vibration.

Solution of the Equations

In the derivation of Equations [6] and [7] there appears no term in θ in either Equation [4] or [5] so that θ becomes an ignorable co-ordinate. Therefore Equation [6] may be integrated at once, giving the expression (the integral of momentum)

$$[I_e + m(R^2 + L^2 + 2RL\cos\varphi)]\dot{\theta} + m(L^2 + RL\cos\varphi)\dot{\varphi} = \text{const} \quad [8]$$

Instead of using Equation [7] as the second equation, we prefer the energy equation (Equation [5] with Equation [4]). Then let there be introduced the following constants

$$a^2 = R/L$$

(as already suggested)

$$\beta = \frac{I_e + mR^2 + mL^2}{2mRL} \quad [9]$$

c and d, as constants of (reduced) momentum and energy.

Then Equations [5] and [8] become much more simply expressed

$$a^2(\beta + \cos\varphi)\dot{\theta} + 1/2(1 + a^2\cos\varphi)\dot{\varphi} = c \quad [10]$$

$$a^2(\beta + \cos\varphi)\dot{\theta}^2 + (1 + a^2\cos\varphi)\dot{\theta}\dot{\varphi} + 1/2\,\dot{\varphi}^2 = d \quad [11]$$

Certain values of these constants c and d must be reckoned in order to proceed. It is seen that at the instant φ is a maximum, call it φ_0, then $\dot{\varphi} = 0$ and thus there must occur together

$$\left.\begin{aligned} \varphi &= \varphi_0 \\ \dot{\varphi} &= 0 \text{ and } \dot{\theta} = \dot{\theta}_0 \end{aligned}\right\} \quad [12]$$

(which may be positive or negative).

By common sense, it is obvious that $\dot{\theta}_0$ is approximately equal to Ω, the constant mean speed of the carrier. It will be shown later how it varies from Ω by some even-valued harmonics. We then have for the constants

$$\left.\begin{aligned} c &= a^2\dot{\theta}_0(\beta + \cos\varphi_0) \\ d &= a^2\dot{\theta}_0^2(\beta + \cos\varphi_0) = c\dot{\theta}_0 \end{aligned}\right\} \quad [13]$$

We eliminate $\dot{\theta}$ between Equations [10] and [11], obtaining

$$\dot{\varphi}^2(1 - e^2\cos^2\varphi) = 2\omega^2(\cos\varphi - \cos\varphi_0) \quad [14]$$

where

$$\left.\begin{aligned} e^2 &= \frac{mR^2}{I_e + mR^2} \\ \omega^2 &= 2e^2\dot{\theta}_0^2(\beta + \cos\varphi_0) \end{aligned}\right\} \quad [15]$$

Note in connection with these introduced constants that e^2 is always less than unity, and that in the case of small angle φ_0 and large carrier I_e

$$\omega \to a\Omega$$

Equation [14] may be integrated, but not in terms of simple functions (unless perhaps a Fourier series). The integral is in fact an inverse hyperelliptic function

$$\sqrt{2}\,\omega(t - t_0) = \int \sqrt{\frac{1 - e^2\cos^2\varphi}{\cos\varphi - \cos\varphi_0}}\,d\varphi \quad [16]$$

where the limits on the integral correspond to any chosen initial position when $t = t_0$, and any subsequent φ at t. The solution of this integral has been presented by the author, and some curves of these hyperelliptic functions have been drawn (9). In that paper it is shown that Equation [14] occurs also in an analogous motion—the motion of a particle oscillating freely in a vertical plane, on the path of an ellipse of eccentricity e. But in Equation [16] when $\varphi = \varphi_0$ the integrand becomes infinite in value, and to avoid this a substitution is made of a variable ζ

$$\sin\varphi/2 = k\sin\zeta \quad [17]$$

where

$$k = \sin\varphi_0/2$$

With this and $t_0 = 0$ and the lower limit of the integral $\varphi = 0$, Equation [16] is written as the hyperelliptic integral L with the two parameters e and k

$$\omega t = L(e, k, \zeta) \quad [18]$$

This is then inverted, and ζ is written as the hyperelliptic amplitude of ωt. With Equation [17] φ can be expressed in terms of the sine of the hyperelliptic amplitude "sham" or

$$\sin\varphi/2 = k\,\text{sham}\,\omega t \quad [19]$$

This is the solution of Equation [14]. The meaning of this solution written in these terms is amplified in the previous paper (9). It is plain that the curve of the function φ is of periodic form with limits $\pm\varphi_0$. But of particular interest is the period.

It is plain from the integral, Equation [16], that for the case $e = 0$ the motion may be expressed in elliptic functions, and the period thus increases with the parameter k. This is also true for all values of e.

However, the factor that has been overlooked by those who have studied this motion before (6, 7) is that the period is decreased by increase of the moment of inertia ratio e. The two effects on the period are shown in Fig. 2 which gives the period T_φ at any amplitude φ_0 as a ratio to the period T_0 of the small angle motion ($k = 0$, $e = 0$)

[4] However, if in this Equation [6] the first term is changed to

$$[I_e + m(L + R\cos\varphi)^2 + mR^2\sin^2\varphi]\ddot{\theta}$$

and then Equation [7] is multiplied by $(1 + R/L\cos\varphi)$ and subtracted from the foregoing Equation [6], the agreement is shown.

[5] Bibliography (7), p. 353.

[6] Ibid., pp. 322–323

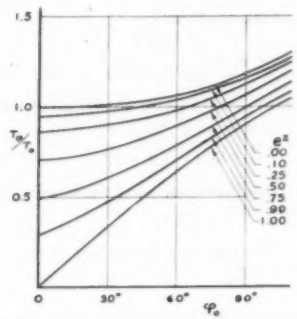

FIG. 2 RATIO OF PERIOD WITH WIDE-ANGLE MOTION OF AMPLITUDE φ_0 TO PERIOD OF SMALL-ANGLE SWING FOR THE CASE $a = 4$

The origins of the lines in Fig. 2 with different e can be seen by setting $k = 0$ in Equation [16] after substituting ζ by Equation [17]. Then the period is

$$T_\varphi = \frac{4}{\omega}\int_0^{\pi/2} \sqrt{1 - e^2}\, d\zeta$$

$$T_\varphi/T_0 = \sqrt{1 - e^2} \quad \text{for} \quad k = 0 \ldots\ldots\ldots [20]$$

As an example of the use of Fig. 2 in the design of a pendulum torsional vibration absorber for resonance, suppose it is desired to find the length of a pendulum for fourth-order "damping" with radius of mounting $R = 2$ in.:

(*a*) By small-angle theory $\sqrt{R/L} = 4$ or $L_0 = 0.125$ in.

(*b*) Assuming a swing of 20 deg amplitude and $e^2 = 0.1$ (i.e., if $I_c = 27$ lb-in.^{2}, $mR^2 = 3.0$ lb-in.^{2}) from the graph, $T\varphi = 0.958\ T_0$ approximately; thus frequency will be $a\Omega/0.958 = 1.044\ a\Omega$. which means we must find a length L such that for resonance

$$1.044a = 1$$
$$R/L = (0.958 \times 4)^2$$

$L = 0.136$ in., or 9 per cent more than the foregoing.

FREE MOTION OF CARRIER

Having found the motion of the pendulum, we should be able to substitute this in one of the equations of motion, and solve for θ. However, since the equation for φ is not very pliable, we shall follow another course. Let us presume a new variable η which gives the relation with φ as

$$a^2(\beta + \cos\varphi)\dot{\eta} + 1/2(1 + a^2\cos\varphi)\dot{\varphi} = 0 \ldots\ldots [21]$$

By observing that the only difference between this and Equation [10] is that $c = 0$, it is plain that η would be the angle of the carrier if it were oscillating against the pendulum, but not rotating at all. In Equation [21] the variables may be separated

$$\eta = -\frac{1}{2a^2}\int \frac{1 + a^2\cos\varphi}{\beta + \cos\varphi}\, d\varphi$$

$$= -\frac{\varphi}{2} + \frac{\beta - 1/a^2}{\sqrt{\beta^2 - 1}} \tan^{-1}\left(\frac{\sqrt{\beta^2 - 1}}{\beta + 1}\tan\varphi/2\right) \ldots [22]$$

for $\pi > \varphi > -\pi$. So that, if the constant of integration is assumed zero, we take the definition of η as

$$\tan\frac{\sqrt{\beta^2 - 1}}{\beta - 1/a^2}(\eta + \varphi/2) = \sqrt{\frac{\beta - 1}{\beta + 1}}\tan\varphi/2 \ldots [23]$$

Let us consider the value of these two coefficients; β is defined in Equation [9] and is usually large; if the maximum likely range of values in any design is probably

$$\left.\begin{array}{c} 40 > I_c/mR^2 > 0.2 \\ 2 \leq a \leq 12 \\ 2.5 < \beta < 3000 \end{array}\right\} \ldots\ldots\ldots\ldots [24]$$

then

In most cases the term $1/a^2$ is small compared with β (see Appendix, Table 1), so on that basis compare the following:

β	$\dfrac{\sqrt{\beta^2 - 1}}{\beta}$	$\sqrt{\dfrac{\beta - 1}{\beta + 1}}$
2	0.866	0.577
4	0.968	0.775
9	0.993	0.894
25	0.99920	0.96077
60	0.99986	0.98347

We divide the subsequent analysis into two cases; for values of β more than 80 (or thereabout), and for values less than 80, but not less than 10, as follows:

Case 1: $\beta > 80$. In this range the two coefficients are so nearly equal to each other and to unity, that Equation [22] can produce no more than a minute angle η (see Equation [28]), which appears as a small difference between two large numbers.

Case 2: $10 < \beta < 80$. Here a small but distinct difference is apparent in the two coefficients in the table. Except for the lowest values of β, we may, however, with slight approximation set

$$\frac{\sqrt{\beta^2 - 1}}{\beta - 1/a^2} = 1$$

while noting

$$\sqrt{\frac{\beta - 1}{\beta + 1}}$$

is nearly unity but not as closely. Equation [23] becomes approximately

$$\tan(\varphi/2 + \eta) = \sqrt{\frac{\beta - 1}{\beta + 1}}\tan\varphi/2 \ldots\ldots [25]$$

η is obviously still an exceedingly small angle.

If the reader is familiar with Landen's transformation for evaluating elliptic integrals (8), a means of trigonometric simplification of this equation will be patent.

Write the equation in the form

$$\tan(\varphi/2 + \eta) = \frac{\lambda - 1}{\lambda + 1}\tan\varphi/2$$

where

$$\lambda = \beta + \sqrt{\beta^2 - 1} = 2\beta \ldots\ldots [26]$$

Then

$$\lambda[\tan(\varphi/2 + \eta) - \tan\varphi/2] = -[\tan\varphi/2 + \tan(\varphi/2 + \eta)]$$
$$\lambda[\sin(\varphi/2 + \eta)\cos\varphi/2 - \sin\varphi/2\cos(\varphi/2 + \eta)]$$
$$= -[\sin\varphi/2\cos(\varphi/2 + \eta) + \sin(\varphi/2 + \eta)\cos\varphi/2]$$

$$\lambda\sin\eta = -\sin(\varphi + \eta)$$

or

$$\lambda\tan\eta = -(\sin\varphi + \cos\varphi\tan\eta)$$

finally

$$\tan\eta = -\frac{\sin\varphi}{\lambda + \cos\varphi} \ldots\ldots [27]$$

Since η is so small, where $\beta >> 1/2 \cos \varphi$, this may be written closely

$$\eta \approx -1/\lambda \sin \varphi \approx -\frac{1}{2\beta} \sin \varphi \quad \ldots\ldots\ldots\ldots [28]$$

A few comparisons between this result and the actual values from Equation [22] are given in the Appendix, Table 2.

Having found η, we return to the two Equations [10] and [21], which are subtracted, giving

$$a^2(\beta + \cos \varphi)(\dot{\theta} - \dot{\eta}) = c \quad \ldots\ldots\ldots\ldots [29]$$

Now substituting $\dot{\theta} = \Omega + \dot{\alpha}$ and using the value found for c

$$(\beta + \cos \varphi)(\dot{\alpha} - \dot{\eta}) = (\beta + \cos \varphi_0)\dot{\theta}_0 - (\beta + \cos \varphi)\Omega \ldots [30]$$

Case (1): $\beta > 80$, giving $\beta + \cos \varphi \approx \beta$. If we allow that $\theta_0 \approx \Omega$, this yields immediately

$$\alpha = \eta \quad \ldots\ldots\ldots\ldots [31]$$

and the relation to φ must be solved through Equation [22] unless Equation [28] is judged adequate.

Case (2): With β not so large, Equation [29] may be integrated for

$$\theta - \eta = \frac{c}{a^2} \int \frac{dt}{\beta + \cos \varphi} + \delta_1$$

where δ_1 is an arbitrary constant. The integrand is expanded as a binomial series in ζ (defined in Equation [17])

$$\theta - \eta = \frac{c}{a^2\beta} \int \frac{dt}{1 \pm \frac{1}{\beta}(1 - 2k^2 \sin^2 \zeta)} + \delta_1$$

$$= \frac{c}{a^2(\beta \pm 1)} \int \left(1 \pm \frac{2k^2}{\beta + 1} \sin^2 \zeta \pm \frac{4k^4}{(\beta + 1)^2} \sin^4 \zeta + \ldots\right) dt + \delta_1$$

The $\pm$ signs take care of the possible phases of 0 and π between φ and α.

Now by Equations [17] and [19], $\sin \zeta = \text{sham } \omega t$. But the meaning of integrals such as

$$\int \text{sham}^3\, \omega t\, dt$$

has not been investigated. However, it is obvious that if sham ωt is expressed as a Fourier sine series, such integrals will yield periodic terms of even-valued harmonics and, therefore, we may write

$$\theta - \eta = \Omega t + \alpha - \eta = \frac{c}{a^2(\beta \pm 1)} [(1 \pm \delta_2)t + (\text{periodic terms})] + \delta_1 \quad \ldots\ldots\ldots\ldots [32]$$

where δ_2 is a constant arising from the integration of the terms in $\text{sham}^n\, \omega t$, and where δ_1 is arbitrary, and in this case zero.

By definition α and η cannot contain anything but periodic terms, hence the linear terms in t must cancel, or

$$\Omega = \frac{c(1 \pm \delta_2)}{a^2(\beta \pm 1)}$$

which defines $\dot{\theta}_0$ through Equations [13] as

$$\dot{\theta}_0 = \left(\frac{\beta \pm 1}{\beta + \cos \varphi_0}\right) \frac{\Omega}{1 \pm \delta_2} \quad \ldots\ldots\ldots\ldots [33]$$

where δ_2 is the very small quantity given approximately by

$$\delta_2 = \frac{k^2}{\beta + 1} + \frac{2k^4}{(\beta + 1)^2} + \ldots\ldots\ldots$$

So finally the oscillating motion of the carrier is related to that of the pendulum by

$$\alpha = \eta + \frac{k^2}{2(\beta \pm 1)} (\text{second and higher even-valued harmonics}) \quad \ldots\ldots\ldots\ldots [34]$$

showing that in any case Equation [28] or [22] gives a very close approximation for α.

BIBLIOGRAPHY

1 "Practical Solution of Torsional Vibration Problems," by W. Ker Wilson, John Wiley & Sons, Inc., New York, N. Y., second edition vol. 2, 1941, p. 512 seq.

2 "Mechanical Vibrations," by J. P. Den Hartog, McGraw-Hill Book Company, Inc., New York, N. Y., third edition, 1948, p. 273.

3 "Crankshaft Torsional Vibration in Radial Aircraft Engines," by E. S. Taylor, *SAE Journal*, vol. 31, 1936, p. 81.

4 "Advanced Dynamics," by S. Timoshenko and D. H. Young, McGraw-Hill Book Company, Inc., New York, N. Y., 1948, pp. 313–314.

5 "Beeinflussung von Drehschwingungen durch Pendelnde Massen," by A. Steiglitz, *Jahrbuch der Deutschen Luftfahrtforschung*, vol. 2, 1938, p. 164. An English translation in NACA Technical Memo. No. 1035, 1942.

6 "Tuned Pendulums as Torsional Vibration Eliminators," by J. P. Den Hartog in S. Timoshenko 60th Anniversary Volume, The Macmillan Company, New York, N. Y., 1938, pp. 23–26.

7 "The Centrifugal Pendulum Dynamic Damper," by F. P. Porter, in "Evaluation of Effects of Torsional Vibration," SAE War Eng. Board, New York, N. Y., 1945, p. 269 seq.

8 "On the Direct Numerical Calculation of Elliptic Functions and Integrals," by L. V. King, University Press, Cambridge, 1924.

9 "Hyperelliptic Function as a Nonlinear Oscillation," by F. R. E. Crossley, *Journal of Mathematics and Physics*, vol. 30, 1952, p. 214.

10 "The Elements of Pendulum Dampers," by R. W. Zdanowich and T. S. Wilson, Proceedings of The Institute of Mechanical Engineers, London, England, vol. 143, pp. 182–210.

Appendix

Table 1 is included, giving values of β for various a and e-values, so that the reader may judge the effect of the approximations suggested in this paper, that either $\beta >> \cos \varphi$ or $\beta \approx a^2/2e^2$ where

$$\beta = \frac{I_c + mR^2 + mL^2}{2mRL} = \frac{1}{2}\left(\frac{a^2}{e^2} + \frac{1}{a^2}\right)$$

$$a^2 = R/L$$

$$e^2 = \frac{mR^2}{I_c + mR^2}$$

TABLE 1 VALUES OF β

e^2	$a = 2$	4	6	8	10
0.05	40.125	160.031	360.014	640.008	1000.005
0.10	20.125	80.031	180.014	320.008	500.005
0.25	8.125	32.031	72.014	128.008	200.005
0.50	4.125	16.031	36.014	64.008	100.005
0.90	2.347	8.920	20.014	35.563	55.561
$\frac{1}{2a^2}$ =	0.125	0.031	0.014	0.008	0.005

TABLE 2 SHOWING EFFICACY OF APPROXIMATION FOR η*

Case 1 $\beta = 16.03125$	φ_0 deg	$-\eta$ *	$\frac{\sin \varphi_0}{\lambda}$	Error, per cent
$a = 4$ $\lambda = 32.03128$	10	0.00542	0.00542	−0.0
$\sqrt{\frac{\beta-1}{\beta+1}} = 0.9394513$	30	0.01567	0.01560	−0.4
	50	0.02425	0.02392	−1.4
$\frac{\beta-1/a^2}{\sqrt{\beta^2-1}} = 0.9980450$	70	0.03011	0.02934	−2.6
	90	0.03268	0.03122	−4.5
Case 2 $\beta = 40.1250$	φ_0 deg	$-\eta$	$\frac{\sin \varphi_0}{\lambda}$	Error, per cent
$a = 2$ $\lambda = 80.23754$	10	0.00264	0.00216	−18.2
$\sqrt{\frac{\beta-1}{\beta+1}} = 0.9753808$	30	0.00768	0.00623	−18.9
	50	0.01200	0.00955	−20.4
$\frac{\beta-1/a^2}{\sqrt{\beta^2-1}} = 0.9940782$	70	0.01521	0.01171	−23.0
	90	0.01704	0.01246	−26.9
Case 3 $\beta = 55.560555$	φ_0 deg	$-\eta$	$\frac{\sin \varphi_0}{\lambda}$	Error, per cent
$a = 10$ $\lambda = 111.1121$	10	0.00155	0.00156	+0.6
$\sqrt{\frac{\beta-1}{\beta+1}} = 0.9821607$	30	0.00447	0.00450	+0.7
	50	0.00686	0.00689	+0.4
$\frac{\beta-1/a^2}{\sqrt{\beta^2-1}} = 0.9999820$	70	0.00844	0.00846	+0.2
	90	0.00901	0.00900	−0.1
Case 4 $\beta = 360.0139$	φ_0 deg	$-\eta$	$\frac{\sin \varphi_0}{\lambda}$	Error, per cent
$a = 6$ $\lambda = 720.0266$	10	0.00013	0.00024	+84.6
$\sqrt{\frac{\beta-1}{\beta+1}} = 0.9986102$	30	0.00037	0.00069	+86.4
	50	0.00061	0.00106	+73.8
$\frac{\beta-1/a^2}{\sqrt{\beta^2-1}} = 0.9999264$	70	0.00070	0.00131	+87.1
	90	0.00075	0.00139	+85.3

* η is recorded in radians:
0.00029 radians = 0° 1′
0.01745 radians = 1° 0′

NOTE: Column 2 shows the calculation through Expression [22], while column 3 shows the approximation of Equation [28].

The larger percentage errors occur (*a*) in the last case with too large a value of β, where η occurs as the small difference of two large numbers; (*b*) in case (2) where a small value of a has made the item $1/a^2$ significant in reducing the value of the second factor to 0.994078.

Correlation of Creep Properties by a Diffusion Analogy[1]

By LEON GREEN, JR.,[2] DOWNEY, CALIF.

The necessity of atom movements for both creep and self-diffusion suggests a method of correlating the constant-stress creep properties of pure metals. The concept of steady-state creep is discarded, and two empirical approximations for the strain-time behavior of pure polycrystalline metals lead to a creep equation defining an activation energy as the only undetermined constant. For cases where the orientation of individual crystals is important, a second constant is required. Application of this equation to published creep data effects a correlation which indicates that the apparent activation energies observed for creep and self-diffusion show a similar temperature dependence. The effect of stress upon the activation energy for several metals is described approximately, but the need for further experiments encompassing lower values of stress is revealed. The qualitative effects of impurities, grain size, cold-working, and surface conditions upon creep as predicted by a diffusion analogy are found to be in agreement with experimental results, but it is noted that the analogy does not hold if creep deformation is obtained as a result of slip.

Introduction

IN most investigations of the creep of metals at elevated temperatures, the data are correlated in terms of an activation energy defined by rate theory (1)[3]

$$\text{rate} \sim e^{-\frac{Q}{RT}} \qquad [1]$$

where Q is the activation energy, R is the gas constant, and T is the absolute temperature. When applied to the process of plastic flow, rate theory is normally introduced by the assumption that

$$d\epsilon/dt = ke^{-\frac{Q}{RT}} \qquad [2]$$

where ϵ is usually taken as conventional "engineering" strain, and k is an empirical constant. This substitution is equivocal, since a typical constant-load creep curve exhibits regions of different creep behavior, as shown in Fig. 1, which have been termed primary, secondary (or steady-state), and tertiary creep.

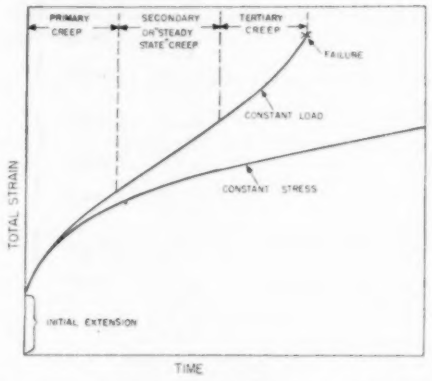

FIG. 1 TYPICAL CREEP CURVES OBTAINED UNDER CONSTANT LOAD AND CONSTANT STRESS
(After Andrade, reference 2.)

Application of Equation [2] thus invites use of the secondary creep rate to determine the activation energy. The classical experiments of Andrade (2), however, demonstrate that a creep curve for the case of constant stress does not exhibit the steady-state region of minimum creep rate, but that the rate decreases continuously, and suggests that the distinction between primary and secondary creep is a fictitious one depending upon an arbitrary choice of time scale (3). The significance of an activation energy based upon a secondary minimum-rate region artificially created by a gradual stress increase is thus questionable. Application of Equation [2] to a constant-stress curve, on the other hand, requires either the introduction of another empirical constant or that the activation energy increase markedly with increasing time, an increase which is difficult to explain.

A usual feature of the strain-rate approach is that the temperature dependence of the activation energy is not mentioned. Since the quantity

$$\frac{\partial\left[\ln\left(\frac{d\epsilon}{dt}\Big/k\right)\right]}{\partial\left[\frac{1}{T}\right]} = -\frac{Q}{R} \qquad [3]$$

is roughly constant over the limited temperature range of most creep experiments, the temperature effect is ordinarily obscured. That the slope given in Equation [3] is not necessarily constant over an extended temperature range, however, has been noted by Malmstrom, Keen, and Green (4). The thermal dependence of the apparent activation energy observed for self-diffusion in metal specimens, on the other hand, is well known, and regimes where lattice, grain-boundary, or surface movements of the atoms predominate have been delineated roughly. Since the creep of a metal under stress also requires atom movements, it would seem

---

[1] This paper is based on studies conducted for the Atomic Energy Commission under Contract AT-11-1-GEN-8.

[2] Atomic Energy Research Department, North American Aviation, Inc. Present address: Aerojet Engineering Corporation, Azusa, Calif. Jun. ASME.

[3] Numbers in parentheses refer to the Bibliography at the end of the paper.

Presented at the National Conference of the Applied Mechanics Division, State College, Pa., June 19–21, 1952, of THE AMERICAN SOCIETY OF MECHANICAL ENGINEERS.

Discussion of this paper should be addressed to the Secretary, ASME, 29 West 39th Street, New York, N. Y., and will be accepted until October 10, 1952, for publication at a later date. Discussion received after the closing date will be returned.

NOTE: Statements and opinions advanced in papers are to be understood as individual expressions of their authors and not those of the Society. Manuscript received by ASME Applied Mechanics Division on November 2, 1951. Paper No. 52—APM-22.

that the apparent activation energy for creep should show an analogous thermal dependence. The empirical approach, however, does not require specification of a particular mode of atom motion, such as the specialized mode required for movement of dislocations, or lattice imperfections, which have been envisaged in many fruitful theoretical studies of the problem of plastic deformation.

Apparently creep was first conceived as a self-diffusion process by Kanter (5), who employed the steady-state concept. Herring (6) has discussed a mechanism of creep by volume diffusion (Fig. 2) which may become predominant at temperatures near the melting point. In this case the strain would be manifested in migration of the grain boundaries and changes in grain shape. At

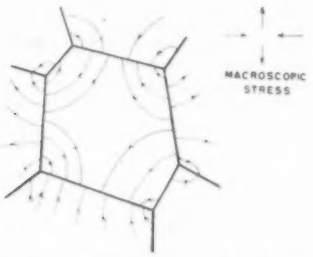

FIG. 2 TYPICAL GRAIN OF POLYCRYSTALLINE SOLID, SHOWING THE (VOLUME) SELF-DIFFUSION CURRENTS TO BE EXPECTED WHEN SOLID IS SUBJECTED TO STRESS
(From Herring, reference 6.)

lower temperatures the atom motion would be localized at the grain boundaries, where movements of the relatively rigid grains would produce boundary thickening. Creep at still lower temperatures might require dislocation activity and presumably would involve slip, a sudden movement of relatively large scale which cannot be considered in the correlation proposed in the following. As mentioned earlier, however, the present empirical approach, in general, will be content with a macroscopic point of view and does not have to specify which of the possible contributing mechanisms is predominant on the microscopic scale.

BASIC ASSUMPTIONS

The basis for the proposed correlation is the assumption that for creep at constant stress and temperature

$$\epsilon = \ln \frac{l}{l_0} = f\left(\frac{t}{\tau}\right) \quad [4]$$

(where l = length of specimen at time t after stress application; l_0 = length of specimen immediately after stress application; τ = a time parameter characteristic of the material under the prevailing conditions of stress and temperature). By analogy with the case of self-diffusion, the "relaxation" time may be represented as

$$\tau = \frac{d^2}{2D} \quad [5]$$

(where d = jump distance for a migrating unit; D = a quantity with the dimensions of diffusivity). Introducing rate theory for description of the "diffusion" constant

$$D = D_0 e^{-\frac{Q}{RT}} \quad [6]$$

(where D_0 = const, same dimensions as D) and approximating D_0 by a Langmuir-Dushman equation

$$D_0 = \frac{Q d^2}{Nh} \quad [7]$$

(where N = Avogadro's number; h = Planck's constant), the characteristic time becomes

$$\tau = \frac{Nh}{2Q} e^{\frac{Q}{RT}} \quad [8]$$

Since strain is a small quantity, the strain-time approximation employed subsequently (Equation [10]) requires the characteristic time parameter for creep to be large in magnitude, as contrasted to the short relaxation time of an atom in the self-diffusion case. Therefore the Q defined by Equation [8] will be larger in magnitude than the activation energy for self-diffusion.

EMPIRICAL CORRELATION

Strain-Time Approximations. The correlation proposed requires constant-stress creep data for pure, annealed polycrystalline metals encompassing a large range of temperatures and stresses. The only published data of this type known to the author are the original lead measurements of Andrade (7) and the recent extensive study of platinum by Carreker (8). To supplement these data the tests of Davis (9) on oxygen-free copper were included, even though the metal was prestrained 8 per cent prior to testing, and the stresses deviated slightly from a constant value.

There is an ever-increasing body of evidence (to which Carreker's data are the most recent contribution) supporting the view that natural strain, constant-stress creep data in the range preceding tertiary creep may be approximated accurately by an equation of the type

$$\epsilon = C t^{\alpha} \quad [9]$$

where C and α are empirical constants.[4] The smooth curves of Andrade and Davis, replotted[5] in terms of natural strain in Figs. 3 to 7, show good agreement with this equation.[6] Because of the small magnitude of the strains, the copper curves (although obtained at constant load) show a large linear region of nearly constant stress before tertiary creep is realized.

Equation [9] suggests that the functional relationship of Equation [4] may be expressed as

$$\epsilon = \left(\frac{t}{\tau}\right)^{\alpha} = \left(\frac{2Qt}{Nh} e^{-\frac{Q}{RT}}\right)^{\alpha} \quad [10]$$

This equation defines a time-independent activation energy in terms of creep data, but is less interesting than a more restricted representation with only one empirical constant. Since a linear

[4] Servi and Grant (10) state that their recent data on aluminum are not well represented by equation [9]. A typical creep curve presented by them (for the case of 99.995 per cent Al at 500 F and 1180 psi) shows good agreement with equation [9] in the "pretertiary" range, however, when the initial extension is subtracted and the remaining creep deformation is presented in terms of natural strain.

[5] The data in Figs. 3 to 7 were taken from enlarged photographic copies of the original published curves. Since Andrade's curves required extrapolation to zero time for determination of the initial elongation, some inaccuracy is possible.

[6] The low-temperature (or high stress) curves for lead, like the low-temperature results of Carreker for platinum (8) show an initial transient portion of rapidly increasing strain which is not pronounced in tests at medium or high temperatures. This behavior (which possibly may be associated with the phenomenon of slip) is of theoretical interest but of small practical importance in high-temperature creep tests, and therefore will not be considered in the following correlation.

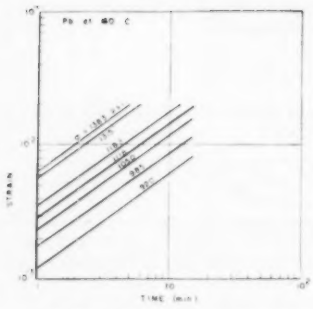

FIG. 3 CREEP OF LEAD AT 160 C

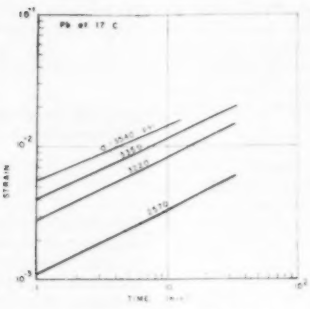

FIG. 4 CREEP OF LEAD AT 17 C

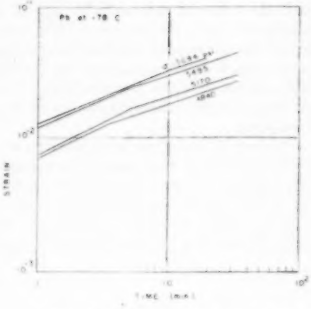

FIG. 5 CREEP OF LEAD AT —78 C

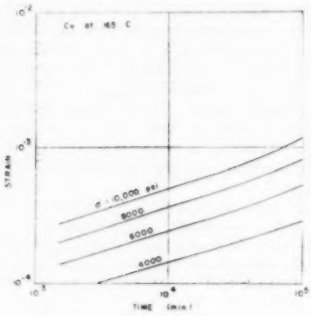

FIG. 6 CREEP OF COPPER AT 165 C

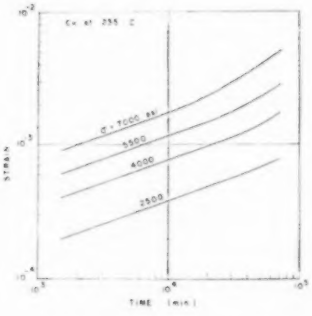

FIG. 7 CREEP OF COPPER AT 235 C

strain-time relationship indicating viscous behavior is approximated near the melting point of a metal, the exponent α must there approach unity. Carreker's results indicated that α varied linearly with temperature (except possibly at very low temperatures), and suggested that the exponent for different metals might be correlated as a function of the reduced temperature T/T_m. For this reason, values of the exponent α obtained for a variety of nominally pure polycrystalline metals under approximately constant stress are assembled in Fig. 8 as a function of T/T_m. Considering that the effects of different grain size, work history, and impurity content have been ignored, the agreement appears reasonably good. Within the accuracy of the purely empirical linear approximation of Fig. 8 the creep equation becomes

$$\epsilon = e^{-\frac{Q}{RT_m}} \left(\frac{2Qt}{Nh}\right)^{\frac{T}{T_m}} \quad \ldots\ldots\ldots\ldots\ldots\ldots [11]$$

in which the activation energy Q is the only undetermined constant. Thus effects of experimental variables may be interpreted in terms of their influence on Q.

It must be noted that the approximation of Fig. 8 appears to be valid only for pure polycrystalline specimens in which the number of grains in the specimen cross section is statistically large enough that the effects due to orientation of individual crystals cancel out. As shown by the single-crystal experiments of Tyndall (11), crystal orientation has a pronounced influence on

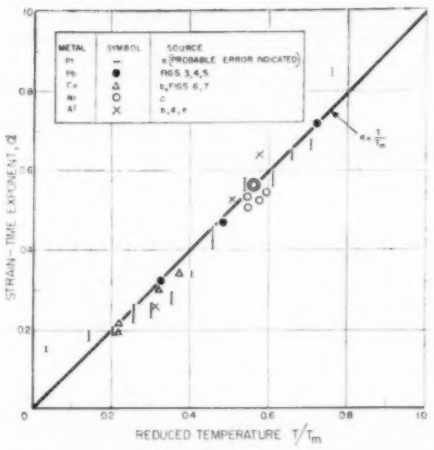

FIG. 8 EXPONENT OF STRAIN-TIME APPROXIMATION VERSUS REDUCED TEMPERATURE FOR SEVERAL NOMINALLY PURE POLYCRYSTALLINE METALS

(*a*, Reference 8; *b*, reference 28; *c*, reference 29; *d*, reference 10; *e*, reference 30.)

the exponent α. It is conceivable that this effect may have contributed to the scatter of Carreker's platinum data in Fig. 8 since his wire specimens contained only 2 to 4 grains per cross section.

Values of the activation energy for lead and copper, calculated from the curves in Figs. 3 to 7, are presented in Fig. 9 as functions of the applied stress. The activation energy is seen to decrease approximately linearly with increasing stress at a rate increasing with increasing temperature. Fig. 10 presents corresponding results calculated from Carreker's strain-time data for platinum,[7] which show similar behavior. Extrapolation to zero stress determines a quantity Q_0, the activation energy in the absence of stress, which is a temperature function. Fig. 11 presents curves of activation energy versus stress for tin and gold calculated from the published data of Tyte (12) and Alexander, Dawson, and Kling (13), respectively. In both cases the data fitted Equation [9], but the specimens were too small for Equation [11] to hold, and so Equation [10] was used in the calculation. The gold filaments with reedlike grain structure used by Alexander, et al., were so small (1 mil diam) that the influence of surface tension was appreciable; the specimens actually contracted while under the smaller loads. For this reason, only the results calculated from the curves obtained under the larger loads are presented in Fig. 11. In spite of this selection, considerable inconsistency is evident.

Influence of Temperature. In self-diffusion studies, activation energies are sometimes correlated in terms of the parameter Q/RT_m (reference 14). Guided by the idea of melting, or disorder, as an important factor in diffusion, Dienes (15) has shown empirically that Q/RT_m is the physically important group. It seemed logical, therefore, to interpret the creep results in terms of the group Q_0/RT_m, as is done in Fig. 12. The corresponding self-diffusion data are also included for comparison, and it may be seen that the creep correlation is at least as convincing as the one for diffusion. It appears that in both cases the group Q/RT_m provides a dimensionless measure of the degree to which local disordering by thermal fluctuations permits lattice movements in the solid. Agreement in both cases probably could be improved by including the effects of grain size in the correlation. It is also evident that, although the activation energy defined by the creep equation is greater in magnitude than Q defined by the diffusion equation, the energies for both manifestations of atom motion vary similarly with temperature.

Influence of Stress. The influence of stress in lowering the re-

[7] Copies of these data (minus the curves for 1450 deg and 1250 deg K) were furnished by Dr. G. J. Dienes.

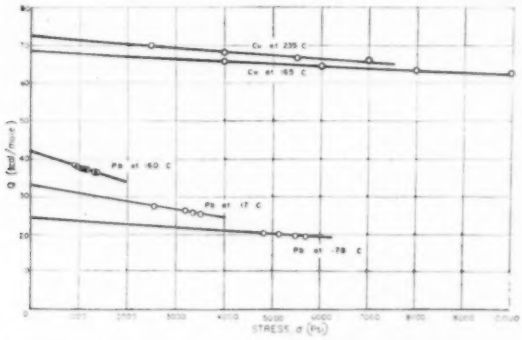

FIG. 9 ACTIVATION ENERGY FOR CREEP OF COPPER AND LEAD VERSUS APPLIED STRESS

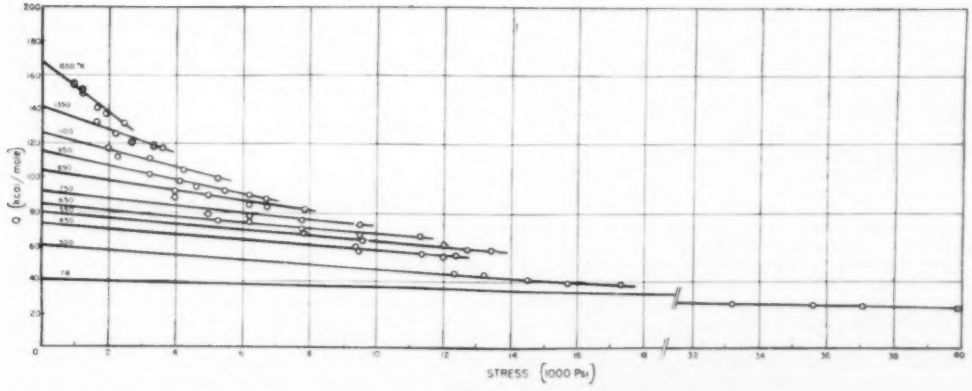

FIG. 10 ACTIVATION ENERGY FOR CREEP OF PLATINUM VERSUS APPLIED STRESS
(From data of Carreker, reference 8.)

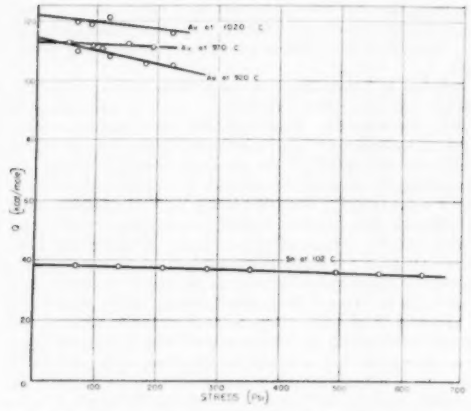

FIG. 11 ACTIVATION ENERGY FOR CREEP OF TIN AND GOLD VERSUS APPLIED STRESS

(From data of Tyte, reference 12, and Alexander, Dawson, and Kling, reference 13.)

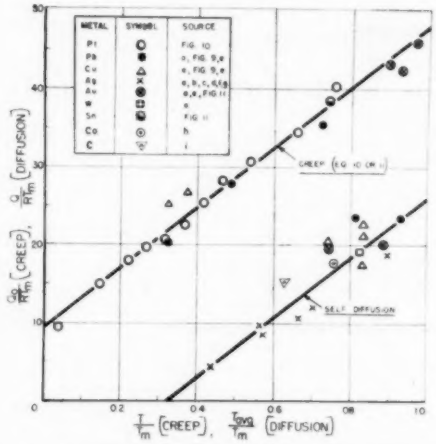

FIG. 12 CORRELATION OF APPARENT ACTIVATION ENERGIES FOR CREEP AND SELF-DIFFUSION AS A FUNCTION OF THE REDUCED TEMPERATURE

(Effect of grain size not considered. *a*, Reference 15; *b*, reference 31; *c*, reference 32; *d*, reference 33; *e*, reference 1, page 540; *f*, reference 34; *g*, reference 35; *h*, reference 36; *i*, reference 37.)

quired activation energy is evident from Figs. 9, 10, and 11. Herring (6) has shown that in the absence of concentration differences, the product of stress and atomic volume is the quantity motivating flux of material. This observation suggested trying to correlate the decrease in activation energy due to stress with the dimensionless group $\sigma V/RT$ (where V is now the molar volume in order to conform with the units of R), as is done in Fig. 13. Since it was evident that the influence of stress in promoting atom movement increased with rising temperature, the abscissa in Fig. 13 was multiplied by Q_0/RT_m, the dimensionless measure of disorder. It may be seen that the resulting tentative correlation is crude, but it is believed that the scatter of the data may be attributed largely to uncertainties in the extrapolations in Figs. 9 and 10, since the small difference $(Q_0 - Q)$ is much more sensitive to extrapolation errors than is Q_0 itself. It is also believed that accurate knowledge of the thermal-expansion coefficient at high temperature (necessary to correct the molar volume) would reduce the deviation of the high-temperature platinum data. In the case of the copper specimens, it is possible that the residual stresses stored by the initial 8 per cent prestretching prior to creep testing may have reduced the relative influence of the additional applied creep stress. It appears that a reliable dimensionless correlation must await further constant-stress creep data on different pure, annealed metals at various temperatures and at stresses ranging low enough to permit accurate determinations of the activation energy decrease.

EFFECT OF OTHER VARIABLES

On the basis of the analogy drawn in the foregoing discussion, certain qualitative predictions (here involving some microscopic speculations) regarding the effects on creep behavior of variables other than stress and temperature may be made and compared with experimental knowledge.

Impurities and Alloying Elements. The simple approximations proposed in the foregoing for the case of a pure metal are not expected to hold for the case of a multicomponent system. The empirical approximation in Fig. 8 possibly may be tested, however, by defining T_m as the temperature at the first appearance of a liquid phase. When this approximation fails, Equation [10] may still be valid as a strain-time relation with two empirical constants.

The proposed picture nevertheless permits qualitative predictions for metals of small impurity content. In the temperature range where grain-boundary movements are governing, impurity atoms concentrated preferentially at the boundaries should impede the atom movements, raise the activation energy, and decrease the creep rate. This effect is usually found experimentally.

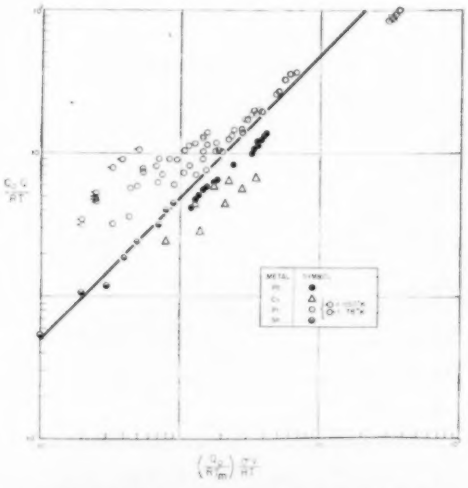

FIG. 13 PROPOSED CORRELATION OF STRESS-INDUCED DECREASE IN ACTIVATION ENERGY FOR CREEP OF VARIOUS METALS

The effect of small amounts of impurities widely dispersed throughout the grains should be small at such temperatures, but might be appreciable in the slip regime.

Grain Size and Work History. Since the disordered fraction of a metal varies inversely as the grain diameter, an increase in grain size (or grain perfection) should raise the activation energy and increase the resistance to medium and high-temperature creep, as is found experimentally (16). At low temperatures where slip deformation prevails, the effect presumably would be oppositely directed. If work hardening can be associated with grain fragmentation, as is indicated by the x-ray studies of Wood and his associates (17, 18), the influence of work history upon creep may be inferred from its influence upon the disordered fraction of the metal. The behavior of metals is interpreted by Wood in terms of a block structure, and he shows that the size of the "operative elements" in whose movements the plastic strain is manifested increases with increasing temperature and decreasing strain rate and approaches the grain size as an upper limit as the strain rate approaches that for pure creep. Since the disordered regions of the metal correspond to the boundaries of such elements, it may be seen from this picture that prior cold-working (or even rapid application of high creep loads) would have the effect of promoting creep at medium and high temperatures. Such an effect observed in the creep of annealed and hard-drawn copper wire has been described by Schmid (19). The analogous increase in diffusion rate with the degree of cold work in the specimen is well known (20).

Surface Conditions. According to the atom-movement idea, the effect of surface conditions upon the creep of a metal should become appreciable only in the limiting case of single-crystal specimens under conditions where lattice movements do not predominate. The inhibition of creep of such specimens by the formation of thin oxide films on the metal surface has been demonstrated by Andrade (21). The effect of surface movements on creep is also possibly indicated by Andrade's much-debated experiments in which a single-crystal cadmium wire was bombarded by alpha rays from a polonium source (22). When the specimen was lightly loaded so that the initial extension was small (1 per cent) and the creep rate was low (0.05 per cent per min), the bombardment effected a fivefold increase in the creep rate, an increase attributed to agitation of the disordered surface atoms. This effect decreased as the load and initial extension were increased, a trend which conforms with the atom-motion requirement, since application of the greater loads presumably gave rise to slip bands, regions of disorder unaffected by the surface bombardment (0.005 mm penetration depth). In the case of an initial extension of 12 per cent under a load producing a creep rate of 0.7 per cent per min, for instance, no change of creep rate as a result of bombardment was noticed.

In contrast to the foregoing effects observed with single crystals, experiments by Pickus and Parker (23), using polycrystalline zinc and nickel, have revealed no dependence of creep rate on surface treatment.

Radiation. Knowledge of the effects of high-energy radiation on the creep of materials would be desirable in the design of nuclear reactors. From the experiments of Martin, Johnson, and Goeddel (24), it is known that the volume self-diffusion of silver is unaffected by bombardment with 10-Mev protons. Creep rates at the temperatures required for lattice movements are not of great engineering interest, however, and speculation regarding the possible influence of radiation in the regime of grain-boundary movements at present must be made in the absence of the corresponding diffusion measurements. In the low-temperature region where work-hardening reduces the creep rate, the hardening produced by radiation (25) might be expected to have a similar effect.

Conclusion

The ultimate object of a correlation such as the one proposed herein is of course the prediction of the creep behavior of a metal from knowledge of its physical properties, history, and the prevailing conditions of stress and temperature. For preliminary design purposes, estimates of even modest accuracy may be valuable. At the present time the correlation between the activation energy, temperature, and stress is not established with accuracy sufficient for this purpose, since the scatter in Figs. 12 and 13 can lead easily to an order-of-magnitude error in the calculated creep strain. It is believed, however, that experiments on various metals under well-controlled conditions of temperature, stress, purity, grain size, and work history possibly may effect a refinement of the correlation to a degree permitting useful estimates of creep relationships. Inclusion of the transient effects which are prominent at low temperatures probably will require recourse to dislocation theory.

Again, it should be emphasized that the correlation of creep properties by the necessarily vague diffusion analogy drawn in the foregoing discussion is a frankly empirical one proposed with possible engineering applications in mind, and that the activation energy so defined is of interest primarily because it shows a reasonable qualitative dependence upon the experimental variables, a dependence apparently predictable from diffusion experiments. It is believed that the foregoing method may be useful for correlative purposes where a minimum of undetermined constants is desirable. The physical process of creep remains incompletely described, however, since the purely empirical approximation of Equation [9], although accurate at medium and high temperatures over the constant-stress range preceding tertiary creep, provides no insight into the fundamental mechanism. It seems possible that the physical picture may be clarified by second-law considerations first proposed by Kauzmann (26). When applied to a constant-stress creep curve by a relation of the type

$$\left(\frac{\partial \epsilon}{\partial t}\right)_\sigma = k\epsilon^{-\frac{Q - T\Delta S}{RT}} \qquad [12]$$

this approach can permit the activation energy to remain constant while an initially large positive entropy change decreases in magnitude with increasing time. This variation implies an ordering process progressing with time, and it is interesting to note that such an ordering (as manifested by a reduction in the broadening of back-reflection spots) of a structure disordered to some degree by the initial load application is indicated by the x-ray studies of Wood and Scrutton (27) using polycrystalline aluminum. Although a considerable amount of experimental work will be required for either a fundamental understanding or a phenomenological description of the creep process from this viewpoint, the desirability of such experiments seems evident.

Acknowledgments

The author wishes to acknowledge the helpful criticisms of G. J. Dienes, P. E. Duwez, and F. E. Faris. The numerical computations were made by Miss Barbara Lemke.

Bibliography

1 "The Theory of Rate Processes," by S. Glasstone, K. J. Laidler, and H. Eyring, McGraw-Hill Book Company, Inc., New York, N. Y., 1941.

2 "On the Viscous Flow in Metals and Allied Phenomena," by E. N. da C. Andrade, Proceedings of the Royal Society of London, series A, vol. 84, 1911, p. 1.

3 "Creep of Metals," by J. D. Lubahn, contained in "Cold Working of Metals," American Society for Metals, 1949.

4 "Some Mechanical Properties of Graphite at Elevated Temperatures," by C. Malmstrom, R. Keen, and L. Green, Jr., *Journal of Applied Physics*, vol. 22, 1951, pp. 593–600.

5 "The Problem of the Temperature Coefficient of Tensile Creep Rate," by J. J. Kanter, Trans. AIME, vol. 131, 1938, pp. 385–418.

6 "Diffusional Viscosity of a Polycrystalline Solid," by C. Herring, *Journal of Applied Physics*, vol. 21, 1950, p. 437.

7 "The Flow of Metals Under Large Constant Stresses," by E. N. da C. Andrade, Proceedings of the Royal Society of London, series A, vol. 90, 1914, p. 329.

8 "Plastic Flow of Platinum Wires," by R. P. Carreker, Jr., *Journal of Applied Physics*, vol. 21, 1950, p. 1289.

9 "Creep and Relaxation of Oxygen-Free Copper," by E. A. Davis, JOURNAL OF APPLIED MECHANICS, Trans. ASME, vol. 65, 1943, p. A-101.

10 "Creep and Stress Rupture Behavior of Aluminum as a Function of Purity," by I. S. Servi and N. J. Grant, *Journal of Metals*, vol. 3, 1951, pp. 909–916.

11 "Creep of Zinc Crystals," by E. P. T. Tyndall, contained in "Plastic Deformation of Crystalline Solids" (Symposium), NAVEXOS-P-834, 1950, pp. 49–59.

12 "The Rate of Viscous Flow of Metals—Part I—Tin," by L. C. Tyte, Proceedings of the Physical Society of London, vol. 80, part 2, 1938, p. 11.

13 "The Deformation of Gold Wire at High Temperature," by B. H. Alexander, M. H. Dawson, and H. P. Kling, *Journal of Applied Physics*, vol. 22, 1951, pp. 439–443.

14 "Diffusion of Metals in Metals," by A. D. LeClaire, contained in "*Progress in Metal Physics*," Interscience Publishers, Inc., New York, N. Y., vol. 1, 1949.

15 "Frequency Factor and Activation Energy for the Volume Diffusion of Metals," by G. J. Dienes, *Journal of Applied Physics*, vol. 21, 1950, pp. 1189–1192.

16 "Properties of Metals at Elevated Temperatures," by G. V. Smith, McGraw-Hill Book Company, Inc., New York, N. Y., 1950, p. 277.

17 "Intrinsic Crystalline Structure and the Strength of Metals," by W. A. Wood, *The Philosophical Magazine*, vol. 42, 1951, p. 310.

18 "Three Basic Stages in the Mechanism of Deformation of Metals at Different Temperatures and Strain Rates," by W. A. Wood, G. R. Wilms, and W. A. Rachinger, *Journal of the Institute of Metals*, vol. 79, 1951, p. 159.

19 "On Plasticity, Crystallographic and Non-Crystallographic," by E. Schmid, International Conference on Physics, London, England, part 2, 1934, p. 161.

20 "The Physics of Metals," by F. Seitz, McGraw-Hill Book Company, Inc., New York, N. Y., 1943, p. 138.

21 "Surface Effect and Structure of Single Crystal Wires," by E. N. da C. Andrade, *Nature*, vol. 164, 1949, p. 536.

22 "Effect of Alpha-Ray Bombardment on Glide in Metal Single Crystals," by E. N. da C. Andrade, *Nature*, vol. 156, 1945, p. 113.

23 "Creep as a Surface Dependent Phenomenon," by M. R. Pickus and E. R. Parker, contained in Symposium on Corrosion of Materials at Elevated Temperatures, ASTM, Special Technical Publication No. 168, 1951.

24 "The Effect of Cyclotron Bombardment on Self-Diffusion in Silver," by A. Martin, R. D. Johnson, and W. Goeddel (to be published).

25 "The Effects of Radiation on Materials," by J. C. Slater, *Journal of Applied Physics*, vol. 22, 1951, pp. 237–256.

26 "Flow of Solid Metals From the Standpoint of Chemical Rate Theory," by W. Kauzmann, Trans. AIME, vol. 143, 1941, pp. 57–81.

27 "The Mechanism of Primary Creep in Metals," by W. A. Wood and R. F. Scrutton, *Journal of the Institute of Metals*, vol. 77, 1950, pp. 423–434.

28 "A Method of Analyzing Creep Data," by R. G. Sturm, C. Dumont, and F. M. Howell, JOURNAL OF APPLIED MECHANICS, Trans. ASME, vol. 58, 1936, p. A-62.

29 "Fifth Technical Report," by T. H. Haslett, E. R. Parker, and M. W. Nathans, AEC No. COO-4, Institute of Engineering Research, University of California, Department of Engineering.

30 Torsion experiment cited in "Plastic Deformation of Crystalline Solids" (Symposium), by T. S. Ke and C. Zener, NAVEXOS-P-834, 1950, p. 185.

31 "Surface Diffusion of Radioactive Silver on Silver," by R. A. Nickerson and E. R. Parker, Trans. ASM, vol. 42, 1950, pp. 376–386.

32 J. H. Hollomon and D. Turnbull, General Electric Research Laboratories Report No. RL-237, 1949.

33 J. H. Hollomon and D. Turnbull, General Electric Research Laboratories Report No. RL-359, 1950.

34 "Lattice and Grain Boundary Self-Diffusion in Silver," by R. E. Hoffman and D. Turnbull, *Journal of Applied Physics*, vol. 22, 1951, pp. 634–639.

35 "Rate of Self-Diffusion in Single and Polycrystals of Silver," by D. Turnbull, *Physical Review*, vol. 76, 1949, p. 471-A.

36 "Cobalt Self-Diffusion: A Study of the Method of Decrease in Surface Activity," by R. C. Ruder and C. E. Birchenall, *Journal of Metals*, vol. 191, 1951, pp. 142–146.

37 "The Diffusion of C^{14} Atoms in AUF Graphite," by M. Feldman, W. Goeddel, G. J. Dienes, and W. Gossen, to be published. (T_m = sublimation temperature.)

Bending With Axial Force of Curved Bars in Plasticity[1]

By ARIS PHILLIPS,[2] STANFORD UNIVERSITY, CALIF.

The problem of symmetrical pure bending with axial force of a curved bar in plasticity is considered. A method is given for finding the axial load and bending moment which produce a given strain distribution. This method is based upon approximating the stress-strain curves by means of broken lines. By increasing the number of sides of these broken lines it is possible to solve our problem with as high accuracy as is desired.

Introduction

IN this paper we consider the problem of symmetrical pure bending with or without axial force of curved bars in plasticity. Our problem is to give a method by means of which we easily can determine the axial load P, and the bending moment M, which produce a given strain distribution in the cross section. The method is quite general and easy to use. It is based upon approximating the stress-strain curves for tension and compression by means of broken lines.[3] By increasing the number of sides of these broken lines we can approximate the stress-strain line with any desired degree of approximation. As the use of the two broken lines instead of the original stress-strain curve is the only approximation entered in the method, we are able to solve our problem with as high a degree of accuracy as is desired.

Let us consider a curved bar with a constant cross section having one axis of symmetry. A small element $abcd$ of this bar, Fig. 1, is loaded in pure bending with axial force. The line joining the centroids of the cross sections is assumed to be a plane curve, and the axis of symmetry of any cross section must lie on this plane. The external forces also lie on this plane of symmetry.

In order to find the stress distribution we assume that transverse cross sections of the bar, which were originally plane and normal to the line joining the centroids, remain plane and normal to the neutral surface after deformation has taken place. We denote with $d\varphi$ the small angle between the two end faces ab and cd of the element of the bar before deformation has taken place. As a result of deformation the cross section cd rotates with respect to ab. We call this angle of rotation $\Delta d\varphi$, and we consider it as positive when it represents a decreasing $d\varphi$. Owing to this rotation the longitudinal fibers on the convex side are compressed, while the fibers on the concave side are extended. However, if the axial load is large compared to the bending moment, then all fibers may be extended or all fibers may be compressed. In this case the neutral surface will lie outside the cross section.

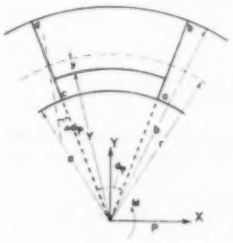

FIG. 1

If nn is the neutral surface, the extension of any fiber at a distance y from the neutral surface will be equal to $y\Delta d\varphi$, where y is positive if directed toward the center of curvature. The corresponding unit elongation is

$$\epsilon = \frac{y}{r - y}\frac{\Delta d\varphi}{d\varphi} \qquad [1]$$

where r is the radius of curvature of the neutral surface. If the distance of the fiber y from the center of curvature is Y, we find

$$y = r - Y \qquad [2]$$

Hence, denoting $\Delta d\varphi/d\varphi$ with ψ, we finally have the formula

$$\epsilon = \left(\frac{r}{Y} - 1\right)\psi \qquad [3]$$

We see that the strain distribution follows a hyperbolic law.

Let us assume that the stress-strain law for tension and compression is represented by means of the equation

$$\sigma = f(\epsilon) \qquad [4]$$

where $\epsilon > 0$ denotes tension while $\epsilon < 0$ means compression. We assume further that if a fiber has a strain ϵ in bending, then the stress of this same fiber can be determined by using Equation [4]. Then we have

$$\sigma = f\left[\left(\frac{r}{Y} - 1\right)\psi\right] \qquad [5]$$

The two equations of statics are

$$\int_{Y=a}^{Y=b} f\left[\left(\frac{r}{Y} - 1\right)\psi\right] B(Y)dY = P \qquad [6]$$

---

[1] The results presented in this paper were obtained in the course of research conducted under a contract sponsored by the Office of Naval Research.

[2] Assistant Professor, Mechanical Engineering Department, Stanford University.

[3] "A General Method of Calculating the Me_{max} Diagram in Plastic Bending of Beams," by Aris Phillips, JOURNAL OF APPLIED MECHANICS, Trans. ASME, vol. 73, 1951, pp. 353–358.

Presented at the National Meeting of the Applied Mechanics Division, State College, Pa., June 19–21, 1952, of THE AMERICAN SOCIETY OF MECHANICAL ENGINEERS.

Discussion of this paper should be addressed to the Secretary, ASME, 29 West 39th Street, New York, N. Y., and will be accepted until October 10, 1952, for publication at a later date. Discussion received after the closing date will be returned.

NOTE: Statements and opinions advanced in papers are to be understood as individual expressions of their authors and not those of the Society. Manuscript received by ASME Applied Mechanics Division, July 2, 1951. Paper No. 52—APM-9.

$$\int_{Y=a}^{Y=b} f\left[\left(\frac{r}{Y}-1\right)\psi\right] B(Y)YdY = M \qquad [7]$$

where $B(Y)$ is the width of the cross section, P is the axial force, and M is the bending moment. Both P and M are considered as acting upon the center of curvature of the bar, that is, at $Y = 0$. From these two equations we can determine two of the four variables—M, P, r, and ψ—if we know the other two. When M and P are known, we first determine r and ψ from Equations [6] and [7]; and then, using Equation [5], we find the stress distribution.

The analytical expression for the broken $\sigma - \epsilon$ line is

$$\left.\begin{aligned} &\sigma = E\epsilon \ldots, && 0 \leqq \epsilon \leqq \epsilon_1 \\ &\sigma = \sigma_i + E_i\epsilon \ldots, && \epsilon_i \leqq \epsilon \leqq \epsilon_{i+1} (i = 1\ 2\ \ldots\ k-1) \\ &\sigma = \sigma_k + E_k\epsilon \ldots, && \epsilon_k \leqq \epsilon \end{aligned}\right\} \ldots [8]$$

for tension, and

$$\left.\begin{aligned} &\sigma = E'\epsilon \ldots, && \epsilon_1' \leqq \epsilon \leqq 0 \\ &\sigma = \sigma_i' + E_i'\epsilon \ldots, && \epsilon_{i+1}' \leqq \epsilon \leqq \epsilon_i' (i = 1, 2, \ldots, l-1) \\ &\sigma = \sigma_l' + E_l'\epsilon \ldots, && \epsilon \leqq \epsilon_l' \end{aligned}\right\} \ldots [9]$$

for compression as explained by the author in another paper.[2] We remark that σ and ϵ are positive for tension and negative for compression.

In the paper mentioned it is shown that we may represent the line defined by Equation [8] as the sum of k perfectly plastic materials

$$\left.\begin{aligned} &\sigma = G_i\epsilon \ldots, && 0 \leqq \epsilon \leqq \epsilon_i \\ &\sigma = p_i = G_i\epsilon_i \ldots, && \epsilon_i \leqq \epsilon \end{aligned}\right\} \ldots [10] \quad (i = 1, 2, \ldots, k)$$

and one elastic material

$$\sigma = G_{k+1}\epsilon \ldots, 0 \leqq \epsilon$$

In these formulas

$$G_i = E_{i-1} - E_i$$

and

$$p_i = \sigma_i - \sigma_{i-1}$$

A similar analysis is valid for the stress-strain line expressed by Equations [9]. In this case we would have l perfectly plastic materials

$$\left.\begin{aligned} &\sigma = G_i'\epsilon \ldots, && \epsilon_i' \leqq \epsilon \leqq 0 \\ &\sigma = p_i' = G_i'\epsilon_i \ldots, && \epsilon \leqq \epsilon_i' (i = 1, 2, \ldots, l) \end{aligned}\right\} \ldots [11]$$

and one elastic material

$$\sigma = G_{l+1}'\epsilon \ldots, \epsilon \leqq 0$$

where

$$G_i' = E_{i-1}' - E_i', \quad p_i' = \sigma_i' - \sigma_{i-1}'$$

Assume now that in tension we have four perfectly plastic materials and one elastic one, whereas in compression we have three perfectly plastic materials and one elastic one. Then the stress-strain law will have the general form shown in Fig. 2.

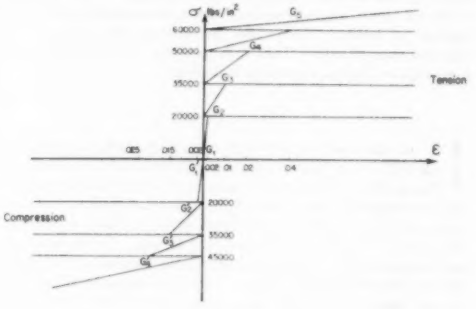

FIG. 2

EXPLANATION OF THE METHOD

In this paper we shall assume that we know r and ψ. Then we also know the strain distribution because of Equation [3]. We want to find the values of P and M which produce this strain distribution.

The method proposed in this paper will be explained by using the stress-strain law shown in Fig. 2 and the cross section shown in Fig. 3 (a). The quantities G_i, P_i, and ϵ_i corresponding to these materials have the values shown in Table 1.

In Fig. 3(b) we see a strain distribution applied on the cross section shown in Fig. 3(a). In order to simplify the presentation of the method we assume that the part of the cross section near

TABLE 1

	1	2	3	4	5	1′	2′	3′	4′	
G_i	10.00	1.50	0.75	0.25	0.10	10.00	1.00	0.40	0.20	$\times 10^4$
P_i	2.00	1.50	1.50	1.00	..	2.00	1.50	1.00	..	$\times 10^4$
ϵ_i	2	10	20	40	..	−2	−15	−25	..	$\times 10^{-4}$

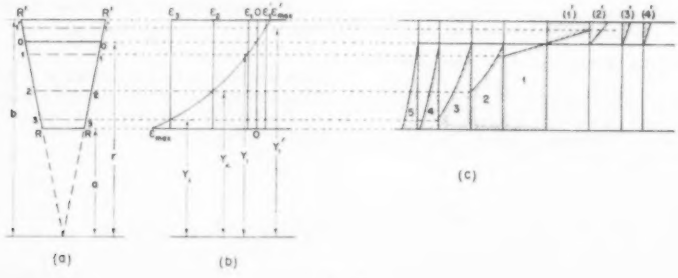

FIG. 3

the concave side of the curved bar is loaded in tension. We remark that the strain line has been superimposed upon the network $\epsilon_4\epsilon_3\epsilon_2\epsilon_1 0\epsilon_1'\epsilon_2'\epsilon_3'$. In this figure ϵ_{max} represents the maximum tensile strain in the cross section, and ϵ_{max}' represents the maximum compressive strain.

For the strain distribution in Fig. 3(*b*) we have $\epsilon_2 < \epsilon_{max} < \epsilon_3$, $\epsilon_3' < \epsilon_{max}' < \epsilon_1'$. The corresponding stress distribution is shown in Fig. 3(*c*), while in Fig. 3(*a*) we see the regions in the cross section where the strain lies between 0 and ϵ_1 (region 0011), between ϵ_1 and ϵ_2 (region 1122), and so forth. From Fig. 3(*c*) we see that the stress distribution in tension is equal to the sum of three perfectly plastic stress distributions (1), (2), and (3), and of two elastic ones (4) and (5). The stress distribution in compression is equal to the sum of one perfectly plastic stress distribution (1′), and of three elastic ones (2′), (3′), and (4′).

The perfectly plastic stress distributions have the following analytical expressions

$$\left.\begin{aligned}
\sigma &= G_i\epsilon = G_i\left(\frac{r}{Y}-1\right)\psi,\ Y_i \leqq Y \leqq r\\
\sigma &= P_i = G_i\epsilon_i = G_i\left(\frac{r}{Y_i}-1\right)\psi,\ a \leqq Y \leqq Y_i\\
\sigma &= G_i'\epsilon = G_i'\left(\frac{r}{Y}-1\right)\psi,\ r \leqq Y \leqq Y_i'\\
\sigma &= p_i' = G_i'\epsilon_i' = G_i'\left(\frac{r}{Y_i'}-1\right)\psi,\ Y_i' \leqq Y \leqq b
\end{aligned}\right\} \quad [12]$$

The elastic stress distributions have the analytical expressions

$$\left.\begin{aligned}
\sigma &= G_i\epsilon = G_i\left(\frac{r}{Y}-1\right)\psi,\ a \leqq Y \leqq r\\
\sigma &= G_i'\epsilon = G_i'\left(\frac{r}{Y}-1\right)\psi,\ r \leqq Y \leqq b
\end{aligned}\right\} \quad [13]$$

From Equations [12] we also find

$$\left.\begin{aligned}
Y_i &= \frac{\psi r}{\psi+\epsilon_i},\quad \epsilon_{max} = \left(\frac{r}{a}-1\right)\psi\\
Y_i' &= \frac{\psi r}{\psi+\epsilon_i'},\quad \epsilon_{max}' = \left(\frac{r}{b}-1\right)\psi
\end{aligned}\right\} \quad [14]$$

from which we can calculate Y_i, Y_i', ϵ_{max} and ϵ_{max}' for a given pair of values ψ and r.

The contribution to the left member of Equation [6] by a perfectly plastic stress distribution, or by an elastic stress distribution is as follows:

1 For $Y \leqq r$ and a perfectly plastic distribution

$$G_i\psi\left[\int_{Y=a}^{Y=Y_i}\left(\frac{r}{Y_i}-1\right)B(Y)dY + \int_{Y=Y_i}^{Y=r}\left(\frac{r}{Y}-1\right)B(Y)\,dY\right] \quad [15]$$

2 For $Y \leqq r$ and an elastic distribution

$$G_i\psi\int_{Y=a}^{Y=r}\left(\frac{r}{Y}-1\right)B(Y)\,dY \quad [15a]$$

3 For $Y \geqq r$ and a perfectly plastic distribution

$$G_i'\psi\left[\int_{Y=r}^{Y=Y_i'}\left(\frac{r}{Y}-1\right)B(Y)\,dY + \int_{Y=Y_i}^{Y=b}\left(\frac{r}{Y_i'}-1\right)B(Y)\,dY\right] \quad [16]$$

4 For $Y \geqq r$ and an elastic distribution

$$G_i'\psi\int_{Y=r}^{Y=b}\left(\frac{r}{Y}-1\right)B(Y)\,dY \quad [16a]$$

Expressions [15a] and [16a] are special cases of Expressions [15] and [16], respectively, for

$$Y_i = a \text{ and } Y_i' = b.$$

The contribution to the left member of Equation [7] is as follows:

1 For $Y \leqq r$ and a perfectly plastic distribution

$$G_i\psi\left[\int_{Y=a}^{Y=Y_i}\left(\frac{r}{Y_i}-1\right)B(Y)\,YdY + \int_{Y=Y_i}^{Y=r}\left(\frac{r}{Y}-1\right)B(Y)\,YdY\right] \quad [17]$$

2 For $Y \leqq r$ and an elastic distribution

$$G_i\psi\int_{Y=a}^{Y=r}\left(\frac{r}{Y}-1\right)B(Y)\,YdY \quad [17a]$$

3 For $Y \geqq r$ and a perfectly plastic distribution

$$G_i'\psi\left[\int_{Y=r}^{Y=Y_i'}\left(\frac{r}{Y}-1\right)B(Y)\,YdY + \int_{Y=Y_i'}^{Y=b}\left(\frac{r}{Y_i'}-1\right)B(Y)\,YdY\right] \quad [18]$$

4 For $Y \geqq r$ and an elastic distribution

$$G_i'\psi\int_{Y=r}^{Y=b}\left(\frac{r}{Y}-1\right)B(Y)\,YdY \quad [18a]$$

Expressions [17a] and [18a] are special cases of [17] and [18], respectively.

Denoting with $G_i\psi k_i$, $G_i'\psi k_i'$, $G_i\psi l_i$, $G_i'\psi l_i'$ the Expressions [15], [16], [17], and [18], respectively, or their special forms [15a], [16a], [17a], and [18a], respectively, we can write Equations [6] and [7] in the form

$$\psi\left[\sum_{i=1}^{i=5}G_ik_i + \sum_{i=1}^{i=4}G_i'k_i'\right] = P \quad [19]$$

$$\psi\left[\sum_{i=1}^{i=5}G_il_i + \sum_{i=1}^{i=4}G_i'l_i'\right] = M \quad [20]$$

If the stress-strain law consisted of n quantities G_i and of m quantities G_i', then in Equations [19] and [20] we would have $\sum_{i=1}^{i=m}$ and $\sum_{i=1}^{i=n}$ instead of $\sum_{i=1}^{i=5}$ and $\sum_{i=1}^{i=4}$, respectively.

The values k_i, k_i', l_i, and l_i' can be determined easily as follows: First we find the functions

$$K_1(Y_0) = \int_{Y=a}^{Y=Y_0}B(Y)\,dY$$

$$K_2(Y_0) = \int_{Y=a}^{Y=Y_0}B(Y)\,YdY$$

$$K_3(Y_0) = \int_{Y=a}^{Y=Y_0}\frac{B(Y)}{Y}\,dY$$

In the case of Fig. 4(*a*) these functions have the values

TABLE 2

		K_1	K_2	K_3	A_i or A_i'	$\bar{A}_i$ or $\bar{A}_i'$	S_i or S_i'	T_i or T_i'	
r =	9.0000	5.6000	40.2668	0.8000	...	...	...	...	A = 5.6000
b =	10.0000	7.5000	58.3336	1.0000	...	...	...	...	A' = 1.9000
Y_1 =	8.4375	4.6191	31.7119	0.6875	0.9808	4.6191	31.7119	0.1125	S = 40.2668
Y_2 =	6.7500	2.0562	12.1698	0.3500	3.5437	2.0562	12.1698	0.4500	S' = 18.0668
Y_3 =	5.4000	0.4160	2.1642	0.0800	5.1840	0.4160	2.1642	0.7200	T = 0.8000
Y_1' =	9.6428	6.7983	51.4416	0.9285	1.1983	0.7016	6.8920	0.1285	T' = 0.2000

$a = 5''$ $b = 10''$ $r = 9''$ $\frac{r}{a} = 1.80$ $\frac{r}{a} - 1 = 0.80$ $\psi = 0.030$ $\epsilon_{max} = 0.0240$

$\frac{r}{b} = 0.90$ $\frac{r}{b} - 1 = -0.10$ $\psi_{cr} = 0.270$ $\epsilon_{max}' = -0.0030$

TABLE 3

	G $\times 10^6$	Y_i	r/Y_i	$r\bar{A}_i/Y_i$	rT_i	A	k_i	Gik_i $\times 10_8$	$r\bar{S}_i/Y_i$	rA_i	S	l_i	G_il_i $\times 10_8$
1	10.00	8.4375	1.0666	4.9267	1.0125	5.6000	0.3392	3.392	33.8239	08.8272	40.2668	2.3843	23.8430
2	1.50	6.7500	1.3333	2.7415	4.0500	5.6000	1.1915	1.7872	16.2259	31.8933	40.2668	7.8524	11.7786
3	0.75	5.4000	1.6666	0.6933	6.4800	5.6000	1.5733	1.1799	3.6068	46.6580	40.2668	9.9960	7.4970
4	0.25	...	...	...	7.2000	5.6000	1.6000	0.4000	...	50.4000	40.2668	10.1332	2.5333
5	0.10	...	...	...	7.2000	5.6000	1.6000	0.1600	...	50.4000	40.2668	10.1332	1.0133
1′	10.00	9.6428	0.9333	0.6548	1.1565	1.9000	−0.0887	−0.8870	6.4323	10.7847	18.0668	−0.8498	−8.4980
2′	1.00	...	...	...	1.8000	1.9000	−0.1000	−0.1000	...	17.1000	18.0668	−0.9668	−0.9668
3′	0.40	...	...	...	1.8000	1.9000	−0.1000	−0.0400	...	17.1000	18.0668	−0.9668	−0.3867
4′	0.20	...	...	...	1.8000	1.9000	−0.1000	−0.0200	...	17.1000	18.0668	−0.9668	−0.1933

$\Sigma G_ik_i = 5.8721 \times 10^6$ $\Sigma G_il_i = 36.6204 \times 10$

$P = 0.17616 \times 10^6$ $M = 10.9861 \times 10^6$

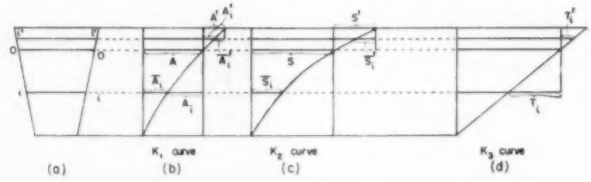

FIG. 4

$$K_1(Y_0) = 0.10\,(Y_0^2 - 25),\quad K_2(Y_0) = \frac{0.20}{3}\,(Y_0^3 - 125),$$

$$K_3(Y_0) = 0.20\,(Y_0 - 5)$$

These functions can be determined by means of analytical or graphical integrations. Their forms are shown in Figs. 4(*b*), 4(*c*), and 4(*d*).

We introduce now the following notations

$$\left.\begin{aligned} A &= K_1(r) - K_1(a), & A_i &= K_1(r) - K_1(Y_i)\\ \bar{A}_i &= K_1(Y_i) - K_1(a), & A' &= K_1(b) - K_1(r)\\ A_i' &= K_1(Y_i') - K_1(r), & \bar{A}_i' &= K_1(b) - K_1(Y_i')\\ S &= K_2(r) - K_2(a), & S' &= K_2(b) - K_2(r)\\ \bar{S}_i &= K_2(Y_i) - K_2(a), & \bar{S}_i' &= K_2(b) - K_2(Y_i')\\ T_i &= K_3(r) - K_3(Y_i), & T_i' &= K_3(Y_i') - K_3(r) \end{aligned}\right\} \quad \ldots [21]$$

With these notations we find

$$\left.\begin{aligned} k_i &= \frac{r}{Y_i}\,\bar{A}_i - A + rT_i, & k_i' &= \frac{r}{Y_i}\,\bar{A}_i - A' + rT_i\\ l_i &= \frac{r}{Y_i}\,\bar{S}_i - S + rA_i, & l_i' &= \frac{r}{Y_i'}\,\bar{S}_i' - S' + rA_i' \end{aligned}\right\} \quad \ldots [22]$$

The significance of notations, Equations [21], is shown in Fig. 4.

Let us assume now that we want to find the values P and M corresponding to a given set of values ψ and r. We first construct the lines K_1, K_2, and K_3. For the cross section shown in Fig. 3(*a*) these lines have been constructed in Figs. 4(*b*), 4(*c*), and 4(*d*), respectively. It is important to note that these lines are independent of the specific selection of ψ and r; they depend only on the cross section and on the position of the center of curvature with respect to the cross section.

Next, using Equations [14] we find the values ϵ_{max} and ϵ_{max}', thus deciding which G_i and G_i' correspond to perfectly plastic materials. In the case of Tables 2 and 3 we have selected $\psi = 0.030$ and $r = 9$. Hence $\epsilon_{max} = 0.0240$ and $\epsilon_{max}' = -0.0030$. Therefore, for the lower side of the cross section we have three plastic materials G_1, G_2, G_3, and two elastic ones G_4 and G_5; and for the upper side of the cross section we have one plastic material G_1', and three elastic ones G_2', G_3', and G_4'. Now we calculate from Equations [14] the values Y_i and Y_i' for the perfectly plastic materials; and then by using Equations [21] we calculate the values A, A', A_1, ... (Table 2). Now from Equations [22] we find the values k_i, k_i', l_i, l_i' and from Equations [19] and [20] we find the values M and P (Table 3).

Plastic Flow in a V-Notched Bar Pulled in Tension[1]

By E. H. LEE,[2] PROVIDENCE, R. I.

A V-notched bar pulled in tension in plane strain as shown in Fig. 1 is considered. The distribution of stress and deformation are determined from the analysis of the motion with large strains as the initial notch width pulls down toward line contact as the test proceeds. The analysis is based upon the theory of flow of a so-called Saint Venant-Mises material, which flows at a constant yield limit given by the Mises criterion, and obeys the Mises flow-type relationship between stress and strain increments. The successive configurations of an initially square grid on the cross section of the notch are obtained to illustrate the strain distribution. This solution is of interest in investigating the initiation of fracture in a notch-bar tension test. In such a test the foregoing type of solution applies until plastic flow is arrested by the appearance of a fracture crack. The variation of the solution with notch angle is of interest in connection with the determination of the technical cohesive strength of a metal using Kuntze's technique. The present solution indicates a contrast with Kuntze's hypothesis, in that it predicts the possibility of a plastic-flow type of rupture at a stress depending only upon the yield stress of the metal.

Introduction

WE consider the plastic flow in a deeply notched bar pulled in tension in plane strain. This condition is obtained with the specimen shown in Fig. 1, if the width b of the bar is large compared with the thickness at the notch root; for

FIG. 1 NOTCHED BAR PULLED IN TENSION

with a deep notch, plastic flow is localized in the vicinity of the root of the notch, and the parts remaining elastic prevent appreciable lateral contraction, thus leading to plastic flow in plane strain. It is considered that the theoretical stress and strain distributions are of interest not only as a theoretical analysis of a problem of plastic flow, but are also of value in interpreting material tests using this type of specimen. Such a test is, in general, terminated by fracture, whereas the theoretical analysis is concerned only with plastic flow and can be carried through until the notch root is pulled down to a line of contact. A theoretical study of the history of the strain distribution which determines localized regions of high strain, may help in assessing the initiation of fracture in such a test.

The theory is based on an ideally plastic material subjected to large strains. Since strains of the order unity occur, it is permissible to neglect elastic strains, and thus to consider elastic material to be rigid. In such problems, in addition to regions of large plastic strain, the yield point is exceeded in material which is confined by surrounding elastic material, so that the plastic strains occurring there are limited to be of the order of elastic strain. To our degree of accuracy these regions will also be considered rigid, so that in the segregation into rigid and plastic areas, the rigid parts may be subject to small plastic strain. This type of analysis is sufficient for most metal-forming problems since it is the regions of large flow only that need to be investigated.

The assumption of ideal plasticity implies plastic flow at a constant stress limit, which is a reasonable approximation for many materials. This must not be thought of as equivalent to neglecting work-hardening, but rather to averaging its effect over the field of flow; for having determined the final strain distribution an average strain magnitude can be used to determine an average yield stress for substitution in the equations based upon the ideal material. In practice it has been found (1)[3] that even with lead, which exhibits a rounded stress-strain curve in the yield region with gradual development of plastic flow, good agreement with experiment is obtained with this type of theory.

Basic Theory

The type of idealized material discussed in the previous section, which is considered rigid until plastic flow occurs at a constant stress limit, is known in the literature as a Saint Venant-Levy-Mises material. The condition for plastic flow is determined by the Mises yield limit

$$(\sigma_y - \sigma_z)^2 + (\sigma_z - \sigma_x)^2 + (\sigma_x - \sigma_y)^2 + 6(\tau_{xy}^2 + \tau_{yz}^2 + \tau_{zx}^2) = 2Y^2 \quad \ldots\ldots [1]$$

adopting the usual notation for stress components in Cartesian co-ordinates, where Y is the yield stress in simple tension. For large plastic flow in plane strain, this law is equivalent to the Tresca law of flow at constant maximum shear stress, without modification of the equations other than the magnitude of the constant which appears in the analysis as the maximum shear stress throughout the field.

The strain components are determined by the Mises incremental type of law, which can be written in the form

[1] This work was sponsored by Watertown Arsenal Laboratory under contract ORD-11.

[2] Professor of Applied Mathematics, Graduate Division of Applied Mathematics, Brown University. Mem. ASME.

Presented at the Annual Conference of the Applied Mechanics Division, The Pennsylvania State College, State College, Pa., June 19–21, 1952, of THE AMERICAN SOCIETY OF MECHANICAL ENGINEERS.

Discussion of this paper should be addressed to the Secretary, ASME, 29 West 39th Street, New York, N. Y., and will be accepted until October 10, 1952, for publication at a later date. Discussion received after the closing date will be returned.

NOTE: Statements and opinions advanced in papers are to be understood as individual expressions of their authors and not those of the Society. Manuscript received by ASME Applied Mechanics Division, June 16, 1950. Paper No. 52—APM-4.

[3] Numbers in parentheses refer to the Bibliography at the end of the paper.

$$\frac{d\epsilon_x - d\epsilon_y}{\sigma_x - \sigma_y} = \frac{d\epsilon_y - d\epsilon_z}{\sigma_y - \sigma_z} = \frac{d\epsilon_z - d\epsilon_x}{\sigma_z - \sigma_x} = \frac{d\gamma_{xy}/2}{\tau_{xy}} = \frac{d\gamma_{yz}/2}{\tau_{yz}} = \frac{d\gamma_{zx}/2}{\tau_{zx}} \quad [2]$$

combined with no volume change

$$d\epsilon_x + d\epsilon_y + d\epsilon_z = 0 \quad [3]$$

We consider flow in plane strain which takes place slowly, so that inertia forces are negligible. Our solution for the stress distribution and the velocity field of flow in the regions of appreciable plastic deformation, therefore, must satisfy the equations of equilibrium and Equations [1], [2], [3] with strain-rate components expressed in terms of the velocity field.

In the case of plane strain with no motion parallel to the z-axis only the three strain components in the plane of flow are nonzero, and only the three stress components in the plane of flow appear in the analysis of the stress distribution. Following Hencky (2), it is convenient to consider the stress field in terms of the trajectories of maximum shear stress, or slip lines, shown in Fig. 2. These orthogonal trajectories are used to define curvilinear co-ordinates α, β. Equations [1], [2], [3] imply that the

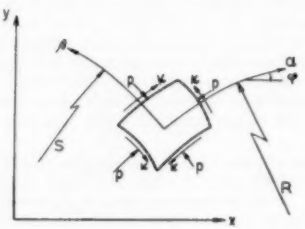

FIG. 2

maximum shear stress κ is constant throughout the field of flow. Therefore, the stress system at every point is determined completely by the slip-line direction, defined by the angle φ, and the average hydrostatic pressure p.

In terms of these variables, the equations of equilibrium take the form[4]

$$\left.\begin{array}{c} p + 2\kappa\varphi \\ \text{is constant along an } \alpha\text{-line} \\ p - 2\kappa\varphi \\ \text{is constant along a } \beta\text{-line} \end{array}\right\} \quad [4]$$

It is convenient also to work in terms of the radii of curvature of the slip lines, R and S shown in Fig. 2. The equations of equilibrium, Equations [4], are equivalent to the differential relations

$$\left.\begin{array}{c} dS + Rd\varphi = 0 \\ \text{along an } \alpha\text{-line} \\ dR - Sd\varphi = 0 \\ \text{along a } \beta\text{-line} \end{array}\right\} \quad [5]$$

If u and v are the velocity components along the slip lines, Equation [2] implies the relations

$$\left.\begin{array}{c} du - vd\varphi = 0 \\ \text{along an } \alpha\text{-line} \\ dv + ud\varphi = 0 \\ \text{along a } \beta\text{-line} \end{array}\right\} \quad [6]$$

The analysis of a metal-forming problem requires the determination of p, φ, R, S, u, and v throughout the field of large plastic flow to satisfy Equations [4], [5], and [6] and the boundary conditions which may involve both stresses and velocities. Adjacent regions considered rigid must be able to withstand the stresses transmitted across the plastic-rigid boundaries and the external boundary tractions, and their rigid-body motion must be compatible with the motion of the adjacent plastic material. In the case of nonsteady motion, these conditions must be satisfied at all stages in the flow as the boundaries change due to the deformation of the material. The solution presented in this paper satisfies these conditions.

Development of the Solution

The slip-line field for the initial plastic flow before the boundaries of the notch have been deformed appreciably is shown in Fig. 3. This field is a modification of those given by Hill (3) for parallel-sided notches with circular roots. The configuration is symmetrical about the horizontal and vertical center lines. The region ABE consists of straight slip lines inclined at $\pi/4$ to AE. The straight slip lines in ECD are inclined at $\pi/4$ to the horizontal, and these two regions are joined by concentric circular arcs and corresponding radii with center E.

This field clearly satisfies the condition of zero shear at the notch boundaries, for the shear stress is zero on surfaces inclined at $\pi/4$ to the slip lines. That the equilibrium equations are satisfied is clear from a consideration of the degenerate forms of Equations [5] when one or both the radii of curvature become infinite, or from individual study of the special types of stress field. For example, the regions in which both sets of slip lines are linear correspond to uniform stress.

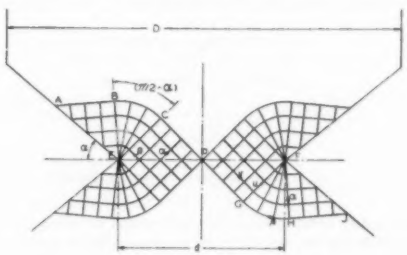

FIG. 3

The free surface AE determines p to equal $-\kappa$ there. Application of Equations [4] then determines

$$p = -\kappa - 2\kappa\left(\frac{\pi}{2} - \alpha\right) \quad [7]$$

in ECD. We can thus determine the stress on the notch center line EF. There is no shear stress, as would be expected by symmetry, and the normal tensile stress is

$$-p + \kappa = 2\kappa\left(1 + \frac{\pi}{2} - \alpha\right) \quad [8]$$

The tensile stress for flow in plane strain without a notch is

[4] Details of this and subsequent analysis of the section are given in (1).

2κ, so that the constraint of the notch increases the stress by the factor $(1 + \pi/2 - \alpha)$.

The assumption of a deep notch requires that the average stress away from the notch

$$2\kappa \left(1 + \frac{\pi}{2} - \alpha\right) \frac{d}{D}$$

where d and D are the dimensions shown in Fig. 3, be less than $2\kappa\gamma$, where γ is a factor of magnitude about 0.5 to allow for the nonuniform distribution of stress in the rigid material adjacent to the notch. This will insure that the specimen does not deform in the region away from the notch root, so that the region outside the slip-line field may be considered as rigid in determining the large local deformation.

In order to consider the associated velocity field of flow, it is convenient to give the upper part of the specimen unit velocity upward, and the lower part unit velocity downward. The magnitude or time variation of this velocity does not influence the solution as long as it remains small and positive, since inertia forces are neglected. By symmetry the material on the center line EF will have no vertical component of velocity. If we now superpose a unit velocity upward on the whole system, the rigid material below the notch is brought to rest, which facilitates study of the motion of the material $DFJHG$ in Fig. 3. The material on the line DF has now a vertical component of velocity of magnitude unity.

The velocity field follows simply from Equations [6]. Since all α-lines are straight, $d\varphi$ is zero along them and u is, therefore, a constant for each line. But since the rigid material below $DGHJ$ is at rest, this constant must be zero for all α-lines in order to maintain continuity. Thus the second of Equations [6] determines v to be constant on all β-lines, which must be $\sqrt{2}$ to produce the required unit vertical component of velocity on DF.

This velocity field develops when the plastic strains first become large relative to elastic strains, but before the boundaries have deformed appreciably. Since the whole boundary FJ moves with the uniform velocity $\sqrt{2}$, the initial deformation of the notch surface will be a kink at J, and at the three points corresponding to J by symmetry.

Since the notch boundaries between these kinks and the root move parallel to themselves, the notch width decreases but the contour retains its shape between the kinks. This suggests that a similar stress configuration may apply for the subsequent motion. The validity of this suggestion will be established if the new stress field extends only in the region of the undisturbed notch boundary shape, for the stress field would not satisfy the stress boundary conditions in the deformed part of the boundary. This configuration is, in fact, found to be satisfactory, and applies at all stages in the deformation. The corresponding stress and deformation fields when the neck has been reduced to one half its initial width are shown in Figs. 4 and 5, for a notch of semi-angle $\alpha = \pi/4$.

In Fig. 4, C corresponds to J in Fig. 3, the point where the notch boundary is first deformed. At the stage depicted in Fig. 4, only the material in $D'E'J'K'$ is flowing plastically. The material below $D'K'J'$ but above the initial plastic-rigid boundary through C has been subject to large flow during the earlier motion, but has now been subject to stress reduction and is left with a distribution of residual permanent strain.

The linearity of the deformed boundary $J'C$ in Fig. 4 is a consequence of the constant velocity of the notch boundary $E'J'$ and of the plastic-rigid boundary $K'J'$ which terminates the plastic flow. The velocity of the latter is constant since its position is determined by the configuration $D'E'J'K'$, which remains geometrically similar throughout the motion, its dimensions being determined by the length $D'E'$, where E' moves with a constant velocity determined from the constant velocity of the notch surfaces. The deformed position of the surface $J'C$ can be deduced from a consideration of the flow velocities and the duration of flow of each element. However, it can be obtained more simply by noticing that the notch will finally be pulled down to line contact between two wedges. The linear sides of these wedges pass through C, and corresponding points on the other faces, so that the condition of no volume change determines the deformed wedge angle by the equal area condition shown in Fig. 6. Looked at from this standpoint, it is evident that the flow in the notched bar is the reverse of that in a wedge pressed

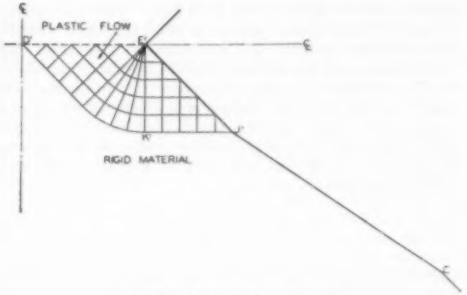

FIG. 4 THE SLIP-LINE FIELD

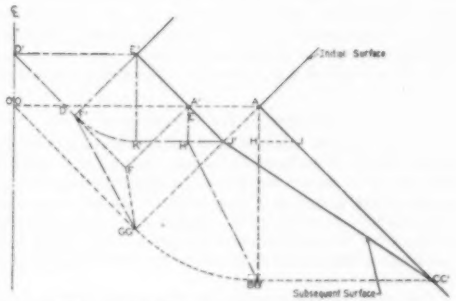

HBCJ	to *H'B'C'J'*	by simple shear
AHJ	to *A'H'J'*	by rigid body motion
ODFG	to *O'D'F'G'*	by simple shear
EDF	to *E'D'F'*	by rigid body motion
EFGBHA	to *E'F'G'B'H'A'*	by more complex motion

FIG. 5 THE DEFORMATION FIELD

FIG. 6

against a smooth surface given by Hill (4). However, the latter is clearly a pseudosteady problem in which the whole configuration and strain distribution is geometrically similar at all stages of the motion, and this indicates that the method of solution will be similar to that for wedge indentation (1). In the case of the notch bar, the strain distribution is of course not similar at all stages in the motion, and the motion from its initial configuration is unsteady. The angle β which determines the deformed surface of the notch has been given by Hill (4) for the wedge problem, and with our notation is

$$\tan \beta = \frac{(1 + \cos \alpha)^2}{\sin \alpha(2 + \cos \alpha)} \quad [9]$$

Since the velocity field is known throughout the motion, integration will give the deformation at any stage. This can be carried out directly by following the motion of a point through the varying velocity field, or by means of the hodograph theory of the unit diagram (see reference 1). Since we are interested in a series of deformation fields as the motion proceeds, the former method was used, and carried out graphically. Some of the more interesting details of this procedure are discussed in the next section.

Analysis of the Deformation

In order to check this solution experimentally, and in order to obtain an idea of the strain distribution from which to study the initiation of fracture, it is of interest to obtain the deformation of a square grid scribed on a cross section of the undeformed bar. This has been carried out for a grid of side 1/16 of the notch width. The deformation at increments of time during which the notch width is reduced by 1/8 of its initial value has been determined.

The major regions in which the deformation field is divided are shown in Fig. 5, in which the types of deformation are listed. These are deduced by consideration of the relative velocity between the stress-field boundaries and the material. For example, the boundary $E'K'$ moves faster than the material particles, so that material to the right of its initial position AB has been only in a region of uniform horizontal velocity or at rest. It has never been in a region which has a vertical component of velocity. This implies that the material initially to the right of AB has either sheared horizontally or moved horizontally as a rigid body. This, in conjunction with the consideration of the motion of the boundary $K'J'$ determines the motion of ABC to $A'H'B'C'J'A'$. Similar considerations apply for the other regions of simple shear or rigid body motion in Fig. 5. This breakdown can be more readily seen from the trajectories in the unit diagram (see reference 1), but space does not permit detailed discussion of this construction here.

The deformation of $EFGBHA$ is complicated by the varying direction of the particle velocity as the flow proceeds. The motion of a particular particle during an increment of time is obtained graphically by drawing the stress-field configuration before and after the time increment. The initial stress field gives the initial direction of motion of the particle, and, since the magnitude of the velocity is known to be $\sqrt{2}$, an approximation to the final position is obtained. A somewhat different velocity direction will be determined by the new particle position and the new stress-field configuration. In obtaining the final position an average velocity direction is used between these two. The time intervals stated at the beginning of this section were found sufficiently small to enable an accurate deformation field to be determined.

This procedure was carried out for each grid point, but the fact that most grid points lie in regions of simple rectilinear motion considerably simplified the construction.

In tracing out the position of the deformed grid lines, more information is required to obtain an accurate configuration than the positions of the grid points. This arises since finite shear occurs across the boundary $D'K'J'$ which produces a finite change in the slope of grid lines there. A knowledge of the particle and boundary velocities enables the change in direction to be determined by a simple graphical construction, and this was used in obtaining the final configuration. Moreover, a knowledge of the deformed directions of the grid lines where they meet the boundary $E'A'$ was required to plot the field accurately. This was obtained by using the unit diagram plot to follow the motion of such a line as it passed through the vertex E'.

The initial net and the deformation fields for four time increments are shown in Figs. 7, 8, 9, 10, 11. In Fig. 11, $t = 4$, the notch has been reduced to one half its initial width. The construction could be continued until only line contact occurs across the notch, but, since in practice plastic flow is arrested at an earlier stage by the initiation of fracture, it was considered not worth while to complete the construction.

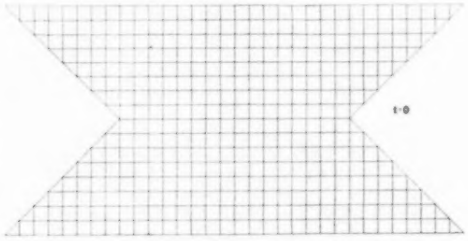

Fig. 7

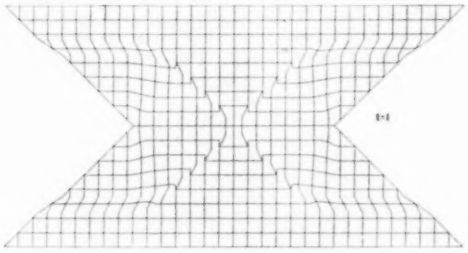

Fig. 8

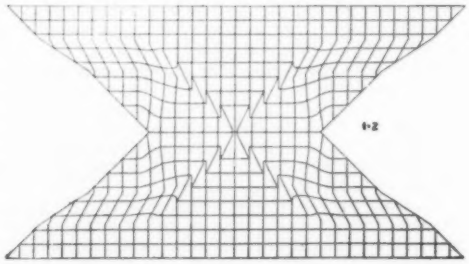

Fig. 9

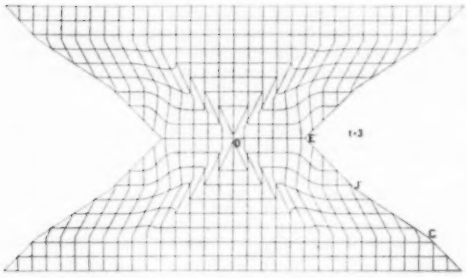

FIG. 10

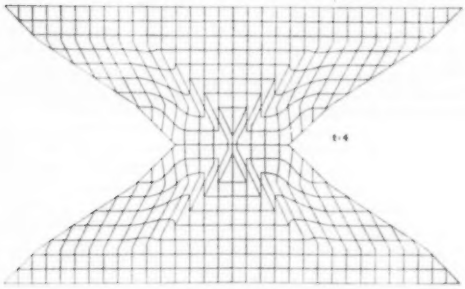

FIG. 11

technological significance of this solution is that of uniqueness of solution. The theory of the deformation of ideal plastic materials does not always lead to unique stress and velocity fields. However, it is usually possible to decide which of two solutions would occur in practice, since one may require a larger force, so that the other will occur first before the external force has reached the value necessary to produce the second type of flow.

In the present case the stress field shown in Fig. 12 can be used to develop a complete solution. The material flow velocities are smaller for this solution, but the plastic region extends further. The initial force required to initiate plastic flow is the same as for the previous solution. However, the point C_1 where the initial deformation of the boundary occurs is further removed from the notch root than the point C in Fig. 6. A similar equal area construction is required in the present case based upon C_1 rather than C. In Fig. 6 the equal area requirement demands that AP is parallel to CO. For this second type of solution with the final notch apex P_1, AP_1 is parallel to C_1O, so that P_1 lies above P. The force for any fixed separation of the ends of the specimen is therefore greater, as is also the distance over which the force must act before complete separation of the two halves occurs. These considerations indicate that the solution we have used which involves a smaller force throughout the motion will occur in practice.

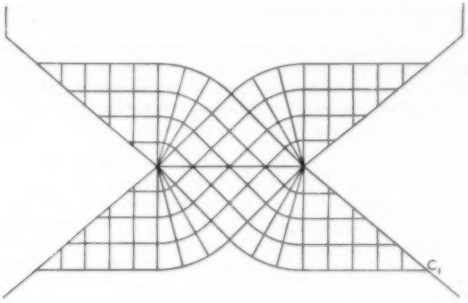

FIG. 12

DISCUSSION OF SOLUTION

The deformation field can perhaps best be assessed from Fig. 10. Large strains have occurred in the regions traversed by the plastic-rigid boundaries and near the notch root E'. There are regions between D' and E', and between E' and J' where no distortion has occurred. It would be of interest to check this deformation with a pattern obtained experimentally. One would expect the same general distribution to be obtained, though the discontinuous changes in direction of the lines across the plastic-rigid boundary would be smoothed by the rounded stress-strain curve of most materials and the influence of work-hardening.

An interesting type of fracture occurs due to the flow near the root of the notch. The flow pattern demands separation of the material at this point, so that material which originally formed the cross section of the notch, now forms the notch surface. This differs from the usual type of fracture in which the energy of local plastic flow, to bring about separation of the surface, must be supplied as well as the surface energy associated with the development of a new surface. The latter is, in fact, very small, and is neglected compared with the energy absorbed in plastic deformation. A discussion of this question has been given by Merchant (5) in connection with a similar separation process occurring in machining. A similar separation occurs when a smooth wedge penetrates a plastic medium (1), but in both this case, and machining, the separation is produced by the pressure of a rigid body between the two parts. In the case of the notched bar it is produced by tension in combination with the shape of the free surface there. It might be pointed out that this separation involves large local plastic strain, so that the details of flow, in this region, may be somewhat modified by work-hardening.

A question which should be considered before turning to the

TECHNOLOGICAL SIGNIFICANCE OF SOLUTION

The application of this solution in studying the initiation of fracture in a notch-bar tension test can be decided only after comparison with experiment, to check what influence the assumptions made have on the deformation field. However, some interesting indications concerning the investigation of the so-called technical cohesive strength are suggested by the range of solutions for varying notch angle.

The basic idea in the material tests carried out by Kuntze (6), is that a cylindrical specimen with a sharp deep notch would fracture without plastic flow at a stress known as the technical cohesive strength. This stress is considered to play a fundamental role in the theory of fracture. Its value is obtained by extrapolating, to zero notch width and zero angle, tests for a range of notch angles and notch depths. This concept is based on the hypothesis that this limiting notch would produce a state of hydrostatic tension which would lead to fracture without plastic flow.

It has been pointed out by Orowan (7) that plastic flow in a deep notch will occur according to a solution analogous to the one discussed here for plane strain, and that the stress at which flow occurs is dependent purely on plastic-flow characteristics. Thus

the greatest stress which can be produced by the constraining effect of the notch is a function of the yield stress, and is not limited only by the cohesive strength of the material.

Similar considerations apply for the plane-strain problem discussed in this paper. The tensile stress of Equation [8] is the maximum stress produced by the constraint of the notch, and, if this is less than the cohesive strength, plastic flow would, in general, be expected before fracture. The amount of flow before the notch-bar parts, if fracture does not occur to arrest the plastic flow, can be measured, roughly, by the dimension OP in Fig. 6, for this represents one half of the over-all extension. The construction of Fig. 6, in which AP is parallel to CO, indicates clearly that this maximum amount of plastic flow decreases with notch semiangle α, and is zero for zero α. Thus, in the limit $\alpha = 0$, our solution predicts a flow type of fracture at the notch stress $2\kappa(1 + \pi/2)$ with zero deformation. This forms an interesting comparison with Kuntze's conjecture that for this case plastic flow would be prevented by hydrostatic tension and that the corresponding stress would be the technical cohesive strength.

It should be emphasized that this limit is just where the assumptions of our solution cease to apply, for strains large with respect to elastic strain were assumed, and the surface energy of the metal was neglected in comparison with the energy absorbed in plastic flow. Clearly these assumptions do not apply in the limit when the plastic flow is zero. Nonetheless, one would expect the deformation to diminish with decreasing notch angle, the solution forming an interesting contrast with Kuntze's hypothesis.

BIBLIOGRAPHY

1 "The Theory of Wedge Indentation of Ductile Materials," by R. Hill, E. H. Lee, and S. J. Tupper, Proceedings of the Royal Society of London, England, series A, vol. 188, 1947, pp. 273–289.

2 "Ueber einige statisch bestimmte Faelle des Gleichgewichts in plastischen Koerpern," by H. Hencky, *Zeitschrift für angewandte Mathematik und Mechanik*, vol. 3, 1923, pp. 241–251.

3 "The Plastic Yielding of Notched Bars Under Tension," by R. Hill, *Quarterly Journal of Mechanics and Applied Mathematics II*, vol. 1, 1949, pp. 40–52.

4 "Some Special Problems of Indentation and Compression in Plasticity," by R. Hill, Proceedings of the Seventh International Congress of Applied Mechanics, vol. 1, 1948, pp. 365–377.

5 "Mechanics of the Metal Cutting Process. I. Orthogonal Cutting and a Type 2 Chip," by M. E. Merchant, *Journal of Applied Physics*, vol. 16, 1945, p. 273.

6 "Kohaesionsfestigkeit," by W. Kuntze, *Mitteilungen der Deutscher Materialprüfungsanstalten*, Sonderheft 20, Berlin, Germany, 1932.

7 "Notch Brittleness and the Strength of Metals," by E. Orowan, Transactions of the Institution of Engineers and Shipbuilders in Scotland, vol. 89, 1945, pp. 165–196.

Experiments on the Plastic Compression of a Block Between Rough Plates

By J. F. NYE,[1] CAMBRIDGE, ENGLAND

Hill, Lee, and Tupper have recently published a theory for the plastic compression of a block between parallel plates. This paper describes experiments designed to check the theory as closely as possible. The theoretical predictions for the average pressure on the plates are very well verified by the experiments. The details of the strain distribution within the block and the positions of the elastic-plastic boundaries are closely compared with the theory.

A NUMBER of attempts have been made to develop a theory describing the plastic compression of a block between parallel rough plates. Following the incomplete solutions given by Prandtl (1),[2] by Geiringer and Prager (2), and by Geiringer (3), Hill, Lee, and Tupper (4) by a numerical procedure have produced a solution which satisfies all the boundary conditions both for stress and displacement.[3] Their solution was first circulated as a departmental government report[4] in 1945, and at their instigation the author carried out a series of experiments to test the theory. The experimental results were also circulated as a report[5] in 1947. Now that the theory has been published in this journal it has been thought worth while to publish the experiments as well.

Few theoretical solutions of plastic flow problems have been fully tested by experiment. Most tests have been partly qualitative and, in particular, have seldom included a quantitative examination of the distribution of strain in the deformed material. Accordingly these experiments were planned to give as complete a check as possible upon the theoretical predictions for the mean pressure on the plates, the distribution of strain, and the position of the plastic-elastic boundaries.

Choice of Material

The material assumed in the theory has a well-defined yield point and shows negligible strain-hardening. A full solution was obtained only by neglecting elastic strains. The material was further assumed to be isotropic throughout the straining, and to obey the Mises criterion of yielding and the Lévy-Mises law of plastic flow under combined stresses. These last two conditions made it desirable that the experimental material should be a metal. There does not seem to be any material, however, that adequately obeys all the requirements of the theory. Lead, for example, which has been chosen in the past on account of its softness, has no sharp yield point and has the further disadvantage that its large grain size causes unwanted local disturbances in strain. Work-hardened copper, on the other hand, has grains of small size and a well-defined yield point, but it is not isotropic and is too hard for experiments of this type.

The compromise adopted was to use rolled tellurium-lead containing 0.05 per cent of tellurium. This alloy is soft, and the rolled material becomes isotropic (at least under metallographic examination) if heated for 4 hr at 150 C. At the same time, the grain size, after the heat-treatment, is limited by the presence of the tellurium to about 0.06 mm. The degree to which the stress-strain curve of this material approaches the ideal may be judged from Figs. 1 and 2. The method of obtaining the stress-strain curves is described in the next section.

The Stress-Strain Curve

Four compression tests with cylindrical specimens were made to establish the stress-strain curve of the annealed tellurium-lead. The specimens were loaded by aid of an ordinary lever machine, and the amount of compression was measured on a dial gage. Vaseline was used as a lubricant between the specimen and the compressing plates. If the rate of strain is too great, creep effects interfere with the measurements; to avoid this, the loading was carried out in steps, and about 5 min was allowed to elapse after each successive loading before the strain reading was taken. Specimen A was compressed by about 10 per cent, and the resulting stress-strain curve is shown in Fig. 1. The change of cross section in the course of compression has been allowed for in computing the stress. The strain is defined as

$$-\frac{\Delta l}{l_0}$$

where l_0 is the original length of the specimen and $-\Delta l$ the decrease in length.

Specimens B and C were each compressed by more than 40 per cent, and the ordinates of the two resulting stress-strain curves were found to agree to within 3 per cent. With these two specimens a certain amount of barreling was observed, indicating that friction on the plates, due to the squeezing out of the lubricant, was causing a nonuniform compression and increasing the load. To estimate the magnitude of this effect the following procedure described by Taylor[6] was used. After a fourth specimen D had been compressed by about 18 per cent, the load was removed from it, new lubricant applied to the plates, and the test continued. In this way barreling was avoided, and a stress-strain curve was obtained which was free from the complicating effect

---

[1] Cavendish Laboratory, University of Cambridge; now at Bell Telephone Laboratories, Murray Hill, N. J.

[2] Numbers in parentheses refer to Bibliography at end of paper.

[3] The present position has been well summarized in "The Mathematical Theory of Plasticity," by R. Hill, Oxford University Press, England, 1950, pp. 226–234. See also "Approximate Solutions of Problems of Plane Plastic Flow," by P. G. Hodge, Jr., JOURNAL OF APPLIED MECHANICS, Trans. ASME, vol. 72, 1950, pp. 257–264.

[4] Theoretical Research Report No. 28/45, by R. Hill, E. H. Lee, and S. J. Tupper, Ministry of Supply.

[5] Theoretical Research Report No. 6/47, by J. F. Nye, Ministry of Supply.

Presented at the National Conference of the Applied Mechanics Division, State College, Pa., June 19–21, 1952, of THE AMERICAN SOCIETY OF MECHANICAL ENGINEERS.

Discussion of this paper should be addressed to the Secretary, ASME, 29 West 39th Street, New York, N. Y., and will be accepted until October 10, 1952, for publication at a later date. Discussion received after the closing date will be returned.

NOTE: Statements and opinions advanced in papers are to be understood as individual expressions of their authors and not those of the Society. Manuscript received by ASME Applied Mechanics Division, July 3, 1951. Paper No. 52—APM-10.

[6] Reference (5), p. 312.

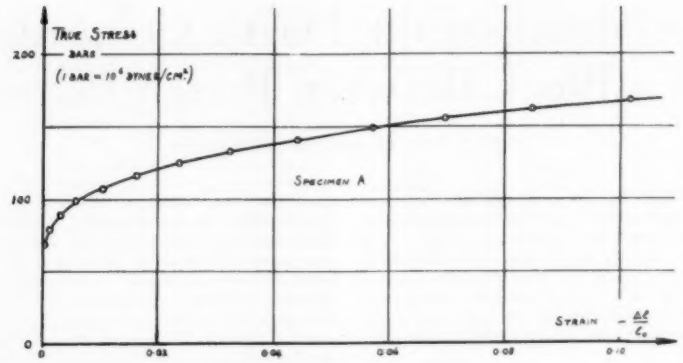

FIG. 1 STRESS-STRAIN CURVE IN COMPRESSION
(Annealed tellurium-lead.)

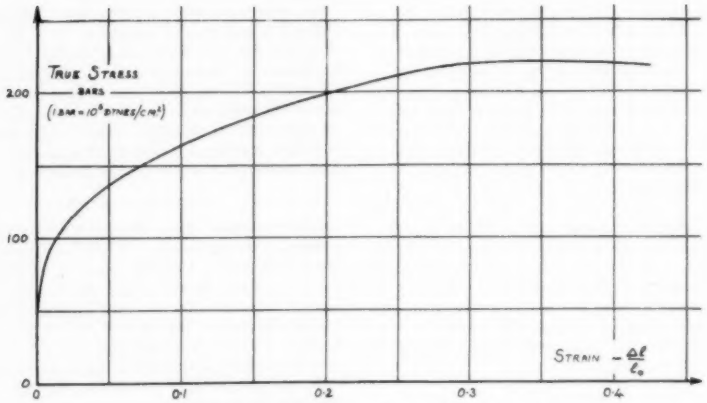

FIG. 2 MEAN STRESS-STRAIN CURVE IN COMPRESSION
(Annealed tellurium-lead.)

of plate friction. At a strain of 0.40 it lay 6 per cent lower than the mean curve of specimens B and C. The best mean of the four curves from specimens A, B, C, and D is drawn in Fig. 2.

It may be mentioned incidentally that the test with specimen D was continued to a compressive strain of more than 0.90 by repeated unloading and relubrication of the plates. At a certain stage, when the specimen was becoming unduly flattened, it was turned down on a lathe and the test continued. The result showed that the true stress-strain curve reaches a maximum of 222 bars [7] at a strain of 0.33, after which it falls gradually to 185 bars. For strains greater than 0.60 the stress remains constant at 185 bars.

DESCRIPTION OF TESTS ON RECTANGULAR BLOCKS BETWEEN ROUGH PLATES

To conform with the theory the rectangular blocks shown in Figs. 3 (*a*) and (*b*), have to be constrained to deform in plane strain, with no motion normal to the plane of the paper, but the metal must be allowed to flow out from between the plates at each side.

[7] 1 bar = 10^6 dynes per sq cm.

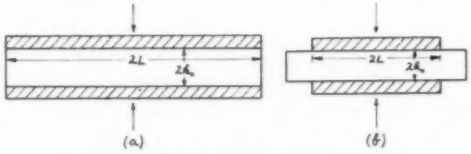

FIG. 3 THE TWO TYPES OF EXPERIMENT

Two types of experiments were performed, with and without a part of the metal projecting beyond the plates, as shown in Fig. 3.

The condition of plane strain was realized by compressing the metal within a trough of hard steel, Fig. 4. It flowed out from between the compressing surfaces in the direction *AA*, while the shoulders *BB* prevented any movement in the perpendicular direction. Each specimen consisted of two blocks *CC* of annealed tellurium-lead milled so as to fit the trough accurately when placed together within it. The combined clearance *DD* was not more than 0.005 in. so that very little displacement perpendicular to the main direction of flow could occur. All the block

surfaces were smoothed, and the interfaces between the two halves, which were to receive grids of squares, were highly polished. Two perpendicular sets of equally spaced lines, 1 mm apart, were scribed lightly on these faces with the help of a dividing engine, the blocks being placed in a carriage and made to slide beneath a fixed stylus. The carriage was provided with adjusting screws in order that the lines could be set accurately (*a*) parallel to the edges of the block, and (*b*) perpendicular to the measuring screw of the dividing engine. By this method lines were ruled so that the average deviation of the spacing from the mean value of 1 mm was 0.01 mm.

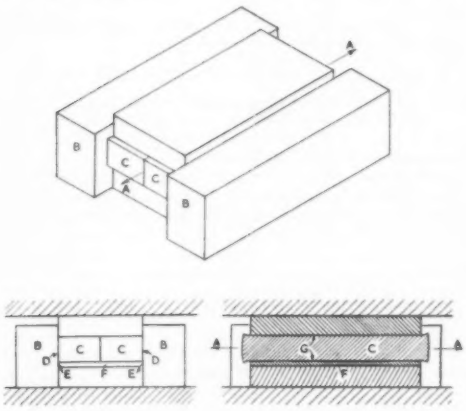

FIG. 4 EXPERIMENTAL ARRANGEMENT FOR COMPRESSING BLOCKS

Since high pressures were exerted on the shoulders *BB* during the compression, it was necessary to design the trough so as to avoid excessive concentrations of stress. The method adopted was to round the steps *EE* and to use a loose plate *F* to provide the lower compressing surface. There were, in fact, several of these plates to allow the compression of blocks of different sizes. As an additional precaution against cracking, the whole trough was surrounded by a substantial steel frame.

Friction on the faces *G* was achieved after various trials by grinding the steel with 120-grade silicon-carbide powder. The faces *DD* were lubricated with vaseline. Compression was carried out by placing the whole apparatus between the plates of an Amsler hydraulic testing machine. The load was increased at 5-min intervals by measured amounts, and at the end of each interval the extent of the compression was read from two dial gages attached at either side of the compression plates of the machine. Four blocks (each consisting of two parts) were compressed, as shown in Table 1.

The following notation will be used:

$2L$ = plate length
$2h_0$ = original height of block
$2h$ = current height
$s = h_0 - h$
$a_0 = \sqrt{2h_0}$
$a = \sqrt{2h}$

x_0, y_0 are original co-ordinates of a material point referred to the center of the block as origin,

x, y are current co-ordinates of the same point,

u_x, u_y are x and y-components of displacement of a point for unit compression ($s = 1$).

Fig. 5 shows the mean pressure p on the plates, deduced directly from the load, plotted against the amount of compression as measured by s/h_0. The change in height s was calculated from the dial gage readings by subtracting the elastic part of the compression. For blocks 2 and 3 the latter was obtained from an assumed value of Young's modulus, and for Nos. 4 and 5 from a curve measured as the blocks were unloaded, the amount of the correction to s/h_0 ranging from 0.008 to 0.01. The permanent compression was also measured after the test with a micrometer and was found to agree well with the dial gage readings.

The accuracy in the measurement of the curves may be judged from the fact that the curves for blocks 2 and 4, which were nearly identical in dimensions, should coincide. The same applies to blocks 3 and 5.

MEAN PRESSURE ON PLATES—COMPARISON WITH THEORY

Fig. 9 of reference (4) shows the distribution of pressure to be expected theoretically on the surface of a block whose ratio of length to height is 6.72 (which is very near to the initial ratio for blocks 3 and 5). The pressure-distribution curves for blocks of length-height ratios varying between 3.64 and 6.72 have been integrated by the authors of reference (4) with the result that within this range the mean pressure p is found to be related to k, the maximum shear stress (equal to $Y/\sqrt{3}$, where Y is the yield stress in compression, if Mises' criterion for yielding is adopted) by the equation

$$p = \left(0.52\,\frac{L}{h} + 1.42\right) k \qquad [1]$$

This equation is similar to that derived from the Prandtl cycloid solution if the condition is introduced that there should be no resultant force on the ends of the block, namely

$$p = \left(0.50\,\frac{L}{h} + 1.57 - \frac{h}{2L}\right) k$$

which, with $L/h = 6.72$, gives

$$p = \left(0.50\,\frac{L}{h} + 1.50\right) k$$

(The last equation differs slightly from that given by integration of the dashed pressure-distribution curve in Fig. 9 of reference (4), in that the elastic region at the center of the block has been taken as bounded by the cycloids through the center rather than by the slip lines given by the numerical computation.) For large values of L/h it is probable that the 0.52 in Equation [1] would approach 0.50.

Confirmation that the mean pressure on the plates is given by Equation [1] is to be found in the measured pressure curves for the four experimental blocks. From them the value of k given by Equation [1] has been plotted as a function of the plastic compression s/h_0, Fig. 6.

TABLE 1 BLOCK COMPRESSION DATA

Block no.	Length before compression, mm	Width, mm	$2L$, mm	$2h_0$ mm	L/h_0	After compression		
						$2h$, mm	s/h_0	L/h
2	69.85	49.8	50.15	11.98	4.19	7.18	0.400	6.99
3	100.65	49.8	101.1	14.98	6.76	12.20	0.185	8.30
4	69.75	49.8	50.15	12.30	4.08	11.511	0.0643	4.35
5	100.5	49.8	101.1	15.05	6.73	13.968	0.0718	7.25

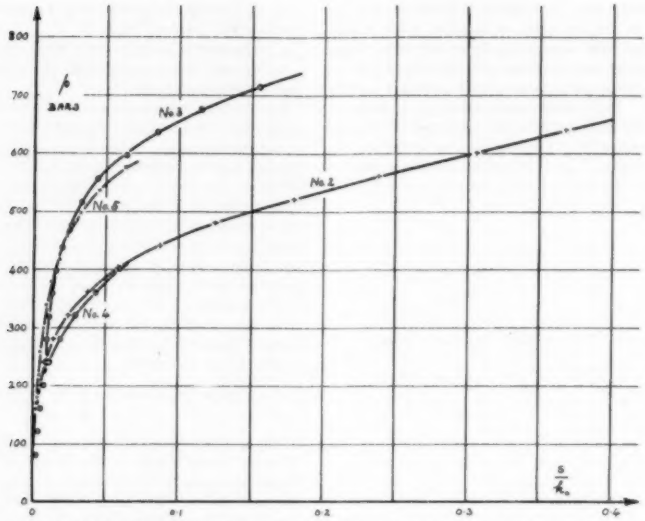

FIG. 5 MEAN PRESSURE ON PLATES AS A FUNCTION OF AMOUNT OF COMPRESSION

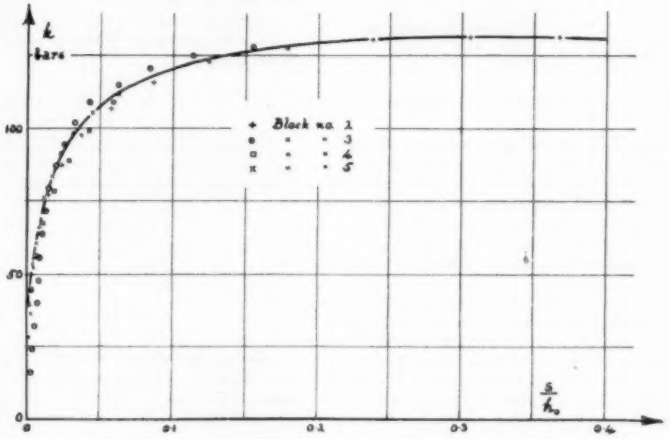

FIG. 6 MAXIMUM SHEAR STRESS AS A FUNCTION OF COMPRESSION, DEDUCED FROM PRESSURE CURVES IN FIG. 5

The theory assumes a material in which k is constant (no strain-hardening), so that the value of k to use in Equation [1] at any given value of the plastic compression is problematical. On the other hand it is remarkable that when k is plotted as a function of s/h_0 the curves for the four blocks all coincide within the limits of experimental error. We may conclude that not only is Equation [1] correct, but that the value of k to be used in it is independent of the length-height ratio of the blocks, at any rate for

$$4.08 \leqslant \frac{L}{h} \leqslant 8.30$$

The curve in Fig. 6 cannot be compared directly with the stress-strain curve in compression in Fig. 2 because it is not known how to relate the abscissas, but it is interesting to note that both curves reach a maximum. The maximum value of Y from Fig. 2 is 221.5 bars and the maximum value of k from Fig. 6 is 131.6 bars, which, when multiplied by $\sqrt{3}$, gives 227.9 bars. The heights of the maxima of the two curves, therefore, agree to within 2.9 per cent. It is rather surprising, and possibly fortuitous, that the maximum in each curve occurs at the same value of the abscissa

$$-\frac{\Delta l}{l_0} = \frac{s}{h_0} = 0.33$$

THEORETICAL STRAIN DISTRIBUTION

The field of slip lines computed for a length-height ratio of

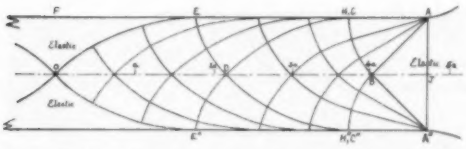

FIG. 7 FIELD OF SLIP LINES FOR A BLOCK OF LENGTH-HEIGHT RATIO 6.72

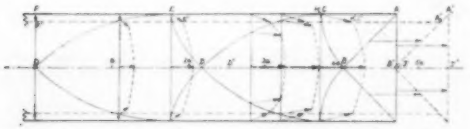

FIG. 8 VELOCITY FIELD CORRESPONDING TO SLIP-LINE FIELD IN FIG. 7, ASSUMING VELOCITY TO REMAIN CONSTANT FOR A COMPRESSION OF 14 PER CENT

6.72 is illustrated in Fig. 7, while Fig. 8 shows the corresponding velocity field calculated by Hill, Lee, and Tupper on the supposition that each point retains its initial velocity throughout a compression of 14 per cent. In Fig. 8 a prime denotes the position of a point after compression. Velocities are referred not to a time scale but to unit velocity of the plates.

The theoretical distribution along the x-axis of the velocity (displacement) component u_x is shown in Fig. 9, and above it is plotted the resulting strain distribution. A discontinuity will be seen at $x_0 = 2.175a_0$ corresponding to the point D of the slip-line field. In Fig. 7 points for which $x_0 > 4.05a_0$ are outside the plastic region and the strain and displacement of this part of the material are those of a rigid body. It is clear that since the section $AA''B$ moves out as a rigid body, the addition to the block of an overhanging part outside the plates should leave the strain distribution unaffected.

Curves showing the theoretical distribution of u_y and $\partial u_y/\partial y_0$ in the direction perpendicular to the plates are given in Figs. 10 and 11, for three different values of x_0. The discontinuity in the curves for $x_0 = 3.029\ a_0$ is again associated with the crossing of the slip line CD.

EXPERIMENTAL STRAIN DISTRIBUTIONS

After the compression the blocks were removed from the trough, sometimes with difficulty, and the two halves carefully separated. In the case of Nos. 2 and 3, both halves had been scribed, and the pressing of one upon the other during the test gave rise to two sets of lines, nearly coincident, on each block. To avoid this, in the tests with Nos. 4 and 5 only one half of each was treated. Photographs of the distorted grids of squares are shown in Fig. 12. The surface of the lead, which was originally highly polished, has become roughened in the regions of plastic distortion and these appear darker than their surroundings in views (*a*) and (*b*). Tracings of the grids on specimens 2, 3, and 5 were made at a magnification of 10 with the aid of a Hilger universal projector; they are reproduced in Fig. 13.

To gain more precise information about the distribution of strain throughout the blocks the spacing of neighboring grid lines was measured on the tracings for blocks 2 and 3, both along the center line $y = 0$, and along various ordinates. It was impossible to avoid a slight relative shear of the compression plates, and for this reason the diagrams in Fig. 13 are slightly unsymmetrical, all the lines being tilted over a little. The mean of the measurements on each side of $x = 0$ was taken in calculating the curves of strain distribution shown in Fig. 14. For block No. 5 greater accuracy in the measurement was necessary owing to the smallness of the compression, and it was found convenient to make use of the traveling stage of the projector. The lines whose spacing was to be measured were brought up in turn to a fixed mark on the projection screen and the movement of the stage read from a micrometer. The displacements and strains measured in this way are plotted in Figs. 10, 11, and 14. In all cases the strain is taken to be $\Delta l/l_0$, where l_0 is the original spacing of lines and Δl the change in spacing. Fig. 14 gives the strain along $y = 0$ plotted against the original abscissa x_0 of each point, while Fig. 11 shows the distribution in the perpendicular direction for the same three values of x_0 as were chosen for the theoretical curves. In plotting these vertical strain distributions a mean of the values in each of the four quadrants was used.

COMPARISON OF THEORETICAL STRAIN-DISTRIBUTION CURVES WITH EXPERIMENT

In comparing the position of the boundaries of the plastic re-

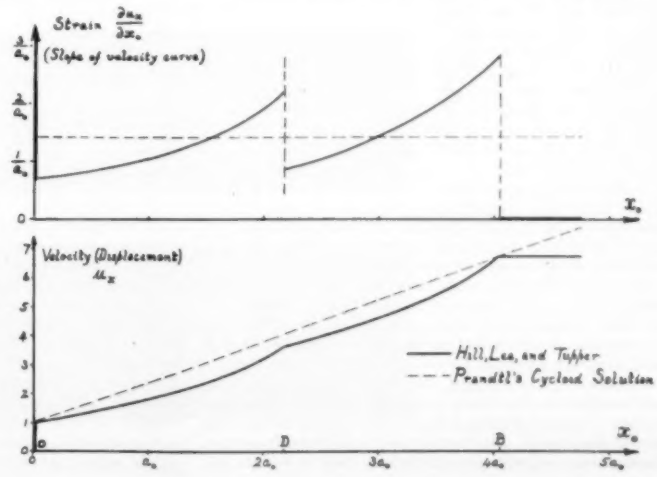

FIG. 9 THEORETICAL DISTRIBUTION OF VELOCITY (DISPLACEMENT) AND STRAIN ALONG AXIS OF BLOCK, INWARD VELOCITY OF UPPER PLATE BEING UNITY

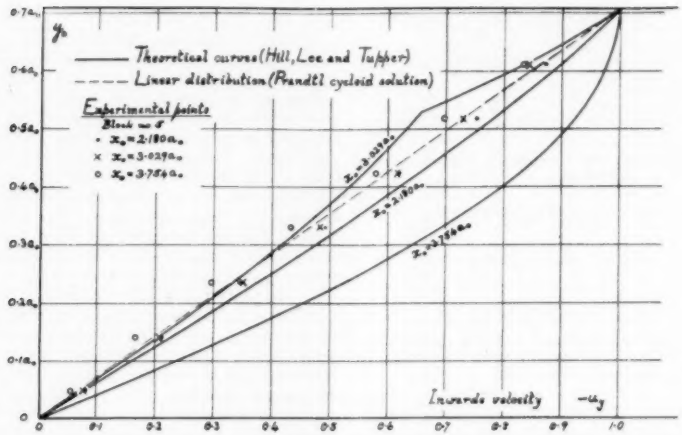

FIG. 10 DISTRIBUTION OF VELOCITY—DISPLACEMENT—PERPENDICULAR TO AXIS OF BLOCK, INWARD VELOCITY OF UPPER PLATE BEING UNITY

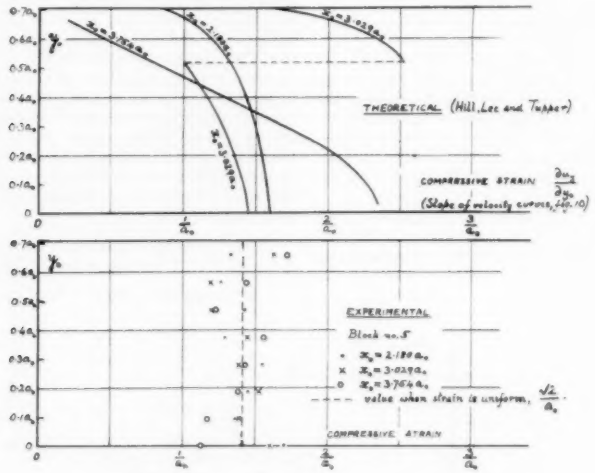

FIG. 11 DISTRIBUTION OF STRAIN PERPENDICULAR TO AXIS OF BLOCK

gions shown in Fig. 7 with the tracings of distorted grids of squares, and also in relating the theoretical curves of velocity and strain distribution to the corresponding measured curves, it is necessary to bear in mind that the theoretical curves refer to infinitesimal displacements or, more precisely, to instantaneous values of the velocities calculated for a certain length-height ratio (6.72). In applying them to a block that has undergone a finite compression there are two complicating factors. One is that as the deformation proceeds L/h is increased, the slip-line field is correspondingly modified, and the plastic boundaries move to new positions in space. Each new slip-line field of course will give rise to a new velocity distribution. But there is another, and more important, consideration; for, even were the velocity field to remain constant and fixed in space, a given material element of the block would not remain at the same place in that field during the course of the compression; it would occupy a succession of different positions in a certain limited range.

Fig. 15 will help to make this clear. In diagram (a) a block with an overhang is shown before compression. Let us consider point B of the slip-line field, Fig. 7. Before the compression it coincides with the element at B_1, A_1B_1 and H_1B_1 both being inclined at 45 deg to Ox. During compression $A_1KLH_1B_1$ moves out as a rigid body and B_1 entirely leaves the plastic region, diagram (b). The element that now coincides with the point B of the slip-line field is B_2, this element having moved out from some point within the plastic region. All the elements within the area $A_1B_1H_1H_2B_2A_2$

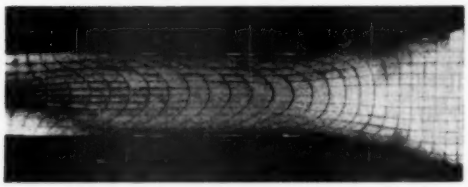

(*a*) Part of block No. 2; undistorted squares can be seen at right

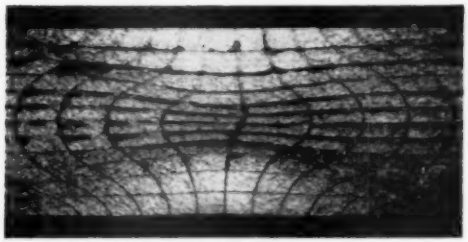

(*b*) Central region in block No. 2; showing "nonplastic" zones

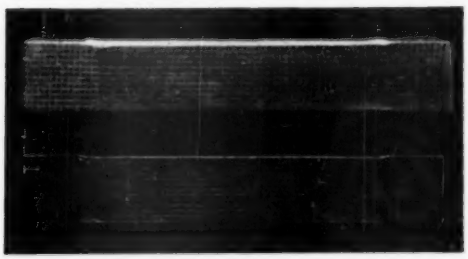

(*c*) Two halves of block No. 4; only upper half was scribed; lines on lower half were imprinted during compression

(*d*) Block No. 5; no overhang; compression = 7.18 per cent

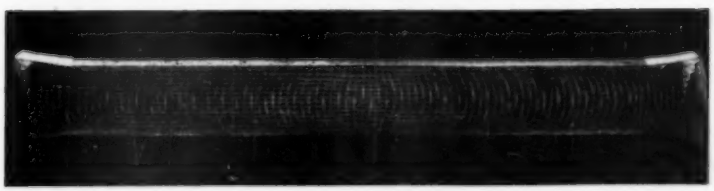

(*e*) Block No. 3; no overhang; compression = 18.5 per cent

FIG. 12 NETS OF SQUARES AFTER DEFORMATION

were plastic at the start of the compression but became rigid in their passage across the plastic boundary. Each element to the left of $A_2B_2H_2$, on the other hand, was always plastic, although situated at different positions in the velocity field during the distortion. That $A_1B_1H_1$ was, in fact, the initial position in the block of the plastic boundary for specimen No. 2 can be seen from Fig. 13 and this conclusion is supported by the upper strain-distribution curve in Fig. 14. The elements designated by B_1 and B_2 in Fig. 15 are marked by the same letters in Fig. 14. In Fig. 15 (*a*) therefore, $OB_2 = 11.8$ mm and $OB_1 = 19.1$ mm for block No. 2.

As expected, the strain is zero to the right of B_1. With block No. 5 the agreement is not so good; this block had no initial overhang. Elements from B_1 to B_2 were in the plastic region for increasingly long periods of the deformation and naturally give rise to the corresponding ascending portions of the strain-distribution curves.

As mentioned previously, the length-height ratio increases during the compression, and the change which this brings about in the slip-line field must be considered. The theoretical slip-line field for a length-height ratio rather greater than 6.72 is indicated in Fig. 16. According to Figs. 8 and 9, discontinuities in velocity gradient should be expected across certain slip lines as, for example, ED and DH. The discontinuity associated with one of these slip lines is only momentary for an element crossing it, and its final effect is a discontinuity in the curvature of a deformed transverse line. The discontinuity in slope of such a line in Fig. 8 is due simply to the assumption of a constant velocity field over a finite time interval. With large compressions the discontinuities become considerably spread out. For example, in block No. 2 the element which originally coincided with point D of the slip-line field was at a distance $2.07\ a_0$ from the center of the block. During the compression this element moved out along Ox past B, and well into the rigid region. Its place was taken by an element which started at a distance of only $0.67\ a_0$ from the center of the block. Thus all elements within the range $0.67\ a_0 \leqslant x_0 \leqslant 2.07\ a_0$ came under the influence of the discontinuity at D at some instant of the compression. With block No. 5 the compression was much smaller and, as is shown by the points marked D_1 and D_2 in Fig. 14, the range was only $1.84\ a_0 \leqslant x_0 \leqslant 2.175\ a_0$. Fig. 14 also indicates the elements which were initially and finally at G.

The theory predicts discontinuities in velocity gradient at 0, D, G, and B. As mentioned previously, the existence of the one at B is clear from the upper curve in Fig. 14. That at D, on the other hand, would not be expected to show for such a large compression as 40.0 per cent. There is, however, no sign of it in the lower curve in Fig. 14 which represents a much smaller compression (7.18 per cent). Nor is the discontinuity in the curve for $x_0 = 3.029\ a_0$ in Figs. 10 and 11 reflected in the experimental points. Indeed, it is noteworthy that for all cases, and particularly for the two blocks of large length-height ratio, there is a substantial region (XX in Fig. 14) over which the strain is independent of x, a fact which can also be seen from the experimental points in Figs. 10 and 11. Over this region the

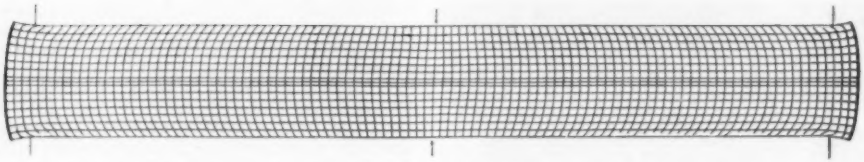

Block No. 5; compressed 7.18 per cent; no overhang; length-height ratio 6.73 before compression

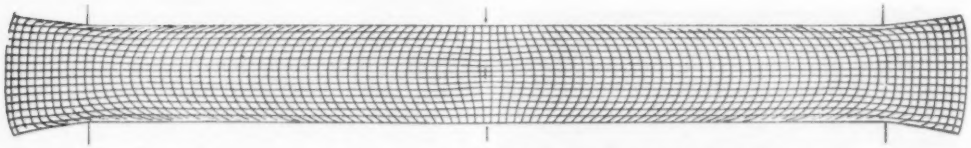

Block No. 3; compressed 18.5 per cent; no overhang; length-height ratio 6.76 before compression

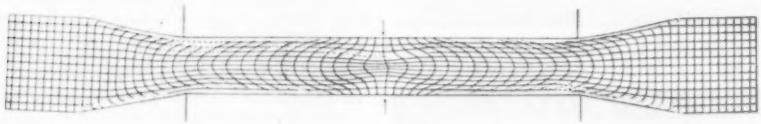

Block No. 2; compressed 40.0 per cent; overhang of 10 mm at each end; compressed length/initial height = 4.19

FIG. 13 TRACINGS OF DISTORTED GRIDS OF SQUARES RULED ON BLOCKS

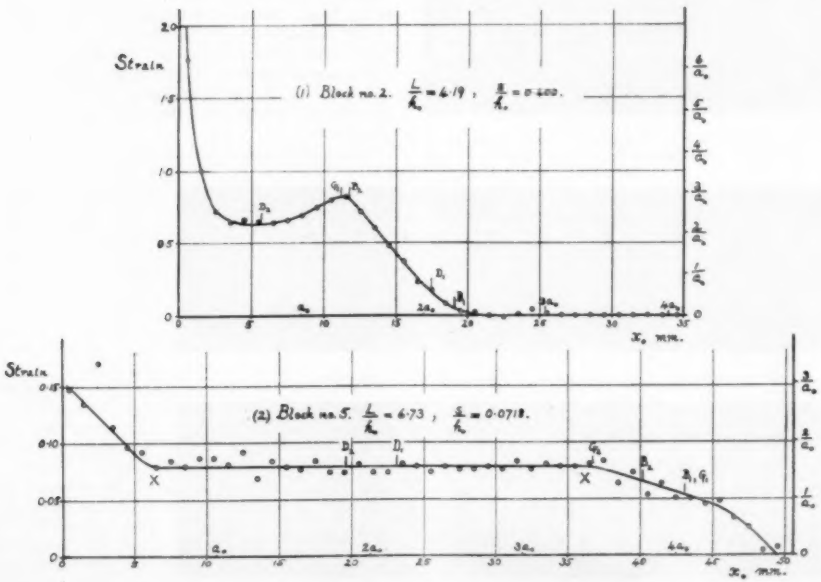

FIG. 14 DISTRIBUTION OF STRAIN ALONG AXIS OF BLOCK MEASURED EXPERIMENTALLY

(B_1, point corresponding to material element originally at B in slip-line field; B_2, point corresponding to material element finally at B in slip-line field; similarly for D_1, D_2, G_1, and G_2.)

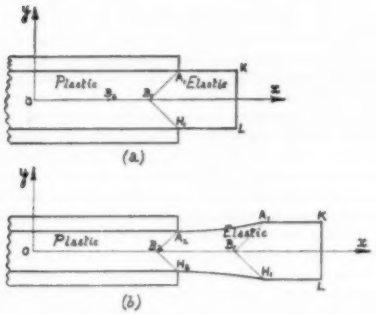

FIG. 15 PLASTIC BOUNDARIES BEFORE AND AFTER COMPRESSION

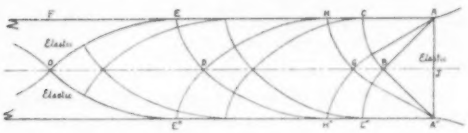

FIG. 16 SLIP-LINE FIELD FOR LENGTH-HEIGHT RATIOS GREATER THAN 6.72

deformed grids of squares show that the distortion consists of a simple shear parallel to Ox, of an amount which varies with y, together with a compression in the direction of Oy. This compression, moreover, is strikingly uniform, as can be seen by a comparison of the experimental points with the broken curves in Figs. 10 and 11. The evenness of spacing of the horizontal grid lines implied by this property is retained even up to the highest compression used (40.0 per cent).

Thus the strain discontinuities propagated along slip lines, predicted by the theory for an ideally plastic material, seem to disappear when a material is used whose stress-strain curve shows a smooth transition from elastic to plastic behavior. This would be expected on general grounds, since a strain discontinuity in a strain-hardening material would imply a stress discontinuity.

In reference (4) an analog of Saint Venant's principle in the theory of elasticity is suggested whereby the stress distribution approaches that given by Prandtl's analysis for a long block in regions far from the edges. A similar principle for the velocity distribution is less likely to hold, for the velocity field has to be built out from the center of the block, and there is a discontinuity in tangential velocity along the bounding slip line OE, Fig. 16, together with discontinuities in velocity gradient across ED, DH, etc. Now it is conceivable, of course, that these discontinuities along slip lines, although propagated, become progressively weaker, but no evidence exists for this at present, and a final answer to the problem must await a more extended calculation of the velocity field. Nevertheless one can say in general terms that if the strain distribution at large distances from the center of the block of ideally plastic material does approach a configuration that is independent of x, it certainly does not do so at all rapidly.

On the other hand, it is plausible to suppose that an analog of Saint Venant's principle applies for the strain distribution in a work-hardening material, for, according to the experimental results given here, the deformation has settled down to a state of strain that does not vary with x at quite a short distance, of the order of h_0, from the central region.

The author has attempted elsewhere a theoretical treatment of this steady state of strain (6). Here the steady state is compared with the predictions of earlier theories. The slip lines in Prandtl's solution were two orthogonal families of cycloids, and it is possible to derive a corresponding velocity distribution in which the velocity component u_x appears as a linear function of x_0. For a given y_0, $\partial u_x/\partial y_0$ is then independent of x_0. This is shown for $y_0 = 0$ by the broken curves in Fig. 9.

Such a velocity distribution implies that the vertical lines should be deformed into similar curves equally spaced in the x-direction. It follows, in view of the assumed incompressibility, that the horizontal lines should remain straight, parallel, and equally spaced after the compression. The vertical lines can be shown to be distorted into halves of ellipses, with semiminor axes of length

$$\frac{h_0^2 - h^2}{h}$$

Incidentally

$$\frac{h_0^2 - h^2}{h} \to 2s \quad \text{as} \quad s \to 0$$

These results are true for large strains of any magnitude.

The experiments show that in the region under consideration nearly all these properties are possessed by the grid lines. In particular, the lines are seen to be spaced equally in both horizontal and vertical directions. However, although it is true that the vertical lines in this region appear to be parts of ellipses, the lengths of the semiminor axes are not $(h_0^2 - h^2)/h$. The discrep-

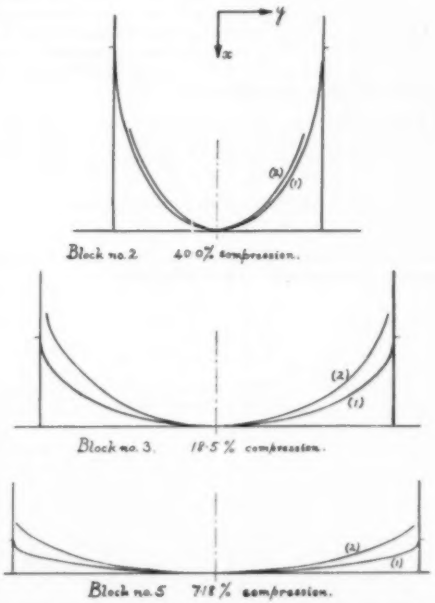

FIG. 17 SHAPE AFTER COMPRESSION OF LINES ORIGINALLY STRAIGHT AND PARALLEL TO y-AXIS
(1, Ellipse predicted by Prandtl's theory; 2, experimental curve.)

ancy, which is no doubt mainly due to strain-hardening, may be judged from Fig. 17. It may also be noted that the observed and calculated curves agree more closely at higher compressions, where the whole of the metal has reached less steeply sloping parts of the stress-strain curve.

As a proof that there is no appreciable change in volume of the deformed material, the following measurements made on block No. 5 in the uniform region 15.5 mm $\geq x_0 \geq$ 35.5 mm may be quoted. The measured compression, s/h_0, together with the observation that the lines parallel to $y = 0$ remained equally spaced, was used to calculate the strain along $y = 0$. If the volume is assumed constant, the strain, as previously defined, is easily seen to be s/h, which in this case is 0.0776. This is to be compared with the measured strain along $y = 0$ in the uniform region, where the mean value is 0.0785, with an average deviation of the measurements from the mean of 0.0028. The actual figure given for the mean will of course be more accurate than this. Within the limits of experimental error, therefore, the volume change was zero.

As predicted by the theory, and by Prandtl's original analysis, two more or less rigid regions are seen at the center of the block. (block No. 2 in Fig. 12 shows this most clearly). The sharp rise of strain along $y = 0$ as x decreases to 0, Fig. 14, and the fact that the strain along $x = 0$ is not zero must be attributed to the continuous transition from elastic to plastic behavior.

It may be recalled that the shape of the part of the body extruded from between the plates was shown by Hill, Lee, and Tupper to be expressed by the differential relationship

$$ydx = Ldy$$

where $y = f(x)$ is the shape of the extruded portion, Fig. 18.

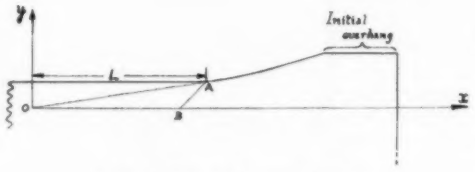

FIG. 18 SHAPE OF EXTRUDED MATERIAL

OA is then a tangent to $y = f(x)$ at A. The latter fact is verified roughly by an inspection of the distorted grids.

CONCLUSIONS

The main conclusions to be drawn from the experiments are as follows: The theory predicts very well the way in which the mean pressure on the plates varies with the geometry of the block and the amount of compression. The lack of a material without strain-hardening makes it more difficult to check the theoretical velocity distribution. There is also the difficulty that the problem is not geometrically similar throughout the compression, and the velocity distribution has only been computed for one instant. Some theoretical conclusions, for instance the position of the outer plastic boundary when the deformed body protrudes beyond the compression plates, appear to be true independently of the precise relationship between stress and strain in the material used. Other predicted effects, as, for example, the existence of discontinuities in velocity gradient propagated along slip lines, do not appear in the experiments and are a direct consequence of the idealized stress-strain curve. The analog of Saint Venant's principle in the theory of elasticity, suggested by Hill, Lee, and Tupper as applying to the stress distribution in an ideally plastic body, appears to hold also for the strain distribution in a real, strain-hardening material.

ACKNOWLEDGMENTS

The author would like to thank Mr. W. J. Cairns for his help in the experiments. He is also indebted to Dr. E. Orowan, F. R. S.; to Dr. E. H. Lee, Dr. R. Hill, and Mr. S. J. Tupper for their advice and for permission to publish the curves giving the results of their theoretical work; and to Prof. J. F. Baker for permission to use the facilities of the Engineering Laboratories, University of Cambridge, England. Acknowledgment is made to the Chief Scientist, Ministry of Supply, for permission to publish this paper

BIBLIOGRAPHY

1 "Anwendungsbeispiele zu einem Henckyschen Satz ueber das plastische Gleichgewicht," by L. Prandtl, *Zeitschrift für angewandte Mathematik und Mechanik*, vol. 3, 1923, pp. 401–406.

2 "Mechanik isotroper Koerper im plastischen Zustand," by H. Geiringer and W. Prager, *Ergebnisse der exacten Naturwissenschaften*, vol. 13, 1934, pp. 310–363.

3 "Fondements mathématiques de la théorie des corps plastiques isotropes," by H. Geiringer, *Mémorial des Sciences Mathématiques*, vol. 86, 1937.

4 "A Method of Numerical Analysis of Plastic Flow in Plane Strain and Its Application to the Compression of a Ductile Material Between Rough Plates," by R. Hill, E. H. Lee, and S. J. Tupper, JOURNAL OF APPLIED MECHANICS, Trans. ASME, vol. 73, 1951, pp. 46–52.

5 "Plastic Strain in Metals," Twenty-Eighth May Lecture, by G. I. Taylor, *Journal of the Institute of Metals*, vol. 62, 1938, p. 307.

6 Ph.D. Dissertation, by J. F. Nye, Cambridge, England, 1948.

A Theory of Plastic Bending From a Statistical Aspect

By HERMANN CRAEMER,[1] ALEXANDRIA, EGYPT

The apparent increase of the yield stress under bending with respect to that under pure tension is explained by the lesser probability that a weak element is situated close to an edge.

Old and New Theories of Plasticity

THERE has been a controversy between the adherents of the so-called old, also classical, and new theories of plasticity. The first pretend that, in a bending test, after the edges have reached the yield stress as determined in a tensile test, yield gradually penetrates into the cross section as shown in Fig. 1(*a*) until the neutral axis is reached. Contrary to this, according to their opponents, who refer to experimental evidence, the stress distribution remains linear until a stress is reached which they call the bending yield stress and which is much higher than the yield stress from the tensile test, whereafter almost suddenly the whole cross section becomes plastic, Fig. 1(*b*). This means that the stress-strain relation is not the same as under pure tension. It is difficult to realize how such a "tele-effect" can work and how the outer fibers are notified that they form part of a cross section under bending and therefore have to change their strength properties.

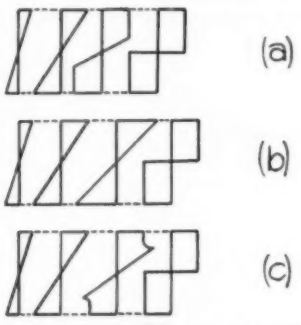

Fig. 1 Stress Distribution at Section of Beam

Now, if we take into account a possible upper yield stress and stick to the stress-strain relation obtained from the tensile test, we arrive at Fig. 1(*c*). It can be shown that when the upper yield stress is just 1.5 times the lower one, for a rectangular bar, Fig. 1(*c*) passes into Fig. 1(*b*). So there is no reason to adopt the foregoing criticized tele-effect. This has been pointed out and verified experimentally by Rinagl.[2]

However, the sequence of stress distributions as shown in Fig. 1(*b*), can be explained without the assumption of an upper yield point if the statistical fluctuation of the strength properties is taken into account. It is well known that, even under apparently perfectly equal conditions, the results obtained from different specimens vary about an average. This, of course, is true also for the different elements of which a test piece can be considered to be composed. What is measured as the yield stress of a bar, thus in reality is a function of the varying, although unknown, properties of its elements.

Let a cross section be composed of $2r$ equal elements, Fig. 2, and let each of them obey Prandtl's idealized plastic stress-strain law with equal modulus of elasticity but varying yield stress, Fig. 3(*a*). If now the specimen is submitted to an equally distributed unit strain, i.e., pure tension, Fig. 2(*a*), the stresses will be equal until the weakest element reaches its yield point. Hereafter the remaining $(2r - 1)$ elements have to carry the excess of the load alone; thus their stress will now increase more rapidly than the load, see point 1 in Fig. 3(*b*). Point 2 in the figure corresponds to the next weakest element and the horizontal line to the state when all elements have yielded. The stress-strain function of a bar thus does not follow the idealized broken line even if those of its elements do. Summarizing, we state that the starting of yield in a tensile bar is controlled by its weakest element.

Now, this is not the case in a bending test with a triangular strain distribution, Fig. 2(*b*). It is quite improbable that just the weakest element would be situated at an edge and thus make

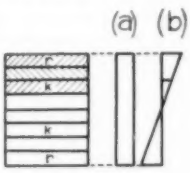

Fig. 2 Strain Distribution at Section of a Beam (*a*, Pure tension; *b*, bending.)

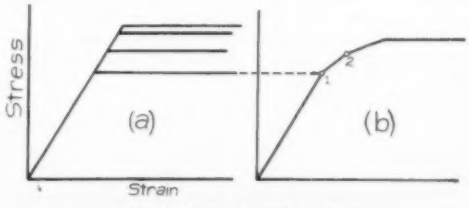

Fig. 3 Stress-Strain Curves

[1] Professor of Engineering, Bulkeley, Immeuble Binoor.

Presented at the National Conference of the Applied Mechanics Division, State College, Pa., June 19–21, 1952, of The American Society of Mechanical Engineers.

Discussion of this paper should be addressed to the Secretary, ASME, 29 West 39th Street, New York, N. Y., and will be accepted until October 10, 1952, for publication at a later date. Discussion received after the closing date will be returned.

Note: Statements and opinions advanced in papers are to be understood as individual expressions of their authors and not those of the Society. Manuscript received by ASME Applied Mechanics Division, December 6, 1951. Paper No. 52—APM-26.

[2] "Yield Limits and Characteristics Under Bending," by F. Rinagl, International Association for Bridge and Structural Engineering, 2nd Congress, Berlin-Munich, Preliminary Publication, Appendix to the volume, 1936, Paper No. I, 3, pp. 1561–1582.

yield start. The probability is much greater that it lies anywhere in the inner part of the beam where the strain and, therefore, the liability to yield is less. What, in turn, can be expected at an edge is an element not with minimum but with intermediate properties. As a consequence, under bending, the edges will with great probability yield under a larger stress than in the tensile test. Sometimes it occurs that a smaller yield stress belongs to a smaller Young's modulus; in such a case the stress in the weakest element is comparatively less than in the stronger ones, i.e., it is to some extent protected against overstressing and the foregoing explained effect is less marked.

This is the qualitative explanation of the observations referred to in the "new" plastic theory.

Statistical Distribution Law for Yield Stresses

To explain them quantitatively we need to assume a statistical distribution law for the yield stresses of the elements. The well-known Gaussian normal distribution leads to cumbersome arithmetic and implies negative values of the yield stress which would be meaningless. Both are avoided by the use of the distribution proposed by Weibull[2] for strength problems; it runs

$$p = \exp\left[-\left(\frac{\sigma}{\sigma_u}\right)^c\right] \qquad [1]$$

Herein "exp" is the exponential function, p is the probability that an element has at least a yield stress equal to σ; σ_u and c are constants. If σ_a is the average (arithmetic mean) and s the standard deviation belonging to the distribution, Equation [1], the ratios σ_a/σ_u and s/σ_a are functions of c only

$$\frac{\sigma_a}{\sigma_u} = F_1(c), \quad \frac{s}{\sigma_a} = F_2(c) \qquad [2]$$

They have been computed in Weibull's paper[2] with the help of gamma-functions, and Table 1 is drawn from it. The last line in the table will be explained later.

TABLE 1

$c =$	2	3	4	8	20	100
$\sigma_a/\sigma_u =$	0.886	0.893	0.906	0.942	0.974	0.994
$s/\sigma_a =$	0.522	0.364	0.281	0.148	0.062	0.0127
$\sigma_{ba}/\sigma_{sa} =$	1.735	1.585	1.495	1.315	1.165	1.05

Now, the probability p_s, that in a tensile bar yield starts at a stress not less than σ, equals the probability that each of its $2r$-elements has a yield stress not less than σ; according to laws of probability (probability of "as well as") this is

$$p_s = p^{2r} \qquad [3]$$

or, using Equation [1]

$$p_s = \exp\left[-2r\left(\frac{\sigma}{\sigma_u}\right)^c\right] \qquad [4]$$

Let σ_{sa} be the average yield starting stress for the tensile piece belonging to the foregoing distribution, and s_s the corresponding standard deviation. The first can be found from Equation [4] in the same way as σ_a was found from Equation [1] and, by just exchanging σ_u for $\sigma_u/(2r)^{1/c}$ and making use of Equations [2], we have

$$\sigma_{sa} = \frac{\sigma_a}{\sqrt[c]{2r}} \qquad [5]$$

and similarly

$$s_s = \frac{s}{\sqrt[c]{2r}} \qquad [6]$$

These, by the way, are the formulas expressing the dependency of strength upon the size of a brittle tensile specimen which, however, lies outside the scope of this paper.

In order that the stresses at the edge of the same piece under bending may reach a value not less than σ when yield starts anywhere, it is necessary that the particular yield stress of each element is at least $(k/r)\sigma$, as is easily understood from Fig. 2(*b*). The probability that this holds for a single element k is according to Equation [1]

$$p_k = \exp\left[-\left(\frac{k}{r}\frac{\sigma}{\sigma_u}\right)^c\right] \qquad [7]$$

whereas the probability that it holds for all of them is

$$p_b = p_1^2\, p_2^2 \cdot \ldots \cdot p_k^2 \ldots p_r^2 \qquad [8]$$

as there are always two elements equally stressed in the top and bottom chord of the beam. Combining Equations [7] and [8] we have

$$p_b = \exp\left[-2\left(\frac{\sigma}{r\,\sigma_u}\right)^c \sum_1^r k^c\right] \qquad [9]$$

From this, too, an average can be obtained by using

$$\frac{\sigma_u\, r}{\sqrt[c]{2\sum_1^r k^c}}$$

instead of σ_u; we find

$$\sigma_{ba} = \frac{r\,\sigma_a}{\sqrt[c]{2\sum_1^r k^c}} \qquad [10]$$

and, correspondingly

$$s_b = \frac{r\,s}{\sqrt[c]{2\sum_1^r k^c}} \qquad [11]$$

This is the average and the deviation of the edge stress when yield starts in a bending test.

Comparing now σ_{ba} and σ_{sa}, we get

$$\frac{\sigma_{ba}}{\sigma_{sa}} = \sqrt[c]{\frac{r^{c+1}}{\sum_1^r k^c}}$$

It is seen that the unknown property σ_u of the elements is eliminated. As to r, it is most reasonable to imagine the piece composed of an infinity of small pieces and, making $r = \infty$, the equation passes into

$$\frac{\sigma_{ba}}{\sigma_{sa}} = \sqrt[c]{c+1} \qquad [12]$$

By inspection of Equations [5], [6], [10], and [11] we see that

$$\frac{s_s}{\sigma_{sa}} = \frac{s_b}{\sigma_{ba}} = \frac{s}{\sigma_a} \qquad [13]$$

i.e., the standard deviation relative to the average remains unchanged when tensile or bending members are considered in-

[2] "The Phenomenon of Rupture," by W. Weibull, Royal Swedish Institution of Engineering, Research Proceeding No. 153, 1939

stead of elements; this is due to the particular form of Weibull's distribution function. When either s_a/σ_{na} or s_b/σ_{ba} are known we can determine c from Table 1, and represent σ_{ba}/σ_{na} as a function of the relative standard deviation.

The results have been inserted in the last line of the table and plotted in Fig. 4.

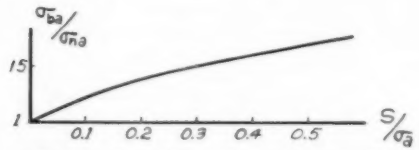

FIG. 4 AVERAGE EDGE STRESS VERSUS STANDARD DEVIATION

A similar reasoning is possible for a circular or a diamond cross section. As there is relatively more material near the neutral axis, the probability of yield under bending would lessen and the corresponding curve would, although starting from the same point, lie higher than that in Fig. 4. More complicated cases, such as stress concentration around a hole, can be examined along the same lines. Contrary to this, in an I-beam, the ratio σ_{ba}/σ_{na} should be very close to 1.0 as most of the material is situated at the edges.

WHEN CROSS SECTION IS FULLY PLASTIC

Finally, we shall examine the case when the whole cross section is fully plastic, i.e., when every element is strained within the horizontal range of the lines of Fig. 3(*a*). In a tensile test piece the apparent stress then will be equal to the average of the yield stresses of its elements. The same is true, however, for the stresses in either the tensile or compressive zone of a beam, if computed after the plastic theory, viz., $4\ M/b\ h^2$ for a rectangle.

Thus there is no distinction between the yield stresses corresponding to full plastic action in the tensile and bending tests. A possible eccentricity in the tensile test as well as a possible deviation in the distance between the interior resultants in compression and tension under bending which may occur due to the nonhomogeneity of the material, have been neglected.

No preciseness, of course, is claimed for the results of this investigation which would be different if another frequency distribution had been assumed. The general trend, however, coincides with what can be expected and it would be informative if experimental data which, mostly, do not state a standard deviation or even distribution would be enlarged in order to make a check possible.

Thermal Stresses in Bodies Exhibiting Temperature-Dependent Elastic Properties[1]

By H. H. HILTON,[2] URBANA, ILL.

Expressions are derived for thermal stresses and strains due to a steady-state temperature gradient in a thick-walled cylinder and a circular thin plate, made of a material having temperature-dependent elastic properties. Two numerical examples are computed for specific temperature gradients and temperature-dependent elastic properties, which yield results showing that the maximum thermal stresses are appreciably lower and the maximum thermal strains are larger than the corresponding values obtained for temperature-independent properties. The validity of the thermal plane-stress assumptions is investigated and it is shown that such solutions, regardless of whether the material properties are temperature-dependent or constant, are only approximations. The smaller the temperature gradient the more closely are the plane-stress assumptions satisfied.

Nomenclature

The following nomenclature is used in the paper:

a, A_n = constants
b = constant
c, C_n = constants
G = shear modulus as a function of the temperature, psi
G_0 = value of shear modulus at room temperature, psi
G_1 = constant
r = radial co-ordinate (nondimensional, radial length divided by radius of hole)
T = temperature above a value which corresponds to zero stress, deg F
T_n = constants
u_i = displacement in the ith direction
z = axial co-ordinate (nondimensional)
α = coefficient of linear thermal expansion as a function of the temperature (in/in-deg F)
α_n = constants
ϵ_{ij} = strain component on the ith face in the jth direction
σ_{ij} = stress component on the ith face in the jth direction
φ = angular co-ordinate (radians)

Introduction

The operating temperatures of modern aircraft propulsion units are of such magnitudes that the existing classical elastic thermal-stress solutions (1)[3] no longer truly describe actual phenomena. These solutions ignore the behavior of material properties under temperature and, consequently, become only approximations at higher temperatures where not only material properties vary appreciably with temperature, Fig. 1, but in addition Hooke's law is no longer applicable even at very low stresses (2, 3).

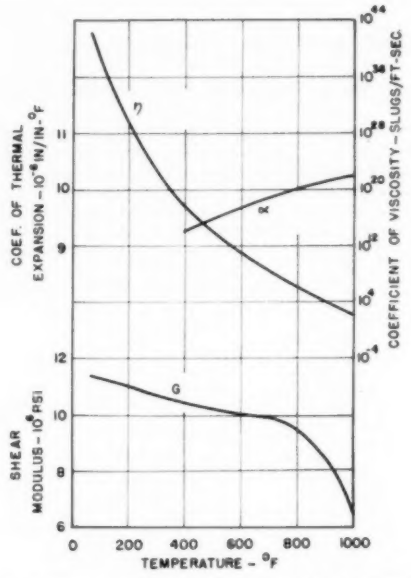

Fig. 1 Variation of Material Properties With Temperature

This anelastic or viscoelastic behavior of metals must be represented by relations between stresses, strains, and their time derivatives (4). Thermal-stress solutions based on temperature-dependent viscoelastic stress-strain relations have been obtained recently by the author (5, 6). It was shown that the elastic thermal stresses and strains (based on temperature-dependent elastic material properties) represent the maximum values in the case of the incompressible viscoelastic Maxwell body.

This paper presents an analysis of thermal stresses and strains, taking into account the variations of the elastic shear modulus and the coefficient of thermal expansion with temperature. The results that are developed establish the initial conditions of the viscoelastic problem and they further serve to indicate

[1] This paper represents a portion of a thesis submitted to the Graduate College of the University of Illinois in partial fulfillment of the requirements for the degree of Doctor of Philosophy in Theoretical and Applied Mechanics.

[2] Assistant Professor, Department of Aeronautical Engineering, University of Illinois. Jun. ASME.

Presented at the National Conference of the Applied Mechanics Division, State College, Pa., June 19–21, 1952, of The American Society of Mechanical Engineers.

Discussion of this paper should be addressed to the Secretary, ASME, 29 West 39th Street, New York, N. Y., and will be accepted until October 10, 1952, for publication at a later date. Discussion received after the closing date will be returned.

Note: Statements and opinions advanced in papers are to be understood as individual expressions of their authors and not those of the Society. Manuscript received by ASME Applied Mechanics Division, September 13, 1951. Paper No. 52—APM-32.

[3] Numbers in parentheses refer to the Bibliography at the end of the paper.

the effect of temperature-dependent material properties on the thermal stresses and strains.

As a fundamental understanding of the problem was desired, the analysis was simplified by treating only rotationally symmetrical bodies with steady-state temperature gradients in the radial direction.

Thick-Walled Cylinder Problem

Consider a long thick-walled, circular cylinder, Fig. 2, subjected to a steady-state temperature gradient $T = T(r)$, which is

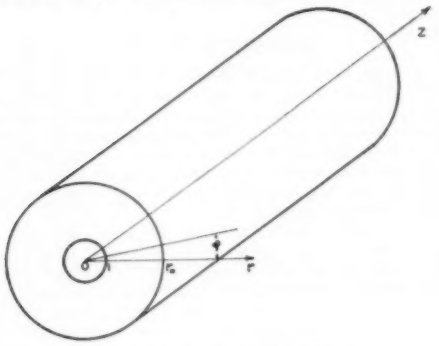

Fig. 2 The Circular Cylinder

symmetrical with respect to the axis of the cylinder and invariable in the axial direction. At a sufficient distance from the ends, the cross sections of the cylinder may be assumed to remain plane. Thus the problem is reduced essentially to a constant-strain problem with rotational symmetry.

The conditions of rotational symmetry are fulfilled only if

$$u_\varphi = \sigma_{r\varphi} = \sigma_{\varphi z} = 0 \quad [1]$$

$$\partial\sigma_{ij}/\partial\varphi = \partial\epsilon_{ij}/\partial\varphi = \partial u_i/\partial\varphi = 0 \quad [2]$$

If the cross sections are to remain plane, then

$$\epsilon_{zz} = \partial u_z/\partial z = \text{const} \quad [3]$$

and since the temperature is independent of both φ and z

$$\partial\sigma_{ij}/\partial z = \partial\epsilon_{ij}/\partial z = 0 \quad [4]$$

These conditions dictate that the shear strains vanish, or

$$\epsilon_{ij} = 0 \quad (i \neq j) \quad [5]$$

Five of the six compatibility equations are now satisfied identically and the remaining one reduces to

$$r(d\epsilon_{\varphi\varphi}/dr) + \epsilon_{\varphi\varphi} - \epsilon_{rr} = 0 \quad [6]$$

The stress-strain relations for the incompressible elastic solid may be written in the form

$$\epsilon_{rr} = (2\sigma_{rr} - \sigma_{\varphi\varphi} - \sigma_{zz})/6G + \alpha T \quad [7]$$

$$\epsilon_{\varphi\varphi} = (2\sigma_{\varphi\varphi} - \sigma_{rr} - \sigma_{zz})/6G + \alpha T \quad [8]$$

$$\epsilon_{zz} = (2\sigma_{zz} - \sigma_{rr} - \sigma_{\varphi\varphi})/6G + \alpha T \quad [9]$$

$$\epsilon_{ij} = \sigma_{ij}/2G, (i \neq j) \quad [10]$$

and where the shear modulus G and coefficient of thermal expansion α are temperature-dependent and, therefore, in this case functions of r.

From Equations [5] and [10] it is seen that the shear stresses vanish.

In the absence of body forces, two of the three equilibrium equations are satisfied identically, with

$$r(d\sigma_{rr}/dr) + \sigma_{rr} - \sigma_{\varphi\varphi} = 0 \quad [11]$$

Using Equations [9] and [11] to eliminate, respectively, σ_{zz} and $\sigma_{\varphi\varphi}$ from Equations [7] and [8], and substituting these new expressions for the strains into the compatibility Equation [6], one obtains

$$d/dr\,[(r/G)(d\sigma_{rr}/dr)] + (2/G)(d\sigma_{rr}/dr) = -6[d(\alpha T)/dr] \quad [12]$$

which may be integrated readily to yield

$$\sigma_{rr} = C_1 \int G\, r^{-3}\, dr + C_2 - 6 \int \{ G\, r^{-3} \int r^2\, [d(\alpha T)/dr]\, dr \}\, dr \quad [13]$$

or

$$\sigma_{rr} = C_1 F_1(r) + C_2 + F_2(r) \quad [13a]$$

Since the inner and outer surfaces of the cylinder (at $r = 1$ and $= r_0$) are free, the normal stresses must vanish, or

$$\sigma_{rr}(1) = \sigma_{rr}(r_0) = 0 \quad [14]$$

from which the constants of integration may be determined as

$$C_1 = \frac{F_2(r_0) - F_2(1)}{F_1(1) - F_1(r_0)} \quad [15]$$

$$C_2 = \frac{F_1(r_0)\, F_2(1) - F_1(1)\, F_2(r_0)}{F_1(1) - F_1(r_0)} \quad [16]$$

The remaining thermal stresses and strains are obtained by substituting Equation [13] into Equations [7], [8], [9] and [11]

$$\sigma_{\varphi\varphi} = C_1\, [r\, F_1(r)]' + [r\, F_2(r)]' + C_2 \quad [17]$$

$$\sigma_{zz} = C_1\, [r\, F_1(r)]'/2 + [r F_2(r)]'/2 + C_1 F_1(r)/2 + F_2(r)/2 + C_2 - 3\alpha GT + 3G\epsilon_{zz} \quad [18]$$

$$\epsilon_{rr} = -(r/4G)\, [C_1 F_1'(r) + F_2'(r)] + 3\alpha T/2 - \epsilon_{zz}/2 \quad [19]$$

$$\epsilon_{\varphi\varphi} = (r/4G)\, [C_1 F_1'(r) + F_2'(r)] + 3\alpha T/2 - \epsilon_{zz}/2 \quad [20]$$

where the primes denote differentiation with respect to r.

The boundary conditions at the ends of the cylinder prescribe either the value of the strain ϵ_{zz} or the stress σ_{zz}.

For instance, if the faces at each end of the cylinder are prevented from displacing, then a condition of plane strain results, i.e., $\epsilon_{zz} = 0$, and σ_{zz}, as given by Equation [18], represents the force per unit area that must be applied at the ends of the cylinder to maintain plane deformation.

Another possibility could be that the resultant of the normal forces over the cross-sectional area vanishes and then the equation

$$2\pi \int_1^{r_0} \sigma_{zz}\, r\, dr = 0 \quad [21]$$

would determine the value of the constant ϵ_{zz}.

In the foregoing solution the dependence of G and α on the temperature and the temperature gradient itself have been arbitrary, so that any desired form may be used. These solutions will be discussed in detail in a later section.

Thin-Plate Problem

Consider next a thin, circular plate with a concentric round hole, subjected to a steady-state radial temperature gradient. Let this plate have the same cylindrical co-ordinates as the thick-walled cylinder in Fig. 2. If the faces of the plate are not

restrained, they must be stress-free and if, in addition, the thickness of the plate is so small as to make any variation of stresses from one face to the other negligible, then one may assume that throughout the entire plate

$$\sigma_{zz} = \sigma_{rz} = \sigma_{\varphi z} = 0 \quad [22]$$

$$\partial\sigma_{ij}/\partial z = \partial\epsilon_{ij}/\partial z = 0 \quad [23]$$

This plane-stress condition, together with the rotational symmetry assumptions of Equations [1] and [2], is equivalent to disallowing any warping of the plate. It will be shown in the Appendix that these conditions cannot be fulfilled and that any solution based on the foregoing is only an approximation.

However, the assumptions of plane stress and rotational symmetry greatly simplify the problem. The correct solution, taking into account the warping of the plate, does not seem to exist even for the simpler case of an elastic material with temperature-independent properties, although solutions for this material have been obtained under the afore-mentioned assumptions (1).

Using the equilibrium condition, Equation [11], to eliminate $\sigma_{\varphi\varphi}$ from the stress-strain laws, Equations [7] and [8], and substituting the resulting strain expressions into the compatibility Equation [6], the following differential equation will result

$$r(d^2\sigma_{rr}/dr^2) + [3 - (r/G)(dG/dr)](d\sigma_{rr}/dr) - (1/2G)(dG/dr)\,\sigma_{rr} = -3G[d(\alpha T)/dr] \quad [24]$$

Unfortunately, this equation cannot be solved with the same generality as the corresponding relation for the thick-walled cylinder, Equation [12]. However, since it is an ordinary equation with variable coefficients, it can be readily solved specifically for any desired physical temperature gradient.

For example, if the circumference of the concentric hole is heated to some temperature T_1 and the heat is allowed to dissipate to a temperature T_2 at the outer radius, then at any point of the plate

$$T = T(r) = T_2 \ln(ar) \quad [25]$$

where the constants T_2 and a are determined from the values T_1 and T_2. (This relationship assumes that the coefficient of thermal conductivity is independent of the temperature and that there is no heat lost at the faces of the plate.)

If one approximates linearly the variation of the shear modulus with temperature and also linearizes the relation for the coefficient of thermal expansion, then

$$G = G_0(A_1 + A_2T) = G_1 \ln(br) \quad [26]$$

$$\alpha = \alpha_0(A_3 + A_4T) = \alpha_1 \ln(cr) \quad [27]$$

where A_n, G_n, α_n, b, and c are constants.

Substituting these expressions into the compatibility condition, Equation [24], using the transformation $y = \ln(br)$, and with the help of the method of Frobenius (7), one finds the solution to be

$$\left.\begin{aligned}\sigma_{rr} = {} & C_4[1 - (\ln br)/2] + (3/8)C_3(\ln br)^2 \\ & + (C_4/8)(\ln br)^2[3\ln(\ln br) - 19/2] \\ & + \sum_{3}^{\infty} \frac{(-1)^{n-1}[4n-5][4(n-1)-5]\cdots[-1](\ln br)^n U_n}{2^n\, n!\,(n-2)!} \\ & - (6/77)\alpha_1 G_1 T_2\{14(\ln br)^2 + [8 + 11\ln(ac/b)](\ln br)^2\}\end{aligned}\right\} \quad [28]$$

where

$$\left.\begin{aligned}U_n = {} & C_3 + C_4 \ln(\ln br) \\ & + C_4\{[4/4n - 5 + 4/4(n-1) - 5 + \cdots + 4/-1] \\ & - [1/n + 1/(n-1) + \cdots + 1/1]\cdots \\ & - [1/(n-2) + 1/(n-3) + \cdots + 1/-1] + 1\}\end{aligned}\right\} \quad [29]$$

It can be shown that the series of Equation [28] converge for $0 < \ln(br) < \infty$, and since this is always the physical case, the solution, Equation [28], is admissible.

The constants C_3 and C_4 are determined from the boundary conditions, Equation [14], and as all other thermal stresses, strains and displacements depend only on σ_{rr}, the problem is solved.

Discussion and Conclusions

Two numerical examples have been computed for a thick-walled cylinder having an outer radius equal to 10 times the inner one and subjected to a temperature gradient varying from 1000 to 900 (Figs. 3 to 6). The temperature dependence of G, Fig. 1, is for 1020 steel and the α versus T curve is for typical austenitic steels as given, respectively, in references (8) and (9), while the viscosity-temperature relation is for "Puron" iron as obtained from reference (2).

Two possible boundary conditions are considered, namely (*a*) the cylinder is heated uniformly to 900 F, then it is clamped at the ends and the 100 F temperature gradient is applied (plane-strain condition, Figs. 3 and 4); (*b*) the same temperature gradient is applied when the body is originally at 70 F with the boundary conditions so arranged as to produce zero resultant axial forces over all faces of the cylinder (constant strain condition, Figs. 5 and 6).

In either case, the effect of a temperature-dependent G and α is to decrease appreciably the maximum thermal stresses and to increase the maximum thermal strains as compared to those based on constant G and α. For the computed cases, the greatest decrease in maximum stresses is 66 per cent and the greatest increase in maximum strains is 4.6 per cent.

It should be noted that the thermal stresses for this temperature gradient are of such magnitudes as to exceed locally the proportional limit of steel, and consequently the numerical values in these regions have no significance beyond showing the influence of the temperature-dependent G and α on the thermal stresses and strains. These numerical examples indicate that the temperature gradient must be smaller in order to make the elastic stress-strain relations applicable. Of course, if a metal with a smaller value of α were considered then the thermal stresses and strains would be reduced accordingly.

In the Appendix it is shown that the thermal plane-stress solution for a thin elastic plate, regardless of whether G and α are temperature-dependent, is only an approximation. The smaller the temperature gradient the more closely are the plane-stress assumptions satisfied. While the series solution of Equa-

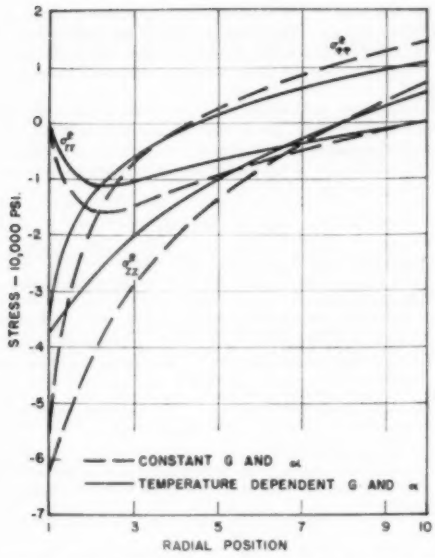

FIG. 3 ELASTIC THERMAL STRESSES IN A THICK-WALLED CYLINDER PLANE-STRAIN CONDITION

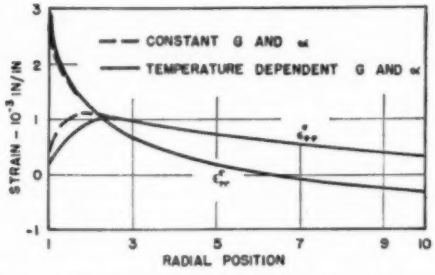

FIG. 4 ELASTIC THERMAL STRAINS IN A THICK-WALLED CYLINDER PLANE-STRAIN CONDITION

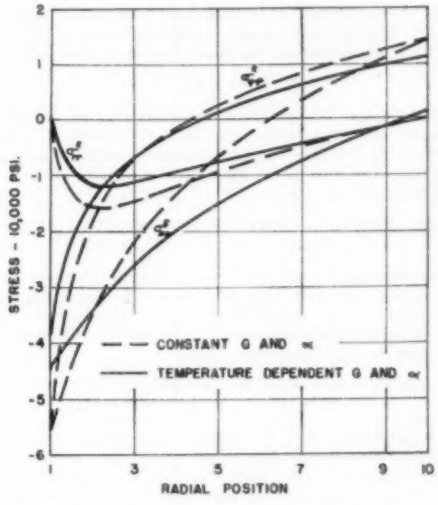

FIG. 5 ELASTIC THERMAL STRESSES IN A THICK-WALLED CYLINDER CONSTANT-STRAIN CONDITION

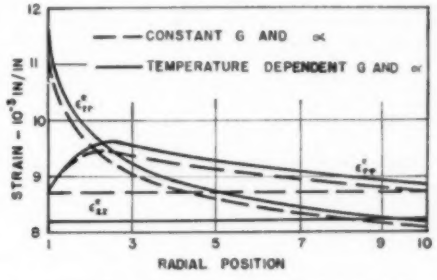

FIG. 6 ELASTIC THERMAL STRAINS IN A THICK-WALLED CYLINDER CONSTANT-STRAIN CONDITION

tion [28] converges as n approaches infinity, it converges extremely slowly for the leading terms and in view of the aforementioned inherent limitations a numerical example has not been computed.

As experimental data showing the distribution of thermal stresses and strains at elevated temperatures are not available in the literature, no comparison could be made between these theoretical analyses and actual results.

ACKNOWLEDGMENT

The author is indebted to Professors A. M. Freudenthal and J. O. Smith, his thesis advisers, for suggesting this line of research and for their other valuable suggestions and kind criticism. The author further wishes to acknowledge gratefully the many inspiring discussions he has had with Dr. P. Torda.

APPENDIX

ON THE LIMITATIONS OF THE THERMAL PLANE-STRESS ASSUMPTIONS

In the formulation of the thin-plate problem, plane-stress and rotational symmetry assumptions were made, which excluded the presence of shearing stresses in the plane of the plate and, consequently, any possible warping of the plate.

It will now be shown that such conditions are physically unattainable in elastic bodies and that results based on these assumptions are only approximations which depart from reality with increasing temperature gradients.

Under the conditions of rotational symmetry, Equations [1] and [2], the shearing strains $\epsilon_{r\varphi}$ and $\epsilon_{\varphi z}$ vanish identically, while the definition of ϵ_{φ} together with Equations [10] and [22] yields

$$\partial u_z/\partial z = -\partial u_r/\partial r \quad [30]$$

But the displacement u_r must be independent of z if Equation [23] is to be satisfied. Therefore, through Equations [2], [23], and [30] the strain ϵ_{zz} must be independent of φ, z, and r, or

$$\epsilon_{zz} = \text{const} \quad [31]$$

Substituting the equilibrium Equation [11] into the stress-strain relations for ϵ_{rr} and $\epsilon_{\varphi\varphi}$, Equations [7] and [8], and in turn introducing the latter into the compatibility condition, Equation [6], one obtains the governing differential equation of the thermal plane-stress problem

$$r(d^2\sigma_{rr}/dr^2) + [3 - (r/G)\,(dG/dr)]\,(d\sigma_{rr}/dr) - (1/2G)\,(dG/dr)\,\sigma_{rr} = -3G\,[d(\alpha T)/dr] \quad [24]$$

This differential equation was solved earlier in the paper.

However, the plane-stress problem is overdeterminate, since one more equation remains which has not yet been used. This is the stress-strain relation for ϵ_{zz}, Equation [9]. Differentiation of Equation [9] with respect to r yields

$$r(d^2\sigma_{rr}/dr^2) + [3 - (r/G)\,(dG/dr)]\,(d\sigma_{rr}/dr) - (2/G)\,(dG/dr)\sigma_{rr} = 6G[d(\alpha T)/dr] \quad [32]$$

If the stress σ_{rr} is to be a solution of the thermal plane-stress problem, then it must satisfy both differential Equations [24] and [32]. This is clearly impossible unless the temperature T is a constant, since G and α are functions of T. If T were constant, then with the boundary conditions, Equation [14], the trivial solution $\sigma_{rr} = 0$ follows.

Even if the problem were simplified further by assuming G and α temperature-independent, T must still be a constant in order that σ_{rr} may satisfy both differential Equations [24] and [32].

The fact that σ_{rr}, as obtained from the solution of the compatibility, Equation [24], does not satisfy the stress-strain law for ϵ_{zz}, Equation [9], means that the strain ϵ_{zz} is not independent of r and therefore the shear strain ϵ_{rz} does not vanish as assumed.

Consequently, the smaller the temperature gradient the more fully are the thermal plane-stress assumptions satisfied. The numerical examples indicate that the temperature gradient must be relatively small, if the elastic thermal stresses are not to exceed the proportional limit.

BIBLIOGRAPHY

1 "Theory of Elasticity," by S. Timoshenko, McGraw-Hill Book Company, Inc., New York, N. Y., 1934.

2 "Anelastic Properties of Iron," by T. S. Kê, *Metals Technology*, T.P. No. 2370, 1948.

3 "Elasticity and Anelasticity of Metals," by C. M. Zener, University of Chicago Press, Chicago, Ill., 1948.

4 "The Inelastic Behavior of Engineering Materials and Structures," by A. M. Freudenthal, John Wiley & Sons, Inc., New York, N. Y., 1950.

5 "Thermal Stresses and Strains in Circular Thin Plates and Thick-Walled Cylinders Exhibiting Temperature Dependent Elastic and Viscoelastic Properties," by H. H. Hilton, PhD thesis, University of Illinois, March, 1951.

6 "Thermal Stresses in Media Exhibiting Temperature Dependent Viscoelastic Properties," by H. H. Hilton, paper presented to the First U. S. National Congress of Applied Mechanics, Chicago, Ill., June, 1951.

7 "Ordinary Differential Equations," by E. L. Ince, Dover Publications, New York, N. Y., 1944.

8 "Poisson's Ratio at High Temperatures," by F. L. Everett and J. Miklowitz, *Journal of Applied Physics*, vol. 15, 1944, pp. 592–598.

9 "Properties of Metals at Elevated Temperatures," by C. S. Smith, McGraw-Hill Book Company, Inc., New York, N. Y., 1950.

The Plane-Stress Problem of Perforated Plates[1]

By G. HORVAY,[2] SCHENECTADY, N. Y.

In an earlier paper[3] it was indicated that perforated plates of triangular layout, with narrow ligaments, as they occur, for instance, in heat-exchanger tube sheets, can be treated in plane-stress calculations as solid sheets of suitable elastic moduli, provided that the stress distribution does not vary appreciably from hole to hole. This paper completes that study by providing suitable curves (Figs. 4, 8), from which deformations and stresses can be read off in terms of the values calculated for solid sheets, for mechanical, thermal, and gravitational loads.

Diffusivity

FIG. 1(*a*) illustrates a honeycomb structure, of the familiar triangular layout. The heat flux that enters the honeycomb on the left, over the width R, follows the vertically hatched path. Hence conductivity k^* of the honeycomb structure, in terms of the conductivity k of solid material is

$$k^* = k\,\frac{3L}{R}\Big/\left(\frac{L}{h}+\frac{L}{2h}+\frac{L}{h}+\frac{L}{2h}\right) = k\,\frac{h}{R} \qquad [1a]$$

We assumed that the ligaments are long and slender, so inaccuracies that result from corners and overlaps in the path are negligible.

From Fig. 1(*a*), it is also seen that the density ρ^* of the honeycomb, as compared with the density ρ of solid material, is in the ratio of $\times\times\times$ hatched area to //// hatched area

$$\rho^*/\rho = \frac{6Lh}{6LR/2} = 2h/R \qquad [1b]$$

hence the diffusivity of the honeycomb is

$$\kappa^* = k^*/\rho^* c = \kappa/2 \qquad [1c]$$

When instead of a honeycomb we deal with a perforated disk as in Fig. 1(*b*), where the ligaments are long and thin, the hexagonal representation, as indicated by the dashed lines, reduces this to the previous structure, and the foregoing formulas still apply except that in Equation [1*a*] the width $2h$ must be replaced by the average ligament width

$$2\bar{h} = L\Big/\int_0^{L/2} d\xi/\eta \qquad [2a]$$

and in Equation [1*b*] it must be replaced by a somewhat different average ligament width

$$2\bar{h} = (4/L)\int_0^{L/2} \eta\, d\xi \qquad [2b]$$

Here η is the ordinate

$$\eta = R - \sqrt{(R-h)^2 - \xi^2} \qquad [3]$$

of the profile of the ligament, as indicated in Fig. 1(*b*). The notation $2h$ is retained for the narrowest width of the ligament, at $\xi = 0$.

The average width $2\bar{h}$ also can be characterized as the uniform width which permits as much extension under tension T as the actual ligament permits. See Fig. 2(*a*), and Equation [2] footnote 3. We shall still need another effective width

$$2h' = L\Big/\left(\int_0^{L/2} 3\xi^2\, d\xi/\eta^4\right)^{1/4} \qquad [4]$$

This is defined as the width of a uniform bar of length L which deflects the same amount in "sidesway bending" [parallel displacement of one end of the bar with respect to the other, see Fig. 2(*c*)], as the actual ligament does.[4] The curves $\bar{h}/h$, h'/h versus the "slenderness ratio"

$$\epsilon = h/R \qquad [5]$$

are plotted in Fig. 3. They can be considered as reliable up to about $\epsilon = 0.2$.

When the ratio ϵ is neither too small nor too large, we have

$$2\bar{h} \sim 2h \qquad [6]$$

and the Relation [1*c*] is approximately valid also for circular holes. As $\epsilon \to 0$, $\kappa^* \to 0$; as $\epsilon \to 1$, $\kappa^* \to \kappa$.

Deformations

The relative density of a perforated plate is determined by the ratio h/R. It is reasonable to expect the plate to exhibit a stiffness proportional to its density, that is, we expect the plate to deform somewhat like a solid plate of effective Young's modulus

$$E^* = AE\bar{h}/R \qquad [7a]$$

where E is the Young's modulus for the solid material, and A is some suitable constant. Likewise we expect the plate to experience maximum stresses of the form

$$\hat{\sigma} = K\,\frac{p}{h/R} = K\sigma_0 \qquad [8]$$

where K is some other suitable constant.[5] The first assertion is

---

[1] The work reported here was carried out under Contract No. W-31-109, Eng-52.

[2] Knolls Atomic Power Laboratory, General Electric Company. Mem. ASME. The Knolls Atomic Power Laboratory is operated by the General Electric Company for the Atomic Energy Commission.

[3] "Thermal Stresses in Perforated Plates," by G. Horvay, Proceedings of the First U. S. National Congress of Applied Mechanics, 1951.

Presented at the National Conference of the Applied Mechanics Division, State College, Pa., June 19–21, 1952, of THE AMERICAN SOCIETY OF MECHANICAL ENGINEERS.

Discussion of this paper should be addressed to the Secretary, ASME, 29 West 39th Street, New York, N. Y., and will be accepted until October 10, 1952, for publication at a later date. Discussion received after the closing date will be returned.

NOTE: Statements and opinions advanced in papers are to be understood as individual expressions of their authors and not those of the Society. Manuscript received by ASME Applied Mechanics Division, June 18, 1951. Paper No. 52—APM-19.

[4] Footnote 3, equation 7.

[5] $\hat{\sigma}$ denotes the maximum ligament stress (irrespective of sign), p the numerically larger of the two principal stresses in the solid plate at a point x, y close to the ligament considered; σ_0 is an abbreviation for p/ϵ. Due to our basic assumption that solid stresses vary but slowly from hole to hole, the precise location of x, y is immaterial. Note that the E^* expression involves $2\bar{h}/2R$ (average ligament width to $2R$ ratio), the $\hat{\sigma}$ expression involves $2h/2R$ (minimum width to $2R$ ratio).

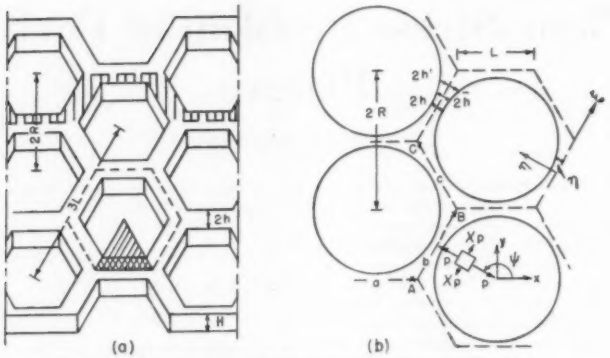

FIG. 1 ILLUSTRATION OF (a) HONEYCOMB, (b) PERFORATED PLATE
(|||| indicates heat path; ××× indicates 1/3 ligament area; //// indicates area of equivalent solid.)

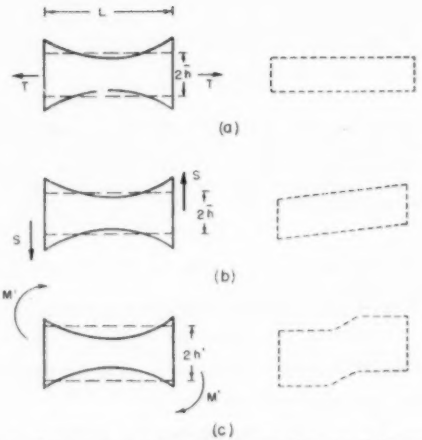

FIG. 2 DEFORMATION OF LIGAMENT UNDER TENSION T, SHEAR S, AND SIDESWAY BENDING MOMENT M'
(Full line = actual ligament. Long dashes = equivalent uniform ligament. Short dashes = deformed shape of equivalent ligament.)

readily verified, for it was shown in equation 21 of footnote 3 that A has the very simple expression

$$A = 1 - \mu^*,\ \mu^* = 1 - \frac{4}{3 + (s/\epsilon) + (1/2\epsilon)}$$

$$= 1 - \frac{4}{3 + 2(1+\mu)n + L^2\bar{h}/4h'^3} \quad \ldots\ldots [7b]$$

where, in accordance with the notation of the previous paper,[6] $sL/\epsilon L$ denotes the ratio of shear deflection of a ligament under unit shear force S to its extension under unit tensile force T, $1/(\epsilon L)$ denotes the ratio of bending deflection of a ligament under unit sidesway bending moment M' to extension under unit tensile force T. The three deformations are sketched in Figs. 2(*a*), (*b*), (*c*). Their expressions on the right of Equation [7*b*] involve the ordinary Poisson ratio μ, the familiar factor n (which ranges from 1.0 to 1.5 but is usually chosen as 1.2), which relates shear strain

[6] Footnote 3, equations 8, 9.

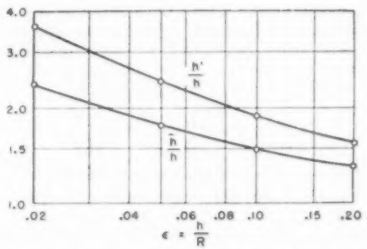

FIG. 3 RATIO OF LIGAMENT WIDTHS, TENSILE AVERAGE TO MINIMUM, $2\bar{h}/2h$, AND BENDING AVERAGE TO MINIMUM, $2h'/2h$, OF A PERFORATED PLATE

to shear stress, and the dimension ratios, $h/\bar{h}$, h/h', and $h/L = \sqrt{3}\epsilon/2$. Term μ^* is the effective Poisson ratio of the perforated plate. Knowing this and E^*, the deformations of the perforated plate can be calculated by solid-plate formulas. Curves for μ^*, E^*/E and $E^*/(1-\mu^*)E$, calculated on the basis of Fig. 3 by Equations [7], are shown in Fig. 4 for $\mu = 0.3$, $n = 1.2$. Since our theory presumes that $\epsilon^2 << 1$, we cannot use Equations [7] for calculating the curves for $\epsilon \geq 0.2$. Knowing however the limiting values at $\epsilon = 1$ ($E^* = E$, $\mu^* = \mu$), the curves are readily faired in (by dashed lines) in the missing range.

STRESSES DUE TO APPLIED MECHANICAL TRACTIONS

The factor K for the stresses is of much more complicated nature. Mainly, because it is not a constant but still depends on ϵ, though not very sensitively (in other words, factoring out the ratio $\sigma_0 = p/\epsilon$ in Equation [8] has not eliminated completely the ϵ-dependence of K), it also depends upon the ratio χ of the principal stresses of the solid plate—we denote the larger principal stress by p, the smaller by χp so that always $|\chi| \leqq 1$ — and it also depends upon ψ, the orientation of stress p with respect to a ligament. Such dependences are to be expected. We know that when the holes are exceedingly small, K must assume the familiar value of the stress concentration factor k for isolated holes

$$K = k = \begin{cases} 2 \\ 3 \text{ for } \chi = \begin{cases} 1 \text{ (isotropic tension)} \\ 0 \text{ (simple tension)} \\ -1 \text{ (pure shear)} \end{cases} \\ 4 \end{cases} \text{ when } \epsilon = h/R = 1 \quad \ldots\ldots [9]$$

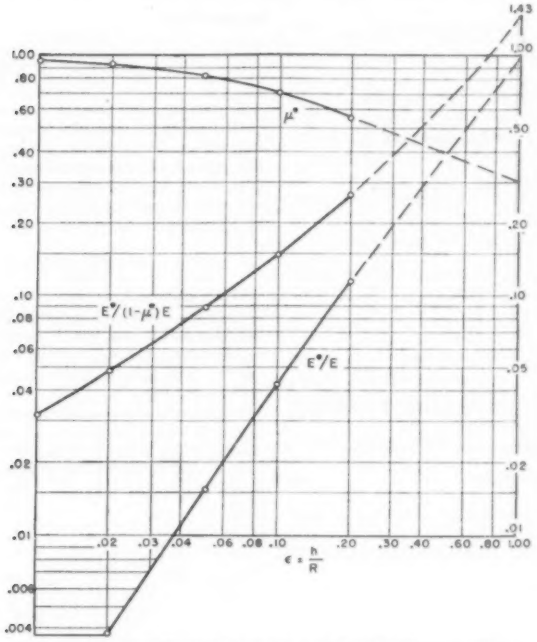

FIG. 4 EFFECTIVE POISSON RATIO μ^* AND YOUNG'S MODULUS E^* OF PERFORATED PLATE FOR $\mu = 0.3$, $n = 1.2$
(Dashed portion is extrapolated.)

This suggests therefore a further split of K into factors

$$K = k\mathbf{T} \qquad [10a]$$

where $\mathbf{T}$ is a "stress-enlargement factor," indicating the ratio of maximum average cross-sectional stress in the ligament to σ_0, while k gives the ratio of maximum local stress to maximum average stress, and is thus a bonafide stress-concentration factor. However, for the narrow ligaments to which our analysis is restricted ($\epsilon^2 << 1$), the excess of k over 1 is insignificant and can be disregarded. For $\epsilon^2 << 1$ therefore

$$K = \mathbf{T}_a(\chi;\ \psi) \qquad (\epsilon^2 << 1) \qquad [10b]$$

The dependence of $\mathbf{T}$ on ψ is also obvious. For a state of simple tension ($\chi = 0$), for instance, if p acts perpendicularly to a ligament, as in Fig. 1(b) where it is perpendicular to b, the ligament will not experience any stresses because all loads are carried by inclined ligaments[7] such as a and c, hence

$$\mathbf{T}_{lig} = 0 \text{ for } \psi = \pi/2 \qquad [11a]$$

If p is parallel to a ligament, then the ligament is subject to simple tension and we have

$$\mathbf{T}_{lig} = 1 \text{ for } \psi = 0 \qquad [11b]$$

In all other cases bending also will occur in the ligaments in addition to tension. Usually, however, we are not interested in the maximum stress, σ_{max}, in one particular ligament, but rather in the maximum of all the stresses that may arise in the six ligaments surrounding a hole; this we denote by $\hat{\sigma} = k\mathbf{T}\sigma_0$, without use of the subscript "lig." Therefore $\mathbf{T}(\psi)$ is the largest of the three values $\mathbf{T}_{lig}(\psi)$, $\mathbf{T}_{lig}(\psi + \pi/3)$, $\mathbf{T}_{lig}(\psi - \pi/3)$.

We are now ready to derive the formula for $\mathbf{T}$. From Figs. 8 to 13 of the earlier paper,[8] it follows that if a solid-plate stress distribution $\widehat{xx}$, $\widehat{xy}$, $\widehat{yy}$, is found to exist, then the ligaments of the perforated plate experience tensions T and sidesway bending moments M' at points A, B, C of Fig. 1(b) as follows (H is the plate thickness)

$$\left.\begin{array}{lll} & T/2RH = & M'/2RHL = \\ A: & \widehat{xx} & \frac{1}{2}\widehat{xy} \\ B: & \frac{1}{4}\widehat{xx} + \frac{\sqrt{3}}{2}\widehat{xy} + \frac{3}{4}\widehat{yy} & -\frac{\sqrt{3}}{8}\widehat{xx} - \frac{1}{4}\widehat{xy} + \frac{\sqrt{3}}{8}\widehat{yy} \\ C: & \frac{1}{4}\widehat{xx} - \frac{\sqrt{3}}{2}\widehat{xy} + \frac{3}{4}\widehat{yy} & \frac{\sqrt{3}}{8}\widehat{xx} - \frac{1}{4}\widehat{xy} - \frac{\sqrt{3}}{8}\widehat{yy} \end{array}\right\} \quad [12]$$

Expressing $\widehat{xx}$, $\widehat{xy}$, $\widehat{yy}$ in terms of the principal stresses p, χp, and the direction ψ of p with respect to the x-axis, see Fig. 1(b), we can write

[7] Remember that our basic assumption, the ligaments are thin, implies that loads are transmitted only at the corners of the skeleton hexagons, such as points A, B, C in Fig. 1(b). (This assumption, combined with that of slow variation of stresses from hole to hole, also insures that only M' [sidesway] type bending moments arise in the ligaments of the plates. See footnote 3.)

$$\left.\begin{aligned}\widehat{xx} &= \frac{1}{2}\,p\,(1+\chi) + \frac{1}{2}\,p(1-\chi)\cos 2\psi \\ \widehat{xy} &= \frac{1}{2}\,p(1-\chi)\sin 2\psi \\ \widehat{yy} &= \frac{1}{2}\,p(1+\chi) - \frac{1}{2}\,p(1-\chi)\cos 2\psi\end{aligned}\right\} \quad \ldots\ldots [13]$$

Hence the stress in the horizontal ligament a becomes

$$\sigma_{hor} = \frac{2M'\xi/L}{\frac{2}{3}H\eta^2} + \frac{T}{2H\eta} = \frac{6M'}{2RHL}\frac{\xi/R}{(\eta/R)^2} + \frac{T}{2RH}\frac{1}{\eta/R}$$

$$= \frac{3}{2}\,p(1-\chi)\sin 2\psi\,\frac{\xi/R}{(\eta/R)^2} + \left[\frac{1}{2}\,p(1+\chi) + \frac{1}{2}\,p(1-\chi)\cos 2\psi\right]\frac{1}{\eta/R} \quad \ldots\ldots [14]$$

and the stresses in ligaments b and c are obtained by replacing ψ by $\psi - \pi/3$ and $\psi + \pi/3$, respectively.

For isotropic loading, $\chi = 1$, Equation [14] reduces to

$$\sigma_{hor} = pR/\eta \quad \ldots\ldots [15]$$

Its maximum (at $\xi = 0$) is

$$\sigma_0 = pR/h = p/\epsilon \quad \ldots\ldots [16a]$$

and we obtain

$$\Upsilon(+1;\ \psi) = \frac{\sigma_0}{p/\epsilon} = 1. \quad \ldots\ldots [16b]$$

By varying ξ in Equation [14] between $-L/2$ and $+L/2$ we can determine the numerical maximum σ_{max} of σ_{hor}. The ratios σ_{max}/σ_0 are plotted in Fig. 5 versus χ and ψ for various values of ϵ. It must be remembered that when ligament a experiences p at 15 deg, then b experiences it at -45 deg, and c at 75 deg; hence the largest of the three σ_{max}, which we denote by $\hat{\sigma}$, is by Fig. 5 for, say, $\epsilon = 0.05$, $\chi = -0.2$

$$\hat{\sigma} = \Upsilon_{0.05}(-0.2, \pi/4)p/\epsilon = 3.9\,p/0.05 = 78\,p \quad \ldots\ldots [17]$$

When ligament a experiences p at 30 deg, then b experiences it at -30 deg, c at 90 deg, and, from Fig. 5, $\Upsilon = 3.65$. When a experiences p at 60 deg, then b experiences it at 0 deg, c at 60 deg, and $\Upsilon = 3.2$. It is thus noticed that Υ depends upon ψ but moderately, ranging, in the present example, from 3.2 to 3.9 as ψ varies from 0 to $\pi/2$.

Therefore it is the simplest procedure to disregard the variation of Υ with ψ altogether and write simply $\Upsilon_s(\chi)$, using the ψ-value which makes Υ the largest. This, by Fig. 5, is evidently $\psi = \pi/4$ for all except very thick ligaments for which our theory ceases to be reliable anyhow. Thus one derives from Equation [14]

$$\Upsilon_s(\chi) = [\Upsilon_s(\chi, \psi)]_{\substack{\text{max with} \\ \text{respect to } \psi}} \simeq \Upsilon_s(\chi, \pi/4)$$

$$= \left[\frac{3}{2}(1-\chi)\frac{\xi h}{\eta^2} + \frac{1}{2}(1+\chi)\frac{h}{\eta}\right]_{max} \quad \ldots\ldots [18]$$

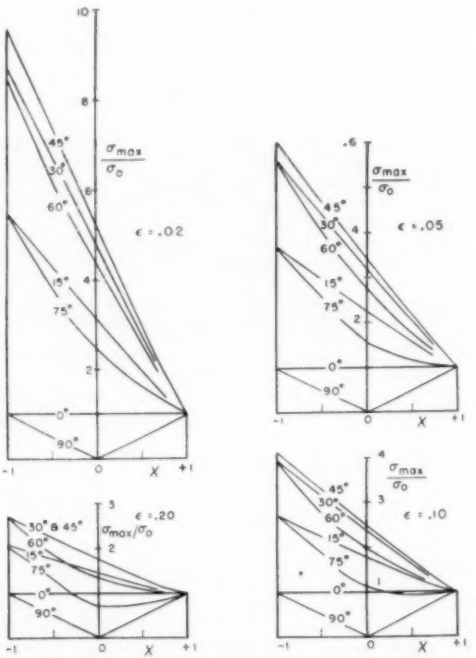

FIG. 5 RATIO OF MAXIMUM LIGAMENT STRESS UNDER ACTION OF PRINCIPAL STRESSES p, χp, TO MAXIMUM STRESS UNDER ISOTROPIC TENSION ($\chi = 1$) AS FUNCTION OF χ AND DIRECTION ψ OF p, FOR VARIOUS ϵ

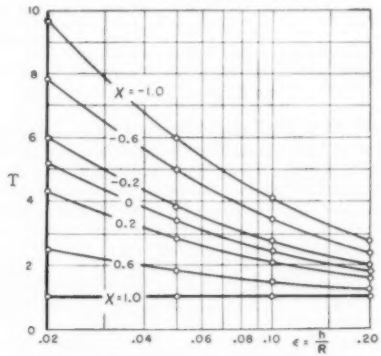

FIG. 6 DEPENDENCE OF STRESS-ENLARGEMENT FACTOR Υ_s ON χ AND ϵ

and the Υ curves so obtained are plotted in Fig. 6.

From Fig. 5 one notices that Υ_s is almost linear in χ. Thus one can write approximately

$$\Upsilon_s(\chi) \simeq \frac{1+\chi}{2}\,\Upsilon_s(1) + \frac{1-\chi}{2}\,\Upsilon_s(-1) \quad \ldots\ldots [19a]$$

where

$$\Upsilon_s(1) = 1,\ \Upsilon_s(-1) = [3\xi h/\eta^2]_{max} \simeq \frac{27/8}{\sqrt{6\epsilon}}\left(1 - \frac{7}{12}\,\epsilon + \ldots\right) \quad \ldots\ldots [19b]$$

The last expression, assumed at the abscissa

$$\xi \simeq R\sqrt{\epsilon\left(\frac{2}{3} - \epsilon + \dots\right)} \quad \dots [19c]$$

is obtained by expansion in powers of ϵ.

It is rather interesting to note that the largest ligament stresses are experienced when $\chi = -1$, and p is aligned at 45 deg. For this case the ligament is subject to pure (sidesway) bending, by moment M'. We may write our maximum stress, therefore, also in the form

$$(\hat{\sigma})_{\max} = M'/\Sigma;\ M' = RHLp;\ \Sigma = \frac{HLh}{3(\xi h/\eta^2)_{\max}} = \frac{HLh}{\mathfrak{T}(-1)} \quad [20]$$

and can refer to Σ as the "apparent section modulus," i.e., the modulus which when divided into the maximum moment gives the maximum stress. (Note that maximum moment occurs at end of ligament, maximum stress not far from center.)

Thermal and Gravitational Stresses

It was shown in the foregoing that the mechanical stresses in a perforated plate produced by applied tractions are related to solid-plate stresses by the formula:

Applied mechanical tractions

$$\hat{\sigma}_a = Kp/\epsilon = k\mathfrak{T}p/\epsilon \quad \dots [21a]$$

We shall now show that if stresses are produced by temperature changes or by gravitational (or centrifugal) body forces the formula must be modified to the following:

Thermal stresses

$$\hat{\sigma}_t = m_t Kp/\epsilon,\quad m_t = E^*/E \quad \dots [21b]$$

Gravitational stresses

$$\hat{\sigma}_g = m_g Kp/\epsilon,\quad m_g = E_a/E \quad \dots [21c]$$

Here m_t, m_g can be referred to as mitigating factors, indicating the extent to which the body forces which arise in a perforated plate are reduced from those which act in a solid plate. It is clear that the gravitational mitigating factor is given by the relative density of the perforated plate

$$m_g = \rho^*/\rho = 2h/R \quad \dots [22a]$$

This also can be written[8] as

$$m_g = E_a/E \quad \dots [22b]$$

Here E_a is the effective modulus of elasticity of the perforated plate for axial (z-direction) loading. The derivation of the expression for m_t is somewhat more involved.

It is shown elsewhere[9] that a thermal-stress problem can be solved as follows: One considers the plate as chopped up into infinitesimal elements so as to permit the strains

$$\epsilon_{x,\text{thermal}} = \epsilon_{y,\text{thermal}} = \alpha\vartheta \quad \dots [23]$$

owing to the temperature change $\vartheta(x, y)$ to develop without stresses. Applying now an hydrostatic tension[10]

$$\widehat{xx_0} = \widehat{yy_0} = -\frac{E\alpha\vartheta}{1-\mu} \quad \dots [24a]$$

restitutes the original size of the elements; these now can be cemented together by use of some good-quality cement. The stresses, Equation [24a], are produced by certain body forces. Compensating body forces

$$(X, Y) = -E\alpha\nabla\vartheta/(1-\mu) \quad \dots [24b]$$

must be applied to maintain proper equilibrium. Superimposition of Equation [24a], of the effect of Equation [24b], and of the effect of normal edge tensions

$$\frac{E\alpha\vartheta}{1-\mu} \quad \dots [24c]$$

(which compensate for the boundary stresses produced by $\widehat{xx_0}$, $\widehat{yy_0}$, X, Y) provides solution of the thermal-stress problem.

If the plate is perforated, an isotropic tension p of magnitude

$$p = -\frac{E^*\epsilon}{1-\mu^*} \quad \dots [25a]$$

[8] "Bending of Honeycombs and of Perforated Plates," by G. Horvay, Journal of Applied Mechanics, Trans. ASME, vol. 74, 1952, pp. 122-123.

[9] "Theory of Elasticity," by S. Timoshenko and J. N. Goodier, McGraw-Hill Book Company, Inc., New York, N. Y., 1951, p. 425.

[10] The minus sign indicates that the stress, for positive ϑ, is actually a compression.

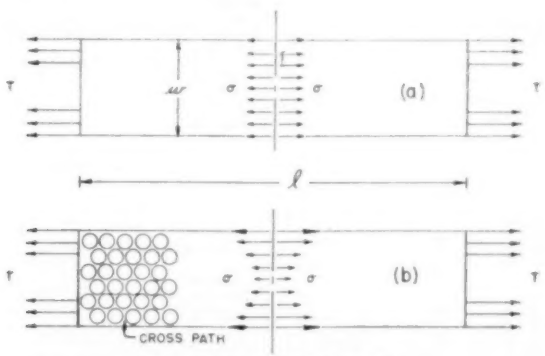

Fig. 7 Propagation of Stresses

Solid plate exhibits no shear lag. b. Perforated plate experiences shear lag.

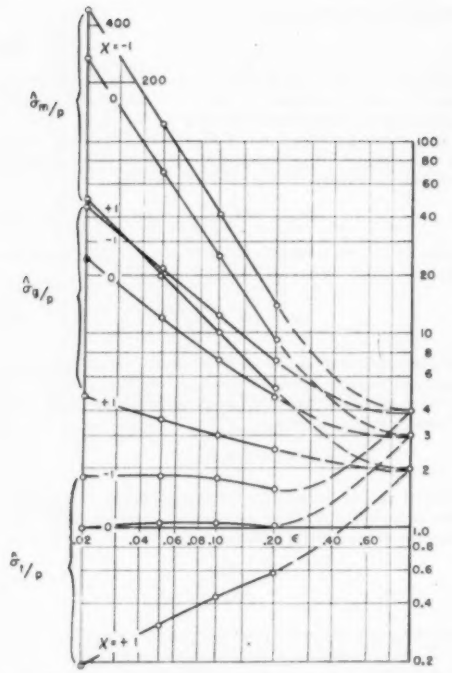

FIG. 8 RATIO OF LARGEST LIGAMENT STRESS $\hat{\sigma}$ OF A PERFORATED PLATE TO PRINCIPAL STRESS p, OF A SOLID PLATE, FOR APPLIED MECHANICAL TRACTIONS m, GRAVITATIONAL LOADS g, AND THERMAL LOADS t, VERSUS ϵ WHEN LOADS ARE APPLIED IN PLANE OF PLATE (Curves are extrapolated by dashed lines to $\epsilon = 1$. $\mu = 0.3$, $n = 1.2$ are used.)

is required to eliminate the isotropic strain $\epsilon = \alpha\vartheta$ (see footnote 3, equation 25). Hence the body forces brought into play are

$$-E^*\alpha\nabla\vartheta/(1-\mu^*) \quad [25b]$$

and the edge tractions are

$$\frac{E^*\alpha\vartheta}{1-\mu^*} \quad [25c]$$

Therefore it follows that the entire analysis for thermal effects remains unchanged if E^*, μ^* replace E, μ in all expressions. The results of thermal-stress calculations are usually expressed in multiples of a reference length $l = R\alpha T$ where displacements are concerned, and in multiples of a reference stress $S = E\alpha T$ where stresses are concerned. T is some reference temperature. The corresponding quantities for the perforated plate are

$$l^* = R\alpha T = l, \qquad S^* = E^*\alpha T = SE^*/E \quad [26$$

Equation [21b] now follows at once.

We must re-emphasize the limitations appertaining to our approach. Tht temperature distribution $\vartheta(x, y)$ must not vary by more than infinitesimal amounts from hole to hole, for the skeleton hexagons in Fig. 1(*b*) now constitute the infinitesimal elements of the body, and subdivision of these is not permitted because otherwise the isotropic relation Equation [25a], would cease to hold. In particular the present formulas do not apply to thermal shock.[11]

In Fig. 8 we plot the stress ratios $\hat{\sigma}_m/p, \hat{\sigma}_g/p, \hat{\sigma}_t/p$ versus ϵ, as obtained from Equations [21] for $\chi = 1, 0, -1$. Linear interpolation is permitted, by Equation [19a], for in-between values of χ. The curves are valid for $\epsilon \lesssim 0.2$. Knowing the limiting values for $\epsilon = 1$ the curves are readily faired in, by dashed lines, in the uncalculated $\epsilon = 0.2$ to $\epsilon = 1$ range. It is rather interesting to note that thermal stresses in perforated plates exceed, by and large, those in solid plates where χ is negative, and are smaller where χ is positive. Stresses caused in the plates by mechanical tractions obviously may reach very large values when the ligaments are slender, and the frequently used design criterion, $\hat{\sigma} \sim \sigma_0 = p/\epsilon$, is shown to be entirely inadequate. Evidently the lack of failures of tube sheets based upon such an unsatisfactory formula must be attributed to the additional strength derived from the outside portions of the attached tubes. No study has been made of this strengthening effect.

ACKNOWLEDGMENT

The author wishes to express his appreciation to Miss O. Podmajersky for carrying out the numerical calculations.

[11] For a treatment of thermal shock see Unclassified KAPL Report 566, Aug. 17, 1951, of which the present paper is a condensed version. Another topic treated in KAPL 566, but not considered in the present paper, is the analysis of perforated plates with heavy reinforcing rims. The limitations of the theory to slowly varying solid stress distributions is much more severe than offhand one would be inclined to believe. This is illustrated schematically in Fig. 7. For the concentrated end loads shown a solid beam will exhibit uniform tension at the center as in (*a*), so long as the length l is appreciably larger (say, 2 or more times) than the height w. A perforated beam will exhibit shear lag, as in (*b*), unless the net width of all the cross-paths connecting top and bottom is about twice the height w. This expected behavior of perforated plates has been confirmed by "Stress-coat" tests.

Thin Rectangular Plates on Elastic Foundation[1]

By H. J. FLETCHER[2] AND C. J. THORNE,[3] SALT LAKE CITY, UTAH

The deflection of a thin rectangular plate on an elastic foundation is given for the case in which two opposite edges have arbitrary but given deflections and moments. Six important cases of boundary conditions on the remaining two edges are treated. The solution is given for general transverse loads which are continuous in one direction and sectionally continuous in the other. By use of the sine transform the solution is obtained as a single trigonometric series. Numerical solutions are obtained for six special cases.

Introduction

THE problem of an infinite plate on an elastic foundation has been treated for several loads and boundary conditions.[4] Murphy has solved the problem of a finite plate simply supported on all edges, and has given numerical results.[5] Timoshenko gives the solution when two edges are clamped and two edges are simply supported.[6]

This paper treats the rectangular plate with two opposite edges having prescribed moments and deflections, and the other two edges having any of the six most important boundary conditions. The method of solution is the same as that used by Deverall and Thorne.[7] Numerical results are given for the two edges clamped, free, and simply supported. Deflections and moments are given for constant load and strip load.

Problem

The deflection $w(x, y)$ of the middle surface of a thin homogeneous isotropic plate must satisfy the following differential equation over the region bounded by the plate in Fig. 1[6]

$$\frac{\partial^4 w}{\partial x^4} + 2\frac{\partial^4 w}{\partial x^2 \partial y^2} + \frac{\partial^4 w}{\partial y^4} = \frac{q(x, y)}{D} - \frac{k'w}{D} \quad [1]$$

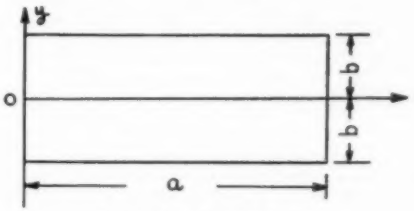

Fig. 1 Plan View of Plate

where

$q(x, y)$ = load per unit area normal to surface of plate

$D = \dfrac{Eh^3}{12(1 - \nu^2)}$

h = thickness of plate

E = Young's modulus

ν = Poisson's ratio of material

k' = foundation modulus

In all problems to be considered, the edge conditions, Fig. 1, will be at $x = 0$

$$w(0, y) = w_1(y) \quad [2]$$

$$M_x|_{x=0} = -D\left[\frac{\partial^2 w}{\partial x^2} + \nu\frac{\partial^2 w}{\partial y^2}\right]_{x=0} = M_1(y) \quad [3]$$

and at $x = a$

$$w(a, y) = w_2(y) \quad [4]$$

$$M_x|_{x=a} = -D\left[\frac{\partial^2 w}{\partial x^2} + \nu\frac{\partial^2 w}{\partial y^2}\right]_{x=a} = M_2(y) \quad [5]$$

The six cases for edge conditions at the other two edges $y = \pm b$ are as follows:

Case 1 Two edges fixed

$$w(x, y) = w_3(x) \text{ at } y = b \quad [6]$$

$$\frac{\partial w}{\partial y} = S_1(x) \text{ at } y = b \quad [7]$$

and

$$w(x, y) = w_4(x) \text{ at } y = -b \quad [8]$$

and

$$\frac{\partial w}{\partial y} = S_2(x) \text{ at } y = -b \quad [9]$$

Case 2 Deflection and moments given, Equations [6] and [8] with

$$M_y = -D\left[\frac{\partial^2 w}{\partial y^2} + \nu\frac{\partial^2 w}{\partial x^2}\right] = M_3(x) \text{ at } y = b \quad [10]$$

and

$$M_y = -D\left[\frac{\partial^2 w}{\partial y^2} + \nu\frac{\partial^2 w}{\partial x^2}\right] = M_4(x) \text{ at } y = -b \quad [11]$$

Case 3 Moments and reactions given, Equations [10] and [11] with

---

[1] This work was supported by the army ordnance department technical report No. 2 of Contract No. DA-04-495-ord 160; RAD Order No. ORDTB, PS 1-13074; Ordnance Project No. TB2-0001.

[2] Graduate Assistant, Department of Mathematics, University of Utah.

[3] Associate Professor, Department of Mathematics, University of Utah.

[4] "Equilibrium of a Thin Plate, Symmetrically Loaded, Resting on an Elastic Foundation of Infinite Depth," by A. H. A. Hogg, *Philosophical Magazine*, vol. 25, 1938, p. 576.

[5] "Stresses and Deflections in Loaded Rectangular Plates on Elastic Foundations," by G. Murphy, Bulletin 135, Iowa Engineering Experiment Station, 1937.

[6] "Theory of Plates and Shells," by S. Timoshenko, McGraw-Hill Book Company, Inc., New York, N. Y., 1940, p. 248.

[7] "Some Thin-Plate Problems by the Sine Transform," by L. I. Deverall and C. J. Thorne, Journal of Applied Mechanics, Trans. ASME, vol. 73, 1951, pp. 152–156.

Presented at the West Coast Conference of the Applied Mechanics Division, Los Angeles, Calif., June 26–28, 1952, of The American Society of Mechanical Engineers.

Discussion of this paper should be addressed to the Secretary, ASME, 29 West 39th Street, New York, N. Y., and will be accepted until October 10, 1952, for publication at a later date. Discussion received after the closing date will be returned.

Note: Statements and opinions advanced in papers are to be understood as individual expressions of their authors and not those of the Society. Manuscript received by ASME Applied Mechanics Division, February 4, 1952.

$$R_y = -D\left[\frac{\partial^3 w}{\partial y^3} + (2-\nu)\frac{\partial^3 w}{\partial y\,\partial x^2}\right] = R_1(x) \text{ at } y = b \quad [12]$$

and

$$R_y = -D\left[\frac{\partial^3 w}{\partial y^3} + (2-\nu)\frac{\partial^3 w}{\partial y\,\partial x^2}\right] = R_2(x) \text{ at } y = -b \quad [13]$$

Case 4 One edge fixed ($y = b$), and one with deflection and moment given ($y = -b$), Equations [6], [7], [8], and [11].

Case 5 One edge with moment and reaction given ($y = b$), and one edge fixed ($y = -b$), Equations [8], [9], [10], and [12].

Case 6 One edge with moment and reaction given ($y = b$), and one edge with deflection and moment given ($y = -b$), Equations [8], [10], [11], and [12].

The Sine Transform

Let $y(x)$ be a function which is equal to its Fourier sine series for $0 < x < a$. The finite Fourier sine transform of $y(x)$ is the function $y_s(\alpha)$ obtained by the linear integral operation defined as follows

$$y_s(\alpha) \equiv S\,[y(x)] = \int_0^a y(x)\sin\alpha x\,dx \quad [14]$$

where $\alpha \equiv n\pi/a$, $(0 < x < a,\ n = 1, 2, \ldots)$.

Since

$$y(x) = \sum_{n=1}^{\infty} b_n \sin\alpha x, \quad (0 < x < a) \quad [15]$$

where

$$b_n = (2/a)\int_0^a y(x)\sin\alpha x\,dx = (2/a)\,y_s(\alpha) \quad [16]$$

we have

$$y(x) = (2/a)\sum_{n=1}^{\infty} y_s(\alpha)\sin\alpha x, \quad (0 < x < a) \quad [17]$$

This expression, Equation [17], for $y(x)$ is the "inverse sine transform" of $y_s(\alpha)$. Repeated integration by parts yields the following formulas for the transforms of second and fourth derivatives

$$S\left[\frac{d^2y}{dx^2}\right] = -\alpha^2 y_s(\alpha) - \alpha[(-1)^n y(a) - y(0)] \quad [18]$$

$$S\left[\frac{d^4y}{dx^4}\right] = \alpha^4 y_s(\alpha) - \alpha\,[(-1)^n y''(a) - y''(0)] + \alpha^3\,[(-1)^n y(a) - y(0)] \quad [19]$$

When writing the sine transform (or inverse transform) of any function, we shall assume that the function has properties necessary for that transform (or inverse transform) to exist.[5] Also, we assume continuity of all derivatives.

The Solution

By taking the sine transform of Equation [1] with respect to x, we have

$$\frac{d^4 w_s(\alpha, y)}{dy^4} - 2\alpha^2\frac{d^2 w_s(\alpha, y)}{dy^2} + (\alpha^4 + k')w_s(\alpha, y) = Q(\alpha, y) \quad [20]$$

where

$$k^2 = +\sqrt{\frac{k'}{D}}$$

where

$$Q(\alpha, y) = \frac{q_s(\alpha, y)}{D} + \alpha\left[(-1)^n\frac{\partial^2 w(a, y)}{\partial x^2} - \frac{\partial^2 w(0, y)}{\partial x^2}\right] - 2\alpha\left[(-1)^n\frac{\partial^2 w(a, y)}{\partial y^2} - \frac{\partial^2 w(0, y)}{\partial y^2}\right] - \alpha^3[(-1)^n w(a, y) - w(0, y)] \quad [21]$$

This may be written

$$Q(\alpha, y) = \frac{q_s(\alpha, y)}{D} + \alpha\left\{(-1)^{n+1}\left[\frac{M_2(y)}{D} + \nu\,w_2''(y)\right] + \frac{M_1(y)}{D} + \nu w_1''(y)\right\} + 2\alpha\,[(-1)^n w_2''(y) - w_1''(y)] - \alpha^3[(-1)^n w_2(y) - w_1(y)] \quad [22]$$

The solution of Equation [20] is

$$w_s(\alpha, y) = C_1\sinh uy\sin vy + C_2\cosh uy\sin vy + C_3\sinh uy\cos vy + C_4\cosh uy\cos vy + G(\alpha, y) \quad [23a]$$

where

$$u = +\sqrt{\frac{\sqrt{\alpha^4 + k'} + \alpha^2}{2}}, \quad v = +\sqrt{\frac{\sqrt{\alpha^4 + k'} - \alpha^2}{2}} \quad [23b]$$

$G(\alpha, y)$ can be expressed in closed form by using the Laplace transform on Equation [20]. The result is

$$G(\alpha, y) = \int_{\tau=0}^{\tau=y}\frac{Q(\alpha, \tau)}{k^2(u^2 + v^2)}\,[u\cosh u(y-\tau)\sin v(y-\tau) - v\sinh u(y-\tau)\cos v(y-\tau)]\,d\tau \quad [23c]$$

The following abbreviations will be used:

$S = \sinh ub$, $C = \cosh ub$, $s = \sin vb$, $c = \cos vb$, $S_2 = \sinh 2ub$, $S_4 = \sinh 4ub$, $c_2 = \cos 2vb$, etc.

In all cases when k' approaches zero

$$C_1\sin vy \to C_1' y\ C_2\sin vy \to C_2' y$$

$$C_3 \to C_3',\ C_4 \to C_4',\ u \to \alpha,\ v \to \frac{k^2}{2\alpha} \to 0$$

where primes refer to the case of no elastic foundation.[7]

The transformed edge conditions, Equations [6] to [13], inclusive, are

$$w_s(\alpha, b) = w_{1s}(\alpha) \quad [24]$$

$$w_s'(\alpha, b) = S_{1s}(\alpha) \quad [25]$$

$$w_s(\alpha, -b) = w_{4s}(\alpha) \quad [26]$$

$$w_s'(\alpha, -b) = S_{2s}(\alpha) \quad [27]$$

$$-w_s''(\alpha, b) + \nu\alpha^2 w_s(\alpha, b) + \alpha\nu[(-1)^n w(a, b) - w(0, b)] = M_{2s}(\alpha)/D \quad [28]$$

$$-w_s''(\alpha, -b) + \nu\alpha^2 w_s(\alpha, -b) + \alpha\nu[(-1)^n w(a, -b) - w(0, -b)] = M_{4s}(\alpha)/D \quad [29]$$

$$-w_s'''(\alpha, b) + (2-\nu)\alpha^2 w_s'(\alpha, b) + (2-\nu)\alpha[(-1)^n w'(a, b) - w'(0, b)] = R_{1s}(\alpha)/D \quad [30]$$

$$-w_s'''(\alpha, -b) + (2-\nu)\alpha^2 w_s'(\alpha, -b) + (2-\nu)\alpha[(-1)^n w'(a, -b) - w'(0, -b)] = R_{2s}(\alpha)/D \quad [31]$$

where

[5] "Modern Operational Mathematics in Engineering," by R. V. Churchill, first edition, McGraw-Hill Book Company, Inc., New York, N. Y., 1944, pp. 267, 269, 37.

$$w_x' = \frac{dw_x(\alpha, y)}{dy}, \text{ etc.}$$

From the edge conditions at the edges $y = \pm b$, we can evaluate the constants C_1, C_2, C_3, and C_4 in Equations [23]. We will give first the values of these constants for certain of the edge functions required to be zero (cases 1*a*—6*a*, inclusive). The values of the constants C_1, C_2, C_3, and C_4 for the edge functions not equal to zero will be written in terms of the corresponding constants for the edge functions equal to zero.

The constants for Cases 1(*a*) — 6(*a*), inclusive, are as follows:

Case 1(*a*)

$$\left.\begin{aligned}
C_1(us_2 + vS_2) &= [G(\alpha, b) + G(\alpha, -b)]\,(uSc - vCs)\\
&\quad - Cc[G'(\alpha, b) - G'(\alpha, -b)]\\
C_2(us_2 - vS_2) &= [-G(\alpha, b) + G(\alpha, -b)]\,(uCc\\
&\quad - vSs) + Sc[G'(\alpha, b) + G'(\alpha, -b)]\\
C_3(-us_2 + vS_2) &= [-G(\alpha, b) + G(\alpha, -b)]\,(uSs\\
&\quad + vCc) + Cs[G'(\alpha, b) + G'(\alpha, -b)]\\
C_4(-us_2 - vS_2) &= [+G(\alpha, b) + G(\alpha, -b)]\,(uCs\\
&\quad + vSc) - Ss[+G'(\alpha, b) - G'(\alpha, -b)]
\end{aligned}\right\} \quad [32]$$

Case 2(*a*)

$$\left.\begin{aligned}
k^2C_1(C_2 + c_2) &= -Cc[G''(\alpha, b) + G''(\alpha, -b)]\\
&\quad - (-Cc\alpha^2 + Ssk^2)\,[G(\alpha, b)\\
&\quad + G(\alpha, -b)]\\
k^2C_2(C_2 - c_2) &= -Sc[G''(\alpha, b) - G''(\alpha, -b)]\\
&\quad - (-Sc\alpha^2 + Csk^2)\,[G(\alpha, b)\\
&\quad - G(\alpha, -b)]\\
k^2C_3(C_2 - c_2) &= +Cs[G''(\alpha, b) - G''(\alpha, -b)]\\
&\quad - (+Cs\alpha^2 + Sck^2)\,[G(\alpha, b)\\
&\quad - G(\alpha, -b)]\\
k^2C_4(C_2 + c_2) &= +Ss[G''(\alpha, b) + G''(\alpha, -b)]\\
&\quad - (Ss\alpha^2 + Cck^2)\,[G(\alpha, b) + G(\alpha, -b)]
\end{aligned}\right\} \quad [33]$$

Case 3(*a*)

$$\left.\begin{aligned}
&C_1\{2\alpha^2k^2(1-\nu)(vs_2 - uS_2) + [\alpha^2(1-\nu)^2 - k^4]\\
&(us_2 + vS_2)\} = [\alpha^2(1-\nu)Cc - k^2Ss]\,[G''''(\alpha, b)\\
&- G''''(\alpha, -b) - (2-\nu)\alpha^2G''(\alpha, b)\\
&+ (2-\nu)\,\alpha^2G''(\alpha, -b)] + \tfrac{1}{2}Sc[\alpha^2(1-\nu)u + k^2v]\\
&- Cs[\alpha^2(1-\nu)v - k^2u]\}\,[G''(\alpha, b) + G''(\alpha, -b)\\
&- \nu\alpha^2G(\alpha, b) - \nu\alpha^2G(\alpha, -b)].\\
&-C_2\{2\alpha^2k^2(1-\nu)(vs_2 + uS_2) + [\alpha^2(1-\nu)^2\\
&- k^4]\,(us_2 - vS_2)\} = [\alpha^2(1-\nu)Sc - k^2Cs]\\
&[G''''(\alpha, b) + G''''(\alpha, -b) - (2-\nu)\alpha^2G''(\alpha, b)\\
&- (2-\nu)\alpha^2G''(\alpha, -b)] + \tfrac{1}{2}Cc[\alpha^2(1-\nu)u + k^2v]\\
&- Ss[\alpha^2(1-\nu)v - k^2u]\}\,[G''(\alpha, b) - G''(\alpha, -b)\\
&- \nu\alpha^2G(\alpha, b) + \nu\alpha^2G(\alpha, -b)]\\
&-C_3\{2\alpha^2k^2(1-\nu)(vs_2 + uS_2) + [\alpha^2(1-\nu)^2 - k^4]\\
&(us_2 - vS_2)\} = [-\alpha^2(1-\nu)Cs - k^2Sc]\,[G''''(\alpha, b)\\
&+ G''''(\alpha, -b) - (2-\nu)\alpha^2G''(\alpha, b) - (2-\nu)\alpha^2G''(\alpha,\\
&-b)] - \tfrac{1}{2}Ss[\alpha^2(1-\nu)u + k^2v] + Cc[\alpha^2(1-\nu)v\\
&-k^2u]\}\,[G''(\alpha, b) - G''(\alpha, -b) - \nu\alpha^2G(\alpha, b)\\
&+ \nu\alpha^2G(\alpha, -b)]\\
&C_4\{2\alpha^2k^2(1-\nu)(vs_2 - uS_2) + [\alpha^2(1-\nu)^2 - k^4]\\
&(us_2 + vS_2)\} = [-\alpha^2(1-\nu)Ss - k^2Cc]\,[G''''(\alpha, b)\\
&- G''''(\alpha, -b) - (2-\nu)\alpha^2G''(\alpha, b)\\
&+ (2-\nu)\alpha^2G''(\alpha, -b)] - \tfrac{1}{2}Cs[\alpha^2(1-\nu)u + k^2v]\\
&+ Sc[\alpha^2(1-\nu)v - k^2u]\}\,[G''(\alpha, b) + G''(\alpha, -b)\\
&- \nu\alpha^2G(\alpha, b) - \nu\alpha^2G(\alpha, -b)]
\end{aligned}\right\} \quad [34]$$

Case 4(*a*)

$$\left.\begin{aligned}
&k^2(us_4 - vS_4)C_1 = -2k^2G(\alpha, b)\,[uSc(2s^2 + C_2)\\
&+ vCs(2c^2 - C_2)] + 2G(\alpha, -b)\,[+uk^2Scc_2\\
&+ vk^2CsC_2 + \alpha Cc(us_2 - vS_2)] + 4k^2CcG'(\alpha, b)\\
&(s^2 + S^2) - 2CcG''(\alpha, -b)\,(us_2 - vS_2)
\end{aligned}\right\} \quad [35]$$

$$\left.\begin{aligned}
&k^2(us_4 - vS_4)C_2 = -2k^2G(\alpha, b)\,[uCc(-2s^2 + C_2)\\
&+ vSs(-2c^2 - C_2)] + 2G(\alpha, -b)\,[+uk^2Ccc_2\\
&- vk^2S_2C_2 + \alpha^2Sc(us_2 + vS_2)] + 4k^2ScG'(\alpha, b)\\
&(c^2 + S^2) - 2ScG''(\alpha, -b)\,(us_2 + vS_2)\\
&k^2(us_4 - vS_4)C_3 = -2k^2G(\alpha, b)\,[uSs(-2c^2 - C_2)\\
&+ vCc(2s^2 - C_2)] + 2G(\alpha, -b)\,[-uk^2Ssc_2\\
&- vk^2CcC_2 - \alpha^2Cs(us_2 + vS_2)] - 4k^2CsG'(\alpha, b)\\
&(c^2 + S^2) + 2CsG''(\alpha, -b)\,(us_2 + vS_2)\\
&k^2(us_4 - vS_4)C_4 = -2k^2G(\alpha, b)\,[uCs(2c^2 - C_2)\\
&+ vSc(-2s^2 - C_2)] + 2G(\alpha, -b)\,[-uk^2Csc_2\\
&+ vk^2ScC_2 - \alpha^2Ss(us_2 - vS_2)] - 4k^2SsG'(\alpha, b)\\
&(s^2 + S^2) + 2SsG''(\alpha, -b)\,(us_2 - vS_2)
\end{aligned}\right\} \quad [35\ (cont.)]$$

Case 5(*a*)

$$\left.\begin{aligned}
\Delta C_1 &= -k^2G(\alpha, -b)\,\{2\alpha^2(1-\nu)\,[u^2Cc(-s^2 + C_2)\\
&+ uvS_2(c^2 - C^2) + v^2Cc(-2s^2 + C^2)]\\
&+ k^2[-u^2Scc_2 + 2uvCc(-c^2 + C^2) - v^2S_2C_2]\}\\
&+ k^2G'(\alpha, -b)\,\{2\alpha^2(1-\nu)\,[uSc(c^2 - 2C_2)\\
&+ vCs(-2c^2 + C^2) + k^2[uCsc_2 - vScC_2]\}\\
&+ [G'''(\alpha, b) - \alpha^2\nu G(\alpha, b) + \alpha^2(1-\nu)G(\alpha, -b)]\\
&\{2\alpha^2(1-\nu)\,(uSc - vCs)\,(-usc + vSC)\\
&+ k^2[u^2Ccc_2 + v^2CcC^2 + 2uvSs(-c^2 + C^2)]\\
&- [G'''(\alpha, b) - (2-\nu)\alpha^2G'(\alpha, b)\\
&+ \alpha^2(1-\nu)G'(\alpha, -b)]\}\,\{-2\alpha^2(1-\nu)Cc\,(-usc\\
&+ vSC) + k^2uScc_2 + k^2vCsC_2\}
\end{aligned}\right\} \quad [36]$$

where Δ is given by

$$\left.\begin{aligned}
\Delta &= \alpha^4(1-\nu)^2(-u^2s_2^2 + v^2S_2^2)\\
&+ \alpha^2(1-\nu)k^2uv(c_4 - C_4) - k^4(u^2c_2^2 + v^2C_2^2)
\end{aligned}\right\}$$

and the other C's are given in terms of C_1

$$\left.\begin{aligned}
&2C_4\{k^2[uScc_2 + vCsC_2] + \alpha^2(1-\nu)Cc(us_2 - vS_2)\}\\
&= G(\alpha, -b)\,[-k^2(uS_2 + vc_2) + \alpha^2(1-\nu)\,\{-us_2\\
&+ vS_2\}] - 2k^2G'(\alpha, -b)\,(-c^2 + C^2) + [G'''(\alpha, b)\\
&- \alpha^2\nu G(\alpha, b) + 2C_1\alpha^2(1-\nu)Ss]\,(-us_2 + vS_2)\\
&+ 2k^2C_1(-uCsc_2 + vScC_2)\\
&C_2(-usc + vSC) = -(uCc - vSs)G(\alpha, -b)\\
&+ C_1vS^2 - C_4uc^2 - ScG'(\alpha, -b)\\
&C_2Sc = C_1Ss - C_2Cs + C_4Cc + G(\alpha, -b)
\end{aligned}\right\}$$

Case 6(*a*)

$$\left.\begin{aligned}
\Delta C_1 &= -G(\alpha, -b)\,[\alpha^2(1-\nu)Cc - k^2Ss]\,\{-[\alpha^2(1\\
&-\nu)u + k^2v]\,[\alpha^2(1-\nu)s_2 + k^2S_2] + [k^2u - \alpha^2(1\\
&-\nu)v]\,[-\alpha^2(1-\nu)S_2 + k^2s_2]\}\,+\,[G''(\alpha, b)\\
&-\alpha^2\nu G(\alpha, b)]k^2\,\{-[\alpha^2(1-\nu)u + k^2v]\,(Sss_2\\
&+ ScC_2) + [k^2u - \alpha^2(1-\nu)v]\,[Ccs_2 - CsC_2]\\
&+ [G''(\alpha, b) - \nu\alpha^2G(\alpha, -b)]\,\}\,-\,[\alpha^2(1-\nu)u\\
&+ k^2v]\,[2Csc^2\alpha^2(1-\nu) + k^2ScC_2] + [k^2u - \alpha^2(1\\
&-\nu)v]\,[-2SC^2c\alpha^2(1-\nu) + k^2Csc_2]\}\\
&+ 2k^2[G''''(\alpha, b) - (2-\nu)\alpha^2G'(\alpha, b)]\,[\alpha^2(1-\nu)Cc\\
&- k^2Ss]\,(c^2 - C^2)
\end{aligned}\right\} \quad [37]$$

$$\left.\begin{aligned}
&2\Delta = k^2\,\{[u\alpha^2(1-\nu) + k^2v]\,[\alpha^2(1-\nu)s_4 + k^2S_4]\\
&+ [\alpha^2(1-\nu)v - k^2u]\,[-\alpha^2(1-\nu)S_4 + k^2s_4]\}\\
&2k^2C_3[-\alpha^2(1-\nu)Cc + k^2Ss]\,(c^2 - C^2) = -G''(\alpha,\\
&-b)\,[k^2c_2S + s_2C\alpha^2(1-\nu)]C - k^2SCG''(\alpha, b)\\
&+ G(\alpha, -b)\,\{k^2SC\alpha^2\nu - 2[-\alpha^2(1-\nu)Cc + k^2Ss]\\
&[\alpha^2Cs + k^2Sc] + \alpha^2\nu k^2SCG(\alpha, b) + 2C_1k^2(s^2 - C^2)\\
&[\alpha^2(1-\nu)Cs + k^2Sc]\\
&2C_4[-\alpha^2(1-\nu)Cc + k^2Ss] = \{G''(\alpha, b) + G''(\alpha, -b)\\
&- \alpha^2\nu G(\alpha, b) - \alpha^2\nu G(\alpha, -b) - 2C_1\\
&[-\alpha^2(1-\nu)Ss - k^2Cc]\}\\
&CsC_2 = +C_1Ss - C_2Sc + C_4Cc + G(\alpha, b)
\end{aligned}\right\}$$

We shall now find the constants C_1, C_2, C_3, and C_4 for Cases 1 to 6, inclusive:

Case 1 In the constants of Case 1(a), replace

$$G(\alpha, b) \text{ by } G(\alpha, b) - w_{3s}(\alpha) \quad [38]$$

$$G(\alpha, -b) \text{ by } G(\alpha, -b) - w_{4s}(\alpha) \quad [39]$$

$$G'(\alpha, b) \text{ by } G'(\alpha, b) - S_{1s}(\alpha) \quad [40]$$

$$G'(\alpha, -b) \text{ by } G'(\alpha, -b) - S_{2s}(\alpha) \quad [41]$$

Case 2 In the constants of Case 2(α), use Equations [38] and [39] and replace

$$G''(\alpha, b) \text{ by } G''(\alpha, b) - \alpha^3\nu w_{3s}(\alpha) - \alpha\nu[(-1)^n w(a, b) - w(0, b)] + M_{3s}(\alpha)/D \quad [42]$$

$$G''(\alpha, -b) \text{ by } G''(\alpha, -b) - \alpha^3\nu w_{4s}(\alpha) - \alpha\nu[(-1)^n w(a, -b) - w(0, -b)] + M_{4s}(\alpha)/D \quad [43]$$

Case 3 In the constants of Case 3(a), replace

$$G''(\alpha, b) \text{ by } G''(\alpha, b) - \alpha\nu[(-1)^n w(a, b) - w(0, b)] + M_{3s}(\alpha)/D \quad [44]$$

$$G''(\alpha, -b) \text{ by } G''(\alpha, -b) - \alpha\nu[(-1)^n w(a, -b) - w(0, -b)] + M_{4s}(\alpha)/D \quad [45]$$

$$G'''(\alpha, b) \text{ by } G'''(\alpha, b) - (2 - \nu)\alpha[(-1)^n w'(a, b) - w'(0, b)] + R_{1s}(\alpha)/D \quad [46]$$

$$G'''(\alpha, -b) \text{ by } G'''(\alpha, -b) - (2 - \nu)\alpha[(-1)^n w'(a, -b) - w'(0, -b)] + R_{2s}(\alpha)/D \quad [47]$$

Case 4 In the constants of Case 4(a) use Equations [38], [39], [40], and [43].

Case 5 In the constants of Case 5(a) use Equations [44], [46], [39], and [41].

Case 6 In the constants of Case 6(a) use Equations [44], [46], [39], and [43].

For example, if in Case 2 a constant moment was applied at the edges one would replace

$$G''(\alpha, b) \text{ by } G''(\alpha, b) + \frac{M_{3s}(\alpha)}{D}$$

where

$$M_{3s}(\alpha) = \int_0^a M_3(x) \sin \alpha x \, dx = \frac{M_3}{\alpha}[1 - (-1)^n] \quad [48]$$

and one would replace

$$G''(\alpha, -b) \text{ by } G''(\alpha, -b) + \frac{M_{4s}(\alpha)}{D}$$

where

$$M_{4s}(\alpha) = \int_0^a M_4(x) \sin \alpha x \, dx = \frac{M_4}{\alpha}[1 - (-1)^n] \quad [49]$$

The final solution is given by

$$w(x, y) = \frac{2}{a} \sum_{n=1}^{\infty} w_s(\alpha, y) \sin \alpha x \quad [50]$$

where $w_s(\alpha, y)$ is given by Equation [23].

Examples

The factor depending on the load is $G(\alpha, y)$. This factor is evaluated for several specific examples from Equation [23c]:

(a) Rectangular strip

$q(x, y) = q$ as indicated is shaded area of Fig. 2.

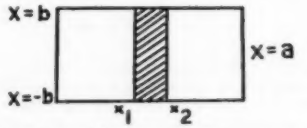

Fig. 2 Constant Load Applied Between x_1 and x_2

$$G(\alpha, y) = \frac{q_0}{D} \frac{1}{\alpha^4 + k^4} \frac{\cos \alpha x_1 - \cos \alpha x_2}{\alpha} \quad [51]$$

(b) Concentrated line strip

$$q(x, y) = \frac{q_0}{dx} \text{ when } x = \xi$$

$$= 0 \text{ elsewhere}$$

$$G(\alpha, y) = \frac{q_0}{D} \frac{1}{\alpha^4 + k^4} \sin \alpha\xi \quad [52]$$

This was obtained by letting x_2 approach x_1 in Equation [51]

(c) Constant load

$$q(x, y) = q_0$$

$$G(\alpha, y) = \frac{q_0}{D} \frac{1}{\alpha^4 + k^4} \frac{1 - (-1)^n}{\alpha} \quad [53]$$

This was obtained by letting $x_1 \to 0$ and $x_2 \to a$ in Equation [51].

(d) Hydrostatic pressure in x-direction

$$q(x, y) = \frac{q_0 x}{a}$$

$$G(\alpha, y) = \frac{q_0}{D} \frac{1}{\alpha^4 + k^4} \frac{(-1)^{n-1}}{\alpha} \quad [54]$$

(e) Hydrostatic pressure in y-direction

$$q(x, y) = \frac{q_0 y}{b}$$

$$G(\alpha, y) = \frac{q_0}{D} \frac{1}{\alpha^4 + k^4} \frac{1 - (-1)^n}{\alpha} \frac{y}{b} \quad [55]$$

(f) No load but constant moments at $x = 0$, and $x = a$

$$M_1(y) = M_1, \; M_2(y) = M_2$$

$$G(\alpha, y) = \frac{\alpha(-1)^n M_2 + \alpha M_1}{D(\alpha^4 + k^4)}$$

The constant-load solution is the same as that in Timoshenko,[6] if one takes w_1, w_2, M_1, M_2, w_3, w_4, S_1, S_2 equal to zero and uses Case 1. In examples (c), (d), (e), (f) one can sum $G(\alpha, y) \sin \alpha x$, giving a particular solution in simple form. These are the solutions corresponding to the one-dimensional problems.

The general equation of a thin isotropic homogeneous plate on an elastic foundation including time dependence is

$$D\nabla^4 W = q - k'W - \rho \frac{\partial^2 W}{\partial t^2}$$

If we assume the load is impressed sinusoidally $q = q_0(x, y) \sin(\omega t + \delta)$ then $W(x, y, t) = w(x, y) \sin(\omega t + \delta)$ is a solution where w satisfies the equation

$$D\nabla^4 w = q - (k' - \rho\omega^2)w$$

If $\omega < \sqrt{k'/\rho}$ this equation is the same as the static case, Equation [1], where k' is replaced by $k' - \rho\omega^2$. Also, if $k' = \rho\omega^2$ this reduces to the case treated by Deverall and Thorne.[7]

The problem of elastically supported edges at $y = \pm b$ also could be solved by the foregoing method.

MOMENTS

1- CLAMPED
2- SIMPLY SUPPORTED
3-FREE
UNITS OF MOMENTS ARE
33.33 Q_0 LB-IN / IN
WHERE Q_0 IS IN LB / IN²

UNITS OF DEFLECTIONS
ARE 6.034×10^{-4} Q_0
LBS. PER SQ. IN. AND
STRIP LOAD IS IN
SHADED AREA

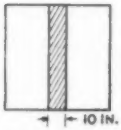

FIG. 3 STRIP LOAD

DISCUSSION OF GRAPHS

All curves are plotted for the following values of the physical constants:

$a = 2b = 60$ in.

$\nu = 0.15$

$h = 6$ in.

$E = 3 \times 10^6$ psi

$k' = 100$ lb per cu in.

The curves would be the same shape if E, h, k' were varied in such a way as to make $Eh^3/k' = 6.48 \times 10^6$ but are reduced by a factor of $1/k'$.

Deflections and moments are symmetric about the two center lines. Hence plots were made only in one quadrant. The values of the hyperbolic functions were computed from the tables compiled by Federal Works Agency, Works Project Administration (WPA).

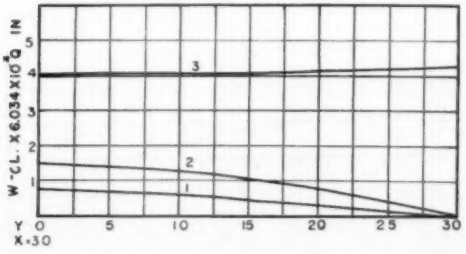

FIG. 4 DEFLECTION AT $x = 30$, CONSTANT LOAD

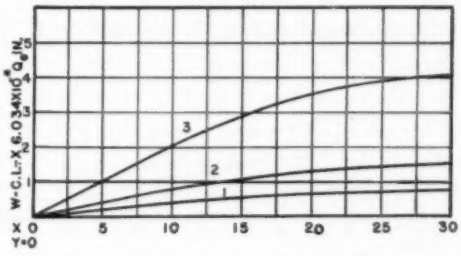

FIG. 5 DEFLECTION AT $y = 0$, CONSTANT LOAD

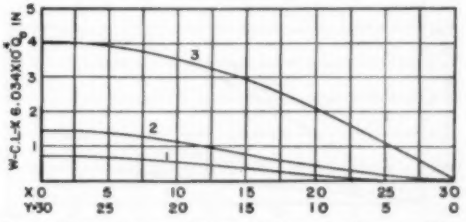

FIG. 6 DEFLECTION ON NEGATIVE DIAGONAL, CONSTANT LOAD

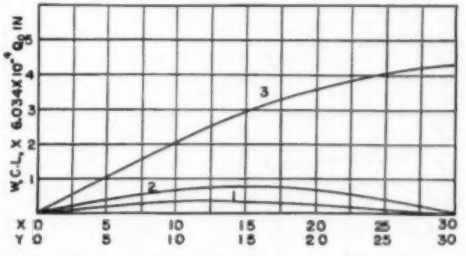

FIG. 7 DEFLECTION ON POSITIVE DIAGONAL, CONSTANT LOAD

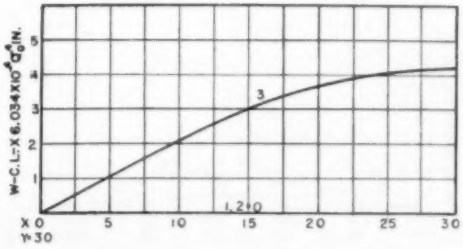

FIG. 8 DEFLECTION AT $y = 30$, CONSTANT LOAD

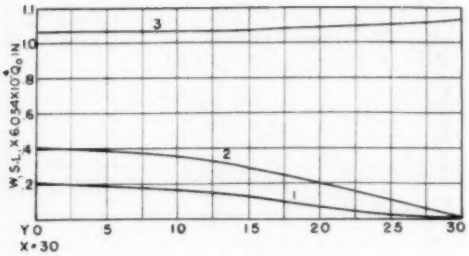

FIG. 9 DEFLECTION AT $x = 30$, STRIP LOAD

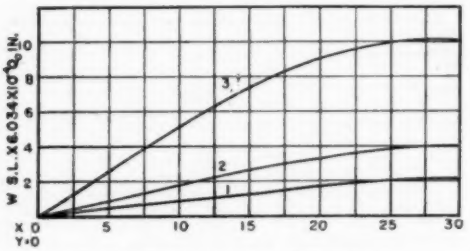

FIG. 10 DEFLECTION AT $y = 0$, STRIP LOAD

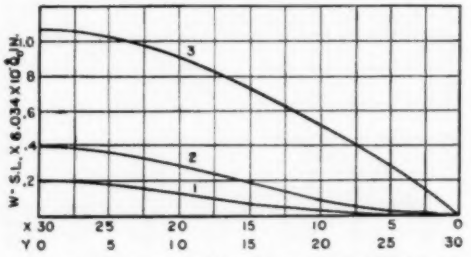

FIG. 11 DEFLECTION ON NEGATIVE DIAGONAL, STRIP LOAD

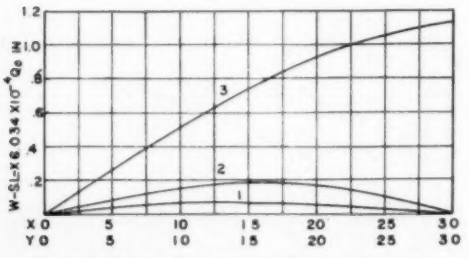

FIG. 12 DEFLECTION ON POSITIVE DIAGONAL, STRIP LOAD

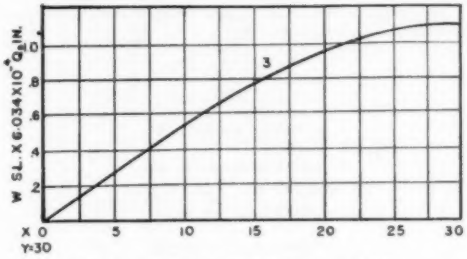

FIG. 13 DEFLECTION AT $y = 30$, STRIP LOAD

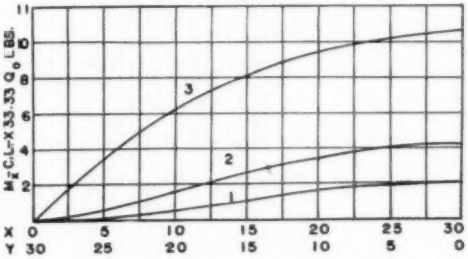

FIG. 14 x-MOMENT ON NEGATIVE DIAGONAL, CONSTANT LOAD

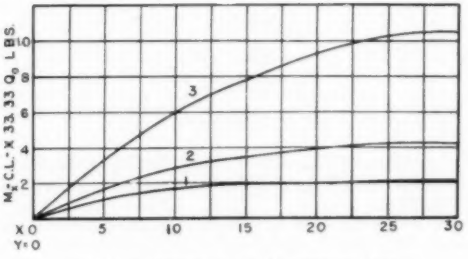

FIG. 15 x-MOMENT AT $y = 0$, CONSTANT LOAD

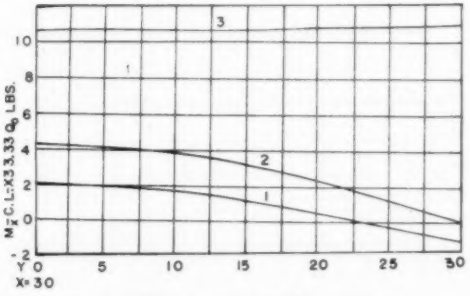

FIG. 16 x-MOMENT AT $x = 30$, CONSTANT LOAD

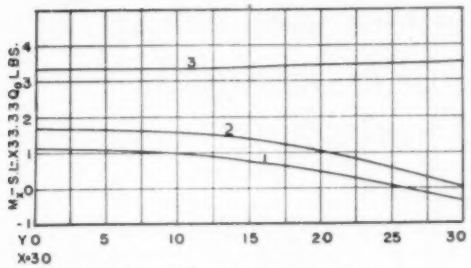

FIG. 17 x-MOMENT AT $x = 30$, STRIP LOAD

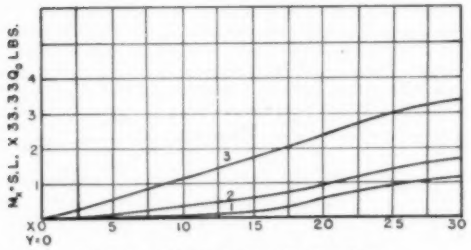

FIG. 18 x-MOMENT AT $y = 0$, STRIP LOAD

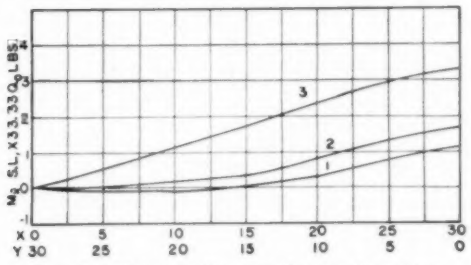

FIG. 19 x-MOMENT ON NEGATIVE DIAGONAL, STRIP LOAD

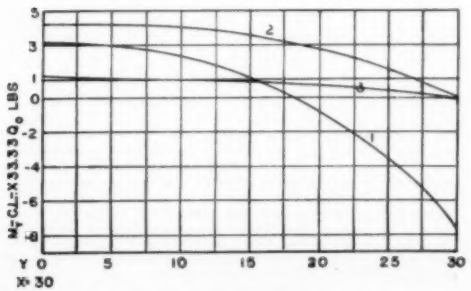

FIG. 20 y-MOMENT AT $x = 30$, CONSTANT LOAD

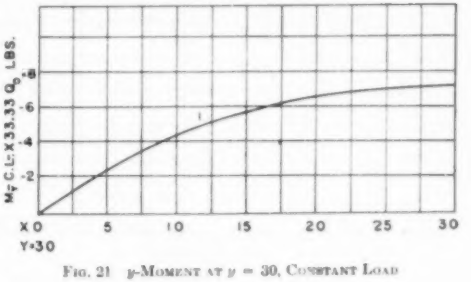

FIG. 21 y-MOMENT AT $y = 30$, CONSTANT LOAD

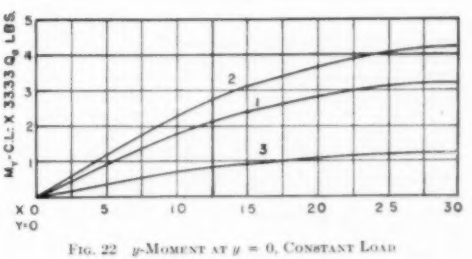

FIG. 22 y-MOMENT AT $y = 0$, CONSTANT LOAD

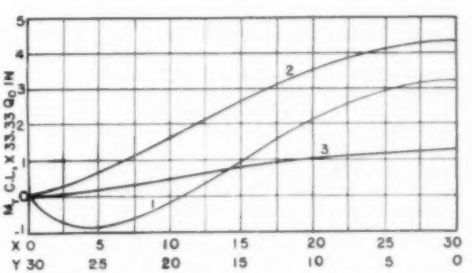

FIG. 23 y-MOMENT ON NEGATIVE DIAGONAL, CONSTANT LOAD

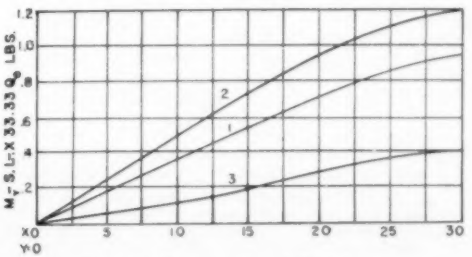

FIG. 24 y-MOMENT AT $y = 0$, STRIP LOAD

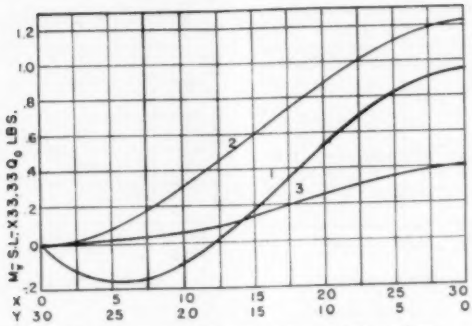

FIG. 25 y-MOMENT ON NEGATIVE DIAGONAL, STRIP LOAD

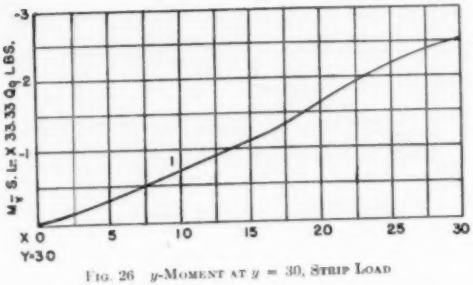

FIG. 26 y-MOMENT AT y = 30, STRIP LOAD

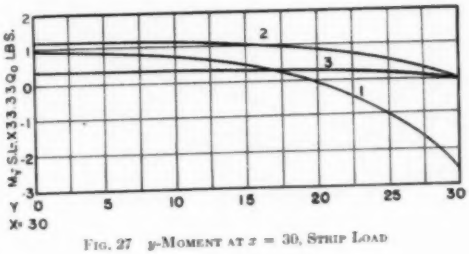

FIG. 27 y-MOMENT AT x = 30, STRIP LOAD

Temperature Development in a Heated Contact With Application to Sliding Contacts

By RAGNAR HOLM,[1] ST. MARYS, PA.

The calculation of the development of the temperature in and around a heated contact is reduced to the use of some simple formulas for certain fundamental variables and to making readings from a diagram. Applications are made to a contact that is heated by the current and to circular or oval heat sources (for example, friction-heated sliding contact-surfaces) stationary or moving on the face of a semi-infinite body. The practicability of the method is due primarily to the fact that the numerical calculations, which are made before using the standard curves, are so simple that the chance of a numerical error is very small.

Nomenclature

The following nomenclature is used in the paper:

a = radius of circular contact spot, cm

b = radius of substituted sphere *Sp*, cm; based upon principle that same amount of generated heat shall cause same average temperature rise in actual and substituted contact, Equation [1] must hold[2] (see Appendix)

$$\pi b = 2a \qquad [1]$$

r = distance from center of contact, cm. Hemispheres r = const are isotherms in case of *Sp*-contact; but in actual case, with a flat contact spot, those hemispheres only approximate the isotherms. Because of this fact Equations [5], [7], and [12] give a good approximation for actual isotherms only if they are at a distance greater than b from any part of contact spot.

z = dimensionless position co-ordinate satisfying

$$r = b(1 + x) \qquad [2]$$

2α and 2β = major and minor axes of an elliptic contact spot. References will be made to a representative circular spot with radius a, where $\alpha = \gamma a$ and $\beta = a/\gamma$. Here γ is a measure of ovalness.[3]

We have $a^2 = \alpha\beta$, and thus the elliptic and the substituted circular areas are equal.

$f(x) = 2 - \dfrac{1}{1 + x}$

$f(\gamma)$ = another function, compare Fig. 4.

$\varphi(x) = \dfrac{x}{1 + x}$

q = rate of heat, watt/cm², conducted into a semi-infinite body per unit area of heat source on its surface

t = time measured from beginning of heating period, sec

t_c = time measured from beginning of cooling period

$\vartheta(t, r)$ = supertemperature at time t and position r, measured in centidegrees from bulk temperature of contact members. This bulk temperature is regarded as remaining constant at its initial value.

$\vartheta_c(t_c, r)$ = supertemperature during cooling of a "stationary" contact region (constriction) which previously was heated up to a steady state

$\vartheta(\infty, r)$ = steady supertemperature at r

$\vartheta_m(t)$ = maximum[5] supertemperature in contact spot at time t. In a stationary heat source $\vartheta_m(t)$ belongs to center of spot.

$\vartheta_m(v)$ = maximum[5] supertemperature under a heat source moving with speed v. $\vartheta_m(v)$ appears between center and rear point of source.

θ_m = steady supertemperature in center of stationary contact spot

$\bar{\theta}$ = average steady supertemperature in stationary contact spot. In the *Sp*-case $\theta_m = \bar{\theta}$.

The indexes *A*, *B*, *S* refer to cases A, B, S, which are defined in the second and third sections; for example, $\bar{\theta}_A$.

z = dimensionless substitution for time

$$z = \frac{\lambda}{c b^2} t = \frac{\pi^2}{4} \frac{\lambda}{c a^2} t \qquad [3]$$

ρ = resistivity of contact material, ohm-cm

λ = heat conductivity, in watt/cm deg

c = heat capacity, joules/cm³ deg

I = current, a

U = contact voltage = voltage between bulks of contact members

v = speed of heat source, cm per sec

μ = coefficient of friction

Introduction

The problem of the temperature and its variation in and around a contact heated by an electric current through it, or by friction,

[1] Stackpole Carbon Company.

[2] Cf. reference (1)[4] equation 11.19, and reference (3) equation 19.

[3] Cf. reference (1) 4E. If ϵ = eccentricity $\frac{1}{\gamma^2} = 1 - \epsilon^2$.

[4] Numbers in parentheses refer to the Bibliography at the end of the paper.

Presented at the National Conference of the Applied Mechanics Division, State College, Pa., June 19–21, 1952, of The American Society of Mechanical Engineers.

Discussion of this paper should be addressed to the Secretary, ASME, 29 West 39th Street, New York, N. Y., and will be accepted until October 10, 1952, for publication at a later date. Discussion received after the closing date will be returned.

Note: Statements and opinions advanced in papers are to be understood as individual expressions of their authors and not those of the Society. Manuscript received by ASME Applied Mechanics Division, July 12, 1951. Paper No. 52—APM-24.

[5] In the *Sp*-case (represented by the Equations [5] to [9]) any r represents an isotherm, and there is no difference between average and maximum temperature for any given r. The words "average" and "maximum" refer especially to the case when the formulas are used to approximate the happening in a moving heat source.

arises frequently in practice. In any case, form and size of the contact surface can be computed only roughly, and more than approximate solutions are not needed. Exact solutions of the mathematical problem have been derived for some idealized cases. However, numerical calculations for these cases with these formulas are very tedious and difficult. It would be of great advantage to have the aid of tables or graphical representations. It is the aim of this paper to provide such means, by making certain approximating simplifications. Compared with other uncertainties, the errors which are involved in this method are negligible.

Since all of the fundamental deductions are available in the literature, it is unnecessary to repeat them here. We confine ourselves to a description of the character of the deductions. Among them we distinguish two classes: Class 1, deductions dealing directly with the assumption of plane contact surfaces in close agreement with actual cases; class 2, deductions dealing with a simplifying model in which the actual curved lines of flow, that start in a plane-contact area and are shown in Fig. 1(*A*), are replaced by straight lines of flow going out from a hemispherical surface, as shown in Fig. 1(*B*). The same idea may be expressed mathe-

(*A*) (*B*)

FIG. 1 CURRENT FLOW LINES: (*A*) AROUND A FLAT CONTACT SURFACE; (*B*) IN THE *Sp*-CASE

matically by replacing the circular contact surface by a sphere *Sp* of infinite conductivity, of zero heat capacity and of suitable radius *b*. Of course, a recipe must be given for the conversion from this model to the actual flat contact. As will be explained in the Appendix, the conversion is possible since the system of isotherms beyond a certain small distance from the contact surface is approximately the same in the actual and in the model case, provided that the ratio of the radius *b* of the sphere *Sp* to the radius *a* of the (circular) contact area is given by Equation [1].

The degree of approximation by which the model results approach class 1 is indicated by the close resemblance of the curves *Sb* and *J-O* in Fig. 2. Taking for granted the use of the *Sp*-model we proceed as follows: Using the equations which are based upon the *Sp*-model, a system of curves representing the development of the temperature in different points in and around the contact is designed in Fig. 2. Merely the use of these curves or interpolations between them would shorten computations considerably, but we shall make a further simplifying step. We shall show that the few curves in Fig. 3 suffice for the computations desired. Because of a similitude between curves in Fig. 2, a conversion to the curves in Fig. 3 can be made by some simple algebraic transformations, Equations [15] to [17]. These transformations have no exact mathematical background; but inspection of the data in Table 1 shows that the results obtained by this method agree with Fig. 2 within sufficiently narrow limits.

The practicability of the transformations mentioned lies in the lumping together of both the time and space variables into a single dimensionless parameter z, the calculation of which is so simple that the chance of a numerical error is reduced practically to zero.

Thus far we have considered a stationary heat source. The problem of a "moving heat source"[6] (MHS) on the surface of a flat semi-infinite body exhibits many differences. There is, for instance, the fundamental difference between the happenings at

[6] The contact area of a sliding contact that produces frictional heat is such a heat source.

TABLE 1

Case	z	$\vartheta_X(r,t)/\vartheta_X$	
	According to Eq. [3]	According to Fig. 2	According to 5th section
A2b	0.5	0.085	0.083
A2b	10	0.447	0.465
A4b	2	0.05	0.05
A4b	40	0.28	0.27
B4b	2	0.14	0.16
B4b	200	0.64	0.65
S2b	0.4	0.04	0.05
S2b	8	0.31	0.29
S4b	16	0.105	0.12

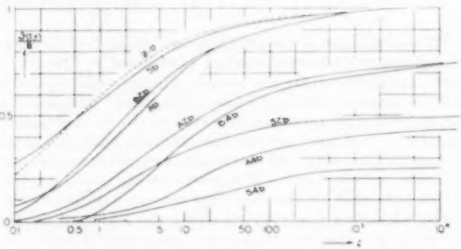

FIG. 2 SUPERTEMPERATURES AS FRACTIONS OF STEADY SUPERTEMPERATURE IN THE CONTACT

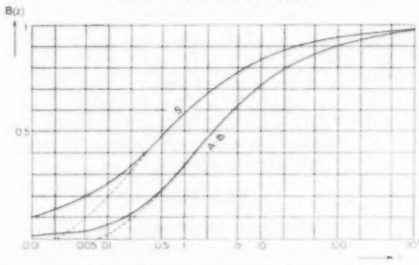

FIG. 3 DIAGRAM FOR SIMPLIFIED CALCULATION

the front and the rear of the heat source. However, if we confine our interest to the average temperature of the contact surface or the maximum temperature near its center, computations can be made on the basis of the rules for a stationary source. The basic idea is that these temperatures will be nearly the same as they are in the case of a stationary heat source with the same dimensions after a heating period of the same duration as the average

TABLE 2 MOVING HEAT SOURCE. COMPARISON BETWEEN RESULTS ACHIEVED WITH SIMPLIFIED METHOD AND CALCULATIONS ACCORDING TO JAEGER'S EXACT BUT COMPLICATED FORMULAS

$\frac{ct}{2A}$	z_0	$B(z_0)$ According to simplified method	$B(z_0)$ Based on Figs. 5 and 6, i.e., on Jaeger's (2) equation [16
	CIRCULAR OR SQUARE HEAT SOURCE		
5	0.39	0.44	0.44
1	1.94	0.66	0.68
0.2	9.7	0.835	0.85
	OVAL HEAT SOURCE WITH $\gamma^2 = 10$		
31.6	0.0613	0.22	0.25
3.16	0.613	0.50	0.52
0.316	6.13	0.79	0.75

time of contact of the points of the MHS.[7] To what degree this is true is illustrated in Table 2 where computations by aid of the

[7] This turns out to be true for a circular but not for an oval heat source; refer to section, Oval Surface Heat Source Moving in Direction of its Major Axis.

recipe given here are compared with calculations according to Jaeger's formulas which apply directly to a moving heat source. It is of minor importance that Jaeger regards a square contact surface and the author a circular one. The deviations revealed by the table certainly lie within the inevitable inaccuracy limits of the determinations of the contact dimensions.

A Contact With Circular Contact Spot Is Heated at $t > 0$ by Traversing Contact Current I — to Find $\vartheta(t,r)$

Only Holm has worked out numerical solutions to this problem.[8] He assumes ρ and λ to be constants and starts from the artificial *Sp*-case. Heat is developed all over the current constriction. It flows off to both sides in the direction from the hottest surface at which $(d\vartheta)/(dr) = 0$. The bulk of the semi-infinite contact members has a great heat capacity; it is supposed to remain on a constant temperature that is labeled $\vartheta = 0$, i.e., ϑ is a supertemperature above the temperature of the bulk. It is shown (1) that for the *Sp*-model suitable transformations convert the problem to solving the equation[9]

$$K\frac{\partial^2 v}{\partial x^2} = \frac{\partial v}{\partial t}$$

for which suitable solutions are known. After a simple manipulation, the final formulas may be written as follows, Equations [4] to [9]. In this shape the equations are particularly fit for numerical checking of the corresponding curves in Fig. 2. Certainly, planimetric evaluation of the integrals cannot be avoided. Such difficulties are inherent in the problem.

$$\hat{\vartheta}_A = \frac{I^2}{8\rho\lambda} \qquad [4]$$

For case A, concerning contact between equal members, the contact surface, which corresponds to $r = b$, is the hottest isotherm.

$$(1+x)\frac{\vartheta_A(t,r)}{\hat{\vartheta}_A} = f(x) - \frac{1}{2\sqrt{\pi z}}\int_0^\infty \left\{ f(\alpha)e^{-\frac{1}{z}\left(\frac{\alpha-x}{2}\right)^2} + \left[f(\alpha) - 2e^{-\alpha}\int_0^\alpha f(\xi)e^{\xi}\,d\xi \right] e^{-\frac{1}{z}\left(\frac{\alpha+x}{2}\right)^2} \right\} d\alpha \qquad [5]$$

Hence $$\vartheta_A(\infty, r) = \frac{2x+1}{(x+1)^2}\hat{\vartheta}_A = \frac{b}{r^2}(2r-b)\hat{\vartheta}_A \qquad [6]$$

as is readily checked. For case B, concerning a contact between a poor thermal and electric conductor (e.g., graphite), to which r, $\vartheta(t,r)$, λ, ρ and c refer, and a perfect conductor (represented, for example, by copper) with the hottest isotherm situated in the poor conductor and corresponding to $r = 2b$

$$(1+x)\frac{\vartheta_B(t,r)}{\hat{\vartheta}_A} = 4\varphi(x) - \frac{4}{\sqrt{\pi}}\left[\int_{-\frac{x}{2\sqrt{z}}}^{\infty} \times \varphi(2\beta\sqrt{z}+x)e^{-\beta^2}\,d\beta - \int_{\frac{x}{2\sqrt{z}}}^{\infty} \varphi(2\beta\sqrt{z}-x)\, e^{-\beta^2}\,d\beta \right] \qquad [7]$$

Hence

$$\vartheta_B(\infty, r) = \frac{4x}{(1+x)^2}\hat{\theta}_A = \frac{4b}{r^2}(r-b)\hat{\vartheta}_A \qquad [8]$$

The calculation of $(d\vartheta)/(dt)$ at $t = 0$ has been made (1) starting from the fundamental differential equation. Putting

$$\frac{d\vartheta(t,r)}{dt} = \frac{\lambda}{c}\frac{d\vartheta}{b^2\,dz}$$

we have for $r = b$

$$\left(\frac{d\vartheta_A}{dz}\right)_{z=0} = 2\hat{\vartheta}_A$$

and for $r = 2b$

$$\left(\frac{d\vartheta_B}{dz}\right)_{z=0} = \frac{\hat{\vartheta}_A}{2} \qquad [9]$$

A Circular Spot Is Heated at $t > 0$ Uniformly at Rate q Watt Per Square Centimeter—to Find $\vartheta(t,r)$

We denote this problem case S where the "S" refers to surface heat source. This case may be substantiated by a circular region on the face of a semi-infinite body being (surface) heated by irradiation at $t > 0$.

The problem of a surface heat source has been treated by some few authors in diversified manners. Equation [10] is well known.[10] It gives the temperature rise $d\vartheta(t,r)$ in a semi-infinite body at the distance r from a surface point where the instantaneous amount dq of heat has been generated at $t = 0$ and $r = 0$, under the condition that otherwise no heat passes through the surface of the body

$$d\vartheta(t,r) = \frac{2\,dq}{c\left(4\pi\frac{\lambda}{c}t\right)^{3/2}}\operatorname{Exp}\left(-\frac{cr^2}{4\lambda t}\right) \qquad [10]$$

The actual heat source may be regarded as composed of points of this kind. This is the procedure which has been used previously (2, 4, 5). Oosterkamp (4) has confined his calculations to the temperature in the center of a stationary circular spot. Jaeger (2) carries out formulas for rectangular sources, stationary and moving.

Holm (3) does not start from Equation [10] but uses again the artifice with the sphere *Sp*, previously mentioned. His resulting formula, Equation [12], is particularly fitted to the simplifying method we here aim at. We use it in the following. The deviation of Holm's result from the others is illustrated by the deviation of the *Sb*-curve from the *J-O*-curve in Fig. 2 which is negligible for the present purpose.

The final average supertemperature in the stationary heat source is[11]

$$\hat{\vartheta}_S = \frac{\pi a q}{4\lambda} = \frac{\pi^2 bq}{8\lambda} \qquad [11]$$

The average supertemperature at the distance r from the center of the heat source[12] is given approximately by Equation [12] when $r = a$ or $r > 2a$, whereas the Equation furnishes a poor approximation when $a < r < 2a$.

$$\frac{\vartheta_S(t,r)}{\hat{\vartheta}_S} = \frac{1-Y}{1+x} \qquad [12]$$

[8] A. Avramescu, thesis, Dresden, Germany, 1937, has given later a solution by means of expansion in Heaviside series, without trying its suitability for numerical calculation.

[9] See reference (1) § 11.

[10] Cf. reference (5), p. 216.

[11] Cf. reference (3), p. 364.

[12] Reference (3) equations 4 to 7. For z-values which make the argument of the erf function larger than 2 the approximation

$$1 - \operatorname{erf}(u) \doteq \frac{e^{-u^2}}{u\sqrt{\pi}}\left(1 - \frac{1}{2u^2}\right)$$ is recommended.

where

$$Y = \operatorname{erf}\left(\frac{x}{2\sqrt{z}}\right) + e^{x+z}\left[1 - \operatorname{erf}\left(\frac{x}{2\sqrt{z}} + \sqrt{z}\right)\right]$$

with, for $r = b$

$$\left[\frac{d\,\vartheta_S}{dt}\right]_{t=0} = \infty \quad \ldots\ldots [13]$$

and

$$\vartheta_S(\infty, r) = \frac{\hat{\theta}_S}{1+x} = \frac{b}{r}\,\hat{\theta}_S \quad \ldots\ldots [14]$$

Numerical Results of Formulas

Numerical results of the equations of the preceding two sections are illustrated in Fig. 2. The indications at the curves will be understood from the following examples:

A4b refers to case A and to distance $r = 4b$.

B2b refers to case B and $r = 2b$, which here defines the hottest isotherm.

S2b concerns heating in a "surface spot" and the temperature at $r = 2b$.

The dashed *J-O*-curve is based upon the formulas by Jaeger and Oosterkamp and represents

$$\frac{\vartheta_m(t)}{\theta_m}$$

with $\theta_m = 1.122\,aq/\lambda$ or $\theta_m = aq/\lambda$, respectively.[13] The factor 1.112 appears because Jaeger assumes a square heat source.

In all cases z is defined according to Equation [3]. The deviations from the *S*-curve are practically negligible.

The Simplified Calculation

We now are prepared for the particular simplification aimed at. Regarding the curve A2b in Fig. 2, one sees that extension of its vertical dimensions by the factor 1/0.75 and moving it to the left a horizontal distance corresponding to the factor 2 brings that curve to an approximate coincidence with Ab. This means a kind of similitude between the curves A2b and Ab. The same kind of similitude exists between all curves belonging to cases A and B, and also between the curves belonging to case S. This fact suggests the attempt to reduce the curves to some few fundamental patterns. Fig. 3 is the result of such an attempt. It shows an *A-B* curve and an *S*-curve, both with dashed branches at small z-values. The reduction of the curves Ab and B2b into one single *A-B* curve is a performance within the error limits. Fig. 3 may be used according to the following directions which, as emphasized in the foregoing, are partly empirical. Their suitability is proved in Table 1 by numerical comparison with data from Fig. 2.

First consider for which case, A, B, or S, and for what distance, r, from the contact (or heat source) center, information is wanted. Express r in the unit b, which is defined by Equation [1]. Observe two singularities which result from the use of the fictitious hemisphere *Sp* in the calculations:

1 The contact surface is not represented by $r = 0$ but by $r = b$.

2 The method is applicable for points "outside" the contact area only when $r \geq 2b$ or $r \geq 4b$, respectively, according to Equations [15].

Calculate $\vartheta_A(\infty, r)$, $\vartheta_B(\infty, r)$, or $\vartheta_S(\infty, r)$ according to Equation [6], [8], or [14], respectively, and the corresponding factor $p(r)$ according to Equations [15]

$$\left.\begin{aligned} p_A(r) &= \frac{1}{2}\left(\frac{r}{b}\right)^2 \text{ for } r \geq 2b \\ p_B(r) &= \left(\frac{r}{2b}\right)^2 \text{ for } r \geq 4b \\ p_S(r) &= 2\left(\frac{r}{b}\right)^2 \text{ for } r \geq 2b \\ p_A(b) &= p_B(2b) = p_S(b) = 1 \end{aligned}\right\} \quad \ldots\ldots [15]$$

Then read off the ordinate $B(z)$ from the concerned curve in Fig. 3 with

$$z = \frac{\pi^2}{4p(r)}\,\frac{\lambda}{c\,a^2}\,t \quad \ldots\ldots [16]$$

When $r > b$ the dashed branches shall be used. Finally, we obtain

$$\vartheta_X(t, r) = B(z)\vartheta_X(\infty, r) \quad \ldots\ldots [17]$$

where $X = A$, B, or S, respectively.

Results which have been achieved in this manner are compared with direct readings from Fig. 2, in Table 1. The differences are practically negligible.

Circular Heat Source Moving on Surface of a Semi-infinite Body

This case is embodied in the contact of a slider moving along the face of a semi-infinite body, when friction heat is produced at a uniform rate all over the contact area. This area is then what we call the heat source.

Jaeger (2) gives a thorough treatment for a square source, starting from Equation [10], but does not deduce formulas for a circular source. Holm (3) uses an approximate method for a circular heat source. We gain a considerable simplification by following Holm and confining ourselves to the "maximum temperature" in the spot. Because of the motion the source covers successively new points of its trail and any point is contacted only a limited time t_v. The average contact time with a circular source is

$$\bar{t}_v = \frac{\pi}{2}\,\frac{a}{v} \quad \ldots\ldots [18]$$

It is plausible that $\bar{t}_v$ plays a similar part for the highest temperature in the contact surface as does (via z) the heating time t for a stationary contact according to Equation [12]. Numerical comparison in Table 2 confirms this.

Substitution of $\bar{t}_v$ in Equation [3] yields

$$z_v = \frac{\pi^2}{8}\,\frac{\lambda}{c\,a\,v} \quad \ldots\ldots [19]$$

Let the corresponding ordinate of the *S*-curve in Fig. 3 be $B(z_v)$. Then the maximum supertemperature under the source varies according to

$$\vartheta_m(v) \approx B(z_v)\,\theta_m = B(z_v)\,\frac{aq}{\lambda} \quad \ldots\ldots [20]$$

where

$$\theta_m = \frac{\pi\,a^2 q}{\pi a \lambda} = \frac{aq}{\lambda}$$

is the steady supertemperature[14] in the center of a surface heated circular spot.

[13] Cf. reference (2), p. 213.

[14] Cf. reference (2) equation [31].

Equation [20] also satisfies Jaeger's results for a square source if aq/λ is replaced by $1.122\ aq/\lambda$, which is the maximum steady supertemperature under a stationary square source. Fig. 5 illustrates the temperature distribution along the axis in the v-direction of a moving square heat source.[15]

Note that in the case when q is produced by irradiation its determination is obvious; but in the case when heat is produced by friction it is a particular problem to determine what portion of it is conducted into the contact member under consideration.

Oval Surface Heat Source Moving in Direction of Its Major Axis

A stationary isothermal oval heat source with an ovalness[16] which is measured by γ has a thermal constriction resistance

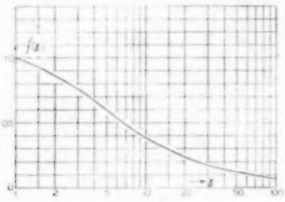

Fig. 4 Function $f(\gamma)$

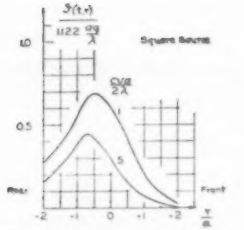

Fig. 5 Distribution of Temperature Along Symmetry Axis of Moving-Square Heat Source, in Direction of Movement

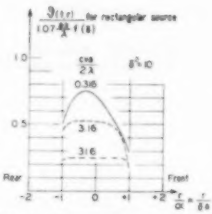

Fig. 6 Distribution of Temperature Along Major Axis of Rectangular Heat Source, Moving in Direction of This Axis

W_γ that is smaller than the constriction resistance W_c of the representing circular contact spot with the radius a. We have

$$W_\gamma = W_c f(\gamma) \quad \ldots\ldots [21]$$

with $f(\gamma)$ according to Fig. 4. The maximum supertemperature appears in the center of a stationary circular heat source and is[17] $\theta_m = aq/\lambda$. Assuming that the factor $f(\gamma)$ still applies when we turn to a surface heated oval spot which is not isothermal we obtain the maximum temperature in it

$$\theta_{m\gamma} = \frac{aq}{\lambda} f(\gamma) \quad \ldots\ldots [22]$$

If the heat source is rectangular, with the ratio γ^2 between the sides, and with $5 < \gamma^2 < 100$, the maximum temperature[18] is

$$\theta_{m\gamma\text{rect}} = 1.07 \frac{aq}{\lambda} f(\gamma) \quad \ldots\ldots [23]$$

In the moving heat source the maximum temperature no longer appears in the center but is displaced behind it. Fig. 6[19] shows the temperature distribution along the major axis of a rectangular heat source. The maximum ordinate

$$\frac{\vartheta_m(v)}{\theta_{m\gamma\text{rect}}}$$

may be expressed as $B(z_v)$, where B is the function that is represented by the full drawn curve S in Fig. 3, if z_v is suitably chosen. One would guess that z_v would be obtained according to Equation [3] by inserting $t = (\pi a\gamma)/(2v)$, the average contact time. But this is not true. In order to determine fairly correct B-values, z_v shall be determined by Equation [19] with $a = \sqrt{\alpha\beta}$. Consequently, we write for an oval heat source

$$\vartheta_{m\gamma}(v) = (aq/\lambda)B(z)f(\gamma) \quad \ldots\ldots [24]$$

making the plausible assumption that $B(z)$ is the same for the oval and rectangular heat sources. Table 2 confirms that the proposed use of Fig. 3 gives fairly good agreement with Jaeger's (2) Equation [16].

Example

Assumptions: An oval contact spot with $a = 5 \times 10^{-3}$ cm and $\gamma^2 = 10$, thus $f(\gamma) = 0.75$ is moving in the α-direction with $v = 200$ cm per sec. The size of this spot would correspond to a load of about $P = 100g$ if the Brinell hardness of the softer contact member is of the order of 20.[20] With q being frictional heat

$$q = \mu\xi \frac{Pv}{\pi a^2}$$

where μ is the coefficient of friction and ξ is the fraction of the heat which is conducted into the stationary semi-infinite contact member. Reasonable values are $\mu = 1$ and $\xi = 0.8$ giving

$$q = 2 \times 10^3 \text{ g/cm sec} = 2 \times 10^4 \text{ watt/cm}^2$$

With $\lambda = 0.45$ watt/cm deg and $c = 3.6$ joule/cm deg, corresponding to material of iron in the semi-infinite stationary contact member, we obtain

$$z_v = 0.49 \text{ and } B(z_v) = 0.47$$

Equation [22] gives

$$\theta_{m\gamma} = 167 \text{ deg}$$

Hence, according to Equation [24]

$$\vartheta_{m\gamma}(v) = 78.5 \text{ deg}$$

Cooling of a Previously Heated Contact Region

The problem of cooling a previously heated contact is of the same importance as the heating process. Holm[21] has proved that those processes follow the same pattern, and that the cooling can be mathematically expressed by

$$\vartheta_c(t_c, r) = \vartheta(\infty, r) - \vartheta(t_c, r) \quad \ldots\ldots [25]$$

Consequently the rules given in the foregoing can be applied also to the cooling problem.

Remark Concerning Acceleration of Chemical Reactions by a Sliding Process

The so-called frictional oxidation and other phenomena have been interpreted as resulting from very high temperatures in sliding contacts. However, according to calculations the tem-

[15] Calculated according to equation [16], reference (2).
[16] Cf. symbols at 2α and reference (1) 4E.
[17] See reference (2) equation [31].
[18] Calculated on the basis of equation [18], reference (2).
[19] Calculated on the basis of equation [16], reference (2).
[20] Cf. reference (1), p. 75.
[21] Reference (1) appendix iv, and reference (3).

peratures of sliding smooth surfaces usually are found to be rather moderate.[22] Any discrepancy is removed by the hypothesis that in sliding contacts the rough treatment of the upper atom layer and particularly of small abraded grains in the contact interspace provides activation energies beyond that which thermodynamic temperature with Maxwellian distribution would produce. In addition, the individual grains may have higher temperature than is calculated for a smooth contact surface.

BIBLIOGRAPHY

1 "Electric Contacts," by R. Holm, H. Geber, Stockholm, Sweden, 1946.

2 "Moving Sources of Heat and the Temperature at Sliding Contacts," by J. C. Jaeger, *Journal of the Royal Society, NSW*, vol. 56, 1942, pp. 203–224.

3 "Calculation of the Temperature in a Contact Heated in the Contact Surface, and Application to the Problem of the Temperature Rise in a Sliding Contact," by R. Holm, *Journal of Applied Physics*, vol. 19, 1948, pp. 361–366.

4 "The Heat Dissipation in the Anode of an X-ray Tube," by W. J. Oosterkamp, Philips Research Reports, vol. 3, 1948, pp. 49–59.

5 "Conduction of Heat in Solids," by H. S. Carslaw and J. C. Jaeger, The Clarendon Press, Oxford, England, 1947.

Appendix

Application of the *Sp*-Model

The *Sp*-model is applicable to the problem of the temperature development in a heated circular contact at the face of a semi-infinite body, if the model defines a heat development that approximates the actual one. The mathematical proof that this is the case is sketched by Holm.[23] We shall not repeat here the mathematical formulas but describe the significance of the deduction. We imagine a set of isothermal surfaces in the actual constriction[24] region, as illustrated in Fig. 7. The surfaces will

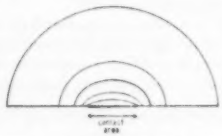

Fig. 7 Isotherms Around a Heated Contact Surface

be equipotentials in the case of an electric current traversing the contact. The choice is made so as to define the same electric (or thermal) resistance between any consecutive pair of isotherms. The corresponding isotherms in the *Sp*-case are hemispheres. Homologous surfaces in the actual and the *Sp*-case include the same resistance. The temperature development will be the same in both cases if the heat capacity C_m of the shell between the isotherms T_m and T_n is approximately equal in the model and the actual constriction. It is proved that this is true if the model has the dimensions prescribed by Equation [1].

We have applied the *Sp*-model to the problem of a moving source, where the model simply provides a picture of isotherms which is suitable for the calculation. Obviously, the curvature of the model contact has nothing to do with the fact that such a surface would not slide.

[22] Cf. Example section, and reference (3).

[23] Cf. reference (1), § 11c.

[24] The concept "constriction," which is fundamental to the theory of contacts, is defined in reference (1), § 3.

Minimum Weight of Tapered Round Thin-Walled Columns

By MORRIS FEIGEN,[1] LOS ANGELES, CALIF.

It is shown that the optimum wall thickness of a cylindrical round tube column is a function of load only and is independent of diameter. The optimum wall thickness of a tapered round thin-walled column is found to be constant along its length. The optimum shape of a tapered round thin-walled column is derived, being that column whose bending stress in the buckled state is constant along its length. The weight ratio of the optimum tapered column to an equal-strength optimum cylindrical column is found to be 0.8924. It is shown that a double truncated cone whose diameter ratio is in the range $0.55 \leqslant D_1/D_2 \leqslant 0.50$ closely approaches the optimum column. If it is specified that no portion of the double truncated cone shall yield, then the weight advantage of the cone over the cylindrical column is rapidly lost as the stress in the cylindrical column approaches the yield stress. In the inelastic range the weight advantage of the tapered column will be less than in the elastic range.

Nomenclature

The following nomenclature is used in the paper:

- A = cross-section area
- C = constant
- d = a length parameter
- D = diameter
- E = modulus of elasticity
- σ = stress
- I = moment of inertia
- k = constant
- K = a nondimensional length parameter
- L = length of a pin-ended column
- M = bending moment
- P = axial compressive load
- t = wall thickness
- x = co-ordinate along column
- y = deflection of column at any point x
- W = weight of column
- m = strength ratio

Introduction

The principles of structural design for minimum weight have been clearly stated by Shanley.[2] As is pointed out by Mr. Shanley, it is in many cases impossible to design a structure of the absolute minimum weight; however, if a theoretical minimum were known, the designer would then be able to estimate how closely his structural design has approached the theoretical minimum. The case of optimization of the cylindrical round thin-walled column has been established[2] but is repeated here, from a slightly different approach, for continuity reasons. Further optimization of the column can be obtained by considering taper, i.e., by removing material from the ends of the column and placing it in the middle where it is more effective.

The basic concept used is that the stress in an optimum structure will be at a maximum in all parts of the structure so that incipient failure can occur simultaneously in all parts of the structure, in effect, a structural "One Hoss Shay." In primary column buckling the governing stress to be held constant for optimization is the bending stress in the buckled state rather than the axial compressive stress. For the thin-walled column of a given length to support a given load the diameter and thickness are so chosen so as to result in a structure that will buckle at the critical load both locally and due to primary column failure at any point along the column.

Cylindrical Columns

For a cylindrical round tube under axial compression the equation for local buckling is given as[3]

$$\sigma_{cr} = \frac{kE}{D/t} \qquad [1]$$

The critical buckling stress σ_{cr} may be expressed in terms of load and area

$$\sigma_{cr} = \frac{P}{A} = \frac{P}{\pi\, Dt} \qquad [2]$$

Equating Equations [1] and [2]

$$t_{opt} = \left(\frac{P}{\pi kE}\right)^{\frac{1}{2}} \qquad [3]$$

This shows that the minimum or optimum thickness is independent of the diameter and depends only upon the required load.

To determine the optimum weight for a given load and a given length, the optimum thickness is chosen and the diameter is allowed to decrease until the tube fails in primary buckling. For a pin-ended column the formula for primary buckling is the well-known Euler formula

$$P = \frac{\pi^2 EI}{L^2} \qquad [4]$$

For a thin-walled tube the moment of inertia is

$$I = \frac{\pi D^3 t}{8} \qquad [5]$$

Substituting Equation [5] into Equation [4] and utilizing Equation [3], the resulting equation solves for D

[1] Associate Engineer, University of California.

[2] "Principles of Structural Design for Minimum Weight," by F. R. Shanley, *Journal of the Aeronautical Sciences*, vol. 16, 1949, pp. 133–149.

Presented at the West Coast Conference of the Applied Mechanics Division, Los Angeles, Calif., June 26–28, 1952, of The American Society of Mechanical Engineers.

Discussion of this paper should be addressed to the Secretary, ASME, 29 West 39th Street, New York, N. Y., and will be accepted until October 10, 1952, for publication at a later date. Discussion received after the closing date will be returned.

Note: Statements and opinions advanced in papers are to be understood as individual expressions of their authors and not those of the Society. Manuscript received by ASME Applied Mechanics Division, March 17, 1952.

[3] "Theory of Elastic Stability," by S. Timoshenko, McGraw-Hill Book Company, Inc., New York, N. Y., 1936.

$$D_{opt} = \left(\frac{8P^{1/3}L^{2}k^{1/3}}{\pi^{2/3}E^{1/3}}\right)^{\frac{1}{3}} \quad [6]$$

Given, then, a thin-walled round tube column of length L, and so designed to carry a load P, the optimum thickness and diameter can be found from Equations [3] and [6].

$$\left(\frac{D}{t}\right)_{opt} = \left(\frac{8k^{2}E}{\pi\left(\frac{P}{L^{2}}\right)}\right)^{\frac{1}{3}} \quad [7]$$

This is the same as Equation [10] in the Shanley paper[5] where P/L^2 is his "structural index."

Tapered Columns

Given a tapered round tube column symmetrical about its mid-length whose diameter varies arbitrarily along its length and whose taper is small (as it will be for any practical column), then the effect of taper upon Equation [1] will be small and Equation [1] is assumed to be valid for the tapered column. Hence, for a tapered column designed to carry a fixed load, the optimum thickness is independent of diameter and the wall thickness along its length is constant. Again, to determine the optimum weight for a given load, length, and shape (distribution of diameter) the optimum thickness is chosen and all diameters are allowed to decrease proportionately until the column fails in primary buckling. The question arises as to whether or not the shape chosen will give an absolute minimum weight. The optimum shape for absolute minimum weight is developed in the next section.

Optimum Shape for Minimum Weight

Given a tapered pin-ended column of length L as shown in Fig. 1, it is assumed the optimum shape will be that shape such that the bending stress will be constant along its length when the column has buckled. Since buckling depends only upon EI and is independent of compressive stress, the optimum distribution of material will be that to give a constant bending stress when the column has buckled. H. Blasius[6] has derived the optimum shape of solid columns using variational principles; however, the assumption stated previously will yield the same differential equation of buckling as obtained by Blasius.[6]

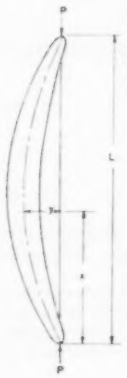

Fig. 1

In order to simplify the approach for determining the optimum shape and computing the resulting weight it is assumed that the column has a constant wall thickness measured normal to the column center line rather than normal to the column surface.

The bending stress σ_b, after buckling has occurred at any point x is given by

$$\sigma_b = \frac{MD/2}{I} = \frac{PyD}{2I} \quad [8]$$

Substituting I from Equation [5][6] and solving for y

$$y = \frac{\pi\sigma_b D^2 t}{4P} \quad [9]$$

Since the bending stress, σ_b, and thickness t, are constant, then for any critical buckling load the diameter must vary as the square root of the buckled deflection curve. In a buckled column the magnitude of the deflection is arbitrary; therefore the deflection can be written as

$$y(x) = C_1\left[\frac{D(x)}{D_2}\right]^2 \quad [10]$$

where D_2 is the diameter at mid-length and $D(x)$ is the diameter at any point x.

The differential equation for buckling is given by

$$EI\frac{d^2y}{dx^2} + P_2 y = 0 \quad [11]$$

Substituting the expression for I and y as given in Equations [5] and [10] and dropping the functional notation

$$\frac{d^2\left[C_1\left(\frac{D}{D_2}\right)^2\right]}{dx^2} + \frac{P_2 C_1\left(\frac{D}{D_2}\right)^2}{E\frac{\pi D^3 t}{8}} = 0 \quad [12]$$

where P_2 is the critical load for the optimum tapered column.

Simplifying

$$\frac{d^2\left(\frac{D}{D_2}\right)^2}{dx^2} + \frac{P_2}{EI_2\left(\frac{D}{D_2}\right)} = 0 \quad [13]$$

where

$$I_2 = \frac{\pi D_2^3 t}{8}$$

Let $\eta = D/D_2$ and $q_2^2 = P_2/(EI_2)$ and substituting in Equation [13]

$$\frac{d^2\eta^2}{dx^2} + \frac{q_2^2}{\eta} = 0 \quad [14]$$

The boundary conditions are

$$x = 0,\ x = L;\ \eta = 0$$

or

$$x = \frac{L}{2};\ \eta = 1,\ \frac{d\eta}{dx} = 0$$

To solve Equation [14] the following substitutions are made

$$\zeta = \eta^2;\ d\zeta = 2\eta d\eta;\ \frac{d\zeta}{dx} = \frac{1}{u}$$

$$\frac{d^2\zeta}{dx^2} = \frac{d\left(\frac{1}{u}\right)}{dx} = \frac{d\left(\frac{1}{u}\right)}{d\zeta}\frac{d\zeta}{dx} = \frac{1}{u}\frac{d\left(\frac{1}{u}\right)}{d\zeta} = \frac{1}{2}\frac{d\left(\frac{1}{u}\right)^2}{d\zeta}$$

After substituting into Equation [14]

$$\frac{d^2\zeta}{dx^2} + \frac{q_2^2}{\eta} = 0$$

[6] "Trager Kleinster Durchbiegung und Stabe Groster Knickfestikeit Bei Gegebenem Materialverbrauch," by H. Blasius, *Zeitschrift für Mathematik und Physik*, vol. 62, Heft 2, September, 1913, pp. 182–197.

[5] Since writing this paper the author has been able to prove, through an extension of Blasius' work, that the assumption of constant stress is valid for the optimum column of arbitrary cross section when the cross-section area varies as a^τ, where a = any cross-section reference dimension and τ is a constant.

[6] This formula for I breaks down as $D \to 0$; however, the assumption is carried through for theoretical purposes only.

or

$$\frac{d\left(\frac{1}{u}\right)^2}{d\zeta} = -\frac{2q_2^2}{\eta} \quad [15]$$

Integrating

$$\left(\frac{1}{u}\right)^2 = -2q_2^2 \int \frac{d\zeta}{\eta} = -4q_2^2 \int d\eta$$

or

$$\left(\frac{1}{u}\right)^2 = 4q_2^2(C_2 - \eta) \quad [16]$$

Taking the square root and substituting for $(1/u)$

$$\frac{d\zeta}{dx} = 2q_2(C_2 - \eta)^{\frac{1}{2}} \quad [17]$$

when

$$x = \frac{L}{2},\ \eta = 1,\ \frac{d\eta}{dx} = 0,\ \text{and}\ \frac{d\zeta}{dx} = 0$$

Therefore $C_2 = 1$.

Making the substitution for C_2 and solving Equation [17]

$$2q_2x = \int \frac{d\zeta}{(1-\eta)^{1/2}} = 2\int_0^\eta \frac{\eta d\eta}{(1-\eta)^{1/2}} \quad [18]$$

Solving Equation [18]

$$q_2x = \frac{4}{3} \pm \frac{2}{3}(2+\eta)(1-\eta)^{\frac{1}{2}} \quad [19]$$

In applying the boundary conditions:

(*a*) For $x = 0$ use the (—) value in Equation [19].
(*b*) For $x = L$ use the (+) value in Equation [19].
Applying the condition (*a*) and the boundary conditions

$$x = 0,\ \eta = 0$$

Applying the condition (*b*)

$$x = L,\ \eta = 0;\ \text{then}\ q_2L = \frac{8}{3}$$

or

$$P_2 = \left(\frac{8}{3}\right)^2 \frac{EI_2}{L^2} \quad [20]$$

where P_2 is the critical buckling load for the optimum-shaped column whose shape given by

$$2 \pm \left(2 + \frac{D}{D_2}\right)\left(1 - \frac{D}{D_2}\right)^{\frac{1}{2}} = \frac{4x}{L}$$

and whose moment of inertia is I_2 at the center.

In general, the critical buckling load of a tapered column can be given by

$$P_2 = \frac{m\pi^2 EI_2}{L^2} \quad [21]$$

where m is the strength ratio between a tapered column and a cylindrical column in which the moment of inertia or diameter at the center is the same. For the optimum column

$$m = \left(\frac{8}{3\pi}\right)^2$$

To find the weight of the optimum-shaped tapered column it is necessary to compare the optimum column to an optimum cylindrical column of equal strength

$$P_2 = \left(\frac{8}{3}\right)^2 \frac{EI_2}{L^2}$$

for the optimum column

$$P_c = \frac{\pi^2 EI_c}{L^2}$$

for a cylindrical column where the subscript c denotes cylinder. But $P_c = P_2$ and $I_c = (\pi D_c^3 t)/8$; therefore $I_2/I_c = (3\pi/8)^2$, since the wall thickness must be the same for each column, or

$$\frac{D_2}{D_c} = \left(\frac{3\pi}{8}\right)^{\frac{2}{3}} \quad [22]$$

The weight of the optimum column (assuming a density of unity) is given by

$$W_2 = 2\int \pi D t_s\, ds \quad [23]$$

where ds is an element of length along the surface of the column and t_s is the wall thickness normal to the surface. However

$$t_s = t\frac{dx}{ds}$$

therefore

$$W_2 = 2\int_0^{L/2} \pi D t dx = 2\pi D_2 t \int_0^{L/2} \frac{D}{D_2}\frac{dx}{d\eta}d\eta \quad [23a]$$

But from Equation [18]

$$\frac{dx}{d\eta} = \frac{3}{8}\frac{L\eta}{(1-\eta)^{1/2}}$$

therefore

$$W_2 = \frac{3}{4}\pi L D_2 t \int_0^1 \frac{\eta^2 d\eta}{(1-\eta)^{1/2}} \quad [24]$$

Solving Equation [24]

$$W_2 = \frac{4}{5}\pi L D_2 t \quad [25]$$

The weight of a cylindrical column is given by

$$W_c = \pi D_c t L \quad [26]$$

The weight ratio W_2/W_c is

$$\frac{W_2}{W_c} = \frac{4}{5}\frac{D_2}{D_c},\ \text{but}\ \frac{D_2}{D_c} = \left(\frac{3\pi}{8}\right)^{\frac{2}{3}}$$

therefore

$$\frac{W_2}{W_c} = \frac{4}{5}\left(\frac{3\pi}{8}\right)^{\frac{2}{3}} = 0.8924 \quad [27]$$

This equation shows that the absolute minimum weight for a thin-walled tapered column is 0.8924 of the weight of an equal-strength optimum cylindrical tube.

Since it is impractical to build a column whose end diameter goes to zero, columns of shapes other than the optimum must be considered.

Various Shaped Tapered Columns

Boyd[7] has investigated, both theoretically and experimentally,

[7] "Tapered Struts, a Theoretical and Experimental Investigation," by J. E. Boyd, Ohio State University, Bulletin No. 25, The Engineering Experiment Station, September 15, 1923.

the critical buckling load P_2 for solid tapered columns of the type to be considered here.

Given a symmetrical tapered column of the type shown in Fig. 2, for which the moment of inertia varies as $I = C_x x^n$, four cases are considered, namely, $n = 1$, $n = 2$, $n = 3$, and $n = 4$.

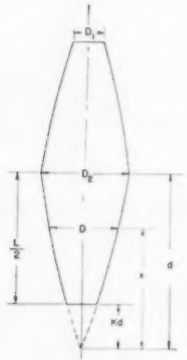

FIG. 2

The differential equation for buckling is

$$EC_x x^n \frac{d^2y}{dx^2} + Py = 0 \quad \ldots\ldots [28]$$

The analytical solutions as given by Boyd[7] are rather complicated; however, the final results can be given in a useful form. If the equation for the critical buckling load is given by

$$P_2 = \frac{m\,\pi^2\,EI_2}{L^2} \quad \ldots\ldots [21]$$

then the results by Boyd can be summarized in Table 1.

TABLE 1 BOYD'S RESULTS[7] FOR SOLID TAPERED COLUMNS

	$n = 1$	$n = 2$	$n = 3$	$n = 4$
K	m	m	m	m
0	0.5860	0.175	0	0
0.01	0.5952	0.2176	0.0142	0.0004
0.05	0.6257	0.2841	0.0687	0.0080
0.10	0.6570	0.3492	0.1300	0.0326
0.20	0.7101	0.4497	0.2419	0.1070
0.30	0.7560	0.5341	0.3459	0.2108
0.40	0.7974	0.6107	0.4452	0.3067
0.50	0.8337	0.6281	0.5416	0.4170
0.60	0.8717	0.7480	0.6359	0.5306
0.70	0.9058	0.8152	0.7284	0.6463
0.80	0.9382	0.8784	0.8194	0.7632
0.90	0.9684	0.9399	0.9085	0.8814
1.00	1.0000	1.0000	1.0000	1.0000

It should be noted here that the results as given in Table 1, although computed for solid columns, are completely general and could be applied to any column with arbitrary cross section as long as the variation in I followed the form $I = cx^n$. Hence these results will be applied to the thin-walled column.

In order to utilize these results and to compute weight ratios, some additional analysis is necessary.

The variation of moment of inertia I at any point x is

$$I = C_x x^n = \frac{\pi D^3 t}{8} \quad \ldots\ldots [29]$$

where D is the diameter at any point x. However

$$I_2 = \frac{\pi D_2^3 t}{8} = C\ d^n$$

therefore

$$C_x = \frac{\pi D_2^3 t}{8 d^n}$$

and

$$I = \frac{\pi\ D_2^3 t}{8}\left(\frac{x}{d}\right)^n = I_2\left(\frac{x}{d}\right)^n \quad \ldots\ldots [30]$$

Therefore

$$I_1 = I_2\left(\frac{Kd}{d}\right)^n = I_2 K^n \quad \ldots\ldots [31]$$

If $\pi D^3 t/8$ is substituted for I, and dividing

$$\frac{D_1}{D_2} = K^{\frac{n}{3}} \quad \ldots\ldots [32]$$

Similarly

$$\frac{D}{D_2} = \left(\frac{x}{d}\right)^{\frac{n}{3}} \quad \ldots\ldots [33]$$

and

$$\frac{D}{D_1} = \left(\frac{x}{Kd}\right)^{\frac{n}{3}} \quad \ldots\ldots [33a]$$

By considering Equation [21] and the expression for I

$$\frac{D_e}{D_2} = m^{\frac{1}{3}} \quad \ldots\ldots [34]$$

and

$$\frac{D_e}{D_1} = \left(\frac{m}{K^n}\right)^{\frac{1}{3}} \quad \ldots\ldots [35]$$

where D_e is the diameter of an equal-strength cylindrical column. To compute the weights for the various columns, Equation [23a] can be utilized

$$W_2 = 2\int_0^{L/2} \pi D t\, dx = 2\int_{Kd}^{d} \pi D t\, dx \quad \ldots\ldots [23a]$$

Let $\xi = x/d$ and utilizing Equation [33]

$$W_2 = 2\pi D_2\, dt \int_K^1 \xi^{n/3}\, d\xi \quad \ldots\ldots [36]$$

The solution is

$$W_2 = \frac{2\pi D_2\, dt}{\frac{n}{3}+1}\left(1 - K^{\frac{n}{3}+1}\right) \quad \ldots\ldots [37]$$

However

$$d = \frac{L}{2}\,\frac{1}{1-K}$$

therefore

$$W_2 = \frac{\pi\ D_2\, tL}{\frac{n}{3}+1}\left(\frac{1 - K^{\frac{n}{3}+1}}{1-K}\right) \quad \ldots\ldots [38]$$

Dividing by W_e, the weight of an equal-strength cylindrical column, substituting for K, and utilizing Equation [34]

$$\frac{W_2}{W_e} = \frac{3}{(n+3)\,m^{1/3}}\left[\frac{1 - \left(\frac{D_1}{D_2}\right)^{\frac{n+3}{3}}}{1 - \left(\frac{D_1}{D_2}\right)^{\frac{3}{n}}}\right] \quad \ldots\ldots [39]$$

$$\frac{W_2}{W_c} = \frac{3}{(n+3)\,m^{1/3}} \left[\frac{1 - K^{\frac{n+3}{3}}}{1 - K^{3/n}} \right] \quad \ldots\ldots [39a]$$

The weight ratios W_2/W_c and diameter ratios D_2/D_c and D_1/D_c for equal-strength columns have been plotted in Figs. 3, 4, and 5. Examining Fig. 3, W_2/W_c versus D_1/D_2, it is noted that the minimum value of W_2/W_c for all columns are close to the optimum. For construction purposes one should choose the type most easily made. The most easily constructed column is the double truncated cone ($n = 3$).

It is also noted in Fig. 3 that the columns for $n = 1$ and $n = 2$ are the only columns which have a finite buckling strength when $D_1 = 0$. The reason for this is that for the other columns the deflection, or bending moment, at the end is increasing faster than the section modulus resulting in an infinite bending stress at the end. The criterion for finite buckling strength when $D_1 = 0$ is, therefore, that the bending stress at $D_1 = 0$ be finite.

From the bending formula

$$\sigma_b = \frac{4Py}{\pi D^3 t} \quad \ldots\ldots [10]$$

If it is specified that $(\sigma_b)_0 \neq \infty$ then $(y/D^3)_0 \neq \infty$, but $(y/D^3)_0$ is indeterminate and to evaluate, both numerator and denominator are differentiated, therefore

$$\frac{\left(\frac{dy}{dx}\right)_0}{\left(2D\frac{dD}{dx}\right)_0} \neq \infty \quad \ldots\ldots [40]$$

For a pin-ended column

$$\left(\frac{dy}{dx}\right)_0 = 0 \text{ and } (D)_0 = 0$$

therefore

$$\left(\frac{dD}{dx}\right)_0 = \infty \quad \ldots\ldots [41]$$

The criterion for finite buckling strength of a column when the end diameter is zero is that the end of the column does not come to a point, or has a horizontal tangent, i.e.

$$\left(\frac{dD}{dx}\right)_0 = \infty$$

It is easily verified from Equation [18] that this condition is satisfied for the optimum column and it is also satisfied for the columns when $n = 1$ and $n = 2$.

Comparison of a Cone With an Equal-Strength Cylinder

As an example, the double truncated cone ($n = ?$) is compared to a cylinder. The material is 75S-T which has a yield stress of 55,000 psi. The data for an optimum cylindrical round tube are taken from Shanley,[2] where stress and weight are plotted versus the structural index (P/L^2).

If it is specified that all compressive stresses remain below the yield point, then the stress at the end of the cone (where stress is a maximum) must be equal to or less than the yield stress σ_y.

The minimum diameter at the end is governed by

$$\sigma_y = \frac{P_2}{\pi D_1 t_{opt}}$$

therefore

$$D_{1(\min)} = \frac{P_2}{\pi \sigma_y t_{opt}} = \frac{P_2}{\pi \sigma_y \left(\frac{P_2}{\pi k E}\right)^{1/2}} = \left(\frac{P_2 k E}{\pi \sigma_y^2}\right)^{\frac{1}{2}} \quad [42]$$

From Equation [8] for a round tube

$$D_{c(\text{opt})} = \left(\frac{8 P_c^{1/3} L^2 k^{1/3}}{\pi^{1/3} E^{1/3}}\right)^{\frac{1}{3}} \quad \ldots\ldots [6]$$

Dividing Equation [42] by Equation [8] and simplifying

$$\left(\frac{D_{1(\min)}}{D_{c(\text{opt})}}\right)^3 = \frac{kE^2 \left(\frac{P_2}{L^2}\right) \pi}{8\sigma_y^3} \quad \ldots\ldots [43]$$

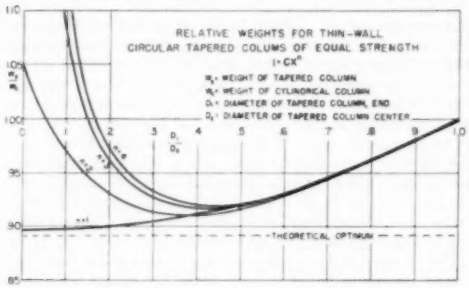

Fig. 3

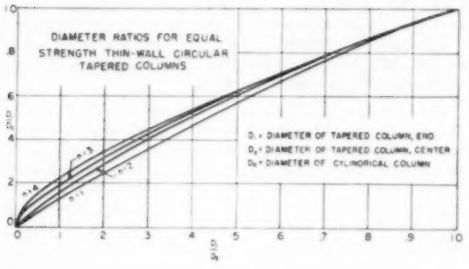

Fig. 4

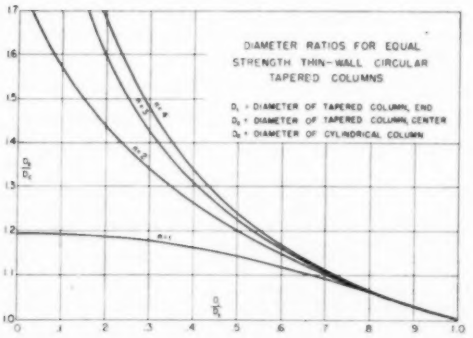

Fig. 5

From Equation [11a] of Shanley's paper[2]

$$\frac{P_2}{L^2} = \frac{8\sigma}{\pi k E^2} \quad [44]$$

Substituting Equation [44] into Equation [43]

$$\frac{D_{1(\min)}}{D_{c(\text{opt})}} = \left(\frac{\sigma}{\sigma_y}\right)^3 \quad [45]$$

where σ is the optimum compressive stress for a cylindrical round tube as a function of P/L^2 for 75S-T as plotted by Shanley.[2]

The optimum D_1/D_2 as determined from Fig. 3 is equal to 0.4 which, utilizing Fig. 4, results in $D_1/D_c = 0.525$, or substituting in Equation [45] and solving for σ

$$\sigma = 55{,}000\,(0.525)^{1/3} = 44{,}300 \text{ psi}$$

From Shanley's[2] fig. 3, a stress of 44,300 psi results in $P/L^2 = 4.85$. For values of $P/L^2 \leqslant 4.85$, the optimum D_1/D_2 is equal to 0.4 resulting (from Fig. 3) in a W_2/W_c equal to 0.917. As P/L^2 increases, the optimum stress, fig. 3,[2] increases resulting in a larger D_1/D_2 and subsequently in a higher W_2/W_c. Stated in other terms, as the load increases and the stress in the cylinder approaches the yield stress, the taper must gradually decrease, approaching ultimately a cylinder.

Taking values from fig. 3,[2] and Figs. 3 and 4 of this paper, the resulting W_2/W_c is plotted versus P/L^2 in Fig. 6. From Fig. 6 it is noted that as P/L^2 increases beyond 4.85 (or $\sigma = 44{,}300$ psi) the weight ratio W_2/W_c increase to 1.0 where the entire column is at the yield stress and the truncated cone has degenerated to a cylinder.

Inelastic Range

The optimum design of cylindrical round tubes can be extended into the inelastic range by using the tangent-modulus formula for primary buckling.[3] For tapered columns, however, the stress and

[3] "Inelastic Column Theory," by F. R. Shanley, *Journal of the Aeronautical Sciences*, vol. 14, May, 1947, pp. 261–268.

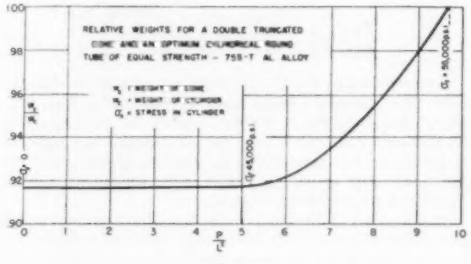

Fig. 6

therefore the tangent modulus varies along the column and the solution of Euler's differential equation will be more difficult. The optimum shape of a tapered column extended into the inelastic range will evidently be a function of the load. When the stress at the small end of the column has passed the knee of the stress-strain diagram the center of the column may still be in the elastic range. This change in effective stiffness can be visualized as a constant modulus with a change in moment of inertia which will effectively reduce the diameter in the inelastic portion. As can be seen from Fig. 3, if the effective diameter ratios are at the optimum point, then the actual diameter ratios will be larger, resulting in a larger weight for the tapered column.

Hence, based upon this physical reasoning, it is felt that under certain conditions in the inelastic range the weight ratio of an optimum tapered column to a cylindrical column will be more nearly equal to unity than for the elastic case. If the stresses in both the tapered column and cylindrical column have passed the knee of the stress-strain curve and they both are at a portion of the stress-strain diagram where the tangent modulus is nearly constant then the weight advantage of the tapered column over the cylindrical column may be regained.

The Characteristics of Fuel Motion Which Affect Airplane Dynamics

By E. W. GRAHAM[1] and A. M. RODRIGUEZ,[2] SANTA MONICA, CALIF.

Problems in aircraft dynamics such as stability and response of the rigid airplane may be affected by fuel motion in the tanks. Such problems also might arise in connection with missiles. In this paper the response of the fuel to simple harmonic motions of a rectangular tank in translation, pitching, and yawing is studied. Using the force and moment expressions, simple mechanical systems equivalent to the fuel are constructed. These systems respond to motions of the tank walls in the same fashion as the fuel, producing identical forces and moments. The use of such mechanical analogies should simplify in many cases the analysis of the complete dynamic system.

Introduction

THERE has been increasing interest recently in aircraft-dynamics problems which are affected by the motion of fuel in partially full tanks (1, 2).[3] The stability and response of a rigid airplane is a problem of this type. It is intuitively apparent that a large mass of fuel with a free surface may have serious dynamic effects on the airplane, particularly if there is a possibility of resonance.

Available Information. The understanding of these problems primarily requires an understanding of the dynamics of fuel motion. A great deal of the necessary information has been available for some time (3*a*), particularly the nature of the free oscillations of liquid in some tanks of simple shape. Extension of this material to include forced oscillations makes it possible to determine the forces communicated to the tank walls by an arbitrary motion of the tank (or airplane). Prior work in this direction initiated by Stewart and Lorell (4) was in part responsible for the present investigation. Related problems have been investigated in the field of seismology. Reference (5) gives experimental results and additional references to theoretical and experimental work in that field.

Reference (6), the unabridged version of the present paper, contains much more information on the mathematical development, and discusses the use of Laplace transforms.

Methods Used. For convenience in solving the complete dynamics problem it may be desirable to replace the fuel by a simple mechanical system. Therefore this paper suggests mechanical systems which produce the same forces and moments as the oscillating fuel when the container is given an arbitrary motion. (The "arbitrary" motion must, of course, fall within the scope of the linearization processes used.) In a previous report (7) the representation of fuel by an equivalent pendulum was discussed. The characteristics of the equivalent pendulum were determined only from consideration of fluid motions in a stationary tank. This was adequate to define the frequency and the product of mass times amplitude of motion for the pendulum, so that forces corresponding to a given amplitude of the fundamental wave motion were duplicated. This provided sufficient information for the study of some stability problems as affected by fuel "sloshing." The present paper offers additional information so that the more general problem of aircraft response to arbitrary disturbances can be considered, including the effect of angular tank motions.

Development of Equations

Co-Ordinate-System. Consider a rectangular tank filled to a depth h with fuel. Let the walls and bottom of the tank be given in irrotational co-ordinates, which are allowed to translate with the tank, by

$$x = \pm \frac{a}{2}, \quad y = \pm \frac{b}{2}, \quad z = -\frac{h}{2} \qquad [1]$$

as shown in Fig. 1. Positive forces, moments, displacements, and rotations are defined according to the conventions of a right-hand system.

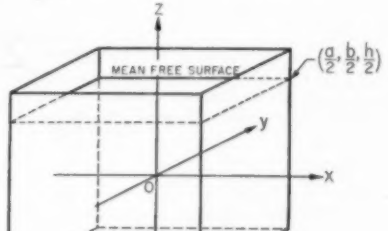

Fig. 1 Diagram of Partially Filled Tank Showing Co-Ordinate System

Assumptions. In order to simplify the problem a number of restrictions are applied concerning the nature of the fluid and the motions of the tank. The fluid is considered incompressible, and is also assumed nonviscous since the tanks are relatively large and baffles are not considered.

All tank motions are restricted to small accelerations compared to gravity. Angular motions are restricted so that they involve only small angular displacements while motion in translation may involve large displacements and velocities. In the case of sinusoidal motion, it is assumed that the frequency of oscillation is not in the immediate neighborhood of a natural free-surface frequency so that the slope of the free surface is small. These

[1] Aerodynamics Consultant, Douglas Aircraft Company, Inc., Santa Monica Division.

[2] Aerodynamicist, Douglas Aircraft Company, Inc., Santa Monica Division.

[3] Numbers in parentheses refer to the Bibliography at the end of the paper.

Presented at the West Coast Conference of the Applied Mechanics Division, Los Angeles, Calif., June 26–28, 1952, of The American Society of Mechanical Engineers.

Discussion of this paper should be addressed to the Secretary, ASME, 29 West 39th Street, New York, N. Y., and will be accepted until October 10, 1952, for publication at a later date. Discussion received after the closing date will be returned.

Note: Statements and opinions advanced in papers are to be understood as individual expressions of their authors and not those of the Society. Manuscript received by ASME Applied Mechanics Division, February 13, 1952.

assumptions allow a linearization of the boundary conditions, which is consistent with the small perturbation methods used in airplane dynamics.

From reference (3*a*, *b*) it can be shown that the velocity potential must then satisfy the following equations

$$\phi_{xx}(x, y, z, t) + \phi_{yy}(x, y, z, t) + \phi_{zz}(x, y, z, t) = 0 \quad [2]$$

$$-\phi_n \text{ (at tank boundaries)} = \text{normal velocity of boundary} \quad [3]$$

$$\phi_{tt}\left(x, y, \frac{h}{2}, t\right) + g\,\phi_z\left(x, y, \frac{h}{2}, t\right) = 0 \quad [4]$$

Equation [3] may be satisfied at the mean positions of the tank boundaries for angular motions of the tank.

Equation [4] combines two linearized free-surface conditions, i.e., the zero-pressure condition

$$g\eta(x, y, t) = \phi_t\left(x, y, \frac{h}{2}, t\right) \quad [5]$$

and the kinematic condition

$$\eta_t(x, y, t) = -\phi_z\left(x, y, \frac{h}{2}, t\right) \quad [6]$$

Tank Motions Considered. Any rigid tank motion of the type considered can be constructed from motions of translation along the x, y, and z-axes and a unique set of rotations about the three axes. It is enough to treat three basic tank motions, i.e., horizontal translation parallel to the x-axis, pitching about the y-axis, and yawing about the z-axis. The first two require only two-dimensional solutions involving x and z, while yawing motion requires a three-dimensional solution.

The motions will be assumed to be sinusoidal in the present development. Solutions for arbitrary tank motions can be constructed from sinusoidal motion by use of the Fourier integral. However, the use of the Laplace transform method (with respect to time) is especially adaptable for arbitrary tank motions. This procedure has been developed in reference (6).

Velocity Potential for Horizontal Motion Parallel to x-Axis. Let the displacement of the tank relative to inertial co-ordinates be

$$X(t) = A \sin \omega t$$

The boundary conditions for the velocity potential become

$$-\phi_x\left(\pm\frac{a}{2}, z, t\right) = A\omega \cos \omega t$$

$$\phi_z\left(x, -\frac{h}{2}, t\right) = 0$$

which leads to the solution

$$\phi = -A\omega \cos \omega t \left\{ x + \sum_{n=0}^{\infty} (-1)^n \frac{4a}{\pi^2(2n+1)^2} \left(\frac{\omega^2}{\omega_n^2 - \omega^2}\right) \times \frac{\sin\left[(2n+1)\frac{\pi}{a}x\right] \cosh\left[(2n+1)\frac{\pi}{a}\left(z + \frac{h}{2}\right)\right]}{\cosh\left[(2n+1)\pi\frac{h}{a}\right]} \right\} \quad [7]$$

where the resonant frequencies ω_n are given by

$$\omega^2 = \omega_n^2 = g(2n+1)\frac{\pi}{a}\tanh\left[(2n+1)\pi\frac{h}{a}\right] \quad [8]$$

Velocity Potential for Pitching About y-Axis. Let the angular displacement of the tank walls in pitch be

$$\theta(t) = B \sin \omega t$$

The boundary conditions for the velocity potential become

$$-\phi_x\left(\pm\frac{a}{2}, z, t\right) = +B\omega z \cos \omega t$$

$$-\phi_z\left(x, -\frac{h}{2}, t\right) = -B\omega x \cos \omega t$$

which leads to the solution

$$\phi = -B\omega \cos \omega t \left\{ \sum_{n=0}^{\infty} (-1)^n \frac{4}{\pi^2(2n+1)^2} \left(\frac{h^2 \sin\left[(2n+1)\frac{\pi}{h}z\right] \sinh\left[(2n+1)\frac{\pi}{h}x\right]}{\cosh\left[(2n+1)\frac{\pi a}{2h}\right]} + \frac{a^2 \sin\left[(2n+1)\frac{\pi}{a}x\right] \cosh\left[(2n+1)\frac{\pi}{a}\left(z - \frac{h}{2}\right)\right]}{\sinh\left[(2n+1)\frac{\pi}{a}h\right]} \right) + \sum_{n=0}^{\infty} (-1)^n \frac{4a}{\pi^2(2n+1)^2} \left(\frac{\omega^2}{\omega_n^2 - \omega^2}\right) \left(\frac{h}{2} - \frac{2a \tanh\left[(2n+1)\frac{\pi h}{2a}\right]}{\pi(2n+1)} + \frac{g}{\omega_n^2} \right) \times \frac{\sin\left[(2n+1)\frac{\pi}{a}x\right] \cosh\left[(2n+1)\frac{\pi}{a}\left(z + \frac{h}{2}\right)\right]}{\cosh\left[(2n+1)\frac{\pi h}{a}\right]} \right\} \quad [9]$$

where the ω_n are given by Equation [8].

Velocity Potential for Yawing About z-Axis. Let the angular displacement of the tank walls in yaw be

$$\psi(t) = C \sin \omega t$$

The boundary conditions for the velocity potential become

$$-\phi_x\left(\pm\frac{a}{2}, y, z, t\right) = -C\omega y \cos \omega t$$

$$-\phi_y\left(x, \pm\frac{b}{2}, z, t\right) = C\omega x \cos \omega t$$

$$\phi_z\left(x, y, -\frac{h}{2}, t\right) = 0$$

which leads to the three-dimensional velocity potential

$$\phi = C\omega \cos \omega t \left\{ \sum_{n=0}^{\infty} (-1)^n \frac{4}{\pi^2(2n+1)^2} \left(\frac{b^2 \sin\left[(2n+1)\frac{\pi}{b} y\right] \sinh\left[(2n+1)\frac{\pi}{b} x\right]}{\cosh\left[(2n+1)\frac{\pi a}{2b}\right]} - \frac{a^2 \sin\left[(2n+1)\frac{\pi}{a} x\right] \sinh\left[(2n+1)\frac{\pi}{a} y\right]}{\cosh\left[(2n+1)\frac{\pi b}{2a}\right]} \right) + \sum_{m=0}^{\infty}\sum_{n=0}^{\infty} (-1)^{m+n} \left(\frac{\omega^2}{\omega_{m,n}^2 - \omega^2}\right) \times \frac{16ab\,[b^2(2n+1)^2 - a^2(2m+1)^2]\ \operatorname{sech}\left[\frac{\pi}{ab}\sqrt{b^2(2n+1)^2 + a^2(2m+1)^2}\, h\right]}{\pi^4(2m+1)^2(2n+1)^2\,[b^2(2n+1)^2 + a^2(2m+1)^2]} \times \sin\left[(2n+1)\frac{\pi}{a} x\right] \sin\left[(2m+1)\frac{\pi}{b} y\right] \cosh\left[\frac{\pi}{ab}\sqrt{b^2(2n+1)^2 + a^2(2m+1)^2}\left(z + \frac{h}{2}\right)\right] \right\} \quad [10]$$

where the resonant frequencies $\omega_{m,n}$ are given by

$$\omega_{m,n} = g\frac{\pi}{ab}\sqrt{b^2(2n+1)^2 + a^2(2m+1)^2} \times \tanh\left[\frac{\pi}{ab}\sqrt{b^2(2n+1)^2 + a^2(2m+1)^2}\, h\right] \quad [11]$$

The two-dimensional part of the potential satisfies the boundary conditions on the tank side walls while the three-dimensional part is needed to satisfy the free-surface condition given by Equation [4].

Equivalent Mechanical Systems. In replacing the fuel by an equivalent mechanical system it is necessary to consider three types of motion:

(*A*) Horizontal translation parallel to the *x*-axis and pitching about the *y*-axis.

(*B*) Horizontal translation parallel to the *y*-axis and pitching about the *x*-axis.

(*C*) Yawing about the *z*-axis.

In order for a mechanical system to be equivalent to the fuel with respect to one of the foregoing types of motion, it must exert the same force and total moment on the tank as the fuel does for that type of motion. Motions of type (*A*) and (*B*) are of the same character so that it is necessary to discuss only one of them.

Motions of Type (A). Consider a mechanical system composed of a fixed mass M and an infinite set of undamped spring masses m_n so constrained as to move parallel to the bottom of the tank and the *xz*-plane. Locate the spring masses at vertical distances z_n and the fixed mass at a vertical distance Z from the origin as shown in Fig. 2. Let the spring constants be given by $k_n = m_n\omega_n^2$ where ω_n is given by Equation [8]. The moving masses may be thought of as point masses while the fixed mass has a distribution such that its moment of inertia about a line parallel to the *y*-axis and passing through $z = Z$ and $x = 0$ is I_y.

The equations of motion of the moving masses in response to sinusoidal tank motion are for horizontal translation

$$m_n(\ddot{x} - A\omega^2 \sin \omega t) = -k_n x \quad [12]$$

and for pitching motion

$$m_n\ddot{x} = -k_n(x - Bz_n \sin \omega t) + m_n g B \sin \omega t \quad [13]$$

From these equations the horizontal force and moment about the *y*-axis are derived. The corresponding force and moment exerted by the fuel are obtained by integrating the pressure and pressure times moment arm, respectively, over the tank boundaries. They are given in nondimensional form in the following, where primed forces and moments refer to the equivalent mechanical system and

$r_1 = \frac{h}{a}$ = tank aspect ratio in *xz*-plane

F_H = horizontal force

W_F = weight of fuel

M_y = moment about *y*-axis

I_{F_y} = effective moment of inertia of the fuel about *y*-axis (moment of inertia with "free" surface fixed)

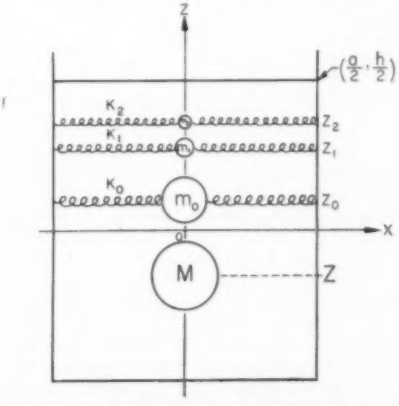

FIG. 2 DIAGRAM OF MECHANICAL SYSTEM REPRESENTING FUEL FOR HORIZONTAL AND PITCHING MOTIONS OF TANK

M_F = mass of fuel

$$f^2 = \frac{h\omega^2}{g}$$

$$f_n^2 = \frac{h\omega_n^2}{g} = (2n+1)\pi r_1 \tanh\left[(2n+1)\pi r_1\right]$$

Horizontal translation

$$\frac{F_H}{W_F} = \frac{A}{h} f^2 \sin \omega t \left\{ 1 + \sum_{n=0}^{\infty} \frac{8 \tanh\left[(2n+1)\pi r_1\right]}{\pi^3 (2n+1)^3 r_1} \frac{1}{\left(\frac{f_n}{f}\right)^2 - 1} \right\}$$

$$\frac{F_H'}{W_F} = \frac{A}{h} f^2 \sin \omega t \left\{ \frac{M}{M_F} + \sum_{n=0}^{\infty} \frac{m_n}{M_F} + \sum_{n=0}^{\infty} \frac{m_n}{M_F} \frac{1}{\left(\frac{f_n}{f}\right)^2 - 1} \right\} \quad \ldots [14]$$

$$\frac{M_y}{W_F h} = \frac{A}{h} f^2 \sin \omega t \left\{ \frac{1}{12 r_1^2} + \sum_{n=0}^{\infty} \frac{8 \tanh\left[(2n+1)\pi r_1\right]}{\pi^3 (2n+1)^3 r_1} \times \left(\frac{1}{2} - \frac{\tanh\left[(2n+1)\frac{\pi}{2} r_1\right]}{(2n+1)\frac{\pi}{2} r_1} + \frac{1}{f_n^2} \right) \frac{1}{\left(\frac{f_n}{f}\right)^2 - 1} \right\}$$

$$\frac{M_y'}{W_F h} = \frac{A}{h} f^2 \sin \omega t \left\{ \frac{M}{M_F} \frac{Z}{h} + \sum_{n=0}^{\infty} \frac{m_n}{M_F} \left(\frac{z_n}{h} + \frac{1}{f_n^2} \right) + \sum_{n=0}^{\infty} \frac{m_n}{M_F} \left(\frac{z_n}{h} + \frac{1}{f_n^2} \right) \frac{1}{\left(\frac{f_n}{f}\right)^2 - 1} \right\} \quad \ldots [15]$$

Pitching motion

$$\frac{F_H}{W_F} = B f^2 \sin \omega t \left\{ \frac{1}{12 r_1^2} + \sum_{n=0}^{\infty} \frac{8 \tanh\left[(2n+1)\pi r_1\right]}{\pi^3 (2n+1)^3 r_1} \times \left(\frac{1}{2} - \frac{\tanh\left[(2n+1)\frac{\pi}{2} r_1\right]}{(2n+1)\frac{\pi}{2} r_1} + \frac{1}{f_n^2} \right) \frac{1}{\left(\frac{f_n}{f}\right)^2 - 1} \right\}$$

$$\frac{F_H'}{W_F} = B f^2 \sin \omega t \left\{ \frac{M}{M_F} \frac{Z}{h} + \sum_{n=0}^{\infty} \frac{m_n}{M_F} \left(\frac{z_n}{h} + \frac{1}{f_n^2} \right) + \sum_{n=0}^{\infty} \frac{m_n}{M_F} \left(\frac{z_n}{h} + \frac{1}{f_n^2} \right) \frac{1}{\left(\frac{f_n}{f}\right)^2 - 1} \right\} \quad \ldots [16]$$

$$\frac{M_y}{W_F h} = B f^2 \sin \omega t \left\{ \frac{I_{Fy}}{M_F h^2} + 2 \sum_{n=0}^{\infty} \frac{8 \tanh\left[(2n+1)\pi r_1\right]}{\pi^3 (2n+1)^3 r_1} \times \left(\frac{1}{2} - \frac{\tanh\left[(2n+1)\frac{\pi}{2} r_1\right]}{(2n+1)\frac{\pi}{2} r_1} + \frac{1}{2 f_n^2} \right) \frac{1}{f_n^2} + \sum_{n=0}^{\infty} \frac{8 \tanh\left[(2n+1)\pi r_1\right]}{\pi^3 (2n+1)^3 r_1} \times \left(\frac{1}{2} - \frac{\tanh\left[(2n+1)\frac{\pi}{2} r_1\right]}{(2n+1)\frac{\pi}{2} r_1} + \frac{1}{2 f_n^2} \right) \frac{1}{\left(\frac{f_n}{f}\right)^2 - 1} \right\} + B \sin \omega t \left\{ \frac{1}{12 r_1^2} \right\}$$

$$\frac{M_y'}{W_F h} = B f^2 \sin \omega t \left\{ \frac{I_y}{M_F h^2} + \frac{M}{M_F} \left(\frac{Z}{h} \right)^2 + \sum_{n=0}^{\infty} \frac{m_n}{M_F} \left(\frac{z_n}{h} + \frac{1}{f_n^2} \right)^2 + \sum_{n=0}^{\infty} \frac{m_n}{M_F} \left(\frac{z_n}{h} + \frac{1}{f_n^2} \right)^2 \frac{1}{\left(\frac{f_n}{f}\right)^2 - 1} \right\} + B \sin \omega t \left\{ \frac{MZ}{M_F h} + \sum_{n=0}^{\infty} \frac{m_n}{M_F} \left(\frac{z_n}{h} + \frac{1}{f_n^2} \right) \right\} \quad \ldots [17]$$

If the forces and moments exerted by the mechanical system are to be identically equal to the forces and moments exerted by the fuel for all forcing frequencies, then the characteristics of the mechanical system must be given by

$$\frac{m_n}{M_F} = \frac{8 \tanh\left[(2n+1)\pi r_1\right]}{\pi^3 (2n+1)^3 r_1} \quad \ldots [18]$$

$$\frac{z_n}{h} = \frac{1}{2} - \frac{\tanh\left[(2n+1)\frac{\pi}{2} r_1\right]}{(2n+1)\frac{\pi}{2} r_1} \quad \ldots [19]$$

$$\frac{M}{M_F} = 1 - \sum_{n=0}^{\infty} \frac{8 \tanh\left[(2n+1)\pi r_1\right]}{\pi^3 (2n+1)^3 r_1} \quad \ldots [20]$$

$$\frac{Z}{h} = -\frac{1}{\left(\frac{M}{M_F}\right)} \sum_{n=0}^{\infty} \frac{m_n}{M_F} \frac{z_n}{h} \quad \ldots [21]$$

$$\frac{I_y}{M_F h^2} = \frac{I_{Fy}}{M_F h^2} - \frac{M}{M_F} \left(\frac{Z}{h} \right)^2 - \sum_{n=0}^{\infty} \frac{m_n}{M_F} \left(\frac{z_n}{h} \right)^2 \quad \ldots [22]$$

$$\frac{hk_n}{W_F} = \frac{8 \tanh^2\left[(2n+1)\pi r_1\right]}{\pi^3 (2n+1)^2} \quad \ldots [23]$$

Equation [22] indicates that the rigid mechanical system has the same moment of inertia about the y-axis as the fuel would have if the free surface were constrained by a tank boundary. This effective moment of inertia of the fuel is found to be

$$I_{F_y} = I_{S_y}\left\{1 - \frac{4}{1+r_1^2} + \frac{768}{\pi^5 r_1(1+r_1^2)} \times \sum_{n=0}^{\infty} \frac{\tanh\left[(2n+1)\frac{\pi}{2}r_1\right]}{(2n+1)^5}\right\} \quad \ldots [24]$$

where I_{S_y} is the moment of inertia about the y-axis of the solidified fuel.

then the yawing moment produced by the mechanical system can be compared to that produced by the fuel. In this comparison, which is made in the following, the primed moment is produced by the mechanical system and

M_z = moment about z-axis or yawing moment
I_{F_z} = effective moment of inertia of fuel about z-axis
I_{S_z} = moment of inertia of solidified fuel about z-axis

$$r_1 = \frac{h}{b} = \text{tank aspect ratio in } yz\text{-plane}$$

$$r_2 = \frac{r_2}{r_1} = \frac{a}{b} = \text{tank aspect ratio in } xy\text{-plane}$$

$$f_{m,n}^2 = \frac{h\omega_{m,n}^2}{g} = \pi r_1\sqrt{r_2^2(2m+1)^2 + (2n+1)^2} \times \tanh\left[\pi r_1\sqrt{r_2^2(2m+1)^2 + (2n+1)^2}\right]$$

$$\frac{aM_z}{gI_{S_z}} = Cr_1 f^2 \sin\omega t\left\{\frac{I_{F_z}}{I_{S_z}} + \sum_{m=0}^{\infty}\sum_{n=0}^{\infty} \frac{768\,[r_2^2(2m+1)^2 - (2n+1)^2]^2 \tanh\left[\pi r_1\sqrt{r_2^2(2m+1)^2 + (2n+1)^2}\right]}{\pi^7 r_1(1+r_2^2)(2m+1)^4(2n+1)^4[r_2^2(2m+1)^2 + (2n+1)^2]^{5/2}} \frac{1}{\left(\frac{f_{m,n}}{f}\right)^2 - 1}\right\} \quad \ldots [30]$$

$$\frac{aM_z'}{gI_{S_z}} = Cr_1 f^2 \sin\omega t\left\{\frac{I_z}{I_{S_z}} + \sum_{m=0}^{\infty}\sum_{n=0}^{\infty}\frac{I_{m,n}}{I_{S_z}} + \sum_{m=0}^{\infty}\sum_{n=0}^{\infty}\frac{I_{m,n}}{I_{S_z}}\frac{1}{\left(\frac{f_{m,n}}{f}\right)^2 - 1}\right\}$$

Approximate expressions for I_{F_y}/I_{S_y}, M/M_F and Z/h which lend themselves to easy calculation are as follows

$$\frac{I_{F_y}}{I_{S_y}} = 1 - \frac{4r_1^2}{1+r_1^2} + 2.510\left(\tanh\frac{\pi}{2r_1} + 0.0043\right) \times \frac{r_1^2}{1+r_1^2}, (r_1 \leqslant 1) \quad \ldots [25]$$

$$\left.\begin{aligned}\frac{M}{M_F} &= 1 - \frac{0.258}{r_1}(\tanh \pi r_1 + 0.0518), \left(r_1 \leqslant \frac{1}{2}\right)\\ \frac{M}{M_F} &= 1.032\, r_1\left(\tanh\frac{\pi}{4r_1} + 0.0518\right), \left(r_1 \geqslant \frac{1}{2}\right)\end{aligned}\right\} \quad \ldots [26]$$

$$\frac{Z}{h} = \frac{1}{2} - \frac{1}{2\left(\frac{M}{M_F}\right)} + \frac{1}{6r_1^2\left(\frac{M}{M_F}\right)} - \frac{0.1643}{r_1^2\left(\frac{M}{M_F}\right)} \times \left(\frac{1}{\cosh \pi r_1} + \frac{1}{3^5\cosh 3\pi r_1} + \ldots\right) \quad \ldots [27]$$

Motion of Type C. Consider a mechanical system composed of a fixed mass with moment of inertia about the z-axis I_z and an infinite set of moving masses constrained to pivot about the z-axis. If the moving masses have moments of inertia $I_{m,n}$ and are attached to torsional springs with spring constants $k_{m,n}$, then if the system is undamped the equations of motion of the moving masses are

$$I_{m,n}\ddot{\psi} = -k_{m,n}(\psi - C\sin\omega t) \quad \ldots [28]$$

where $C \sin \omega t$ is the angular displacement of the tank in yaw. If the spring constants are related to the natural frequencies of fuel oscillation by

$$k_{m,n} = I_{m,n}\,\omega_{m,n}^2 \quad \ldots [29]$$

If the two yawing moments are to be identical for all forcing frequencies, then

$$\frac{I_{m,n}}{I_{S_z}} = \frac{768\,[r_2^2(2m+1)^2 - (2n+1)^2]^2}{\pi^6(1+r_2^2)(2m+1)^4(2n+1)^4[r_2^2(2m+1)^2 + (2n+1)^2]} \times \frac{\tanh\left[\pi r_1\sqrt{r_2^2(2m+1)^2 + (2n+1)^2}\right]}{\pi r_1\sqrt{r_2^2(2m+1)^2 + (2n+1)^2}} \quad \ldots [31]$$

$$\frac{I_z}{I_{S_z}} = \frac{I_{F_z}}{I_{S_z}} - \sum_{m=0}^{\infty}\sum_{n=0}^{\infty}\frac{I_{m,n}}{I_{S_z}} \quad \ldots [32]$$

where I_{F_z} is given by Equation [24] if r_1 is replaced by r_2.

Mechanical Systems for Combinations of Tank Motions. A single mechanical system, that will respond the same as the fluid to all tank motions, cannot, in general, be constructed from the simple mechanical systems discussed without introducing negative moments of inertia. However, it is always possible to construct a single mechanical system that will represent the fluid response to both yawing motion and motion of type (A) or yawing motion and motion of type (B). Consider the mechanical system that represents motions of type (A); the fixed mass can be distributed in the yz-plane so that the center of gravity remains fixed and its moment of inertia is I_{F_x} about the z-axis and I_y about an axis passing through $z = Z$ and parallel to the y-axis. The moment of inertia I_{F_x} can then be separated into the components I_x, $I_{0,0}$, $I_{0,1}$, and so on, of the mechanical system representing the response of the fluid to yawing motion.

Description of Mechanical Systems

In the preceding section equivalent mechanical systems were derived and shown to produce the same forces and moments as the fuel in response to tank motions. Their characteristics were derived in terms of tank aspect ratios $r_1 = h/a$, $r_2 = h/b$, and $r_3 = a/b$. Some of these characteristics of the mechanical systems have been computed and are shown in Figs. 3 through 10.

Fig. 3 shows the ratio of the fixed mass and first two moving masses to the total fuel mass as a function of tank aspect ratio r_1. The ratio M/M_F was computed from Equation [26]. The moving masses associated with the higher harmonics are too small to plot except very near $r_1 = 0$. The ratio of m_n to m_0 is approximately $1/(2n + 1)^2$ for small r_1 and $1/(2n + 1)^3$ for large r_1. These ratios are plotted on a logarithmic scale in Fig. 4 versus the frequency ratios f_n/f_0.

Fig. 5 shows the vertical location of the fixed mass and first two moving masses as functions of r_1. Z/h was computed from Equation [27]. The ratio Z/h becomes infinite for the shallow tank but Z remains finite approaching the value $0.461a$ for $r_1 = 0$.

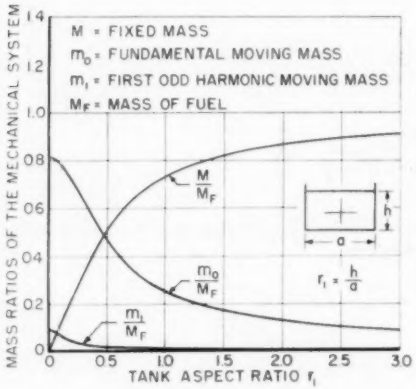

Fig. 3 Magnitudes of Masses in Mechanical System as a Function of Tank Proportions

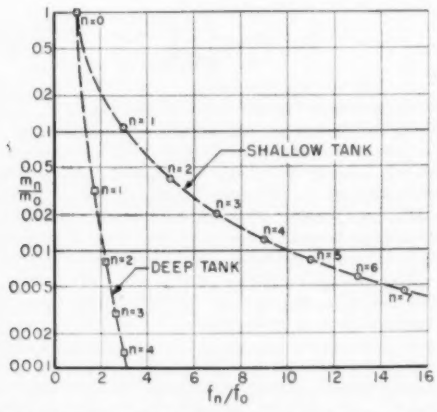

Fig. 4 Magnitudes of Moving Masses as a Function of Their Natural Frequencies

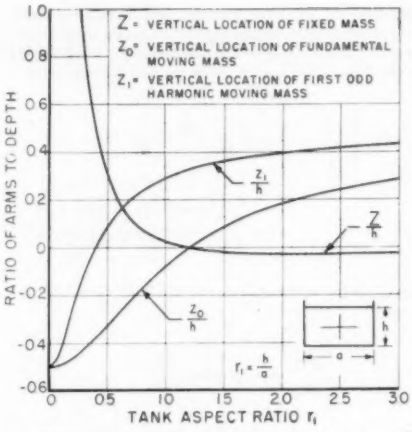
Z = VERTICAL LOCATION OF FIXED MASS
Z0 = VERTICAL LOCATION OF FUNDAMENTAL MOVING MASS
Z1 = VERTICAL LOCATION OF FIRST ODD HARMONIC MOVING MASS
RATIO OF ARMS TO DEPTH
TANK ASPECT RATIO r1
Z1/h
Z/h
Z0/h
r1 = h/a

Fig. 5 Vertical Locations of Masses as a Function of Tank Proportions

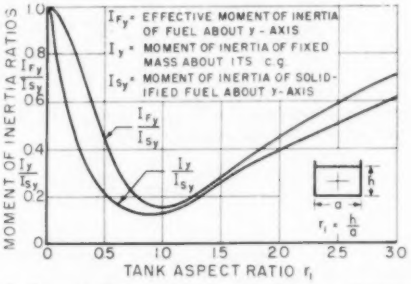
IFy = EFFECTIVE MOMENT OF INERTIA OF FUEL ABOUT y-AXIS
Iy = MOMENT OF INERTIA OF FIXED MASS ABOUT ITS c.g.
ISy = MOMENT OF INERTIA OF SOLIDIFIED FUEL ABOUT y-AXIS
MOMENT OF INERTIA RATIOS
TANK ASPECT RATIO r1
IFy/ISy
Iy/ISy
r1 = h/a

Fig. 6 Pitching Moment of Inertia Ratios as a Function of Tank Proportions

Moment of inertia ratios I_y/I_{S_y} and I_{F_y}/I_{S_y} were computed from Equations [22] and [25] and are shown in Fig. 6. I_{F_y}/I_{S_y} for $r_1 > 1$ was computed by replacing r_1 by $1/r_1$ in Equation [25].

Fig. 7 shows the nondimensional spring constants hk_n/W_F associated with the first three moving masses.

Fig. 8 is a plot of the horizontal force produced by the mechanical system in response to horizontal oscillation divided by the force that would be produced by the fuel if it were solidified. The ratio is plotted against the dimensionless forcing frequency f for $r_1 = 0.25$.

When yawing motion is considered, it is probably sufficiently accurate to consider only the masses with moments of inertia $I_{0,0}$, $I_{1,0}$, $I_{0,1}$, $I_{2,0}$, and $I_{0,2}$ as moving masses and the rest as part of the fixed mass. The ratios of these moments of inertia to I_{S_z} have been computed from Equation [31] for $r_1 = r_3 = 0$. They are plotted against r_3 in Figs. 9 and 10. I_{F_z}/I_{S_z} was computed from Equation [25]. I_z/I_{S_z} is zero in the shallow tank case.

Discussion

Some problems arise concerning the proper use of the preceding material, and a few of these will be discussed.

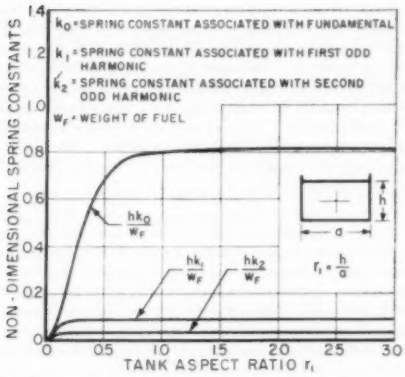
k_0 = SPRING CONSTANT ASSOCIATED WITH FUNDAMENTAL
k_1 = SPRING CONSTANT ASSOCIATED WITH FIRST ODD HARMONIC
k_2 = SPRING CONSTANT ASSOCIATED WITH SECOND ODD HARMONIC
W_F = WEIGHT OF FUEL
NON-DIMENSIONAL SPRING CONSTANTS
TANK ASPECT RATIO r_1
$\frac{hk_0}{W_F}$
$\frac{hk_1}{W_F}$
$\frac{hk_2}{W_F}$
$r_1 = \frac{h}{a}$

FIG. 7 SPRING CONSTANTS FOR MECHANICAL SYSTEM AS A FUNCTION OF TANK PROPORTIONS

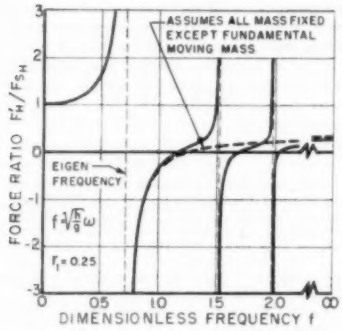

FIG. 8 FORCE EXERTED BY MECHANICAL SYSTEM AS A FUNCTION OF FREQUENCY OF FORCED HORIZONTAL OSCILLATION

Mechanical Systems. For aircraft having a vertical plane of symmetry through the longitudinal axis, the longitudinal stability and the lateral-directional stability can be treated independently.

In order to handle the longitudinal stability it is necessary to know the forces and moments produced by translation of the tank and by pitching motions. A single mechanical system has been set up to represent the tank for both of these motions.

The lateral-directional case is more complicated since, in general, the effects of rolling motion, translation, and yawing must be considered. A single mechanical system has been devised to represent the fuel tank for all of these motions, provided the translation is confined to the plane of the rolling motion. The more general case, involving also longitudinal translation (which would appear with wing-tip tanks), cannot, in general, be represented by a single system of the present type, unless imaginary dimensions are introduced. In such a case different systems could be used to obtain forces and moments in different planes.

It is also possible to use the Laplace transforms of the forces and moments directly, without regard to mechanical systems, if the transform method is being used for the complete problem.

In some cases, particularly where tanks are located far from the CG of the airplane, the effect of angular motions of the tank may be negligible by comparison with the effect of translation of the tank. In such cases some simplifications may be possible.

Approximate Mechanical Systems. The forces and moments produced by the higher harmonics of the fluid motion will be negligible in many cases. This means that the equivalent mechanical system frequently can be assumed to consist of one fixed mass and one moving mass.

If the airplane has a natural frequency quite close to a higher harmonic of the fluid motion, it might be assumed that it would be necessary to retain the moving mass corresponding to this harmonic. However, consideration of the practical limitations on wave heights may alter the picture. These limitations may arise from the effects of viscosity, cavitation, or through the presence of nonlinearities in free-surface boundary conditions. For example, in reference (3c) a limitation on the ratio of wave height to wave length is suggested. Such a "limit" might mark the introduction of splashing with consequent energy dissipation.

Tanks of Different Shape. Tanks of other than rectangular shape could be studied. Stewart and Lorell (4) have studied the forced oscillations in a cylindrical tank of circular cross section with free surface normal to the axis. Some information on the

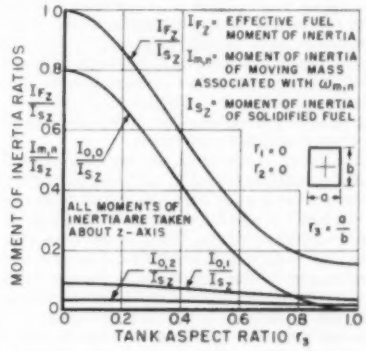
I_{F_Z} = EFFECTIVE FUEL MOMENT OF INERTIA
$I_{m,n}$ = MOMENT OF INERTIA OF MOVING MASS ASSOCIATED WITH $\omega_{m,n}$
I_{S_Z} = MOMENT OF INERTIA OF SOLIDIFIED FUEL
ALL MOMENTS OF INERTIA ARE TAKEN ABOUT Z-AXIS
$r_1 = 0$
$r_2 = 0$
$r_3 = \frac{a}{b}$
MOMENT OF INERTIA RATIOS
TANK ASPECT RATIO r_3

FIG. 9 YAWING MOMENT OF INERTIA RATIOS FOR SHALLOW TANK

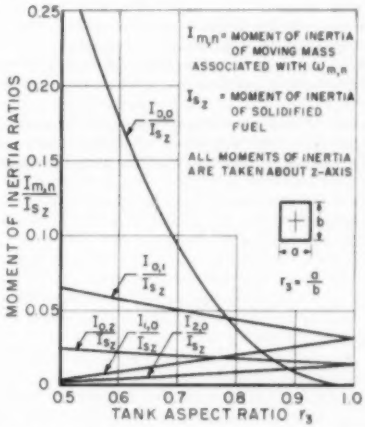
$I_{m,n}$ = MOMENT OF INERTIA OF MOVING MASS ASSOCIATED WITH $\omega_{m,n}$
I_{S_Z} = MOMENT OF INERTIA OF SOLIDIFIED FUEL
ALL MOMENTS OF INERTIA ARE TAKEN ABOUT Z-AXIS
$r_3 = \frac{a}{b}$
MOMENT OF INERTIA RATIOS
TANK ASPECT RATIO r_3

FIG. 10 DETAILS OF YAWING MOMENTS OF INERTIA OF MOVING MASSES FOR SHALLOW TANK

free oscillations in a few other tanks of simple shape is given in the appendix to reference (7). Few cases involving variable tank depth have been solved exactly. Although there are mathematical difficulties in getting exact solutions to many cases which appear physically simple, it is still possible to get approximate theoretical solutions in such cases. Also, it should be comparatively easy to determine experimentally the fundamental frequency for a tank of arbitrary shape.

Baffle Locations. If the oscillations of the fluid produce large forces on the tank walls, baffles may be required to dissipate the fluid energy rapidly. These baffles probably should be placed in regions which show high velocities in the unbaffled condition. For example, consider the fundamental mode in a rectangular tank undergoing horizontal oscillations. Here the highest vertical velocities of the fluid occur at the ends of the tank in the free surface, and the highest horizontal velocities occur at the center of the tank in the free surface. Baffles should be most effective in these locations.

Effective Value of g. If the fuel tank experiences a large constant acceleration normal to the mean free surface, then the value of g is effectively changed. If the effective value of g is quadrupled, then the natural frequencies of fluid oscillation are doubled. If the effective value of g approaches zero, as in a free fall, then the natural frequencies approach zero. Such effects probably would be of interest in connection with missile dynamics, and might be of importance in aircraft maneuvers.

To get the correct equivalent mechanical systems and force and moment expressions it is only necessary to replace g by the effective value of g in the formulas. (This results in the introduction of an effective fuel weight also.)

Variable Normal Accelerations. It has been mentioned that a constant acceleration normal to the mean free surface changes the effective value of g and alters the natural frequencies of the fluid in the tank. It also can be shown that variable normal accelerations may alter the amplitude of the wave motion. In particular, a periodic normal acceleration of the correct frequency may feed energy into an existing wave motion. This occurs through a nonlinear coupling, and the equivalent mechanical system does not correctly represent the fluid to this order. Such terms are not ordinarily considered in airplane dynamics.

Nonlinearities. When the amplitude of the fuel motion is large the effect of nonlinearity may become important. The nonlinearity is associated with boundary conditions at the free surface, not with the Laplace equation, which is linear. The mathematical difficulties introduced by the nonlinear effects are too great to permit investigation here. The region of applicability of the linearized equations can best be determined by experiment.

Viscosity. The effects of viscosity are small for unbaffled tanks of the size considered in aircraft. If baffles were present this certainly would not be the case, since the actual flow pattern can be radically different from the potential flow pattern in such cases, and heavy damping may be introduced. For this reason it is of little interest to investigate the potential flow pattern where baffles are involved. The scope of the paper therefore is limited primarily to determining whether or not baffles may be necessary. It is then possible to suggest locations where baffles might be found most effective. This is based entirely on the velocity distribution in the unbaffled tank, it being assumed that the greatest energy dissipation would be produced by locating baffles in the regions of highest velocity.

Conclusions

In many cases it is practicable to replace the fuel by spring-mass systems for purposes of dynamic analysis. These spring-mass systems correctly represent the fuel even for angular motions of the tank. When many types of tank motion must be considered simultaneously these equivalent systems may become complicated, and possibly lose physical significance through the necessity for negative moments of inertia.

It seems probable that masses corresponding to higher harmonics of the fuel motion often may be neglected (or considered as fixed mass). This type of approximation is, of course, very important in simplifying calculations, and deserves further study.

When equivalent mechanical systems are introduced, any desired method may be used for solving the complete dynamics problem. Laplace transform methods may be used in conjunction with the mechanical systems or without reference to them. In either case terms corresponding to higher harmonics probably can be omitted.

BIBLIOGRAPHY

1 "An Analytical Approach to the Fuel Sloshing and Buffeting Problems of Aircraft," by Harold Luskin and Ellis Lapin, *Journal of the Aeronautical Sciences*, vol. 19, April, 1952, pp. 217–228.

2 "A Theoretical Analysis of the Effects of Fuel Motion on Airplane Dynamics," by A. A. Schy, NACA Technical Note 2280, January, 1951.

3 "Hydrodynamics," by H. G. Lamb, Dover Publications, New York, N. Y., sixth edition, 1945.

(a) Articles 227, 228, 257, 258, 259, 190, 191, 178, 179.
(b) Article 20.
(c) Article 250.

4 "Forces Produced by Fuel Oscillation," by Jack Lorell, Jet Propulsion Laboratory Progress Report 20-149, Pasadena, Calif., 1951.

5 "Hydrodynamic Experiments With Rigid Cylindrical Tanks Subjected to Transient Motions," by L. S. Jacobsen and R. S. Ayre, Bulletin of the Seismological Society of America, vol. 41, no. 4, October, 1951.

6 "The Characteristics of Fuel Motion Which Affect Airplane Dynamics," by E. W. Graham and A. M. Rodrigues, Douglas Aircraft Company Report No. SM-14212, November 27, 1951.

7 "The Forces Produced by Fuel Oscillation in a Rectangular Tank," by E. W. Graham, Douglas Aircraft Company Report No. SM-13748, Revised April 16, 1951.

A Mathematical Analysis of the Relaxation Type of Vehicle Suspension

By JOSEPH GALLAGHER[1] and ENRICO VOLTERRA,[2] CHICAGO, ILL.

The responses of the relaxation type of vehicle suspension to steady and transient disturbances are analyzed. The results are compared with the corresponding responses for the standard type of vehicle suspension. The relaxation suspension system shows a definite improvement over the standard suspension system in the response to transient disturbances, as the initial shocks following a sudden wheel movement are reduced greatly. In the particular case of critical adjustment of a relaxation suspension system the maximum amplitude of the transient vibration is approximately 30 per cent lower than that of the standard-type system at critical adjustment. The amplitude and phase-angle curves presented in the paper for the steady-state motion, together with the transient-state-response analysis, permit the design of a relaxation-type suspension system with known vibrational characteristics in both states.

Nomenclature

The following nomenclature is used in the paper:

$x_1(t)$ = displacement of wheel
$x_2(t)$ = displacement of vehicle
$x_3(t)$ = displacement of damper piston
$x = (x_3 - x_1)$ = relative displacement
X_1 = amplitude of motion of wheel
X_2 = amplitude of motion of vehicle
X_3 = amplitude of motion of damper piston
k_1 = spring constant of main spring
k_2 = relaxation spring constant
c = coefficient of viscous damping
M = mass of vehicle carried by one wheel
t = time
U = step function
U' = unit impulse
U'' = unit doublet
L = Laplace transformation
$\mathfrak{x}(s)$ = transform of $x(t)$
L^{-1} = inverse transformation
k_{2c} = critical value of relaxation spring
c_c = critical value of viscous damping
$h = \frac{k_2}{k_{2c}}$ = relaxation factor
$\zeta = \frac{c}{c_c}$ = damping factor
$Z(s)$ = impedance transform
a = triple root of $Z(s)$
α = real root of $Z(s)$
δ = real part of conjugate root
ρ = imaginary part of conjugate root
s = distance from wave crest
v = velocity of vehicle
l = wave length of road disturbance
$\omega = \frac{2\pi v}{l}$ = frequency of road variation
φ = phase angle between relative motion and road motion
β = phase angle between steady vibration and road motion
$\Omega = \frac{k_2}{c}$
$\omega_{11}^2 = \frac{k_1}{M}$ = natural undamped frequency of vehicle
$\omega_{22}^2 = \frac{k_2}{M}$
$r = \frac{\omega}{\omega_{11}}$
$\theta = 3\sqrt{3}\,\frac{h}{\zeta}$
$\gamma = \sqrt{8h}$

Introduction

In a recent paper by Bourcier de Carbon (1)[3] a new type of vehicle suspension, called the "relaxation type," is described. It consists of a spring connected in parallel with a spring and a dashpot connected in series. This new type of suspension presents considerable advantages in comparison with the standard type of suspension consisting of a spring connected in parallel with a dashpot.

The object of the paper is to present a mathematical study of this new type of suspension by analyzing its responses to steady and transient disturbances and by comparing the results with the corresponding responses for the standard type of suspension. Curves giving the principal results of the analysis are presented.

In an Appendix the responses of the standard type of vehicle suspension to transient disturbances are analyzed. By comparing the impulsive responses of the two systems, it appears that one of the chief advantages of the relaxation system over the standard type is that the former gives no instantaneous jump or displacement when an impulse is applied. The sudden displacement of a vehicle with a standard suspension system is, in fact, due to the high instantaneous velocity of the damper piston relative to its cylinder. As a consequence, an instantaneous force is transmitted to the vehicle. In the case of the relaxation system, on the other hand, this sudden force cannot be transmitted instantaneously to the vehicle owing to the presence of the relaxation spring between dashpot and vehicle.

Aside from this obvious improvement of passenger comfort, the results of the analysis indicate that the maximum displacements for the relaxation type are lower than for the standard type,

[1] Graduate Student, Illinois Institute of Technology.
[2] Associate Professor of Mechanics, Illinois Institute of Technology. Mem. ASME.

Presented at the West Coast Conference of the Applied Mechanics Division, Los Angeles, Calif., June 26–28, 1952, of The American Society of Mechanical Engineers.

Discussion of this paper should be addressed to the Secretary, ASME, 29 West 39th Street, New York, N. Y., and will be accepted until October 10, 1952, for publication at a later date. Discussion received after the closing date will be returned.

Note: Statements and opinions advanced in papers are to be understood as individual expressions of their authors and not those of the Society. Manuscript received by ASME Applied Mechanics Division, October 18, 1951.

[3] Numbers in parentheses refer to the Bibliography at the end of the paper.

in the particular case of a critically adjusted relaxation suspension system the maximum amplitude of transient vibration being approximately 30 per cent lower than that of a critically adjusted standard type.

The steady state of the relaxation suspension system is also analyzed in the paper, on the usual assumption that the wheel of the vehicle is moving over a sinusoidal profile.

The analysis of the responses of the relaxation type of vehicle suspension presented in this paper supplies the data necessary for the design of relaxation-type suspension systems with known vibrational characteristics in both states.

Transient Motion of a Relaxation Suspension System

Fig. 1 shows the model of a relaxation suspension system. The mass M represents the mass of the vehicle, k_1 the constant of the spring coupled in parallel with a system of a spring (of constant k_2) in series with a dashpot (of constant c). In the following analysis the spring forces will be considered linear and the damping viscous.

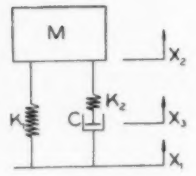

Fig. 1

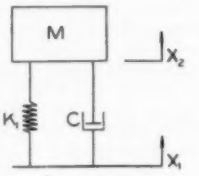

Fig. 2

Fig. 2 shows the model of a standard type of suspension system.

The equation of motion for the mass M is

$$M\frac{d^2x_2(t)}{dt^2} + k_1x_2(t) + k_2x_2(t) - k_2x_3(t) = k_1x_1(t) \quad \ldots\ldots [1]$$

whereas consideration of the forces acting on the damper piston, whose mass is neglected, leads to

$$-k_2x_2(t) + k_2x_3(t) + c\frac{dx_3(t)}{dt} = c\frac{dx_1(t)}{dt} \quad \ldots\ldots [2]$$

In studying the transient motion, the general method of impulsive response will be used. The response of the mass M will be found when the co-ordinate x_1 performs a unit impulse, i.e., a displacement which can be considered to be the limiting case of a displacement of $1/R$ units acting for a time duration of R seconds as R approaches zero. The response of the mass M to an arbitrary displacement x_1 of the wheel can be built up by superposition of the responses to unit impulses.

Let the co-ordinate x_1 perform the motion defined by

$$x_1(t) = U'(t) = \lim_{R\to 0}\left[\frac{1}{R}\,U(t) - \frac{1}{R}\,U(t-R)\right] \quad \ldots [3]$$

(see Fig. 3). $U(t)$ is a step function defined as zero for $t < 0$ (2) and unity for $t > 0$. Substituting Equation [3] into Equations [1] and [2]

$$\left.\begin{aligned} M\frac{d^2x_2(t)}{dt^2} + k_1x_2(t) + k_2x_2(t) - k_2x_3(t) &= k_1U'(t) \\ c\frac{dx_3(t)}{dt} + k_2x_2(t) - k_2x_3(t) &= c\frac{dU'(t)}{dt} \end{aligned}\right\} \quad \ldots [4]$$

The Laplace transformation will be used for solving Equations

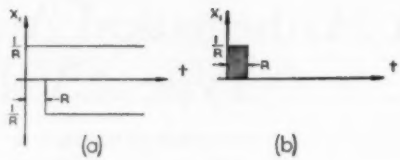

Fig. 3

[4] for the co-ordinate x_2. The system will be considered to be at rest at time $t = 0$.

Let the transforms of the co-ordinate x_2 and x_3 be

$$L[x_2(t)] = \mathfrak{X}_2(s) \qquad L[x_3(t)] = \mathfrak{X}_3(s) \quad \ldots\ldots [5]$$

Hence

$$\mathfrak{X}(s) = \int_0^\infty e^{-st}\,x(t)dt$$

and

$$\left.\begin{aligned} L\left[\frac{d^2x(t)}{dt^2}\right] &= s^2\mathfrak{X}(s) & L[U'(t)] &= 1 \\ L\left[\frac{dx(t)}{dt}\right] &= s\mathfrak{X}(s) & L[U''(t)] &= s \end{aligned}\right\} \quad \ldots\ldots [6]$$

Applying the Laplace transformation to the differential Equations [4] and making use of Equations [5] and [6]

$$\left.\begin{aligned} Ms^2\mathfrak{X}_2(s) + k_1\mathfrak{X}_2(s) + k_2\mathfrak{X}_2(s) - k_2\mathfrak{X}_3(s) &= k_1 \\ cs\mathfrak{X}_3(s) + k_2\mathfrak{X}_3(s) - k_2\mathfrak{X}_2(s) &= cs \end{aligned}\right\} \quad \ldots\ldots [7]$$

The differential Equations [4] are thus reduced to the algebraic Equations [7] in the transforms $\mathfrak{X}_2(s)$ and $\mathfrak{X}_3(s)$. From Equations [7]

$$\mathfrak{X}_3(s) = \frac{f(s)}{Z(s)} = \frac{c(k_1+k_2)s + k_1k_2}{Mcs^3 + Mk_2s^2 + c(k_1+k_2)s + k_1k_2} \quad \ldots [8]$$

The classical method for finding the inverse function involves a contour integration in the complex plane. The value of this contour integral equals the sum of the residues of the function $e^{st}x_3(s)$ (3).

From Equation [8] it follows that the values of the residues of this function will depend on the nature of the roots of the impedance function $Z(s)$. It will, therefore, be of interest to determine how the parameters of the system affect these roots.

As far as the stability of the ensuing motion of the system is concerned, it is known (4, 5) that if the real parts of the roots of Equation [8] are negative, the system is dynamically stable. By Hurvitz' criterion of stability (6) it is known that an algebraic equation with real coefficients

$$f(x) = p_0 + p_1x + p_2x^2 + \ldots\ldots\ldots\ldots + p_nx^n = 0 \quad \ldots [9]$$

has all roots with negative real parts if, and only if, the n-determinants of the polynomial Equation [9] are positive, provided that $p_0 > 0$.

The determinants for a polynomial of third degree are

$$D_1 = p_0;\ D_2 = \begin{vmatrix} p_1 & p_0 \\ p_3 & p_2 \end{vmatrix}; \qquad D_3 = \begin{vmatrix} p_1 & p_0 & 0 \\ p_3 & p_2 & p_1 \\ 0 & 0 & p_3 \end{vmatrix} \quad \ldots\ldots [10]$$

From Equation [8] the polynomial is

$$Z(s) = Mcs^3 + Mk_2s^2 + c(k_1+k_2)s + k_1k_2 \quad \ldots\ldots [11]$$

Comparing Equations [11] and [9], one gets for the coefficients

$$p_0 = k_1k_2;\ p_1 = c(k_1 + k_2);\ p_2 = k_2M;\ p_3 = Mc \quad [12]$$

Substituting the expressions given by Equations [12] in the determinants given by Equations [10] and expanding

$$D_1 = c(k_1 + k_2);\ D_2 = ck_2^2M;\ D_3 = ck_2^2M^2 \quad [13]$$

As p_0 given by Equations [12] together with the values of the determinants given by Equations [13] are positive, the system is dynamically stable.

It is well known from the case of a simply damped system of one degree of freedom that the transition from periodic motion takes place when the discriminant of the impedance function equals zero. Then the impedance equation for the system has one double root.

In our case the values of the parameters which cause the impedance transform Equation [11] to have one triple root are of interest. If the impedance transform is to have one triple root $s = -a$, then

$$(s + a)^3 = s^3 + 3as^2 + 3a^2s + a^3 \quad [14]$$

must equal the impedance transform which, by dividing numerator and denominator of Equation [8] by Mc, becomes

$$Z(s) = s^3 + \frac{k_2}{c}s^2 + \frac{k_1 + k_2}{M}s + \frac{k_1k_2}{Mc} \quad [15]$$

By equating Equations [14] and [15]

$$3a = \frac{k_2}{c} \quad [16]$$

$$3a^2 = \frac{k_1 + k_2}{M} \quad [17]$$

$$a^3 = \frac{k_1k_2}{Mc} \quad [18]$$

The value of the triple root given by Equation [17] is

$$a = \frac{1}{\sqrt{3}}\sqrt{\frac{k_1 + k_2}{M}} \quad [19]$$

Substituting the value of a given by Equation [19] into Equations [16] and [18], one is led to

$$c = \frac{1}{\sqrt{3}}k_2\sqrt{\frac{M}{k_1 + k_2}} \quad [20]$$

$$c = 3\sqrt{3}\,\frac{k_1k_2}{k_1 + k_2}\sqrt{\frac{M}{k_1 + k_2}} \quad [21]$$

Equating Equations [20] and [21]

$$k_2 = 8k_1 \quad [22]$$

Substituting Equation [22] into Equation [20] one obtains for c

$$c = \frac{8}{3\sqrt{3}}\sqrt{Mk_1} \quad [23]$$

The values of k_2 and c given by Equations [22] and [23] are those which cause the impedance transform given by Equation [15] to have a triple root. The motion performed by the system is a transition between oscillatory and nonoscillatory conditions, and the corresponding values of k_2 and c are known as "critical values" and will be designated by

$$k_{2c} = 8k_1 \quad [24]$$

$$c_c = \frac{8}{3\sqrt{3}}\sqrt{Mk_1} \quad [25]$$

Introducing the dimensionless ratios h and ζ defined by

$$h = \frac{k_2}{k_{2c}},\quad \zeta = \frac{c}{c_c} \quad [26]$$

and the natural undamped frequency of the mass M: $\omega_{11} = \sqrt{k/M}$ into Equation [8] for the transform $\bar{x}_2(s)$ equation

$$\bar{x}_2(s) = \frac{\omega_{11}^2(1 + 8h)s + 3\sqrt{3}\,\frac{h}{\zeta}\,\omega_{11}^3}{s^3 + 3\sqrt{3}\,\frac{h}{\zeta}\,\omega_{11}s^2 + \omega_{11}^2(1 + 8h)s + 3\sqrt{3}\,\frac{h}{\zeta}\,\omega_{11}^3} \quad [27]$$

is obtained.

The nature of the inverse function of $\bar{x}_2(s)$ given by Equation [27] and, therefore, the motion of the mass M depends on whether h and ζ are $\gtrless 1$. From a practical point of view, the motion when h and ζ are $\leqslant 1$ is of interest and will be considered in the following analysis.

Transient Motion for Critical Adjustments of Parameters

In this case the impedance function has one triple root defined by Equation [19]. When $k_2 = 8k_1$, Equation [19] becomes

$$a = \frac{1}{\sqrt{3}}\sqrt{\frac{k_1 + 8k_1}{M}} = \sqrt{3}\,\omega_{11} \quad [28]$$

Equation [27] for the transform $\bar{x}_2(s)$ when $h = \zeta = 1$, becomes

$$\bar{x}_2(s) = \frac{9\omega_{11}^2s + 3\sqrt{3}\,\omega_{11}^3}{(s + \sqrt{3}\,\omega_{11})^3} \quad [29]$$

Equation [29] may be written as

$$\bar{x}_2(s) = \frac{9\omega_{11}^2s}{(s + \sqrt{3}\,\omega_{11})^3} + \frac{3\sqrt{3}\,\omega_{11}^3}{(s + \sqrt{3}\omega_{11})^3} \quad [30]$$

The inverse transform of these functions are available from tables (2)

$$\left.\begin{aligned} L^{-1}\left[\frac{1}{(s + a)^3}\right] &= \frac{1}{2}t^2e^{-at} \\ L^{-1}\left[\frac{s}{(s + a)^3}\right] &= \frac{1}{2}(2te^{-at} - at^2e^{-at}) \end{aligned}\right\} \quad [31]$$

Applying the inverse transforms given by Equations [31] to Equation [30], after some simplifications the following equation is obtained

$$x_2(t) = 9\omega_{11}^2te^{-\sqrt{3}\omega_{11}t} - 3\sqrt{3}\,\omega_{11}^3\,t^2e^{-\sqrt{3}\omega_{11}t} \quad [32]$$

As Equation [32] shows, the impulsive response of the relaxation suspension system in the case of critical adjustment of the parameters is a function only of the natural undamped frequency ω_{11} of the system. Fig. 4 gives the impulsive response calculated from Equation [32] for critical adjustment of the parameters k_2 and c. The response is calculated for a static deflection of the vehicle of 3, 6, and 9 in. According to B. S. Cain (7), good passenger railroad cars have been built with a static deflection of less than 6 in., but tests indicate that improvements can be obtained by increasing the static deflection to about 12 in. Fig. 5 gives the response of a critically adjusted standard suspension system for the same values of the static deflection.

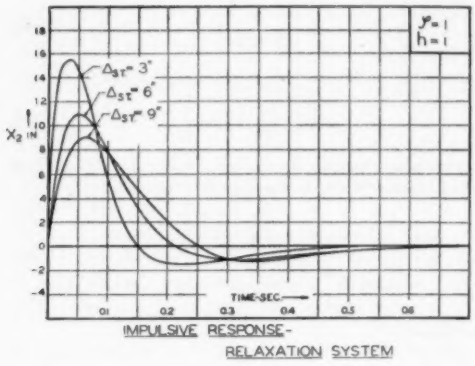

FIG. 4

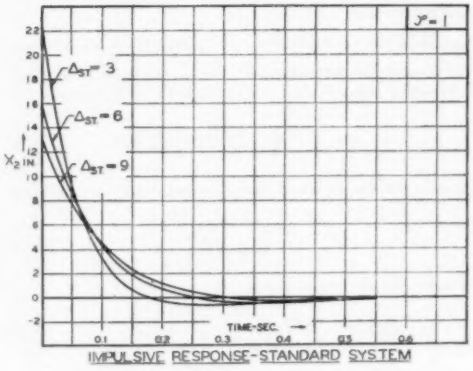

FIG. 5

TRANSIENT MOTION FOR LESS THAN CRITICAL ADJUSTMENT OF PARAMETERS

In the case in which k_2 and c are less than their critical values, the transient motion is oscillatory, and Equation [15] has one real root and two conjugate imaginary roots, which will be designated by

$$s_{(1)} = -\alpha,\ s_{(2)}_{(3)} = -\delta \pm i\rho \quad \ldots\ldots [33]$$

These roots are obtained easily from the impedance transform by Cardan's method for given values of h, ζ, and ω_{11}. In this case the transform $\mathfrak{X}_2(s)$ given by Equation [27] becomes

$$\mathfrak{X}_2(s) = \frac{\omega_{11}^2(1+8h)s + 3\sqrt{3}\,\frac{h}{\zeta}\,\omega_{11}^2}{(s+\alpha)\,(s+\delta+i\rho)\,(s+\delta-i\rho)} \quad \ldots\ldots [34]$$

Expanding Equation [34], one gets

$$\mathfrak{X}_2(s) = \frac{\omega_{11}^2(1+8h)s}{(s+\alpha)[(s+\delta)^2+\rho^2]} + \frac{3\sqrt{3}\,\frac{h}{\zeta}\,\omega_{11}^2}{(s+\alpha)[(s+\delta)^2+\rho^2]} \quad \ldots [35]$$

The following inverse function can be found by means of partial fractions

$$L^{-1}\left\{\frac{1}{(s+\alpha)[(s+\delta)^2+\rho^2]}\right\} = \frac{e^{-\alpha t}}{[(\alpha-\delta)^2+\rho^2]} + \frac{e^{-\delta t}\sin(\rho t-\varphi)}{\rho\sqrt{(\alpha-\delta)^2+\rho^2}} \quad \ldots\ldots [36]$$

where

$$\varphi = \tan^{-1}\frac{\rho}{\alpha-\delta} \quad \ldots\ldots [37]$$

By the same method, the following inverse can be found

$$L^{-1}\left\{\frac{s}{(s+\alpha)[(s+\delta)^2+\rho^2]}\right\} = -\frac{\alpha e^{-\alpha t}}{[(\alpha-\delta)^2+\rho^2]} - \frac{\delta e^{-\delta t}\sin(\rho t-\varphi)}{\rho\sqrt{(\alpha-\delta)^2+\rho^2}} + \frac{e^{-\delta t}\cos(\rho t-\varphi)}{\sqrt{(\alpha-\delta)^2+\rho^2}} \quad \ldots\ldots [38]$$

where φ is given by Equation [37].

By using Equations [36] and [38] the inverse of Equation [35] is found to be

$$x_2(t) = \frac{(B-A\alpha)e^{-\alpha t}}{[(\alpha-\delta)^2+\rho^2]} + \frac{e^{-\delta t}}{\rho\sqrt{(\alpha-\delta)^2+\rho^2}}\,[A\rho\cos(\rho t-\varphi) - A\delta\sin(\rho t-\varphi) + B\sin(\rho t-\varphi)] \quad \ldots [39]$$

where φ is given by Equation [37] and A and B by

$$A = \omega_{11}^2(1+8h), \quad B = 3\sqrt{3}\,\frac{h}{\zeta}\,\omega_{11}^2 \quad \ldots\ldots [40]$$

Equation [39] may be written in the following form

$$x_2(t) = \frac{(B-A\alpha)e^{-\alpha t}}{[(\alpha-\delta)^2+\rho^2]} + \frac{\sqrt{(B-A\delta)^2+(A\rho)^2}}{\rho\sqrt{(\alpha-\delta)^2+\rho^2}}\,e^{-\delta t}\sin(\rho t-\varphi-\gamma) \quad \ldots\ldots [41]$$

where γ is given by

$$\gamma = \tan^{-1}\frac{-A\rho}{B-A\delta}$$

Equation [41] determines the impulsive response of a relaxation suspension system for values of the parameters k_2 and c less than the critical values. As Equation [41] shows, the motion depends on the values of h, ζ, and ω_{11}. From Equation [41] Figs. 6 and 7 have been calculated. Fig. 6 gives the impulsive response of the relaxation system for $\zeta = c/c_c = 1$ and $h = k_2/k_{2c} = 1, 0.5, 0.25, 0.125$, and for a statical deflection of 3 in. (approximately standard railroad practice for passenger cars). Fig. 7 gives the impulsive response for $h = k_2/k_{2c} = 1$ and $\zeta = c/c_c = 1, 0.5, 0.25, 0.125$, and for the same statical deflection of 3 in.

For comparative purposes, Fig. 8 shows the impulsive response of a standard system for $\zeta = c/c_c = 1, 0.75, 0.5, 0.25$, and for the same static deflection in Figs. 6 and 7.

STEADY-STATE MOTION OF A RELAXATION SUSPENSION SYSTEM

In the analysis of the steady-state motion of the relaxation suspension system, we shall consider, as is common practice (8), that the vehicle is moving over a road having an approximately sinusoidal profile given by the equation

$$x_1(t) = X_1\cos\frac{2\pi v}{l} \quad \ldots\ldots [42]$$

where l is the wave length and s the distance from a wave crest

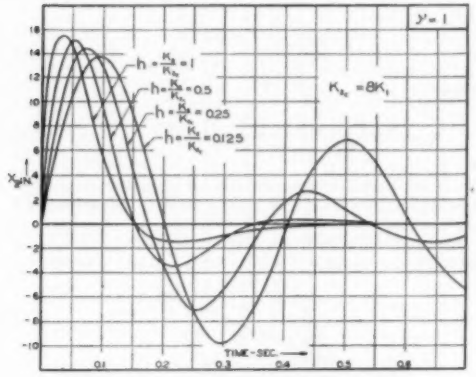

IMPULSIVE RESPONSE - RELAXATION SYSTEM

FIG. 6

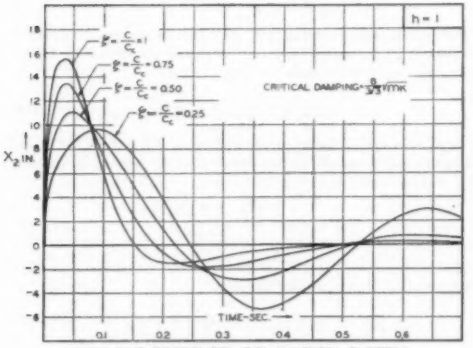

IMPULSIVE RESPONSE - RELAXATION SYSTEM

FIG. 7

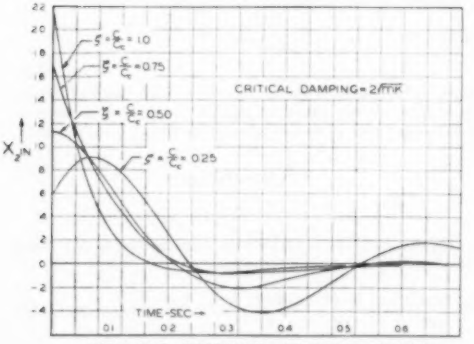

IMPULSIVE RESPONSE - STANDARD SYSTEM

FIG. 8

(see Fig. 9). If the wheels are small enough so that the hub has the same harmonic displacement as the road surface, and if $s = vt$ (v being the velocity of the vehicle), the motion of the hub (coordinate x_1) may be written as

$$x_1(t) = X_1 \cos \omega t \quad \ldots\ldots\ldots\ldots\ldots\ldots [43]$$

where

$$\omega = \frac{2\pi v}{l}$$

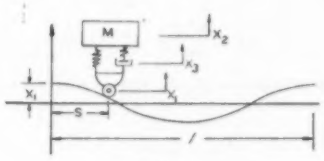

FIG. 9

The equations governing the motion of the system are Equations [1] and [2]. Equation [2] may be written as

$$\frac{k_2}{c}(x_3 - x_1) = \frac{k_2}{c}(x_3 - x_1) + \frac{d}{dt}(x_3 - x_1) \ldots\ldots [44]$$

Multiplying Equation [44] by the factor $e^{\frac{k_2}{c}t}$

$$\frac{k_2}{c} e^{\frac{k_2}{c}t}(x_2 - x_1) = \frac{k_2}{c} e^{\frac{k_2}{c}t}(x_3 - x_1) + e^{\frac{k_2}{c}t}\frac{d}{dt}(x_3 - x_1)$$

$$= \frac{d}{dt}\left[e^{\frac{k_2}{c}t}(x_3 - x_1)\right] \ldots\ldots [45]$$

Integrating Equation [45] from $t = 0$ (instant at which the motion begins) and $t = t$, one gets

$$x_3 - x_1 = \frac{k_2}{c} e^{-\frac{k_2}{c}t} \int_0^t e^{\frac{k_2}{c}\tau}[x_3(\tau) - x_1(\tau)]d\tau \ldots [46]$$

By partial integration, Equation [46] becomes

$$(x_3 - x_2) = -e^{-\frac{k_2}{c}t} \int_0^t e^{\frac{k_2}{c}\tau} \frac{d}{d\tau}[x_3(\tau) - x_1(\tau)]d\tau [47]$$

Substituting Equation [47] into Equation [1], Equation [1] becomes

$$M\frac{d^2x_2(t)}{dt^2} + k_1[x_2(t) - x_1(t)] + k_2 e^{-\frac{k_2}{c}t} \int_0^t e^{\frac{k_2}{c}\tau} \frac{d}{d\tau}$$

$$[x_2(\tau) - x_1(\tau)]\,d\tau = 0 \ldots\ldots\ldots [48]$$

Introducing into Equation [48] the relative displacement $x = x_2 - x_1$

$$M\frac{d^2x(t)}{dt^2} + k_1 x(t) + k_2 e^{-\frac{k_2}{c}t} \int_0^t e^{\frac{k_2}{c}\tau} \frac{dx(\tau)}{d\tau} d\tau$$

$$= -M\frac{d^2x_1(t)}{dt^2} \ldots\ldots\ldots [49]$$

Replacing $x_1(t)$ by the equation of the road profile, Equation [43], Equation [49] becomes

$$M\frac{d^2x(t)}{dt^2} + k_1x(t) + k_2e^{-\frac{k_2}{c}t}\int_0^t e^{\frac{k_2}{c}\tau}\frac{dx(\tau)}{d\tau}\,d\tau = M\omega^2X_1\cos\omega t \quad [50]$$

Equation [50] is identical with the equation for forced vibrations of a single-degree-of-freedom hereditary system, in the case in which the generalized force is sinusoidal (9).

Differentiating Equation [50]

$$M\frac{d^3x(t)}{dt^3} + k_1\frac{dx(t)}{dt} - \frac{k_2}{c}\left[k_2e^{-\frac{k_2}{c}t}\int_0^t e^{\frac{k_2}{c}\tau}\frac{dx(\tau)}{d\tau}\,d\tau\right] + k_2\frac{dx(t)}{dt} = -M\omega^2X_1\sin\omega t \quad [51]$$

By replacing in Equation [51] the expression in brackets by its equivalent expression

$$k_2e^{-\frac{k_2}{c}t}\int_0^t e^{\frac{k_2}{c}\tau}\frac{dx(\tau)}{d\tau}\,d\tau = -M\frac{d^2x(t)}{dt^2} - k_1x(t) + M\omega^2X_1\cos\omega t$$

obtained from Equation [50], one finally obtains the equation

$$\frac{d^3x(t)}{dt^3} + \frac{k_2}{c}\frac{d^2x(t)}{dt^2} + \left(\frac{k_1}{M} + \frac{k_2}{M}\right)\frac{dx(t)}{dt} + \frac{k_1k_2}{cM}x(t) = \frac{k_2}{c}\omega^2X_1\cos\omega t - \omega^2X_1\sin\omega t \quad [52]$$

Introducing the following notation into Equation [52]

$$\omega_{11}^2 = \frac{k_1}{M};\quad \omega_{22}^2 = \frac{k_2}{M};\quad \Omega = \frac{k_2}{c} \quad [53]$$

Equation [52] becomes

$$\frac{d^3x(t)}{dt^3} + \Omega\frac{d^2x(t)}{dt^2} + (\omega_{11}^2 + \omega_{22}^2)\frac{dx(t)}{dt} + \Omega\omega_{11}^2x(t) = \Omega\omega^2X_1\cos\omega t - \omega^3X_1\sin\omega t \quad [54]$$

Let us assume the particular solution (forced vibration) of Equation [54] to be of the form

$$x(t) = X\cos(\omega t - \varphi) \quad [55]$$

Substituting Equation [55] into Equation [54]

$$X = \omega^2X_1\frac{\sqrt{\{\Omega^2(\omega_{11}^2 - \omega^2) - \omega^2[\omega^2 - (\omega_{11}^2 + \omega_{22}^2)]\}^2 + (\Omega\omega\omega_{22}^2)^2}}{\Omega^2(\omega_{11}^2 - \omega^2)^2 + \omega^2[\omega^2 - (\omega_{11}^2 + \omega_{22}^2)]^2} \quad [56]$$

$$\varphi = \tan^{-1}\frac{\Omega\omega\omega_{22}^2}{\Omega^2(\omega_{11}^2 - \omega^2) - \omega^2[\omega^2 - (\omega_{11}^2 + \omega_{22}^2)]} \quad [57]$$

Introducing the following notations

$$\theta = \frac{\Omega}{\omega_{11}} = 3\sqrt{3}\,\frac{h}{\zeta};\quad r = \frac{\omega}{\omega_{11}} \quad [58]$$

$$\gamma = \frac{\omega_{22}}{\omega_{11}} = \sqrt{\frac{k_2}{k_1}} = \sqrt{8}h \quad [59]$$

(where h and ζ are given by Equations [26]) into Equations [56] and [57], the expressions for the relative amplitude X and phase angle φ become

$$X = X_1r^2\Phi \quad [60]$$

and

$$\varphi = \tan^{-1}\frac{\theta r\gamma^2}{\theta^2(1 - r^2) - r^2[r^2 - (1 + \gamma^2)]} \quad [61]$$

where

$$\Phi = \frac{\sqrt{\{\theta^2(1 - r^2) - r^2[r^2 - (1 + \gamma^2)]\}^2 + (\theta r\gamma^2)^2}}{\theta^2(1 - r^2)^2 + r^2[r^2 - (1 + \gamma^2)]} \quad [62]$$

The factor Φ given by Equation [62] has previously been calculated (9) as a function of r for various values of the parameters θ and γ.

The amplitude of the forced vibration X_2 can be found from the vector diagram shown in Fig. 10, when X_1, X, and φ are known.

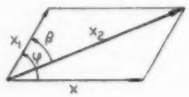

FIG. 10

In fact, from Fig. 10 one has

$$X_2^2 = X_1^2 + X^2 + 2X_1X\cos\varphi \quad [63]$$

Substituting into Equation [63] the expression for the relative amplitude X given by Equation [60], the amplitude of forced vibration X_2 of the vehicle becomes

$$X_2 = X_1\sqrt{1 + (r^2\Phi)^2 + 2r^2\Phi\cos\varphi} \quad [64]$$

The phase angle β between the motion of the hub of the wheel (amplitude X_1) and the forced vibration of the vehicle (amplitude X_2) can be found from Fig. 10 to be

$$\beta = \cos^{-1}\frac{X_1^2 + X_2^2 - X^2}{2X_1X_2} \quad [65]$$

Substituting for X and X_2 the expressions given by Equations [60] and [64] Equation [65] becomes

$$\beta = \cos^{-1}\frac{1 + r^2\Phi\cos\varphi}{\sqrt{1 + (r^2\Phi)^2 + 2r^2\Phi\cos\varphi}} \quad [66]$$

The ratio between the amplitude of the forced vibration X_2 and the amplitude of the disturbance X_1 (Equation [64]) is represented graphically in Figs. 11, 12, and 13, for values

$$\theta = 3\sqrt{3}\,\frac{h}{\zeta}$$

equal to 0.1, 1, and 10, and for values $\gamma = \sqrt{8}h$ ranging from 0.25 to 4. The values of the phase angle β (Equation [66]) are given for the same sets of values of θ and γ in Figs. 14, 15, and 16.

Appendix

TRANSIENT RESPONSE OF STANDARD SUSPENSION SYSTEM

The standard type of vehicle suspension is represented in Fig. 2. The equation of motion of the system is

$$M\frac{d^2x_2(t)}{dt^2} + c\left[\frac{dx_2(t)}{dt} - \frac{dx_1(t)}{dt}\right] + k_1[x_2(t) - x_1(t)] = 0 \quad [67]$$

Let the co-ordinate x_1 perform a unit impulse $U'(t)$ previously defined. Replacing the co-ordinate x_1 by $U'(t)$, Equation [67] becomes

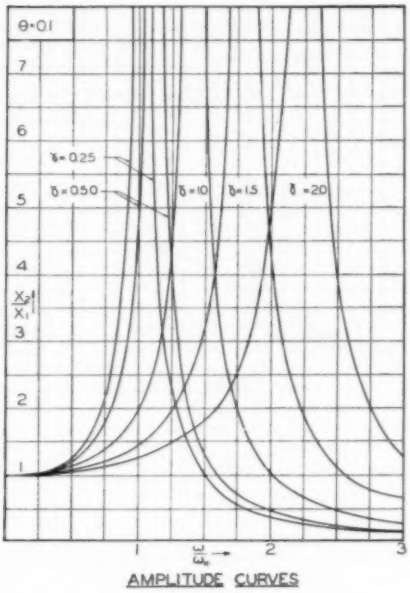

FIG. 11

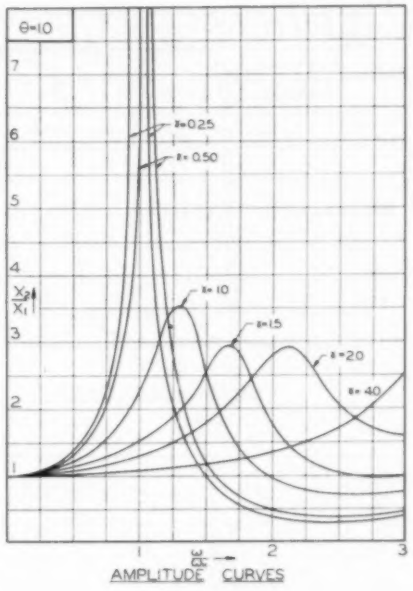

FIG. 12

$$M\frac{d^2x_2(t)}{dt^2} + c\frac{dx_2(t)}{dt} + k_1x_2(t) = k_1U'(t) + cU''(t) \quad [68]$$

If the system is supposed at rest when the impulse is applied, the Laplace transform of Equation [68] is

$$Ms^2\mathfrak{X}_2(s) + cs\mathfrak{X}_2(s) + k_1\mathfrak{X}_2(s) = k_1 + cs \quad [69]$$

Solving Equation [69] for the transform $\mathfrak{X}_2(s)$, one obtains

$$\mathfrak{X}_2(s) = \frac{k_1 + cs}{Ms^2 + cs + k_1} \quad [70]$$

Introducing the following notation

$$c_c = 2M\omega_{11},\ \omega_{11}^2 = \frac{k_1}{M},\ \zeta = \frac{c}{c_c} \quad [71]$$

into Equation [70]

$$\mathfrak{X}_2(s) = \frac{\omega_{11}^2 + 2\omega_{11}\zeta s}{s^2 + 2\omega_{11}\zeta s + \omega_{11}^2} \quad [72]$$

In the critically adjusted system, ζ equals 1, and Equation [72] becomes

$$\mathfrak{X}_2(s) = \frac{\omega_{11}^2 + 2\omega_{11}s}{(s + \omega_{11})^2} \quad [73]$$

The inverse of Equation [73] is readily found to be

$$x_2(t) = 2\omega_{11}e^{-\omega_{11}t} - \omega_{11}^2te^{-\omega_{11}t} \quad [74]$$

Equation [74] is the impulsive response of the standard suspension system and was used to calculate the curves for critical response of the system given in Fig. 5.

In the case in which ζ is less than 1 (c less than $2M\omega_{11}$), the de-

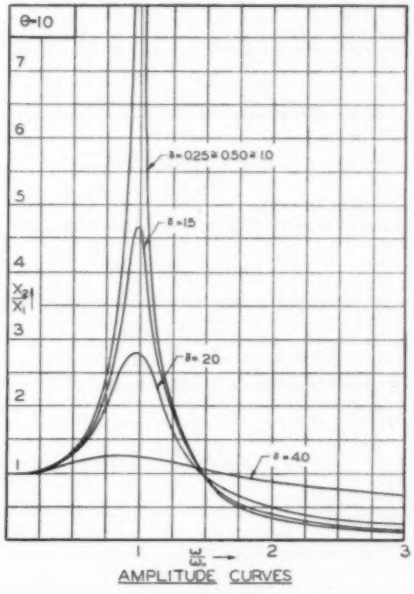

FIG. 13

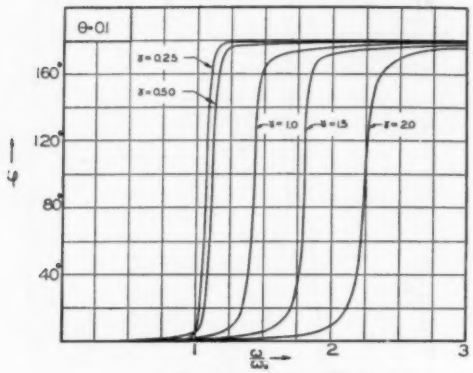

PHASE ANGLE CURVES

FIG. 14

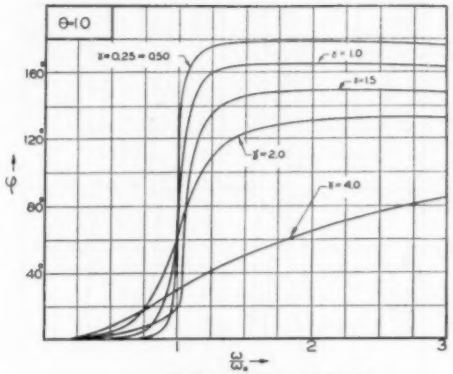

PHASE ANGLE CURVES

FIG. 16

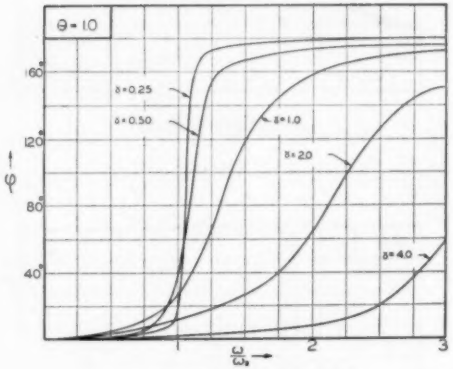

PHASE ANGLE CURVES

FIG. 15

nominator of Equation [72] has two conjugate imaginary roots given by

$$s = -\xi \pm i\eta \quad \ldots\ldots [75]$$

Using the roots given by Equation [75], Equation [72] becomes

$$x_\xi(s) = \frac{\omega_{11}^2 + 2\omega_{11}\zeta s}{(s+\xi)^2 + \eta^2} \quad \ldots\ldots [76]$$

The inverse of Equation [76] is readily found to be

$$x_\xi(t) = \frac{\omega_{11}}{\eta}\sqrt{(\omega_{11} - 2\zeta\xi)^2 + (2\zeta\eta)^2}\, e^{-\xi t} \sin(\eta t - \varphi) \quad \ldots\ldots [77]$$

where

$$\varphi = \tan^{-1}\frac{-2\zeta\xi}{(\omega_{11} - 2\zeta\xi)}$$

Equation [77] gives the impulsive response of the standard suspension system for less than critical damping in the system and was used to calculate the curves given in Fig. 8.

BIBLIOGRAPHY

1 "Perfectionnement à la suspension des véhiculesroutiers. Amortisseur á relaxation," by Christian Bourcier de Carbon, Comptes-Rendus de l'Académie des Sciences de Paris, France, vol. 225, 1947, pp. 722–724.

2 "Laplace Transformation. Theory and Engineering Applications," by W. T. Thomson, Prentice-Hall, Inc., New York, N. Y., 1950.

3 "Modern Operational Mathematics in Engineering," by Ruel V. Churchill, McGraw-Hill Book Company, Inc., New York, N. Y., 1944.

4 "Mathematical Methods in Engineering," by Th. von Kármán and Maurice A. Biot, McGraw-Hill Book Company, Inc., New York, N. Y., 1940.

5 "Mechanical Vibrations," by J. P. Den Hartog, McGraw-Hill Book Company, Inc., New York, N. Y., 1940.

6 "Theory of Equations," by J. V. Uspensky, McGraw-Hill Book Company, Inc., New York, N. Y., 1948.

7 "Vibrations of Rail and Road Vehicles," by B. S. Cain, Pitman Publishing Corporation, New York, N. Y., 1940.

8 "Vibration Analysis," by N. O. Myklestad, McGraw-Hill Book Company, Inc., New York, N. Y., 1944.

9 "Vibrations of Elastic Systems Having Hereditary Characteristics," by Enrico Volterra, JOURNAL OF APPLIED MECHANICS, Trans. ASME, vol. 72, 1950, pp. 363–371.

Limit Design of a Full Reinforcement for a Circular Cutout in a Uniform Slab[1]

By H. J. WEISS,[2] W. PRAGER,[3] AND P. G. HODGE, JR.[4]

A thin square slab with a central circular cutout reinforced by a concentric ring is subjected to uniform tensions T_x and T_y on the exterior edges. It is desired to determine the dimensions of the reinforcement if the slab is not to collapse under any load which could be supported by a similar slab without any cutout or reinforcement. It is assumed that the slab and reinforcement are made of a perfectly plastic material which satisfies the Tresca yield criterion of maximum shearing stress, and that the dimensions of the reinforcement are such that it may reasonably be approximated by a curved beam. Under these assumptions, an upper bound on the necessary thickness of the reinforcement for any given radius is obtained. Certain practical limitations of the theory are discussed.

Statement of Problem

CONSIDER first a uniform plane square slab of side $2d$ and thickness h, subjected to uniform tensions T_x and T_y on its edges, Fig. 1. At time $t = 0$ let T_x and T_y be sufficiently small so that the deformations in the slab are all very small compared to 1. Then, let the tensions be slowly increased proportionally, so that at time t they are $\lambda(t)\ T_x$, $\lambda(t)\ T_y$ where $\lambda(t)$ is a monotonically increasing function and $\lambda(0) = 1$. For some critical value of λ, the deformations no longer will be considered small. It will, of course, be necessary to adopt some definite criterion of "small" deformations. Such a criterion might be that the total greatest extension of the slab be less than some small constant times $2d$. The resulting critical tensions will be called a "yield load" and will be denoted by $\lambda_1 T_x$, $\lambda_1 T_y$. Any load less than a yield load will be called a "safe load."

Next, consider the same slab with a central circular cutout of radius a, Fig. 2. The material which has been cut out formerly participated in carrying the load on the slab. Therefore its removal will weaken the slab, so that the yield load will now be $\lambda_2 T_x$, $\lambda_2 T_y$ where $\lambda_2 < \lambda_1$.

Finally, let the cutout be reinforced by a concentric annulus of thickness δ, inner radius a, and total thickness H, Fig. 3. Since $H > h$, this will have the effect of strengthening the cutout slab so that the critical tensions will now be $\lambda_3 T_x$, $\lambda_3 T_y$, where $\lambda_3 > \lambda_2$.

The problem then is to determine the smallest value of H for which the reinforced cutout slab will have the same critical tensions as the original slab, i.e., such that $\lambda_3 = \lambda_1$.

The preceding problem is a completely defined "physical"

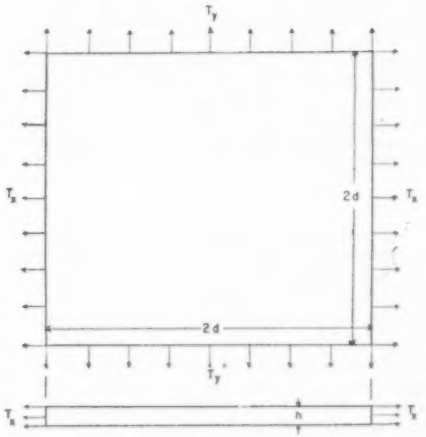

Fig. 1 Plane Slab

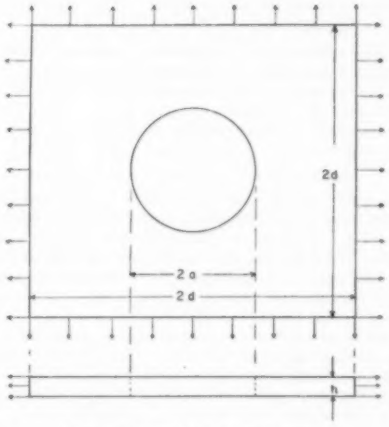

Fig. 2 Plane Slab With Cutout

---

[1] The results presented in this paper were obtained in the course of research conducted under Contract N7onr-35810 between the Office of Naval Research and Brown University.

[2] Assistant Professor of Applied Mathematics, Brown University, Providence, R. I.

[3] Professor of Applied Mechanics, Brown University. Mem. ASME.

[4] Assistant Professor of Mathematics, University of California, Los Angeles, Calif. Jun. ASME.

Presented at the West Coast Conference of the Applied Mechanics Division, Los Angeles, Calif., June 26–28, 1952, of The American Society of Mechanical Engineers.

Discussion of this paper should be addressed to the Secretary, ASME, 29 West 39th Street, New York, N. Y., and will be accepted until October 10, 1952, for publication at a later date. Discussion received after the closing date will be returned.

Note: Statements and opinions advanced in papers are to be understood as individual expressions of their authors and not those of the Society. Manuscript received by ASME Applied Mechanics Division, March 4, 1952.

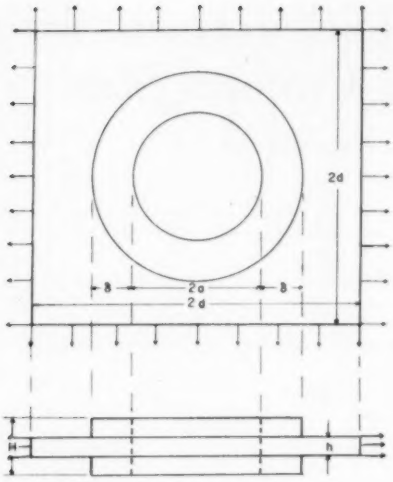

FIG. 3 PLANE SLAB WITH REINFORCED CUTOUT

problem. For a given slab of a given material, and for a given tension ratio T_x/T_y there will exist a unique answer which could, for example, be determined experimentally (1).[5] However, if general results are desired, such a procedure would be expensive and time-consuming. Therefore it is desired to find some mathematical method which can be used to predict the correct value of H for a slab of a material with given properties.

The solution of a physical problem by mathematical methods involves essentially three steps which shall be taken up in order in the succeeding sections.[6] These steps are as follows:

1 The definition of a mathematical model which describes the salient features of the physical problem.

2 Manipulation of the components of the model in accord with the laws of mathematics.

3 Interpretation and evaluation of the results in terms of the physical problem.

PREREQUISITES OF A MATHEMATICAL MODEL

The mathematical model of a physical problem consists of an idealization of the actual problem into well-defined mathematical components. Consider first the problem of the slab without a cutout. The actual physical slab is three-dimensional and contains minor surface irregularities; the mathematical model will be a two-dimensional plane square. The physical tensions are applied through clamps of some sort which produce certain nonuniform stress distributions near the edges; the model has uniform tensions applied at the edges. The physical material is neither completely homogeneous nor isotropic and has a complicated stress-strain curve; the model is taken to be homogeneous and isotropic and some simplified stress-strain curve is assumed; and so on. The process of constructing a mathematical model is such a common one that it is often done unconsciously.

[5] Numbers in parentheses refer to the Bibliography at the end of the paper.

[6] A more complete discussion of the relation between the physical and mathematical approach to a problem will be found in many mechanics texts, for example (2). The present discussion is included because of the comparatively recent development of the theory of limit analysis, and the consequent uncertainty in the minds of many engineers as to value of the theory.

Obviously, the solution of a problem with these simplifications will not be the precise solution of the original physical problem. However, if the choice of model has been a good one, the results will be nearly the same. It follows that a successful mathematical model must satisfy two conditions simultaneously:

1 The formulation must be sufficiently simple so that mathematical results can be obtained.

2 The results must be sufficiently accurate for the purpose for which they are intended.

It may be that there is no common ground for these two requirements, i.e., that the most complicated mathematical problem which can be solved will yield physical results which are unsatisfactory. In this case the theoretical engineer will try to apply more powerful mathematics to overcome his previous mathematical difficulties. The experimental engineer, on the other hand, will use the mathematical results so far obtained to design economical and informative experiments. In either case, the time spent in obtaining the first inadequate mathematical results has not been wasted.

MATHEMATICAL MODEL FOR THE PROBLEM

It is convenient to consider the reinforced slab as consisting of a cylindrical hub joined to the unreinforced slab, Fig. 4(*a*). At a moderate distance from the hub the state of stress in the slab is approximately plane. Near the hub, however, the state of plane stress cannot subsist, and this hub itself cannot be in a state of plane stress. Thus a solution of the problem so defined would

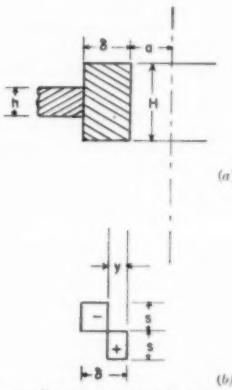

FIG. 4 (*a*) "HUB" AND SLAB; (*b*) FULLY PLASTIC STRESS DISTRIBUTION FOR HUB

require the consideration of three-dimensional stress distributions and consequently would be rather difficult. A cruder model is therefore proposed in which the hub is treated as a curved beam with rectangular cross section of depth δ and width H while the slab is considered to be in a state of plane stress throughout. In the elastic range this approximation has proved very successful (3). Obviously, it will be satisfactory only if H/h is not too great, since otherwise the question of the carrying width of the hub will arise.

Next, the behavior of the material must be considered. Most actual materials have stress-strain curves of the type indicated in Fig. 5(*a*) or 5(*b*). The stress-strain curve for the mathematical model is given in Fig. 5(*c*). The essential simplification is that the idealized (perfectly plastic) curve will tolerate even infinite

strains with no increase in stress above the yield stress. Thus the idealized curve is a rather poor approximation to Fig. 5(*a*), but appears to be a reasonable one for Fig. 5(*b*), *provided that the strains remain small*. This proviso will not necessarily be enforced, so that any results must be viewed with suspicion. However, on the basis of the argument in the preceding section the present approach appears to be worth developing.

The yield stress occurring in the ideal stress-strain diagram, Fig. 5(*c*), must be extended to two-dimensional states of stress.

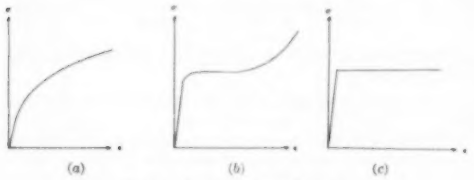

FIG. 5 STRESS-STRAIN CURVES
(*a*, *b*, Real materials; *c*, perfectly plastic material.)

The Tresca yield condition (4) is here adopted and may be represented conveniently by the hexagon *ABCDEF* in Fig. 6. Here σ_1, σ_2 are the principal stresses in the plane of the problem, the third principal stress normal to this plane being zero, and s is the yield stress in simple tension. Plane states of stress at the yield limit are represented by points on the sides of the hexagon. In particular, the vertex *A* represents a state of uniaxial tension, the vertex *B* a state of biaxial tension, and the center *G* of the side *A-F* a state of pure shear.

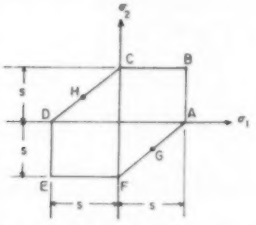

FIG. 6 TRESCA'S YIELD CONDITION FOR PLANE STRESS

Finally, the criterion for "small deformations" must be incorporated into the model. Let the original tensions T_x, T_y be such that the slab, Fig. 3, is everywhere elastic; i.e., the stress point is everywhere in the interior of the yield hexagon, Fig. 6. As λ increases, plastic regions, i.e., regions where the stress point is on the yield hexagon, will develop. At first the deformation of the material within these regions remains restricted by the surrounding elastic material which is not capable of large deformations. When the plastic regions extend entirely across the slab, however, large (infinite) deformations become possible. The yield loads will be defined as the loads λT_x, λT_y for which such large deformations first become possible. For the plane slab, Fig. 1, plastic behavior obviously occurs instantaneously throughout the slab when λT_x, λT_y correspond to any point on the hexagon in Fig. 6.

In conclusion, then, the following mathematical problem is to be solved. A cylindrical hub of inner radius a, and thickness δ is rigidly attached to a centered cutout of radius $a + \delta$ in a square slab of thickness h and side $2d$. The whole is made of a perfectly plastic material satisfying the Tresca yield condition. It is desired to find the minimum height H of the cylindrical hub such that the plate will not suffer infinite deformations under any load within the hexagon of Fig. 6.

LIMIT-DESIGN THEOREM

The solution to the problem is based on a limit-design theorem recently proved by Drucker, Greenberg, and Prager (5). According to this theorem, a given system of loads can be considered as safe, if stresses can be found which (*a*) are in equilibrium with the given loads and (*b*) do nowhere reach the limits set by the yield criterion. In the applications of this theorem the considered stresses may be allowed actually to reach the limits set by the yield criterion. While the existence of an equilibrium system of stresses of this type does not permit the conclusion that the given loads are safe, it establishes the fact that safe loads can be obtained by reducing all given loads by a fixed, arbitrarily small percentage.

YIELD CONDITION FOR HUB

Within the framework of beam theory, the state of stress at a generic cross section of a beam is specified by the stress resultants, that is, bending moment, axial force, and shear force. For solid cross sections, the shearing stresses caused by the shear force are negligible in comparison with the axial stresses caused by bending moment and axial force and will be neglected in the model. By the yield condition, Fig. 6, the intensity of these axial stresses is restricted to the interval from $-s$ to s. This condition imposes certain restrictions on the bending moments and axial forces which the beam can support.

To find limiting combinations of bending moment and axial force, consider a fully plastic stress distribution of the type shown in Fig. 4(*b*): part of the cross section is stressed to the yield limit in tension, the rest to the yield limit in compression. Let y denote the depth of the layer stressed in tension or the depth of the layer stressed in compression, whichever is smaller, and let the bending moments be computed about the center line. The absolute values of bending moment M and the axial force N corresponding to such a fully plastic stress distribution are then given by

$$|M| = Hy(\delta - y)s \quad [1]$$

$$|N| = H(\delta - 2y)s \quad [2]$$

Elimination of y between these equations leads to

$$4sH|M| + N^2 \leq s^2H^2\delta^2 \quad [3]$$

as the yield condition for the stress resultants. In particular if $N = 0$, the bending moment is limited by

$$|M| \leq M_0 = sH\delta^2/4 \quad [4]$$

and if $M = 0$, the axial force is limited by

$$|N| \leq N_0 = sH\delta \quad [5]$$

With M_0 and N_0 defined in this manner, the yield condition [3] may be written in the form

$$\left|\frac{M}{M_0}\right| + \left(\frac{N}{N_0}\right)^2 \leq 1 \quad [6]$$

When M/M_0 and N/N_0 are used as rectangular co-ordinates, Fig. 7, the domain of safe stress resultants is bounded by two parabolic arcs.

The loads which the slab transmits to the hub may be considered as safe if stress resultants M, N can be found which (*a*)

are in equilibrium with these loads, and (*b*) do nowhere reach the limits set by the yield condition [6].

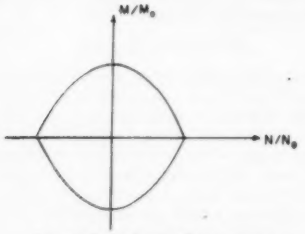

FIG. 7 SAFE STRESS RESULTANTS

BIAXIAL TENSION

The case of biaxial tension furnishes a particularly simple illustration of this approach. Here, an equilibrium distribution of stresses in the slab which do not violate the Tresca condition is obtained by assuming the slab to be in a uniform state of biaxial tension represented by the point B in Fig. 6. Under this assumption, the slab transmits to the hub a uniformly distributed radial force hs per unit length of the circumference of radius $a + \delta$. This load can be equilibrated in the hub by a constant axial force.

$$N = (a + \delta)hs \quad \ldots\ldots [7]$$

Since this axial force must not exceed the value N_0 of Equation [5], the hub must be designed so that

$$H\delta = (a + \delta)h \quad \ldots\ldots [8]$$

or

$$\frac{H}{h} = \frac{1 + (\delta/a)}{\delta/a} \quad \ldots\ldots [9]$$

UNIAXIAL TENSION

In the case of uniaxial tension, it is not quite so easy to find stress resultants in the hub which satisfy the conditions for the limit-design theorem. Here, an equilibrium distribution of stresses in the slab which do not violate the Tresca condition is obtained by assuming the slab to be in a uniform state of uniaxial tension represented by the point A in Fig. 6. The stress resultants in the hub can then be determined from equilibrium considerations if the bending moment at the cross section $\theta = 0$ is known, Fig. 8. Indeed, the equilibrium of that portion of the system which lies, say, below the x-axis in Fig. 8, requires the equal axial forces at the cross sections $\theta = 0$ and $\theta = \pi$ to vanish so that the bending moment X is the only nonvanishing stress resultant at the cross section $\theta = 0$.

In terms of this statically indeterminate quantity, the stress resultants M and N at a generic cross section θ are obtained by considering the equilibrium of the portion $xOAB$ in Fig. 8. One finds

$$M = X + \frac{1}{2} sah(a + \delta) \sin^2 \theta \quad \ldots\ldots [10]$$

$$N = sh(a + \delta) \sin^2 \theta \quad \ldots\ldots [11]$$

With the use of Equations [4] and [5], Equations [10] and [11] can be written as follows

$$\frac{M}{M_0} = \frac{X}{M_0} + 2\frac{h}{H}\frac{a}{\delta}\left(\frac{a}{\delta} + 1\right)\sin^2 \theta \quad \ldots\ldots [12]$$

$$\frac{N}{N_0} = \frac{h}{H}\left(\frac{a}{\delta} + 1\right)\sin^2 \theta \quad \ldots\ldots [13]$$

In view of the last of these equations, the first is equivalent to

$$\frac{M}{M_0} = \frac{X}{M_0} + 2\frac{a}{\delta}\frac{N}{N_0} \quad \ldots\ldots [14]$$

and the yield condition [6] assumes the form

$$\left|\frac{X}{M_0} + 2\frac{a}{\delta}\frac{N}{N_0}\right| \leq 1 - \left(\frac{N}{N_0}\right)^2 \quad \ldots\ldots [15]$$

For the discussion of the Inequality [15], the following facts are of importance:

1 The ratios X/M_0 and N/N_0 cannot exceed 1 in absolute value.

2 According to Equation [13], the ratio N/N_0 is nonnegative and monotonically increasing in the interval $0 \leq \theta \leq \pi/2$ which alone needs to be considered on account of the symmetry of the problem.

3 According to Equation [12], the ratio M/M_0 is monotonically increasing in this interval so that the ratio X/M_0 must be negative if the bending moment is to be kept small at $\theta = \pi/2$ where the axial force assumes its maximum value.

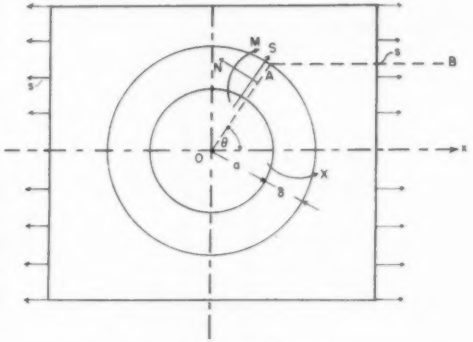

FIG. 8 UNIAXIAL TENSION

To discuss the Inequality [15], plot each side as a function of N/N_0. The parabola in Fig. 9 represents the right-hand side of Inequality [15]; the line representing the left-hand side depends on the values of a/δ and X/M_0. For instance, the line A-B-C corresponds to the values $a/\delta = 1$, $X/M_0 = -0.75$. In this case, the highest value of N/N_0 for which Inequality [15] remains satisfied is given by the abscissa of the point C. According to Equation [13], this maximum value of N/N_0 equals (h/H) $[(a/\delta) + 1]$ and is assumed at $\theta = \pi/2$. Since the line A-B-C is based on a specific value of a/δ, the abscissa of the point C furnishes a compatible value of h/H. If H is to be kept as small as possible for the given a, h, and the assumed δ, the ratio h/H and hence the abscissa of C should be maximized. This is accomplished by replacing the line A-B-C by the line A'-B'-C', i.e., by choosing $X/M_0 = -1$.

Not for all values of a/δ, however, does the choice $X/M_0 =$

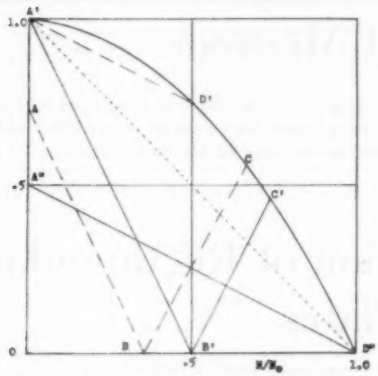

FIG. 9 DISCUSSION OF INEQUALITY [15]

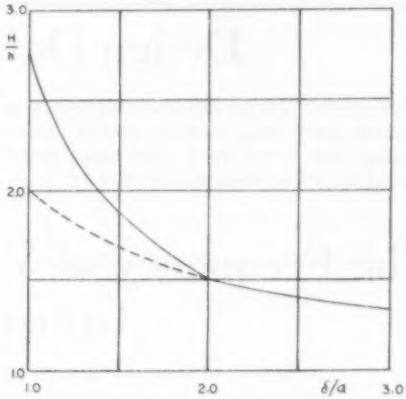

FIG. 10 DIMENSIONS OF SAFE REINFORCEMENTS

—1 lead to the most favorable design. The line A'-D' in Fig. 9 corresponds to the values $a/\delta = 1/4$, $X/M_0 = -1$, and yields 0.5 as the largest value of N/N_0 for which Inequality [15] remains satisfied. The line A''-D'', on the other hand, corresponds to the same value of a/δ but to $X/M_0 = -0.5$, and yields 1.0 as the largest admissible value of N/N_0.

Obviously, the line A'-D'' in Fig. 9, which corresponds to $a/\delta = 1/2$, $X/M_0 = -1$ represents the border-line case separating these two manners of choosing X/M_0.

When $a/\delta \geq 1/2$, one must choose $X/M_0 = -1$. The largest admissible N/N_0 is then found by substituting this value of X/M_0 into Inequality [15] and using the equality sign

$$-1 + 2\frac{a}{\delta}\frac{N}{N_0} = 1 - \left(\frac{N}{N_0}\right)^2 \quad \ldots\ldots [16]$$

or

$$\frac{N}{N_0} = -\frac{a}{\delta} + \sqrt{\left(\frac{a}{\delta}\right)^2 + 2} \quad \ldots\ldots [17]$$

Equating this to the value of N/N_0 obtained by setting $\sin\theta = 1$ in Equation [13], and solving for H/h, one finds that

$$\frac{H}{h} = \frac{1 + (\delta/a)}{\sqrt{[1 + 2(\delta/a)^2]^{1/2} - 1}} \text{ for } \frac{\delta}{a} \leq 2 \quad \ldots\ldots [18]$$

On the other hand, when $\delta/a \geq 2$, the discussion based on Fig. 9 shows that the maximum value of N/N_0 can be made to equal 1 by a suitable choice of X/M_0; thus

$$\frac{H}{h} = \frac{1 + (\delta/a)}{\delta/a} \text{ for } \frac{\delta}{a} \geq 2 \quad \ldots\ldots [19]$$

The full line in Fig. 10 shows H/h versus δ/a according to Equations [18] and [19]; the dotted line corresponds to Equation [9]. It is seen that a reinforcement which is safe for uniaxial tension is also safe for biaxial tension.

OTHER CASES OF LOADING

The points on and inside the hexagon in Fig. 6 represent safe states of loading for a uniform slab without cutout. From the symmetry of the hexagon with respect to the origin and from its convexity the following results are obtained:

(*a*) If T_x, T_y is a safe load, then $-T_x$, $-T_y$ is also a safe load.[7]

(*b*) If T_x', T_y' and T_x'', T_y'' are each safe loads, then $\mu T_x' + (1-\mu)T_x''$, $\mu T_y' + (1-\mu)T_y''$ is a safe load for any $0 \leq \mu \leq 1$.

It is readily seen that any safe state of loading can be obtained from the stress-free state (the origin in Fig. 6), the state of uniaxial tension (points A or C in Fig. 6), and the state of biaxial tension (point B in Fig. 6), by means of the operations indicated under (*a*) and (*b*). Since the domain of safe stress resultants for the hub, Fig. 7, is also convex and symmetric with respect to the origin, it follows that a reinforcement which is safe when the slab is stressed to its capacity in uniaxial tension and in biaxial tension, will also be safe when the slab is stressed to its capacity in any other manner. Thus the reinforcement designed according to the full line in Fig. 10 restores the yield strength of the slab with cutout to the full value of the uniform slab without cutout for any type of loading represented by a point on the hexagon in Fig. 6.

BIBLIOGRAPHY

1 "Welded Reinforcement of Openings in Structural Steel Members" (First Progress Report), by D. Vasarhelyi and R. A. Hechtman, Contract NObs-50238, University of Washington, Seattle, Wash.

2 "Principles of Mechanics," by J. L. Synge and B. A. Griffith, McGraw-Hill Book Company, Inc., New York, N. Y., 1949. Sec. 1.1.

3 "On Stresses in a Plate With a Circular Hole," by S. Timoshenko, *Journal of The Franklin Institute*, vol. 197, 1924, pp. 505–516.

4 "Mémoire sur l'écoulement des corps solides," by H. Tresca, *Mémoires présentes par divers savants*, vol. 18, 1868, pp. 733–799.

5 "Extended Limit Design Theorems for Continuous Media," by D. C. Drucker, H. J. Greenberg, and W. Prager, *Quarterly of Applied Mathematics*, vol. 9, 1952, pp. 381–389.

[7] The possibility of buckling is not considered in the mathematical model, and must be discussed separately in relation to the physical problem.

Design Data and Methods

It is important that the data contained in technical papers be made readily available to designing engineers. In order to satisfy these needs of industry, this section of the Journal includes a concise presentation of data and information drawn chiefly from papers previously published by the Applied Mechanics Division of The American Society of Mechanical Engineers.

The Frequency of Vibration of Rectangular Isotropic Plates

By R. F. S. HEARMON,[1] PRINCES RISBOROUGH, AYLESBURY, BUCKS, ENGLAND

The object of the present paper is to collect the theoretical estimates available for calculating the frequency of vibration of rectangular isotropic plates subjected to various boundary conditions.

Nomenclature

The following nomenclature is used in the paper:

a, b = lengths of sides of plate.
$D = Eh^3/12(1 - \nu^2)$
E = Young's modulus of elasticity
f = frequency of vibration
h = plate thickness
$k = \omega/\sqrt{D/\rho h a^4} = \omega a^2\sqrt{M/D}$
$k' = \omega/\sqrt{D/\rho h b^4} = \omega b^2\sqrt{M/D}$
$M = \rho h$ = mass per unit area of plate material
m, n = positive integers
$r = a/b$
θ = skew angle (see Table 4)
ρ = density of plate material
ν = Poisson's ratio of plate material
$\omega = 2\pi f$ = angular frequency

Solving the Differential Equation

The differential equation to be solved, and the mathematical expressions for the boundary conditions are discussed by Timoshenko (1),[2] who gives the exact solution for a plate with all edges simply supported as

$$\omega a^2\sqrt{M/D} = \pi^2(m^2 + r^2n^2) \quad \ldots\ldots\ldots\ldots [1]$$

A solution also has been given by Voigt (2) for a plate with two opposite edges simply supported and the other two free, but this solution does not appear to have been evaluated numerically.

Apart from these two treatments, exact solutions are not available, and the frequencies have to be estimated by an approximate procedure, usually that of Rayleigh-Ritz (1). Ritz himself (3) calculated the frequencies of a square plate with all edges free up to the 35th mode, and his results have been compared with experiment by Waller (4). The values obtained by the approximate procedure depend somewhat on the value assumed for Poisson's ratio, and the extent of this dependence for the square plate with all edges free is discussed by Waller. Ritz assumed $\nu = 0.225$ in his calculations, but the value assumed by the other workers quoted in the present paper is $\nu = 0.3$.

In 1938, Iguchi (5) summarized and extended his earlier work in an important paper which has been overlooked in recent discussions. Iguchi calculated the fundamental frequencies for values of r of 0, 1/5, 2/5, 1/2, 2/3, 1, 3/2, 2, 5/2, 3, ∞, and for the following edge conditions:

(*a*) One edge clamped, remainder simply supported.
(*b*) Opposite edges clamped, remainder simply supported.
(*c*) All edges clamped.

Iguchi also calculated the frequencies of the modes of a square plate up to the 9th for edge conditions (*a*), to the 18th for edge conditions (*b*), and to the 6th for edge conditions (*c*).

More recently, Young (6) independently calculated the frequencies of the modes of a clamped square plate up to the 6th, and up to the 5th for the following edge conditions:

(*d*) One edge clamped, remainder free (cantilever plate).
(*e*) Adjacent edges clamped, remainder free.

Barton (7) later extended Young's calculations for the cantilever plate to values of r of 1/2, 1, 2, 5, and also has given the frequencies of the first two modes of the rhombus-shaped cantilever plate (skew cantilever plate). Barton has compared his solutions with experimental values, and finds good agreement, the experimental values, however, being, as expected, lower than the calculated values. It also appears that the agreement becomes poorer for the skew cantilever plate as the departure from the square shape becomes more pronounced.

Numerical Results

The available numerical results are summarized in Tables 1 to 4. The diagrams in these tables give the edge conditions, using the abbreviations F = free, S = simply supported, and C = clamped. The quantity entered in Tables 1, 3, and 4 is $k = \omega a^2\sqrt{M/D}$ and in Table 2 is either k, or $k' = \omega b^2\sqrt{M/D}$. Ritz actually cal-

[1] Officer in Charge, Physics Section, Forest Products Research Laboratory.

[2] Numbers in parentheses refer to the Bibliography at the end of the paper.

Discussion of this paper should be addressed to the Secretary, ASME, 29 West 39th Street, New York, N. Y., and will be accepted until October 10, 1952, for publication at a later date. Discussion received after the closing date will be returned.

Note: Statements and opinions advanced in papers are to be understood as individual expressions of their authors, and not those of the Society. Manuscript received by ASME Applied Mechanics Division, September 20, 1951.

TABLE 1 k FOR MODES OF A SQUARE PLATE

Edge Conditions	Authority	Mode Number 1	2	3	4	5	6
F F F F	Young	3·494	8·547	21·44	27·46	31·17	
C F C F	Young	6·958	24·08	26·60	48·05	63·14	
F F F F	Ritz	14·10	20·55	23·91	35·96	61·60	65·24
S S S S	Eqns.	1·974	4·934	7·896	9·869	12·83	16·78
S S S S	Iguchi	23·65	51·68	58·65	86·13	100·3	113·2
C S C S	Iguchi	28·95	54·78	69·32	94·59	102·2	129·1
C C C C	Iguchi	35·98	73·40	108·2		132·2	165·0
C C C C	Young	35·99	73·41	108·3	131·6	132·3	165·1

TABLE 2 k AND k' FOR FUNDAMENTAL MODE OF RECTANGULAR PLATES (IGUCHI)

S S S S	b/a	1·0	1·5	2·0	2·5	3·0	∞
	k	19·74	14·26	12·34	11·45	10·97	9·87
C S C S	b/a	1·0	1·5	2·0	2·5	3·0	∞
	k	23·65	18·90	17·33	16·63	16·26	15·43
	a/b	1·0	1·5	2·0	2·5	3·0	∞
	k'	23·65	15·57	12·92	11·75	11·14	9·87
C S C S	b/a	1·0	1·5	2·0	2·5	3·0	∞
	k	28·95	25·05	25·83	25·27	22·99	22·37
	a/b	1·0	1·5	2·0	2·5	3·0	∞
	k'	28·95	17·37	15·69	12·13	11·36	9·87
C C C C	b/a	1·0	1·5	2·0	2·5	3·0	∞
	k	35·98	27·00	24·57	23·77	23·19	22·37

culated[3] $\lambda = k^2/16$; Iguchi calculated k/π^2, and their results have been converted accordingly. Values of k for simply supported plates, calculated from Equation [1], have been included in Tables 1 and 2 for comparison with the remaining results.

The agreement between the calculations of Iguchi and Young for the clamped square plate is very close, but it appears that Iguchi missed the mode for which Young found $k = 131.6$.

The Ritz procedure gives upper limits to the frequencies, and references to papers dealing with the convergence and accuracy of the method are quoted by Young (6). Weinstein (8) later pointed out that it is also possible to calculate lower limits to the frequencies, and in this way to estimate the accuracy of the results. For the first ten modes of a clamped square plate, he states that the errors range from 0.39 to 6.1 per cent.

It is worthy of note that when, as in Table 3, the modes are numbered in order of ascending frequency for the square plate ($a/b = 1$), the frequencies do not always ascend with increasing mode number for other values of a/b. Each mode in Table 3

[3] It should be noted that the 4π in the denominator of the Ritz equation [56] is in error; it should be 2π.

TABLE 3 k FOR MODES OF RECTANGULAR CANTILEVER PLATES (BARTON)

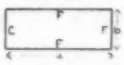

a/b	Mode Number 1	2	3	4	5
½	3·508	3·372	21·96	10·26	24·65
1	3·494	8·547	21·44	27·46	31·17
2	3·472	14·93	21·61	94·49	48·71
3	3·450	34·73	21·52	563·9	105·9

TABLE 4 k FOR MODES OF SKEW CANTILEVER PLATES (BARTON)

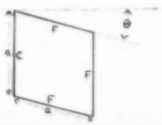

Mode Number	θ 15°	30°	45°
1	3·60	3·96	4·82
2	8·87	10·19	13·75

corresponds with a given pattern of nodal lines; for example, the first mode has a single nodal line along the clamped edge, and the second mode has two nodal lines, one along the clamped edge and the other perpendicular to it, bisecting the rectangle. The frequencies of these modes vary differently with a/b; the first and third decrease slightly with increasing a/b, whereas the frequencies of the other modes increase, and for this reason the progression of k with mode number is irregular for values of a/b other than 1.

ACKNOWLEDGMENT

Acknowledgment is made to the Department of Scientific and Industrial Research for permission to publish this paper.

BIBLIOGRAPHY

4 "Vibration Problems in Engineering," by S. Timoshenko, second edition, D. van Nostrand Company Inc., New York, N. Y., 1937.

2 "Bemerkung zu dem Problem der transversalen Schwingungen rechteckiger Platten," by W. Voigt, *Göttingen Nachrichten*, 1893, p. 225.

3 "Theorie der Transversalschwingungen einer quadratischen Platten mit freien Rändern," by W. Ritz, *Annalen der Physik*, Leipzig, vol. 28, 1909, p. 737.

4 "The Vibrations of Free Square Plates. Part 1, Normal Vibrating Modes," by M. D. Waller, Proceedings of the Physical Society of London, vol. 51, 1939, p. 831.

5 "Die Eigenwertprobleme für die elastische rechteckige Platte," by S. Iguchi, Memoirs of the Faculty of Engineering, Hokkaido Imperial University, vol. 4, 1938, p. 305.

6 "Vibration of Rectangular Plates by the Ritz Method," by D. Young, JOURNAL OF APPLIED MECHANICS, Trans. ASME, vol. 72, 1950, p. 448.

7 "Vibration of Rectangular and Skew Cantilever Plates," by M. V. Barton, JOURNAL OF APPLIED MECHANICS, Trans. ASME, vol. 73, June, 1951, p. 129.

8 "Vibration of Rectangular Plates by the Ritz Method," by Dana Young, discussion by A. Weinstein, JOURNAL OF APPLIED MECHANICS, Trans. ASME, vol. 73, June, 1951, p. 229.

Brief Notes

On the recommendations of the Executive Committee of the ASME Applied Mechanics Division, it has been decided to initiate a section devoted to brief notes on technical matters in mechanics. These notes must not be longer than 750 words (about 2½ double-spaced typewritten pages, including figures) and will be subject to the usual review procedure prior to publication. After approval such notes will be published in the next issue of the Journal. The notes should be submitted to the Secretary of the ASME Applied Mechanics Division.

An Exact Solution for a Rectangular-Plate Problem

By J. G. SUTHERLAND,[1] URBANA, ILL.

THE problem considered is that of an interior panel of a plate which is continuous over a rectangular grid of flexible beams supported at their intersections by columns. If parallel beams are of equal stiffness and are equally spaced, and if the lateral load is uniformly distributed over the whole plate, the bending in all interior panels may be assumed to be identical. Under these conditions only one interior panel need be considered. From symmetry, the slope of the deflection surface at a panel boundary in the direction of the normal to the boundary must be zero, and the shearing force in the plate at the boundary must be equal to one half of the pressure on the supporting beam. For co-ordinate axes directed along the beams, these considerations lead to the following boundary conditions

$$(\partial w/\partial x)_{x=a} = (\partial w/\partial y)_{y=b} = 0 \quad \ldots\ldots [1]$$

and

$$\left.\begin{aligned} \frac{a\lambda_b}{2c}\left[\frac{\partial^4 w}{\partial y^4}\right]_{x=a} &= \left[\frac{\partial^3 w}{\partial x^3} + (2-\mu)\frac{\partial^3 w}{\partial x\,\partial y^2}\right]_{x=a} \\ \frac{a\lambda_a}{2}\left[\frac{\partial^4 w}{\partial x^4}\right]_{y=b} &= \left[\frac{\partial^3 w}{\partial y^3} + (2-\mu)\frac{\partial^3 w}{\partial x^2\partial y}\right]_{y=b} \end{aligned}\right\} \quad \ldots\ldots [2]$$

where

w = lateral deflection of plate

$\lambda_a = EI_a/aD$ = ratio of beam rigidity to plate rigidity for each of beams parallel to x-axis

$\lambda_b = EI_b/bD$ = ratio of beam rigidity to plate rigidity for each of beams parallel to y-axis

$c = a/b$ = ratio of panel length (along x-axis) to panel width (along y-axis)

μ = Poisson's ratio

In addition to the foregoing boundary conditions, the deflection function w must be zero over the columns, and must satisfy the differential equation

$$\nabla^2\nabla^2 w = q/D \quad \ldots\ldots [3]$$

where

q = intensity of uniform load on plate

It is easily verified that all of the requirements mentioned are satisfied by the deflection function

$$w = \frac{q}{24D}\left[\frac{x^2(a-x)^2}{1+c\lambda_a} + \frac{y^2(b-y)^2}{1+\lambda_b/c}\right] \quad \ldots\ldots [4]$$

for cases in which

$$\lambda_a\lambda_b = 1 \quad \ldots\ldots [5]$$

Although this solution is limited in generality by virtue of Equation [5], it is felt that it is of interest in view of the limited number of exact solutions available in closed form.

The foregoing solution can be generalized for cases in which the uniformly loaded panel is restrained or loaded by any moments which are uniform along its boundaries. In these cases, however, the solutions are exact only if Poisson's ratio is zero. Assuming that on the boundaries $x = 0$ and $x = a$ there is a restraining moment given by $M_1 = C_1\theta_1$, where $\theta_1 = (\partial w/\partial x)_{x=0} = -(\partial w/\partial x)_{x=a}$, and similarly for the boundaries $y = 0$ and $y = b$, $M_2 = C_2\theta_2$, we have then

$$\frac{w}{q/D} = \frac{1}{24(1+c\lambda_a)}\left[(a^3x - 2ax^3 + x^4) - \frac{a^2x(a-x)}{1+2D/aC_1}\right] + \frac{1}{24(1+\lambda_b/c)}\left[(b^3y - 2by^3 + y^4) - \frac{b^3y(b-y)}{1+2D/bC_2}\right] \quad [6]$$

Like Equation [4], this expression is limited to cases for which $\lambda_a\lambda_b = 1$. It should be noted that λ_a and λ_b are still defined in terms of the moment of inertia of a beam which was assumed to support boundaries of two similar adjacent panels. If the stiffness constants C_1 and C_2 become very large, this expression reduces to that given by Equation [4]. When C_1 and C_2 are very small, the solution is that for a plate which is not continuous over the beams, that is, for the case in which there is no bending moment in the plate along the panel boundaries.

The foregoing solutions were obtained originally from the application of an energy method to the more general case of a plate continuous over flexible beams. The results of this latter investigation will be included in the author's doctoral dissertation.

[1] Research Assistant in Civil Engineering, University of Illinois.

Discussion of this paper should be addressed to the Secretary, ASME, 29 West 39th Street, New York, N. Y., and will be accepted until October 10, 1952, for publication at a later date. Discussion received after the closing date will be returned.

NOTE: Statements and opinions advanced in papers are to be understood as individual expressions of their authors, and not those of the Society. Manuscript received by ASME Applied Mechanics Division, April 24, 1952.

Discussion

Supersonic Flow With Variable Specific Heat[1]

H. H. Korst.[2] The author treats the case of an oblique plane shock based upon the classical fundamental equations (assumptions 4 through 7 in the author's paper) for a semiperfect gas that satisfies the state equation $p = \rho g R T$ (assumptions 1 through 3) but has variable specific heat. He derives correction coefficients for the principal thermodynamic properties and the normal component of the Mach number to take care of deviations from results as they are usually presented under the assumption of constant specific heats. As the influence of the temperature level becomes significant, a universal dimensionless presentation of the results is no longer possible. This application of variable specific heats to the conventional treatment of plane shock constitutes an interesting refinement in this type of analysis. The author has brought out the significance of this factor in the range of conditions covered by the paper.

It might be worth mentioning that the author's computations can be utilized for the discussion of the influence of variable specific heat on the geometrical configuration of the shock. The vector diagram of the velocities, as it results from the continuity

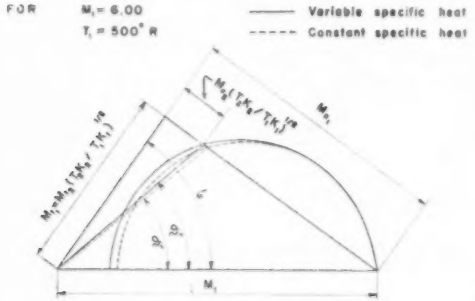

Fig. 1 Shock Polar Diagram

equation and the momentum equation, yields the following well-known relations

$$M_{n1} = M_1 \sin \sigma$$

$$M_{n2} = M_1 (T_1/T_2)^{1/2} \cos \sigma \tan (\sigma - \vartheta) (k_1/k_2)^{1/2}$$

where σ is the shock angle and ϑ the deflection angle, so that M_{n1} and M_{n2} can be eliminated and replaced by the variables σ and ϑ. One obtains for constant specific heat

$$\tan (\sigma - \vartheta)_c = M_{n2_c} (T_2/T_1)_c^{1/2} / \cos \sigma M_1$$

and for variable specific heat

$$\tan (\sigma - \vartheta)_v = \tan (\sigma - \vartheta)_c A(M_{n2}) A(T_2/T_1)^{1/2} (k_2/k_1)^{1/2}$$

The correction factors $A(M_{n2})$ and $A(T_2/T_1)$ are defined in the author's paper. Shock polars $\vartheta = \vartheta(\sigma, M_1, T_1)$ can be computed for different values of the parameters M_1 and T_1. Fig. 1 of this discussion gives evidence of the change in the shock configuration for air of a free-stream temperature of $T_1 = 500$ R, and $M_1 = 6.0$ due to variable specific heat as compared with the idealized case of constant specific heat. While relatively little difference exists for weak shocks with small deflection angles, the limiting wedge angle is considerably larger in the case with variable specific heat. The limits for a regular shock reflection consequently are shifted.

[1] By F. P. Durham, published in the March, 1952, issue of the Journal of Applied Mechanics, Trans. ASME, vol. 74, pp. 57–62.

[2] Professor of Mechanical Engineering, University of Illinois, Urbana, Ill.

Linear Bending Theory of Isotropic Sandwich Plates by an Order-of-Magnitude Analysis[1]

E. H. Lee.[2] In presenting this paper the author stated that the constancy of the direction cosines along its length of a line initially normal to the undisturbed plate surfaces implies that plane sections remain plane. This is certainly too stringent a deduction. Plane sections comprising planes generated by normals to the undeformed surface, in general, will become ruled surfaces, and one cannot even put on the restriction that, in general, they will be developable.

Author's Closure

The statement referred to by Professor Lee was used in a sense customarily employed in discussing the characteristics of sandwich plates. As such the deduction does not appear to be too stringent.

Bending of Honeycombs and of Perforated Plates[1]

I. Malkin.[2] The author's "Brief Note" is virtually a new version of his comments on a previous paper by the writer.[3] In this new version he proposes a simplified computation of the fictitious elastic constants derived by the writer for the case of a tube sheet of triangular layout (see point 2 in the following). His statements give rise to objections as follows:

1 He contends that his constants E_0, μ_0 represent the fictitious elastic constants of an equivalent isotropic plate, but no justification is given for such a claim.

2 He states that the writer "first considered the problem of determining" the elastic constants (of the equivalent isotropic plate). This statement is inaccurate; it narrows unjustifiedly the scope of the writer's work:[3] reduction of the bending problem of the hexagonal grid to the problem of an isotropic plate in bending plus determination of the corresponding fictitious elastic

[1] By George Gerard, published in the March, 1952, issue of the Journal of Applied Mechanics, Trans. ASME, vol. 74, pp. 13–15.

[2] Professor of Applied Mathematics, Graduate Division of Applied Mathematics, Brown University, Providence, R. I. Mem. ASME.

[1] By G. Horvay, published in the March, 1952, issue of the Journal of Applied Mechanics, Trans. ASME, vol. 74, pp. 122–123.

[2] Standards and Design Engineer, Foster Wheeler Corporation, New York, N. Y.

[3] "Notes on a Theoretical Basis for the Design of Tube Sheets of Triangular Layout," Trans. ASME, vol. 74, April, 1952, pp. 387–396.

constants. This work was done by the writer in March, 1946, as can be proved from the files of his company.

3 The author speaks of an "unfortunate slip" in the writer's derivations; the writer could not find any slips in his calculations and he maintains that his formulas are correct.

4 Neither of the two constants computed by the author agrees with the corresponding constants derived by the writer.

5 The problem of the plate and that of the grid in bending require consideration of bending and twisting stresses, but in Mr. Horvay's Fig. 2, he introduces into his beam element 01 a bending moment only, without justifying the omission of the torque.

6 He emphasizes convenience of derivation of formulas; the main thing is, however, not the convenience of derivation, but reliability of the results, which, in turn, calls for services of a reliable guide (the Hamiltonian principle[3]).

7 A serious inaccuracy occurs at the very beginning of the author's "Note," where he says that the hexagonal grid "can be treated in bending calculations as an isotropic solid plate," and so on. The correct definition of the reduction of the hexagonal grid to the isotropic plate in bending is given in the lines between the Equations [16] and [17], [18] in the writer's paper.[2] The equivalence between grid and plate is valid only in so far as the determination of the deflection is concerned, but not for the remainder of the bending calculations. A noncritical reader may conclude from the author's Note the possibility of figuring the stresses in a perforated plate in the same manner as in a solid plate, if only some fictitious elastic constants are being used, which is entirely incorrect. In this connection the writer considers it most appropriate to call attention to the fact that correct stress calculations in tube sheets (and adjacent elements) on the basis of his previous work[2] have been carried out by him in two further papers, "Stress Analysis of a Tubular Air Heater," and "Stress Analysis of a Pressure Vessel Tube Chamber"; the reasons for their not being published yet cannot be discussed here.

Author's Closure

The author is indebted to Mr. Malkin for the stimulating discussion and his keen interest in the paper. Mr. Malkin and the author agree in claiming equivalence between hexagonal grid work and solid plate. Since the end results differ—Malkin's equivalent plate constants can be written in the form

$$\mu' = (1 - K)/(3 + K), \quad E' = (1 - \mu')Eh/R \quad \ldots [1]$$

while the author finds

$$\mu_b = (1 - K)/(1 + 3K), \quad E_b = (1 - \mu_b)Eh/R \quad \ldots [2]$$

one of the two analyses must be incorrect. In the above

$$C = GJ = KB$$
$$B = EI = E(2hH^2/12) = 2h\,I_sE \quad \ldots [3]$$

denote torsional and bending stiffness, respectively, of a ligament (such as 01 in Fig. 1), and I_s is the moment of inertia (per inch) of a solid plate of height H.

Malkin leads off his derivation by writing the strain energy of beam 01 in Fig. 1 in the form

$$U_1 = \frac{1}{2} B\kappa_x^2 L + \frac{1}{2} C\kappa_{xy}^2 L \quad \ldots [4]$$

where κ_x, κ_{xy} are curvature and twist. Then he obtains U_2, U_3 for beams 02, 03, expresses their respective curvatures in terms of $\kappa_x, \kappa_{xy}, \kappa_y$; finally compares the resultant energy

$$U_1 + U_2 + U_3 = (3L/16)(3 + K)B\,[(\kappa_x + \kappa_y)^2 + 4(\kappa_{xy}^2 - \kappa_x\kappa_y)(1 + K)/(3 + K)] \quad \ldots [5]$$

with the energy

$$U = \{3LRH^3 E'/24(1 - \mu'^2)\}\,[(\kappa_x + \kappa_y)^2 + 2(1 - \mu')(\kappa_{xy}^2 - \kappa_x\kappa_y)] \quad \ldots [6]$$

of a solid plate, of area $2R \times 3L/2$, which incurs the curvatures κ_x, κ_{xy}, κ_y. By choosing the solid plate constants μ', E' as in Equation [1], equality of the two expressions [5] and [6] is established.

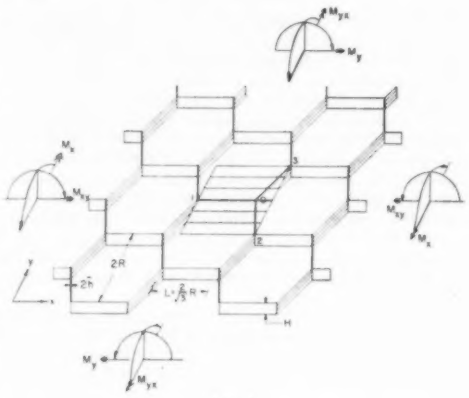

Fig. 1

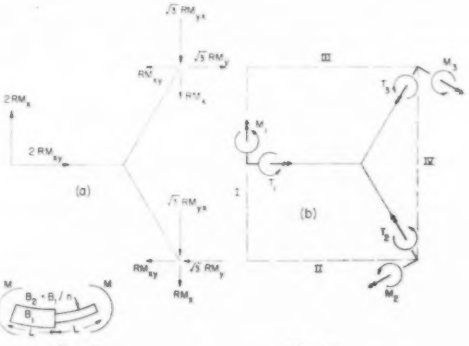

Fig. 3 Fig. 2

The author, on the other hand, considers the behavior of the gridwork in Fig. 1 under action of edge moments M_x, M_y, $M_{yx} = M_{xy}$ per inch. He determines, by means of Figs. 2(*a*)*, and (*b*), the bending moments and torques

$$M_1 = 2RM_x$$
$$T_1 = 2RM_{xy}$$
$$M_2 = \frac{1}{2}R(M_x + 3M_y) + \sqrt{3}\,RM_{xy}$$
$$T_2 = \frac{1}{2}\sqrt{3}\,R(M_y - M_x) - RM_{xy} \quad \ldots [7]$$

* In Fig. 2(*a*) the arrow of the moment vector $\sqrt{3}\,RM_{yx}$ acting at point 3 should point up.

$$M_1 = \frac{1}{2} R(M_x + 3M_y) - \sqrt{3}\, RM_{xy}$$

$$T_1 = \frac{1}{2} \sqrt{3}\, R(M_x - M_y) - RM_{xy}$$

which act on the three beams 01, 02, 03; then calculates the corresponding bending and twist angles

$$\varphi_k = M_k L/B \qquad \psi_k = T_k L/C \quad \ldots\ldots\ldots\ldots [8]$$

By using the definitions, $\varkappa_x$ = change in deflection angle with respect to x axis between faces I and IV per distance $3L/2$, $\varkappa_y$ = change in deflection angle with respect to y axis between faces II and III per distance $2R$, $\varkappa_{xy}$ = change in deflection angle with respect to y axis between faces I and IV per distance $3L/2$, and $\varkappa_{yx}$ = change in deflection angle with respect to x axis between faces II and III per distance $2R$, he obtains

$$\varkappa_x = \frac{\varphi_1 + (\varphi_2 + \varphi_3 - \sqrt{3}\,\psi_2 + \sqrt{3}\,\psi_3)/4}{3L/2} = \left(\frac{3/2}{B} + \frac{1/2}{C}\right) RM_x - \left(\frac{1/2}{C} - \frac{1/2}{B}\right) RM_y$$

$$\varkappa_y = \frac{(\sqrt{3}\,\varphi_2 + \sqrt{3}\,\varphi_3 + \psi_2 - \psi_3)/2}{2R} = \left(\frac{3/2}{B} + \frac{1/2}{C}\right) RM_y - \left(\frac{1/2}{C} - \frac{1/2}{B}\right) RM_x$$

$$\varkappa_{xy} = \frac{\psi_1 + (\sqrt{3}\,\varphi_2 - \sqrt{3}\,\varphi_3 + \psi_2 + \psi_3)/4}{3L/2} = \left(\frac{1}{B} + \frac{1}{C}\right) RM_{xy} \quad \ldots\ldots [9]$$

$$\varkappa_{yx} = \frac{(\varphi_2 - \varphi_3 - \sqrt{3}\,\psi_2 - \sqrt{3}\,\psi_3)/2}{2R} = \left(\frac{1}{B} + \frac{1}{C}\right) RM_{xy}$$

(φ, ψ, $\varkappa$ are considered as positive in the same sense as the corresponding M, T.) By comparing these expressions with the moment-curvature relations

$$\left.\begin{aligned} E_b J_x \varkappa_x &= M_x - \mu_b M_y \\ E_b J_x \varkappa_y &= M_y - \mu_b M_x \\ E_b J_x \varkappa_{xy} &= (1 + \mu_b)\, M_{xy} \end{aligned}\right\} \quad \ldots\ldots\ldots\ldots [10]$$

of a solid plate of constants μ_b, E_b, he finds that equality between Equations [9] and [10] is established when Equation [2] holds.

The same result is obtained when one calculates the strain energy

$$\left.\begin{aligned} U_1 + U_2 + U_3 &= \frac{1}{2} M_1\varphi_1 + \frac{1}{2} T_1\psi_1 + \ldots \\ &= (M_1^2 + M_2^2 + M_3^2)L/2B + (T_1^2 + T_2^2 + T_3^2)L/2C \\ &= \frac{3}{2}\left(\frac{3/2}{B} + \frac{1/2}{C}\right) R^2 L(M_x + M_y)^2 + 3\left(\frac{1}{B} + \frac{1}{C}\right) R^2 L\,(M_{xy} - M_x M_y) \end{aligned}\right\} \quad \ldots [11]$$

of the three beams and equates it to the strain energy

$$U = (3RL/2E_bJ_x)\,[(M_x + M_y)^2 + 2(1 + \mu_b)\,(M_{xy}^2 - M_x M_y)] \quad \ldots\ldots\ldots\ldots [12]$$

of a solid plate, of constants E_b, μ_b, and area $3RL$.

The author's results are clearly right, because they express the actual deformations that occur between faces I, IV and faces II, III, of Fig. 2. Since Malkin's derivation is free of numerical errors, it must be surmised that his analysis is based on false premises. What is the fallacy in Malkin's arguments? To reveal this, consider the analogous, but simpler and more obvious, problem of determining an equivalent B_{eq} for the composite beam of Fig. 3. By writing, as the author does

$$2LM^2/B_{eq} = 2U = M^2L/B_1 + M^2L/B_2 \quad \ldots\ldots [13a]$$

one obtains

$$2/B_{eq} = 1/B_1 + 1/B_2 = (n + 1)/B_1 \quad \ldots\ldots [13b]$$

by writing, as Malkin does,

$$2L\varkappa_1^2\, B_{eq} = 2U = B_1\varkappa_1^2 L + B_2\varkappa_2^2\, L = B_1(1 + n)\varkappa_1^2 L \quad \ldots [14a]$$

one obtains

$$2\, B_{eq} = (n + 1)\, B_1 \quad \ldots\ldots [14b]$$

Obviously, expression [13b] has general usefulness in calculating deflections of beams which are made up of successive sections $B_1B_2B_1B_2B_1 \ldots$; on the other hand, expression [14b] is without physical or mathematical significance.

Besides providing the right deflections, the author's approach furnishes also the ligament stresses. For, once the solid plate problem has been solved, M_x, M_y, M_{xy} are also known; hence so are the moments and torques Equations [7], which act on the individual beams. But then the ligament stresses can be calculated by elementary beam formulas.

It is of interest to mention some special values of K and μ_b which are of frequent occurrence (in all cases it is assumed that $R \gg h$):

$$\left.\begin{aligned} &\text{Cylindrical ligament, } K = 1/(1 + \mu), \quad \mu_b = \mu/(4 + \mu) \\ &\text{flat rectangular bar } (H \ll 2h), \quad K = 2/(1 + \mu),\ \mu_b = -(1 - \mu)/(7 + \mu) \\ &\text{square bar } (H = 2h), \quad K = 0.844/(1 + \mu), \quad \mu_b = (0.16 + \mu)/(3.53 + \mu) \\ &\text{tall rectangular bar } (H \gg 2h), \quad K = 2\,(2h/H)^2/(1 + \mu), \quad \mu_b = 1 - 8(2h/H)^3\,[1 + \mu + 6(2h/H)^2] \end{aligned}\right\} \quad [15a, b, c, d]$$

Use[5] of formula [15d] is restricted to the case $H < R$, because of the requirement (of the underlying analysis) that the ligaments be long and slender. For the case $H \gg R$ the plane stress formula, Equation [7] of the paper in footnote [6] is appropriate. (The author plans to investigate intermediate cases more fully at a later time.)

The requirement $R \gg h$ can also be moderated somewhat but then the average ligament width $2h$ or the effective ligament length L must be defined with greater care than was done by the author.[1] (One can, for instance, follow Malkin's Fig. 3 of footnote 3.) Another vital restriction on the use of the method is the requirement that the loads on the plate vary but slowly from hex to hex. A discussion of this restriction is likewise given in the paper.[4]

[6] "The Plane Stress Problem of Perforated Plates," by G. Horvay Presented at ASME Applied Mechanics Division Conference State College, Pa., June 19–21, 1952. Paper No. 52—APM-19.

On the Direction of Fatigue Cracks in Polycrystalline Ingot Iron[1]

R. E. PETERSON.[2] The crack behavior discussed in this paper, in the writer's opinion, would be applicable to conditions existing during the initial stage of crack development. As is well known, slip lines form in accordance with maximum resolved shear stress;[3] these lines broaden under repeated stress and finally develop into cracks which are the source of the gross crack which later spreads across the section. The region of initial failure in a low-carbon steel is shown in Fig. 1[4] of this discussion. The angles which the slip lines make with a line perpendicular to the tension-compression direction should be within the region of approximately ±45 deg, since the slip lines represent traces of planes approximately tangent to a 45-deg cone. We see from

FIG. 1 FATIGUE CRACK IN LOW-CARBON STEEL

Fig. 1 that the slip lines are in the range mentioned. The average angle is zero, and consequently, as pointed out by the author, the shear cracks should (and do) zigzag about a line normal to the tension-compression direction. It is of interest to note that a large number of cycles was required, about 30,000 in this case,[4] before the slip lines became visible at 340X, and a considerably larger number of cycles, about 550,000 cycles in this case, until a crack started.

The point which the writer is leading up to is that there appear to be two different processes involved in the formation of a gross fatigue crack. The one, described in the foregoing, has to do with the development of shear cracks in a relatively small number of grains located at the most highly stressed region.

Another involves the spread of the crack across the section. Here we are dealing essentially with a "notched" (cracked) specimen. The crack apex travels rapidly through the grains as the crack opens and closes in response to tension-compression cycles. As seen under a microscope, the region about the crack apex becomes grayish in appearance, evidently due to general plastic flow, but with no sharp slip lines of the kind shown in Fig. 1. As mentioned, such sharp lines require considerable cycling (time), which is not attained due to the rapid crack progress. Sections taken through a crack tend in many cases to show, at some depth, a nearly straight crack, which appears to be governed by the tensile stress, Fig. 2, herewith. Incidentally, it may be

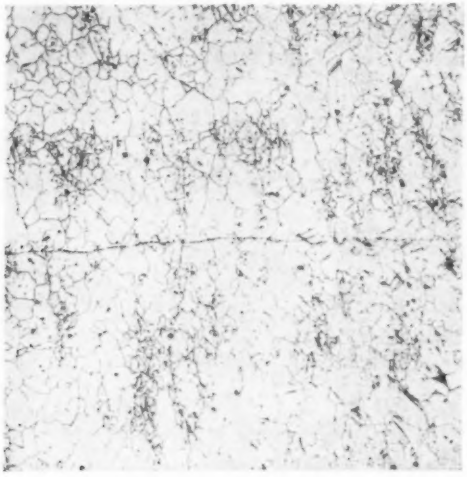

FIG. 2 FATIGUE CRACK IN DISCALOY

preferable to study a sectioned crack rather than a surface crack since this avoids any possible surface-finishing effects. In view of the foregoing, it would be of interest to compare data of the kind presented by the author for different sections of cracks of considerable length.

If crack propagation (not crack origin) is due to normal stress, the 45-deg helical crack in torsion, of course, would be expected. In the harder steels, free from directional effect, one always obtains 45-deg cracks as a result at repeated torsion. However, in soft materials one obtains 45-deg cracks for stresses near the endurance limit (long life), but at relatively high stresses (short life) there is a tendency to obtain cracks in the shear direction[5] instead of 45 deg. This would seem to be tied in with plastic behavior in some way, but the writer has no clear explanation of this result. Perhaps the author has some ideas in this regard.

Far too little attention has been paid to the mechanics of crack propagation. It is hoped that this valuable paper will stimulate further work in this field.

[1] By F. A. McClintock, published in the March, 1952, issue of the JOURNAL OF APPLIED MECHANICS, Trans. ASME, vol. 74, pp. 54–56.

[2] Manager, Mechanics Department, Research Laboratories, Westinghouse Electric Corporation, Pittsburgh, Pa.

[3] "Crystalline Structure in Relation to Failure of Metals—Especially by Fatigue," by H. J. Gough, Proceedings of the ASTM, vol. 33, part 2, 1933, p. 3.

[4] Discussion of paper by A. V. DeForest, JOURNAL OF APPLIED MECHANICS, Trans. ASME, vol. 58, 1936, p. A-116.

[5] "Handbook of Experimental Stress Analysis," John Wiley & Sons, Inc., New York, N. Y., 1950, footnote to p. 606.

Author's Closure

Mr. Peterson's micrograph of a fatigue crack in Discalloy is very interesting, for it points out that the author's theory does not account for the facts in all materials. The author wonders whether the difference between Mr. Peterson's two micrographs may not be due to the difference in material as well as, or possibly instead of, being due to the stage of crack growth. The experimental data of the paper were based on the center 90 deg of the main crack of each specimen and hence include developments at a fairly late stage. If the cracks tend to straighten out at a later stage, that could explain the fact that the cracks might be a little more nearly perpendicular to the axis than predicted by the theory. The author regrets that the specimens are not available for studying the crack directions over varying lengths and at various depths, as Mr. Peterson suggests.

As for the possible effect of plastic behavior on crack direction, one is inclined to turn to the theory of plasticity for some treatment of a thin cavity in a generally elastic solid. Such problems have not been treated, however, and the author has been informed that they are considered quite difficult.

A Contribution to the Theory of the Development and Stability of Detonation in Gases[1]

Edward Adams Richardson.[2] It might be of interest to learn of a much earlier study of this problem carried on somewhat qualitatively in the spring of 1922. An outline thereof was published later by the writer.[3] As the assumptions, then used to correlate the data in some six papers which were highly conflicting (in appearance), were later used, apparently independently, by another, and more broadly,[4] they should be of interest.

Two assumptions were made: (*a*) The phenomena of chemical reactions in gases must be governed by laws of the distribution of particle velocities such as those underlying the kinetic theory of gases. (*b*) Dissociation of a particle must be regarded as a quantumlike process, since if the maximum energy absorbable on collision is less than the minimum energy to dissociate, according to any one of n possible ways, the collision is elastic; if the energy is greater for a given collision than that required for the kth way but less than for the $k + 1$ way, dissociation will be by the kth way.

Now, for a given temperature a probability curve of particle velocity may be set up. On such a curve, lines can be drawn at the first—kth—nth manner of dissociation, and the probability of a given order of dissociation being possible must be calculated. A very low probability, multiplied by the number of collisions per second, results in what may be very frequent occurrences. If the frequency so determined is high enough, at least first-order reaction can occur. A flame front traveling into unreacted gases tends to be governed in speed by the order of reaction and the density of energy liberation made possible. If by any means the temperature ahead of the flame front increases, then a re-evaluation of probabilities becomes necessary. The curve of probabilities has the same general shape as before, but the most probable velocity is now appreciably higher; hence the area under the curve between, say, the second order and infinity becomes enough to produce substantially second-order reaction. If this corresponds to a greater rate of energy liberation per unit of volume when taken with the rate of first-order reaction, the flame front can speed up.

A flame front is a thin region in which dissociation and reaction are occurring, with a preponderance of energy in the direction co-ordinate paralleling travel, with particles of high velocity being shot into the region ahead, which if sufficiently numerous, produce sufficient energy to maintain the motion. The higher particle velocities are too few, so the "fires" they start cannot be maintained, the steady motion being governed by a balance between dissociation and heat liberation adequate to maintain the work of dissociation at flame-front velocities. It is a kinetic equilibrium.

Now, temperatures may rise in one of two ways; either by reactions behind the flame front expanding the gases there behind and increasing the flame-front velocity and energy, or more likely by the reflection of the shock waves setting up pressures and temperatures which suddenly increase at the meeting of flame front and shock wave. Nothing of moment occurs until a temperature level suddenly brings into substantial importance a new order of reaction, accompanied by much larger rates of energy liberation. If such occurs, the rate of flame acceleration becomes large—so large in the case of detonation that the "jump" in velocity appears almost instantaneous. But no matter how large the velocity, the tendency to a kinetic balance of dissociation and energy liberation will always be associated with substantial constancy of velocity of the flame front or of the detonation wave, and that velocity will be less than the highest probable velocities, greater than the particle velocity for the next lower state of dissociation.

At the time, this qualitative explanation was tested quantitatively in accounting for the slowing of the detonation wave in a tube when the gases in the tube were raised in temperature by small amounts, an effect observed, but not accounted for, in the literature of the time.

The explanation herein given is not necessarily opposed to the author's analysis. It does tend, I think, to clarify the physical processes involved. Obviously, a detonation wave tends to have a higher velocity than sound; hence no other shock wave can precede the detonation wave. The physical picture in the foregoing is more general than the concept of two discontinuities.

The writer of this discussion was seeking ways to avoid detonation in internal-combustion engines. He found them and embodied his findings in a patent[5] covering the methods described in his previous paper.[3] Tests thereof confirmed the theory behind the method; hence he lost interest in any further study of detonation.

Several Approximate Analyses of the Bending of a Rectangular Cantilever Plate by Uniform Normal Pressure[1]

F. S. Shaw.[2] The author is to be commended for his work since, in those cases where exact solutions are not known, comparisons of this nature are extremely useful. At the same time care should be taken in evaluating the comparisons.

---

[1] By A. K. Oppenheim, published in the March, 1952, issue of the Journal of Applied Mechanics, Trans. ASME, vol. 74, pp. 63–71.

[2] Partner of Edward, (Nellie), and George Richardson of Bethlehem, Pa. Mem. ASME.

[3] "Heating Fuels for Injection Engines," by Edward Adams Richardson, Engineering Bulletin No. 16 of The Pennsylvania State College, April, 1933, under the auspices of the Oil and Gas Power Division of the ASME.

[4] "Introduction to Chemical Physics," by J. C. Slater, McGraw-Hill Book Company, Inc., New York, N. Y., and London, England, 1939.

[5] U. S. Patent No. 1,876,168, Process of Preparing Fuels for Use, issued September 6, 1932, to E. A. Richardson.

[1] By W. A. Nash, published in the March, 1952, issue of the Journal of Applied Mechanics, Trans. ASME, vol. 74, pp. 33–36.

[2] Department of Aeronautical Engineering and Applied Mechanics Polytechnic Institute of Brooklyn. Brooklyn, N. Y.

To obtain reasonable accuracy with a straightforward use of finite-difference approximations to derivatives, it is usually found that rather more mesh points are desirable than have been used by the author.

Again, when using collocation methods for satisfaction of boundary conditions, i.e., satisfaction of such conditions at a small finite number of points on the boundary, it is desirable to examine, in some way or another, the results given by such solutions at boundary points intermediate to the "collocation" boundary points. It occasionally happens that in between the collocation points the solutions oscillate quite wildly.

Author's Closure

The author would like to thank Dr. Shaw for his interest in this application of numerical methods to the problem of the rectangular cantilever plate. As emphasized in the paper, the results hold only for a plate subject to uniform normal pressure and having a span-to-chord ratio of 1:2; other cases would have to be dealt with individually and it is probable that more mesh points would be necessary in some cases, particularly those involving unsymmetric loadings. In the numerical solution of the problem discussed in the paper the values of the bending moment and edge reaction at points intermediate to the mesh points shown were computed and found to be negligibly small.

On the Axisymmetric Problem of the Theory of Elasticity for an Infinite Region Containing Two Spherical Cavities[1]

H. Poritsky.[2] The authors have added one further interesting case to the impressive list of stress problems solved by them; in this case the solution, though exact, is not in finite form.

The writer would like to ask what general criteria the authors could suggest for separability of the type suggested by Equation [17] of the authors' paper for the Laplace or the repeated Laplace equation, namely, where solutions exist which are of the form $\mu A(\alpha)B(\beta)C(\gamma)$, that is, a product of a fixed function μ by functions of the independent variables, $A(\alpha)$, $B(\beta)$, $C(\gamma)$, satisfying proper ordinary differential equations.

In view of the extreme complexity of the solution found and the large amount of algebraic manipulation required in applying it, it is proper to ask whether it would not be simpler to apply an alternative procedure, similar to a method utilized by A. E. Green for plates with circular holes.[3] For the region external to two spheres S, S_1 with centers at O, O_1 on the z-axis, this method, when applied to harmonic functions which are axially symmetric about the z-axis, proceeds as follows:

Let the center O of S be at the origin $z = 0$, the center O_1 of S_1 at $z = a$. One starts with the two series

$$V = \sum A_n P_n(\cos\theta)/R^{n+1} + \sum B_n P_n(\cos\theta_1)/R_1^{n+1}$$

where R, R_1 are the distances from O, O_1 and θ, θ_1 the colatitude angles based on spherical co-ordinates with O, O_1 as poles. To apply proper boundary conditions on S one expands the terms of the second series in positive powers of R, utilizing the Neumann-type expansion

$$\frac{P_n(\cos\theta_1)}{R_1^{n+1}} = \frac{1}{a^{n+1}} + \frac{(n+1)RP_1(\cos\theta)}{a^{n+2}} + \frac{(n+1)(n+2)}{2!}\frac{R^2P_2(\cos\theta)}{a^{n+3}} + \cdots$$

The second series is then rearranged so that terms with like Legendre polynomials in $\cos\theta$ are grouped together, and the boundary conditions over S are applied. Similarly, one applies the boundary conditions over S_1 by expanding the A_n-terms in positive powers of R_1 and rearranging in Legendre polynomials in $\cos\theta_1$. In this manner one is led to an infinite number of equations in the two sets of coefficients A_n, B_n. These equations are solved by a method of successive approximations, based on the fact that the coefficients in the diagonal terms are much larger than the remaining coefficients.

Quite similar methods are applicable to the repeated Laplace equation and to regions with more than two spherical cavities.

The writer has not had any experience with the foregoing method as applied to the region exterior to several spheres and to elastic problems, but he once applied an analogous method to a harmonic problem for the region exterior to a cylinder and between parallel planes, and found the convergence very gratifying.

Authors' Closure

The authors greatly appreciate Dr. Poritsky's interesting comments. In connection with his first question, reference is made to Böcher's book[4] which contains a pertinent discussion. Further references are cited in a more recent paper on the same subject.[5]

With regard to the second question, it is certainly correct that the scheme outlined by Dr. Poritsky provides an alternative approach to the problem under consideration. Whether this approach is simpler is difficult to foresee. In the present problem it would involve four, rather than two, infinite sets of initially unknown coefficients, and would lead to a doubly infinite system of equations; in contrast, the method which was adopted yields a single infinite system which has a maximum of ten unknowns in each equation. Moreover, it would seem questionable whether expectations as to the speed of convergence derived from experience with a Dirichlet problem, are justified. An obvious important advantage of Dr. Poritsky's suggestion is the fact that the proposed method remains applicable to any number of cavities, whereas the approach based on spherical dipolar co-ordinates is confined to the case of two cavities.

It perhaps should be pointed out that the algebraic complexity of the solution given stems from various rearrangements of the initial aggregates of component solutions. These rearrangements were undertaken in order to accelerate the convergence of the solution. It would have been possible to leave the solution in a form whose simpler appearance is maintained at the sacrifice of a more favorable convergence. Incidentally, the authors believe that the algebraic work could now be shortened considerably by means of an alternative stress-function approach.[6]

---

[1] By E. Sternberg and M. A. Sadowsky, published in the March, 1952, issue of the Journal of Applied Mechanics, Trans. ASME, vol. 74, pp. 19–27.

[2] Consulting Engineer, General Electric Company, Schenectady, N. Y. Mem. ASME.

[3] "General Bi-Harmonic Analysis for a Plate Containing Circular Holes," by A. E. Green, Proceedings of the Royal Society, series A, vol. 176, 1940, pp. 121–139.

[4] "Ueber die Reihenentwicklungen der Potentialtheorie," by Maxime Böcher, B. G. Teubner, Leipzig, Germany, 1894.

[5] "Separation of Laplace's Equation," by N. Levinson, B. Bogert, and R. M. Redheffer, *Quarterly of Applied Mathematics*, vol. 7, 1949, pp. 241–262.

[6] "Pure Bending of an Incomplete Torus," by M. A. Sadowsky and E. Sternberg; now in preparation.

Analysis of Straight and Curved Beam-Columns[1]

R. PLUNKETT.[2] Practical methods for the solution of problems of this type are of great importance to the designer, and the authors are to be congratulated on developing another simple method for the solution of beam-column problems. However, it is well to point out the limitations of such methods; this one suffers from the limitations of being applicable only when the axial loads are relatively small in comparison with the critical buckling load. Equation [2] is developed from the "principle of least work" and neglects one of the terms. Since, generally speaking, the energy due to direct compression is negligible in comparison with that due to bending, this term will be neglected in the following.

Putting a load q at point s, the total bending moment at s' is

$$M(s') = W(s') + P(s')\,\delta(s') + qm(s, s') \quad [1]$$

The internal energy is

$$U = \int_0^l \frac{M^2(s')}{2EI}\,ds'$$

By Castigliano's theorem

$$\delta(s) = \frac{\partial U}{\partial q} = \int_0^l \frac{M}{EI}\,\frac{\partial M}{\partial q}\,ds'$$

but

$$\frac{\partial M}{\partial q} = P(s')\,\frac{\partial \delta(s')}{\partial q} + m(s,s')$$

or, letting $q = 0$

$$M(s) = W(s) + P(s)\int_0^l \frac{M(s')[m(s,s') + P(s')\delta(s,s')]\,ds'}{E(s')\,I(s')} \quad [2]$$

where

$$\delta(s, s') = \frac{\partial \delta(s')}{\partial q}$$

is the added deflection at s' due to a unit load at s. This is not an easy quantity to figure but can be seen to be important as P approaches the critical load. For the illustrative problem this amounts to about 0.09 in the coefficient m_{44}, Table 2 of the paper, changing this number to 4.89. Thus for this problem it is negligible. To get an idea of the order of magnitude of this effect, the axial loading is about $^1/_3$ of the critical; the writer solved the same problem by Newmark's[3] method and got bending moments about 1 per cent greater than those shown by this paper. It is felt that Newmark's method is simpler than that of Southwell,[4] and in this problem took somewhat less numerical work than the method proposed by the authors.

It also should be pointed out that the foregoing analysis is valid only if the axial loads do not deflect with the beam, which is difficult to visualize. This is a minor point and may be taken care of in Equation [1] of this discussion.

AUTHORS' CLOSURE

The authors wish to thank Mr. Plunkett for pointing out important limitations of the method presented. While the method is strictly valid only for axial loads that do not deflect with this beam, it will usually give conservative results for other types of axial loading. This is always the case if the bending moments are everywhere of one sign.

The relative merits of numerical methods are perhaps greatly dependent upon the skills of the persons using them. The numerical work of the example problem as originally solved was much shorter than the published solution. At the request of the editorial committee, it was reworked the way which might be used by a person not very familiar with Southwell's method.

---

[1] By C. M. Tyler, Jr., and J. G. Christiano, published in the September, 1951, issue of the JOURNAL OF APPLIED MECHANICS, Trans. ASME, vol. 73, pp. 283–284.

[2] General Electric Laboratory, General Electric Company, Schenectady, N. Y. Jun. ASME.

[3] "Numerical Procedure for Computing Deflections, Moments, and Buckling Loads," by N. M. Newmark, Trans. ASCE, vol. 108, 1943, p. 1161.

[4] "Relaxation Methods in Engineering Science," by R. V. Southwell, Oxford University Press, New York, N. Y. and London England, 1940, p. 40.

Book Reviews

Engineering Materials

ENGINEERING MATERIALS, Their Mechanical Properties and Applications. By Joseph Marin. Prentice-Hall, Inc., New York, N. Y., 1952. Cloth, 5½ × 8½ in., ix and 491 pp., illus., tables, problems, bibliography, name and subject indexes, $8.70.

REVIEWED BY NICHOLAS GROSSMAN[1]

LABORATORY courses have been an integral and essential part of engineering curriculums, with their own time-hallowed traditions and foibles. Most engineering students are subjected to classes in strength of materials and laboratory exercises in testing materials, later followed by some form of machine design. The failure of the students to grasp the fundamental principles and the over-all harmony cannot be entirely blamed on them, because frequently the laboratory exercises and classroom recitations are not properly synchronized. Professor Marin's new book is a great forward step in bringing a closer co-ordination among the several undergraduate subjects in the general field of the mechanics of materials. While the book is a self-contained entity, it presumes an elementary knowledge of strength of materials, and then proceeds to present an organized structure on empirical and analytical information.

The book is divided into three major sections dealing with mechanical properties in general, the properties of specific materials, and the testing of materials. The tradition of dealing with "engineering" materials and then giving cursory treatment to all nonmetallic materials has been carried over into the present work. In the past this may have been justified, but the renaissance of wood, wood laminates and sandwich materials, a host of new synthetics, developments in ceramics, sintered products, and refractory materials, advances in prestressed reinforced concretes would suggest either their inclusion as materials of voting age, or a more modest title for the book.

The author makes no clear attempt to separate the general mechanical properties and the empirical methods of obtaining them. The reviewer does not imply that such a clear-cut differentiation is essential, but since the author outlined such a grouping it should have been carried out. Definitions are always a thorny topic, and it is unfortunate that they are not treated more profoundly in this book. The author selected the term "total stress" to designate force and "unit stress" to mean force per unit area, with similar connotation calling the elongation or deformation "total strain." The concept of elasticity is introduced quite indirectly, and while the term "plasticity" reappears throughout the book, the reviewer was unable to find any attempt to properly define it.

The first part deals with mechanical properties in general. The welcome innovation was a strong bid to show the reader the engineering utilization of these properties as they are introduced. Copious numerical examples are given throughout, and a set of problems are appended to each chapter. While the reviewer did not have sufficient time to solve all these problems, he feels that the numerical examples and the set of problems are an outstanding feature of the book and should recommend it to all instructors who have been searching for a suitable textbook for materials engineering. The reviewer felt that properties like wear, corrosion resistance, hardness, and fretting have been somewhat neglected. Connection between tension and torsion is a frequently encountered question not treated in the book. The chapter on combined stresses is outstanding in clarity and completeness, with proper references to existing engineering codes and Government specifications. The section on stress concentration is incomplete due to the omission of the three-dimensional cases, and stress intensifiers in torsion. The section on impact is a thorough one including tension, torsion, and bending impact properties. The section on creep and temperature properties is noteworthy, because the author introduces the low-temperature embrittlement of certain metals, with the transition temperature concept as a separate phenomenon, divorced from impact—and this is a refreshing (and in the reviewer's opinion, correct) approach. The treatment of creep in tension, torsion, and under combined stress is clear and complete.

The second part treats the structure and properties of specific materials, mostly metals. The topics dealing briefly with the elementary concept of the structure of matter, manufacturing and forming, and some metallography, make the unit self-contained and sufficiently complete for the purposes of this book.

The last part describes the testing machines and the more common type of measuring devices used in materials testing. The reviewer feels that a more balanced redistribution of the subject matter would improve the general appeal of the book; there are about seven pages devoted to combined stress-testing machines, in addition to some other special testing apparatus enumerated, while hardness testing is dispensed with on three pages.

The subject index is not adequate for readers who wish to use this as a reference book, and more detailed topics with cross references are desirable.

The reviewer opinions that Professor Marin has accomplished his avowed purpose in treating the mechanical properties of materials in a more analytical and more vigorous fashion than textbooks of the past and succeeds in filling the gaps between mechanical properties and application to design.

[1] Mechanical Engineer, The M. W. Kellogg Company, New York, N. Y. Mem. ASME.

Soil Testing

SOIL TESTING FOR ENGINEERS. By T. William Lambe. John Wiley & Sons, Inc., New York, N. Y., 1951. Cloth, 8½ × 11 in., ix and 165 pp., illus., $5.

REVIEWED BY RALPH E. FADUM[2]

THE text treats in a comprehensive manner practically all of the important laboratory soil tests for engineering purposes. Especially noteworthy is the author's treatment of the highly important consolidation and shearing-strength tests. The inclusion of numerous examples, typical data sheets, derivations of formulas, and a generous number of illustrations should be particularly helpful to the user of this text.

The text is well documented and is written on a level such that it should be reasonably suited to the needs of the advanced undergraduate student and the graduate student. It should also be of value as a reference for practicing engineers and soil-testing technicians.

The text justifies the author's objective as stated in the preface: "to fulfill the need of a text for the teaching of soil testing."
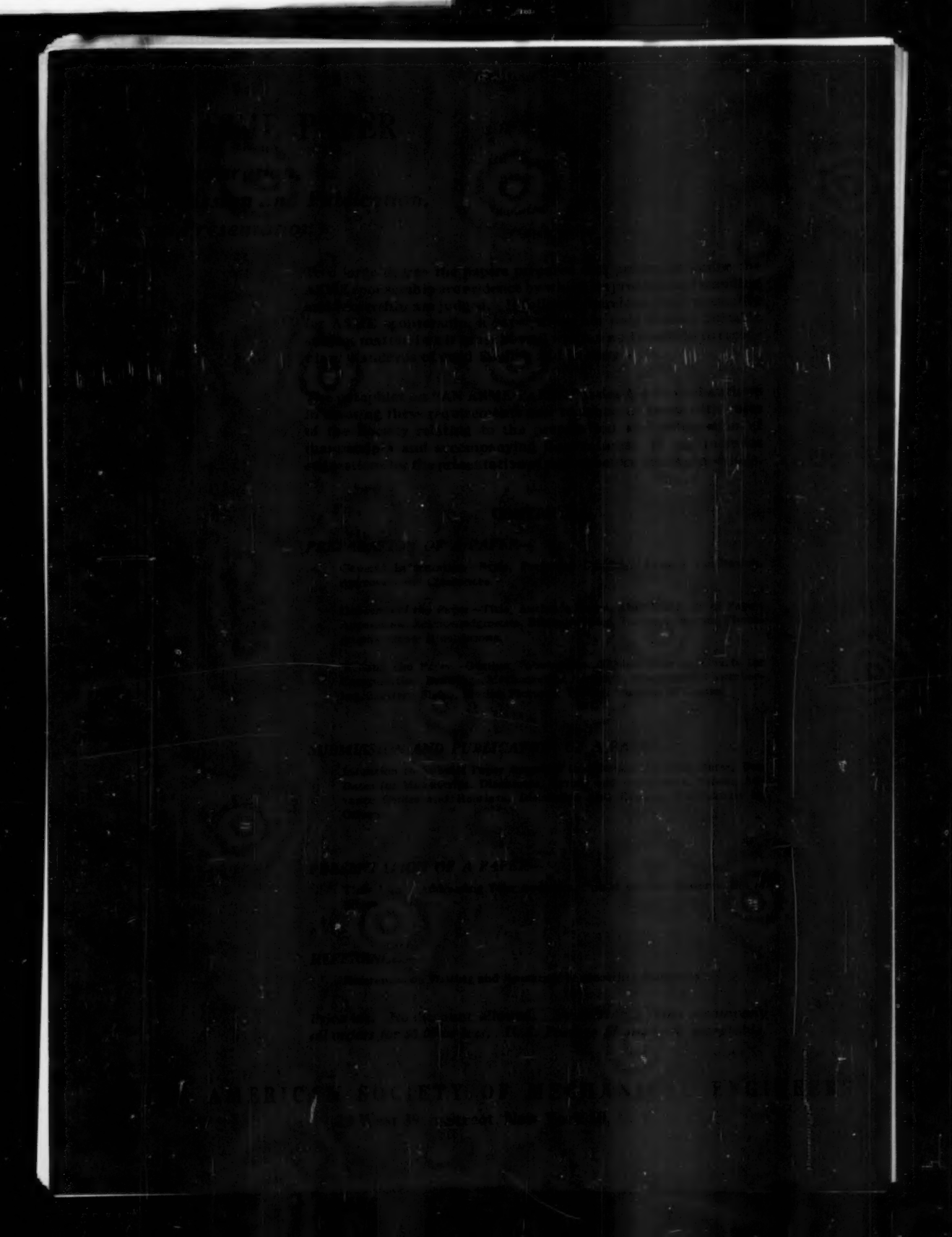
[2] Head, Department of Civil Engineering, North Carolina State College of Agriculture and Engineering of the University of North Carolina, Raleigh, N. C.